

Refractories Handbook

edited by
Charles A. Schacht



Refractories Handbook

MECHANICAL ENGINEERING
A Series of Textbooks and Reference Books

Founding Editor

L. L. Faulkner

*Columbus Division, Battelle Memorial Institute
and Department of Mechanical Engineering
The Ohio State University
Columbus, Ohio*

1. *Spring Designer's Handbook*, Harold Carlson
2. *Computer-Aided Graphics and Design*, Daniel L. Ryan
3. *Lubrication Fundamentals*, J. George Wills
4. *Solar Engineering for Domestic Buildings*, William A. Himmelman
5. *Applied Engineering Mechanics: Statics and Dynamics*, G. Boothroyd and C. Poli
6. *Centrifugal Pump Clinic*, Igor J. Karassik
7. *Computer-Aided Kinetics for Machine Design*, Daniel L. Ryan
8. *Plastics Products Design Handbook, Part A: Materials and Components; Part B: Processes and Design for Processes*, edited by Edward Miller
9. *Turbomachinery: Basic Theory and Applications*, Earl Logan, Jr.
10. *Vibrations of Shells and Plates*, Werner Soedel
11. *Flat and Corrugated Diaphragm Design Handbook*, Mario Di Giovanni
12. *Practical Stress Analysis in Engineering Design*, Alexander Blake
13. *An Introduction to the Design and Behavior of Bolted Joints*, John H. Bickford
14. *Optimal Engineering Design: Principles and Applications*, James N. Siddall
15. *Spring Manufacturing Handbook*, Harold Carlson
16. *Industrial Noise Control: Fundamentals and Applications*, edited by Lewis H. Bell
17. *Gears and Their Vibration: A Basic Approach to Understanding Gear Noise*, J. Derek Smith
18. *Chains for Power Transmission and Material Handling: Design and Applications Handbook*, American Chain Association
19. *Corrosion and Corrosion Protection Handbook*, edited by Philip A. Schweitzer
20. *Gear Drive Systems: Design and Application*, Peter Lynwander
21. *Controlling In-Plant Airborne Contaminants: Systems Design and Calculations*, John D. Constance
22. *CAD/CAM Systems Planning and Implementation*, Charles S. Knox
23. *Probabilistic Engineering Design: Principles and Applications*, James N. Siddall
24. *Traction Drives: Selection and Application*, Frederick W. Heilich III and Eugene E. Shube
25. *Finite Element Methods: An Introduction*, Ronald L. Huston and Chris E. Passerello
26. *Mechanical Fastening of Plastics: An Engineering Handbook*, Brayton Lincoln, Kenneth J. Gomes, and James F. Braden
27. *Lubrication in Practice: Second Edition*, edited by W. S. Robertson
28. *Principles of Automated Drafting*, Daniel L. Ryan
29. *Practical Seal Design*, edited by Leonard J. Martini
30. *Engineering Documentation for CAD/CAM Applications*, Charles S. Knox

31. *Design Dimensioning with Computer Graphics Applications*, Jerome C. Lange
32. *Mechanism Analysis: Simplified Graphical and Analytical Techniques*, Lyndon O. Barton
33. *CAD/CAM Systems: Justification, Implementation, Productivity Measurement*, Edward J. Preston, George W. Crawford, and Mark E. Coticchia
34. *Steam Plant Calculations Manual*, V. Ganapathy
35. *Design Assurance for Engineers and Managers*, John A. Burgess
36. *Heat Transfer Fluids and Systems for Process and Energy Applications*, Jasbir Singh
37. *Potential Flows: Computer Graphic Solutions*, Robert H. Kirchhoff
38. *Computer-Aided Graphics and Design: Second Edition*, Daniel L. Ryan
39. *Electronically Controlled Proportional Valves: Selection and Application*, Michael J. Tonyan, edited by Tobi Goldoftas
40. *Pressure Gauge Handbook*, AMETEK, U.S. Gauge Division, edited by Philip W. Harland
41. *Fabric Filtration for Combustion Sources: Fundamentals and Basic Technology*, R. P. Donovan
42. *Design of Mechanical Joints*, Alexander Blake
43. *CAD/CAM Dictionary*, Edward J. Preston, George W. Crawford, and Mark E. Coticchia
44. *Machinery Adhesives for Locking, Retaining, and Sealing*, Girard S. Haviland
45. *Couplings and Joints: Design, Selection, and Application*, Jon R. Mancuso
46. *Shaft Alignment Handbook*, John Piotrowski
47. *BASIC Programs for Steam Plant Engineers: Boilers, Combustion, Fluid Flow, and Heat Transfer*, V. Ganapathy
48. *Solving Mechanical Design Problems with Computer Graphics*, Jerome C. Lange
49. *Plastics Gearing: Selection and Application*, Clifford E. Adams
50. *Clutches and Brakes: Design and Selection*, William C. Orthwein
51. *Transducers in Mechanical and Electronic Design*, Harry L. Trietley
52. *Metallurgical Applications of Shock-Wave and High-Strain-Rate Phenomena*, edited by Lawrence E. Murr, Karl P. Staudhammer, and Marc A. Meyers
53. *Magnesium Products Design*, Robert S. Busk
54. *How to Integrate CAD/CAM Systems: Management and Technology*, William D. Engelke
55. *Cam Design and Manufacture: Second Edition; with cam design software for the IBM PC and compatibles, disk included*, Preben W. Jensen
56. *Solid-State AC Motor Controls: Selection and Application*, Sylvester Campbell
57. *Fundamentals of Robotics*, David D. Ardayfio
58. *Belt Selection and Application for Engineers*, edited by Wallace D. Erickson
59. *Developing Three-Dimensional CAD Software with the IBM PC*, C. Stan Wei
60. *Organizing Data for CIM Applications*, Charles S. Knox, with contributions by Thomas C. Boos, Ross S. Culverhouse, and Paul F. Muchnicki
61. *Computer-Aided Simulation in Railway Dynamics*, by Rao V. Dukkipati and Joseph R. Amyot
62. *Fiber-Reinforced Composites: Materials, Manufacturing, and Design*, P. K. Mallick
63. *Photoelectric Sensors and Controls: Selection and Application*, Scott M. Juds
64. *Finite Element Analysis with Personal Computers*, Edward R. Champion, Jr., and J. Michael Ensminger
65. *Ultrasonics: Fundamentals, Technology, Applications: Second Edition, Revised and Expanded*, Dale Ensminger
66. *Applied Finite Element Modeling: Practical Problem Solving for Engineers*, Jeffrey M. Steele
67. *Measurement and Instrumentation in Engineering: Principles and Basic Laboratory Experiments*, Francis S. Tse and Ivan E. Morse

68. *Centrifugal Pump Clinic: Second Edition, Revised and Expanded*, Igor J. Karassik
69. *Practical Stress Analysis in Engineering Design: Second Edition, Revised and Expanded*, Alexander Blake
70. *An Introduction to the Design and Behavior of Bolted Joints: Second Edition, Revised and Expanded*, John H. Bickford
71. *High Vacuum Technology: A Practical Guide*, Marsbed H. Hablanian
72. *Pressure Sensors: Selection and Application*, Duane Tandeske
73. *Zinc Handbook: Properties, Processing, and Use in Design*, Frank Porter
74. *Thermal Fatigue of Metals*, Andrzej Weronki and Tadeusz Hejwowski
75. *Classical and Modern Mechanisms for Engineers and Inventors*, Preben W. Jensen
76. *Handbook of Electronic Package Design*, edited by Michael Pecht
77. *Shock-Wave and High-Strain-Rate Phenomena in Materials*, edited by Marc A. Meyers, Lawrence E. Murr, and Karl P. Staudhammer
78. *Industrial Refrigeration: Principles, Design and Applications*, P. C. Koelet
79. *Applied Combustion*, Eugene L. Keating
80. *Engine Oils and Automotive Lubrication*, edited by Wilfried J. Bartz
81. *Mechanism Analysis: Simplified and Graphical Techniques, Second Edition, Revised and Expanded*, Lyndon O. Barton
82. *Fundamental Fluid Mechanics for the Practicing Engineer*, James W. Murdock
83. *Fiber-Reinforced Composites: Materials, Manufacturing, and Design, Second Edition, Revised and Expanded*, P. K. Mallick
84. *Numerical Methods for Engineering Applications*, Edward R. Champion, Jr.
85. *Turbomachinery: Basic Theory and Applications, Second Edition, Revised and Expanded*, Earl Logan, Jr.
86. *Vibrations of Shells and Plates: Second Edition, Revised and Expanded*, Werner Soedel
87. *Steam Plant Calculations Manual: Second Edition, Revised and Expanded*, V. Ganapathy
88. *Industrial Noise Control: Fundamentals and Applications, Second Edition, Revised and Expanded*, Lewis H. Bell and Douglas H. Bell
89. *Finite Elements: Their Design and Performance*, Richard H. MacNeal
90. *Mechanical Properties of Polymers and Composites: Second Edition, Revised and Expanded*, Lawrence E. Nielsen and Robert F. Landel
91. *Mechanical Wear Prediction and Prevention*, Raymond G. Bayer
92. *Mechanical Power Transmission Components*, edited by David W. South and Jon R. Mancuso
93. *Handbook of Turbomachinery*, edited by Earl Logan, Jr.
94. *Engineering Documentation Control Practices and Procedures*, Ray E. Monahan
95. *Refractory Linings Thermomechanical Design and Applications*, Charles A. Schacht
96. *Geometric Dimensioning and Tolerancing: Applications and Techniques for Use in Design, Manufacturing, and Inspection*, James D. Meadows
97. *An Introduction to the Design and Behavior of Bolted Joints: Third Edition, Revised and Expanded*, John H. Bickford
98. *Shaft Alignment Handbook: Second Edition, Revised and Expanded*, John Piotrowski
99. *Computer-Aided Design of Polymer-Matrix Composite Structures*, edited by Suong Van Hoa
100. *Friction Science and Technology*, Peter J. Blau
101. *Introduction to Plastics and Composites: Mechanical Properties and Engineering Applications*, Edward Miller
102. *Practical Fracture Mechanics in Design*, Alexander Blake
103. *Pump Characteristics and Applications*, Michael W. Volk
104. *Optical Principles and Technology for Engineers*, James E. Stewart

105. *Optimizing the Shape of Mechanical Elements and Structures*, A. A. Seireg and Jorge Rodriguez
106. *Kinematics and Dynamics of Machinery*, Vladimír Stejskal and Michael Valášek
107. *Shaft Seals for Dynamic Applications*, Les Horve
108. *Reliability-Based Mechanical Design*, edited by Thomas A. Cruse
109. *Mechanical Fastening, Joining, and Assembly*, James A. Speck
110. *Turbomachinery Fluid Dynamics and Heat Transfer*, edited by Chunill Hah
111. *High-Vacuum Technology: A Practical Guide, Second Edition, Revised and Expanded*, Marsbed H. Hablani
112. *Geometric Dimensioning and Tolerancing: Workbook and Answerbook*, James D. Meadows
113. *Handbook of Materials Selection for Engineering Applications*, edited by G. T. Murray
114. *Handbook of Thermoplastic Piping System Design*, Thomas Sixsmith and Reinhard Hanselka
115. *Practical Guide to Finite Elements: A Solid Mechanics Approach*, Steven M. Lepi
116. *Applied Computational Fluid Dynamics*, edited by Vijay K. Garg
117. *Fluid Sealing Technology*, Heinz K. Muller and Bernard S. Nau
118. *Friction and Lubrication in Mechanical Design*, A. A. Seireg
119. *Influence Functions and Matrices*, Yuri A. Melnikov
120. *Mechanical Analysis of Electronic Packaging Systems*, Stephen A. McKeown
121. *Couplings and Joints: Design, Selection, and Application, Second Edition, Revised and Expanded*, Jon R. Mancuso
122. *Thermodynamics: Processes and Applications*, Earl Logan, Jr.
123. *Gear Noise and Vibration*, J. Derek Smith
124. *Practical Fluid Mechanics for Engineering Applications*, John J. Bloomer
125. *Handbook of Hydraulic Fluid Technology*, edited by George E. Totten
126. *Heat Exchanger Design Handbook*, T. Kuppan
127. *Designing for Product Sound Quality*, Richard H. Lyon
128. *Probability Applications in Mechanical Design*, Franklin E. Fisher and Joy R. Fisher
129. *Nickel Alloys*, edited by Ulrich Heubner
130. *Rotating Machinery Vibration: Problem Analysis and Troubleshooting*, Maurice L. Adams, Jr.
131. *Formulas for Dynamic Analysis*, Ronald L. Huston and C. Q. Liu
132. *Handbook of Machinery Dynamics*, Lynn L. Faulkner and Earl Logan, Jr.
133. *Rapid Prototyping Technology: Selection and Application*, Kenneth G. Cooper
134. *Reciprocating Machinery Dynamics: Design and Analysis*, Abdulla S. Rangwala
135. *Maintenance Excellence: Optimizing Equipment Life-Cycle Decisions*, edited by John D. Campbell and Andrew K. S. Jardine
136. *Practical Guide to Industrial Boiler Systems*, Ralph L. Vandagriff
137. *Lubrication Fundamentals: Second Edition, Revised and Expanded*, D. M. Pirro and A. A. Wessol
138. *Mechanical Life Cycle Handbook: Good Environmental Design and Manufacturing*, edited by Mahendra S. Hundal
139. *Micromachining of Engineering Materials*, edited by Joseph McGeough
140. *Control Strategies for Dynamic Systems: Design and Implementation*, John H. Lumkes, Jr.
141. *Practical Guide to Pressure Vessel Manufacturing*, Sunil Pullarcot
142. *Nondestructive Evaluation: Theory, Techniques, and Applications*, edited by Peter J. Shull
143. *Diesel Engine Engineering: Thermodynamics, Dynamics, Design, and Control*, Andrei Makartchouk
144. *Handbook of Machine Tool Analysis*, Ioan D. Marinescu, Constantin Ispas, and Dan Boboc

145. *Implementing Concurrent Engineering in Small Companies*, Susan Carlson Skalak
146. *Practical Guide to the Packaging of Electronics: Thermal and Mechanical Design and Analysis*, Ali Jamnia
147. *Bearing Design in Machinery: Engineering Tribology and Lubrication*, Avraham Harnoy
148. *Mechanical Reliability Improvement: Probability and Statistics for Experimental Testing*, R. E. Little
149. *Industrial Boilers and Heat Recovery Steam Generators: Design, Applications, and Calculations*, V. Ganapathy
150. *The CAD Guidebook: A Basic Manual for Understanding and Improving Computer-Aided Design*, Stephen J. Schoonmaker
151. *Industrial Noise Control and Acoustics*, Randall F. Barron
152. *Mechanical Properties of Engineered Materials*, Wolé Soboyejo
153. *Reliability Verification, Testing, and Analysis in Engineering Design*, Gary S. Wasserman
154. *Fundamental Mechanics of Fluids: Third Edition*, I. G. Currie
155. *Intermediate Heat Transfer*, Kau-Fui Vincent Wong
156. *HVAC Water Chillers and Cooling Towers: Fundamentals, Application, and Operation*, Herbert W. Stanford III
157. *Gear Noise and Vibration: Second Edition, Revised and Expanded*, J. Derek Smith
158. *Handbook of Turbomachinery: Second Edition*, Revised and Expanded, edited by Earl Logan, Jr., and Ramendra Roy
159. *Piping and Pipeline Engineering: Design, Construction, Maintenance, Integrity, and Repair*, George A. Antaki
160. *Turbomachinery: Design and Theory*, Rama S. R. Gorla and Aijaz Ahmed Khan
161. *Target Costing: Market-Driven Product Design*, M. Bradford Clifton, Henry M. B. Bird, Robert E. Albano, and Wesley P. Townsend
162. *Fluidized Bed Combustion*, Simeon N. Oka
163. *Theory of Dimensioning: An Introduction to Parameterizing Geometric Models*, Vijay Srinivasan
164. *Handbook of Mechanical Alloy Design*, edited by George E. Totten, Lin Xie, and Kiyoshi Funatani
165. *Structural Analysis of Polymeric Composite Materials*, Mark E. Tuttle
166. *Modeling and Simulation for Material Selection and Mechanical Design*, edited by George E. Totten, Lin Xie, and Kiyoshi Funatani
167. *Handbook of Pneumatic Conveying Engineering*, David Mills, Mark G. Jones, and Vijay K. Agarwal
168. *Clutches and Brakes: Design and Selection, Second Edition*, William C. Orthwein
169. *Fundamentals of Fluid Film Lubrication: Second Edition*, Bernard J. Hamrock, Steven R. Schmid, and Bo O. Jacobson
170. *Handbook of Lead-Free Solder Technology for Microelectronic Assemblies*, edited by Karl J. Puttlitz and Kathleen A. Stalter
171. *Vehicle Stability*, Dean Karnopp
172. *Mechanical Wear Fundamentals and Testing: Second Edition, Revised and Expanded*, Raymond G. Bayer
173. *Liquid Pipeline Hydraulics*, E. Shashi Menon
174. *Solid Fuels Combustion and Gasification*, Marcio L. de Souza-Santos
175. *Mechanical Tolerance Stackup and Analysis*, Bryan R. Fischer
176. *Engineering Design for Wear*, Raymond G. Bayer
177. *Vibrations of Shells and Plates: Third Edition, Revised and Expanded*, Werner Soedel
178. *Refractories Handbook*, edited by Charles A. Schacht

179. *Practical Engineering Failure Analysis*, Hani M. Tawancy, Anwar UI-Hamid, and Nureddin M. Abbas
180. *Mechanical Alloying and Milling*, C. Suryanarayana
181. *Mechanical Vibration: Analysis, Uncertainties, and Control, Second Edition, Revised and Expanded*, Haym Benaroya
182. *Design of Automatic Machinery*, Stephen J. Derby
183. *Practical Fracture Mechanics in Design: Second Edition, Revised and Expanded*, Arun Shukla
184. *Practical Guide to Designed Experiments*, Paul D. Funkenbusch

Additional Volumes in Preparation

Mechanical Engineering Software

Spring Design with an IBM PC, Al Dietrich

Mechanical Design Failure Analysis: With Failure Analysis System Software for the IBM PC, David G. Ullman

Refractories Handbook

edited by
Charles A. Schacht
*Schacht Consulting Services
Pittsburgh, Pennsylvania, U.S.A*



MARCEL DEKKER, INC.

NEW YORK • BASEL

Although great care has been taken to provide accurate and current information, neither the author(s) nor the publisher, nor anyone else associated with this publication, shall be liable for any loss, damage, or liability directly or indirectly caused or alleged to be caused by this book. The material contained herein is not intended to provide specific advice or recommendations for any specific situation.

Trademark notice: Product or corporate names may be trademarks or registered trademarks and are used only for identification and explanation without intent to infringe.

Library of Congress Cataloging-in-Publication Data

A catalog record for this book is available from the Library of Congress.

ISBN: 0-8247-5654-1

This book is printed on acid-free paper.

Headquarters

Marcel Dekker, Inc., 270 Madison Avenue, New York, NY 10016, U.S.A.
tel: 212-696-9000; fax: 212-685-4540

Distribution and Customer Service

Marcel Dekker, Inc., Cimarron Road, Monticello, New York 12701, U.S.A.
tel: 800-228-1160; fax: 845-796-1772

Eastern Hemisphere Distribution

Marcel Dekker AG, Hutgasse 4, Postfach 812, CH-4001 Basel, Switzerland
tel: 41-61-260-6300; fax: 41-61-260-6333

World Wide Web

<http://www.dekker.com>

The publisher offers discounts on this book when ordered in bulk quantities. For more information, write to Special Sales/Professional Marketing at the headquarters address above.

Copyright © 2004 by Marcel Dekker, Inc. All Rights Reserved.

Neither this book nor any part may be reproduced or transmitted in any form or by any means, electronic or mechanical, including photocopying, microfilming, and recording, or by any information storage and retrieval system, without permission in writing from the publisher.

Current printing (last digit):

10 9 8 7 6 5 4 3 2 1

PRINTED IN THE UNITED STATES OF AMERICA

Preface

This book was developed to provide a comprehensive source of a broad range of technical aspects of refractories to be used by the refractory manufacturers, refractory material engineers, refractory lining designers, and industrial users of refractories. Basic industry processing materials from the bowels of the earth require high-temperature processing and the use of refractories. Refractories are necessary to insulate and control the process temperature and to minimize heat loss from the process. They are required to insulate the vessel or support structure from the process temperature to prevent overheating and deterioration of the support structure. Without the support or structure, the high-temperature process cannot be contained.

The first three chapters provide the fundamentals of refractories. Refractories deteriorate from either or both chemical and mechanical effects. The fundamentals of refractory material properties are addressed in Chapter 1. Fracture mechanics or those aspects of the mechanical deterioration of refractories are provided in Chapter 2. Chapter 3, on the corrosion of refractory brick, looks at the chemical deterioration of refractories.

Several of the fundamental types of refractory brick are addressed in Chapters 4 through 9. Included here are alumina-silica, magnesite, silica, dolomite, and spinel-containing brick. Because of the high thermal conductivity of carbonaceous refractories described in Chapter 8, carbonaceous refractory linings are basically designed as a cooling system rather than as an insulating system.

Castables continue to gain popularity as a refractory lining system in many of the basic industries. Chapters 10 through 12 are devoted to castables, with each

chapter discussing different aspects of castables. These three chapters are intended to capture most of the significant factors of castable lining design.

Chapter 13 is devoted to the thermomechanical aspects of refractory linings. Although brick refractory lining systems are primarily addressed, nearly all the fundamental concepts of brick lining design can be directly applied to castable lining design. Fundamental considerations include the classification of load types, fundamentals of refractory strength, selecting the best refractory based on static compressive stress–strain data, the fundamentals of cylindrical lining behavior, and fundamentals of expansion allowance.

Chapters 14 and 15 give examples of refractory lining systems used in the petrochemical and steel industries, respectively. Both chapters are written by authors with many years of experience in these industries and provide valuable insight in the design of lining systems.

Chapter 16 discusses all the various tests that can be conducted on refractories to determine the thermal and mechanical material properties, as well as tests to determine such properties as spalling resistance and other inferential properties. Spalling tests are defined as inferential, because the refractory shape is not subjected to the complete stress–strain operating environment during testing. However, these tests are very valuable in ranking candidate refractory materials.

Chapter 17 deals with the installation of refractories. Although there are numerous types of lining system geometries and combinations of refractory materials, this chapter is intended to give an overview of the basic aspects that should be considered in refractory lining installation.

Charles A. Schacht

Contents

<i>Preface</i>	<i>iii</i>
<i>Contributors</i>	<i>xi</i>
1. Properties of Refractories <i>Subrata Banerjee</i>	1
2. Fracture of Refractories <i>Richard C. Bradt</i>	11
3. Corrosion of Refractories <i>Denis A. Brosnan</i>	39
4. Alumina-Silica Brick <i>Denis A. Brosnan</i>	79
5. Magnesite Refractories <i>Richard A. Landy</i>	109
6. Silica Brick Material Properties <i>Charles A. Schacht and James C. Hays</i>	151
7. Dolomite Refractories <i>Colin Richmond</i>	183

8.	Carbonaceous Refractories <i>Albert J. Dzermejko</i>	201
9.	Spinel-Containing Refractories <i>S. Zhang and W. E. Lee</i>	215
10.	Refractory Castables <i>Leonard Krietz</i>	259
11.	Unshaped Refractory Products <i>Rudolf Krebs</i>	287
12.	Surface Chemistry as a Tool for the Development of Advanced Refractory Castables <i>André A. Studart and Victor C. Pandofelli</i>	335
13.	Thermomechanical Considerations for Refractory Linings <i>Charles A. Schacht</i>	369
14.	Refractory Applications in Refineries and Circulating Fluid Bed Reactors <i>M. S. Crowley</i>	395
15.	Byproduct Coke Oven Battery Heating Wall Refractories—Damage and Causes of Failure <i>Roger L. Rueckl</i>	415
16.	Testing of Refractory Materials <i>Sarah Baxendale</i>	435
17.	Refractory Lining Design and Installation <i>Charles A. Schacht and Michael Maupin</i>	475
	<i>Index</i>	491

Contributors

Subrata Banerjee, Ph.D. Answer Technology, Inc., Wheaton, Illinois, U.S.A.

Sarah Baxendale, B.Sc. Process and Materials Division, CERAM Research, Stoke-on-Trent, Staffordshire, England

Richard C. Bradt, Ph.D. Alton N. Scott Professor of Engineering, Department of Metallurgical and Materials Engineering, The University of Alabama, Tuscaloosa, Alabama, U.S.A.

Denis A. Brosnan, Ph.D. National Brick Research Center, College of Engineering and Science, and Department of Materials Science and Engineering, Clemson University, Clemson, South Carolina, U.S.A.

M. S. Crowley, Ph.D., P.E. M. S. Crowley Ltd., Crete, Illinois, U.S.A.

Albert J. Dzermejko, B.S. Consulting Engineer, Schaumburg, Illinois, U.S.A.

James C. Hays, B.S., P.E. Civil & Environmental Consulting, Inc., Pittsburgh, Pennsylvania, U.S.A.

Rudolf Krebs, Dipl. Ing. Retired, St. Augustin, Germany

Leonard Krietz, B.S. Department of Research & Development, Plibrico Company, Chicago, Illinois, U.S.A.

Richard A. Landy, Ph.D. Consultant, Landy & Associates, State College, Pennsylvania, U.S.A.

W. E. Lee, D. Phil Department of Engineering Materials, The University of Sheffield, Sheffield, England

Michael Maupin, B.S., M.B.A. Maupin Enterprises, LLC, Northville, Michigan, U.S.A.

Victor C. Pandolfelli, Ph.D. Department of Materials Engineering, Federal University of São Carlos, São Carlos, Brazil

Colin Richmond, Ph.D.* Consultant, LWB Refractories, York, Pennsylvania, U.S.A.

Roger L. Rueckl, B.S. Independent Refractory Consultant, Apollo, Pennsylvania, U.S.A.

Charles A. Schacht, Ph.D., P.E. Schacht Consulting Services, Pittsburgh, Pennsylvania, U.S.A.

André R. Studart, Ph.D. Department of Materials Engineering, Federal University of São Carlos, São Carlos, Brazil

S. Zhang, Ph.D. Department of Engineering Materials, The University of Sheffield, Sheffield, England

**Current affiliation:* Independent Consultant, Ripon, North Yorkshire, England

1

Properties of Refractories

Subrata Banerjee

Answer Technology, Inc., Wheaton, Illinois, U.S.A.

I. INTRODUCTION

Refractory materials, by definition, are supposed to be resistant to heat and are exposed to different degrees of mechanical stress and strain, thermal stress and strain, corrosion/erosion from solids, liquids and gases, gas diffusion, and mechanical abrasion at various temperatures. Different refractories are designed and manufactured so that the properties of the refractories will be appropriate for their applications. In most cases, refractory properties can be predicted from the results of appropriate tests; for others, knowledge and experience predict the refractory properties where direct tests correlating the properties are not available. The testing of refractory properties can, in most cases, indicate the performance of a refractory in actual application. Hence, appropriate testing of refractories for predicting properties, closely simulative to their applications, is of great importance. In this chapter, the importance of the refractory properties is covered so that performance in actual application will closely resemble their characteristic properties.

Refractories are mostly used (70%) in basic metal industries. In iron and steel making in integrated plants, iron is made in the blast furnace. Here iron is formed from the reduction of iron ore by carbon in the presence of limestone, which helps in forming the slag. Inside the blast furnace, the refractories experience abrasion in the upper part and intense heat and molten slag and metal contacts in the lower region. After the metal and slag are formed, they come out through a tap hole, which is opened and closed intermittently as the liquid iron is formed. The property requirement of the tap hole material should be such that the hole can be conveniently drilled for tapping molten iron and slag out and then the hole can be plugged for the process to be repeated when the iron

will be ready to be tapped. After the molten iron and slag comes out of the tap hole, it flows through the trough in the cast house, where the iron and slag are separated. Iron goes through the iron runner into the receiving ladles, and slag goes through the slag runner in the slag ladle or slag pit. Thus, the properties of the trough should be that it resists the impact and splashing of the molten iron and slag. It also should have sufficient resistance to the molten iron and slag interface where the refractory is affected most. The property requirements in the cast house refractories are thus well defined.

In the steel-making process by the basic oxygen furnace (BOF), the molten iron from the blast furnace combined with some scrap iron is purified from the impurities such as C, S, P, Mn, etc. by blowing oxygen through the molten iron either by lances from the top or by blowing oxygen through pipes at the bottom. In the process, the molten metal experiences vigorous stirring along with intense heat. The refractory properties in the BOF should be such that it resists the molten slag (basic) and the high temperature generated in the process. Basic refractories (MgO-based) containing carbon are used, which provides the required properties of high temperature and resistance to basic slag.

Properties of refractories required in the electric arc furnace (EAF) are slightly different than those of BOF. In the electric arc furnace, steel is primarily made from scrap iron. Here the refractory properties should be that it can tolerate the mechanical impingement of the scrap iron and the arcing created from the electric current. Arcing in the lining sometimes experiences intense heat in localized areas, called “hot spots.” The refractory property requirement is to have good mechanical strength, high refractoriness, and basic slag resistance.

In recent years, most of the metallurgical operations have usually been done in ladle metallurgical furnaces (LMF). The property requirements of these refractories are thus more stringent than classical ladle refractories. The refractory properties should be such that it will be able to resist the alloying operations along with reheating the molten metal when needed. The stringent property requirements of the ladle and tundish tubes (shrouds), slide gates, and nozzles should allow the operator to continue the process at the desired level. There are specific refractory property needs for the refractories used in the tundish backup and working lining. The working lining should be able to resist the steel and slag contacts and have enough shrinkage so that the lining should be able to deskill conveniently and completely.

In other primary metal industries such as aluminum, the refractory properties requirements are quite different than steel making. Although the temperature of aluminum refining and alloying process is much lower than steel, it has the unique problem of penetration in the refractories. Hence, the refractory should be designed so that it has a nonwetting characteristic to molten aluminum. The nonwetting properties are introduced in the refractories by special additives.

In hydrocarbon industries, the property requirements of the refractories are different than those of metal industries. Although the temperature in petrochemical refining is much lower than in metal industries, the refractories suffer a high rate of abrasion due to the flow of high-velocity particles at a continuous rate. Hence, the major characteristic requirement of these refractories is abrasion resistance. Also, the refractories need to be able to conserve heat. Hence, there are defined ranges of thermal conductivity for different regions of the process so that the processes conserve energy during the conversion processes.

In the glass-making process, the refractories in the glass tank are in constant contact with the molten glass, and this poses different kinds of requirements for the refractory. Since glass in the molten state is quite fluid and tends to go through the refractory pores, the most needed characteristic should be nonporous refractories, and hence fused refractories are used in molten glass contact areas.

It is obvious that the property requirements of refractories vary significantly according to the application and use in different processes. Hence, individual refractories need to be designed with characteristic properties for specific systems since the requirements vary with different high-temperature processes.

Refractories are broadly divided into two categories—shaped (bricks and cast shapes) and unshaped (monolithic) refractories. There are two kinds of shaped refractories—the primary kind is like brick or similar shapes and the other kind is the shapes made from monolithic refractories, where they are dictated by the properties of the monolithic refractories. For shaped refractories (like brick making), attaining maximum density after the shapes are formed is the goal of the process.

There are different kinds of monolithic refractories, namely plastics, ramming mixes, mortars, coatings, castables/pumpables, and gunning mixes. The physical characteristics of plastics and ramming mixes are their ease of ramming to consolidate to proper density. For mortars and coatings, they should have appropriate consistency to be used as desired for the specific applications. For gunning mixes, the material should have good adhesion to the gunned surface, low rebound, and appropriate properties as designed. For castable/pumpable refractories, the primary characteristics are particle size distribution, which in effect controls the flowability along with proper addition of minor ingredients and controls the workability; setting and strength development upon curing and heating; and the bonding system, which dictates the high-temperature properties.

Since the development of vibratable and pumpable castables, methods have been standardized for measuring the flowability of a castable, which can predict the flow characteristics. The test consists of filling up a cone with the castable refractory and then letting it flow under vibration for a specified time. The predetermined flowability characteristics define the castable's use in actual applications.

Refractory properties can be classified as follows:

Physical

Density

Porosity

Strength

Abrasion

Thermal

Thermal shock

Thermal conductivity

Thermal diffusivity

Chemical

Corrosion/erosion

II. PHYSICAL PROPERTIES

Physical property requirements for shaped and unshaped refractories are different. For shaped refractories, the main requirements are their density and porosity and dimensional tolerance. Monolithic (unshaped) refractories, on the other hand, have to be characterized with different parameters. For plastics refractories, the workability and aging characteristics are the prime requirements, whereas, for ramming mixes, the rammability with proper compaction is the main requirement. For castable/pumpable refractories, the prime requirement is the flowability at a specific water addition with or without vibration. In recent years, castable/pumpable refractories have been the most predominant monolithic refractories for most applications. Significant work has been done with castable/pumpable refractories since the development of low and ultralow cement castables. The development of sol-gel bonded refractories introduced the pumpable characteristics of castables. Since then, the low and ultralow cement castables have been designed to have self-flow and pumpable characteristics. This is achieved by careful selection of grain sizing of the castable components. Specific grain size distribution parameters are required in flowability for a castable to make it self-flowable and pumpable. The setting parameters are supposed to be associated with the flowability since adverse effects may take place if the castable/pumpable does not satisfy the setting parameters.

Refractory materials are characterized by their physical properties, which often indicate the use and performance of refractory materials. The physical appearance of a refractory material sample, submitted for testing, is quite important since the results of testing of a refractory will be as good as the sample submitted for testing. The predictability of refractory uses in specific applications is, in most cases, dictated by past experience. In general, the basic physical

properties can often indicate whether a refractory material can be used for intended applications. The following basic physical properties are often used to predict, select, and prescribe refractories for specific applications:

- Density and porosity
- Strengths—cold and hot, their importance
- Abrasion

The above properties are determined by standard ASTM (1) tests, and hence the materials are classified and characterized according to their physical test results. The significance and characterization of the above tests can be summarized as follows:

Density and Porosity (ASTM D-20). The values of density and porosity determined by standard methods are used to recommend or predict the use of refractories for specific uses. In general, the higher the density, the lower the porosity. Also, other physical properties, such as strength, abrasion, and gas permeability, are often related to the density and porosity of the refractory.

Strengths. Cold and hot, their importance—The physical strengths, in both cold and hot conditions, are often characterized as measures of the use of a refractory. Cold strengths indicate the handling and installation of the refractory, whereas hot strengths indicate how the refractory will perform when used at elevated temperatures. Initial strength develops in refractory materials during the forming process. For shaped refractories, the strengths often develop during the physical processing of the products and sometimes followed by higher temperatures where the refractory goes through a firing process. For monolithic refractories, the initial strength develops during the installation or forming process (for precast shapes), and the final strength develops while in application.

In recent years, more importance has been given to high-temperature strengths of refractories rather than cold strengths since refractories are used at elevated temperatures and not at room temperatures.

Strengths of refractories are measured as cold compressive strength, cold modulus of rupture, or hot modulus of rupture. Hot modulus of rupture provides the best indication of the performance of a refractory material in use.

Cold Compressive Strength (ASTM C-133). The cold compressive strength of a refractory material is an indication of its suitability for use of refractories in construction. It is a combined measure of the refractory for the strength of the grains and also of the bonding system.

Cold Modulus of Rupture (ASTM C-133). The cold modulus of rupture of a refractory material indicates the flexural strength and its suitability for use in construction. It is indicative of the strength of the bonding system of the refractory product. Since the test is done at room temperature, it can only show its

suitability and its use in construction. It provides no indication of how the refractory will behave at elevated temperatures.

Hot Modulus of Rupture (ASTM C-583). The hot modulus of rupture provides the indication of a refractory material about its flexural strength at elevated temperatures. Since refractories are used at elevated temperatures, the hot modulus of rupture is the true indicator of the suitability and performance of a refractory at high temperatures. Hence, in recent years, the hot modulus of rupture has been prescribed and required by users as the most important test criterion for selection and use of refractories.

Abrasion Resistance (ASTM C-704). This is a measure of the resistance of a refractory material when high-velocity particles abrade the surface of the refractory. It measures the strength of the bond and the refractory particles and its resistance to the flow of high-velocity particles across its surface. The need for good abrasion resistance of refractory materials is most evident in petrochemical industries where fine particles impinge the refractory surface at high velocities at moderately elevated temperatures. A direct correlation between abrasion resistance and cold crushing strength has recently been established. Thus, the cold crushing strengths can provide, and have a direct indication about, the predictability of a refractory material regarding its resistance to abrasion.

III. THERMAL PROPERTIES

A. Thermal Expansion

This is a measure of the refractory about its linear stability when it is exposed to different ranges of high temperatures and then cooled to room temperatures. It is defined as a permanent linear change (ASTM C-113) and is measured by the changes in the longest linear dimensions. Most refractory materials expand when heated. Hence, when refractories are installed at room temperatures, the whole structure tightens up when heated. But if the temperature reaches higher than the softening temperature of the bonding system, the structure may distort or collapse. Hence, refractory systems should always be designed in such a way that the maximum temperature attainable in the system is lower than the softening or melting temperature of the refractory ingredients (grains and bonding system). Often cracks are observed in monolithic refractory systems when cooled, but, in most cases, the apparent cracks visible on cooling close up after the system is heated up.

B. Thermal Shock

This is measure of the refractory property when the refractory is exposed to alternate heating and cooling. It is an important property for a refractory material. Most high-temperature processes experience heating and cooling. Both refractory grains and the bonding system expand while being heated and contract during cooling. Having similar grains in the structure, the thermal shock resistance depends on the matrix bonding the grains. Thus, refractories having structures with built-in microcracks of defects show better thermal shock resistance than with rigid systems. In some refractories, the bonding system, by nature, possesses microstructural defects or cracks that provide better thermal shock resistance.

There are two standard methods for determining the thermal shock resistance of refractory materials. For brick shapes, thermal shock resistance is measured by “Ribbon Thermal Shock Testing” (ASTM C-1100), and for monolithic refractories the standard method is ASTM C-1171. These tests clearly differentiate among refractory materials about their resistance to thermal shocks.

A clear difference is exhibited in castables where the different bonding systems are a low-cement castable and sol–gel bonding with similar alumina contents (2) as exhibited in Figure 1.

C. Thermal Conductivity

Thermal conductivity is a measure of the refractory regarding its ability to conduct heat from the hot to the cold face when it is exposed to high temperatures. There are three different methods of determining thermal conductivity of refractory materials. ASTM C-210 is the standard method for determining

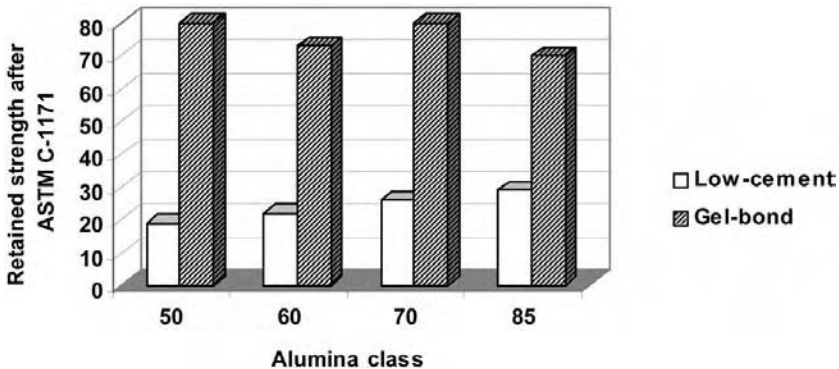


Figure 1 Retained strength of low-cement and gel-bond castables with similar alumina contents (grains) as per ASTM C-1171.

thermal conductivity of refractories; ASTM C-202 is the standard method for determining thermal conductivity of refractory brick; and ASTM C-1113 is the standard method for determining thermal conductivity of refractories by hot wire. The thermal conductivity tests are particularly important for insulating refractories where the thermal gradients from the hot face to the cold face dictate the use of a refractory material for the specific uses.

D. Thermal Diffusivity

The thermal diffusivity property is particularly useful for carbon-containing materials. ASTM C-714 is the standard method for determining thermal diffusivity of carbon and graphite by the thermal pulse method.

IV. CHEMICAL PROPERTIES

The chemical properties of a refractory are defined by the chemical analysis of the refractory grains, by the nature of the bonding, and also by the ability of the refractory to resist the action of liquids when exposed to high temperatures.

The chemical properties of a refractory material are primarily dictated by the chemical composition of the refractory. The bonding system of the refractory plays a vital role in dictating its properties. When refractories are exposed to corrosive liquids at high temperatures, the extent of corrosion/erosion depends on the refractory grains and the chemical bonding system of the refractory.

Refractory corrosion may be caused by mechanisms such as dissolution in contact with liquid, a vapor–liquid or solid-phase reactions (3). It may also occur due to penetration of the vapor or liquid in the pores, resulting in an alternate zone. In most cases, corrosion is the result of some combination of these factors. The nature and rate of dissolution of a refractory in a liquid can be calculated from a phase equilibrium diagram. A concentration gradient occurs in the refractory composition at the boundary region when the refractory comes in contact with the molten slag. The refractory components diffuse through the interfacial film and dissolve in the liquid. The interfacial film influences the rate of dissolution. The larger the concentration gradient, the faster the dissolution rate and thus the refractory dissolves more readily.

Corrosion/erosion resistance is one of the most important characteristics of refractories, which are exposed to molten metal and slag. Hence, the design of the tests closely simulating the conditions that the refractories experience during use is of great importance.

During the formulation of a refractory, close attention is given to a refractory composition in choosing the refractory grains and the bonding system. Thus, refractories used in an iron-making process will differ from that of a steel-making

process since the nature of the metal and slag is different in these cases. In iron making, the metal and liquid slag is primarily neutral or slightly acidic in nature, whereas the slag is distinctively basic in the steel-making process. Refractories chosen for iron making are based on alumina and silica, whereas magnesia-base refractories are the choice for steel making.

Since the exposure of refractories to molten metal/slag is a dynamic process, the tests simulating the conditions also need to be dynamic. For steel-making refractories, the rotary slag test (ASTM C874) provides close simulation of the conditions in steel-making refractories.

For iron-making refractories, primarily for blast furnace cast house applications, a dynamic slag test in an induction furnace (4, 5) has been designed that closely simulates the conditions in a blast furnace trough. The test method is designed to compare refractories with that of a standard whose corrosion/erosion characteristics are known. The test is done in an induction furnace, where a natural movement of the metal occurs in the furnace due to the inductive force in the furnace. Four specimen bars with dimensions of $205 \times 38 \times 38$ mm are hung from a holding rod rotating at a speed of 8 to 10 revolutions per minute. After pre-heating above the molten slag/iron in the furnace, the specimens are dipped in the liquid slag and iron until sufficient corrosion/erosion is visible on the specimens. The specimens are then pulled out and cooled, the relative wears are visually compared, and then the areas around the maximum wear are measured. This gives the comparative corrosion/erosion behavior of the specimens tested. This test has been found to be the best simulative behavior of blast furnace cast house refractories.

V. CERAMIC PROPERTIES

Ceramic properties of a refractory material are defined by its nature or reaction when exposed to heat. Refractories behave differently when exposed to heat, depending on the type of the refractory and how it has been formed. For fired bricks, the ceramic reactions and bonds have already been instituted by high-temperature firing. Hence, when they are exposed to high temperature, they do not exhibit any further change. However, for unfired refractories, the formulations are designed so that the ceramic reactions are supposed to take place at those temperatures. Thus, for fired bricks like fireclay, high-alumina, magnesia-chrome-type bricks, which are already fired at high temperatures, do not exhibit any further ceramic reaction when exposed to high temperatures. But for unfired refractories, like magnesia-carbon bricks and alumina-carbon bricks, the formulations are designed so that the ceramic properties will be developed at use temperatures.

For monolithic refractories, the formulations are made so that the ceramic properties develop when they are exposed to high temperatures. Monolithic refractories, like plastics, ramming mixes, dry vibratables, mortars, and coatings,

are already prepared and are to be applied as received. By contrast, castables and gunning mixes are supposed to be mixed with water or the liquid bond for application. Thus, for monolithic refractories, in particular, it is of interest to find the ceramic reactions that take place at or before service temperatures.

In phosphate-bonded plastics, the progressive reactions that take place while it is being heated are provided in detail (6). Depending on the bonding system, the ceramic reactions for gunning mixes take place at high temperatures for specific applications. Thus, the organic bonding in gunning mixes acts only to help in adherence of the material on the gunned surface. With heat the organic bonding will burn out, leaving the ceramic bonding to take over at higher temperatures. For castables and gunning mixes containing high-alumina hydraulic cements (calcium aluminates), the initial strength development occurs by the hydraulic process, while the ceramic bondings take place at higher temperatures (7).

Recent developments in low- and ultralow-cement castables/pumpables, the effects of the ultrafine particles are of great significance. The water requirements are low since the ultrafine silica fume particles (mostly used in these compositions) occupy part of the space of water. Although the silica fume helps in reducing water requirements in the castable, it affects high-temperature properties due to the formation of anorthite and gehlinit phases at temperatures around 1250°C–1400°C. The effects are somewhat minimized in ultralow cement castables due to the use of lesser quantity of calcium aluminate cement.

Due to the recent development of sol–gel bonded refractories (2), the high-temperature properties of castable/pumpable refractories have improved significantly since the high-temperature phases are no longer low-melting. It forms mullite only at higher temperatures (since there is no CaO or MgO) and thus provides better properties at elevated temperatures.

REFERENCES

1. ASTM – ASTM Book of Standards.
2. Banerjee S. Versatility of gel-bond pumpable/castable refractories. ALAFAR XXVIII Congress, Aruba, 1999:13–24.
3. Banerjee S. Monolithic Refractories. World Scientific Publications Private Ltd and The American Ceramic Society, 1998:222–223.
4. Banerjee S, Singh KN, Youmans CT. Use of pumpable castable in Bethlehem steel blast furnace at Sparrows Point. Steel World Quarterly, Oct 1994.
5. Banerjee S, Anderson MW, Singh JP, Poeppel RB. Reaction of iron and slag with refractories. UNITECR '93 Proc. 3, 1481–1492.
6. Banerjee S. Monolithic Refractories. World Scientific Publications Private Ltd and The American Ceramic Society, 1998:151.
7. Banerjee S. Monolithic Refractories. World Scientific Publications Private Ltd and The American Ceramic Society, 1998:51–52.

2

Fracture of Refractories

Richard C. Bradt

The University of Alabama, Tuscaloosa, Alabama, U.S.A.

I. ABSTRACT

Fracture of refractories is considered from the traditional strength point of view and from the perspective of fracture mechanics. Strength and fracture toughness are related through the aggregate sizing of refractories, which illustrates the importance of the microstructural aspects of the refractory aggregate to the strength. The J-integral analysis methodology and the wedge-splitting experimental technique are both reviewed as they are useful to address the nonlinear load-displacement character of refractories. The latter is associated with the concept of a rising R-curve, which is discussed from the phenomenological point of view. The rising R-curve is directly related to the refractory aggregates through toughening mechanisms that are active in the crack process zones, both in front of and behind an extending crack.

The refractory toughening processes are responsible for the nonlinear portions of the stress-strain and load-displacement curves, or diagrams and the rising R-curves. Thermal shock damage, which is originally addressed from the conventional strength viewpoint, is then considered within the rising R-curve concept. It is concluded that the refractory aggregates, their size and distribution in a refractory body, assume an absolutely critical role in refractory fracture phenomena. This is because of the crucial role that aggregates assume in the following wake region of a crack. The aggregate distribution must be the focus of microstructural design for improved fracture characteristics when all other factors are equal in a refractory body.

II. INTRODUCTION

Fracture has always been a critical problem for refractories during their use. It has not been a field that is without progress, as can be appreciated by referring to previous reviews (1, 2). However, it is an extremely complicated topic, for industrial refractories are diverse multiphase composites that are utilized under dynamic conditions. In addition, the large volumes required for metallurgical process vessel linings have constrained many commercial refractories to use mineral systems that contain natural impurities, many of which are silicates. During refractory processing, the silicates develop into bonding grain boundary phases that frequently dominate the fracture process at the elevated temperatures of refractory applications. These special features elevate refractories to a unique technical position in the hierarchy of materials, a position that is a combination of ceramics, geology, mineralogy, and engineering composite technology. Unfortunately, this special blend of science and technology has not always been a particularly active area for fundamental research. Refractories lie within the realm of industrial technology where commercial profit is the goal in contrast to an understanding of the scientific technical phenomena.

The composite nature of refractories separates the refractory fracture process from that of single-phase, fine grain size, high-strength brittle structural ceramics and more closely associates refractory fracture with the fracture of engineering composite materials. For example, similar to high-tech composites, refractories generally exhibit rising R-curves during crack extension or propagation. Of course, commercial refractories are dynamic high-tech composites (3). Thus, in addition to the direct brittle fracture phenomenon, one must also have some understanding of the development of a crack process zone about the crack and the role of R-curves during the fracture process. Unfortunately, the R-curve phenomenon has not been extensively nor systematically studied in any refractory system, so many implications can only be inferred from other studies of the phenomenon such as those on the simple structural ceramic systems.

Fracture is one of the two most common modes of failure for the refractory linings of modern industrial processing vessels. The other is chemical attack, or corrosion by the material that the refractories are containing within the process vessel, often molten metals or glasses at very high temperatures. With molten metals, a unique corrosion process is also common from the slags protecting the liquid metals from the atmosphere. Often these slag/refractory reactions are so intense and so problematical that special types of refractories, different from those in the rest of the process vessel lining, must be employed at the slag lines of metallurgical vessels.

Fracture failures of refractories are of several varieties, including simple mechanical overload as may develop from impact during the loading of the

process vessel with scrap metal. Thermal stress fracture during cooling or heating, particularly the initial heat-up of a vessel or during rapid thermal cycling between heats, is another type of failure. In the case of refractory concretes or castables, the situation of explosive fracture from moisture entrapment is also a major concern (4). These fractures may be catastrophic and result in the complete loss of the refractory lining. Sometimes thermal shock simply causes surface spalling and a significant reduction of the lifetime, or campaign, of the lining. However, fracture need not always be disastrous; it may just result in the development of a crack pattern in the process vessel lining. Those crack surfaces may be held together and closed by the vessel lining compressive stresses that develop from thermal expansion when the vessel is heated to operating temperatures.

III. REFRACTORY STRENGTHS

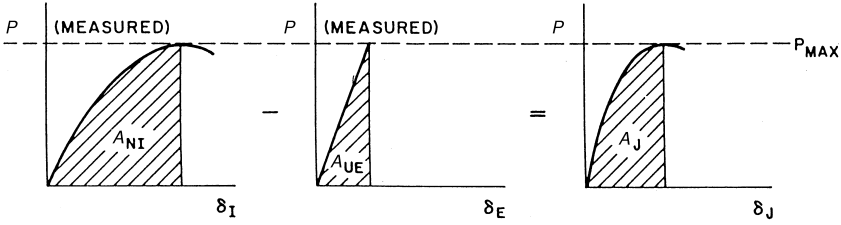
Even today, after nearly a half-century of fracture mechanics, fracture of refractories remains closely associated with the mechanics concept of strength as defined in undergraduate strength of materials courses. Strengths of refractories are usually reported in terms of the three-point bend strength or the flexural strength, frequently called the modulus of rupture (MOR). In the case of refractories, there exists a standard test for this simple strength measurement. It is based on the familiar formula:

$$\sigma_f(\text{MOR}) = 3PL/2bh^2, \quad (1)$$

where σ_f is the strength in three-point bending, L is the length of the test span, b is the specimen width, and h is the specimen height. The fracture load is P . It specifies the tensile stress at the bottom of the flexing bend test beam. Although perhaps 80% or 90% of the refractory strengths that have been reported in the literature were obtained on the basis of tests using Eq. (1), this approach leaves much to be desired. It is complicated by the specimen preparation, the flaw distribution in the refractory, and the rate at which the testing load is applied during the actual strength test (5). Some researchers have developed an appreciation for another strength test, the Brazil test. In that test a cylindrical specimen is diametrically loaded in compression to produce an internal tensile failure aligned with the specimen diameter. However, the Brazil test is not discussed here.

In principle, Eq. (1) is strictly applicable only when the load-displacement curve is fully linear elastic to failure, similar to the middle diagram in Figure 1, which illustrates an unnotched J-integral measurement test specimen. Unfortunately, only rarely are the load-displacement curves determined during the normal strength measurements of refractories. Often the displacement is not

LOAD DISPLACEMENT CURVES



SPECIMENS



$$J_{Ic} = \frac{2}{bB} \int_0^{\delta_J} P d\delta$$

$$J_{Ic} = \frac{2}{bB} (A_{NI} - A_{UE})$$

$$J_{Ic} = \frac{2}{bB} (A_J)$$

Figure 1 The illustrated compliance technique for J-integral determination. (From Ref. 18.)

monitored at all. It is not an unreasonable conclusion that much of the refractory bend strength data in the literature is suspect. However, as a consequence of many years of utilization of strength data based on this type of bending or flexural strength measurement, refractories applications engineers have developed a methodology for refractory lining design based on the data from these types of tests. This type of strength test will undoubtedly remain a part of refractory fracture for the foreseeable future and probably beyond that time.

Equation (1) can be converted to fracture mechanics terminology through the familiar Griffith equation, which in the analogous form to the above equation is

$$\sigma_f(\text{MOR}) = K_{Ic} Y C^{-1/2}, \tag{2}$$

where K_{Ic} is the fracture toughness, Y is a geometric factor equal to $\pi^{-1/2}$ in the classical, center crack Griffith derivation, and C is the critical flaw size (6). When refractories fail in a brittle elastic manner, where the load-displacement curve is clearly linear elastic to failure, then both Eqs. (1) and (2) are satisfactory representations for the strength. However, when refractories do not fail in a brittle linear elastic manner, such as when an extensive nonlinear region develops prior to fracture, then the use of these two equations is not the best practice for strength determinations. They are, however, used with regularity in the refractories field with general disregard for their limitations.

Before proceeding with the actual fracture process in refractories, it is important to consider the strength and toughness levels of industrial refractories in a global sense. This calibrates the reader and provides some understanding of the real importance of the strengths of refractories in service. For the most part, refractory linings, or systems, are not subjected to severe load-bearing conditions; their function is primarily one of containment. Refractories do not have a major structural role in their applications. For these reasons, refractories do not need to be very strong—just strong enough to maintain their integrity. In fact, from the thermal shock damage perspective, as will be discussed later, high strength can actually be a serious detriment to thermal shock damage resistance for many refractory applications.

Strengths for various types of refractories are not tabulated here, but their general level of strength will be discussed for the purpose of comparison relative to other materials. Typically, refractories have room-temperature bend, or flexural strengths as expressed through measurements using Eq. (1) in the range of approximately 10–40 MPa (\sim 1500 to 6000 psi). It is important to realize that refractories are not very strong by any standards or comparisons. However, refractories do not need to be very strong, for they do not generally serve a major structural load-bearing function. Often the refractory linings of process vessels are coupled to the structural steel shell of that process vessel, or supported by elaborate anchoring systems to the process vessel superstructure. In most applications, refractories must do little more than support their own weight, which usually is not very significant. In some other instances, refractories may be designed to be in a stress state of compression, where they are somewhat stronger, although not very strong.

Refractories are utilized at elevated temperatures, so there is naturally an interest in the change of their strength with increasing temperature. When the strength of refractories is measured by the three-point bend test and done so as a function of temperature, then the bend or flexural strength invariably exhibits a maximum that is associated with the softening of the silicate bonds. This strength maximum is usually not a very large one. It is usually observed between 600°C and 1400°C, depending on the particular refractory type, its silicate content, and the specific chemistry of that silicate. At more elevated temperatures, above this strength maximum, the strength of the refractory rapidly decreases to only a few MPa and exhibits distinctly nonlinear load-displacement curves. Thus, although refractories are never very strong, they become even weaker at highly elevated temperatures, but they are noticeably less brittle as well. In addition, the loading rate dependence of strength at elevated temperatures becomes quite complicated. The coupling of the loading rate and temperature effects on strength has been previously addressed (2, 5). It is not a simple interdependency, but one that varies considerably from one refractory system to another.

When attempting to understand the fundamentals that govern the strengths of refractory systems, it is important to realize that although many refractories can be considered brittle materials at low temperatures ($< 600^{\circ}\text{C}$), once the temperature of the strength maximum is exceeded, refractories no longer remain very brittle. The silicates soften and impart a significant degree of "plasticity." Brittle fracture of refractories is not a major problem at elevated temperatures where a distinctly viscous, or plastic deformation, type of response occurs under most loading conditions. Furthermore, although literature exists reporting the high-temperature strengths of refractories, these strength values should only be accepted with reservations and only applied to design situations with a considerable degree of caution. Most of those strengths were probably not properly measured.

IV. THE FRACTURE TOUGHNESS/STRENGTH RELATIONSHIP

The studies of Nakayama in the 1960s developed the work-of-fracture test and applied it to refractories. He introduced energy concepts related to the extension of a single crack to refractory fracture (7). In the 1970s and 1980s, following Nakayama's lead, researchers realized that the approach to understanding the fracture of refractories was to conduct measurements on individual or single cracks, instead of, or in addition to, the common bend strength measurements. The path to understanding was to use the fracture mechanics approach of a single crack. Sakai and Bradt have reviewed and discussed numerous fracture mechanics test specimens and related them to the work-of-fracture measurement (8). There have been a number of measurements of the fracture toughnesses of refractories. The K_{Ic} -values were determined by the single-edge crack, or notched-beam bend specimen, where the normal three-point bend specimen was simply notched straight across at the half height with a thin diamond blade. From this simple bend test of an artificially cracked (diamond saw notched) specimen, the fracture toughness is then calculated from the equation

$$K_{Ic} = (3PLC^{1/2}/2bh^2)f\{c/h\}, \quad (3)$$

which bears a close resemblance to a combination of Eqs. (1) and (2) and where the parameters have the same identities. The $f\{c/h\}$ polynomial is related to the ratio of the crack length to the specimen thickness, although most researchers have used a straight through sawed artificial crack of a depth of one half of the specimen thickness. Several have tabulated this function (9, 10).

The fracture toughness can be measured by this test at low temperatures where fractures are predominantly brittle and the load-displacement curve is

essentially linearly elastic to failure. That toughness can be plotted versus the strength as measured by the three-point bend test for a group, or class of refractories, such as fireclays, or high aluminas. The result is a straight line that passes through the origin. The slope of this line, as indicated by Eq. (2), is the geometric constant, Y , multiplied by the square root of the critical flaw size, C . Flaw sizes estimated from the slopes of these plots are generally of the same size as the largest aggregates in the refractory. This is not surprising, for it has long been known that refractory mixes with larger top size aggregates have lower strengths than those containing just fine aggregates. It is evident that the intrinsic flaws in a refractory body are related to, or scale in size with, the largest aggregates in that refractory. It is an important point for understanding the strength of refractories and the role of the aggregates in the refractory mix.

It is desirable to comment on the values of the fracture toughness that have been reported for refractories, if for no other reason than to appreciate their susceptibility to fracture. Although it is usually not appropriate to group aluminosilicates and basic refractory bricks, or shapes together with refractory castables, in this instance it is not a technical disaster to do so because of the broad generality that is intended by this calibration process. The reason is that refractories are not very tough by any standards. The fracture toughnesses of refractories usually are in the range of about 0.2 to $1.5 \text{ MPa} \cdot \text{m}^{1/2}$, not very large toughnesses. Refractory castables are at the lower portion of this range and fired bricks at the higher end. For comparison, the toughness of window glass is $0.75 \text{ MPa} \cdot \text{m}^{1/2}$ and that of most cast irons is about $20 \text{ MPa} \cdot \text{m}^{1/2}$, although some are lower and some are higher. The toughest steels are more than $200 \text{ MPa} \cdot \text{m}^{1/2}$ (6).

The rather low fracture toughness values for refractories are to be expected, for refractories are not very strong and their intrinsic flaws are quite large, as evidenced by the readily visible large aggregates (flaws) in refractory bodies. Although the fracture toughness is by no means the complete situation for the fracture of refractories, its low values clearly send the message that the crack initiation resistance of refractories is not very large. Cracking and fracture may be expected to be of concern for industrial refractories in many of their applications.

V. THERMAL STRESS FRACTURE

When fracture occurs as a consequence of the thermal stresses generated during the temperature changes that a refractory lining experiences during its initial heating, or during thermal cycling of day-to-day operational practices, the extent of damage during fracture is governed by an energy criterion. This is illustrated by Hasselman in his classical papers (11,12). Generally, for refractories, one

might expect these microstructures to experience quasi-static crack extension during any thermal shock, but kinetic crack growth is also a consideration, although probably much less so and is often unlikely. Similar equations address both situations. For kinetic crack growth, Hasselman derives and defines the kinetic thermal shock damage resistance parameter, R''' , as

$$R''' = E\gamma_{\text{wof}}/\sigma_f^2, \quad (4)$$

where E is the elastic modulus and γ_{wof} is the work-of-fracture as measured originally by Nakayama (7) and subsequently by Tattersall and Tappin (13). Hasselman similarly defines a quasi-static crack growth damage resistance parameter, R_{st} , which he expresses as

$$R_{\text{st}} = (\gamma_{\text{wof}}/E\alpha^2)^{1/2}, \quad (5)$$

where α is the coefficient of thermal expansion and the other parameters are as previously noted. These have been recently reviewed by Rodrigues and Pandofelli with specific reference to refractory castables (14).

Although it is not immediately obvious, Eqs. (4) and (5) have the same general dependency on the elastic modulus and strength. When the thermoelastic stress is expressed in simple form for total linear restraint in one dimension, it is of the form

$$\sigma = \alpha E f(T), \quad (6)$$

which, when squared on both sides, indicates that

$$\sigma^2 \sim \alpha^2 E^2. \quad (7)$$

Combining Eq. (7) with (5) for $E\alpha^2$ reveals that both R''' and R_{st} are inversely related to the strength squared divided by the elastic modulus, E . This quantity, (σ^2/E) , is essentially the stored elastic strain energy in an object at the stress level σ (15). It is the driving force for fracture or crack extension. It is not surprising that whether the thermal shock damage crack growth is either kinetic or quasi-static, the crack must still be driven by the stored elastic strain energy of the system.

The above analysis explains why the evolution of industrial refractory strengths over history has not been focused toward the development of high-strength refractories. The thermal stress damage resistance decreases as the strength increases and it does so as the square of the strength. High-strength refractories are much more susceptible to thermal shock damage. Refractory manufacturers have known this for some time as their ceramic engineers increased the thermal shock damage resistance of fireclays by adding large aggregates from crushed rejected "bats" to the refractory mix. Refractory engineering pioneers often expressed the thought that the large hard aggregates acted as ther-

mal shock crack stoppers (16). The aggregates may have functioned somewhat in that role, but it is more likely that the beneficial effect of the crushed brick aggregates was primarily one of introducing large flaws into the refractory microstructure and thus reducing the strength and the stored elastic strain energy available for thermal shock crack propagation. Now it is recognized that the strong large aggregates also assume an important role in the creation of a rising R-curve in refractories and will decrease the extent of crack propagation, a point discussed later. No matter how multifaceted the role of the aggregates may be, it is now obvious that where thermal shock damage resistance is a concern, then a stronger refractory is not necessarily a better refractory.

VI. NONLINEAR FRACTURE AND THE J-INTEGRAL APPROACH

Linear elastic, brittle fracture of refractories occurs only at room temperature, or at moderately elevated temperatures. Even at room temperature, many refractories, especially castables or other monolithics, will exhibit an extensive nonlinear portion of the load-displacement curve prior to failure in a normal bend strength test, and most certainly in a fracture mechanics test with a large artificial crack. The load-displacement curve for a typical strength test resembles that in the first diagram of Figure 1. This nonlinear form is the result of inelastic phenomena occurring in the region of the crack or fracture, both in the crack front process zone ahead of the main crack (microcracking) and also in the following wake region behind the crack front across the newly formed fracture surfaces (aggregate bridging). Typically, after the usual linear elastic region during initial loading, an extensive bending of the curve occurs and a nonlinear region develops that soon reaches a maximum value in the load-displacement curve. This general load-displacement characteristic of nonlinearity also occurs for many metals, but it is a consequence of the extensive plastic zone that develops surrounding the crack tip frontal region during yielding and dislocation plastic flow. The point is that the nonlinear stress-strain or load-displacement curve is a general load-displacement phenomenon in many materials, one that is not restricted to only industrial refractories.

To address this nonlinear inelastic phenomenon, Rice formulated a concept known as the J-integral (17). The J-integral is based on a path-independent energy-line integral that encompasses the crack region. It was initially applied to metals to extend the concepts of linear elastic fracture mechanics and to address the issue of the extensive plastic flow in the vicinity of the crack tip during loading. However, the general principles of the concept are universal and not restricted to any specific material nor to any particular nonlinear mechanism. Homeny et al. applied this parameter to the fracture of refractories

in the late 1970s (18). It seems only natural to apply the J-integral concept and experimental methodology to the fracture of refractories, but the concept has never received the universal acceptance that one might have anticipated. However, since it is basic in principle and will undoubtedly gain favor in some form in the future, perhaps in a related test of some sort, the simple experimental compliance method for J-integral determination is reviewed here.

Figure 1, after Homeny et al. (18), illustrates the basic principles of the experimental compliance technique for determining the J-integral. An artificially cracked or notched specimen and a geometrically identical but unnotched specimen are required. The notched specimen is loaded just past its maximum load, to clearly identify the nonlinear regime and its load-displacement curve is recorded. Then the area, A_{NI} is determined to the displacement point of the maximum load. Next, the similar, but unnotched specimen is loaded to the same P_{MAX} -value so that the stored elastic strain energy in the specimen, A_{UE} , can be determined and then subtracted from the energy of the notched specimen. The difference of the two, the remaining energy, is then used to calculate the critical value of the J-integral, J_{IC} , at the maximum load experienced by the notched specimen. This is the compliance technique as described by Rice et al. (17), Mindess et al. (19), and Roedig et al. (20).

This technique results in a J_{IC} -value that has the units of J/m^2 and thus requires comparison with a G_{IC} -value rather than a stress intensity-based fracture toughness, a K_{IC} . When Homeny et al. measured the J_{IC} -values and the K_{IC} -values for the same aluminosilicate refractories, according to Eq. (3), and then converted them to G_{IC} -values, they observed that the J_{IC} -values consistently exceeded the G_{IC} -values, often by as much as a factor of four or more. It is obvious that the J-integral technique is capable of measuring the energy demands of the crack process zone in refractories. Furthermore, the J-integral has a fundamental meaning for the microstructural condition associated with the maximum load. These are critical issues at the very heart of the microstructural design of refractories. It must be concluded that the J-integral has considerable potential for advancing the understanding of the fracture process, its relationship to microstructural design, and numerous related phenomena in refractory materials.

When Homeny et al. compared the energies from the J-integral method to twice the total work-of-fracture for the same refractories, $2\gamma_{wof}$, the latter was generally much larger, often four or five times as large (18). It is evident that when large cracks develop in refractory specimens, then there is considerable energy dissipation in the vicinity of the advancing crack front, probably both in the frontal process zone and in the following wake region. The fact that Homeny et al. did these experiments on laboratory-scale specimens that were only a few centimeters in their dimensions and that the fully developed process zone for their refractories would probably have been larger than the entire actual test specimen, suggests that the evolution of the process zone of refractories is a

fruitful area for future research. It is certainly one where a greater understanding will be beneficial to refractory microstructural development, especially for the strength and thermal shock damage resistance of refractories.

VII. WORK-OF-FRACTURE

The development of the work-of-fracture test and its subsequent application to fireclay refractories by Nakayama and Ishizuka were the seminal works that redirected the research on the fracture of refractories to that of using large single cracks similar to fracture mechanics research on metals (21). The work-of-fracture test remains one of the simplest tests that one can apply to refractories. However, similar to the previous comments above regarding the specimen size, it is now realized that the crack region process zone size for refractories can be quite large and many laboratory-scale work-of-fracture specimens are simply not large enough to permit an assessment of the full development of the crack process zone. In spite of this shortcoming, the work-of-fracture test will be discussed because of its simplicity and the extension of its concepts to current fracture tests that are much more popular. Its principles are essential ones to understand refractory fracture, especially thermal shock fracture and spalling.

A key issue to the work-of-fracture test is to provide a specimen geometry that encourages stable crack growth, that is a crack extension that the test machine is able to completely monitor during crack growth through the microstructure of the test specimen. It is also desirable to have a stiff, low-compliance testing machine to promote stable crack growth. Nakayama achieved both, the latter by building his own machine. For the former, Nakayama notched a simple three-point bend specimen at the center of its length to leave a triangular, or chevron, type of remaining ligament section such that the sharp apex of the triangular section was on the tensile side of the bend specimen during testing. When done properly, this promotes a stable load-displacement test curve as the crack grows through the test specimen. This crack stability issue is important and has been discussed at length by Nakayama et al. (22). The energy, or work-of-fracture, is then simply

$$\text{work-of-fracture} = \gamma_{\text{wof}} = \int \frac{P du}{2A}, \quad (8)$$

where the integral, $\int P du$, is simply the area under the load-displacement curve and A is the cross-sectional area of the remaining ligament of the specimen after notching. The factor of 2 is included because when a specimen is fractured, then two newly created fracture surfaces result. This is similar to the energies or areas under the curves in Figure 1. Although a chevron type of notch seems to be preferable nowadays, any triangular form of remaining specimen ligament that

encourages the initiation of stable crack growth at low applied loads is quite satisfactory.

Initially, it was considered that the work-of-fracture was a material constant, much like the elastic modulus, or the fracture toughness. The discovery of rising R-curves, which are discussed later, and the concept of a fully developed crack region process zone about an advancing crack have cast considerable doubt upon that original notion. Although discussion of this may be premature to the R-curve and crack process zone discussion later, it is nevertheless necessary. The work or energy to create a crack is dependent on the development of the energy-consuming process zone in the region of the crack. In a refractory with a rising R-curve, that process zone is a function of the crack size, or length, usually increasing in size with increasing crack length, but reaching a plateau value at its fullest stage of development. In most laboratory-scale work-of-fracture tests, the test specimen is just not sufficiently large enough to generate the plateau value or equilibrium configuration (steady state) of the crack process zone as the crack is extending, thus the energy for fracture, the work-of-fracture is continually increasing as the crack is growing. Unless the experimentalist has very large test specimens, ones where the steady-state condition of the crack process zone is achieved and then the work-of-fracture is normalized on a unit crack length basis in this plateau value or constant-size process zone region, the measured work-of-fracture may be expected to increase with increasing crack length and test specimen size as well. This dilemma relates to the fundamental origin of the rising R-curve and also applies to other similar materials such as structural concretes.

Some discussion is in order with regard to the use of the single edge crack notched-beam test previously described with regard to Eq. (3) for measuring the fracture toughness in an experimental manner such as to simultaneously extract a work-of-fracture value from the same experiment. In fact, many experimentalists like to extract these two items concurrently from the same test sample. Because of the efficiency of getting two pieces of data from only one test, researchers have found this test to be attractive. Many have used this technique with some modest degree of success, for many refractories are so well microstructurally designed to dissipate energy during crack growth that there is little or no difficulty obtaining a stable fracture from a straight through notch. If one is using a stiff testing machine, then a chevron specimen notch is not necessary. It seems easy.

Several dangers to generating data in this fashion exist, the most prevalent being the wandering of the propagating crack from the plane originally defined by the diamond-sawed notch. This generates a larger real fracture surface area than the apparent area of the notch plane. When this occurs, it produces erroneously large work-of-fracture values. Of course, the triangular notch has a restraining, a guiding effect on the propagating crack that is absent from a straight through notch. As straight through notches have a strong tendency to produce semistable

cracks, it is possible that the time response of the test machine may not be sufficiently high to fully monitor the crack growth during the notch-beam test. Some of the energy dissipation in the specimen may not be recorded. For these reasons, the author does not recommend using the single-edge crack notched-beam test to generate both fracture toughness and work-of-fracture results simultaneously.

As with the strength and the fracture toughness, it is appropriate to consider some of the work-of-fracture values of refractories in a global sense, if only to calibrate readers and refractory researchers. If one considers the work-of-fracture of glass, or that of the cleavage planes of single crystals, then the values are not too different from their thermodynamic surface free energies, only 1 or 2 J/m². For these materials the energies for crack initiation and propagation are virtually equal. Many fine grain size, high-strength structural advanced ceramics have work-of-fracture values that are at the level of about 10 J/m². Refractories generally have much larger work-of-fracture values. At room temperature, the more brittle, densely fired refractories have work-of-fracture values of about 30 J/m² and the microstructurally well-designed refractories have work-of-fracture values of about 100 J/m², or more. It should be apparent that refractories are substantially more resistant to crack growth than to crack initiation, by a factor of 10 or more.

Finally, when work-of-fracture values are measured as a function of temperature, the values in the vicinity of the strength maximum, or perhaps slightly above in temperature, are very large. The maxima in the work-of-fracture values at these elevated temperatures are often greater than 1000 J/m². This is predominantly from the presence of the viscous silicates. As expected, testing at still higher temperatures where the silicates are more fluid, or less viscous, reveals a substantial decrease in the work-of-fracture values to levels of only a few J/m².

VIII. FRACTURE TEST DEVELOPMENTS TO ADDRESS TESTING CONCERNS

As more refractories development included the fracture testing of refractories, it became evident that there were problems with obtaining representative results for the usual laboratory-scale test specimens. This was quite obvious with work-of-fracture specimens, as the scatter of individual results from multiple tests on the same refractory body yielded widely ranging results with unacceptably large confidence intervals. It was not difficult to understand the reason for this problem, as a simple visual examination of the fracture surfaces related the test results to the character of the fracture surfaces. Coarse aggregates were observed to be very important in the fracture process, often causing very large work-of-fracture values when the aggregate was near to the apex of the chevron, or remaining triangle ligament. It became evident that the coarse aggregate microstructure of

refractories would not allow for a representative sampling of the refractory for the small laboratory-scale specimens. Undoubtedly, one of the reasons was that it did not allow for complete development of the crack process zone region. Neither the microcracking and crack branching in front of the advancing crack, nor the bridging phenomena in the wake of the crack system, reached a steady-state configuration. A much larger test specimen was clearly in order to properly assess the coarse aggregate refractory structures. Of course, entire bricks, some a meter in dimension, are available as potential test specimens for many types of refractories.

Researchers at VRD in Leoben, Austria, have promoted the wedge-splitting fracture test where much larger specimens are possible and better specimen averaging and a much greater degree of crack process zone development are possible (23, 24). Although this test has not presently received widespread acceptance, nor has it been exploited to its fullest, it has the promise to provide considerable additional insight into the refractory fracture process. Unfortunately, several researchers using the wedge-splitting specimen test have chosen to redefine some of the standard fracture terminology and have created confusion for those without familiarity with the field. Systematic, orderly tests with this technique for different refractory microstructure variations are in order, and as a function of temperature to further elucidate the important fracture mechanisms.

The wedge-splitting test has some features in common with the previously noted J-integral compliance method. It merits further description for those who may wish to employ it for future refractory fracture testing. Figure 2 illustrates a schematic of the test specimen after Buchebner and Hartmut (24). It is evident that the name of the test, wedge-splitting, is quite a representative description. It has an elaborate fixture arrangement within a starter notch configuration and two side notches to restrict crack wandering during the actual test. It is loaded in compression and is able to generate fracture parameters from analysis of the load-displacement curve. Because of the specimen size and the large fracture surface area, there is generally no difficulty in obtaining fully stable fractures for refractories, and thus a reliable record of the total energy for crack propagation through the specimen is easily obtained with a stiff testing machine.

Figure 3 illustrates typical load-displacement curves for wedge-splitting refractory specimens. Depicted is a refractory of the "brittle" variety (perhaps a high fired superduty fireclay) and a "tough," or more energy-consuming, variety (such as a highly microcracked 70% alumina). When the load-displacement curve is integrated, analogous to Eq. (8), it is possible to obtain the total work-of-fracture. Some researchers using this technique have defined it as the specific fracture surface energy and used a G_F instead of the total work-of-fracture, $2\gamma_{wof}$. This may be a convenient nomenclature if it is intended to later relate this result to the strain energy release rate, G_C , or perhaps even a form of some variant of J_C ,

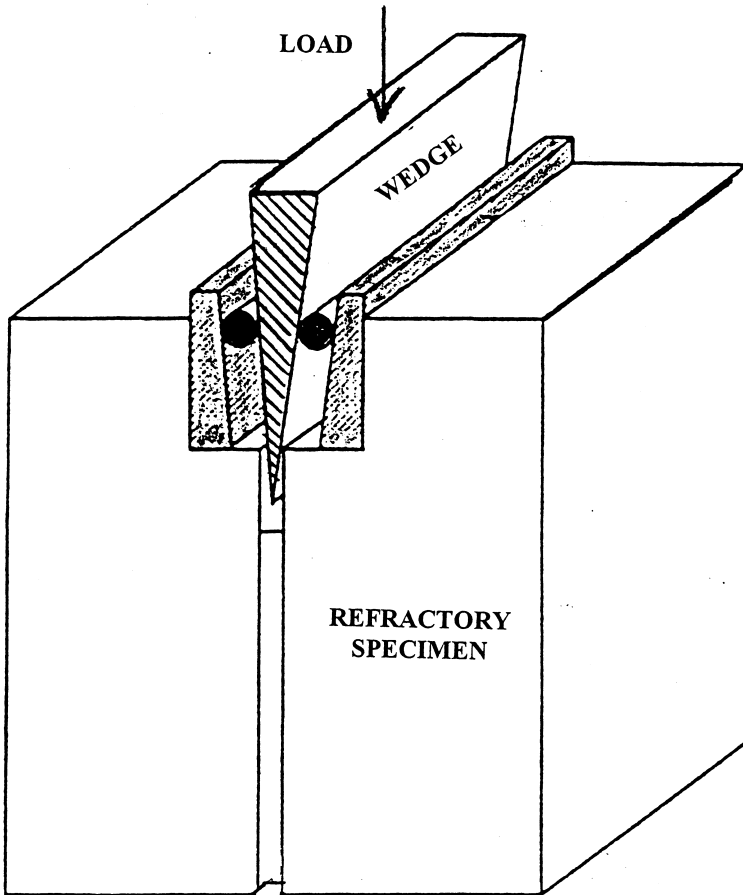


Figure 2 The wedge-splitting test specimen and configuration for fracture measurements. (From Ref. 24.)

but the experimental measurement is clearly that of the work-of-fracture as specified originally by Nakayama (7).

As the load-displacement curves are typically stable ones for the wedge-splitting specimens, they exhibit an initial linear elastic region and a moderate nonlinear region, which is followed by a maximum load value, similar to the first of the diagrams in Figure 1 for the J-integral, then a long tail of decreasing load with increasing displacement. It is also possible to use the maximum of this load-displacement curve for additional information, although the value of this

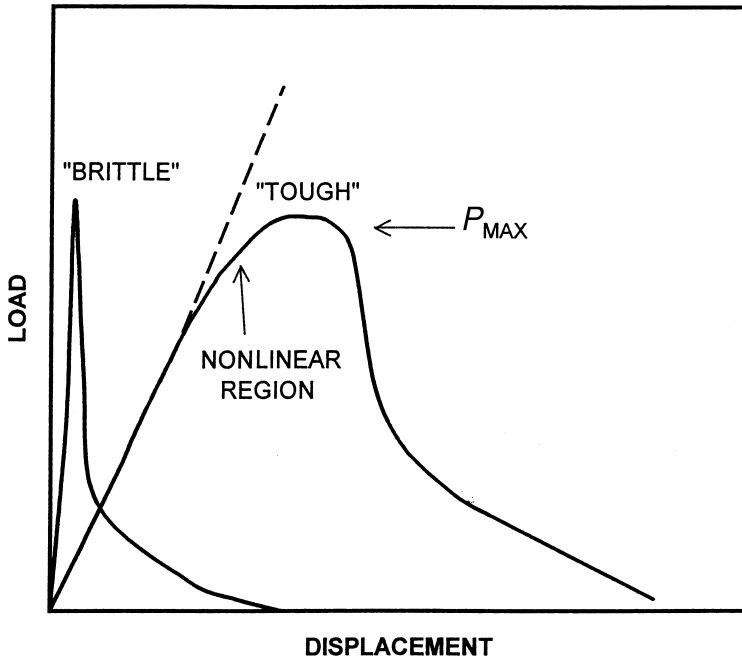


Figure 3 Schematic load-displacement curves for refractories in the wedge-splitting test.

information remains to be fundamentally demonstrated. Some researchers have suggested that the integration of the load-displacement curve to the peak as a measure of the strain energy release rate, G_C , is

$$G_C = \int \frac{P \, du}{2A} \Big|_0^{P_{\max}} \quad (9)$$

where the integral is taken to the maximum load, P_{\max} , and A is the remaining ligament or the eventual fracture surface area. This approach would have more merit if all test specimens in the universe were the same size. However, it should be recalled that a similar type approach is utilized in the J-integral compliance technique where the stored elastic strain energy in the test specimen at the maximum load is subtracted to specifically identify the crack process zone energy. As the stored elastic strain energy will vary with the test specimen size and the particular refractory material, it must be accounted for independently from the observed area under the load-displacement curve. This suggests that simply attributing the maximum load to a G_C quantity is not fundamentally correct. How-

ever, the G_C -value determined in this way may be a satisfactory approximation for development purposes within a single class of refractories such as mag-chrome or alumina-magnesia-carbon.

A particularly interesting and quite practical approach to utilize the above results from the wedge-splitting test is to assess the ratio of the area under the stable fracture curve from the initial loading point to the maximum, referred to as G_C above, and the total area of the stable load-displacement curve that yields the quantity referred to above as G_F . The ratio of the two quantities may be used to define a toughness, ductility, or flexibility ratio as

$$\text{ratio} = G_F/G_C. \quad (10)$$

This ratio will have a large value, >10 , for those refractories with high energy consumption during crack propagation relative to the energy required for crack initiation. This ratio is really nothing more, actually less on a fundamental basis because of the problems with G_C , than the well-known ratio relating the work-of-fracture and the single-edge notched-beam fracture surface energy:

$$\text{ratio} = \gamma_{\text{wof}}/\gamma_{\text{nbt}} = 2E\gamma_{\text{wof}}/K_{\text{Ic}}^2, \quad (11)$$

where the K_{Ic} -value is that determined by the single-edge cracked notched-beam test as previously noted and described by Eq. (3). The E is the elastic modulus of the refractory. When the separate issues of energy for propagation and initiation are expressed as above, it becomes quite obvious as to just why industrial experimentalists have attempted to obtain both K_{Ic} and γ_{wof} from a single test specimen, such as the single-edge cracked notched-beam test. The use of the wedge-splitting test specimen also may eventually accomplish this goal.

It is appropriate to note that either of the two ratios expressed by Eqs. (10) and (11) is a measure of the energy requirement for crack propagation divided by a quantity related to the energy required for crack initiation. The higher this ratio, the better the thermal shock damage resistance of the refractory and the greater the ability of the refractory to adapt to thermal and mechanical strains in service. The latter is frequently because the microstructure of the refractory is able to accommodate extensive internal cracking processes and still retain its mechanical integrity. The latter indirectly relates to the extent of the long tail portion of the load-displacement curve, either in the original work-of-fracture test or the wedge-splitting test. As pointed out by Buchebner and Hartmut (24), this is desirable for applications such as rotary cement kilns where the original perfect roundness of the steel kiln shell is changed throughout its lifetime from natural degradation processes.

IX. THE CRACK PROCESS ZONE FOR REFRACTORIES

It must be apparent, even obvious, that very interesting energy-absorbing phenomena occur in the vicinity of the cracks of refractories and that these consume a large amount of energy as the crack front advances (25). These events occur in two different regions: the process zone in front of the advancing crack and the following wake region that trails the advancing crack front. Once a crack begins to propagate, it develops a steady-state frontal process zone, but the region behind the crack continues to increase. The fact that large cracks are more difficult to propagate than short cracks suggests that the following wake region is more important to the crack growth resistance (26).

Figure 4 schematically illustrates the total process zone about the crack, both in front of and following behind the advancing crack front. In the front of the crack, where researchers once believed that all of the "action" occurred, microcracking is prevalent and there is usually considerable crack branching, much of the latter associated with the linking-up of microcracks in the region. The size of this frontal process region varies from one refractory material to another, but a simple estimate using a Dugdale-like approach suggests that this crack front region, or frontal process zone, may be quite large, far larger than most laboratory-scale test specimens when it is fully developed. This indicates that small laboratory-scale test specimen results may not produce absolute num-

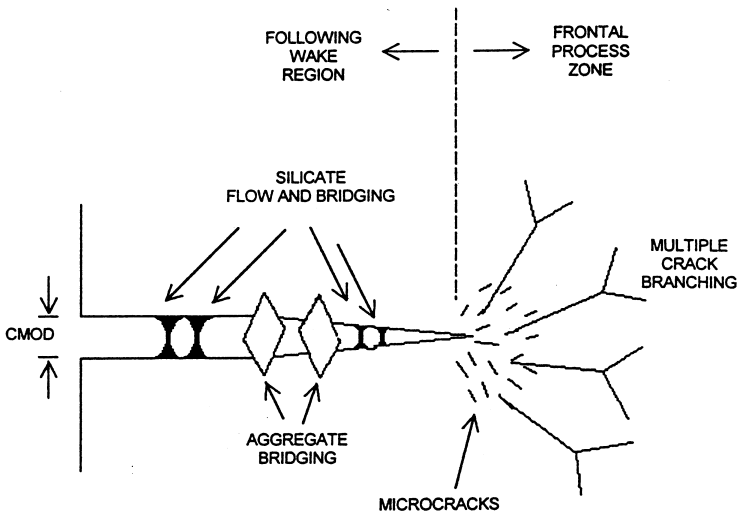


Figure 4 Schematic of the crack process zone for refractory materials.

bers, for the crack process zone, front and back, is only partially developed. Because of these size effects, laboratory-scale testing may only yield values for comparison between different refractory microstructures tested at the same sample size and under the identical testing conditions. Of course, even then, if the elastic moduli of the different refractory specimens vary widely, additional problems are created using some of the test techniques. This is because different amounts of elastic strain energy are stored in the sample and must be accounted for in addressing the microstructural energy-absorbing processes, or events as they relate to the load-displacement curves.

The other important region about an advancing crack front in refractories is the region behind the crack front. In brittle materials the crack opening displacement (COD) is not very large and neither is the crack mouth opening displacement (CMOD). Refractory microstructural elements such as the large aggregates are able to interact across the newly formed crack surfaces. It now appears that the phenomena occurring in the following wake region of the crack are the most important of all of the fracture, or cracking related phenomena in refractories. Certainly, they are the ones that contribute to the R-curve phenomenon described in the following section. Perhaps many things happen just past an advancing crack, but in refractories, the two believed to be the most important are refractory aggregate bridging and silicate ligament bonding, both of which are schematically illustrated in Figure 4.

Silicate ligament bridging of the crack surfaces is only of consequence to refractory fracture at elevated temperatures where the glassy silicates become viscous and can flow and form bonding ligaments between the newly created fracture surfaces. Of course, it is necessary that these silicate ligaments have some strength so as to be able to hold the forming crack faces together. They do, but only over a limited temperature range, for once the temperatures get too high, the viscosity of the silicates decreases and they are no longer strong enough to contribute to any significant bonding of the newly formed crack surfaces. This is probably the reason why there is a strength maximum as a function of temperature and a maximum in the work-of-fracture for silicate-containing refractory bodies. Of course, extensive bonding across the fracture surfaces of a crack of this general nature is not unfamiliar. It is the reason that fibers are used in high-technology fiber composites and also the reason that metal fibers are added to refractory castables. Those materials, similar to refractories, may crack but retain much of their integrity and remain coherent to a large extent.

The bridging role of the aggregates behind the advancing crack front is monumental to the crack growth resistance of refractory materials. Homeny and Bradt demonstrated the importance of the aggregate distributions with direct reference to the thermal shock damage resistance, comparing continuous and gap-sized aggregate distributions (27). Although the truly fundamental import-

ance of these microstructural components has been recognized for many years, it was not fully appreciated until recently that the aggregate contributions occurred in the following wake region after the crack front had actually passed. The details of the aggregate bridging mechanisms that contribute to the crack growth resistance are still not fully appreciated, nor completely understood. At least three have been suggested, namely bridging across the newly created crack surfaces; wedging of the aggregates behind the crack, which requires a bridging phenomenon, and the frictional effects of pullout of the aggregates from one side of the passing crack. The last obviously occurs with some regularity when one examines a refractory fracture surface and sees the large aggregates protruding as a consequence of cracks bypassing them and looping around them. Of course, this last process only occurs when the aggregates are stronger than their matrix bonding. Perhaps it was this latter observation that led the refractory pioneers to view the aggregates as crack stoppers (16). In any event, it is desirable to have aggregates as large and as strong as possible, not only to encourage crack bypass, but to otherwise consume energy during the bridging phenomena following the crack.

There are many opportunities for improving the crack growth resistance of refractories from the structural and microstructural design of the aggregates. First and foremost is the particle size distribution of the aggregate portion of the refractory batch mix (27). It is evident that to bridge the crack, an aggregate must be at least as large as the crack opening displacement, the COD, or perhaps rather the crack mouth opening displacement, the CMOD, if the aggregate is to bridge the crack at a large distance behind the advancing crack front. This has led to one refractory installation concept of using very large aggregates in refractory castable linings and then infiltrating the interstices between the aggregates with a free-flowing castable. It works well in areas such as ladle bottoms.

A natural extension of the aggregate size concept is the geometrical aspect of the aggregates. It seems obvious that angular aggregates should have a mechanical interlocking effect that is greater than spherical aggregates. Experience with the use of fiber additions to castables indicates that length and aspect ratio are important. Probably, larger aspect ratios will give improved crack growth resistance, but mixing this type of geometrical fiber addition into a refractory castable or concrete is not very easy. Stronger aggregates should be better than weak ones, and rough surfaces on the aggregates should be preferred to smooth ones. The chemistry of the bonding with the silicates in the refractory is also very important. It is now almost universally recognized that the phenomena occurring behind the advancing crack front, in the following wake region of a crack, are the most important effects to the crack growth resistance of refractories. It remains to specifically identify and then fully quantify those phenomena to produce more crack growth-resistant refractory microstructures.

X. R-CURVES FOR REFRACTORIES

The consequences of rising R-curve behavior for refractories have been known for some time. Adams et al. (26) were the first to experimentally demonstrate this phenomenon for a series of aluminosilicate refractories when they observed that long cracks were much more difficult to extend than short cracks. In its simplest form, the phenomenon is just that as a crack grows larger, or extends, it gets more difficult for it to grow, or extend further, because of greater opportunities for interactions in the larger following wake region of the crack. The R-curve is a resistance curve, a crack growth resistance curve as schematically shown in Figure 5.

Figure 5 depicts the concept of an increasing or rising R-curve and contrasts it with the brittle flat R-curve that one might expect to observe for glass, or for a fine grain size ceramic specimen. A flat R-curve as observed for a perfectly brittle material is the horizontal dashed line in Figure 5. The crack growth resistance, the *R*-value, is constant with crack length, the horizontal axis. In this instance the *R*-value is just $2\gamma_f$ where γ_f is the fracture surface energy. The diagram shows the crack growth or extension portion to the right of the zero as ΔC . The initial crack size of the test specimen is designated as C_i and lies at the left-hand end of the horizontal axis. The dashed line marked as *G* is the strain energy release rate and for a perfectly brittle material crosses the flat *R*-curve at

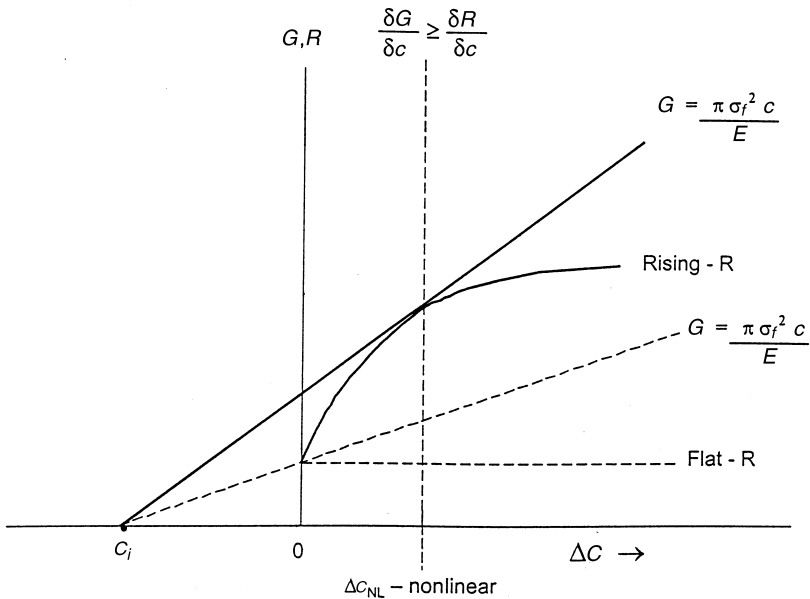


Figure 5 Schematic of a rising or increasing R-curve in contrast with a flat one.

$C = 0$. For a perfectly brittle material, the fracture criterion of $G = R$ has been met and the material will fail catastrophically, producing a load-displacement trace similar to the middle diagram in Figure 1, perfectly linear elastic to failure.

However, for a material with a rising R-curve, as depicted by the heavy solid line curving upward from the intersection of the two dashed lines on the vertical axis of G and R , once $G = R$ and crack growth begins, the R -value increases. R immediately exceeds G and the crack is arrested, for when $R > G$, the crack cannot propagate. A series of many G lines from the dashed one to the solid one occurs for increasing loading of the crack, but the rising nature of the R-curve immediately causes R to exceed G every time that $R = G$, and a sort of quasi-static crack growth process occurs with increasing stress. Eventually, the rising R-curve begins its asymptotic trend to the value for a fully developed crack process zone (both front and back of the crack front) and the G-curve is able to approach and exceed it tangentially. The failure criterion is then determined by the equality of the slopes of the two curves. Failure occurs when $(dG/dc) \geq (dR/dc)$, as depicted on the crack growth diagram in Figure 5.

It can be seen that the presence of an increasing or a rising R-curve has two obvious effects on the fracture of a refractory. First, it creates the need for a higher stress to meet the fracture criterion. It makes the refractory stronger before it fails catastrophically. Second, it generates a nonlinear type of behavior during loading to failure. This nonlinear region is clearly marked ΔC_{NL} for nonlinear crack growth in Figure 5. It corresponds to the nonlinear region of the normal load-displacement plot, the deviation from linear elastic behavior just prior to the load maximum. It is this nonlinear region that Gogotsi et al. have used to define a brittleness ratio, which they later applied to thermal shock damage resistance (29). The extent of strength increase and the extent of the nonlinear region will depend on the individual refractory and the temperature at which it is measured. Of course, it also depends on the crack process zone and the aggregates in that process zone that affect the bridging phenomena in the following wake region after the crack front has passed. It determines the rate of rise for the R-curve of that refractory.

In general, R-curves are not measured for refractories, as many researchers either do not understand them or simply believe that they are too much trouble to bother to determine. After all, integration of the R-curve just yields the total work-of-fracture, so why bother with the details? The reason is that if one does determine the complete R-curve, then it may be possible to directly correlate the R-curve phenomena with specific microstructural features of the refractory as the advancing crack interacts with those structural features. Sakai and Bradt (29) have described a simple graphical technique for determination of the complete R-curve and how it can be derived from the stable load-displacement plot such as that presented in Figure 4 for the wedge-splitting specimen. The load-displacement curves of wedge-splitting specimens appear ideally suited to

R-curve determination. If such load-displacement data are analyzed, the relationships of the rising R-curve features or level to the microstructure of the refractory, its aggregate character, may indeed prove to be very interesting, undoubtedly revealing a great deal about the crack growth process in refractories.

XI. THE RISING R-CURVE AND THERMAL SHOCK DAMAGE RESISTANCE

It should be apparent that the energy balance approach to thermal shock damage originally advanced by Hasselman (11) nearly a half-century ago directly relates to the energy consumption by the nonlinear processes in the crack region process zone and the concept of an increasing, or rising, R-curve. Obviously, if a crack consumes more energy as a consequence of an increasing or rising R-curve, then it will not propagate as far and the resulting thermal shock damage will be decreased. In fracture mechanics terms, the rising R-curve causes $R > G$ and the crack arrests with less extensive penetration into the refractory body. This repetitive $R > G$ event is what Hasselman referred to as quasi-static crack growth. Strength losses will not be as large as for a flat R-curve material for there is no kinetic crack growth. Unfortunately, in industrial situations, as noted in Figure 5, the value of G depends on the stress, σ , which is a time-dependent quantity during temperature changes such as the thermal cycling of a refractory lined processing vessel. This considerably complicates the analysis, but it does not negate the requirement for a crack growth-resistant refractory for improved thermal shock damage resistance and the fact that a rising R-curve is highly desirable for refractory materials.

Without introducing additional diagrams for crack extension, or growth in a transient thermal stress field, the role of the rising R-curve on improved thermal shock damage resistance can be visualized in a manner analogous to the G, R versus ΔC diagram in Figure 5. When a thermal shock crack encounters a steeply rising R-curve of crack growth resistance, it reacts just like any other crack would. It experiences arrest when $R > G$, an event that repeatedly occurs with incremental crack extension. The result is that instead of kinetic crack growth and a large decrease in the strength after a thermal stress event, the strength of the refractory is only gradually decreased, even during the severest of possible thermal shocks. Crack growth occurs in a quasi-static manner, just as Hasselman originally predicted, long before R-curves were known to exist, or measured in any ceramic systems. Refractories that are well designed microstructurally should never exhibit kinetic crack growth, nor a precipitous loss of strength in a severe thermal shock test. Rather, the strength loss with increasing severity of thermal shock is always gradual for well-designed refractories. Sometimes

there is practically no strength degradation for the very low-strength refractories. This is because those refractories, such as the ones in the highly microcracked 70% alumina class, have extensive nonlinear load-displacement regions and if their R-curves were measured, they would undoubtedly exhibit very steeply rising R-curves conducive to crack arrest.

The connections between the concepts and phenomena of nonlinear load-displacement during strength tests, the existence of a rising R-curve, and an increased thermal shock damage resistance have been known for several decades. The first connections were those advanced by Gogotsi and his co-workers in the late 1970s, (28, 30). Unfortunately, at that time the ideas were not given much attention, for the era was one of “pure” fracture mechanics applied to ceramics, including refractories, and Gogotsi had a unique mechanics approach involving an unconventional definition of the brittleness of ceramics through nonlinear strength plots. However, Gogotsi and his co-workers did clearly relate the nonlinear character of strength measurements to good, or improved, thermal shock damage resistance. However, he did not relate this to R-curves, for the concept of an R-curve was not known at the time.

The next significant work that addressed the problem was in about 1990, over a decade after the nonlinear concepts were first advanced by Gogotsi and over a decade ago. Steinbrech and co-workers clearly demonstrated that the primary contributions to the rising R-curve in alumina ceramics was behind the crack front, in the following wake region (31). About the same time, Swain began addressing the R-curve effect on thermal shock damage (32, 33). Then Sakai and Ichikawa directly tied the phenomena of microcracking in advance of the crack front and crack bridging behind the crack front to increases in the work of fracture (34). By the mid-1990s, all of the fundamentals were established to directly associate nonlinear load-displacement with crack region process zone phenomena and rising R-curves leading to improved thermal shock resistance of ceramics and refractories. Now, a decade later, the experimental measurements relating to these concepts have not yet become everyday activities for refractory development, but it is clear that they should be, and they eventually will become so. It is only a matter of time.

Included in the proceedings of a NATO conference on the thermal shock of advanced ceramics (35) are several papers addressing the connection of increased thermal shock damage resistance and the nonlinear effects of rising R-curves. Unfortunately, those papers either are of a totally theoretical nature or are applied to advanced structural ceramics materials, not to real refractories. Few, if any, of the advanced ceramics are capable of generating as strongly rising R-curves as are commonplace for most microstructurally well-designed refractories. To this day, approximately a decade after all of the basic principles have been in place and confirmed, at least in a partial sense for advanced ceramics, the necessary parallel studies in true refractory systems have not been completed.

It should be evident, even to the casual reader, that refractory microstructural design of refractories should be focused toward optimizing the nonlinear load-displacement character and the rate of rise of the R-curve. It is obvious that one route to this goal is with design of the aggregate distribution to maximize the crack bridging phenomena in the following wake region of an extending crack. This is the logical approach to the improved thermal shock damage resistance of refractories. In the case of refractories, this microstructural design is directly related to the aggregate character, its size distribution, its strength, and its bonding to the refractory matrix. Although several generalities may apply to all refractory aggregate distributions, such as to make the aggregate as large as possible consistent with manufacturing the refractory and achieving other properties at an adequate level for industrial performance, one should naturally expect that every refractory system will be somewhat different. The same aggregate distributions that maximize the rise of R-curves for bricks or other fired shapes will probably not optimize exactly the same for castables. Perhaps each class of refractories will require detailed systematic study of the effects of its aggregate character on the R-curves of that particular class of refractories? The refractory technical community has hardly begun the extensive effort necessary to understand the development of rising R-curves and their most important role in the development of more thermal shock-resistant refractories.

XII. SUMMARY AND CONCLUSIONS

Fracture of refractories has been addressed here from both the conventional strength and the fracture mechanics approaches, considering several techniques for experimental measurements. The relation between the strength and the fracture toughness of refractories is noted to be related to the aggregate size in the refractory. The aggregates, their size, size distribution, and bonding character are critical to the intrinsic flaws in refractories and directly affect the strength through that parameter.

It is noted that the aggregates have a major role in the crack bridging mechanisms in the following wake of an extending crack in refractories. This leads to the development of the rising R-curve phenomenon, which is related to the nonlinear stress-strain and load-displacement characteristics of refractories. These characteristics of refractories impart improved thermal shock damage resistance to them. When all of the refractory crack “toughening” processes are considered, it is evident that the aggregates dominate the crack bridging in the wake region. It must be concluded, therefore, that the aggregates, their size, and size distribution as well as their strength, their geometry, and their bonding to the matrix are critical to the fracture-related properties of refractories.

Acknowledgments

The author would like to extend his gratitude to all of his former students who conducted research on refractories with him and thus taught him about the fracture of these interesting materials known as refractories. The support of AISI, DOE, TRI, and other sponsored research on refractories is gratefully acknowledged. His current graduate students doing refractory theses and dissertations have been a particular inspiration, and he extends a special thanks to them, Flavia N. Cunha, Faiz Al-Musalami, and Joaquin Aguilar-Santillan. Finally, he would like to thank Chuck Schacht for asking him to contribute this article and for sending him the frequent reminder e-mails, which made the completion of this work the only rationale alternative.

REFERENCES

1. Bradt RC. Fracture testing of refractories, past, present and future. Proc. 2nd Int. Symp. on Refractories. Vol. I. Tokyo, Japan: TARJ, 1987:661–668. Reprinted in *Taikabutsu* 1988; 40(1): 14–18 and in *Bull Amer Cer Soc* 1988; 67(7): 1176–1179.
2. Bradt RC. Elastic moduli, strength and fracture characteristics of refractories. In: Singh JP, Banerjee S, eds. *Microstructure and Properties of Refractories. Key Engineering Materials*. Vol. 88. Aedermannsdorf, Switzerland: Trans Tech Publications, 1993:165–192.
3. Bradt RC. Twenty-first century refractories, dynamic high-tech composites. Zhong X. et al., ed. Proc 2nd Chinese Intl. Ref. Symp. 1992:15–21. Also published in Chinese in the *J Chin Cer Soc* 1993; 21(2):169–175.
4. Gitzen WH, Hart LD. Explosive spalling of refractory castables bonded with calcium aluminate cement. *Bull Amer Cer Soc* 1961; 40(8):503–507, 510.
5. Crouch AG, Jolliffe KH. The effect of stress rate on the rupture strength of alumina and mullite refractories. *Proc Brit Cer Soc* 1970; 15:37–46.
6. Hertzberg RW. *Deformation and Fracture of Engineering Materials*. New York, NY: J. Wiley & Sons, 1976:229–542.
7. Nakayama J. Bending method for direct measurement of fracture surface energy of brittle materials. *Japan J App Phys* 1964; 3(7):422–423.
8. Sakai M, Bradt RC. Fracture toughness testing of brittle materials. *Intl Mat Reviews* 1993; 38(2):53–78.
9. Brown WF. Jr., Srawley JE. Plane strain crack toughness testing of high-strength metallic-materials. ASTM STP 410. Philadelphia, PA: ASTM, 1967:13–15.
10. Munz D, Fett T. *Ceramics: Mechanical Properties, Failure Behaviour, Materials Selection*. Berlin, Germany: Springer-Verlag, 1999:25–27.
11. Hasselman DPH. Elastic energy at fracture and surface energy as design criteria for thermal shock. *J Amer Cer Soc* 1963; 46(10):535–540.
12. Hasselman DPH. Unified theory of thermal shock. *J Amer Cer Soc* 1969; 52(11): 600–604.

13. Tattersall HG, Tappin G. Work of fracture and its measurement in metals and ceramics. *J Mat Soc* 1966; 1(3):296–301.
14. Rodrigues JA, Pandofelli VC. Thermal treatment temperature and its influence on the thermal shock parameters of refractory castables. *Interceram*. 2002; 51(May): 186–189.
15. Popov EP. *Engineering Mechanics of Solids*. Upper Saddle River, NJ: Prentice Hall, 1999:111–115.
16. Dulberg I. Personal communication, Snow Shoe, PA: J.H. France Refractories 1970.
17. Rice JR. A path independent integral and the approximate analysis of strain concentration by notches and cracks. *J App Mech* 1968; 35(6):379–386.
18. Homeny J, Darroudi T, Bradt RC. J-integral measurements of the fracture of 50% m alumina refractories. *J Amer Cer Soc* 1980; 63(5–6):326–331.
19. Mindess S, Lawrence FV, Kesler CE. The J-Integral as a fracture criterion for fiber reinforced concrete. *Cem Concr Res* 1977; 7(6):731–742.
20. Roedig M, Kleist G, Schiffers H, Nickel H. The J-integral applied to carbon. *Proc. of the Fifth London Intl. Carbon and Graphite Conf. Vol. I*. London: Society of Chemical Industries, 1978:51–62.
21. Nakayama J, Ishizuka M. Experimental evidence for thermal shock damage resistance. *Bull Amer Cer Soc* 1966; 45(7):666–669.
22. Nakayama J, Abe H, Bradt RC. Crack stability in the work-of-fracture test, refractory applications. *J Amer Cer Soc* 1981; 64(11):671–675.
23. Harmuth H. Stability of crack propagation associated with fracture energy determined by wedge splitting specimen. *Theor and App Fract Mech* 1995; 23(2):103–108.
24. Buchebner G, Harmuth H. Magnesite-hercynite bricks—an innovative burnt basic refractory. *Proc. UNITECR 1999*. Berlin, Germany: Berlin, German Refractories Association 1999:201–203.
25. Bradt RC. Problems and possibilities with cracks in ceramics. *Sci Ceram Vol. 11*. Göteborg, Sweden: Swedish Ceramic Society, 1981:349–360.
26. Adams TA, Landini DJ, Schmacher CA, Bradt RC. Micro- and macro-crack growth in alumina refractories. *Bull Amer Cer Soc* 1981; 60(7):730–735.
27. Homeny J, Bradt RC. Aggregate distribution effects on the mechanical properties and thermal shock behavior of model monolithic refractory systems. In: Fisher RE, ed. *Adv. in Ceramics. New Developments in Monolithic Refractories*. Vol. 13. Westerville, OH: Amer Cer Soc, 1985:110–130.
28. Gogotsi GA, Grushevsky YL, Strellov KK. The significance of non-elastic deformation in the fracture of heterogeneous ceramic materials. *Ceramurgia* 1978; 4(2):113–118.
29. Sakai M, Bradt RC. Graphical methods for determining the nonlinear fracture parameters of silica and carbon refractory composites. In: Bradt RC et al. eds. *Fract Mech of Ceramics, Vol VII*, New York, NY: Plenum Publishing Corp., 1986:127–142.
30. Gogotsi GA. The significance of non-elastic deformation in the thermal shock fracture of heterogeneous ceramic materials. In: Schnieder GA, Petzow G, eds. *Thermal Shock and Thermal Fatigue Behavior of Advanced Ceramics*. NATO ASI Series E: Applied Sciences. Vol. 241. Dordrecht, The Netherlands: Kluwer Academic Publishers, 1993:279–291.

31. Steinbrech RW, Reichi A, Schaarwachter W. R-curve behavior of long cracks in alumina. *J Amer Cer Soc* 1990; 73(7):2009–2015.
32. Swain MV. R-curve behavior and thermal shock resistance of ceramics. *J Amer Cer Soc* 1990; 73(3):621–628.
33. Lutz EH, Swain MV. Interrelation between flaw resistance, R-curve behavior and thermal shock strength degradation in ceramics. *J Amer Cer Soc* 1991; 74(11):2859–2868.
34. Sakai M, Ichikawa H. Work-of-fracture of brittle materials with microcracking and crack bridging. *Int J Fracture* 1992; 55(1):65–80.
35. Schneider GA, Petzow G, eds. *Thermal Shock and Thermal Fatigue Behavior of Advanced Ceramics*. NATO ASI Series E: Vol. 241. Dordrecht, The Netherlands: Kluwer Academic, 1993.

3

Corrosion of Refractories

Denis A. Brosnan

Clemson University, Clemson, South Carolina, U.S.A.

I. INTRODUCTION

Refractories are used at elevated temperatures for structural purposes, and they are used in many cases to contain a high-temperature corrosive environment. This corrosive environment usually contains liquid (melted) phases that participate in *chemical reactions* with the refractory at elevated temperatures resulting in refractory consumption or wear. It is usually not immediately obvious, but the oxidation and reduction state of the environment (as “redox” conditions or oxygen “activity”) can participate in and influence the chemical reactions that take place. Along with chemical reactions during corrosion, *physical changes* occur that may be *accelerated* by the corrosion process.

Corrosion of refractories can be defined for the purposes of this discussion as follows: Corrosion of refractories is refractory wear by loss of thickness and mass from the exposed face of the refractory as a consequence of chemical attack by a corroding fluid in a process in which the refractory and the corroding fluid react, approaching chemical equilibrium in the zone of contact between the refractory and the fluid.

It is an essential point that corrosion reactions proceed in a direction toward localized chemical equilibrium. This means that phase equilibrium diagrams can be used to analyze corrosion situations and to predict chemical strategies to minimize corrosion and wear rates. This gives persons interested in refractory corrosion two options. The first is to view corrosion as a chemical and physical process without a detailed application of phase equilibrium diagrams—called the “phenomenological approach.” The second is to use the information in the phenomenological approach *and* to use phase equilibrium diagrams. This latter option is required for a full understanding of refractory corrosion.

There are many types of refractory systems—fusion cast and/or bonded brick in a “working” lining placed in front of a backup or “safety” lining (or simply placed against a “shell”), thick-wall applications of concretes (and other monolithics) where the lining thickness is usually on the order of 75 mm or greater, and thin-wall applications of monolithics where the lining thickness is typically less than about 25 mm. It is beyond the scope of this chapter to cover every type and application possible. There are, fortunately, a few fundamental principles that the investigator can apply to any corrosion situation, and it is a purpose of this chapter to provide those fundamental principles.

A. First Fundamental Principle on Refractory and Slag Compatibility

The first fundamental principle is that “acid” refractories tend to resist “acid” slags better than “basic” slags and, conversely, “basic” refractories tend to resist “basic” slags better than “acid” slags. The definitions of acidity and basicity in room-temperature solution chemistry and of refractory chemistry at elevated temperature have a key difference.

1. Definition of Acidity and Basicity in Solution Chemistry at Room Temperature

An acid contains an excess of hydrogen ions (H^+) over hydroxyl ions (OH^-) considering a “baseline” defined as neutrality (a “pH” of 7.0). An acidic substance contributes hydrogen ions to a chemical solution to make it more acidic, whereas a basic substance contributes hydroxyl ions to make it more basic.

2. Definition of Acidity and Basicity in Corrosion Chemistry at Elevated Temperature

An acidic material contains an excess of silica content (SiO_2) over basic materials (usually CaO) considering a “baseline” defined as neutrality (a CaO/SiO_2 ratio of 1.0). An acidic material contributes SiO_2 in a corrosion reaction, whereas a basic material contributes CaO or MgO in a corrosion reaction.

This leads to the observation that acid refractories are more “compatible” with acid slags, that is, acid materials experience less corrosion loss against acid slags as compared to basic slags. In a like manner, basic refractories are more compatible with basic slags than with acid slags.

In a strict definition of compatibility, mineral phases will not react at elevated temperature if they are compatible. This means that on a microscopic basis, they will “stand beside” one another or coexist at equilibrium without reacting to form new substances. In general usage, the term “more compatible” just means “less reactive.”

There are more complex definitions of acidity and basicity for high-temperature chemistry than those given above. For example, in steel refining, the term “V”-ratio is used where a ratio exceeding 1.0 implies a basic chemistry (usually a basic slag chemistry), and a ratio below 1.0 implies an acid chemistry. In definitions of this sort, the “V-ratio” can be expressed in terms such as the following:

$$V = \frac{\text{CaO} + \text{MgO} + \text{FeO} + \text{MnO} + \dots}{\text{SiO}_2 + \text{P}_2\text{O}_5 + \text{Al}_2\text{O}_3 + \text{Fe}_2\text{O}_3 + \text{Mn}_2\text{O}_3 + \dots}$$

In many cases, it is convenient to use three-component phase equilibrium diagrams in analyzing corrosion situations. The major refractory component can be visualized as one apex (corner) of the triangle, with CaO and SiO₂ as the other components (apices). In these analyses, it is convenient to use the simple CaO/SiO₂ ratio. In more complex analyses using advanced thermodynamic software, it may be more accurate to use the V-ratio to define “equilibrium” conditions.

Corrosion reactions should be viewed as attempts by the system to achieve compatibility by progressing toward equilibrium. Refractories are rarely at chemical equilibrium on a microscopic scale since they are typically made from mixtures of different minerals. However, at the immediate corrosion interface between the refractory and the slag, the localized volume elements may be at or close to chemical equilibrium.

B. Second Fundamental Principle on Porosity and Corrosion Rates

Most refractories contain void space or porosity. This porosity may be open pores that can be penetrated by a fluid media (i.e., “apparent” porosity) and/or it may be closed porosity that is not easily penetrated by fluid media. If a refractory contained no porosity (or brick joints, expansion joints, or construction joints), the corrosion reaction is limited only to the face exposed to the corrosive media (called the hot face). When porosity is present, particularly when open porosity is present, the corrosive media can penetrate the refractory, causing destructive reactions behind the hot face.

Most investigators have found that slag corrosion rates *increase linearly* with the percentage of apparent porosity within the refractory. This is usually true within a limited range of apparent porosity—for example, in the range 12–16% apparent porosity—but it is not necessarily true at high apparent porosities (>20%).

It is for this reason that attention is directed toward achieving higher densities in refractories, i.e., obtaining the lowest possible apparent porosities. Higher-density refractories usually exhibit lower wear rates. Understandably, very high-density refractories may exhibit less spalling resistance, leading to

higher wear rates by another process such as thermal shock. This points to the fact that corrosion loss is one part of many possible contributors to an overall wear rate for a furnace lining. Usually one wear process, such as corrosion, is the dominant wear process.

Because corrosive fluids can penetrate the refractory, such penetration usually results in disruption and even destruction of the “matrix” of the refractory. The matrix is the area of “sintered fines” that hold together “bonded” bricks and monolithic refractories. Usually, the matrix contains more impurities and more porosity than aggregate particles. Therefore, corrosion affects the “weakest” component of the refractory at a higher rate than denser or higher-purity particles. In extreme cases of matrix attack, rapid erosion of coarse refractory aggregate can occur.

II. PHENOMENOLOGICAL DESCRIPTION OF CORROSION

A. Introduction

The phenomena that occur during refractory corrosion are well known to anyone who has been around a furnace containing reactive process components such as slags or glasses. It is obvious that the reactive component, hereafter called the “slag,” must contact the refractory’s exposed surface or hot face at an elevated temperature. It is at this interface that corrosion begins and continues throughout the life of the lining.

The situation is illustrated by considering a cross section of the slag and refractory interface (Figure 1). The refractory has a temperature gradient from the hot to cold face—meaning that the highest temperature is at the hot face and temperature declines across the refractory thickness toward its back or cold side. Slag is shown penetrating the refractory until a “freeze plane” is reached. The freeze plane is the location in the refractory where the temperature is sufficiently low to cause the slag to solidify.

The hot face of the refractory is coated with slag. In most metallurgical applications, this coating is relatively thin (~ 2 – 5 -mm thickness). In some vertical wall refractory construction where the refractory is not in contact with a metal bath or slag pool, slag can accumulate in thick sections (> 25 mm).

In some cases, two distinct slag layers can be observed on the outside of the refractory after a used material is sectioned. There may be a fluid “outer layer” over a “viscous appearing” inner layer with the latter directly contacting the surface of the refractory. The inner layer is typically influenced by solution of the refractory in the slag with the added components increasing the viscosity of the slag. There may be eroded particles of the refractory in the inner layer, which can be seen with the aid of a microscope. The two-layer situation is usually seen where liquid slag runs down a vertical refractory wall.

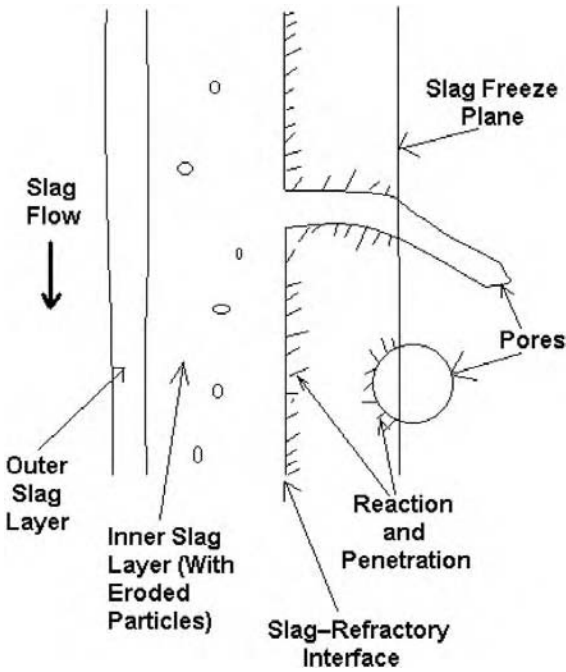


Figure 1 Cross section of the slag–refractory interfacial area.

Two-dimensional representations in drawings or photomicrographs of the hot face zone cannot reveal the three-dimensional structure underlying the area of the section. For this reason, many pores appear to be isolated, but they may be connected to the hot face through a channel under the observed plane. For this reason, pores that are apparently isolated can be filled with slag.

Slag reacts with the refractory, forming new phases at the immediate hot face. Reaction also takes place behind the hot face, where slag contacts the refractory at the pore walls. In metallurgical applications, metal can sometimes be seen penetrating the refractory along with slag.

B. Third Fundamental Principle on Reactions and Temperature Gradients

A key concept of this principle is that the temperature gradient affects the extent of phenomena seen in slag corrosion. In a very steep temperature gradient, very little penetration of slag is seen, with corrosion reactions more or less restricted to the immediate slag and refractory interface. Mobility of fresh slag (reactant) to

the slag–refractory interface may be limited, and transport of reaction products away from the slag–refractory interface may be slow. Steep gradients are seen in thin-wall refractory linings such as those used in utility boilers featuring water or steam cooling at the furnace shell.

In conventional refractory designs, the lining is at least one brick thickness (>225 mm), and the lining typically features a safety lining for a total thickness of at least 450 mm. The slag freeze plane may be located in a zone of 40–75 mm behind the hot face. In some cases, slag may penetrate up to 150 mm behind the hot face.

C. Thin Wall (Steep Temperature Gradient)

The corrosion situation in a thin-wall refractory lining is illustrated in Figure 2. Here the refractory corrosion reactions occur primarily at the immediate hot face, and there is little or no slag penetration. Microscopic examinations usually show

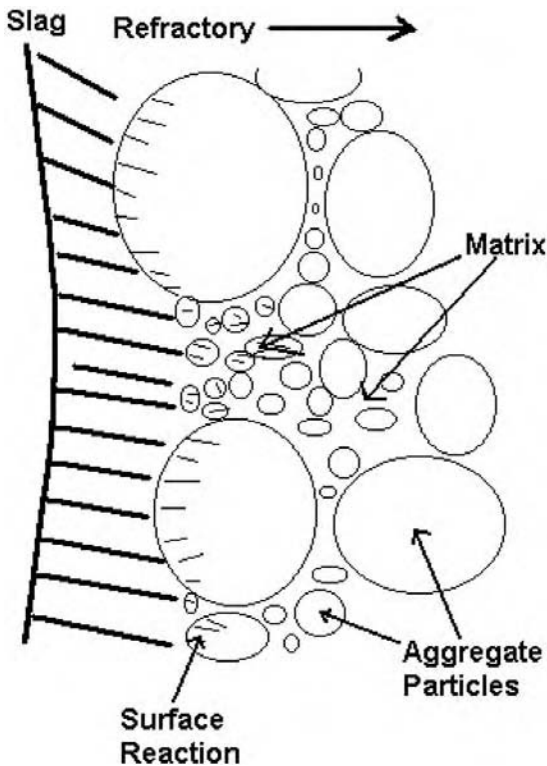


Figure 2 Stage I of slag attack (showing a bonded refractory).

that penetration is confined to a depth of less than 100 microns (0.1 mm) behind the exposed hot face. This situation may be called “Stage I” of slag attack, where reactions occur at the immediate hot face.

It is found that the hot face temperature primarily affects the rate of corrosion reactions. If the hot face temperature is held just below the point that the products of corrosion become liquid (melt), corrosion will be very slow or nonexistent. Most authorities believe that if the hot face is maintained at no more than 20°C above this melting temperature (called a lowest eutectic temperature), reasonable corrosion rates will be observed. However, when the hot face temperature is more than 20°C above the eutectic, corrosion is rapid.

In some applications like utility boilers, “button fusion tests” are run to determine the slag melting temperature. A much more accurate test is to determine the eutectic or “solidus” temperature using thermal analysis. The solidus is recognized on heating with the appearance of an endothermic reaction (melting). The reaction temperature between slag and refractory can be determined by conducting a thermal analysis test of a mixture of ground refractory and ground slag.

Thin-wall refractory designs rarely exhibit more extensive corrosion phenomena than are described as “Stage I” of corrosion. Therefore, the primary process variable affecting corrosion is hot face temperature. Secondary variables influencing corrosion rates include slag impingement velocity and slag chemistry. With respect to chemistry, the refractory will be soluble in the slag up to a certain extent (or percentage). If the slag is “satisfied” with respect to the chemistry of the refractory, slag corrosion should be minimal. The term “satisfied” means that the slag has reached the chemical solubility limit of major refractory constituents in the slag. Usually, the slag is not satisfied, i.e., it is corrosive. Attempts to make additions to the slag to obtain a satisfied chemistry (to minimize corrosion) are usually not economical.

There are a few cases of thick-wall designs where the refractory is so resistant to slag corrosion that corrosion reactions are restricted to the hot face region. Usually, these involve fusion cast refractories employed in furnaces that remain hot during their service life (minimal thermal cycling from hot to cold).

D. Thick Wall (Relatively Broad Temperature Gradient)

Thick-wall refractory designs begin to exhibit corrosion on their initial coating of slag at elevated temperatures. The initial process of corrosion is Stage I (Figure 2). Because of the broad temperature gradient, the refractory is penetrated by slag. Penetration is aided by capillary suction as the smallest pores in the refractory (diameter < 10 microns) draw the liquid slag behind the hot face.

In time, extensive corrosion of the refractory takes place so that the refractory is at “Stage II” of corrosion (Figure 3). Stage II is characterized by two phenomena: (1) full penetration of the refractory and (2) extensive disruption

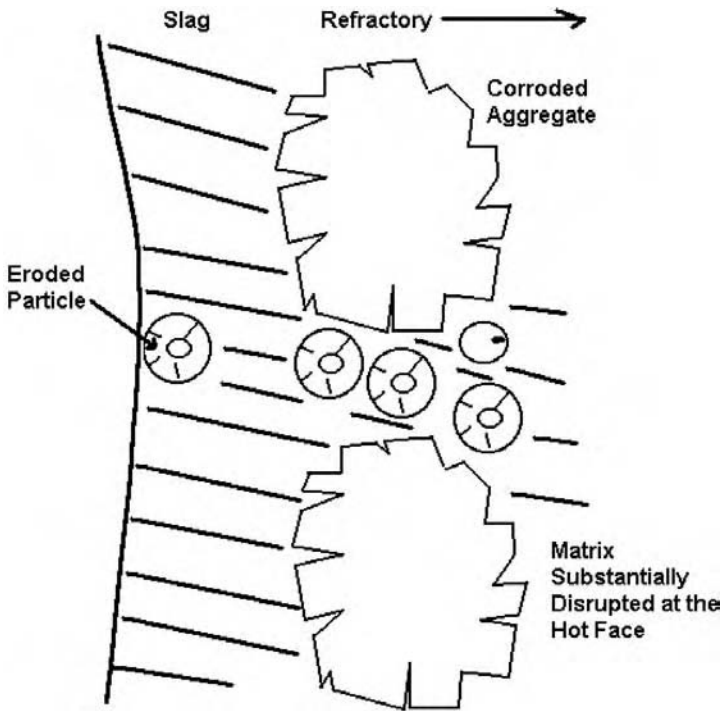


Figure 3 Stage II of the corrosion process (showing a bonded refractory).

by corrosion of the hot face region. Stage II follows Stage I only if there is a sufficiently broad temperature gradient to allow penetration.

In Stage II, the coarse aggregate in a bonded refractory exhibits penetration—particularly along grain boundaries (boundaries between crystals making up polycrystalline aggregate particles). The direct bonding between the matrix and the aggregate particles is disrupted, but this bonding still exists.

Slag penetration in Stage II can result in densification spalling. This type of spalling occurs because the thermal expansion coefficient in the slag penetrated zone is different than that in the unpenetrated cold face region. On continued thermal excursions (cooling and heating), spalling can occur at the line of demarcation between penetrated and unpenetrated areas. The residual lining, after spalling, then begins the corrosion process anew, progressing from Stage I to Stage II again.

Toward the end of the refractory lining's life, or in cases of relatively slow corrosion rates and where densification spalling has not taken place, the refractory hot face zone may progress to a final stage of corrosion that may be called "Stage III" (Figure 4). In this case, bonding in the hot face region and up to 2 to

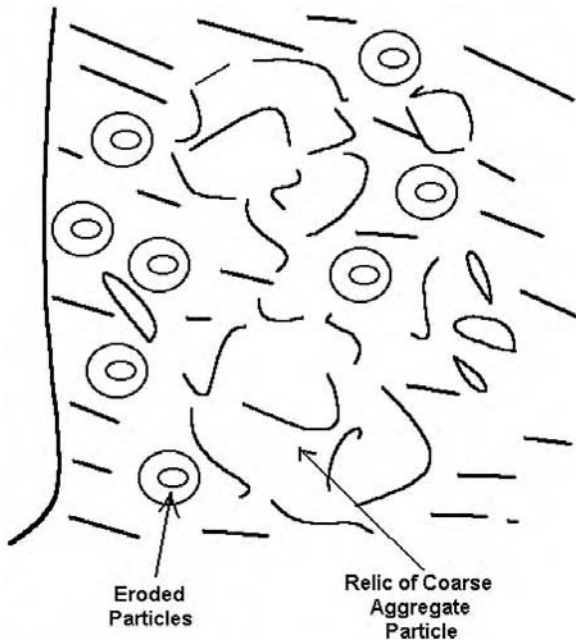


Figure 4 Stage III of the corrosion process.

4 mm behind the hot face is minimal. The slag itself “appears” to be the only phase holding the residual aggregate particles in place. This is probably a result of the higher viscosity of the slag in the hot face region created as a consequence of dissolution of the refractory in the slag.

Because of the influence of slag viscosity maintaining some coherence in the hot face zone in Stages II and III with thick-wall designs, a key process variable affecting corrosion rate is hot face temperature. Many investigators recommend a hot face temperature not more than 20°C above the solidus temperature between the slag and the refractory. Such temperature restrictions are impractical in many thick-wall refractory designs.

III. EQUILIBRIUM CONSIDERATIONS AND PHASE DIAGRAMS

A phase diagram is a map showing equilibrium phases present as a function of composition and temperature. The phase diagram essentially shows the melting relationships in a given chemical system. It is beyond the scope of this chapter

to provide a detailed description of phase diagrams and their interpretation (see Ref. 1).

Even without a complete understanding of phase diagrams, they can be used in a “simplified method” to analyze corrosion. This method provides a “first approximation” of the corrosion potential of the system. This technique will be illustrated using the $\text{Na}_2\text{O}-\text{Al}_2\text{O}_3-\text{SiO}_2$ system (Figure 5). In the chapter on alumina-silica brick, two consequences of Na_2O exposure are mentioned for alumina-silica brick including “glazing” (corrosion to form melted phase) and expansions. This discussion will only consider corrosion of the refractory to form liquids during corrosion.

The first step is to locate the point on the diagram representing the refractory main constituents. For this discussion, we will use a 40% Al_2O_3 superduty brick in contact with a corrosive phase consisting of 20% Na_2O and 80% SiO_2 . Both these compositions are indicated in Figure 5, with a circle indicating

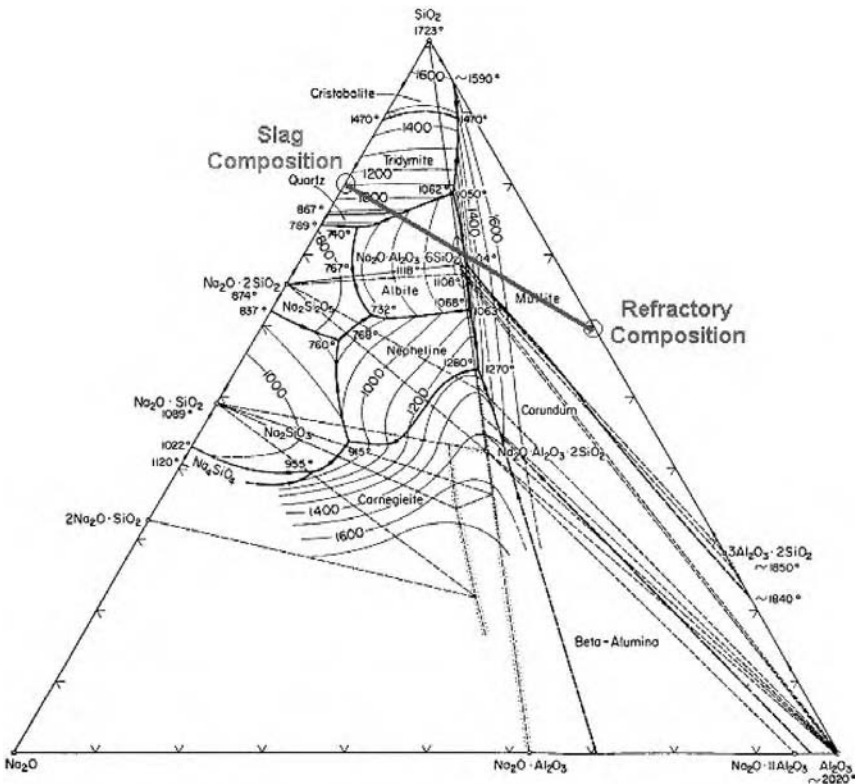


Figure 5 $\text{Na}_2\text{O}-\text{Al}_2\text{O}_3-\text{SiO}_2$ phase diagram used in a corrosion example.

the approximate composition of the slag and another circle indicating the approximate composition of the brick (on the $\text{Al}_2\text{O}_3\text{--SiO}_2$ composition line or “join”).

The second step is to draw a line between the slag composition and the brick composition (indicated in Figure 5). It is *essential* to recognize that all potential reaction products between the refractory and the slag at equilibrium must be located on the line in Figure 5 joining refractory and slag compositions.

The analysis of the corrosion potential is as follows:

1. At the slag–refractory interface, the composition must move from that of the refractory in a direction toward the composition of the slag, i.e., the local composition moves in a “northwesterly” direction.

2. The compound at equilibrium between the slag composition and the refractory composition is “albite,” or $\text{Na}_2\text{O} \cdot \text{Al}_2\text{O}_3 \cdot 6\text{SiO}_2$, melting at 1104°C . Therefore, at equilibrium, the localized melting point of corrosion products at the hot face is 1104°C . Note that albite is contained in the “compatibility” triangle between SiO_2 , mullite ($3\text{Al}_2\text{O}_3 \cdot 2\text{SiO}_2$), and albite. The compatibility triangle establishes the phases that may be present at equilibrium. Mullite and SiO_2 (as glass or vitrified phase) are intrinsic to the refractory. Albite is formed as a consequence of corrosion reactions.

3. The line joining the refractory and the slag crosses temperatures as low as about 1000°C . This implies that nonequilibrium liquids could be formed at this low temperature during corrosion. In Stage I of corrosion, such nonequilibrium liquids are expected. Only in Stage II of corrosion will sufficient refractory be dissolved in the slag to allow observation of the equilibrium corrosion product.

4. The line joining the refractory and the slag composition crosses the $\text{Na}_2\text{O} \cdot 2\text{SiO}_2\text{--SiO}_2\text{--Na}_2\text{O} \cdot \text{Al}_2\text{O}_3 \cdot 6\text{SiO}_2$ compatibility triangle near the ternary (3-component) eutectic or lowest melting temperature of 740°C . This implies that liquids melting as low as 740°C could be formed during nonequilibrium conditions.

Considerable qualification is needed when performing this type of analysis. One is that the refractory contains other components than Al_2O_3 and SiO_2 —notably fluxes like K_2O and Fe_2O_3 . These components can lower the melting points predicted by the diagram. Additionally, the slag may contain other components, changing the melting relationships. The analysis still has considerable value for use in a first approximation.

IV. SELECTED MODELS FOR SLAG ATTACK ON REFRACTORIES

A. Konig’s Model

In 1971, Konig related the corrosion rate of refractories in the bosh area of blast furnace walls to the temperature gradient in the wall. This analysis

includes an assumption that the temperature gradient controls the temperature at the slag–refractory interface (see Figure 6, where the interface temperature is labeled T_s). Because the shell of a blast furnace is water-cooled in the area of the bosh, König’s analysis is appropriate for thin-wall refractory with a steep temperature gradient fixed by the process (furnace) temperature and cold face temperature.

König created a heat balance by assuming that the heat flux into the refractory surface must equal the heat flux through the furnace shell. If the heat flux into the refractory surface exceeds the heat flux out of the shell, the interface temperature (T_r) must increase, causing increased corrosion rates until the heat balance is maintained once again. Terms used in König’s analysis are given in Table 1.

The slag–refractory interface temperature becomes T_c (critical temperature) when the heat flux into the refractory equals the heat flux out of the shell. In other words, T_c “creates” or “maintains” an “equilibrium thickness” in the lining. If the actual temperature is above T_c , rapid corrosion (recession) of the refractory is expected until a dynamic equilibrium is once again achieved.

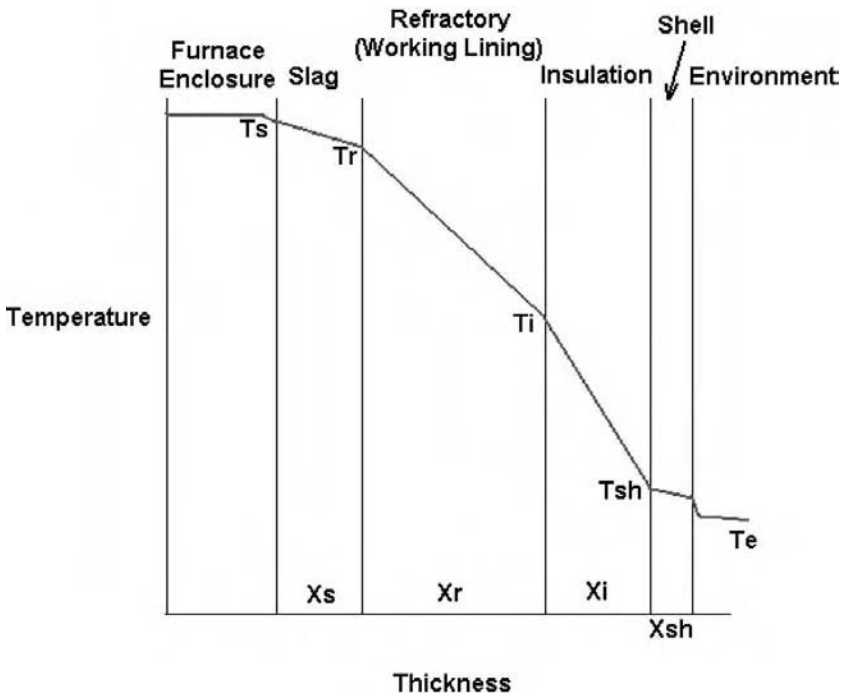


Figure 6 König’s thermal model.

Table 1 Terms Used in Konig’s Analysis

Term	Definition
Q_1	Heat flux into the refractory surface
Q_2	Heat flux through the furnace shell
A	Area of the exposed refractory in the furnace
T	Time at elevated temperature
T_i	Temperature where i = slag surface (s), refractory–slag interface (r), insulation hot face (i), or shell (sh)
x_i	Thickness of component where i = slag layer (sl), refractory working lining (r), insulation (i), or shell (sh)
k_i	Thermal conductivity where i = refractory working lining (r), insulation (i), or shell (sh)
T_c	Critical temperature at the slag–refractory interface
f_i	A film coefficient for convective heat transfer where i = furnace environment (F) or room environment (E)

The heat flow into the refractory surface is described by the equation

$$Q_1 = f_F A t (T_F - T_s).$$

The heat flux out of the furnace shell is

$$Q_2 = k_{eff} A t (T_r - T_E),$$

where k_{eff} is the effective (overall) thermal conductivity through the refractory, insulation, shell, and film contribution in the room environment.

From heat-transfer theory, the relationship for k_{eff} is

$$k_{eff} = \frac{1}{f_E + \frac{x_r}{k_r} + \frac{x_i}{k_i} + \frac{x_{sh}}{k_{sh}}}$$

At equilibrium, $Q_1 = Q_2$ and $T_r = T_c$, so that algebraic manipulation provides a relationship for the “equilibrium thickness” (x_r) of the working lining as

$$x_r = k_r \left[\frac{1}{f_F} \times \frac{(T_c - T_E)}{(T_F - T_{sl})} - \left(f_E + \frac{x_i}{k_i} + \frac{x_{sh}}{k_{sh}} \right) \right].$$

Konig’s relationship for the equilibrium thickness provides the following insight:

The equilibrium thickness x_r increases linearly as the thermal conductivity of the refractory increases.

The equilibrium thickness x_r increases as the thermal conductivity of the insulation increases. This is why conductive ramming materials are used behind high thermal conductivity basic refractories to ensure the best possible cooling effect of the shell.

The equilibrium thickness x_r increases as the T_c of the refractory–slag system increases, i.e., as more slag-resistant refractories are used. This usually means the use of higher-purity refractories, namely higher alumina content or higher MgO purity.

The equilibrium thickness x_r changes as the heat transfer into the lining or out of the shell changes, i.e., as the film coefficients change.

In attempts to apply Konig's analysis to the blast furnace, Herron and Beechan (3) found that corrections were necessary if the refractory's thermal conductivity changes dramatically with increasing temperature. The model was found to describe the behavior of refractories in cyclone burners and in boiler applications where the initial wall thickness of refractory was ~ 25 mm.

B. The Model of Endell, Fehling, and Kley

In a classic reference, Endell, Fehling, and Kley developed an empirical relationship for slag corrosion in a thick-walled refractory lined vessel with slag flowing down a vertical refractory wall. While this work was performed in 1939, it remains the classic reference on slag corrosion despite its empirical nature. In the corrosion studies, the authors used an arrangement where a solid fuel burned within a reaction chamber (liberating heat) with resulting ash (slag) impingement on walls. Terms used in the analysis are given in Table 2.

Table 2 Terms in the Analysis of Endell, Fehling, and Kley

Term	Definition
R	Slag attack rate, i.e., refractory recession, in cm/s
L_0	Solubility of refractory in slag in kg of refractory/kg of slag
T	Absolute temperature of the refractory hot face
η	Slag viscosity in poises
f	Fraction of ash adhering to the refractory wall—interpreted as slag impingement
H	Heat liberated in the furnace chamber in kcal/m ³ -hr
A	Ash content of the fuel in grams per gram of ash
C	A constant for the furnace geometry

The mathematical relationship for slag attack rate is

$$R = CL_0 \left(\frac{T^{2/3}}{\eta^{8/9}} \right) (fHA)^{1/9}$$

The empirical model of Endell, Fehling, and Kley for thick-wall refractory linings provides the following information:

There is a very *strong dependence* of refractory corrosion rates on *hot face temperature*. In fact, temperature is the most important process variable that can be considered in furnace design or process control.

The slag attack rate *increases linearly* with the *solubility of the refractory in the slag*. While modern high Al₂O₃ or high MgO products were not included in the original research, recent practices have shown that corrosion rates can be reduced if the slag chemistry (principally CaO/SiO₂ ratio) is adjusted to reduce solubility of the refractory in the slag.

In essence, the corrosion rate is inversely proportional to slag viscosity. This is probably why refractories exhibit some coherence in Stage III of slag attack because solution of refractory in the slag has increased viscosity at the slag–refractory interface.

In their concluding remarks, Endell, Fehling, and Kley recommend maintaining a hot face temperature of no more than about 30°C above the solidus or eutectic temperature between the refractory and slag. The authors further recommend that a temperature gradient in thick-wall linings should not exceed 10°C/cm or 50°F/in. While these criteria are difficult to maintain given the other purposes for furnaces in processing, they establish criteria for reducing corrosion rates.

V. CASE STUDIES OF CORROSION

A. Alumina-Silica Brick in Ferrous Foundry Applications

1. Introduction

Slag used in ferrous foundry applications is found to contain lime (CaO), silica (SiO₂), iron oxide (FeO), and other oxide constituents. *As a first approximation*, the slag can be assumed as a binary mixture of alumina and silica as they are usually the major components of the slag. The major components of the brick can be represented using the binary Al₂O₃–SiO₂ phase diagram, and this allows the corrosion situation to be analyzed using the three-component CaO–Al₂O₃–SiO₂ phase diagram (Figure 7).

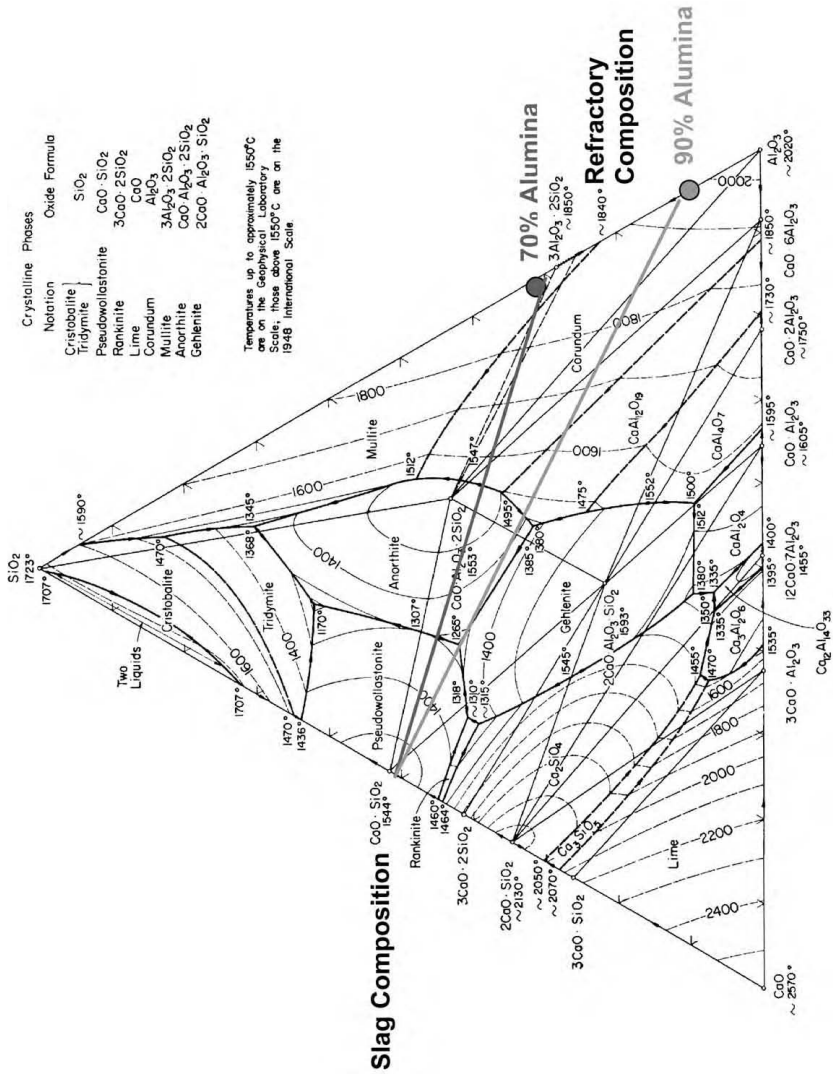


Figure 7 Representation of corrosion of alumina-silica brick in foundry/steel-making slag.

Cases of corrosion of 70% Al_2O_3 and 90% Al_2O_3 brick are analyzed below using Figure 7. The composition of the brick is plotted on the Al_2O_3 – SiO_2 binary (two-component) side of the diagram. Then, a line is drawn to the expected slag composition using the average CaO/SiO_2 ratio of the slag. For this discussion, the slag is assumed to have a CaO/SiO_2 ratio of ~ 1.0 .

A few things are very clear on looking at the lines joining the brick composition and the slag composition in Figure 7:

1. Both “joins” between brick and slag pass very close to the ternary eutectic at 1265°C , implying that the slag and refractory compositions will produce liquid phases, i.e., exhibit corrosion, whenever they are in intimate contact and when this temperature is reached. Other fluxing oxides typically reduce this temperature by as much as 50°C .

2. The effect of lime- (CaO) rich phases penetrating the brick is to render the mullite “binder” in the refractory as a nonequilibrium phase, i.e., the binder is dissolved into the penetrating slag phases and corrosion products. In 70% Al_2O_3 brick, the mullite is stable until the local composition reaches $\sim 20\%$ CaO , while in 90% Al_2O_3 brick, the mullite disappears when the local composition reaches $\sim 8\%$ CaO .

The phase diagram has provided a first approximation of the reaction temperature between the slag and refractory for corrosion to begin, i.e., when the liquid phase is produced as a product of corrosion reactions. This is analogous to the critical temperature in König’s analysis or the “baseline” temperature in the analysis of Endell, Fehling, and Kley.

The joins between refractory composition and slag composition in Figure 7 could have been constructed to analyze the situation with higher slag basicity, i.e., CaO/SiO_2 of 1.5 or 2.0. In this situation, the lines would cross close to the ternary peritectic at 1380°C . This eutectic mixture between anorthite and gehlenite has the special name of “melilite.” The binary join between anorthite and gehlenite is shown in Figure 8, where it is easier to see the solidus temperature, or the temperature above which corrosion begins. Thus, higher CaO – SiO_2 ratios increase the initial reaction temperature between the slag and refractory with respect to formation of liquid phases and the beginning of corrosion.

B. Case Study: 70% Al_2O_3 Brick in an Electric Arc Furnace Roof

A microscopic study of 70% alumina brick after service in the roof of an electric arc furnace was performed to determine the reason for a premature failure of the brick in the roof. Several pieces of brick after service exhibited minimal thickness (Figure 9). In brick selected from other areas of the roof, a greater residual thickness of brick was observed. Cracks were found on saw-cut surfaces of most used

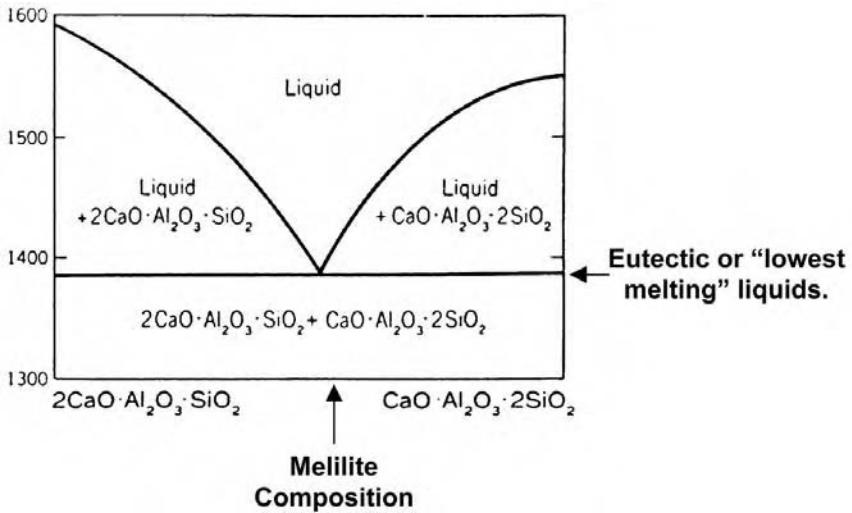


Figure 8 Binary phase diagram between gehlenite ($2\text{CaO} \cdot \text{Al}_2\text{O}_3 \cdot \text{SiO}_2$) and anorthite ($\text{CaO} \cdot \text{Al}_2\text{O}_3 \cdot 2\text{SiO}_2$).

brick from this furnace campaign, and cracks were arranged approximately parallel to the hot face.

The bricks were sectioned, and polished sections were produced for reflected light examination on an optical microscope. In the area of the immediate hot face, i.e., at the slag-brick interface, there was ample evidence of corrosion reactions (Figure 10). Recognizing that the "native" phases in the brick are



Figure 9 Seventy percent alumina brick after a short arc furnace campaign.



Figure 10 Microstructure at the immediate slag–brick interface (130×).

bauxite, clay (grog), and mullite, there is no mullite visible at the immediate hot face. Phases in the hot face in Figure 10 include hercynite or FeAl_2O_4 (labeled “S”), calcium hexaluminate or $\text{CaO} \cdot 6\text{Al}_2\text{O}_3$ (light gray needles), lathlike corundum crystals exsolved from the liquid on cooling, corundum crystals (Al_2O_3) in a relic bauxite grain (lower right field), and a dark gray background of calcium aluminosilicate glass.

At a position of about 2 to 4 mm behind the hot face, slag penetration has taken place through the pore structure of the brick, and the position where mullite crystals appear was easily noticed because of their extreme crystal growth (Figure 11). The mullite crystals are seen as large, light gray laths at a pore

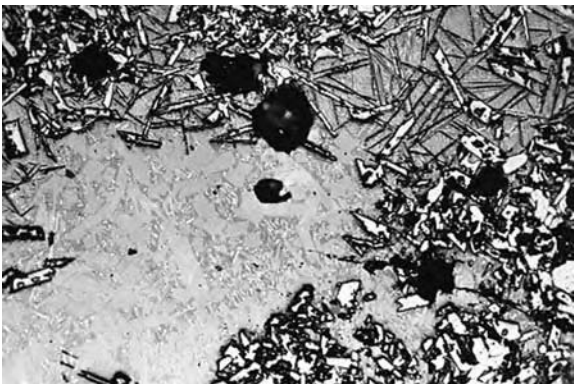


Figure 11 Position where mullite crystals appear behind the hot face (130×).

wall surrounded by relic bauxite grains. Small calcium hexaluminate crystals are located in the glass phase between mullite crystals.

The appearance of mullite signifies the position where the CaO content of the penetrating phase is below about 20%. This is a consequence of the “dilution” of the slag by the corrosion of the brick and the lesser amount of slag as distance is traversed away from the hot face.

At a position of about 10 mm behind the hot face of the brick, slag penetration stopped. Near the cold face of the brick, the microstructure of the brick was normal for a 70% Al_2O_3 brick product made using a mixture of calcined bauxite and clay. The conclusion from this study was that the normally expected corrosion reactions were found to take place, and the accelerated wear was likely due to poor thermal shock resistance, resulting in enhanced spalling that ultimately shortened the campaign of the electric furnace roof.

In summary, the corrosion processes for the 70% Al_2O_3 brick were as follows:

1. Slag coated the surface of the hot refractory, and corrosion began as the surface temperature exceeded about 1265–1380°C. The reaction can be expressed in words as “Calcium (iron) alumino-silicate slag reacts with 70% alumina refractory forming a gehlenite-anorthite glass with solution of mullite and bauxite in the slag.”

2. Slag penetrated the refractory, filling the pores with liquid and dissolving the bond phase (mullite) until the local CaO content of the slag dropped below about 20%. Behind this area, mullite reappeared and exhibited crystal growth to a progressively lower extent until the freeze plane for slag in the brick was attained.

C. Case Study: 90% Al_2O_3 Brick from a Metal Contact Zone in a Ferrous Foundry Furnace

In another case study involving a different foundry, a 90% Al_2O_3 brick was examined for evidence of corrosion after service in a ferrous foundry furnace hearth/lower sidewall application. The premature failure was in a “skewback” brick at the furnace hearth that was supporting the lower furnace sidewalls. A photograph of a brick after service is shown in Figure 12. Because of the extreme wear of the brick, it was suspected that corrosion was a cause of failure.

The 90% Al_2O_3 brick was made using fused alumina aggregate bonded in a matrix of mullite and glass. The calcium-iron-alumino-silicate slag dissolved all of the mullite in the immediate hot face of the refractory and showed evidence of solution of the fused alumina aggregate particles (Figure 13). Phases other than corundum (from the fused alumina—labeled “A”) were hercynite (labeled “H”), calcium hexaluminate, and glass. The fused alumina aggregate appears to dissolve in the slag and form hercynite (iron aluminate spinel) at the aggregate’s periphery.



Figure 12 Ninety percent Al_2O_3 brick after ferrous foundry service.

The slag liquid penetrated the refractory to a depth of 10 to 20 mm behind the hot face. At a depth of about 8 to 10 mm behind the hot face, mullite appeared in the microstructure, indicating that the CaO content of the penetrating slag dropped below about 8% (Figure 14). In the upper field of this photomicrograph,

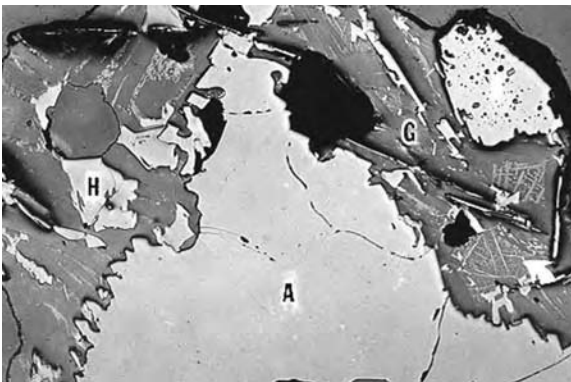


Figure 13 Immediate slag–brick interface of the used 90% alumina brick (130 \times).

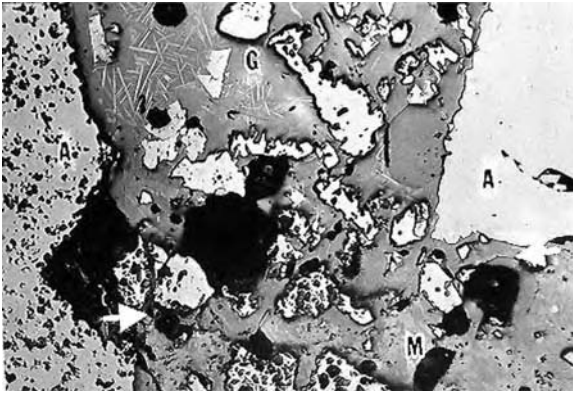


Figure 14 Area where mullite reappears behind the hot face (130 \times).

glass or slag (labeled “G”) penetrated between fused alumina aggregate particles (labeled “A”). Needlelike crystals of calcium hexaluminate are dispersed in the glass phase. In the lower field, mullite (labeled “M”) appears as clusters of individual crystals dispersed in a glass phase somewhat altered in chemistry by the slag penetration.

In this case, it was determined that the corrosion reactions were those normally expected in a ferrous foundry, i.e., chemical solution of the bond phase of the brick with penetration behind the hot face. Large “veins” of solidified metal were found within the used brick, indicating mechanical failure in service followed by metal penetration.

D. Basic Brick in Steel-Making Applications

1. Introduction

A 90% MgO class fired, pitch-impregnated brick was examined after a short campaign in a basic oxygen furnace producing carbon steel. The slag composition can be viewed as a high CaO/SiO₂ ratio liquid containing a substantial amount of iron oxide. Because the major component of the brick was MgO, the ternary system CaO–MgO–SiO₂ can be used to view the corrosion processes as a first approximation (Figure 15).

In the case of the 90% MgO class refractory, the brick contained 95.5% MgO, 2.7% CaO, and 1.4% SiO₂. This implies that the “native” silicate in the brick is dicalcium silicate (2CaO · SiO₂)—a very refractory second phase providing for a part of the bonding in a product where direct sintered bonds between adjacent MgO aggregate particles predominate. In service, a transient period

It is interesting that as the slag basicity increases (i.e., as the CaO/SiO_2 ratio increases), corrosion reactions begin at a higher temperature. This is one reason that steel makers wish to have solution of limestone slag additions as early as possible in a refining cycle to retard slag corrosion.

3. For a CaO/SiO_2 ratio of 2.0, the lowest eutectic temperature is at $\sim 1790^\circ\text{C}$. Without considering the iron oxide and other components of the slag, this implies that the reaction product between the slag and the brick is above most steel-making temperatures. However, the iron oxide plays an important role, significantly reducing the temperature of the reaction products.

E. The Role of Iron Oxide in Corrosion

One consequence of iron oxide in steel-making slag is to significantly reduce the melting temperatures predicted by only considering the $\text{CaO}-\text{MgO}-\text{SiO}_2$ phase diagram. Some of the reaction products commonly found between basic refractories and steel-making slag are given in Table 3.

Table 3 Reaction Products Between Steel Making Slag and Basic Refractories with Melting Points for Full Melting or Partial Melting (Peritectic Reactions)

System $\text{CaO}-\text{MgO}-\text{Al}_2\text{O}_3-\text{SiO}_2$		System $\text{FeO}-\text{MgO}-\text{Al}_2\text{O}_3-\text{SiO}_2$	
Mineral	Melting temperature ($^\circ\text{C}$)	Mineral	Melting temperature ($^\circ\text{C}$)
$2\text{MgO} \cdot \text{SiO}_2$ (forsterite)	1900	$\text{FeO} \cdot \text{SiO}_2$ (fayalite)	1205
$\text{CaO} \cdot \text{MgO} \cdot \text{SiO}_2$ (monticellite)	1485	$\text{FeO} \cdot \text{MgO} \cdot \text{SiO}_2$ (iron monticellite)	1230
$3\text{CaO} \cdot \text{MgO} \cdot 2\text{SiO}_2$ (merwinite)	1575	$2\text{CaO} \cdot (\text{Fe}_2\text{O}_3, \text{Al}_2\text{O}_3) \cdot \text{SiO}_2$ (iron gehlenite)	1285
$2\text{CaO} \cdot \text{SiO}_2$ (dicalcium silicate)	2130	$\text{FeO} \cdot \text{Al}_2\text{O}_3 \cdot 5\text{SiO}_2$ (iron cordierite)	1210
$3\text{CaO} \cdot \text{SiO}_2$ (tricalcium silicate)	2070	$2\text{CaO} \cdot \text{Fe}_2\text{O}_3$ (dicalcium ferrite)	1489
$\text{CaO} \cdot \text{Al}_2\text{O}_3 \cdot 2\text{SiO}_2$ (anorthite)	1553	$4\text{CaO} \cdot \text{Al}_2\text{O}_3 \cdot \text{Fe}_2\text{O}_3$ (brownmillerite)	1395
$2\text{CaO} \cdot \text{Al}_2\text{O}_3 \cdot \text{SiO}_2$ (gehlenite)	1593	$6\text{CaO} \cdot 2\text{Al}_2\text{O}_3 \cdot \text{Fe}_2\text{O}_3$	1365
$\text{CaO} \cdot \text{Al}_2\text{O}_3 \cdot 2\text{SiO}_2$ and $2\text{CaO}-\text{Al}_2\text{O}_3-\text{SiO}_2$ (melilite)	1380		

It is immediately obvious that most of the iron-containing compounds melt in the area of 1200–1350°C while most of the calcium silicate phases melt above 1485°C. It is also true that melting can typically begin below these indicated temperatures by as much as 50°C due to the effect of other impurities and due to the presence of multicomponent eutectics not seen on three-component diagrams.

The corrosion process between calcium-iron-silicate slag and magnesia-containing refractories can depend on the mobility and concentration of reactants. A photomicrograph of the immediate slag–brick interface region in a brick from a steel-making furnace location *above the metal line* is shown in Figure 16. Here the reaction products are “mixed” iron spinel or $(\text{MgO}, \text{FeO}) \cdot (\text{Al}_2\text{O}_3, \text{Fe}_2\text{O}_3)$, dicalcium silicate ($2\text{CaO} \cdot \text{SiO}_2$), and dicalcium ferrite ($2\text{CaO} \cdot \text{Fe}_2\text{O}_3$). Because of the high concentration of iron oxide dust in the furnace atmosphere and the lack of persistent slag attack (or flow), the spinel phase formed a sort of “barrier coating” over the face of the brick.

By contrast, a brick from a slag line application exhibited a very different corrosion process (Figure 17). Here the products of corrosion appear to be dicalcium ferrite ($2\text{CaO} \cdot \text{Fe}_2\text{O}_3$) penetrating around individual magnesium oxide crystals (rounded gray crystals) with isolated pockets of black-appearing dicalcium silicate ($2\text{CaO} \cdot \text{SiO}_2$) present in the slag layer. Magnesium oxide crystals appear to be eroded from the refractory surface in response to the extremely high temperatures and the intensity of the slag contact.

In these cases, the microstructures at the reaction interface are extremely different despite the fact that the bricks were in the same furnace. In the upper sidewall, reaction with iron oxide and lime-containing dust contributed to the corrosion process. By contrast, in the slag line, persistent contact with flowing slag caused corrosion and erosion processes to take place.

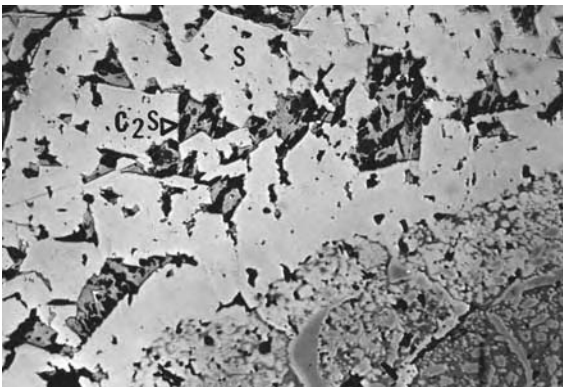


Figure 16 Corrosion interface in an MgO brick from an upper sidewall location (130×).

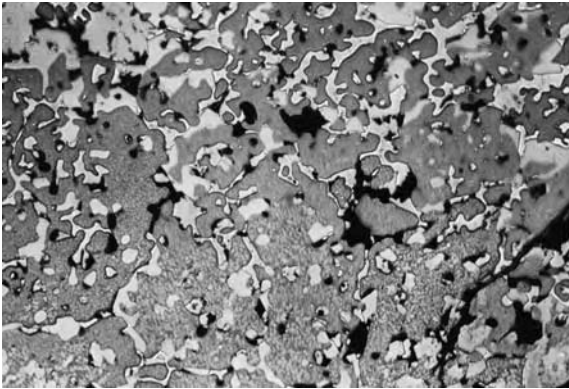


Figure 17 Corrosion interface in an MgO brick from a slag line location (130 \times).

F. Case Study: 90% MgO Burned-Impregnated Brick After Service in the Basic Oxygen Steel-Making Furnace

A used brick from a “bottom tuyere pedestal” (also called a “bottom plug”) is shown in Figure 18. The bottom plug contains tuyeres where oxygen is injected into the molten metal bath to facilitate the refining process. The bricks are exposed to the localized high temperatures from the exothermic reaction between the oxygen and the metal. It is notable that this brick exhibits a layer apparently in the process of spalling away from the brick hot face.

The hot face region of the brick is shown in Figure 19 at low magnification. The immediate slag–brick interface is in the upper field of the photomicrograph. The slag phase penetrating among individual MgO crystals is dicalcium ferrite, forming a thin “dense layer” in the outer zone of the brick. Behind the dense layer, a zone of porosity is noted as “black areas”—areas where the impregnated carbon phase in the brick was removed by oxidation.

Further behind the hot face in Figure 19, a large void is seen in the lower left of the photomicrograph. As will be seen in the following, this void resulted from a defect in the formulation of the brick. With prolonged exposure to heat, the defect in a precursor to the “peeling” away of the surface by spalling, as is seen in Figure 18.

The corrosion process is seen in a field near the immediate hot face (Figure 20). Here dicalcium ferrite (bright phase) and dicalcium silicate penetrate around individual MgO crystals from aggregate particles. Several smaller rounded MgO crystals are in the final phase of dissolution. Even though dicalcium silicate is a “compatible” phase with MgO, it will still dissolve MgO—as



Figure 18 Ninety percent MgO burned impregnated brick after service in a BOF bottom plug.

is evident from the photomicrograph. Thus, the corrosion process can, in part, be represented as solution of MgO in $2\text{CaO} \cdot \text{SiO}_2$.

Further behind the hot face, a zone was discovered where the “matrix” of fines (and carbon) shrunk away from the aggregate particles (Figure 21). This created voids at the periphery of the coarse aggregate particles in the brick, and these voids eventually consolidated, leading to the larger void of Figure 19. These voids lead to the peeling away of layers during service (spalling of thin layers) causing excessive wear. When confronted with the evidence, the developers of the brick were amazed that this separation took place because they had not seen it in laboratory “coking box” experiments. Eventually, the idea was advanced that the coking box temperature of about 1000°C was quite a bit different than the service temperature of the brick (1600°C).

In other case studies, magnesia-chrome and dolomite refractories were examined after service in an argon-oxygen-decarburization (AOD) reactor producing stainless steel. In this instance, slag specimens were collected during typical refining cycles, and bricks were examined after the end of the service campaign.

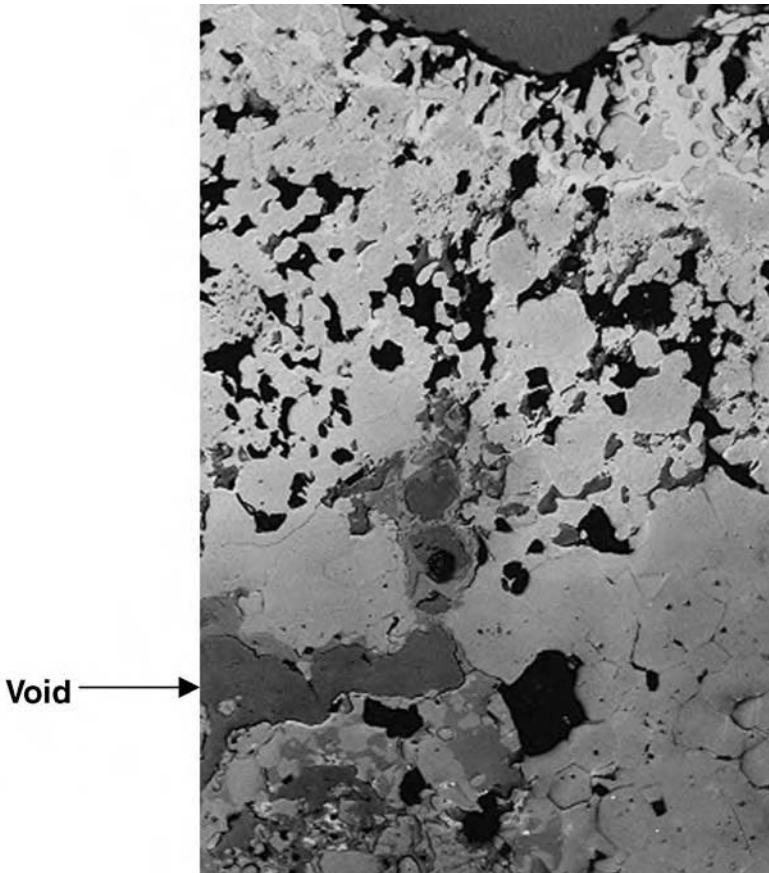


Figure 19 Hot face region of the MgO brick (50 \times).

The AOD refining cycle of slightly over one hour includes an initial period (decarburization cycle) where silicon is oxidized in the metal, producing a very viscous or “chunky” slag. A photomicrograph of this early slag shows clusters of spinel phases or $(\text{MgO}, \text{FeO}) \cdot (\text{Cr}_2\text{O}_3 \cdot \text{Al}_2\text{O}_3 \cdot \text{Fe}_2\text{O}_3)$ and bright metal droplets interdispersed in a calcium silicate glass (Figure 22).

The angular spinel crystals and metal droplets are shown at higher magnification in Figure 23. The “chunky” nature of the slag is due to the viscosity of the slag created by the high concentration of spinel crystals.

The early AOD slag also contained eroded masses of MgO crystals. One such fragment can be seen in the lower left field of Figure 22 and in a photomicrograph taken using a scanning electron microscope (Figure 24). In this latter

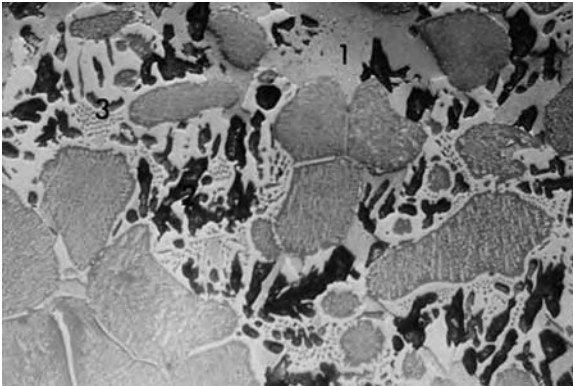


Figure 20 Field in the hot face zone (130×).

picture, spinel crystals in a continuum of calcium silicate glass surround a dark gray mass of MgO in the center of the photomicrograph.

The AOD refining cycle also includes a short “reduction period” where argon is injected into the metal to recover chromium from the slag. In effect, the spinel phases are substantially reduced. This cycle also employs an increased slag CaO/SiO₂ ratio to facilitate chromium recovery.

A photomicrograph of a reduction slag is shown in Figure 25. Only a few spinel crystals protrude from the glass, indicating high efficiency of reduction. The slag shows sign of water etching during polishing consistent with the solubility of merwinite and/or gehlinitite (see Table 3).

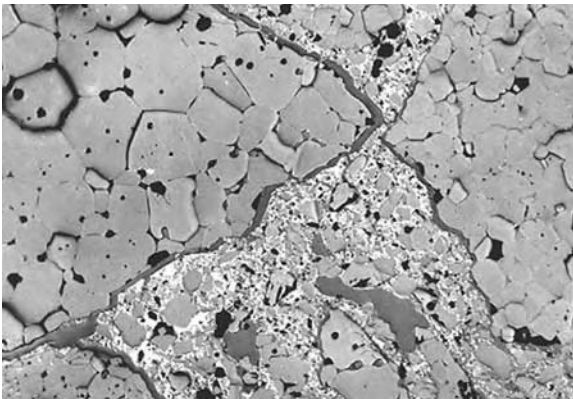


Figure 21 Field near the cold face (130×).

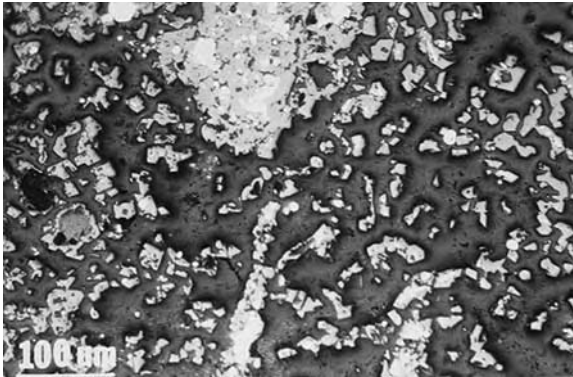


Figure 22 Early AOD slag (50×).

Fired magnesia-chrome bricks were used in early AOD linings. Despite a more recent trend to use magnesia-carbon products in these furnaces, the examination of magnesia-chrome brick illustrates several principles of corrosion processes. One brick from a midbarrel location in a 50-ton AOD reactor is shown in Figure 26. The continuous glassy slag coating on the hot face is typical for AOD service.

The immediate hot face area of the magnesia-chrome brick is shown in Figure 27. A chromite grain (labeled “Cr”) is in the center of the photomicrographs with a coarse magnesia aggregate particle to the left of the field. The slag layer is at the top of the photomicrograph. It is apparent from the “jagged” nature of the brick surface that the corrosion process has preferentially removed the matrix of the refractory, leaving coarse grains to protrude into the slag layer.

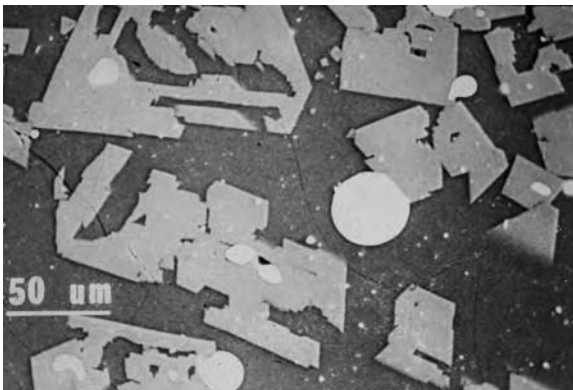


Figure 23 Detail of early AOD slag.

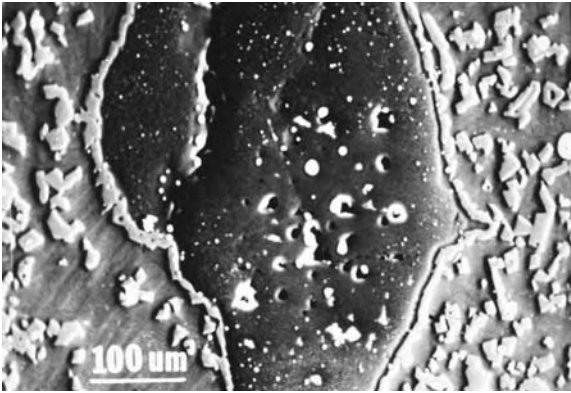


Figure 24 Eroded MgO mass in AOD slag.

What appears to be “corrosion” of the periphery of the chromite grains can also be seen at this low magnification.

A detailed view of the hot face region is shown in Figure 28 (slag layer toward the top of the field). Here, merwinite or $3\text{CaO} \cdot \text{MgO} \cdot 2\text{SiO}_2$ can be seen toward the top of the field (labeled “m”). The other slag silicate is monticellite or $\text{CaO} \cdot \text{MgO} \cdot \text{SiO}_2$. Both of these are expected as compatible phases for slag in the CaO/SiO_2 range of 1.0–1.5 in contact with MgO containing refractories (see Figure 15).

The corroded appearing edges of the chromite grains are “secondary” spinels that did not exist at the service temperature of the brick in the hot face region. The process was dissolution of the constituents of the chrome ore (Al_2O_3 , Cr_2O_3 ,

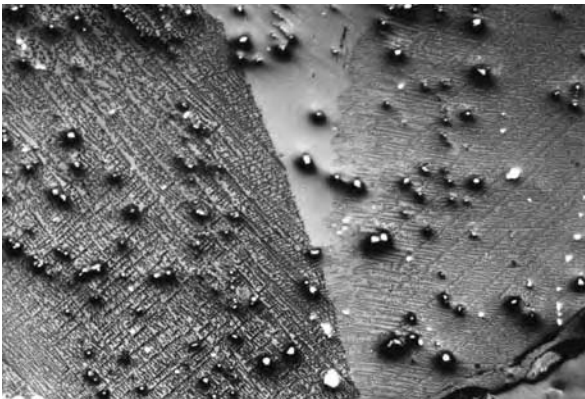


Figure 25 AOD reduction slag (130 \times).



Figure 26 Used magnesia chrome brick after AOD service.

and Fe_2O_3) in the penetrating slag followed by preferential precipitation around the chromite grains on cooling of the lining for the last time. These spinels did not form on the “top” of the chromite grains in the immediate slag–brick interface because of the rapid quenching after the last heat of steel was made. Metal droplets are also seen in Figure 28. These may have formed, in part, due to reduction of oxides in the chromite to the metallic state.

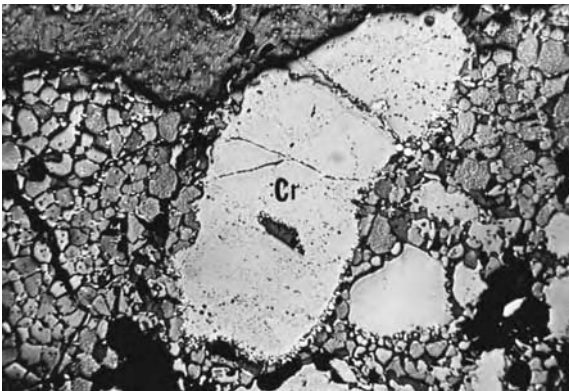


Figure 27 Slag–brick interface (50 \times).



Figure 28 Detail of the hot face region (130 \times).

The corrosion process can be summarized as follows:

Solution of MgO in the slag phases, penetration of slag into the brick, and disruption of the direct bonding behind the hot face.

Solution of chromite in the slag phases and partial chemical reduction of oxides to the metallic state.

In magnesia-chrome brick and other bonded refractories, slag penetration can occur to a depth of 75 mm or more behind the hot face. While significant chemical corrosion is usually limited to a depth of less than about 25 mm behind the hot face, the presence of the slag changes the physical properties of the brick due to shrinkage of the refractory and other processes. If the thermal expansion coefficient in the penetrated zone becomes different than that in the cold face region, spalling can occur near the interface between the penetrated and “unpenetrated” or cold face zones. Used brick can exhibit cracks in this zone and even larger voids where cracks have apparently joined. This phenomenon is called “densification spalling,” and it can result in the spalling loss of sections of about 75 mm in thickness.

G. Dolomite Brick in AOD Service

Dolomite refractories were used in AOD service in the early stages of development of the AOD process. Dolomite brick contain “islands” of MgO crystals in a continuum of CaO. The hot face region of a used dolomite brick after AOD service is shown in Figure 29. In this photomicrograph, the immediate hot face is to the right of the photomicrograph. The central area of the photomicrograph is the affected zone where corrosion has resulted in reaction of

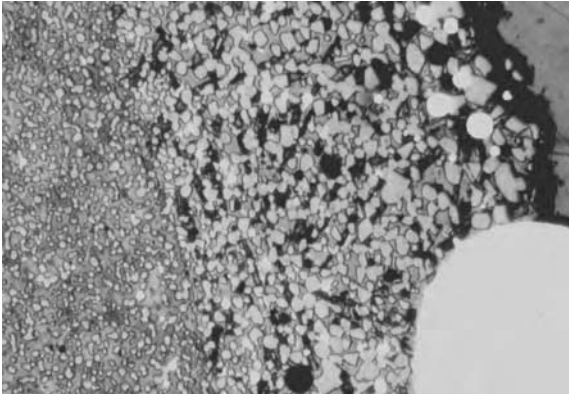


Figure 29 Dolomite brick after AOD service (130 \times).

slag with the CaO continuum in the brick, forming dicalcium silicate and tricalcium silicate (the black phase etched with water in polishing). Metal droplets are apparent in this region. Aside from chemical corrosion, spalling is also known to occur in AOD service.

H. Gas-Phase Reactions

The gas phase in a furnace may be the partial or even sole contributor to corrosion reactions or other deterioration in refractories. Some of the processes that have been recognized include

1. Alkali transport to refractory surfaces resulting in surface reaction and penetration
2. Reduction of the refractory and gas-phase corrosion
3. Alternating oxidation and reduction, causing sequential dimensional changes in refractories that may enhance spalling.

The potential for alkali to cause “glazing” on the surface has been previously discussed (see Figure 5). It is less well recognized that alkali compounds can volatilize in furnace atmospheres, resulting in transport of the volatile species to the surface of the refractory where vapor-phase penetration may also occur.

The melting points of sodium and potassium reaction products with aluminosilicate refractories are given in Table 4. The melting points of the phases themselves are not indicative of the very low eutectic temperatures found in the system. For example, the lowest eutectic in the system $\text{Na}_2\text{O}-\text{Al}_2\text{O}_3-\text{SiO}_2$ (Figure 5) is 732°C.

The sidewall of a sawdust-fired tunnel kiln producing facing brick is shown in Figure 30. In the central section of the picture, the effect of the plume of

Table 4 Alkali Phases Found in Used Refractories

Phase	Melting Point (°C)
$\text{Na}_2\text{O} \cdot \text{Al}_2\text{O}_3 \cdot 6\text{SiO}_2$ (albite)	1100
$\text{Na}_2\text{O} \cdot \text{Al}_2\text{O}_3 \cdot 2\text{SiO}_2$ (carnegite)	1526
$\text{K}_2\text{O} \cdot \text{Al}_2\text{O}_3 \cdot 6\text{SiO}_2$ (carnegite)	1220
$\text{K}_2\text{O} \cdot \text{Al}_2\text{O}_3 \cdot 4\text{SiO}_2$ (leucite)	1686
$\text{K}_2\text{O} \cdot \text{Al}_2\text{O}_3 \cdot 2\text{SiO}_2$ (kaliophilite)	>1700

combustion from the top burner position nearest the wall is seen (kiln draft from right to left). A black slag is seen coating the fireclay brick with white salt deposits visible in this picture taken after seven years of service. There was only surface glazing of the brick in the sidewall of the kiln. Glazing is also shown on the insulating firebrick surface in the crown of the kiln (Figure 31).

The sidewall brick had expanded due to alkali attack to the point that they were replaced. In addition, the insulating firebrick in the crown exhibited both surface glazing and “sheet” spalling. Sheet spalling is well known, and it usually results from a subsurface expansion reaction caused by penetration of an agent in the gas phase that subsequently reacts with the refractory.

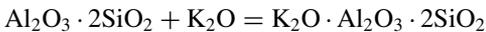
Alkali halides are volatilized in kiln atmospheres. They undergo hydrolysis reactions in a moist high-temperature environment, forming alkali oxide species.

**Figure 30** Sidewall of sawdust fired tunnel kiln after seven years of service.



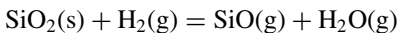
Figure 31 Crown of sawdust fired tunnel kiln after seven years showing surface glazing and sheet spalling.

These oxides can cause glazing or expansion. The expansion reaction with potassium is particularly deleterious for refractories, with the reaction given as



where $\text{Al}_2\text{O}_3 \cdot 2\text{SiO}_2$ is metakaolin (a decomposition product of fireclay) and the reaction product is kaliophylite. The volume expansion due to formation of kaliophylite is on the order of 15% (linear expansion of $\sim 5\%$). As potassium is a product of combustion of sawdust, reactions of this type are expected as the cause of the problems in the sidewalls of tunnel kilns fired with sawdust and as the cause of the sheet spalling (Figure 31).

Gas-phase corrosion is also known in refractories containing SiO_2 . It has long been recognized that products containing SiO_2 can be “reduced” by hydrogen or by penetration of aluminum metal. The gas-phase reduction by hydrogen can be represented as



where (s) signifies a solid phase and (g) signifies a gaseous phase.

Refractories exposed to hydrogen (or carbon monoxide) can experience gas phase removal of SiO_2 through the process of forming silicon monoxide. For example, at 1000°C , a CO/CO_2 ratio of about 10^{-5} will be sufficient to reduce SiO_2 . Mullite reduction and silica loss at temperatures exceeding 1500°C have been seen in petroleum calcining kilns.

VI. LABORATORY SLAG TESTS

Laboratory slag tests have been developed over the years for evaluating corrosion potential. These slag tests range from a “static” cup test to the “dynamic” rotary slag test. The terms “static” and “dynamic” refer to whether the slag is stationary or whether it moves over the refractory surface, respectively. Some of the test methods are summarized in Table 5. The rotary slag apparatus is shown during a test in Figure 32. The slag is running out of the apparatus into a well while a technician is checking the temperature using an optical pyrometer.

Microscopic studies have shown that the same types of reactions occur in the rotary slag test as in brick examined after service in metallurgical furnaces. The slag–brick interface area in a magnesia-chrome brick from a rotary slag test using a steel-making slag is shown in Figure 33.

The corrosion process in Figure 33 includes solution of the MgO in the slag consisting primarily of monticellite. The periphery of chromite grains appears to

Table 5 Laboratory Slag Tests

Test	Type	Reference or comment
Cup	Static	The test usually consists of a ~50 mm diameter hole core drilled or formed into the refractory that is packed with slag and heated to a selected test temperature for a set time. The test only reflects the isothermal reaction and penetration potential between the slag and the refractory
Drip	Dynamic	Slag drips over a surface with evaluation of the depth of a “notch” cut in the surface by corrosion. The test is described in ASTM C 768. The test reflects the isothermal reaction potential between the slag and refractory when there is a constant supply of unreacted or “fresh” slag
Rotating spindle	Dynamic	Refractory bars or rods ~25 × 25 × 200 mm are partially immersed in a crucible containing slag while the specimen is rotating. The test reflects isothermal reaction potential of a flowing slag without a constant supply of “fresh” slag
Rotary	Dynamic	Beveled refractory shapes (formed by saw cutting) or monolithic materials constitute a lining of a small rotary furnace that is constantly fed with slag. After the test, the specimens are examined for corrosion loss and slag penetration. This test is described in ASTM C 768. The test reflects corrosion under a temperature gradient with a constant supply of “fresh” slag



Figure 32 Rotary slag test for refractories.

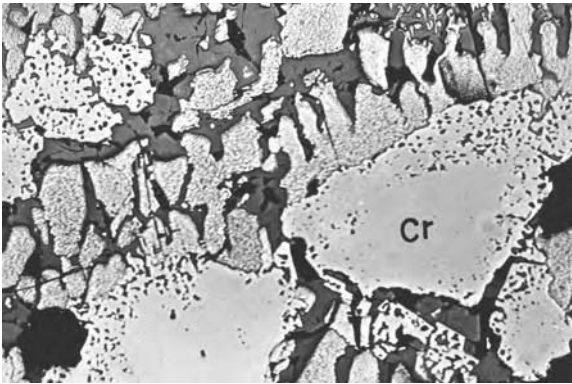


Figure 33 Slag–brick interface in a magnesia-chrome brick after a rotary slag test.

be attacked, but the “porous” spinel phases were formed on recrystallization from the melt when the refractories cooled after the test. The elongated nature of MgO crystals is typical under the influence of the steep temperature gradient in the rotary slag test.

VII. CONCLUDING COMMENTS

Slag corrosion by liquids occurs whenever a threshold temperature is exceeded, which is usually when melting occurs between the refractory and the slag. Corrosion results in solution of refractory constituents in the liquid phase, result-

ing in loss of thickness of the refractory lining. The rate of corrosion is dependent on the chemical environment and on the hot face temperature of the refractory.

Models for the corrosion process point to the fact that hot face temperature is the most important variable in controlling refractory life. To reduce corrosion loss, the usual approach is to employ higher-purity refractories or lower-porosity refractories (such as fusion cast brick) because precise limits on hot face temperature are not practical given process goals. In new furnace designs, consideration should be given to hot face temperature control as a strategy to attain the most economical refractory cost.

Corrosion is primarily a chemical process, and the potential for corrosion can be estimated by reference to phase equilibrium diagrams. These diagrams can allow prediction of the “threshold temperature” for liquid formation. Microscopic techniques allow identification of particular corrosion reactions. Corrosion can also take place through gas-phase reactions. The most fundamental way to limit corrosion is to understand the chemical and physical processes involved in corrosion and to formulate strategies to minimize these processes.

Dedication

This chapter is dedicated to the memory of Mr. Walter S. Treffner, the long-time research director of the former General Refractories Company (USA). Mr. Treffner was an accomplished microscopist and a dignified researcher in the field of refractories. Mr. Joseph L. Stein, former president of General Refractories (USA), is acknowledged for substantial inspiration of the author’s work.

REFERENCES

1. Burgeron C, Risbud, S. Introduction to Phase Equilibria in Ceramics. Columbus, OH: The American Ceramic Society, Inc., 1984.
2. Konig VG. Stahl u. Eisen 1971; 91(2):63–69.
3. Herron R, Beechan, C. Ceramic Engr & Sci Proc 2(11–12):1126–1140.
4. Endell K, Fehling R, Kley R. J Am Ceram Soc 1939; 22:105–116.

4

Alumina-Silica Brick

Denis A. Brosnan

Clemson University, Clemson, South Carolina, U.S.A.

I. INTRODUCTION

With the advent of the Iron Age, people began learning in earnest how to construct furnaces that could withstand sustained temperatures exceeding the melting point of iron (1535°C). At the melting point of iron, magnetite (Fe_3O_4) can be reduced to iron at an oxygen partial pressure of about 10^{-7} atmospheres—an atmosphere easily reached in a furnace packed with a form of carbon such as coke or charcoal. Of course, carbon-saturated iron has a melting point of 1152°C, but the iron must be at a higher temperature to attain sufficient fluidity for casting.

With the advent of a larger demand for iron objects in commerce, modern ferrous metallurgy was born. It cannot be overemphasized that the iron and steel industries, with ever-increasing demands for better refractory products to combat more severe service conditions, drove the innovations with alumina-silica brick over history. All other industries consuming alumina-silica brick, including non-ferrous metals and minerals processing, benefited from this progression of technology.

Alumina-silica bricks have the attributes of being relatively inexpensive—at least compared to most basic brick. In addition, alumina-silica brick can be used in situations where modern castable refractories have disadvantages. While some castable products have achieved physical properties meeting or exceeding those of brick, there is still a responsibility with castables for correct installation, curing, and preheating. If time or local skills for installation are constraints, brick may be a preferred solution. In some types of furnaces, the use of bricks may be preferred to avoid mechanical or thermal shock damage that reduces furnace life. Finally, tradition with use of bricks still influences some product decisions in applications like ceramic kilns, incinerators, and smaller boilers.

The technology of alumina-silica brick is relatively uncomplicated. In other words, the phase relationships and properties listed in the specifications are straightforward. With more in-depth study, the researcher finds that natural raw materials and their inherent variability always influence the average properties and variance in properties in the refractory brick as-manufactured. In addition, no two refractory plants are ever exactly the same because processing equipment influences the quality of the end product. Finally, alumina-silica bricks are manufactured on a tonnage scale, meaning that the products exhibit variability in properties attributable to this scale of manufacture. All this contributes to the correct observation that one product in the same “class” can be better than a competitive product of the same class. The differences between the “good” and “not-as-good” products are usually not revealed in physical property tests alone. Further testing or experience is required to understand the fine points of why one product may be better than another one.

II. A BRIEF HISTORICAL PERSPECTIVE

The earliest refractories used in furnaces were natural stones quarried into brick-like shapes and natural clays and sands used as rammed lining components. Bricklike shapes were used because of the thousands of years of practice using stone and clay masonry in buildings. Thus, it was natural that brick furnace linings would become larger than simple enclosures.

People found that some natural stones and some clays had better thermal resistance than others. In particular, some stones or clays exhibited better “refractoriness” than others. A simple definition of refractoriness is that the material will not melt or deform (shrink) under prolonged service in the furnace environment in service. Excessive shrinkage almost always results in the opening of joints in a furnace, cracking, increased susceptibility to thermal shock, and a host of other problems.

It became fairly obvious that chemical analysis of the natural material was linked to its refractoriness just because lighter colors, for example, indicated less iron content and generally greater refractoriness. Certain clays became known as “fireclay” because of their resistance to high temperature. Clays in certain regions of various countries became preferred for use in refractory products based on their reputation as successful raw materials for refractories.

In time, conveniently located natural stone products were depleted. This resulted in production of hand-molded fireclay bricks. With the onset of the industrial age, fabrication of bricks in mechanical presses began. Sufficient temperature could be reached in downdraft kilns to produce qualities of refractory brick in the late 1800s not too unlike those available today.

With the advent of phase equilibrium diagrams after about 1920, the modern era of alumina-silica brick began. At that point, scientific principles guided the development of fireclay brick rather than trial and error with different sources of raw materials. World War II was particularly influential in the history of alumina-silica bricks as it marked the development of refractories in North America based on bauxite as an alternative to the basic refractories that were suddenly unavailable from Europe. The development of the Bayer process for manufacturing aluminum brought about the manufacture of calcined and tabular alumina—generating a new line of “high-alumina” brick. Processing technology in grinding, separation, mixing, pressing, and firing increased dramatically after World War II, giving “modern” plants a technology edge over older facilities.

Developments with refractory concrete or “castable” eventually caused alumina-silica brick consumption to peak and begin a decline starting in the late 1970s and the early 1980s. Technical improvements in all types of refractory products caused a reduction in refractory consumption rates. The end result has been a decline in production of alumina-silica refractories. In today’s global economy, alumina-silica bricks are primarily produced in emerging countries and exported to “developed” countries. While the production and consumption patterns have shifted, there remains a need for an understanding of the technology in today’s world.

III. THE TECHNOLOGY OF ALUMINA-SILICA REFRACTORIES

A. Phase Relationships in the System $\text{Al}_2\text{O}_3\text{--SiO}_2$

The technology of alumina-silica refractories is traditionally explained using the alumina (Al_2O_3)–silica (SiO_2) phase equilibrium diagram (Figure 1). A phase diagram is essentially a “map” of temperature versus composition showing “phases” or discrete areas/volume elements of similar composition within a material at equilibrium and at a given temperature. The idea is that certain compositions will produce certain qualities of refractories. The diagram in Figure 1 shows composition in mole percent and temperature in degrees Celsius. There are updated representations of this system, but the essential facts remain the same.

The *essential facts* from this phase diagram are the following:

1. One compound known as *mullite* ($3\text{Al}_2\text{O}_3 \cdot 2\text{SiO}_2$) is formed as a reaction product or consequence of heating mixtures of alumina and silica. The theoretical composition of mullite is 71.6% Al_2O_3 and 28.4% SiO_2 on a weight basis (or 60 mole percent Al_2O_3). Mullite is a very refractory compound exhibiting a melting point of 1850°C. As the mullite content of a refractory increases as the composition approaches 72% Al_2O_3 , the refractoriness of the material usually increases due to the presence of the mullite. Near the theoretical composition of mullite, a mullite solid solution (denoted “mullite ss”) forms.

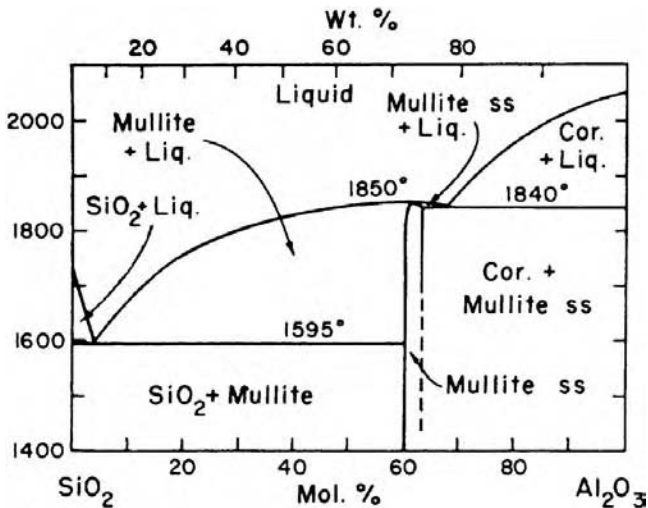


Figure 1 The alumina-silica phase equilibrium diagram. (From Ref. 2.)

2. The diagram has a “solidus” line at 1595°C, meaning that compositions ranging from just below 100% SiO₂ (>0% Al₂O₃) to the mullite composition (60 mole % Al₂O₃ or ~72 weight % Al₂O₃) exhibit solid phases (for example, cristobalite—a form of SiO₂—or glass and mullite) unless the temperature exceeds 1595°C (the binary eutectic temperature between SiO₂ and mullite). The term “glass” signifies the presence of a vitreous and noncrystalline phase. It can be present along with a small percentage of “free” or uncombined crystalline silica. Above 1595°C, a refractory in this composition range would be obviously useless as it would be partially liquid phase or melted (denoted as “Liq.” in Figure 1).

3. Above about 72% Al₂O₃, the solidus line is located at 1840°C, indicating compositions in the range of just above 72% Al₂O₃ to just below 100% Al₂O₃ exhibit no melting until 1840°C is exceeded. As the composition approaches 100% Al₂O₃, *the refractoriness of the material usually increases*. Pure Al₂O₃ (corundum—labeled “Cor.” in Figure 1) has a melting point of about 2050°C.

The Al₂O₃–SiO₂ phase diagram can be used to explain the “classes” of alumina-silica brick in terms of generalized “refractoriness.” These classes are given in Table 1 along with comments on the use of the products. It is easy to see that as you progress across the chart to the right (increase the Al₂O₃ content of the refractory), the refractoriness *increases* either because the mullite content increases and/or because the solidus temperature jumps up above 60 mole % Al₂O₃. The refractoriness increases because the glass content (quantity of vitrified phase) decreases, leading the material to have higher resistance to shrinkage on prolonged high-temperature exposure.

Table 1 Classes of Alumina-Silica Brick Explained in Terms of the Al_2O_3 - SiO_2 Phase Equilibrium Diagram

Al_2O_3 range in most standards	Common terminology <i>Phases</i>	General performance <i>in the absence of slag corrosion or alkali attack conditions</i>
Less than 50% Al_2O_3	Fireclay (Chamotte) <i>Phases on phase diagram:</i> mullite and glass (can contain “free SiO_2 ”)	Usually made from 100% fireclay Highest-quality grades usable to about 1600°C (“super-duty” brick) Typically contain 38%–42% Al_2O_3 and are based on fireclay minerals
50% Al_2O_3 or 60% Al_2O_3	Sillimanite, andalusite, or kyanite <i>Phases on phase diagram:</i> Major phase—mullite and minor phase—glass (can contain “free SiO_2 ”)	Cannot be made from 100% clay since clays do not contain sufficient Al_2O_3 Made from 60% alumina minerals and contain some fireclay. Can be made with bauxite and clay Can be used in excess of 1700°C
70% Al_2O_3	Mullite <i>Phases on phase diagram:</i> Major phase—mullite. Products made with bauxite contain corundum, mullite, and glass	Made either from “bauxitic clay” or calcined bauxite and clay Can be used in excess of 1750°C
80% Al_2O_3 and 85% Al_2O_3	Bauxite <i>Phases on phase diagram:</i> The major phase is corundum, with a minor quantity of mullite and glass	Made from calcined bauxite Usually used in aluminum contact refractories
90% Al_2O_3	Alumina <i>Phases on phase diagram:</i> The major phase is corundum, with a substantially minor quantity of mullite and glass. Brick for molten iron contact usually contain fused Al_2O_3 for enhanced abrasion resistance	Made from tabular and/or fused synthetic (Bayer process) alumina aggregates Can be used in excess of 1800°C

There are natural “lines of demarcation” on the chart. Since refractory fireclays typically contain a maximum of 38% to 40% Al_2O_3 , the refractories made solely from clay are in the fireclay class and have use limits approaching 1600°C (Table 1). Minerals with the next-highest alumina content include sillimanite, kyanite, and andalusite—all containing about 60% Al_2O_3 . Therefore, brick in the 50% and 60% Al_2O_3 classes must substantially contain these latter minerals, giving them higher use temperatures. The next mineral substance containing higher alumina used in refractories is calcined (burned) bauxite that forms a basis for 80% and 85% Al_2O_3 class products. For higher alumina content, synthetic or Bayer process calcined and sintered (tabular) alumina must be used. Tabular alumina aggregates and calcined alumina are used in products in either the 90% or 99% Al_2O_3 classes of refractory brick.

Any discussion of alumina-silica refractories must include the effects of “fluxing” oxides in the raw materials as they affect properties of the refractory. In natural clays, alkali is present in various forms—with the alkali content expressed as sodium oxide (Na_2O) or potassium oxide (K_2O). Both of these powerful fluxes are influential in the firing of fireclay brick and with respect to their performance in service. Other fluxes such as calcium oxide (CaO), iron oxide (FeO or Fe_2O_3), and titanium dioxide (TiO_2) are present. More flux generally means more glass will be present in the fired refractory. It is for this reason that fireclay brick, in particular, may exhibit better service performance (for example, greater spalling resistance) if they contain lower levels of flux; i.e., greater mullite content increases spalling resistance and greater glass content decreases spalling resistance.

As a final note on phase equilibria, refractories are usually not at thermochemical equilibrium. This means nonequilibrium phases may be present. An example might be a fireclay brick containing calcined bauxite aggregate (as a contaminant) with an overall composition of 50% Al_2O_3 . This fired brick will contain corundum even though the phase diagram says it should not be present. Given an unusually long time during the firing process, the corundum would disappear (forming mullite). Phase diagrams always indicate the *direction* for potential reactions in refractories, but they do not provide assurance that the reactions will go to completion.

B. Refractory Raw Materials

Raw materials for use in alumina-silica brick are available throughout the world in discrete deposits found useful in refractories. The typical chemical analyses for materials used as “major mix constituents” are given along with calcination temperature in Table 2. Calcination, if employed, renders the material as volume stable to resist shrinkage up to the original calcination temperature. Many other raw materials are used in manufacturing refractories serving distinct purposes. For example, in brick manufacture, “bond clay” is used to promote cohesion in the pressed mass so the brick can be lifted off the press for subsequent drying and firing. Bond clay

Table 2 Typical Raw Materials Used in Alumina-Silica Brick

Information	Fireclay (calcined basis)	Andalusite	Calcined refractory bauxite (Guyana)	Tabular alumina
Usual calcination temperature, °C	Can be used as calcined aggregate (1450°C+) or as raw clay	Not calcined	1450°C	>1750°C
Chemical analysis, %				
Al ₂ O ₃	39.7	61.3	88.7	99.5
SiO ₂	54.0	37.4	6.5	<0.1
TiO ₂	2.80	0.25	2.84	Tr.
Fe ₂ O ₃	1.90	0.48	1.43	0.05
MgO	0.30	0.13	0.31	0.05
CaO	0.20	0.20	0.15	0.07
Na ₂ O	0.20	0.08	Tr.	0.25
K ₂ O	0.60	0.06	Tr.	Tr.
LOI	0.15	0.13	0.05	0.04

is typically an aluminous clay exhibiting plasticity when wet. An excellent review of raw materials used in refractories is available by Nishikawa (1).

Refractory producers may have a unique or “standard” compliment of raw materials in their inventory to produce all of their alumina-silica brick products. Any one producer may have a special material that is unavailable to other producers. In North America, this was the case for Missouri diaspore until its depletion in the 1960s. As another example, one refractory producer had special bauxitic kaolin in Alabama used to produce 70% Al₂O₃ brick, and the deposit was subsequently depleted in the 1980s. In both cases cited, the producer with the special raw material had a competitive advantage during the life of its particular mineral deposit.

C. Special Changes in Raw Materials on Heating

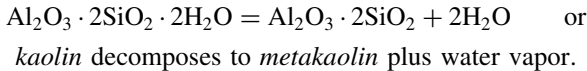
1. Fireclay

The chemical and physical changes in clay materials on heating and cooling are reported in a number of classic references (3). These changes are summarized, in brief, as follows:

1. *Dehydroxylation* of clay minerals in the range of 400°–600°C involving decomposition of clay crystals with consequent release of water vapor.

2. *Inversions* and *conversions* of “free” silica (SiO_2) phases that involve potentially destructive volume changes. The well-known alpha-to-beta quartz inversion is seen at 573°C .
3. *Partial fusion* and *permanent shrinkage* at temperatures approaching “red heat” (above 950°C).

The dehydroxylation of clay can be represented by the nonreversible chemical reaction for kaolinite (the major mineral in fireclay):



It is well known that, on additional heating, the metakaolin forms mullite at about 1020°C . In doing this, excess silica is released in a sequence of steps by metakaolin with the end result being mullite dispersed in a vitreous (glassy) phase.

It is also well known that fireclay contains a small amount of “free” or *uncombined* silica—usually as quartz in the mineral deposit. However, quartz is not the only mineral of pure silicon dioxide (SiO_2). The other silica minerals are *tridymite* and *crystalite*. In fact, quartz can be “converted” into either tridymite and/or crystalite on heating.

The form of quartz in the earth is called alpha (α) quartz. It is also called “low quartz” because it occurs at ambient temperatures in natural minerals. On heating of α -quartz, a new form called beta (β) quartz is formed at 573°C at 1 atm of pressure. The process is called an “inversion” because it involves a slight change in separation of silicon and oxygen atoms while maintaining the same spatial arrangement or crystal structure. This inversion is reversible, i.e., it occurs on heating or cooling if free quartz is present.

The densities of α -quartz and β -quartz are 2.65 g/cm^3 and 2.60 g/cm^3 , respectively. This means a lower-density quartz form is created on heating, forcing a volume increase to take place. The volume change on inversion of α -quartz to β -quartz is small, just 2%, implying a linear expansion of about 0.7%.

On further heating, quartz is *converted* to either tridymite or crystalite in a nonreversible transformation. The complete transformation scheme for silica (SiO_2) is given in Figure 2. Inversions are illustrated by a circle on a horizontal line representing one of the three forms of silica (quartz, tridymite, and crystalite). The inversions only involve a slight change in atomic separations, and an inversion is reversible. “Conversions” are changes involving formation of an entirely new mineral with a new crystal structure, and vertical arrows illustrate the conversions. The densities of all silica forms are given on the diagram.

The actual conversions of silica are influenced by the impurities in clay, meaning that the actual conversion temperatures are different than those published in textbooks for pure silica. For example, fireclay brick can contain crystalite if they are fired above about 2250°F (1230°C). The transformation

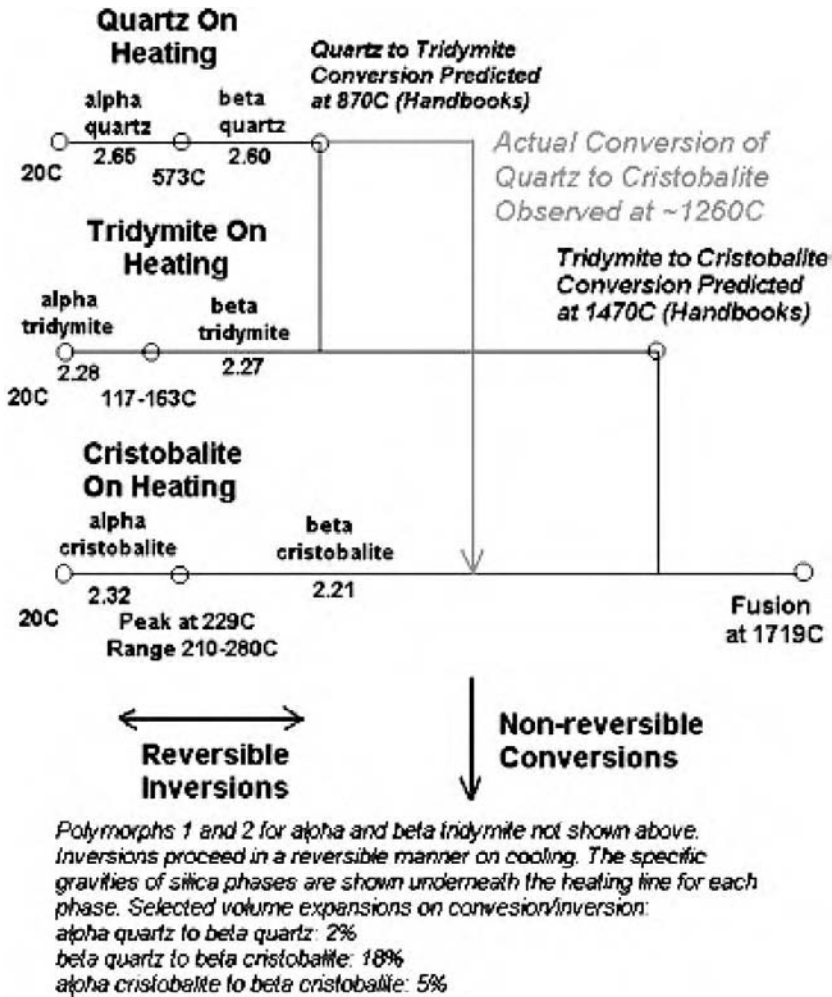


Figure 2 Changes in silica on heating.

from β -quartz to β -cristobalite causes a total permanent volume expansion of 13%. This is counterbalanced in fireclay brick manufactured by shrinkage during vitrification.

The problem with free cristobalite in fireclay refractories is that it causes deterioration in refractories on continued reheating and cooling in a process called "dunting." Dunting results in cracking and eventual fragmentation of refractories that contain too much cristobalite. The cause is the volume expansion

during inversion of α -cristobalite to β -cristobalite on heating of 5% (or shrinkage on cooling). It is well known that dunting can occur well after the refractory has cooled, in a process called “delayed dunting.”

2. Recrystallization of Sillimanite Minerals and Bauxite on Heating

The sillimanite family members, used to produce 50% and 60% alumina class brick, all exhibit characteristic permanent expansions on heating due to decomposition of the mineral and the formation of mullite. This is usually of interest in alumina-silica brick on heating the brick for the first time (during manufacture). The decomposition temperatures and expansions are given in Table 3.

If the brick is fired below the decomposition temperature of the mineral and used above the decomposition temperature of the mineral, the expansion will be realized in service. This could be detrimental to the refractory if there is inadequate expansion allowance in the lining. In certain cases, limited “after expansion” is important to obtaining good refractory life—as in rotary kiln applications.

There is a different situation with calcined refractory-grade bauxite. The original calcination temperature is approximately 1450°C, and this is a normal peak firing (sintering) temperature for bauxite-based refractory bricks. If these bricks are used above the original calcination and firing temperature, further “recrystallization” takes place, resulting in significant expansions. For example, the permanent linear expansion on exposing these products to temperatures reaching 1600°C is in the range of 2%–4%. The actual mechanism contributing to the expansion is likely additional mullite formation and growth of corundum crystals within the bauxite aggregates.

D. Alumina-Silica Brick Manufacturing

Alumina-silica bricks are manufactured from a blend of sized raw material aggregates and clays by mixing, forming, drying, and firing. These are traditional processes in manufacturing any ceramic product. Since refractories are used at

Table 3 Changes on Heating of Sillimanite Family Minerals

Mineral	Decomposition temperature (°C)	Volume expansion (%)
Sillimanite	1530–1625	5.6
Andalusite	1350–1500	4.9
Kyanite	1325–1410	18.8

elevated temperatures, they are particularly sensitive to contamination. Segregation of particle sizes also leads to low bulk density in brick products.

Throughout history, many fireclay bricks have been made by the extrusion process or by extrusion followed by “repressing.” Extrusion always means higher water contents must be used in processing to obtain plasticity, meaning that the product will have higher apparent porosity than a dry pressed product. Modern super-duty fireclay and high-alumina brick are made by dry pressing. Dry pressing has the attribute of producing generally finer pore sizes and structures in the fired product as compared to extruded products. This impacts fracture toughness and thermal shock behavior of the brick.

The best alumina-silica bricks are made in plants with common attributes. If an inspection trip is made to a refractory plant, here are the attributes worth looking for:

Raw material storage—Storage should be free of opportunities for contamination by inadvertent mixing of lower-quality raw materials with higher-quality raw materials.

Particle sizing and sized material storage—How many aggregate storage bins are observed for a particular raw material? A modern dry-pressed brick should contain at least four size fractions of the major raw material: coarse, medium, fine, superfine, etc.

Mixing—Is a modern high-intensity mixer used in production? Muller mixers (with large wheels) were obsolete in the 1970s.

Conveyance—Are conveyors covered to prevent contamination? If bucket elevators are used, is the manufacturer trying to prevent particle size segregation?

Presses—Are the presses computer-controlled, and do they automatically compensate for thickness variance in pressed brick?

Kilns—Are the kilns computer-controlled? Do they have modern high-velocity burner systems?

The most modern high-alumina brick plant is designed to minimize contamination and particle size segregation. This ultimately results in a smaller variance in physical properties in products made in such plants as compared to products from older or dirtier plants.

IV. PROPERTIES AND MICROSTRUCTURE OF HIGH-ALUMINA BRICK

A. Fireclay Brick

Fireclay bricks are classed in standards based on their refractoriness or ability to withstand high temperatures without shrinking and spalling. In North America,

the classes were “low heat duty,” “medium heat duty,” “high heat duty,” and “super duty.” The general composition and typical properties are given in Table 4. One measure of refractoriness is permanent linear change (PLC)—the permanent shrinkage (or expansion) on heating to a specified temperature for a specified time with no load applied. Many people refer to PLC as “reheat expansion” or “reheat shrinkage.”

A typical fireclay refractory brick will exhibit reversible thermal expansion of 3/32" (2.38 mm) per foot (305 mm) of length on heating from room temperature to 2400°F (1315°C). This is equivalent to a thermal expansion coefficient of $6.0\text{exp}(-6)/^{\circ}\text{C}$, i.e., 6.0×10^{-6} mm/mm/°C or $3.35\text{exp}(-6)/^{\circ}\text{F}$, i.e., 3.35×10^{-6} in./in./°F.

Most brick manufacturers recommend an “expansion allowance” (expansion joint allowance) equivalent to 3/32 in. for fireclay brick linings for each foot of lining length (horizontal traverse). This prevents undue loading and damage to the fireclay bricks in the wall due to superimposed stress if the lining is constrained from movement when heated.

Permanent expansion or shrinkage usually affects the hot face region of the refractory (hot side). In linings where movement is expected—as in rotary kilns—consideration must be given to the combined potential for reversible thermal expansion and for permanent expansions or shrinkage.

There is usually not a clear-cut link between composition and properties for fireclay brick products. This is because a multitude of factors determines the “refractoriness” of the clay used in the manufacture of fireclay bricks.

Table 4 Typical Composition and Properties of Fireclay Brick

	Low-duty 1000°C max.	Medium- duty 1200°C max.	High-duty 1400°C max.	Super-duty 1600°C max.
<i>Chemical analysis</i>				
Al ₂ O ₃	25.4	29.3	37.0	41.9
SiO ₂	68.1	62.9	57.8	53.2
Fe ₂ O ₃	1.5	2.3	1.3	1.0
TiO ₂	1.5	2.9	2.3	2.2
Na ₂ O + K ₂ O	1.5	1.5	1.3	1.2
<i>Physical properties</i>				
Bulk density, g/cm ³	2.00	2.10	2.11	2.35
Apparent porosity, %	19.0	20.5	18.0	12.5
Modulus of rupture, MPa	5.2	3.8	9.7	8.5
Crushing strength, MPa	28	32	35	22
PLC, 5 hr. @ 1400°C			-0.2 to +0.2	
PLC, 5 hr. @ 1600°C				0.0 to -1.2
Load test, 172 kPa and 1.5 hr			0.5 to 1.5 @ 1350°C	1.5 to 3.0 @ 1450°C

Like most ceramic products, certain strength properties usually improve as bulk density improves. However, as density improves, spalling resistance may decline. It is best to look for combinations of properties that contribute to success, such as density and PLC together.

The microstructure of a fireclay brick is shown in Figure 3 at very low magnification in reflected light. This brick was fabricated by dry pressing of calcined aggregates and a raw clay blend. Considerable shrinkage of the “matrix” around coarse aggregate particles has created obvious cracks around the aggregate particles.

At higher magnification, the nature of pores in a typical fireclay brick can be seen (Figure 4). The elongated nature of most pores in the calcined aggregate particle is seen along with rounded pores. The continuum of mullite and glass cannot be seen at this magnification. Etching techniques and higher magnification must be used to reveal the mullite crystals.

Fireclay bricks are susceptible to alkali attack, and the usual route for alkali to enter the refractories is through vapor-phase permeation of the refractory brick through the hot face. Two consequences are possible: (1) fluxing of the surface (“glazing”) and (2) formation of new phases resulting in expansion of the refractory.

Glazing of the surface of the refractory and within the refractory immediately behind the hot face is possible given sufficient surface temperature of at least 1125°C and given accumulation of sufficient alkali. The lowest melting liquid phases that form compounds expected when alkali contacts fireclay are given in Table 5. Even lower melting liquids may exist as nonequilibrium or transient phases.

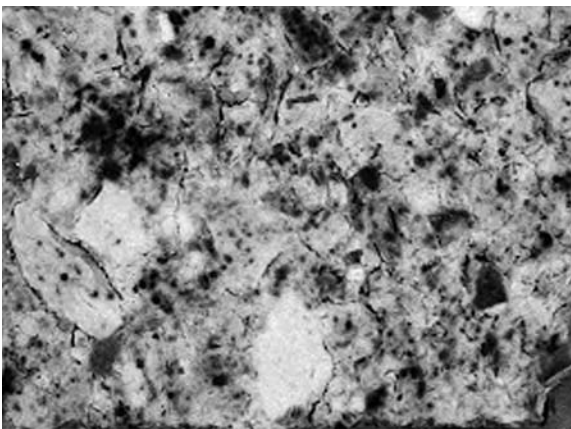


Figure 3 Microstructure of superduty fireclay brick (5×).

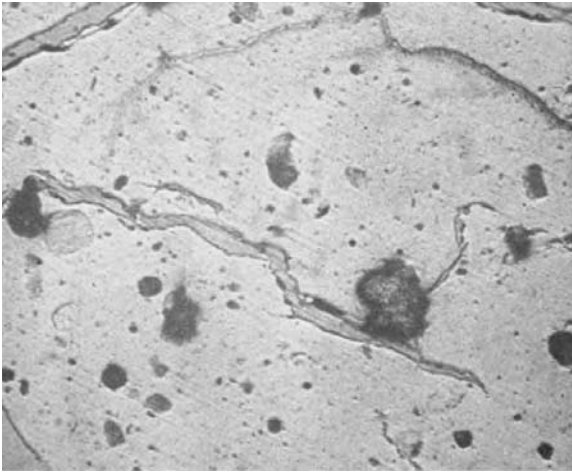


Figure 4 Fireclay brick at high magnification (130 \times).

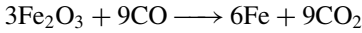
The expansion of fireclay brick is observed in alkali-rich atmospheres and at temperatures at or below where glazing is expected or where there is prolonged alkali exposure with low concentration of alkali in a furnace atmosphere. It is well known that a new phase called kaliophilite ($K_2O \cdot Al_2O_3 \cdot 2SiO_2$) will form in fireclay refractories exposed to potash (K_2O) vapor. This causes a localized volume expansion of about 15% that can result in cracking and “disintegration” within the refractory. Potash vapor is particularly expected in combustion atmospheres where wood is the primary fuel and where glazing of ceramic ware is practiced. Alkali resistance tests can be found in standards for refractories.

Fireclay brick are also subject to carbon monoxide “disintegration” due to their iron oxide content. The mechanism is formation of iron carbide (Fe_3C) when the fireclay brick is exposed to carbon monoxide (CO) gas in the temperature

Table 5 Alkali Phases Formed at the Hot Face of Alumina-Silica Brick Resulting in Localized Melting

Alkali	Phase expected	Melting point of phase ($^{\circ}C$)
Na_2O	Albite $Na_2O \cdot Al_2O_3 \cdot 6SiO_2$	1118
Na_2O	Carnegite $Na_2O \cdot Al_2O_3 \cdot 2SiO_2$	1399
K_2O	Sanidinite $K_2O \cdot Al_2O_3 \cdot 6SiO_2$	1510
K_2O	Leucite $K_2O \cdot Al_2O_3 \cdot 4SiO_2$	1693

range of about 400°–800°C. The formation of iron carbide causes “destruction” of the refractory structure. Carbon monoxide disintegration tests are found in refractory standards. Reactions usually given for this process are



and subsequently



Spalling or thermal shock damage of fireclay refractories has always been a concern of furnace designers and operators. It is not always obvious which brand of fireclay brick will exhibit the best spalling resistance from physical property data alone. Three different brands of fireclay brick are given with their physical properties and spalling loss in laboratory tests in Table 6.

It is apparent from Table 6 that chemical analysis and PLC alone do not correlate with spalling behavior. However, alkali content apparently affects subsidence under load, and it provides improved spalling resistance. This shows that even apparent minor differences in alkali content are important in the performance of fireclay brick. The alkali content of the brick influences the glass content of the brick, and higher glass contents are detrimental to spalling resistance.

Table 6 Spalling Behavior of Three Fireclay Brick Brands

	Conventional	High density	Premium
<i>Chemical analysis</i>			
Al ₂ O ₃	50.8	53.2	52.9
Alkalis	1.5	1.2	1.2
<i>Physical properties</i>			
Bulk density, g/cm ³	2.18	2.34	2.34
PLC, 5 hr. @ 1480°C	0 to -0.6	0 to -1.2	-0.3 to -1
Subsidence under load %, 5 hr. @ 1450°C, 172 kPa	-3 to -5	-1.5 to -3	-1.5 to -2.5
Subsidence under load %, 100 hr. @ 1450°C, 172 kPa	-10 to -14	-6 to -10	-2 to -6
Panel spalling loss %, 1650°C, preheat	3 to 8	2 to 6	0 to 3

B. Semicordierite Brick and Kiln Furniture

Kiln furniture, setter block for kiln cars, and ceramic components are frequently manufactured in a composition close to that of a synthetic mineral named cordierite ($2\text{MgO} \cdot 2\text{Al}_2\text{O}_3 \cdot 5\text{SiO}_2$). Pure cordierite contains 13.7% MgO, and it exhibits a low thermal expansion coefficient of $3\text{exp}(-6)/^\circ\text{C}$. Because of its low thermal expansion coefficient, cordierite materials usually have excellent thermal shock characteristics.

Pure cordierite is an expensive material, and it is known that less pure materials containing some cordierite also exhibit low thermal expansion coefficients. For this reason, “semicordierite” materials are frequently used as kiln furniture and car deck block in ceramic kilns. In some cases, alumina-silica brick compositions are also used for the same product applications. Properties of some products used in kiln furniture/deck block applications are shown in Table 7. The maximum use temperature of these products is typically 1200°C or higher.

Table 7 Composition and Properties of Kiln Furniture/Deck Block Products

	Semicordierite pyrophyllite aggregate (extruded)	Semicordierite pyrophyllite aggregate high fired (extruded)	Semicordierite clay aggregate (pressed)	Semicordierite clay aggregate (pressed)
<i>Chemical analysis</i>				
Al_2O_3	36.2	33.3	32.0	37.7
SiO_2	57.4	61.8	59.1	45.7
Fe_2O_3	1.6	1.3	2.9	1.7
MgO	3.0	2.0	0.9	12.8
<i>Physical properties</i>				
Bulk density, g/cm^3	2.13	2.12	2.13	2.04
Apparent porosity, %	18	20	19	23
Compressive strength, MPa	41.4	20.7	38.5	53.8
Subsidence under load, %, 100 hr., 172 kPa, 1315°C	-2.0	-1.0	NA	NA
Coefficient of thermal expansion	$3.3\text{exp}(-6)/^\circ\text{C}$	$3.1\text{exp}(-6)/^\circ\text{C}$	$5.9\text{exp}(-6)/^\circ\text{C}$	$2.8\text{exp}(-6)/^\circ\text{C}$

NA = not available.

The relationship between MgO content and thermal expansion coefficient is seen in Table 7. At very low MgO content, the thermal expansion coefficient approaches that of fireclay brick or mullite [$\sim 6\exp(-6)/^{\circ}\text{C}$]. The microstructures of typical products of this type are shown in Figures 5 and 6.

The microstructure of the extruded semicordierite material exhibits “slit-shaped” pores as are typical of extruded clay products (Figure 5). It is not obvious from this photomicrograph that the size of the pyrophyllite aggregate particles is large—in some cases approaching 3 to 4 mm. By contrast, the microstructure of the pressed semicordierite material exhibits fireclay aggregate particles surrounded by a matrix of sintered clay with pores that are primarily rounded (Figure 6). Many authorities attribute improved thermal shock resistance to the presence of fine rounded pores. For that reason, it is possible that the pressed product containing $\sim 0.9\%$ MgO (Table 7) might exhibit similar performance with the extruded product containing 3.0% MgO.

A typical contaminant in semicordierite brick is cristobalite formed as “free” silica or as quartz in the raw materials is converted to cristobalite when the refractory is fired to temperatures of at least 1300°C . By reference to an $\text{MgO}-\text{Al}_2\text{O}_3-\text{SiO}_2$ phase equilibrium diagram (not shown), one can see that free cristobalite is an equilibrium phase unless the composition of the product is exactly that of pure cordierite. Excessive cristobalite content can cause “dunting” and reduce the life of kiln furniture/block. Cristobalite can be conveniently determined using X-ray diffraction or thermal analysis techniques.

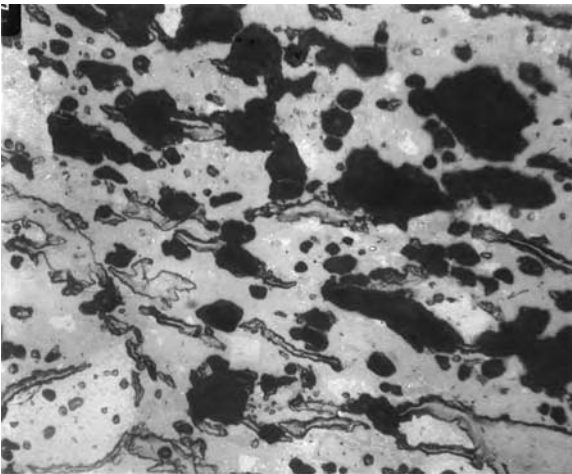


Figure 5 Microstructure of extruded pyrophyllite based semicordierite brick (100 \times).

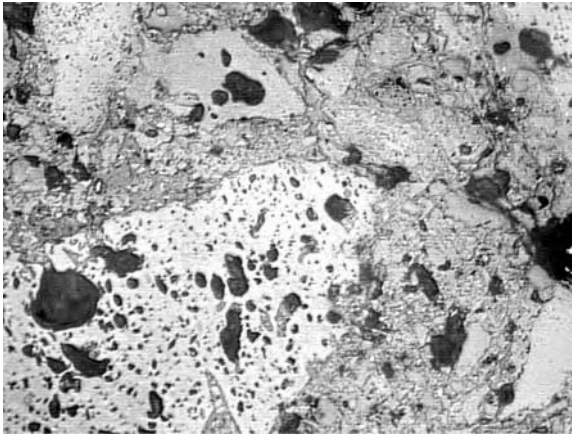


Figure 6 Microstructure of pressed clay-based semicordierite brick (100 \times).

C. Insulating Firebrick

Insulating firebricks (IFB) were developed in the 1930s, and they were the predominant form of insulation until the development of insulating castable and fiber refractories. There are two types of brick: (1) brick based on clay and gypsum using the burnout of sawdust to create high porosity (and thereby provide better insulating value) and (2) brick based on lightweight aggregate and clays. Like all alumina-silica brick, insulating firebricks have a duty rating (service limit). This duty rating is commonly used in the product names—as in K-20 for a 2000°F (1093°C) duty limit. Some data on IFBs are given in Table 8.

It is important to note that the permanent linear change data are based on a 24-hour test exposing the brick to the test temperature. For long-term exposures near the rated service temperature, shrinkage may occur sufficiently to allow joint opening. For this reason, it can be important to use IFBs with a higher duty rating than seems required by the process temperature alone.

Insulating firebricks are susceptible to alkali attack. The products made using gypsum and sawdust burnout material (indicated by high CaO contents) may undergo an expansion reaction in a service environment containing alkali. In some cases, this reaction has been deleterious and reduces service life. By contrast, the IFB made with lightweight aggregate may experience surface glazing in an alkali environment.

Insulating firebricks remain a choice for construction and repair when castable or fiber products may not be preferred. IFBs constitute the working lining of many furnace structures. Construction is usually convenient since most IFBs can be cut with a hacksaw. Caution should be used in selecting IFBs when abrasion resistance or impact resistance is required.

Table 8 Composition and Properties of Selected Insulating Firebrick

Use Limit	K-20 2000°F (1093°C)	K-23 2300°F (1260°C)	K-26 2600°F (1427°C)	JM-30 3000°F (1649°C)
<i>Chemical Analysis</i>				
Al ₂ O ₃	39	39	58	73.4
SiO ₂	44	44	39.1	25.1
Fe ₂ O ₃	0.4	0.4	0.7	0.5
CaO	16	16	0.1	—
Alkalis	0.4	0.4	1.7	0.9
<i>Physical Properties</i>				
Bulk density, g/cm ³	0.48	0.50	0.85	1.01
PLC, %, @ indicated temperature after 24 hr	0 @ 1066°C	0 @ 1232°C	-0.2 @ 1400°C	-0.6 @ 1620°C
Subsidence under load, % @ indicated temperature, 1.5 hr., 69 kPa	0 @ 1066°C	-0.2 @ 1204°C	-0.2 @ 1204°C	-0.1 @ 1204°C
Thermal expansion coefficient/°C	5.4exp(-6)	5.4exp(-6)	NA	NA

D. Fifty Percent and 60% Alumina Class Brick

Refractory bricks in the 50% and 60% Al₂O₃ classes exhibit improved refractoriness over fireclay products. There are two fundamental mineral mixtures used in producing these classes of brick, and the physical properties of the products depend, in part, on which mineral mixture was used in the manufacture.

The most straightforward way to produce brick in this class is to use 50% Al₂O₃ or 60% alumina aggregates (i.e., bauxitic kaolin or andalusite). Another way to produce these classes of products is to use a mixture of bauxite and fireclay. This latter method has been termed the “bauxite dilution” method. In other words, bauxite (at 88% Al₂O₃) is diluted with calcined fireclay and raw clay (at ~40% Al₂O₃) to produce the required alumina content. Properties of these types of refractories are given in Table 9.

It is important to state that refractories containing bauxite or andalusite typically exhibit high reheat expansion while clay bricks do not. In refractories containing andalusite and also containing clay, this tendency for high reheat expansion may not be observed. Thus, there is a fundamental difference in the bricks within the same class with respect to permanent expansion characteristics. In linings requiring the extreme tightness—as in rotary kiln applications—the reheat expansion may be extremely important in good lining life.

Table 9 Composition and Properties of 50% and 60% Al₂O₃ Class Brick

	50% Al ₂ O ₃ clay base	50% Al ₂ O ₃ bauxite base	60% Al ₂ O ₃ clay base	60% Al ₂ O ₃ bauxite base	60% Al ₂ O ₃ andalusite base
<i>Chemical analysis</i>					
Al ₂ O ₃	50.5	49.5	58.1	62.1	58
SiO ₂	44.5	49.5	38.2	32.5	39
Fe ₂ O ₃	1.3	1.3	1.2	1.2	1.5
TiO ₂	2.3	2.5	2.2	2.6	0.2
Alkalis	0.8	0.7	0.1	0.8	≤0.3
<i>Physical properties</i>					
Bulk density, g/cm ³	2.38–2.45	2.37	2.52	2.50–2.59	2.55
Apparent porosity, %	11–16	17.5	14.3	17–20	≤15
Modulus of rupture, Mpa	13.8–20.7	7.6–12.4	18.2	10.3–15.2	
Crushing strength, Mpa	48–69	28–55	58	34.5–62	≥60
PLC, 5 hr. @ 1600°C	+0.5 to +1.5	–1.0 to +1.0	–0.1	+2 to +4	
Panel spalling loss, %, 1650°C, preheat	<5	3–8	<2	3–5	

By contrast, high reheat expansion may be associated with high spalling tendency, i.e., low spalling resistance. In this regard, bricks produced from bauxitic kaolin, i.e., “clay base,” may have superior spalling resistance. This is because of their finer texture, namely smaller average pore size, and due to the absence of permanent expansion reactions on heating.

The TiO₂ content of bricks may indicate the fact that they contain calcined bauxite aggregate (if ≥2.5%). Bauxite can also be recognized on a broken or saw-cut surface as a gray-appearing aggregate to the naked eye.

E. Seventy Percent Alumina Brick

After World War II, 70% Al₂O₃ class refractories became a “workhorse” in industrial furnaces because of their high use or duty ratings and because of their durability in many processes where slag corrosion or other reactions take place. This class of refractories can be produced either from bauxitic clays exhibiting 70% Al₂O₃ or by using appropriate mixtures of bauxite (88% Al₂O₃) and fireclay (~40% Al₂O₃). As in the case of 60% Al₂O₃ brick, the mineral base of the firebrick makes a profound difference in physical properties and thermal response of 70% Al₂O₃ class brick.

The chemical composition and physical properties of the two types of 70% alumina brick are given in Table 10. The brick based on calcined bauxite exhibits much higher reheat expansion (PLC) and higher spalling loss than the brick based on bauxitic clay. On the other hand, the brick based on calcined bauxite may have superior performance where erosion resistance is required.

The microstructures of the two types of 70% Al₂O₃ brick are shown in Figures 7 and 8. In Figure 7, the brick is made from calcined aggregates, which exist, surrounded by a finely textured matrix. The distribution of medium-size particles around coarse aggregates is excellent. This microstructure suggests excellent spalling resistance.

By contrast, the brick made from calcined bauxite has a completely different appearance. The dark bauxite particles predominate the microstructure, but a calcined clay aggregate particle is evident in the lower right of the photomicrograph of Figure 8. A glassy matrix containing mullite surrounds all particles. A comparison of Figures 7 and 8 provides graphic evidence that brick in the same alumina class can have completely different compositions, and the microstructures alone suggest that key reheat (PLC) properties of these brick will be different.

F. Eighty Percent and 85% Alumina Brick

Bricks in the 80% and 85% Al₂O₃ class were originally developed for use in aluminum melting and holding furnaces. It is rare that they find application in

Table 10 Composition and Properties of 70% Al₂O₃ Class Brick

	Bauxitic clay base	Calcined bauxite/clay mix
<i>Chemical analysis</i>		
Al ₂ O ₃	71.8	70.1
SiO ₂	22.9	23.6
Fe ₂ O ₃	2.3	2.0
TiO ₂	0.2	3.0
Alkalis	0.3	0.3
<i>Physical properties</i>		
Bulk density, g/cm ³	2.51	2.60
Apparent porosity, %	21.0	20.0
Modulus of rupture, Mpa	9.3	9.7
Crushing strength, Mpa	57.6	38–65
PLC, 5 hr. @ 1600°C	+0.9	+2–+4
Panel spalling loss, %, 1650°C, preheat	0	≤15

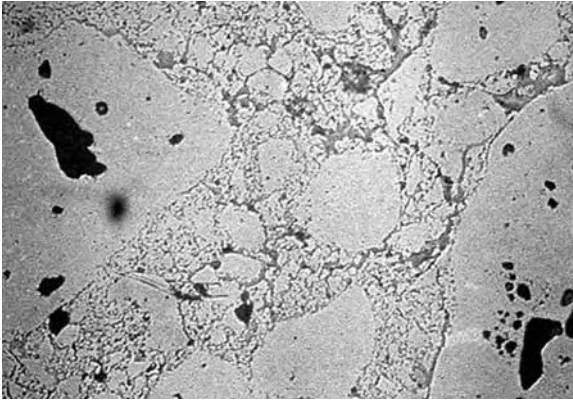


Figure 7 70% Al_2O_3 brick based on bauxitic kaolin.

other types of furnaces. These bricks are based on calcined bauxite, as it is the closest mineral in alumina content to their overall composition.

The properties of 80% and 85% Al_2O_3 brick are given in Table 11. The resistance to aluminum attack is, in part, due to the resistance of the bauxite to solution in molten aluminum and to salt fluxes that may cover the metal bath. Generally speaking, these bricks have not been successful in ferrous foundry or incinerator applications. The reason may be the relatively poor refractoriness of the bond phase (glass and mullite) holding together very refractory calcined bauxite aggregate particles. In an aggressive slagging situation, the bauxite aggregate is eroded out of the brick, and wear rates are usually unacceptably high.

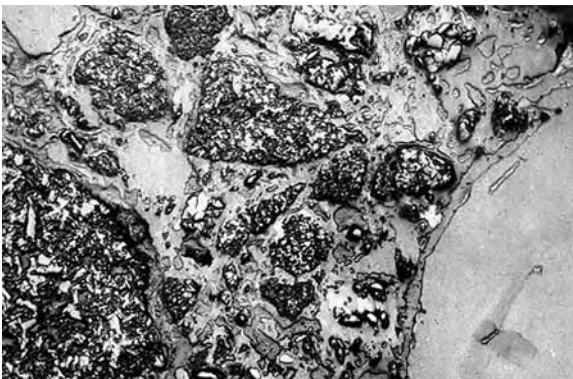


Figure 8 70% Al_2O_3 brick based on calcined bauxite and clay.

Table 11 Composition and Properties of 80% and 85% Al₂O₃ Class Brick

	80% Al ₂ O ₃	85% Al ₂ O ₃
<i>Chemical analysis</i>		
Al ₂ O ₃	79.9	84.1
SiO ₂	13.6	7.3
Fe ₂ O ₃	1.2	1.1
TiO ₂	3.6	2.6
Alkalis	0.6	0.2
<i>Physical properties</i>		
Bulk density, g/cm ³	2.72–2.82	2.82–2.92
Apparent porosity, %	15–18	14–17
Modulus of rupture, MPa	11–17	27
Crushing strength, MPa	48–69	83–110
PLC, 5 hr. @ 1600°C	+0.5 to +1.5	–0.5 to +0.5
Panel spalling loss, %, 1650°C, preheat	0–5	0–5

G. Ninety Percent and 99% Alumina Class Brick

Bricks in the 90% and 99% alumina classes are among the highest strength and erosion resistant of refractory bricks. They are made from synthetic (Bayer process) alumina aggregates, and some types may contain fused alumina for special erosion resistance. It is not surprising that there are several distinct types of brick in the 90% Al₂O₃ class.

The composition and properties of bricks in the 90% Al₂O₃ class are given in Table 12. The type denoted “Fused alumina—mullite matrix” is a product designed in the 1950s for channel induction furnaces for iron foundries. The fused alumina provides very high erosion resistance to flowing molten iron. The microstructure of this type is shown in Figure 9, where fused alumina aggregate particles (white with rounded black pores) are surrounded by a gray matrix containing a lighter mullite phase. Rounded pores are seen in Figure 9 with surface detail created by polishing media on resin impregnant (used for polishing purposes).

The type denoted as “Tabular alumina—corundum matrix” is made from coarse supercalined alumina aggregates and reactive calcined alumina fines to produce a “direct bonded” microstructure where alumina-to-alumina bonding (corundum-to-corundum) predominates. This provides an obvious increase in hot modulus of rupture (Table 12). The microstructure of this type of brick is shown in Figure 10. In the lower field, a tabular alumina aggregate particle resides, and it is connected to the matrix through bonds with smaller corundum crystals.

There is a practical limit on alumina content of about 96% Al₂O₃ (and 3.7% SiO₂) in refractory brick for the highest-temperature applications.

Table 12 Composition and Properties of 90% Al₂O₃ Class Brick

	Fused alumina-mullite matrix	Tabular alumina-corundum matrix	Alumina chrome	Alumina chrome spall resistant
<i>Chemical analysis</i>				
Al ₂ O ₃	91.4	90.1	89.7	83.0
SiO ₂	8.1	9.5	0.5	2.0
Fe ₂ O ₃	0.3	0.1	0.2	0.1
Cr ₂ O ₃	0.0	0.0	9.0	11.2
TiO ₂	Trace	Trace	0.1	Trace
Alkalis	0.2	0.2	0.1	0.2
<i>Physical properties</i>				
Bulk density, g/cm ³	2.72–2.82	2.98	3.17	3.20
Apparent porosity, %	15–18	16	17.8	17.5
Modulus of rupture, MPa	11.7–17.2	16.1	31	11
Modulus of rupture @ 1482°C, MPa	≤5.2	9.1	13	10
Crushing strength, MPa	48.2–68.9	78.2	86	84
PLC %, 5 hr. @ 1705°C	0 to +1.5	–0.2		
PLC %, 5 hr. @ 1816°C			+0.7	–0.1
Panel spalling loss, %, 1650°C, preheat	0–5	0–2	0–2	0

At compositions of higher alumina content, the products cannot be sintered in conventional gas-fired kilns at sufficient temperatures to have good density and PLC (reheat) properties. While 99% Al₂O₃ class bricks exist, they are primarily used for low-temperature applications such as in chemical processes.

In the late 1970s, alumina-chrome bricks were developed. Chromic oxide (Cr₂O₃) functions as a “sintering aid,” allowing for direct bonding to be achieved at gas-fired kiln temperatures without resorting to the use of silica as a sintering aid. The end result is a more refractory product than others in the 90% Al₂O₃ class because the alumina-chrome bricks exhibit only minimal SiO₂ contents. The hot modulus of rupture of these products is extremely high (Table 12). The fired alumina chrome brick are of a “ruby” red color due to the formation of an Al₂O₃–Cr₂O₃ solid solution during firing of the refractory brick.

A “spalling resistant” alumina-chrome product was subsequently developed, and it found immediate application in a number of industrial furnaces including incinerators. While the means of providing additional spalling resistance are proprietary methods, they may include use of second phases like zirconia (ZrO₂) to provide additional fracture toughness.

Mullite Matrix

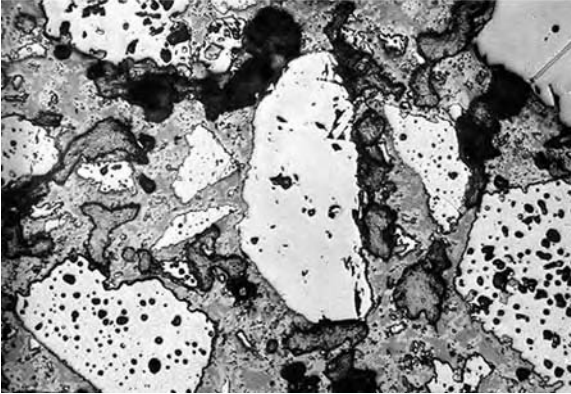


Figure 9 90% Al_2O_3 brick based on fused alumina.

V. SELECTED CASE STUDIES WITH FIRECLAY AND HIGH-ALUMINA BRICK

A. Reaction with Corrosive Materials at Elevated Temperatures

One of the “weaknesses” of alumina-silica brick is their potential for reaction with basic slag or other corrosives to form melted phases or liquid at relatively low temperatures. The reaction potential can be illustrated by considering the

Corundum Matrix

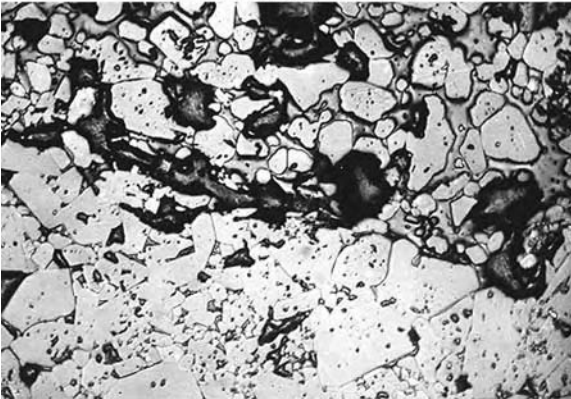


Figure 10 90% Al_2O_3 brick based on tabular alumina.

Table 13 Melting Temperatures for Corrosive Phases with Al_2O_3 - SiO_2 Brick

Corrosive material	Reaction product	Melting point of reaction product, °C
Na_2O	Albite $\text{Na}_2\text{O} \cdot \text{Al}_2\text{O}_3 \cdot 6\text{SiO}_2$	1118
	Carnegite $\text{Na}_2\text{O} \cdot \text{Al}_2\text{O}_3 \cdot 6\text{SiO}_2$	1399
K_2O	Sanidine $\text{K}_2\text{O} \cdot \text{Al}_2\text{O}_3 \cdot 6\text{SiO}_2$	1510
	Leucite $\text{K}_2\text{O} \cdot \text{Al}_2\text{O}_3 \cdot 4\text{SiO}_2$	1693
CaO	Anorthite $\text{CaO} \cdot \text{Al}_2\text{O}_3 \cdot 2\text{SiO}_2$	1553
	Gehlenite $2\text{CaO} \cdot \text{Al}_2\text{O}_3 \cdot \text{SiO}_2$	1593
	Melilite $\text{CaO} \cdot \text{Al}_2\text{O}_3 \cdot 2\text{SiO}_2$ and $2\text{CaO} \cdot \text{Al}_2\text{O}_3 \cdot \text{SiO}_2$	1280
FeO and Fe_2O_3	Iron gehlenite $2\text{CaO} \cdot \text{Fe}_2\text{O}_3 \cdot \text{SiO}_2$	1285
	Iron cordierite $2\text{FeO} \cdot 2\text{Al}_2\text{O}_3 \cdot 5\text{SiO}_2$	1210
	Fayalite $2\text{FeO} \cdot \text{SiO}_2$	1205
	Brownmillerite $4\text{CaO} \cdot \text{Al}_2\text{O}_3 \cdot \text{Fe}_2\text{O}_3$	1410
	Dicalcium ferrite $2\text{CaO} \cdot \text{Fe}_2\text{O}_3$	1449
	Calcium hexaluminate $\text{CaO} \cdot 6\text{Al}_2\text{O}_3$	1850
With Al_2O_3	Hercynite $\text{FeO} \cdot \text{Al}_2\text{O}_3$	1780

reaction products expected for alumina-silica brick in the presence of lime (CaO) (Table 13).

Strictly speaking, the information in Table 13 should be viewed as a “guideline” because actual melting may occur at lower temperatures than indicated by the melting points of the compound. Actual melting occurs on heating at the lowest eutectic point in the system, as revealed on multicomponent phase equilibrium diagrams. More information on how to estimate these initial melting temperatures is given in Chapter 3. Nevertheless, the information indicates that low-temperature melting is expected in the presence of certain corrosive materials.

One example is the situation where a basic slag (containing CaO) is in contact with a fireclay brick. In this situation, one might expect liquid formation near the melting point of anorthite (1553°C) or melilite (1280°C). In fact, melting actually is seen at about 1170°C . This only illustrates that lime (CaO) is a powerful *flux* on fireclay brick. It is true that as the Al_2O_3 content of the brick increases, the relationships with CaO change. For example, lime in contact with a 60% Al_2O_3 brick would be expected to form gehlenite (melts at 1593°C),

but lime-silica mixtures (slags) would still form lower melting liquids even with 60% Al_2O_3 brick.

This limited discussion only points to the well-known fact that basic slags/minerals react with neutral to slightly acidic Al_2O_3 - SiO_2 brick, resulting in corrosive wear of the refractory. The rate of the reaction differs among classes of brick, with the higher Al_2O_3 brick usually exhibiting the slowest corrosion rates at elevated temperatures.

It is interesting that alumina-silica bricks are attacked by acids in chemical applications at room temperature. For example, 70% Al_2O_3 bricks have been known to exhibit service of only several weeks in hot hydrochloric and sulfuric acids. "Acid-proof" bricks are commonly used in chemical service, and these bricks last longest if they exhibit extremely low apparent porosities and if their composition exhibits extremely low alkalis. Alkali phases form glasses in manufacturing that are more readily soluble in acid media, so the bond phase in acid-proof brick must contain higher alumina content and lower alkali content.

B. Sawdust-Fired Ceramic Kiln (with Alkali Attack)

A significant number of ceramic kilns producing clay-facing brick are fired with sawdust fuel in North America. It has been long recognized that wood-fired boilers experience potassium attack on refractories as K_2O vapors are present in the combustion atmosphere. These vapors penetrate the refractory, providing for two types of deleterious wear processes. These are (1) glazing of the brick and deposition of slag on the surface of the brick near the "burners" and (2) expansion of the brick over a long period.

In tunnel kilns of length 50–100 meters, expansion progressed over a period to the point that the interior walls made of fireclay brick typically buckle inward. In about seven years of service, the brick must be replaced to continue operation.

In the same kilns, crown (roof) brick (insulating firebrick) in flat, suspended construction exhibited "sheet" spalling in seven years of service. Sheet spalling is loss of refractory thickness of about 25 mm (1 in.) over a large area (many bricks). The sheet spalling was apparently a result of expansion reactions between the IFB and the alkali in the kiln atmosphere.

C. Rotary Kiln Application of 70% Al_2O_3 Brick and Andalusite Brick

Rotary kilns have been lined with 70% Al_2O_3 brick for many years, and a typical choice has been calcined bauxite/clay base types. These bricks provide sufficient permanent expansion to keep the lining tight against the shell of the rotary kiln. This, in turn, prevents movement of brick as the kiln rotates.

The 70% Al_2O_3 class bricks typically develop a “cobblestone street” appearance in service. This appearance is not necessarily an indication of an impending failure of the lining. In one instance, an inexperienced operator decided to replace the 70% Al_2O_3 bricks with andalusite/clay bricks that had “superior” spalling resistance in laboratory tests. The result was an unusually premature failure of the new lining. Because the andalusite/clay bricks had only a small permanent expansion, the bricks became loose during kiln rotation, resulting in progressive loss of the lining by bricks “falling out” of the lining. While the replacement of the old 70% Al_2O_3 lining was done for a few good reasons, the person making the decision did not consider all the criteria that contributed to many years of success with the 70% Al_2O_3 lining practice.

D. Incinerator Application of 70% Al_2O_3 and Alumina-Chrome Brick

Incinerator designers have used 70% Al_2O_3 brick for years in the primary and secondary combustion chambers of the kilns. For a long time, the 70% Al_2O_3 bricks would experience rapid wear in the fireball regions of the secondary combustion chamber where conditions reach in excess of 1750°C. This is also an area where corrosive lime-alumina-iron oxide-silica slags coat the refractory walls.

The 70% Al_2O_3 bricks were replaced with alumina-chrome bricks (Table 11), and service was extended. The alumina-chrome bricks initially exhibited excessive spalling loss, resulting in the development of the “spall-resistant” alumina-chrome bricks. These latter bricks have been a resounding success in incinerator service.

VI. HEALTH AND SAFETY CONSIDERATIONS WITH ALUMINA-SILICA BRICK

Alumina-silica brick of 60% Al_2O_3 class or lower (including fireclay) can contain a small amount of “free” or uncombined crystalline silica. Not all refractory bricks contain free silica, as its presence complicates manufacture of the brick, and certain silica phases—like cristobalite—contribute to accelerated wear.

It is well known that free silica, as quartz or cristobalite, is a respiratory hazard. Since cristobalite is the expected phase in fired alumina-silica brick, it is of the most potential concern. It is inexpensive to determine if a brick contains quartz or cristobalite. The issue is sawing of the brick during masonry construction. Wet sawing eliminates dust exposure, and it should be used if there are concerns about silica exposure.

Alumina-chrome bricks can form traces of hexavalent chromium (Cr^{+6}) if the bricks are used above 1250°C and are in contact with lime-rich phases.

Used refractories might be checked for hexavalent chromium to ensure that any required disposal regulations are met.

REFERENCES

1. Nishikawa A. *Technology of Monolithic Refractories*. Plibrico Japan Company Limited, 1984.
2. Aramaki S, Roy R. "Revised Phase Diagram for the System $\text{Al}_2\text{O}_3\text{-SiO}_2$ ". *J Am Ceram Soc* 1962; 45(5):229–242.
3. Grimshaw RW. *The Chemistry and Physics of Clays*. Techbooks 1971.

FURTHER READING

For general information on refractories: Kirk-Othmer. "Refractories". *Encyclopedia of Chemical Technology* 20:1–37 (1982, or most recent edition).

Refractories Manual. The American Foundrymen's Society, 1989.

For technical information on clay, alumina, and mullite: "Structural Oxides I: Al_2O_3 and Mullite". In: Lee WF, Rainforth WM, eds. *Ceramic Microstructures*. Chapman and Hall, 1994.

Alumina as a Ceramic Material, Special publication No. 4, The American Ceramic Society, 1970.

"Microstructure of Complex Ceramics". In: Fulrath R, Pask J, eds. *Ceramic Microstructures*. Krieger Publishing Company, 1976.

For historical information: *Refractories: The Hidden Industry*. The American Ceramic Society, 1987.

5

Magnesia Refractories

Richard A. Landy

Landy & Associates, State College, Pennsylvania, U.S.A.

I. INTRODUCTION

A. Definitions

A magnesia refractory is defined by the American Society for Testing and Materials (ASTM) as “a dead-burned refractory material consisting predominantly of crystalline magnesium oxide” (1). Furthermore, ASTM defines “dead-burned” as “the state of a basic refractory material resulting from a heat treatment that yields a product resistant to atmospheric hydration or recombination with carbon dioxide” (2). The chemical formula for magnesium oxide is MgO. However, no dead-burned magnesium oxide contains 100 wt. % MgO. Chemical assays of any such refractory raw material show some level (generally less than 30 wt. % total) of silica, lime, iron oxide, alumina, and boron oxide, that, mineralogically, occur (1) in triple-point pockets and films between the MgO crystallites in the dead-burned magnesium oxide material as, for example, various calcium silicates, calcium magnesium silicates, calcium boron silicates, and calcium aluminates; (2) as lime and iron oxide solid-solutions in the magnesia crystallites; and (3) sometimes, as magnesioferrite exsolution intergrowths, within the magnesium oxide crystallites themselves.

Also, ASTM defines basic refractories as “refractories whose major constituent is lime, magnesia, or both, and which may react chemically with acid refractories, acid slags, or acidic fluxes at high temperatures” (3). (In a postscript, the definition mentions that “commercial use of this term [basic refractories] also includes refractories made of chrome ore or combinations of chrome ore and dead-burned magnesite.”) Conversely, basic refractories exhibit excellent chemical resistance to other basic refractories, basic slags, or basic fluxes at high temperatures. Lime and magnesia also hydrolyze in water to form hydroxides, so the

designation of these so-called basic refractories is truly meant to characterize their chemical behavior.

B. Terminology

Magnesium oxide raw materials and products can be referred to interchangeably as one of four names or terms (4) and, thereby, lead to some confusion for people unfamiliar with commercial industry vernacular: (1) MgO; (2) magnesia; (3) periclase; and (4) magnesite. Technically, (1) MgO is the chemical formula for pure magnesium oxide; (2) magnesia is the chemical name applied to the oxide of magnesium; (3) periclase is the mineral name for magnesium oxide (this mineral is rarely found in nature, but is presently applied to high-grade [generally, less than 10 wt. % impurities], dead-burned magnesium oxide products produced synthetically from, for example, seawater or underground brines); and (4) magnesite is the mineral name for magnesium carbonate, MgCO_3 , and was one of the original sources for magnesium oxide used in refractory products (magnesite has to be dead-burned to remove the carbon dioxide, but the name has carried over to the dead-burned product of the magnesium carbonate—current U.S. terminology is to use magnesite for dead-burned magnesium oxide produced from naturally occurring magnesite, especially those raw materials with impurities greater than 5 wt. %, but its use secularly is not so differentiated).

II. MAGNESIA REFRACTORY RAW MATERIALS

A. General Concepts and Terminology

Generally, every refractory is composed of four major structural elements that are depicted in Figure 1 (5):

1. The primary building blocks of refractory bodies are given the name **grains** or **aggregates**; these components comprise raw materials larger than about 200 μm and constitute, by weight, about 70% of a refractory product. Several carefully graded sizes of aggregates are used to construct a close-packed product texture.
2. **Matrix** or **filler** materials smaller than 150 μm are then used to pack the spaces among the gapped aggregates.
3. The terms **binder**, **bond**, or **cement** are used to describe the structural unit that eventually adheres the aggregates and/or matrix ingredients together to form the refractory product's strength.
4. There is always unfilled space remaining in the refractory body, and these open volumes are called **pores**.

Some raw materials of refractory products can be used directly, can be partially altered from naturally occurring mineral deposits, or are produced

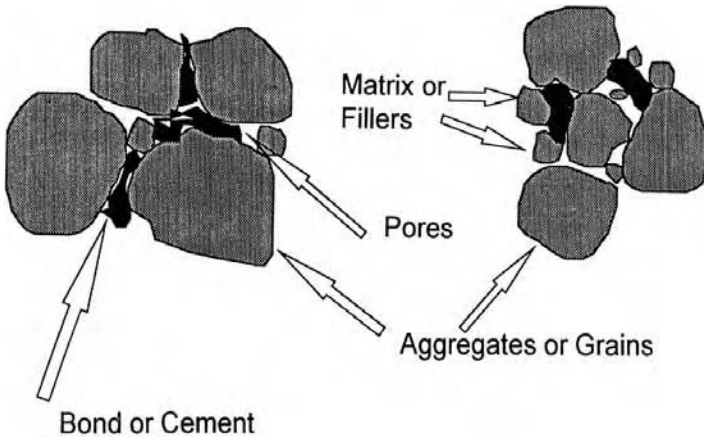


Figure 1 Schema of the four textural elements of a refractory and their respective relationships. [From Ref. 5. Reprinted with permission of the Canadian Ceramics Society (M. Rigaud).]

synthetically by various combinations of chemical processing and heat treatment. If the heat treatment is mild ($\sim 900\text{--}1300^\circ\text{C}$), the raw material is described as being **calcined**; if the heat treatment is more robust ($\sim 1500\text{--}2200^\circ\text{C}$), the raw material is then described as being **sintered** (dead-burned materials are in this group); and if the heat treatment proceeds to a molten state (e.g., for MgO, in excess of 2800°C), then the raw material is said to be **fused**.

B. Dead-Burned Magnesium Oxide (6, 7)

1. Sources of Magnesium Oxide

The principal magnesia refractory raw material is obviously magnesium oxide. Magnesium oxide has a very high melting point of about 2800°C . This characteristic, together with its resistance to basic slags, ubiquitousness, and moderate cost, makes magnesium oxide products the choice for heat-intensive, metallurgical processes such as for the production of metals, cements, and glasses.

Since magnesium oxide does not occur extensively in nature, this material has to be obtained from other sources that are available in commercial quantities. The first source is from sintering naturally occurring magnesite, a mineral whose world reserves exceed 10^{10} mt; the theoretical wt. % of MgO is 47.6, so about half the weight of magnesite is lost due to CO_2 evolution during sintering or dead-burning.

Magnesite occurs in nature in two distinct textures: macrocrystalline and cryptocrystalline. When high-purity, macrocrystalline magnesite, as found in

China, North Korea, and Russia, is simply subjected to heat treatment, a low-density, sintered product is produced and is not favorable for premium-quality refractory usage; the use of additional, more costly processes, such as fine grinding, briquetting, and modern shaft kilns for sintering, is required to produce a product suitable for the refractories industry. However, macrocrystalline magnesite deposits occurring with minor levels of iron oxide (this magnesite variety is called breunnerite) exist in Austria and Slovakia, do sinter to high density, and are quite suitable for certain refractory applications.

On the other hand, the high reactivity of high-purity, fine-grained ($\sim 1 \mu\text{m}$), cryptocrystalline magnesite leads to this type of magnesite rather easily sintering to a high-density grain that is necessary for producing various refractory products. Greece and Turkey were major sources for high-performance, refractory-grade, dead-burned magnesia in the 1960s and 1970s; in the late 1980s, a cryptocrystalline source, claimed to be the largest single deposit of this type in the world, was found in Australia.

The other very large, almost limitless, commercial source of high-purity magnesium oxide is obtained by processing seawater, inland brines, or salt deposits, all containing the soluble compound magnesium chloride (MgCl_2); these final products are referred to as "synthetic magnesia." The introduction of new processing technologies (increasing the CaO/SiO_2 wt. ratio, reducing the boron content, using high-vacuum techniques in dewatering the filter cake, and using higher-pressure briquetting) in the mid-1970s resulted in magnesium oxide qualities that exceeded previously available commercial, synthetic grains and led the refractories producers to employ these newer grades, and the naturally occurring and standard-quality, synthetic, magnesium oxide products largely fell out of favor. The largest seawater facilities of this type are found in Japan, while other important plants are located in Great Britain, the United States, and Ireland. Inland brine operations are found in the United States, Mexico, and Israel, while underground magnesium chloride salt deposits over 1000 m below ground level are recovered in The Netherlands.

Finally, a secondary source of magnesium oxide is from the mining and sintering of brucite deposits; this mineral is composed of magnesium hydroxide, $\text{Mg}(\text{OH})_2$, and has a theoretical MgO of about 70 wt. %. A major source of brucite was located in Nevada.

2. Production of Dead-Burned Magnesia

This section only outlines the generalities of the manufacturing processes since there are quite diverse procedures employed for each of the manifold occurrences described in the previous section.

Exploration, drilling, assaying, and selective mining, either open-pit or underground, are the first four important steps for naturally occurring magnesite

or brucite deposits. To produce high-grade grains, moderate grinding followed by beneficiation techniques using froth flotation or heavy media is then required to remove gangue minerals before dead-burning in either rotary or shaft kilns. If the gangue minerals can't be removed sufficiently to produce high-grade magnesia, then fine grinding must be performed before beneficiation; consequently, high-pressure briquetting is required for this fine-grained output in order to form a suitable pellet for dead-burning. Low-grade products can be manufactured by just coarse crushing the mined ore followed by dead-burning in crude shaft or rotary kilns. Products briquetted prior to dead-burning are delivered to major refractory manufacturers as peach-pit-sized raw materials; materials that are just dead-burned are generally less than 35 mm in size after firing.

When seawater is used as the source, the water is initially pretreated to remove the carbonic acid; inland brines don't require this step (M. Wajer, personal communication, 2002). Then, these waters are mixed with calcined limestone or calcined dolomite in large reaction tanks; the use of calcined dolomite almost doubles the overall percentage of magnesium recovered per unit of processed water. Magnesium hydroxide precipitates out, and the resultant slurry is washed, thickened, and dewatered using very high-vacuum drum filters. The resulting filter cake can be fed directly to a rotary kiln and dead-burned to produce a standard-quality, dead-burned magnesia, but, more likely, the filter cake is calcined in multiple-hearth furnaces to produce a highly active magnesia. Following high-pressure briquetting, the pellets are dead-burned in rotary or shaft kilns, with the latter used for the premium magnesia products.

In The Netherlands, solution mining of underground magnesium salt deposits produces magnesium chloride brine that then goes through the process just described to produce dead-burned magnesia (8). In Israel, Dead Sea water, after solar evaporation in shallow ponds to increase the brine concentration, is initially processed through a special ion exchanger to remove boron, and then the brine is thermally decomposed in the Aman spray roaster to MgO and hydrochloric acid, the latter a byproduct recovered for fertilizer. The MgO is then hydrated to magnesium hydroxide, washed, vacuum drum-filtered, calcined in a multihearth furnace, and dead-burned in a shaft kiln (Dead Sea Periclase web site, 2002).

Synthetic dead-burned magnesias will always be briquetted and thus available to the refractory industry as peach-pit-sized particles or portions thereof.

The ultimate refractory-grade magnesia is manufactured by electromelting previously produced refractory grades of magnesia, calcined magnesia, or even raw, naturally occurring magnesite. The resulting furnace charge or ingot is allowed to cool and crystallize slowly, resulting in the large periclase crystal sizes that are highly sought after for maximum slag resistance. The inner core produces the best product, while the crust is usually recycled due to its small crystallite size. The well-crystallized material is then crushed and sized into a variety of fractions for subsequent refractory-grade use.

3. Key Dead-Burned Magnesium Oxide Characteristics

MgO Content. The MgO content of dead-burned magnesium oxide is generally included in the grade and/or brand of the particular commercial product. Obviously, its overall purity plays an important role in determining what MgO content is suitable for a particular end use. The MgO content of an aggregate is, by and large, but not entirely, directly proportional to its slag resistance. Many impurities, as mentioned previously, are located in triple-point and thin-film accessory mineral deposits between MgO crystallites composing the aggregates or grains; these accessory minerals have lower melting temperatures than MgO. Therefore, the amount of impurities plays a major role in keeping the MgO crystallites apart in the aggregate and not available for high-strength, crystallite-to-crystallite direct bonding during the production sintering process. In metallurgical applications at high temperatures, grain-boundary softening leads to loss of MgO aggregate strength and affords critical pathways for slag attack, whereby corrosive agents breach around the excellent resistance of the MgO crystallites; as a consequence, the rationale for using an MgO refractory body may become meaningless when moderate to large quantities of such impurity phases are present.

Since the mid-1980s, the trend has been to obtain the highest MgO content possible in commercially produced MgO grains.

MgO Impurities. As mentioned in the introduction, a chemical analysis of a sample of commercial MgO aggregate will yield the following principal impurities: SiO₂ (silica); CaO (lime); Al₂O₃ (alumina); Fe₂O₃ (iron oxide); and B₂O₃ (boric oxide). These impurities do not exist in the MgO aggregates as independent oxides per se. Rather, they combine together and/or with MgO from the MgO crystallites to form minerals that, under equilibrium conditions, can be predicted from phase equilibrium relationships in the MgO–CaO–SiO₂–Al₂O₃–FeO–Fe₂O₃ system and generally confirmed by X-ray diffraction analyses. These minerals can be distributed in one or more of the following locations: (1) in triple points or as films along crystallite boundaries in the MgO aggregates; (2) as solid solutions in the magnesia crystallites; and (3) as spinellitic exsolutions in the magnesia crystallites.

However, complicating these general points are the phenomena of the solid solutions or solubilities of CaO and/or iron oxide, respectively, in the MgO crystallites themselves. Although the lime solubility in the MgO phase is relatively small, the effect is particularly important in very high MgO-content materials (9–12). This fact is due to the impact that lime solubility has on altering the CaO/SiO₂ wt. ratio determined by chemical assay and subsequent phase equilibrium assumptions; this ratio, in turn, controls the nature of the calcium silicate minerals that occur in the grains.

The importance of the CaO/SiO₂ wt. ratio can be appreciated from studying the MgO–CaO–SiO₂ phase diagram; its representation is seen in Figure 2

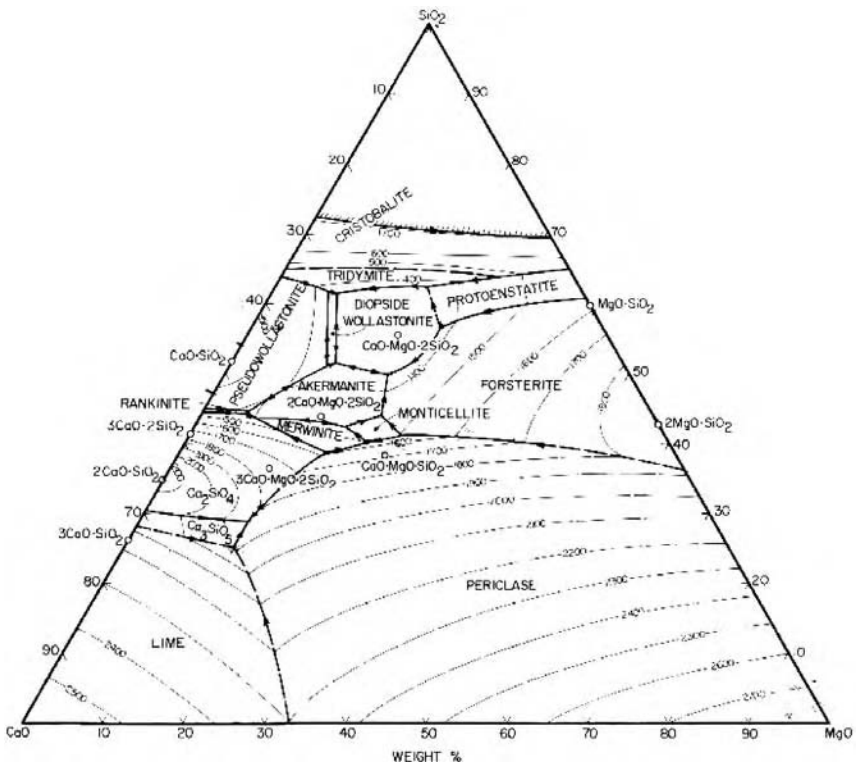


Figure 2 MgO–CaO–SiO₂ phase diagram. (From Ref. 13.)

(13). As mentioned earlier, the CaO/SiO₂ wt. ratio controls which minerals exist in the MgO aggregates. If the wt. ratio of CaO/SiO₂ is greater than 2.8, tricalcium silicate, Ca₃SiO₅, and free CaO can exist as the impurity or accessory phases with initial liquid formation in the MgO aggregate occurring at ~1850°C. An exact 2.8 ratio can yield only tricalcium silicate. If the wt. ratio of CaO/SiO₂ is between 2.8 and 1.87, tricalcium silicate and dicalcium silicate, Ca₂SiO₄, can be present, while the temperature of initial liquid formation is ~1790°C; at just 1.87, only dicalcium silicate can exist. From 1.87 to 1.4 wt. ratio of CaO/SiO₂, dicalcium silicate and merwinite, Ca₃MgSi₂O₈, can be represented and an initial liquid can appear in the magnesia aggregate at 1575°C. At just 1.4 CaO/SiO₂ wt. ratio, only merwinite can be present. A CaO/SiO₂ wt. ratio of 1.4 to 0.93 can produce a combination of merwinite and monticellite, CaMgSiO₄; with this accessory-phase mineral assemblage with MgO, liquid can begin to be generated if the temperature reaches ~1490°C. Only monticellite is present at 0.93. Finally, a CaO/SiO₂ wt. ratio of less than 0.93 can yield the

accessory-phase minerals monticellite and forsterite (Mg_2SiO_4), and a temperature of $\sim 1500^\circ\text{C}$ can begin to initiate melting in the MgO grain.

Liquid formation usually signals initial signs of destruction and, consequently, deterioration of the refractoriness of the MgO grains, so, as discussed in the previous paragraph, the value of the CaO/SiO_2 wt. ratio plays a significant role in this feature. Obviously, the amount of available lime is a critical factor. Since lime can be dissolved in solid solution in the MgO crystallites, this circumstance complicates the overall phase assemblage; moreover, the amount of lime in solid solution in the MgO crystallites, in the presence of silicates, increases with the increasing lime content of the silicate; i.e., as the CaO/SiO_2 wt. ratio increases from 1.4 to over 3, the CaO in solid solution in MgO increases from 0.2 wt. % CaO to ~ 2 wt. % CaO. So, the solid solution of CaO in MgO causes the CaO/SiO_2 wt. ratio in the calcium silicates in the interstices of the MgO grains to decrease, and the refractoriness of the MgO aggregates is reduced. In addition, as the overall silica content decreases, this effect increases the impact on the CaO/SiO_2 wt. ratio, so lime solubility in MgO can cause a very significant lowering of the CaO/SiO_2 wt. ratio and, in very pure MgO aggregates, a dramatic lowering of the temperature of initial melting; this lowering is much greater than anticipated if the lime solubility in MgO is ignored.

Iron oxide is also capable of dissolving in solid solution in the MgO crystallites; its phase equilibrium relationship depends on the oxygen partial pressure of the system, but formation of magnesiowustite, $(\text{Mg},\text{Fe})\text{O}$, and magnesioferrite, $(\text{Mg},\text{Fe})\text{Fe}_2\text{O}_4$, solid solutions commonly occur in MgO crystallites even with low levels of iron oxide being present. At higher iron oxide levels and with the CaO/SiO_2 wt. ratio less than ~ 2 , the iron spinel reacts with the calcium-magnesium silicate accessory phases to further contribute to the amount of liquid that can be formed at a particular temperature. Under these conditions, alumina also reacts with MgO to form spinel, which then also adds to the liquid formation. Even when the CaO/SiO_2 wt. ratio is greater than 2, these impurities cause a loss of refractoriness of the MgO grains; lime reacts with alumina and/or iron oxide to form calcium aluminates, calcium ferrites, or calcium-iron aluminates (14). For these reasons, these impurities need to be kept low.

One further point about the need to keep the iron oxide content of MgO grains low. In the presence of carbon in magnesia-carbon refractories, iron oxide reacts with carbon; therefore, this carbon oxidation-iron oxide reduction reaction contributes to the loss of carbon from the refractory, an undesirable effect that is explored in a later section.

Boric oxide is also a very undesirable impurity. Researchers in the 1960s and 1970s found that one of the major reasons for the excellent hot strength of dead-burned Grecian magnesite, which had such a dramatic effect on the increased life of pitch-impregnated, burned MgO brick manufactured from this material and used in the impact pads of basic oxygen furnaces in the

mid-1960s and early 1970s, was its inherent low boron content (less than 0.005 wt. % as B_2O_3). Subsequently, control of the boron content of synthetic magnesia aggregate to less than 0.02 wt % as B_2O_3 (ideally, less than 0.01 wt. %) was critical to producing a high CaO/SiO₂ product that could produce a burned MgO brick with hot properties similar to brick made with dead-burned Grecian magnesite. Subsequent research found that, apparently, boron combines with other impurities, such as CaO, to form very low temperatures of liquid formation, and the liquid formed possesses a very low wetting angle with MgO, resulting in a very thin, interstitial film around most of the MgO crystallites in commercial MgO grains, which prevents direct-bonded, MgO crystallite-to-MgO crystallite microstructure. There is, however, one aspect where the boron-compound film around the magnesia crystallites comes in handy: Magnesia's hydration resistance increases with the presence of that boron-compound film around the magnesia crystallites, so, where moisture may be present in an application, like electric arc furnace subhearth and furnace or ladle safety linings, bricks composed with these particular raw materials fit a special need.

Quality magnesia-carbon brick for basic oxygen furnaces or steel ladles should have their MgO grain impurities less than 2.5 wt. %, with the highest-quality grain containing preferably less than 1 wt. % impurities. The CaO/SiO₂ wt. ratio should be in excess of 2.5, preferably greater than 3. Overall, the SiO₂, Al₂O₃, and Fe₂O₃ should be as low as possible, 0.1 to 0.2 wt. % at the most. B₂O₃ must be below 0.02 wt. %, with less than 0.01 wt. % preferable. Suitable MgO aggregates for manufacturing conventional, forsterite-containing, direct-bonded, magnesia-chrome brick have different properties; CaO/SiO₂ wt. ratio should be about 1, with CaO and SiO₂ each around 0.8 wt. % or less. Al₂O₃ and Fe₂O₃ may be 0.1 wt. % each. B₂O₃ may be up to about 0.15 wt. %. Other applications require different MgO specifications; for example, the standard MgO ramming mix for electric arc furnace hearths is based on using dead-burned, high-iron breunnerite (Austrian or Slovakian origin).

MgO Crystallite Size. Since chemical reactions, such as in refractory corrosion, are a function of available surface area, one would have to assume that the MgO crystallite size is important. Indeed, research plus results from refractory service over the last 15 years corroborate this characteristic. Prior average crystallite size of dead-burned magnesium oxide ranged from 25 to 100 μm; current synthetic, dead-burned magnesium oxide products are available with crystallites ranging from 100–200 μm. Moreover, when the best corrosion resistance is needed, the industry trend is to use refractories containing at least some fused MgO whose crystallite size can be measured in the several mm range and individual MgO grains can be composed of fragments of single MgO crystals.

Bulk Density of MgO Grains. The true specific gravity of periclase is 3.58. Therefore, the closer the bulk density of a sample of a MgO aggregate is

to that value, the lower its total porosity (open and closed pores). In refractory technology, generally, the densest body offers the best resistance to corrosion by slags and is the strongest to resist abrasion. Desired commercial MgO grains for products destined for basic oxygen furnaces and steel ladles should have bulk densities greater than 3400 kg/m^3 , while those for magnesia-chrome bricks should be greater than 3300 kg/m^3 .

Thermal Expansion of MgO. The coefficient of thermal expansion of an essentially pure MgO refractory is very high; for example, at 1425°C , the linear expansion of a fused MgO or isostatically pressed and fired MgO of 99 wt. % minimum purity with a minimum bulk density of 3180 kg/m^3 is about 2%. Of course, incorporating other refractory raw materials with magnesia in a refractory body will alter this value. Care is required in using these materials to account for this property in an engineering sense.

4. Chemical and Physical Properties of Dead-Burned Magnesias

Dead-burned magnesias can be used as aggregates as well as matrices for refractory products. Table 1 (15) shows the brand name, country of origin, chemical composition, and bulk density for a number of selected commercial dead-burned magnesias from naturally occurring sources, while Table 2 (16) exhibits the same information for several selected dead-burned synthetic and fused magnesias.

C. Chrome Ore

1. General

Chrome ore has been a widely used refractory raw material for many years; in particular, the steel industry greatly expanded its use in the late 1950s after

Table 1 Typical Properties of Several Selected Magnesia Sinters

Brand	Country	MgO (wt. %)	CaO (wt. %)	SiO ₂ (wt. %)	Fe ₂ O ₃ (wt. %)	Al ₂ O ₃ (wt. %)	B ₂ O ₃ (wt. %)	Bulk density (kgm ⁻³)
Kumas 96A	Turkey	96.5	2.2	1.0	0.2	0.02	<0.01	3400
Magnesitas M30	Brazil	96.5	1.0	0.95	0.7	0.1	<0.01	3350
QM9090	China	92.5	1.3	3.5	1.0	1.5	<0.01	3250
Radex S.L.	Austria	90.0	3.0	1.0	5.0	1.0	<0.01	3350
Jelsava S	Slovakia	88.0	2.7	0.9	7.5	0.5	<0.01	3250
QMAG 1	Australia	96.5	2.0	0.5	0.1	0.15	<0.01	3400

Source: Ref. 15. (Copyright 1994, with permission from Elsevier Science.)

Table 2 Typical Properties of Several Selected Synthetic Magnesia Sinters (S) and Fused Magnesia Grains (F)

Brand	Country	MgO (wt. %)	CaO (wt. %)	SiO ₂ (wt. %)	Fe ₂ O ₃ (wt. %)	Al ₂ O ₃ (wt. %)	B ₂ O ₃ (wt. %)	Bulk density (kgm ⁻³)
Premier LC (S)	Ireland	97.4	1.9	0.2	0.15	0.109	0.04	3440
DSP (S)	Israel	99.4	0.5	0.05	0.04	0.03	0.005	3430
UBE 99HD (S)	Japan	99.03	0.68	0.15	0.06	0.07	0.01	3430
Penoles 99 ADS (S)	Mexico	98.8	0.8	0.15	0.50	0.15	0.005	3410
Nedmag 99 (S)	The Netherlands	98.5	0.65	0.2	0.40	0.15	0.02	3440
Martin Marietta 98 (S)	United States	97.5	2.2	0.7	0.20	0.02	0.02	3400
Tateho KMA (F)	Japan	98.5	0.5	0.2	0.20	0.1	0.005	3500
Liaoning (F)	China	98.0	1.0	1.0	0.60	0.5	0.001	3450

Source: Ref. 16. (Copyright 1994, with permission from Elsevier Science.)

laboratory and post-mortem studies revealed that bricks with “direct bonding” between the chrome ore and magnesia aggregates, in which the two grains are joined predominantly by a solid-state diffusion mechanism, produced a brick that outperformed earlier magnesia-chrome brick in open-hearth furnace roofs. Since then, direct-bonded magnesia-chrome bricks have enjoyed good success in steel ladles, cement kilns, and copper converters.

Chrome ores have good resistance to slag attack; this raw material has been considered to be chemically neutral (17). In combination with magnesia, the magnesia-chrome products have excellent refractoriness and spalling resistance. However, under fluctuating temperature and oxygen partial pressure or both, the chromite grains expand or grow continuously, eventually causing the chrome-containing products to become more porous and distort the furnace steel superstructures. Also, chrome ore may have poor resistance to iron oxide attack, and, in the presence of calcium-containing furnace burdens, soluble, hexavalent chromium compounds are formed, leading to an environmentally unfriendly product re disposal problems due to its potentially carcinogenic characteristics.

“Chrome ore” and “chromite” are terms used synonymously in the refractory industry; three grades of chrome ore are sold for industrial usage: metallurgical, refractory, and chemical. Only the refractory grade is discussed here.

2. Sources and Production of Chrome Ore

Refractory-grade chrome-ore deposits are found in a number of areas throughout the world, but the major mines are located in the Transvaal in South Africa and in the

Zambales mountain range on Luzon Island, Philippines. Lesser deposits are found in the Mediterranean regions, specifically Turkey and Albania, and in Russia.

In South Africa's Transvaal's province is the famous geologic formation, the vast Bushveld igneous complex, a norite lopolith (saucer shape) in which stratiform layering is very well developed; differentiation of a basic magma has produced dipping beds of different compositions including several thin chromite-containing strata composed of well-developed chromite crystals ranging from several mm and finer (18–20). Hundreds of million tons of chromite ore are in reserve. Two chromite seams (1- to 1.5-m thick) are currently of economic interest at a large number of locales throughout the region. Both seams are physically and chemically consistent and are underground-mined. The chrome-ore seams are drilled, assayed, and blasted and then transported to mine shafts. Once above ground, the run-of-mine ore is crushed and screened to various size fractions; some ore may be fine-ground. The +10-mm size fraction is beneficiated by means of a dense, heavy-media process, while silica is removed from finer-size fractions by using gravity and elutriation separation techniques. A number of specially sized fractions are available to the refractories industry; the major sizes are –1 mm, –600 μm , and –200 μm .

The Philippine chrome ore, better known as Masinloc chrome ore, is the world's largest produced high-alumina, refractory-grade chromite (21). It is also reported to be the world's largest single chromite outcrop. The Masinloc chrome-ore belt is a pseudo-stratiform deposit lying in a thick gabbro sequence of the Zambales ultramafic complex. Perhaps 10 million mt or more of ore are in reserve. After exploratory drilling, assaying, and mapping, mining is performed using open-pit or underground techniques. Following mining, the massive chrome ore is cleaned and concentrated by several methods: washing, hand sorting, screening, and gravity concentration. Grinding followed by concentrating machines such as heavy-media separation equipment, jigs, vibrating tables, and spirals produces the concentrates or fines. A number of product sizes, from lump size (150 mm), +2 mm, –2 mm, down to –200 μm , are available for refractories use.

3. Key Chrome Ore Characteristics

A dichotomy in the physical and chemical properties exists between the two just-described sources. The Philippine chrome ore produces a massive type, allowing a considerable range of fraction sizes ranging from 150 mm down to finer sizes, while the Transvaal ore is granular with much smaller sizes available. Secondly, the Philippine chrome ore can be characterized as low chrome oxide and iron oxide content with high alumina and magnesia, with the Transvaal showing high chrome oxide and iron oxide with low alumina and magnesia. The SiO_2 content of the Philippine variety varies with the size, ranging from about 6 wt. % for

the lump ore to about 2 wt. % for the $-200\ \mu\text{m}$ size; in contrast, the Transvaal chrome ore varies between 0.7 wt. % and 1 wt. % silica.

4. Properties of Refractory-Grade Chrome Ores

The dominant phase in chrome ore is a mineral that has a spinel structure with a complicated chemical composition due to almost unlimited solid-solution substitutions. Its overall chemical composition can be best understood by considering the general formula for spinel, AB_2O_4 , where A represents a divalent cation, most often Fe^{++} and/or Mg^{++} , and B represents a trivalent cation, generally Fe^{+++} , Al^{+++} , and/or Cr^{+++} ; therefore, the general formula can be written as $(\text{Fe},\text{Mg})(\text{Fe},\text{Al},\text{Cr})_2\text{O}_4$. Another representation of the spinel composition is to consider a right triangular prism with the lower triangular area having end-member apices magnetite (FeFe_2O_4), ferrochromite (FeCr_2O_4), and hercynite (FeAl_2O_4), and the upper triangular area having the end-member apices magnesioferrite (MgFe_2O_4), picrochromite (MgCr_2O_4), and spinel (MgAl_2O_4); then the composition of the chromite would occur at some point within this triangular volume and can be considered to be a mixture of these end members.

One or more silicate gangue minerals accompany the chromite in the ore; these minerals may range from anhydrous magnesia-lime olivines, pyroxenes, and amphiboles to hydrous serpentine varieties.

Chemical compositions of a grade of Transvaal chrome ore and a grade of Masinloc chrome ore are shown in Table 3 (22).

Finally, with respect to particle packing of refractories, chrome ores need to be considered as both aggregate and matrix components.

D. Magnesio-Chrome Grains

These materials occur as either a sintered (also called “prereacted” or “co-clinkered”) or a fused grain. The former is produced by co-grinding calcined magnesia and milled, low-silica chrome ore, granulating or briquetting this mixture, drying, and dead-burning in either a rotary or shaft kiln (23). Sources are available in the United States and Austria. The fused grain is also manufactured by blending the two aforementioned raw materials and then fusing them in a Higgins-type or tilt-pour electric furnace followed by carefully slow-cooling to allow the growth of large magnesia crystallites containing large exsolutions of spinel-solid solutions outlined by partial spinel-solid solution crystals. Manufacturers of fused magnesia-chrome grains are located in Canada, the United States, and several countries in Europe. Various sizes of these products can be furnished to refractory producers.

As with chrome ore, magnesia-chrome grains, in the presence of calcium-containing contaminants, may lead to the formation of soluble, hexavalent chromium compounds and carcinogenic concerns.

Table 3 Typical Chemical Properties of South African Transvaal and Philippine Masinloc Chrome Ores

Oxide	South African Transvaal (wt. %)	Philippine Masinloc (wt. %)
Cr ₂ O ₃	44.5	34.0
Fe ₂ O ₃	28.3	17.0
Al ₂ O ₃	16.7	27.0
MgO	10.0	17.0
CaO	0.3	0.4
SiO ₂	0.7	2.0

Source: Ref. 22. [Reprinted with permission of the Canadian Ceramics Society (M. Rigaud).]

Both grades have particle sizes less than 2 mm.

Various combinations of magnesia and chrome ore can be produced. The properties of both a typical sintered and a fused magnesia-chrome raw material used for producing a number of different refractory products appear in Table 4 (24).

These refractory raw materials can be used as both aggregates and matrix materials.

E. Magnesium Aluminate Spinel

Magnesium aluminate spinel, MgAl₂O₄, or simply spinel, the actual mineral name for this particular spinel composition, causes a thermal-expansion

Table 4 Properties of Sintered and Fused Magnesia-Chrome Grains

	Sintered magnesia- chrome grain	Fused magnesia-chrome grain
Chemical composition, wt. %		
Cr ₂ O ₃	15.2	20.0
Fe ₂ O ₃	7.9	12.4
Al ₂ O ₃	13.1	7.4
MgO	62.2	60.0
CaO	0.6	0.4
SiO ₂	1.0	0.6
Grain bulk density, kgm ⁻³		
	3200	3800

Source: Ref. 24. [Reprinted with permission of the Canadian Ceramics Society (M. Rigaud).]

mismatch with magnesia, leading to a lower coefficient of thermal expansion and, thus, improved thermal shock resistance of the refractory products containing this raw material. Also, this spinel does not expand under alternating temperature and oxygen partial-pressure conditions. Moreover, the use of the spinel with magnesia can lead to refractory products with improved impact strength and slag corrosion resistance. Finally, the formation of carcinogenic compounds in contact with calcium contaminants is not a problem with this raw material.

The stoichiometric composition for spinel is 28.3 wt.% MgO and 71.7 wt. % Al₂O₃. However, a rather wide, solid-solution region exists for this mineral, and a range in spinel composition can be produced from magnesia-rich to alumina-rich varieties depending on the application requirements; this latter concept can be understood by referring to the MgO–Al₂O₃ phase diagram, Figure 3 (25). As can be seen, spinel compositions can be produced from ~40 wt. % MgO–60 wt. % Al₂O₃ (magnesia-rich), through its stoichiometry to ~7 wt. % MgO–93 wt. % Al₂O₃ (alumina-rich).

The various spinels can be produced in three ways for use in refractory products. In all cases, the starting raw materials for their manufacture involve a specific mixture of magnesia (calcined or dead-burned) and alumina

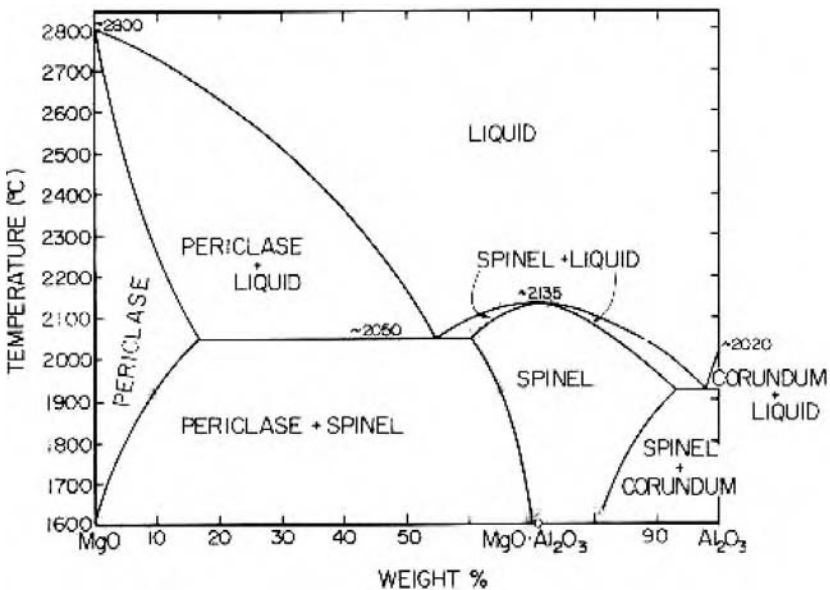


Figure 3 Phase diagram for the system MgO–Al₂O₃. (From Ref. 25.)

(Bayer-process calcined or calcined bauxite) that fall in the range discussed above. In the first instance, the fine magnesia and alumina can be co-ground, granulated and ball-formed or briquetted, dried, and dead-burned in a rotary or shaft kiln resulting in a sintered product (R. Racher, personal communication, 2002). Several U.S. producers manufacture these types of spinel raw materials. Second, fused spinel grains are produced in the United States, Europe, and Japan by fusing the magnesia and alumina raw materials in a Higgins-type or tilt-pour electric arc furnace at temperatures in the range of $\sim 2300^{\circ}\text{C}$.

Various sizes of these two spinel types are available for commercial purposes; following cooling after being produced, either type can be crushed and ground and subsequently screened or sieved.

The third manner for spinel production is for the refractory manufacturer to batch fine magnesia and alumina in the mix recipe itself; therefore, the spinel is formed in situ during a subsequent refractory manufacturing process, such as firing a brick in a kiln, or during service when temperatures approach those required for reaction (greater than $\sim 1500^{\circ}\text{C}$).

Spinel can also be employed as aggregates as well as particles for the matrix of refractories.

Properties of several commercial spinel sinters and a fused spinel appear in Table 5 (26).

F. Carbon Black and Graphite

1. General

These materials are the major sources of carbon added to refractories. They need to be treated as a part of the solid aggregate or matrix portion from a grain-sizing standpoint with respect to theoretical sizing.

2. Carbon Black (27)

Carbon blacks are formed in the absence of air by thermal decomposition of natural gas in a previously heated chamber containing refractory checkerwork. The process is batch-type; the brickwork is heated, and then the natural gas is introduced to make the carbon blacks. A number of companies produce these materials, with the Texas Panhandle being a major manufacturing location.

A number of types of carbon blacks are available for commercial use, but the refractories industry generally uses a thermal black. The thermal black's main properties of interest to the refractory technologist are the mean particle size and surface area; for particle-packing purposes, the thermal black sizing needs to be compatible with the sizing of the ball-milled portion of the other refractory raw materials used in the batch, while the surface area needs to be as low as possible in order to minimize the level of liquid binder to be added to the batch. A medium

Table 5 Properties of Sintered and Fused Spinel Grains

	Sintered spinel grain A	Sintered spinel grain B	Sintered spinel grain C	Fused spinel grain A
<i>Chemical composition, wt. %</i>				
Al ₂ O ₃	66.0	76.0	90.0	65.9
MgO	33.0	23.0	9.0	33.0
Fe ₂ O ₃	<0.1	<0.1	<0.1	<0.1
CaO	<0.4	<0.3	<0.25	0.3
SiO ₂	<0.09	<0.06	<0.05	0.5
Na ₂ O	<0.05	<0.15	<0.17	na
<i>Physical properties</i>				
Grain bulk density, kgm ⁻³	3270	3250	3300	3370
Major phase (XRD)	Spinel	Spinel	Spinel	Spinel
Minor phase (XRD)	Periclase	None	Corundum	Periclase

Source: Ref. 26. [Reprinted with permission of the Canadian Ceramics Society (M. Rigaud).]

thermal carbon black is often specified for pitch-bonded or resin-bonded magnesia-carbon brick.

3. Graphite (28, 29)

Graphite is the mineral name for one of the two polymorphs of carbon and is developed naturally from carbonaceous sediments that have undergone intense metamorphism (high pressure and temperature) and have been converted into gneisses and schists; during this transformation, the carbonaceous material crystallizes as graphite particles throughout these metamorphic rocks in a percentage range from 2 to 20 wt. %.

Graphite can be liberated from the other metamorphic rock minerals by drilling, assaying, blasting, loading into trucks, and hauling to an ore-dressing plant where it is concentrated. The concentration process consists of crushing to a size (-600 μm to -300 μm) to liberate the graphite from the gangue minerals, separating the graphite from the gangue in froth flotation tanks or water columns, dewatering the graphite in rotary vacuum filters or centrifuges, and drying the graphite in steam-tube dryers. This concentration process will produce up to 96 wt. % graphite purity. Purity levels up to 99.8 wt. % graphite require additional chemical processing: acid or acid-base leaching of the previous concentrate followed by further washing.

Major sources of natural graphite are found in Mexico, Brazil, Norway, Germany, China, Madagascar, Sri Lanka, Rhodesia, and Canada. The graphite producers and distributors have divided natural graphites into three classes for commercial purposes: (1) flake—a scaly or lamellar form with each flake

being a separate, crystalline particle in the metamorphic rocks; (2) crystallite—found in rocks as veins or pockety accumulations that are foliated, bladed, columnar, or fibrous (these particles tend to be less flexible than the flake form); and (3) amorphous—these deposits occur in metamorphic rocks as minute, blocky, cryptocrystalline, graphite particles.

All three graphite classes or forms are very well crystallized and produce excellent X-ray diffraction patterns. Within each commercial class, there are many grades; these grades are usually based on particle size and carbon content (purity). For refractory usage, the coarsest grades with wide particle-size distributions are required. The highest carbon content is needed for many applications, and the remaining ash composition is important as well; ashes from the same geographical area are similar, but quite different, between areas. The ashes need to be examined for refractoriness and compatibility with the refractory body; avoid graphites with ashes containing high levels of alkalis and other fluxes. The graphites should have good oxidation-loss ratios in the range of 0.1 to 0.5%. Other important graphite properties include moisture content and volatile levels.

Finally, the “wettability” of the graphite grade with the batch binder is extremely important. During froth flotation, some processes use chemical conditioners that can be phobic with binders; these particular chemicals associated with the graphite can cause severe problems in batch mixing and forming.

Avoid breathing graphite dust; residual quartz particles from the original metamorphic rocks may be related to certain health issues (silicosis and cancer).

Table 6 (30) exhibits properties for each of the three classes of natural graphites.

4. The Magnesia-Carbon Paradox

Carbon, in any form, plays a vital role in minimizing the penetration of steel-making slags into the microstructure of magnesia-carbon refractories; at the same time, MgO becomes incompatible with carbon at these same steel-making temperatures. This incongruity is discussed below.

Barthel (31) contrasted the wear in basic oxygen furnace test panels between burned magnesia brick and the same brick that had been pitch-impregnated; although the initial rate of wear was less in the carbon-free brick, the pitch-impregnated magnesia brick ultimately had a lower overall rate of wear. The importance of carbon in minimizing slag attack was supported shortly thereafter by Herron et al. (32), whose work concluded that slag penetration, and, conversely, overall slag attack, was inversely proportional to the amount of residual carbon (from coked pitch) in the pores of pitch-impregnated, burned magnesia brick and due to the nonwetting of the residual carbon by the infiltrating slag. A number of researchers subsequently studied the role of carbon.

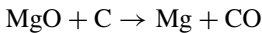
Table 6 Properties of Each Major Class of Graphite

Class	Amorphous	Crystalline	Flake
Origin	Mexico	Sri Lanka	Canada
Carbon content, wt. %	83	96	96
Ash content, wt. %	17	4	4
Ash chemical composition, wt. %			
SiO ₂	51.8	41.2	40.4
TiO ₂	0.5	0.5	0.4
Al ₂ O ₃	35.8	22.4	15.5
Fe ₂ O ₃	10.4	12.5	24.2
CaO	0.3	15.0	11.0
MgO	1.0	ND	5.3
K ₂ O	0.1	1.9	1.7
Na ₂ O	0.1	2.5	0.7
Screen analysis, wt. %			
+50M	27	57 (+40M)	95
-50M + 100M	27	40 (-40M + 100M)	2
-100M + 200M	18	2	1
-200M	28	1	2

Source: Ref. 30. [Reprinted with permission of the Canadian Ceramics Society (M. Rigaud).]

One author argued that the flow of gases toward the hot face from the carbon oxidation tended to inhibit the slag penetration (33); still others revealed that the formation of a dense zone of magnesia almost immediately behind the brick's hot face formed a barrier to the slag (34, 35).

This latter microstructural feature formed as a result of the instability of MgO with carbon at steelmaking temperatures. The diagram representing free energy as a function of temperature indicates that magnesia is stable in contact with carbon below ~1800°C (36). However, thermodynamic calculations indicate that the reaction



can take place even at lower temperatures (e.g., the partial pressure of Mg in contact with carbon at 1600°C is 10³ Nm⁻²). Brezny and Landy's experiments confirmed these calculations and postulated that immediately behind the brick hot face the magnesium vapor would react with oxygen to form a magnesia-dense zone, a microstructural feature they that observed in BOF and laboratory post-mortem examinations (37). In another study, Carniglia, using a diffusion-limited model for the kinetics of the MgO-C reaction, discovered that oxidizing agents, such as ferric oxide, carbon dioxide, and carbon monoxide, in the basic oxygen furnace appeared to cause the majority of the carbon diminution at or below 1650°C, but he found that the MgO-C reaction is not insignificant (38).

He concluded, in line with Brezny and Landy's work, that Mg reoxidation should be limited to the very thin, slag-penetrated region immediately behind the hot face as well as in the slag phase.

Therefore, vaporization of magnesia in contact with carbon can occur at and below steel-making temperatures; furthermore, Carniglia predicted increasing refractory wear rates in basic oxygen steel-making processes with increasing temperature or decreasing partial pressure of oxygen. In fact, Japanese steel-makers quickly learned to limit the maximum operating temperature in basic operating furnaces in order to minimize this reaction.

In addition to retarding slag penetration and attack, graphite contributes to brick longevity in other ways; the oxidation resistance of the carbon phase is improved over that of carbon black, and the thermal conductivity of the brick is greatly increased, which causes the slag's freeze plane to move closer to the hot face, minimizing the slag penetration, as well as increasing the brick's thermal shock resistance (39).

G. Metals and Other Nonoxide Powders

1. Types of Metals and Nonoxide Powders

In the late 1970s to early 1980s, silicon carbide, SiC, was used in manufacturing the initial magnesia-carbon refractories. Aluminum, magnesium, and silicon metals and their alloys quickly replaced this compound; these materials continue to be predominantly used today. Lately, some boron compounds, such as B₄C, CaB₆, ZrB₂, and TiB₂, have been introduced (40). These materials are produced worldwide in specialty facilities as very pure metals and nonoxide compounds; they are then ground to a very fine ($-44\ \mu\text{m}$) sizing. Care must be exercised in using these very fine materials in refractories, particularly during the batching and mixing or blending processes; metals, such as aluminum and magnesium, can spontaneously explode in combination with the oxygen in the air.

2. Reasons for Employing Metals and Nonoxide Powders in Magnesia Refractories

Adding these materials to resin-bonded magnesia-carbon refractories has improved their oxidation resistance, mechanical strength, and corrosion resistance (41). Oxidation of the carbon phase, carbon black or graphite, is a concern for magnesia-carbon refractories when used in basic oxygen furnace linings or steel ladle slaglines. This destructive brick mechanism is attenuated when the above-named metals and nonoxide powders are incorporated in these refractories' manufacture. Materials that minimize oxidation are called anti-oxidants. In magnesia refractories containing carbon, anti-oxidants react with oxygen to form gases whose counterflow retards the penetrating oxygen diffusion; simultaneously, a spinel phase can be formed in the thin reaction zone at the brick

hot face, which acts to seal the brick porosity, additionally, impeding oxygen diffusion into the brick microstructure (42).

New carbide phases formed in the brick matrix during these anti-oxidant reactions with oxygen bolster the brick's mechanical properties.

Finally, the spinel phase formed at the hot face also tends to impede the infiltration of liquid slags into the brick's microstructure, which reduces the impact of slag corrosion.

The thermodynamics of these magnesia-carbon-metal reactions are thoroughly discussed by Rymon-Lypinski (43, 44).

H. Dead-Burned Dolomite (Doloma)

This raw material is discussed thoroughly in another chapter in the present volume.

I. Forsterite

Forsterite is the naturally occurring, magnesia end member of the olivine solid-solution series. Its stoichiometric chemical formula is Mg_2SiO_4 , although some ferrous iron oxide (up to 10 wt. %) is contained in solid solution in the forsterite structure. Its major refractory characteristics are a melting temperature of $\sim 1750^\circ C$, low heat conductivity, and relatively high resistance to liquid iron and steel and both basic and acid slags.

Most of the world's commercial forsterite comes from Norway, where it is mined in an open-pit quarry; its reserves are estimated to run in the billion of tons (45). Forsterite is associated with little gangue material and is quite friable, so it is easily dressed for commercial use by the simple process of crushing, washing, and screening into a number of ready-to-use sizing grades. Forsterite does not have to be precalcined to be used.

The principal use of forsterite refractories is in Europe, but applications throughout the world have been reported. Its main uses are as steel-making refractories for tundish boards, sprays, and back fillings; ladle safety linings for dolomite brick; and in electric arc furnace safety linings and roof brick. In industrial furnace applications, forsterite is employed in alloy foundries and glass tank regenerators.

J. Binders

1. General

These raw materials are added to the refractory mixes to hold the various aggregates and matrix particles together in a form that can be handled with minimum breakage. Generally, for brickmaking, they are liquid; some need to be heated to

liquify, and some may be added as soluble salts that dissolve in water or as solids that disperse and develop plasticity. Their mission during the mixing or blending process is to coat as many grains and fine particles as possible so that they can produce a maximum number of particle-to-particle bonds; if added as acids, the binders are meant to react with the particles they coat to form a reaction-salt bond. Some bonds are temporary, only designed for green strength to handle from presses after forming, during drying or curing, and stacking for firing in kilns; other bonds have sufficient green strength to be handled after forming and then develop additional strength after curing or tempering. For monolithics, such as gun mixes, the binders are added as solids and thoroughly blended dry with the other ingredients; then water is added as the mixes are sprayed during an original construction or repair job. The bond development between particles takes place as the gun mix is being propelled from the gun equipment to the surface being treated, sometimes aided by the heat from the furnace interior if the gunning is hot. Binders will be split into two categories for these discussions.

2. Inorganic Binders

This group includes materials such as various clay minerals including kaolinites and montmorillonites; soluble sulfates and sulfuric acid; sodium silicates; calcium aluminate cements; soluble phosphates, polyphosphates, and phosphoric acid; and borates and boric acid.

3. Organic Binders

This category includes materials such as pitches, resins, lignins and lignosulfonates, dextrans and starches, celluloses, waxes, and polyvinyl alcohol. Only the major two organic binders, pitches and resins, are further briefly discussed.

Pitches. Pitches are derived from either coal or petroleum. Both have been used in the refractories industry, but these binders have fallen out of favor due to their cancer-causing aspects; both pitches contain dangerous polycyclic aromatic hydrocarbons. Since 1986 and the advent of material safety data sheets, employers have been obligated to educate and train their employees with regard to the nature of materials they're handling, and, therefore, these pitches have become a very sensitive raw material to the workers. However, for thoroughness and historical purposes, their major properties will be reviewed. There are several primary manufacturers of pitches in the United States. Pitches with the highest carbon residue after coking (simulating their state in service), as measured by the Conradson coking value (CCV), are desired; coal-tar pitches typically average ~60 wt. % CCV, while petroleum pitches yield ~50 wt. % CCV. The softening point for these pitches is over 100°C, so the pitches, aggregates, coarser fines, the mixers or blenders, hoppers over the presses, and

the presses themselves must be heated before using as well. The coal-tar pitches contain ~ 6 wt. % quinoline insolubles (small, solid, organic particles), while petroleum pitches do not have any of these insolubles.

Petroleum pitch is used also for impregnating previously shaped refractories because petroleum pitch does not contain the quinoline insolubles that can block pores in the refractory body and limit the pitch penetration. In this manner, a carbon source can be added to formed refractories such as burned magnesia brick and, thus, enhance this brick's slag resistance.

Resins (46). Resins originally were derived from coal, but presently most resins emanate from petroleum sources; there are several resin manufacturers in the United States as well as throughout the world. Environmentally, resins are favored over pitches; however, resins need to be stored and handled properly, so their material safety data sheets must be reviewed prior to using. Two major thermosetting phenolic resins are used in the refractories industry; novolacs and resoles. Novolacs require the addition of hexamethylene tetramine for polymerization during curing, while resoles contain a built-in catalyst. Novolacs feature ~ 60 wt. % CCV, while resoles, ~ 70 wt. % CCV. Only very mild, elevated temperatures are required in production, so using resins saves energy over the use of pitches. This feature is another advantage, in addition to the environmental issue, favoring resins over pitches. Care does need to be paid to the wettability of graphite by resins; as mentioned earlier, some chemicals used in the graphite beneficiation process can impact this feature.

III. MANUFACTURE OF MAGNESIA REFRACTORIES

A. General

The overall process of refractories manufacturing is much like that of baking a cake. When one wants to bake a pie or cake, he or she has in mind the reason for making this dessert. A recipe is then selected that best matches the occasion, and a visit to a grocery store is made to purchase the ingredients. Back home, the cook carefully measures each component based on the recipe instructions; some have to be sifted before using further. Each constituent is carefully placed sequentially into a mixing bowl. Following careful mixing, the resulting cake batter or pie mix is placed into a selected pan or dish and then baked at a specified temperature for a prescribed amount of time.

In a like manner, the refractory technologist considers a particular refractory application; he, like his customer, desires a long, lasting refractory life at an economical cost to the consumer. The technologist contemplates the overall environmental and wearing mechanisms to which the refractory will be exposed including temperatures, gas pressures, chemically corrosive agents and/or

mechanical stresses. Based on her experience and theory, she prepares her recipe for this refractory end use from the list of raw materials discussed in the previous section.

In addition, throughout the entire manufacturing process, each step must be carried out in accordance with total quality-control principles defined by ISO 9000–9004 or Malcolm Baldrige paradigms; readers unfamiliar with these concepts need to consult these documents.

B. Raw Materials

The raw materials will be ordered by a purchasing official based on the specifications derived from the refractory technologist. They will arrive at the refractory plant in bulk in covered hopper railroad cars or trucks; as a liquid in railroad or truck tankers; or on pallets of dry, bagged materials or drums. The bulk materials generally are discharged into below-ground bins that supply various types of feeders, elevators, and belts for conveying to appropriate bulk storage silos or piles; sometimes, the bulk materials are discharged onto concrete pads and handled by front-end loaders. The pallets are stacked neatly in rows in the raw-material warehouses. All storage space must be clean and dry. Analyses certifying compliance with specifications based on the required number of samples per batch must accompany each shipment as set forth in advance between the quality assurance departments of the purchaser and the raw material supplier. Initially, the refractory manufacturer's quality-control personnel must sample and test each received batch to verify the supplier's data until confidence is built up between the two parties and the supplier becomes certified. Tests may include various chemical assays and bulk densities.

C. Crushing, Grinding, and Screening

Many of the bulk raw materials, such as dead-burned magnesia, dead-burned doloma, and chrome ore, must be sized for the particular recipe to be produced. The technologist wants to produce a densely packed refractory, so he must have several graded, aggregate sizes to attain that density following the teachings of, for example, Furnas (47); these concepts are based on the theory that each distinct particle-size class is capable of packing to 60% of theoretical density, and that, if the particle-size ratios are great enough between each particle-size class, each distinct particle class will fill 60% of the remaining porosity, and so forth. One aggregate size combination, for example, could be $-9.5\text{ mm} + 6.7\text{ mm}$, $-6.7\text{ mm} + 3.4\text{ mm}$, $-3.4\text{ mm} + 1.2\text{ mm}$, $-1.2\text{ mm} + 300\text{ }\mu\text{m}$, $-300\text{ }\mu\text{m}$ and finer, and $-75\text{ }\mu\text{m}$ and finer.

Most modern, fully integrated refractory producers have a portion of their plant designed for such crushing, grinding, and screening. The coarser sizings can

be obtained, if not available from the raw-material supplier, by crushing the as-received raw-material briquettes or fragments in coarse crushers, such as jaw crushers, gyratory and cone crushers; intermediate pulverizers, such as cage disintegrators and hammer mills; and fine grinding mills, such as rod mills and ball mills. Screening or sieving these fractions is accomplished by passing each fraction over single or multidecked, stationary screens or dynamic screens, such as inclined or horizontal vibrating screens, oscillating sieves, or reciprocating units. Again, all product fractions must be sieve-tested for conformity with internal specifications such as the specific sizing and its screening efficiency. Final products for each raw-material-size fraction are conveyed to individual holding bins or hoppers in the batching area.

D. Batching

The batching area is usually characterized by a batch weigh-hopper on wheels or tracks capable of traversing under rows of multiple hoppers or bins, each holding a specific size fraction of a specific raw material. Some batching systems are automated, while others are manual. In either event, the batch-card weights for each ingredient of a mix recipe are formulated based on the sieve analyses for the specific raw-material fractions being held in the hoppers or bins.

If a pitch binder or similar is to be used in the mixing, the coarser fractions or the total batch have to be heated prior to discharging into the mixer; for the former, a rotating, gas heater might be satisfactory, while preheating the total batch requires a salt-bath-type heater in order to prevent the fines from being elutriated during heating.

E. Mixing

The batch is then discharged into an appropriate mixer. A number of mixers are employed in the refractories industry. The most common type is a muller mixer, a mixing bowl fitted with one or two heavy wheels that rotate while the mixer bowl revolves or the rotating wheels revolve while the mixer bowl is stationary. This equipment produces a kneading action to the batch materials in which that portion of the batch proceeding directly under the wheels is squeezed and pressed producing a “de-airing” action together with intimate mixing of those ingredients. This type of processing is necessary, particularly when graphite is a mix component. Another mixer type is one that has a bowl fitted with a high-intensity rotor, ribbon blades, or screw. These latter mixers usually produce a uniform mix faster than the muller type, but de-airing is not as good.

In general, initially the binder is added to coat the coarser grains or aggregates of the mix, then the recipe fines are added to be picked up in the sticky binder around these coarser grains. Studies have to be conducted for each recipe

to optimize the mixer type-time requirements-mix temperature in order to yield a properly mixed batch with well-distributed components so that each unit of the mix will have the same, randomly arranged percentage of each ingredient as the next.

At this point, the mix batch is conveyed to the press feed-hopper if a brick or a formed piece is to be made. If a monolithic is being produced, the mix batch goes to a holding hopper or bin over a bagger; after filling, the bags are palletized and shrink-wrapped before shipment to customers. Also, samples of the final monolithic product are taken for monitoring various quality characteristics such as chemical properties as well as grain sizing and other pertinent physical characteristics.

F. Pressing or Forming

A formed or pressed refractory piece may be manufactured using a number of different processes. Special, large, complex pieces might be formed by hand molding using an air hammer. Simple geometric shapes, such as straights, keys, wedges, arches, and combinations of these (i.e., key wedges, key arches, or key-arch wedges), are formed by using toggle presses, friction presses, or hydraulic presses; each piece of equipment has advantages. Toggle presses can turn over about six to eight strokes a minute, so they are very high-volume presses; these were very popular in the 1960s to 1980s. Hydraulic presses can produce very high forming pressures and are easily automatically programmed for various steps including de-airing cycles; these presses are replacing toggle presses. Friction (also called screw or impact) presses can be considered as falling between the two others; they were employed in early manufacturing of resin-bonded, magnesia-carbon brick containing large percentages of graphite (up to 50 wt. %).

Typically, the highest possible forming pressures are used in order to obtain brick with the highest bulk densities; recall that brick recipes were designed to yield maximum particle packing so forming pressure also plays a very important element in the overall process. Typical refractory recipes require forming pressures of 50 to 100 Mpa, but resin-bonded, magnesia-carbon refractories with high amounts of graphite may need higher forming pressures of greater than 100 Mpa; also, multiple de-airing cycles will be needed to produce a lamination-free product. Some pressing chambers are enclosed to allow for vacuum pressing to assist with de-airing (48).

Process quality parameters monitored here are brick dimensions and weight and, consequently, brick bulk density; statistical process control techniques are particularly easy to employ at this point of the process.

The type of binder used in the mix recipe will determine how a brick is handled following pressing; most bricks are placed or slid onto flat, individual trays that can be then placed onto steel racks, while other bricks can be stacked several bricks high on drying cars.

G. Drying, Curing, or Tempering

Following off-bearing from the press, inorganic-bonded bricks designed to be sold as chemically bonded or designated for subsequent firing to produce a burned brick are dried at low temperatures ($\sim 150^{\circ}\text{C}$) in order to develop the green strength of the temporary binder-magnesia component reaction.

Resin-bonded brick are processed to temperatures in the range of $\sim 135^{\circ}\text{C}$ to cure the resin bonds. Pitch-bonded brick have to be heated to $\sim 290^{\circ}\text{C}$ to develop appropriate green strength, primarily in the brick's outer areas, in order to be handled during shipment and installation without breaking.

Heating in batch or tunnel ovens can be used for any of these bricks. After cooling, some bricks have completed their manufacturing cycle; see the last part of this section for final procedures. Bricks for burning are appropriately stacked on kiln cars and sent to the kilns.

H. Burning

Burning or firing can be carried out in batch-type or tunnel kilns that are gas- or oil-fired; in some instances, oxygen partial pressures in the heat-up stages are controlled. Temperatures attained during this process can range from 1500°C to 1750°C depending on the type of brick being produced. For example, burned magnesia bricks that are subsequently pitch-impregnated are exposed to the lower temperature, while direct-bonded magnesia-chrome bricks require the upper temperature. Other bricks need intermediate temperatures. Overall heat-up, at-temperature, and cool-down kiln schedules take two to three days. Following cool-down, the bricks are unloaded and await final processing; see the last part of this section for details.

I. Post-Treatments

Some examples of post-treatments are (1) burned magnesia brick may be subsequently pitch-impregnated prior to use; (2) brick for cement kilns may have cardboard spacers glued on one or two brick faces; and (3) resin-bonded magnesia-carbon brick may be subjected to a heating cycle and then pitch-impregnated.

J. Final Inspection and Palletizing

The last processing step for all shaped refractories involves careful inspection for product defects and compliance with proper workmanship standards; randomly selecting finished units for further testing, such as dimensions, weight, and other physical and chemical properties, according to a predetermined quality sampling plan; palletizing; and shrink-wrapping before shipment to the customer.

All pallets carry a date-made code. The palletized brick can be stored in cool, dry, clean warehouses before such shipment.

IV. CLASSIFICATIONS OF MAGNESIA REFRACTORIES

A. Refractory Forms

Two forms of refractories products are universally recognized: (1) formed or pre-shaped refractories, which includes bricks of numerous shapes such as keys, wedges, and arches; and (2) monolithics, which includes mortars and cements, plastics, ramming mixes, castables, and gunning mixes. Various classifications exist for these products.

B. Standard Industrial Classifications

The U.S. Government Census Bureau has several standard industrial classifications (SIC) that are used for reporting annual refractories industry statistics involving basic and, in particular, magnesia products: SIC 3297, Nonclay Refractories; and SIC 3274, Lime (49). These classifications are quite general, confusing, and not very helpful.

C. American Society for Testing and Materials Standard Classifications

A more useful reference is ASTM C455, Standard Classification of Chrome Brick, Chrome-Magnesite Brick, Magnesite-Chrome Brick, and Magnesite Brick; except for all-chrome brick, its purpose is to describe classes distinguished by obvious differences in magnesium oxide (MgO) content (50). Table 7 from this standard presents the essence of this standard. Also, in a just-approved ASTM standard, C1547, Standard Classification of Fusion-Cast Refractory Blocks and Shapes; Table 8 exhibits the classification of magnesia-containing refractories for magnesia-spinel and magnesia-chromite compositions (A.D. Davis, Jr., personal communication, 2002).

D. International Organization for Standardization Classifications

The International Organization for Standardization (ISO) has established an extensive classification for various types of dense-shaped refractory products, ISO 1109–1975; Table 9 replicates the section applicable to shaped basic products (51). Another ISO standard, ISO 10081-1:1991, Basic Refractory Products—Classification, Part 1: Products Containing Less Than 7% Residual

Table 7 ASTM's Classification of Chrome Brick,^a Chrome-Magnesite Brick, Magnesite-Chrome Brick, and Magnesite Brick According to MgO Content

Class	MgO Content, % ^b	
	Nominal	Minimum
Chrome-magnesite and magnesite-chrome brick ^c		
30	30	25
40	40	35
50	50	45
60	60	55
70	70	65
80	80	75
Magnesite brick ^c		
90	90	86
95	95	91
98	98	96

Source: Ref. 50. (Reprinted with permission, copyright ASTM International.)

^aChrome brick is a refractory brick manufactured substantially or entirely of chrome ore.

^bIgnited basis.

^cThis classification applies to both chemically bonded and burned brick.

Carbon, not only classifies by refractory type, but also by MgO content or principal oxides content; this classification is shown in Table 10 (52). ISO 1927–1984 covers the ISO classification for dense and insulating monolithic refractories; Class IV applies to basic materials, but, like the SIC standards, this standard uses only general types of products with differentiation within the class limited to the principal basic material of the monolithic mixtures—magnesia, chrome ore, spinel, forsterite, dolomite, or other alkaline earth oxides (53).

Table 8 ASTM's Classification of Fusion-Cast Magnesia-Containing Refractories by Types and Content of MgO and Spinel

Class	Spinel content (vol. %)	MgO content (vol. %)
Magnesia-spinel (46–50 wt. % MgO)	65–75 (as MgAl ₂ O ₄)	25–35 (as MgO)
Magnesia-chromite (18–22 wt. % Cr ₂ O ₃)	37–43 (as chromite spinel)	48–56 (as Mg _{1-x} Fe _x O)

Source: A.D. Davis, Jr. Personal communication. (Reprinted with permission, copyright ASTM International.)

Table 9 ISO's Classification of Dense-Shaped, Basic Refractory Products

Products	Limiting content of principal constituents	Criteria of subdivision with general observations
Magnesite	MgO > 80%	Products in which the principal constituent is magnesite
Magnesite-chrome	55% < MgO < 80%	Products in which the principal constituents are magnesite and chromite
Chrome-magnesite	25% < MgO < 55%	Products in which the principal constituents are chromite and magnesite
Chromite	Cr ₂ O ₃ > 25%	Products in which the principal constituent is chromite
Forsterite	MgO < 25%	Products in which the principal constituent is forsterite
Dolomite		Products in which the principal constituent is dolomite

Note: In view of recent and possible future developments in basic products, new subdivisions and new criteria of classification may become necessary.

Source: Ref. 51. (The terms and definitions taken from ISO 1109:1975 Refractory Products, Classification Table, are reproduced with the permission of the International Organization for Standardization, ISO. These standards can be obtained from any ISO member and from the web site of the ISO Central Secretariat at the following address: www.iso.org. Copyright remains with ISO.)

E. Other Classifications

Other classification standards exist, notably British Standards Institution (BSI) 7225, a series of classifications that follow ISO practices (54). China, Japan, and Australia, among others, also have developed industry standards and may be of interest to users in those nations.

V. MAGNESIA REFRACTORIES: THEIR APPLICATIONS AND EXAMPLES

A. Evolution of Magnesia Refractories Applications in the United States

In the United States, magnesia refractories are used in a multitude of heat-processing industries, but the greatest quantity is used by the steel industry. Within this industry, the types and amounts of magnesia refractories have dramatically changed over the years and continue to evolve as the steel-making process technology, which requires magnesia refractories, matures. For example, the major application of magnesia refractories in the 1950s and 1960s was in

Table 10 ISO’s Classification of Basic Refractory Products Containing Less Than 7% Residual Carbon by Types and Groups

Types	Groups [MgO (% m/m)] ^a					
Magnesia	98	95	90	85	80	
Magnesia doloma	80	70	60	50		
Doloma					40	30
Magnesia spinel ^b	80	70	60	50	40	30
Forsterite				50	40	
Magnesia chrome ore	80	70	60	50	40	30
Chrome ore					MgO < 30	
					Cr ₂ O ₃ ≥ 30	
Lime					CaO ≥ 70	

Source: Ref. 52. (The terms and definitions taken from ISO 10081-1 : 1991 Basic Refractory Products, Table 4.1 Types and Groups, are reproduced with the permission of the International Organization for Standardization, ISO. These standards can be obtained from any ISO member and from the web site of the ISO Central Secretariat at the following address: www.iso.org. Copyright remains with ISO.)

^aThe analysis is carried out on the calcined products and the residual carbon is determined as in ISO 10060-1.

^bMagnesia spinel: MgO–MgO · Al₂O₃.

constructing open-hearth furnaces. The open hearths were lined with an array of magnesia refractories; the most predominant types were chemical-bonded, burned, direct-bonded, and fusion-cast magnesia-chrome brick and magnesia ramming mixes, while magnesia and doloma fettling and gun products were used extensively for bottom and wall maintenance, respectively.

The development of the basic oxygen steel-making furnace (BOF) in the late 1950s and early 1960s ushered in pitch-bonded doloma, doloma-magnesia, magnesia-doloma, and magnesia brick (the latter with purity levels from 70 to 95 wt % MgO) for construction of the vessel linings; magnesia and doloma gun mixes continued to be used as maintenance materials. In the late 1960s, high-strength, pitch-impregnated, burned magnesia bricks were developed based on using Greek magnesite or its equivalent with their magnesia levels in the range of 95 wt % MgO; these bricks were used in place of pitch-bonded types in the higher-wear areas of BOF linings such as impact pads. As the basic oxygen process for steel production expanded and the open-hearth process waned during the late 1960s and into the 1970s, the most widely used magnesia-chrome brick used in the latter were surpassed by all-magnesia brick in the former, either the previously mentioned pitch-impregnated, burned magnesia or pitch-bonded magnesia in the remainder of these same BOF vessels. Magnesia gunning materials were used extensively to maintain these linings, and BOF lining lives with these particular magnesia refractories reached the high hundreds to low thousands.

However, as the usage of all-magnesia brick surpassed the magnesia-chrome brick, magnesia-chrome brick continued to be used in other steel-making process applications. For example, with the increased production of steel in mini-mills, the amount of magnesia-chrome brick in electric arc furnaces (EAFs) also increased correspondingly; these furnaces were lined initially with fusion-cast magnesia-chrome brick in the high-wear hot spots (walls nearest to the electrodes), direct-bonded and rebonded magnesia-chrome brick in the remainder of the sidewalls, and chemical-bonded and direct-bonded magnesia-chrome brick in the roofs. Moreover, with the steel production shifting away from open hearths, stainless steel-making technology made a significant advancement in the late 1960s by the introduction of the argon-oxygen-decarburization (AOD) refining process duplexed with scrap melting in EAFs, and direct-bonded and rebonded fused-grain magnesia-chrome brick found a new usage in these AOD reactors. Currently, direct-bonded magnesia-chrome bricks still line small AOD vessels, but fired doloma bricks are the product of choice for large AODs (S. Miglani, personal communication, 2002).

In the mid-1970s, the Japanese introduced resin-bonded magnesia-carbon refractories for EAF hot spots. Within a short time period, graphite became the principal carbon ingredient for these resin-bonded magnesite-carbon bricks, and graphite contents up to 35 wt % were tried in the EAF hot spots. Before long, however, experiments commenced with water-cooled panels in EAF upper sidewalls. From the mid-1980s and continuing until the present time, a typical EAF wear lining for the production of carbon and low-alloy steels consists of water-cooled panels in the upper and middle sidewalls from just above the slag lines and several resin-bonded magnesia-graphite qualities in the slaglines and lower hot-spot sidewalls. Typically, such brick for the hot spots are composed of 15 wt. % graphite with various combinations of premium-quality, sintered and fused-grain magnesias and one to three anti-oxidants, while the noncritical areas have the same level of graphite with only sintered magnesia and one to two anti-oxidants (S. Miglani, personal communication, 2002). A hydration-resistant, burned magnesite brick is used to construct the subhearth with the overlying hearth made from either pitch-impregnated, burned magnesite brick or a dry, vibratable, Austrian-type magnesite. Water-cooled panels now also compose the bulk of the EAF roof with high-alumina castables with or without spinel additions in the delta section. Linings for EAFs used in stainless steel production differ from those just described for the production of carbon and low-alloy steels in that several varieties of direct-bonded and rebonded fused-grain magnesite-chrome (~60 wt. % MgO) brick and/or resin-bonded magnesia-graphite brick are used in the slagline and lower hot-spot sidewalls. EAF linings are repaired and maintained with various magnesia and doloma products.

Shortly after the introduction of resin-bonded magnesia-carbon brick in EAFs, this brick type was applied in the early 1980s to the high-wear trunnion areas of BOFs with surprisingly good results. These trials began a period of new and upgraded magnesia-carbon (based on graphite) developments as well

as experimentation in BOF zoning that has lasted to the present. Coupled with the brick developments and new zoning designs, technology changes in steel-making practices, in particular, implementation of slag-splashing technology to coat of the BOF bottoms and walls between heats and the introduction of secondary ladle metallurgy, have succeeded in extending BOF lining life into the high thousands and tens of thousands. Currently, BOF high-wear trunnions are lined with resin-bonded magnesia-carbon brick containing 15 wt. % high-purity graphite. In some cases, 99 wt. % MgO, premium-quality, sintered magnesia is used, but, where extreme conditions exist, various quantities and qualities of fused-grain magnesia replace some or all of the premium-quality, sintered magnesia. In addition, several anti-oxidants are used in these bricks. In the bottom and non-critical areas of the BOFs, resin-bonded magnesia-carbon bricks with 15 wt. % graphite and standard-quality, sintered magnesia with one anti-oxidant are employed. The lining for the BOF cone contains a resin-bonded magnesia-carbon brick with 5 wt. % carbon black and standard-quality, sintered magnesia reinforced with two anti-oxidants (S. Miglani, personal communication, 2002). Again, these linings are repaired and maintained with magnesia gunning mixes.

The advent of secondary ladle metallurgy in the 1970s and the subsequent technological changes to the current ladle metallurgical furnace (LMF) designs have seen a radical transition of ladle wear lining refractories from fireclay brick to bauxite castable or brick (some containing a small addition of magnesia aggregate) in the working bottom and barrel and resin-bonded magnesia-carbon brick or, sometimes, direct-bonded magnesia-chrome brick in the working slagline.

Moreover, the application of magnesia refractories in LMF slaglines now represents the largest utilization for this class of refractories in steel-making; EAFs consume the second-largest quantity of magnesia refractories, while BOF usage, which for the last 30 or so years represented the largest amount of magnesia refractories consumption, has currently fallen even behind the EAF application (S. Miglani, personal communication, 2002). Degassers, processing units that have gained popularity in the past 20 years due to the recent push for “clean steel,” are now the largest consumers of magnesia-chrome refractories, primarily direct-bonded or rebonded fused-grain types (A. Ketner and S. Miglani, personal communication, 2002).

A very important and highly specialized use of burned high-magnesia shapes is for small to medium-sized slide-gate plates for steel ladles with bore size less than 50 mm; the thermal expansion of magnesia is too high for large plates or bores, causing the latter to crack in service. In addition, burned high-magnesia, tundish slide-gate plates and porous upper nozzles are fabricated to control the flow of Mn- or Ca-treated liquid steel into continuous casting molds.

Practically all consumable tundish linings are made from sprayable magnesia mixes; where these magnesia spray materials are not used, dry, vibratable magnesias are employed. Forsterite may be part of these mix recipes.

The use of burned magnesia-spinel brick in the sintering or burning zone and adjacent transitional areas of cement kilns represents the biggest application of magnesia refractories in the nonsteel-making or so-called industrial industries (A. Ketner and S. Miglani, personal communication, 2002). Demand for higher throughputs and energy conservation in the cement industry over the years, particularly in the past 40 years, has led to kiln technology changes, such as transitioning from long, wet and dry kilns to short, preheater and precalcining units and has greatly affected refractory lining practices (55). One hundred years ago, super-duty fireclay or high-alumina brick lined the above-mentioned areas; then, about 70 years ago, chemical-bonded chrome-magnesia brick superseded these products (56). In the 1950s, burned magnesia-chrome brick came into vogue, while direct-bonded magnesia-chrome and doloma bricks were successfully introduced in the 1960s (57). About 30 years ago, burned magnesia-spinel (initially, in situ spinel and, later, sintered or fused spinel) brick appeared, and this trend was accelerated after 1986 when material safety data sheets highlighted the environmental problems of the various magnesia-chrome brick.

Another major environ for magnesia refractories usage in industrial processes is glass tank regenerators. For soda-lime glasses, chemical-bonded high-magnesia bricks (95–98 wt. % MgO) with a low lime/silica ratio have been used successfully in the upper checkers for many years; today, in addition to the aforementioned bricks still being recommended, burned high-magnesia bricks (95–98 wt. %) with a high lime/silica ratio may be employed in these areas, or, if high temperatures and batch carryover exist, burned creep-resistant magnesia-zircon bricks have been introduced recently and have yielded substantially better results than the former magnesia types (58, 59). In the intermediate checkers where operating temperatures exist above the temperature of alkali condensation, chemical-bonded or burned high-magnesia bricks (90–94 wt. % MgO) have been used in the past, whereas today conventional burned high-magnesia bricks (95–97 wt. %) with a low lime/silica ratio are recommended. In the lower checkers where alkali condensation does take place, burned and unburned forsterite, chrome, chrome-magnesia, and magnesia-chrome brick types have been employed in the past (60); the current concept is to use several burned high-magnesia brick types (95–96 wt. % MgO) with either low or high lime/silica ratios in order to have chrome-free regenerator packages, but, if there's a serious condensate-zone problem, then a burned condensate-resistant magnesia-zircon brick is a better choice for that area as well (61). For the regenerator top walls, target walls, and crown, co-sintered magnesia-chrome brick gradually had replaced conventional burned magnesia-chrome brick for these applications over the past 25 years or so, but today the emphasis is on chrome-free brick, so burned high-magnesia (96 wt. %) with a high-lime/silica ratio is being recommended with burned creep-resistant magnesia-zircon brick for severe carryover with high temperatures. These comments are general

considerations; the glass composition, lime/silica ratio of the batch carryover, type of fuel system, regenerator design, temperature profile throughout the regenerators, and operations, among other factors, may require recommendations of brick types different than just stated.

The last major industrial application for magnesia refractories to be covered is in copper processing, particularly in copper converting that takes place almost exclusively in Peirce-Smith converters. In the 1940s, the wear lining of most of these cylindrical vessels was composed of burned magnesia brick, while the trend in the 1950s was to employ burned chrome-magnesia brick (62). Since then, the tendency has been to construct these copper converter wear linings with either silicate-bonded chrome-magnesia brick or direct-bonded magnesia-chrome brick with the exception of the tuyere zone, a section that starts about 50 cm below a single line of 30–50 tuyeres and extends for about 150 cm above the tuyere line (63). This tuyere area is always lined with higher-quality refractories than the rest of the converter; e.g.,

Table 11 Selected Properties of Some Widely Used Magnesia-Carbon Brick

Brick type	Pitch-impregnated burned magnesia	Resin-bonded magnesia-C	Resin-bonded magnesia-C	Resin-bonded magnesia-C	Resin-bonded magnesia-C
<i>Physical properties</i>					
Bulk density, kg/m ³	3150	2900	3020	2930	2980
As-received					
Apparent porosity, %					
As-received		3.8	4.0	5.0	5.5
Coked		7.4		10.0	11.0
Ignited	15.0				
Modulus of rupture, Mpa					
@21°C	2.3	12.4	17.2	12.4	13.8
@1400°C		11.7	16.5	8.3	12.4
@1540°C	8.6				
<i>Chemical composition, wt. %</i>					
Carbon	5	14	3.2	12.7	9.5
(Carbon-free basis)					
MgO	96.0	81.0	94.0	77.2	86.0
CaO	2.2		2.0		
Al ₂ O ₃	0.1		3.3		
Fe ₂ O ₃	0.3		0.2		
SiO ₂	1.1		0.4		
Typical application	BOF charge pad	BOF non-critical barrel areas	BOF cone	EAF hot spots	LMF slag line/freeboard

Source: Ref. 67. (Reprinted with permission, © ANH Refractories Company.)

if silicate-bonded chrome-magnesia bricks are used for the bulk of the furnace wear lining, then direct-bonded magnesia-chrome bricks are used for the tuyere section wear lining, while if direct-bonded magnesia-chrome bricks are used for the bulk of the wear lining, then rebonded co-sintered or fused-grain magnesia-chrome bricks are used for the tuyere section wear lining (64). Recently, concerns over the disposal problems with spent magnesia-chrome refractories, as mentioned in other applications, have led to research programs and test panels of magnesia-spinel brick for these converters with some success (65, 66).

B. Examples of Magnesia Refractories

As seen from the many applications just described, refractory manufacturers produce a wide range of magnesia products with a spectrum of chemical and physical properties. Table 11 (67) depicts selected properties for several widely used magnesia-carbon brick types, while Table 12 (68) shows selected properties for an assortment of other popular magnesia refractory bricks.

Table 12 Selected Properties of Popular Non-carbon Magnesia Brick

Brick type	Chemical-bonded magnesia	High-fired magnesia	Direct-bonded magnesia-chrome	Rebonded fused-grain magnesia-chrome	Burned magnesia-spinel
<i>Physical properties</i>					
Bulk density, kg/m ³	2980	3030	3270	3300	2910
As-received					
Apparent porosity, %					
As-received	8.6	13.3	15.0	13.0	17.4
Coked					
Ignited					
Modulus of rupture, Mpa					
@21°C	11.7	16.3	4.1	10.3	5.0
@1260°C					6.0
@1480°C		11.9	2.8	4.8	
<i>Chemical composition, wt. %</i>					
MgO	98.0	96.2	59.0	62.0	82.4
CaO	0.8	2.5	0.8	0.8	1.5
Al ₂ O ₃	0.2	0.1	6.9	6.3	15.2
Fe ₂ O ₃	0.3	0.3	13.0	12.0	0.2
Cr ₂ O ₃			20.0	18.0	
SiO ₂	0.7	1.0	0.3	0.6	0.4
Typical application	Glass tank top checkers	Glass tank top checkers	Small AODs	EAF stainless steel slaglines	Cement kilns

Source: Ref. 68. (Reprinted with permission, © ANH Refractories Company.)

Acknowledgments

Thanks for the many contributions made by A. Ketner and S. Miglani, former colleagues and current employees of the author's former employer (ANH Refractories Company, née North American Refractories Company), in helping the author verify relative refractory usage and corroborate the current refractory products mentioned in various applications in Section V; some of their major contributions are specifically referenced. S. Miglani also reviewed Section V for context and correlated generic refractory descriptions with current products. T.A. Leitzel, another former colleague, read that part of Section V dealing with continuous casting refractories. The author also wants to thank C.R. Beechan (until recently a former supervisor of refractories research for Bethlehem Steel Corporation) for his critical review and constructive comments of that part of Section V detailing the evolution of magnesia refractories in the steel-making industry. Finally, M. Rigaud, CIREP Chair, Refractory Materials, Ecole Polytechnique, Montreal, critiqued the details of refractories for copper converters in Section V and offered several useful facts.

The author has taken a number of figures and tables from the literature and would like to thank the following publishers of these materials for permission to reproduce them here: Canadian Ceramics Society [Figure 1 (Ref. 5), Table 3 (Ref. 22), Table 4 (Ref. 24), Table 5 (Ref. 26), and Table 6 (Ref. 30)], Addison-Wesley [Figure 2 (Ref. 13) and Figure 3 (Ref. 25)], Elsevier Science [Table 1 (Ref. 15) and Table 2 (Ref. 16)], ASTM [Table 7 (Ref. 50) and Table 8 (personal communication from A.D. Davis, Jr.)], ISO [Table 9 (Ref. 51) and Table 10 (Ref. 52)], and ANH Refractories Company [Table 11 (Ref. 67) and Table 12 (Ref. 68)].

REFERENCES

1. ASTM C 71–93: Standard terminology relating to refractories. Annual Book of ASTM Standards, Section 15: General Products, Chemical Specialties, and End Use Products, Volume 15.01: Refractories, Carbon and Graphite Products, Activated Carbon, Advanced Ceramics. Philadelphia: ASTM, 1995:15–18.
2. ASTM C 71–93: Standard terminology relating to refractories. Annual Book of ASTM Standards, Section 15: General Products, Chemical Specialties, and End Use Products, Volume 15.01: Refractories, Carbon and Graphite Products, Activated Carbon, Advanced Ceramics. Philadelphia: ASTM, 1995:15–18.
3. ASTM C 71–93: Standard terminology relating to refractories. Annual Book of ASTM Standards, Section 15: General Products, Chemical Specialties, and End Use Products, Volume 15.01: Refractories, Carbon and Graphite Products, Activated Carbon, Advanced Ceramics. Philadelphia: ASTM, 1995:15–18.

4. Neely JE. Refractory materials classification: Magnesite. In: Rigaud M, Landy RA, eds. *Pneumatic Steelmaking: Volume Three, Refractories*. Warrendale, PA: ISS, 1996:35–40.
5. Landy RA, Vert T, Rigaud M. Refractories, a practical overview for the selection and uses. Hamilton, Ontario: Presentation to the Can Cer Soc, Feb. 22–23, 1997:30.
6. Brezny B, Landy RA. Magnesium oxide in refractories. In: Bloor D, Brook RJ, Flemings MC, Mahajan S, eds. *The Encyclopedia of Advanced Materials*. Vol. 2. Tarrytown, NY: Pergamon, 1994:1418–1423.
7. Howard-Smith IH. Magnesite and magnesite are basic to modern society. Queensland Metals Corp. N.L. technical paper, 1989:1–41.
8. Anonymous. Top quality magnesite from Holland. Billiton Refractories BV sales brochure. 1987:1–6.
9. Doman RC, Barr JB, McNally RN, Alper AM. Phase equilibria in the system CaO-MgO. *J Am Ceram Soc* 1963; 46:313–316.
10. Henney JW, Jones JWS. The solid solubility of CaO and SiO₂ in MgO and its effects on the MgO-CaO-SiO₂ system at 1750°C. *Trans Brit Ceram Soc* 1969; 68:201–203.
11. Jones DG, Melford DA. Comparison of the high-temperature constitution of sea-water magnesites with that of natural Greek material. *Trans Brit Ceram Soc* 1969; 68:241–247.
12. Hatfield T, Richmond C, Ford WF, White J. Compatibility relationships between the periclase and silicate phases in magnesite refractories at high temperatures. *Trans Brit Ceram Soc* 1970; 69:53–58.
13. Muan A, Osborn EF. *Phase Equilibria Among Oxides in Steelmaking*. Reading, MA: Addison-Wesley, 1965:92–94.
14. Rigby GR, Richardson HM, Ball F. The mineralogical composition of magnesite bricks. *Trans Brit Ceram Soc* 1947; 46:313–329.
15. Brezny B, Landy RA. Magnesium oxide in refractories. In: Bloor D, Brook RJ, Flemings MC, Mahajan S, eds. *The Encyclopedia of Advanced Materials*. Vol. 2. Tarrytown, NY: Pergamon, 1994:1419.
16. Brezny B, Landy RA. Magnesium oxide in refractories. In: Bloor D, Brook RJ, Flemings MC, Mahajan S, eds. *The Encyclopedia of Advanced Materials*. Vol. 2. Tarrytown, NY: Pergamon, 1994:1420.
17. Muan A, Osborn EF. *Phase Equilibria Among Oxides in Steelmaking*. Reading, MA: Addison-Wesley, 1965:191–193.
18. Lindgren W. *Mineral Deposits*. 3rd ed. New York: McGraw-Hill, 1933:784–786.
19. Pirsson EB, Knopf A. *Rocks and Rock Minerals*. 3rd ed. New York: John Wiley, 1947:189–190.
20. Anonymous. Chrome ore. Samancor sales brochure, circa 1993.
21. Besa RA, Dela Cruz SD. Masinloc chromite operation today and the future. *Minerals in the Refractories Industry: Assessing the Decade Ahead*. Pittsburgh, 1982:1–23.
22. Landy RA, Vert T, Rigaud M. Refractories, a practical overview for the selection and uses. Presentation to the Can Cer Soc, Hamilton, Ontario, Feb 22–23, 1997:53.
23. Neely JE, Boyer WH, Martinek CA Jr. Sintered magnesite-chrome grains for new type of refractories. *Am Ceram Soc Bull* 1970; 49:710–713.
24. Landy RA, Vert T, Rigaud M. Refractories, a practical overview for the selection and uses. Presentation to the Can Cer Soc, Hamilton, Ontario, Feb 22–23, 1997:53.

25. Muan A, Osborn EF. Phase Equilibria Among Oxides in Steelmaking. Reading, MA: Addison-Wesley, 1965:45–46.
26. Landy RA, Vert T, Rigaud M. Refractories, a practical overview for the selection and uses. Presentation to the Can Cer Soc, Hamilton, Ontario, Feb 22–23, 1997:52.
27. Mantell CL. Carbon and Graphite Handbook. New York: Interscience Publishers, 1968:76–105.
28. Mantell CL. Carbon and Graphite Handbook. New York: Interscience Publishers, 1968:61–71.
29. Keenan WM. Refractory materials classification: Graphite. In: Rigaud M, Landy RA, eds. Pneumatic Steelmaking: Volume Three, Refractories. Warrendale, PA: ISS, 1996:42–46.
30. Landy RA, Vert T, Rigaud M. Refractories, a practical overview for the selection and uses. Presentation to the Can Cer Soc, Hamilton, Ontario, Feb 22–23, 1997:68.
31. Barthel H. Effect of carbon in tar-impregnated burnt magnesia brick on the wear of basic oxygen furnace linings. Stahl und Eisen 1966; 86:81–88.
32. Herron RH, Beechan CR, Padfield RC. Slag attack on carbon-bearing basic refractories. Amer Ceram Soc Bull 1967; 46:1163–1168.
33. Robinson PC. Some observations on unused and used refractories from oxygen steel-making vessels. Refractories J 1966; 42:218–222.
34. Brezny B, Landy RA. Microstructural and chemical changes of pitch-impregnated magnesite brick under reducing conditions. Trans J Brit Ceram Soc 1972; 71: 163–170.
35. Carniglia SC. Limitations on internal oxidation-reduction reactions in BOF refractories. Amer Ceram Soc Bull 1973; 52:160–165.
36. Muan A, Osborn EF. Phase Equilibria Among Oxides in Steelmaking. Reading, MA: Addison-Wesley, 1965:3–5.
37. Brezny B, Landy RA. Microstructural and chemical changes of pitch-impregnated magnesite brick under reducing conditions. Trans J Brit Ceram Soc 1972; 71:163–170.
38. Carniglia SC. Limitations on internal oxidation-reduction reactions in BOF refractories. Amer Ceram Soc Bull 1973; 52:160–165.
39. Brezny B, Landy RA. Magnesium oxide in refractories. In: Bloor D, Brook RJ, Flemings MC, Mahajan S, eds. The Encyclopedia of Advanced Materials. Vol. 2. Tarrytown, NY: Pergamon, 1994:1418–1423.
40. Humbold K. Boron compounds in carbon-bonded refractories. Ceram Ind 1995; 47–50.
41. Brezny B. Refractory materials selection: Effects of brick properties on BOF lining life. In: Rigaud M, Landy RA, eds. Pneumatic Steelmaking: Volume Three, Refractories. Warrendale, PA: ISS, 1996:116–125.
42. Humbold K. Corrosion resistant refractories. Ceram Ind 2000; 34–38.
43. Rymon-Lypinski T. Reactions of metal additives in magnesium-carbon brick in an oxygen convertor: Part 1, the possible reaction sequences in the systems MgO-C-Al, MgO-C-Mg, and MgO-C-Si in various atmospheres. Stahl und Eisen 1988; 108:1049–1055.
44. Rymon-Lypinski T. Reactions of metal additives in magnesium-carbon brick in an oxygen convertor: Part 2, formation of metal sub-oxides and magnesia vapor. Stahl und Eisen 1988; 108:1055–1059.

45. McCracken WH. Olivine: an under-used raw material. *Ceram Ind* 1993; 57–58.
46. Gardziella A, Rigaud M. Refractory materials selection: Additives. In: Rigaud M, Landy RA, eds. *Pneumatic Steelmaking: Volume Three, Refractories*. Warrendale, PA: ISS, 1996:46–50.
47. Furnas CC. Grading aggregates. I. Mathematical relations for beds of broken solids of maximum density. *Ind Eng Chem* 1931; 23:1052–1058.
48. Barna GL. Refractory materials classification: Manufacturing. In: M Rigaud, RA Landy, eds. *Pneumatic Steelmaking: Volume Three, Refractories*. Warrendale, PA: ISS, 1996, 50–58.
49. *Standard Industrial Classification Manual*, Office of Management and Budget, USGPO, 1972:169–171.
50. ASTM C455–84: Standard classification of chrome brick, chrome-magnesite brick, magnesite-chrome brick, and magnesite brick. *Annual Book of ASTM Standards, Section 15: General Products, Chemical Specialties, and End Use Products, Volume 15.01: Refractories, Carbon and Graphite Products, Activated Carbon, Advanced Ceramics*. Philadelphia: ASTM, 1995:85–86.
51. ISO 1109, Refractory products—classification of dense shaped refractory products. International Standards Organization. Committee TC-33 on Refractories, 1975.
52. ISO 10081-1, Basic refractory products—Classification—Part 1: Products containing less than 7% residual carbon. International Standards Organization. Committee TC-33 on Refractories. 1991.
53. ISO 1927, Prepared unshaped refractory materials (dense and insulating)—Classification. International Standards Organization. Committee TC-33 on Refractories. 1984.
54. British Standard 7225, Classification of refractories series. British Standards Institution. Technical Committee RPM/11.
55. Gonsalves GE, Duarte AK, Brant PORC. Magnesia-spinel brick for cement rotary kilns. *Amer Ceram Soc Bull* 1993; 72:49–54.
56. Seebold JW, Peris A. A new basic refractory. *Rock Products* 1972; 113–116.
57. Seebold JW, Peris A. A new basic refractory. *Rock Products* 1972; 113–116.
58. Anonymous. Magnesia-zircon bricks for top and condensate zone checkers. North American Refractories Company sales brochure, NSB 95–04, 1995.
59. Weichert T, Schmalenbach B. Magnesia-zircon brick: Experiences and development. Didier-Werke AG technical paper, circa 1995.
60. Siefert AC, McEvoy RJ. Basic regenerator refractories in a borosilicate glass wool furnace. *Amer Ceram Soc Bull* 1955; 34:334–336.
61. Anonymous. Magnesia-zircon bricks for top and condensate zone checkers. North American Refractories Company sales brochure, NSB 95–04, 1995.
62. Lathe FE, Hodnett L. Data on copper converter practice in various countries. *Trans Met Soc AIME* 1958; 212:603–617.
63. Rigby AJ. Refractories for copper. North American Refractories Company Sales Meeting Presentation. Tuscon, AZ, 1997.
64. Rigby AJ. Refractories for copper. North American Refractories Company Sales Meeting Presentation. Tuscon, AZ, 1997.

65. Crites MD, Karakus M, Schlesinger ME, Somerville MA, Sun S. Interaction of chrome-free refractories with copper smelting and converting slags. 38th Annual Conference of Metallurgists. Montreal, Aug 22–26, 1999; Allaire C, Rigaud M, eds. *Advances in Refractories for the Metallurgical Industries III*. Montreal: CIMM, 203–213.
66. Schlesinger ME, Karakus M, Crites MD, Somerville MA, Sun S. Chrome-free refractories for copper production furnaces. In: Stett MA, ed. *Advances in Refractories*. Vol. III, Westerville, OH: UNITCER. Amer Ceram Soc, 1997:1703–1709.
67. ANH Refractories Company Data Sheets, 2002.
68. ANH Refractories Company Data Sheets, 2002.

6

Silica Brick Material Properties

Charles A. Schacht

Schacht Consulting Services, Pittsburgh, Pennsylvania, U.S.A.

James C. Hays

Civil & Environmental Consulting, Inc., Pittsburgh, Pennsylvania, U.S.A.

I. INTRODUCTION

We present here the most current thermal and mechanical material property data of normal density, 112 pcf (identified as KN), and high density, 116 pcf (identified as KD), silica brick used in coke oven walls. Coke ovens are used to produce coke for processing iron ore in blast furnaces to make iron. The property tests on the silica brick were conducted by RWTUV, Essen, Germany, and three other testing facilities to be cited below. The testing program was coordinated during 1999 by Dr. Hans-Dieter Potsch at RWTUV with the assistance of Dr. Uhlig and is documented in (1). The tests were conducted on brick samples, mortar samples, and brick/mortar composite samples. The brick/mortar composite samples reflect the behavior brick and mortar joints in the actual coke oven walls. This data can also be applied to other silica brick/mortar joint refractory lining systems.

A considerable number of silica brick-only, mortar-only, and brick/mortar samples were tested. As a result of page limitations in this chapter, representative typical sample data are provided. Average data from a large number of samples are presented in some instances. Due to the nature of silica refractory brick manufacturing, it is expected that there will be some variation from brick to brick in material property values. However, the data presented here can be used to provide insight into the trends of mechanical material properties of silica brick. The unique brick sample data, mortar-only sample, and brick/mortar composite data on refractory material properties in this chapter are typically not found in the literature.

A considerable range of mechanical material property tests was conducted at the RWTVU facilities, including cold static compressive stress–strain (SCSS) of brick-only and composite samples, cold crushing strength (S_C) of brick-only, creep in compression (CIC) of brick-only and composites, thermal expansion (TE) of brick-only, and modulus of rupture (MOR) of brick-only.

Testing at the Institute of Refractory and Ceramics (DIFK) facilities at Bonn, Germany, consisted of hot compressive stress–strain (SCSS) of brick-only. These tests were coordinated by Dr. Jorgen Portsckhe at DIFK.

The testing at the Didier facilities at Weisbaden, Germany, was hot static compressive stress–strain (SCSS) of brick-only and composites and hot crushing strength of brick-only and composites.

The testing at the Lemmens facility at Koln, Germany, was cold sonic tests of brick-only samples to determine Poisson's ratio of the brick.

The SCSS tests were conducted to determine Young's modulus (or modulus of elasticity, MOE) and can be used to define the complete stress–strain behavior up to ultimate failure at room temperature and elevated temperatures. The ultimate crushing strength (S_C) was also obtained from the peak compressive stress in the stress–strain curve. The brick specimens were hollow and cylindrical. They were nominally 2 in. (50 mm) in height and had an OD of 2 in. (50 mm) and an ID of $\frac{1}{2}$ in. (12.5 mm). Brick/mortar composite samples were also tested. The brick/mortar composite samples consisted of a split brick sample with a total nominal height of $1\frac{3}{4}$ in. (45 mm) and about a $13/64$ in. (5 mm) mortar joint between the two splits. The composite samples provided valuable information on the role of the mortar joint in the behavior of the brick/mortar joint lining system. The silica mortar was identified as Silica 11/55. In both the brick and composite samples, the loading rate was 29 psi (0.2 MPa) per second up to the crushing strength for the lower test temperatures and to the maximum crushing strain at the higher temperatures. Several samples of each silica KD and KN brick-only, mortar-only, and composite samples were prepared and tested at room temperature, 260°C (500°F), 538°C (1000°F), 816°C (1500°F), 1094°C (2000°F), and 1205°C (2200°F). All of the samples were subjected to an initial preload of 277 psi (1.91 MPa). The initial preload allowed the test machine platens to be properly seated on the test samples. The SCSS data curves are highly useful for engineers who wish to model and evaluate the thermomechanical behavior of silica brick lining systems using finite element method computer programs.

The CIC tests were conducted using a sample size similar to the SCSS test samples except for the sample OD. The brick sample size used for the creep in compression tests were the same as those used in the SCSS tests. The brick/mortar composite samples were also the same as those used in the SCSS tests. The creep samples were subjected to a constant compressive load of 0.689 MPa (100 psi). The heatup rate of the CIC samples was set at 1.8°F/min (1°C/min)

to the holding temperature. Separate samples had holding temperatures of 1500°F (816°C), 2000°F (1094°C), and 500°F (1372°C). The samples were held at these temperatures for 100 hr. The plots of percent expansion (TE) and the resulting coefficient of thermal expansion were also provided.

MOR tests were conducted on a sample size of 6 in. (152 mm) in length and a square cross section of 1 by 1 in. (25 by 25 mm). The support span was 5 in. (125 mm). The loading was applied at a stress rate of 22 psi (0.15 MPa) per second. The MOR was evaluated at room temperature, 500°F (260°C), 1000°F (538°C), 1500°F (816°C), 2000°F (1094°C), and 2500°F (1372°C).

Poisson's ratio tests were conducted using dynamic methods. The dynamic method was defined as an "impulse excitation of vibration." The sample size was 150 mm in length and a cross section of 15 by 25 mm. The tests were conducted at room temperature. Brick/mortar composite samples were not tested.

II. STATIC COMPRESSIVE STRESS–STRAIN (SCSS) TEST RESULTS

Figures 1 through 24 are the SCSS data curves for the silica KD and KN brick samples and brick/mortar composite samples. The data associated with the SCSS test data and each figure are described in Table 1.

A. Silica KD Brick Sample SCSS Data

Figures 1 through 6 show the SCSS data curve for the temperature defined. The elevated temperature curves (Figures 2 through 6) define the initial tangent Young's modulus or MOE (E_O , slope line with circle) and the secant modulus (E_S , slope line with solid square). E_S reflects the slope to the point of maximum crushing stress on the SCSS data curve. S_C is the maximum stress or crushing stress for the test temperature defined. Refer to Table 1 for the values of E_O , E_S , and S_C .

B. Silica KD Brick/Mortar Composite Sample SCSS Data

Figures 7 through 12 show the SCSS data curve for the temperature defined. These plots are similar to the SCSS data shown in Figures 1 through 6. The brick/mortar composite E_O and E_S values are less than those of brick-only E_O and E_S . The lesser slope is due to two reasons: First, the brick/mortar composite has a lower S_C . Second, the crushing strain (ϵ_C) of the brick/mortar composite is greater than the brick-only crushing strain. It is expected that the brick/mortar composite is softer than the brick-only.

Table 1 Summary of Sample Data for SCSS Tests (see Figs. 1 through 24)

Figure no.	Sample silica type	Sample temp. (°F)	Sample length, L_0 (in.)	Maximum compressive stress, S_c (psi)		Elastic MOE, E_O (psi $\times 10^6$)	Secant MOE, E_S (psi $\times 10^6$)	Ratio, E_O/E_S
1	KD	RT		7,898	0,908	0,715	1,27	
2		500	1,9732	6,220	1,49	1,21	1,23	
3		1000	1,9724	8,526	2,35	1,80	1,31	
4		1500	1,9736	7,758	1,87	0,768	2,43	
5		2000	1,9736	4,930	1,86	0,881	2,11	
6		2200	1,9681	3,857	1,91	0,514	3,72	
7	KD with mortar joint	RT		4,495	0,329	0,250	1,32	
8		500	1,9701	4,074	0,467	0,411	1,14	
9		1000	1,9673	5,075	0,732	0,649	1,13	
10		1500	1,9717	5,365	0,653	0,321	2,04	
11		2000	1,9740	5,554	0,633	0,352	1,80	
12		2200	1,9740	4,306	0,845	0,290	2,91	
13	KN	RT		4,876	0,575	0,454	1,27	
14		500	1,9689	2,798	1,41	1,07	1,32	
15		1000	1,9677	5,017	1,66	1,38	1,20	
16		1500	1,9704	5,075	1,01	0,312	3,24	
17		2000	1,9704	2,581	0,946	0,322	2,94	
18		2200	1,9665	2,610	1,21	0,281	4,30	
19	KN with mortar joint	RT		3,109	0,252	0,229	1,10	
20		500	1,9783	3,625	0,580	0,451	1,28	
21		1000	1,9720	5,350	1,05	0,816	1,28	
22		1500	1,9677	4,916	0,663	0,257	2,58	
23		2000	1,9779	3,509	0,527	0,287	1,84	
24		2200	1,9795	2,740	0,663	0,228	2,90	

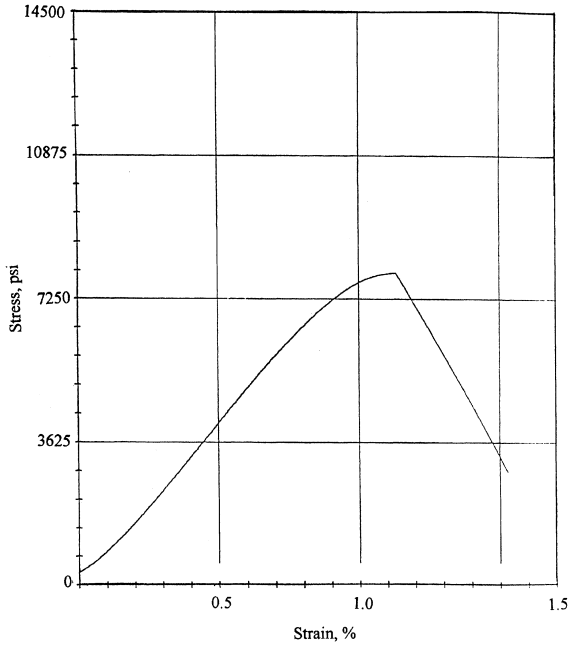


Figure 1 Compressive stress–strain data silica KD brick sample at room temperature.

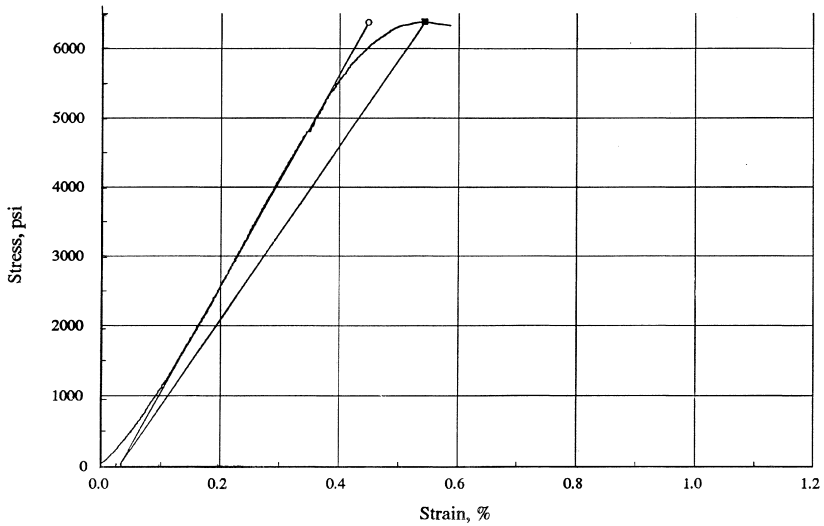


Figure 2 Compressive stress–strain data silica KD brick sample at 500°F.

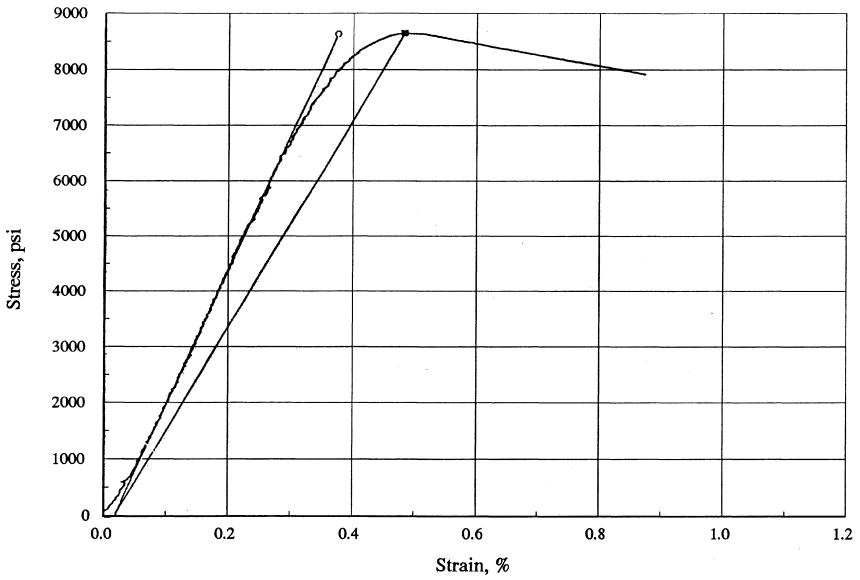


Figure 3 Compressive stress–strain data silica KD brick sample at 1000°F.

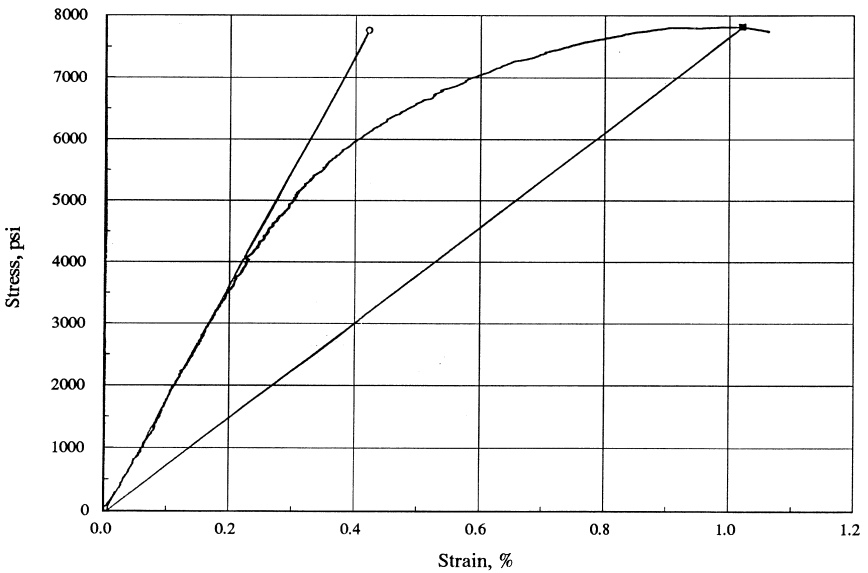


Figure 4 Compressive stress–strain data silica KD brick sample at 1500°F.

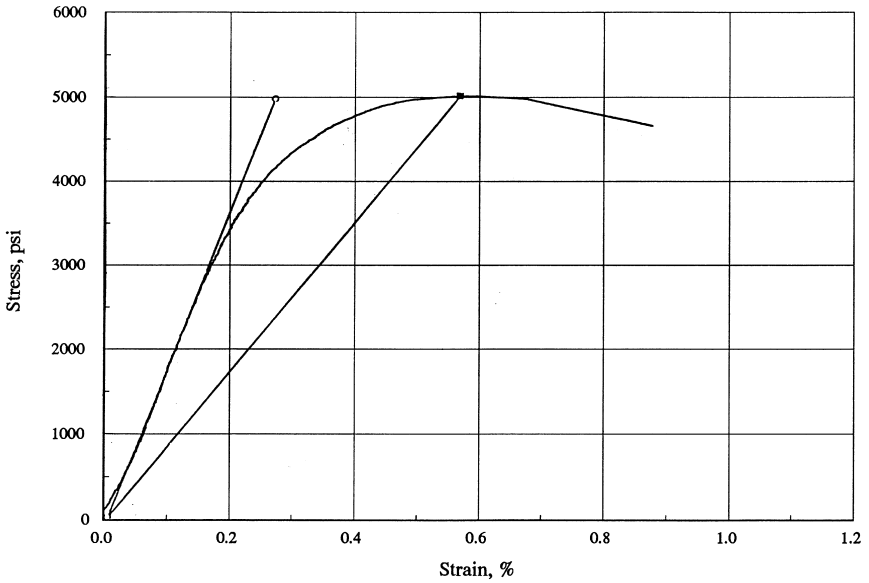


Figure 5 Compressive stress–strain data silica KD brick sample at 2000°F.

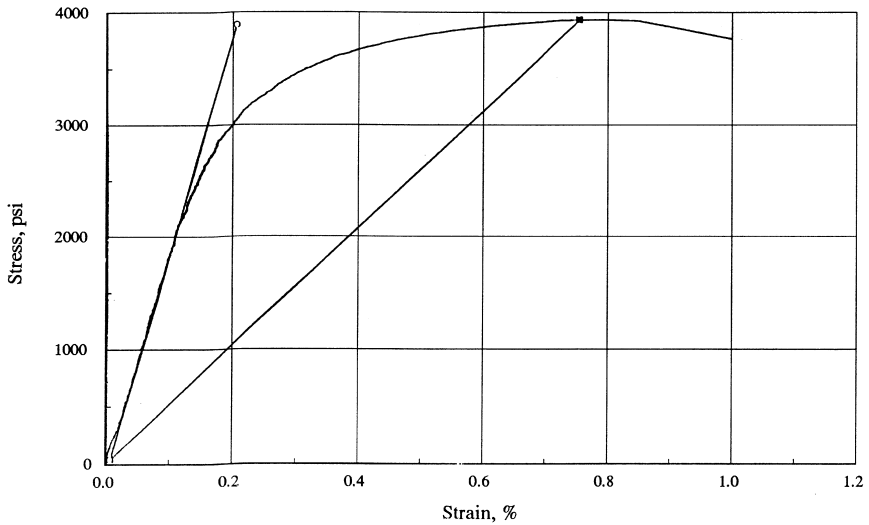


Figure 6 Compressive stress–strain data silica KD brick sample at 2200°F.

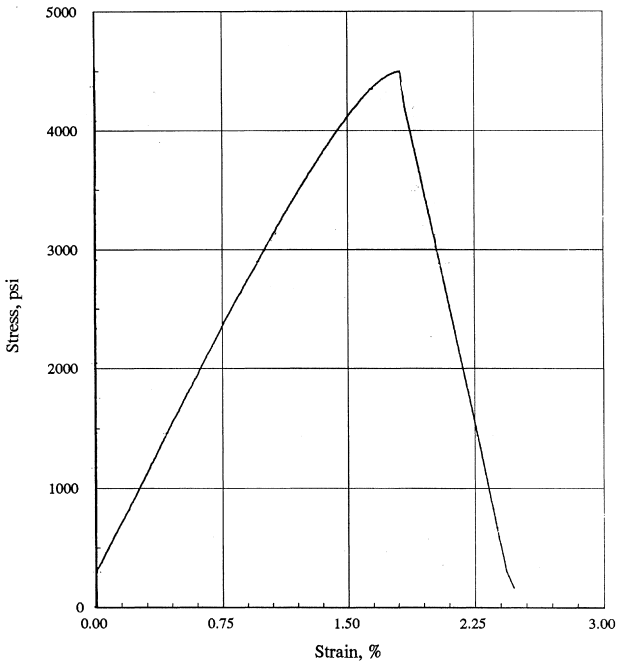


Figure 7 Compressive stress-strain data silica KD brick/mortar sample at room temperature.

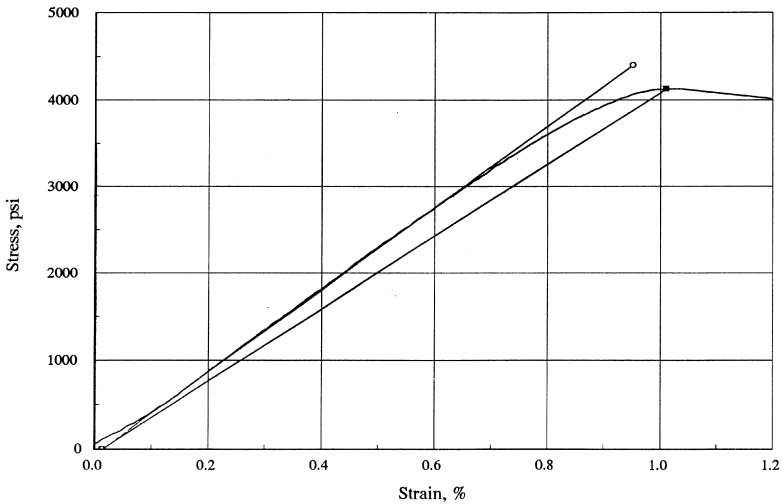


Figure 8 Compressive stress-strain data silica KD brick/mortar sample at 500°F.

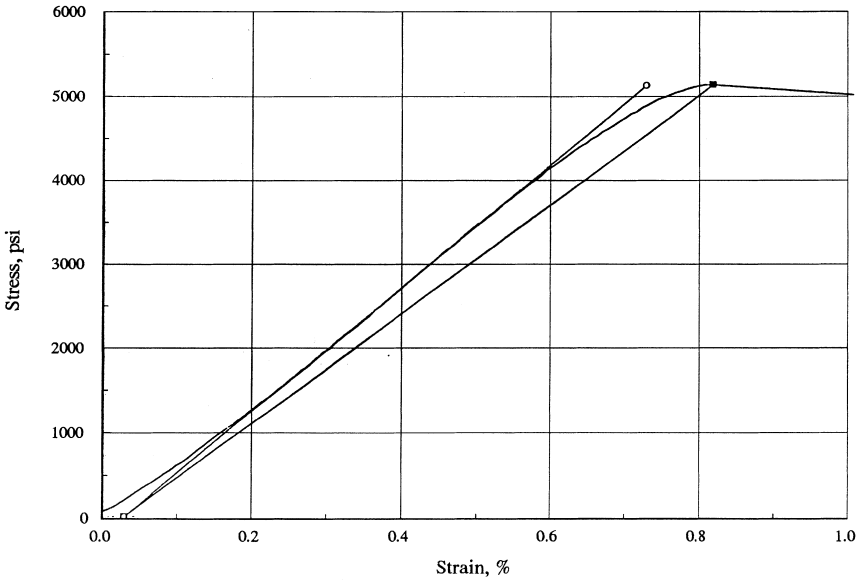


Figure 9 Compressive stress–strain data silica KD brick/mortar sample at 1000°F.

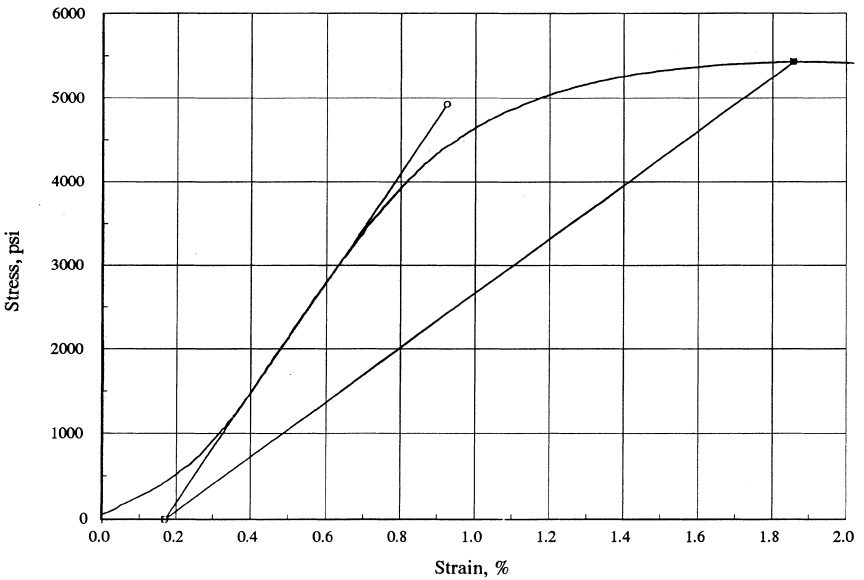


Figure 10 Compressive stress–strain data silica KD brick/mortar sample at 1500°F.

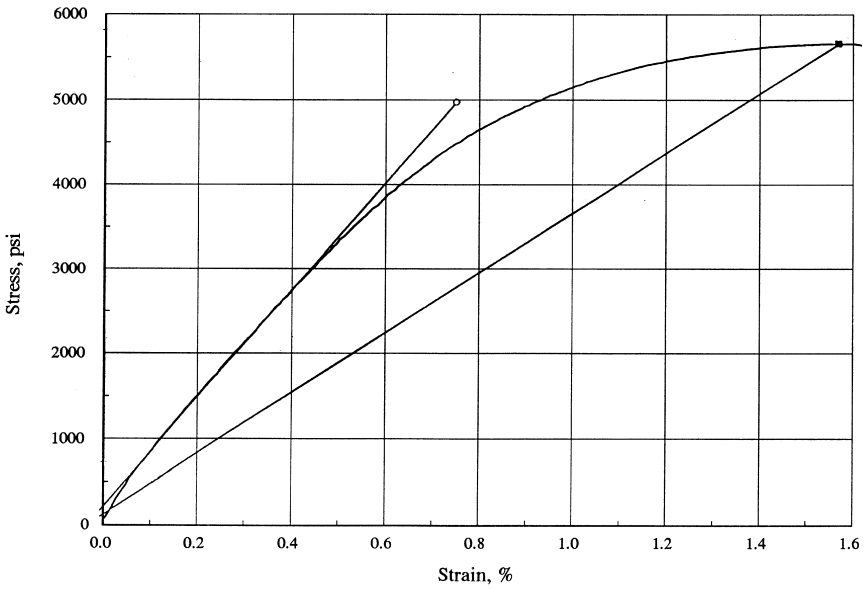


Figure 11 Compressive stress-strain data silica KD brick/mortar sample at 2000°F.

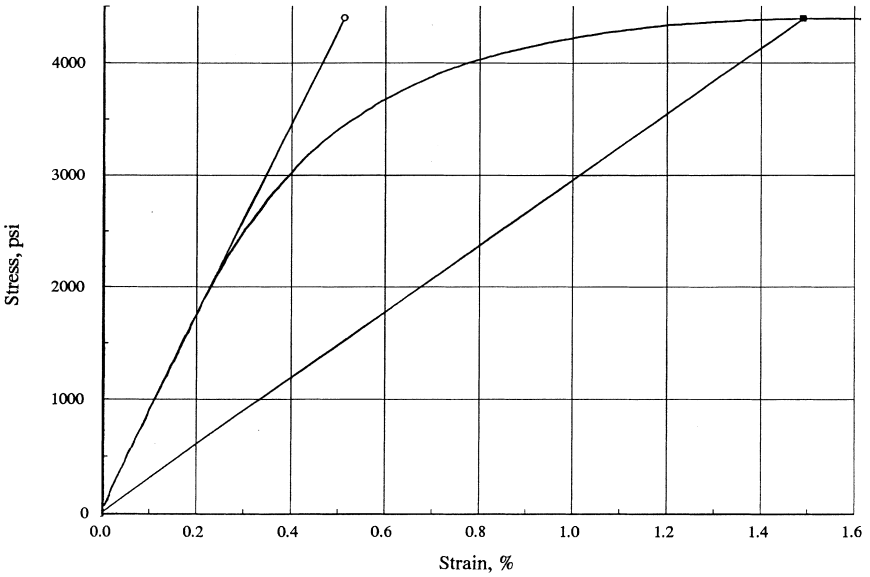


Figure 12 Compressive stress-strain data silica KD brick/mortar sample at 2200°F.

C. Silica KN Brick Sample SCSS Data and Silica KN Brick/Mortar Composite Sample SCSS Data

Figures 13 through 18 show the SCSS data for the KN brick-only samples. Figures 19 through 24 show the SCSS for the KN brick/mortar composite samples. As expected, the lower density of the KN brick results in lower E_O and E_S values.

III. INTERPRETATION OF TEST DATA FOR SILICA KD

The following sections interpret the thermal expansion data and the SCSS data.

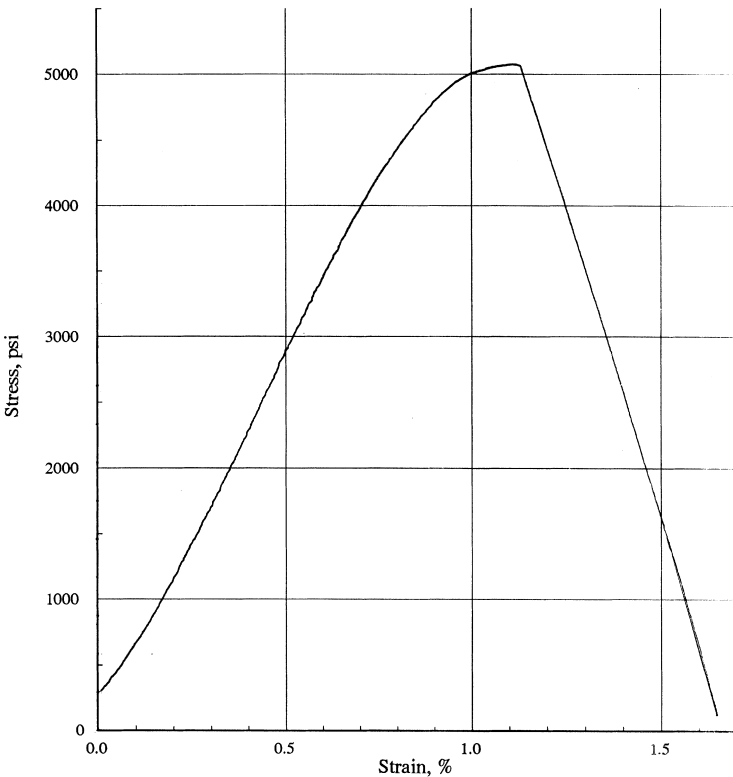


Figure 13 Compressive stress–strain data silica KN brick sample at room temperature.

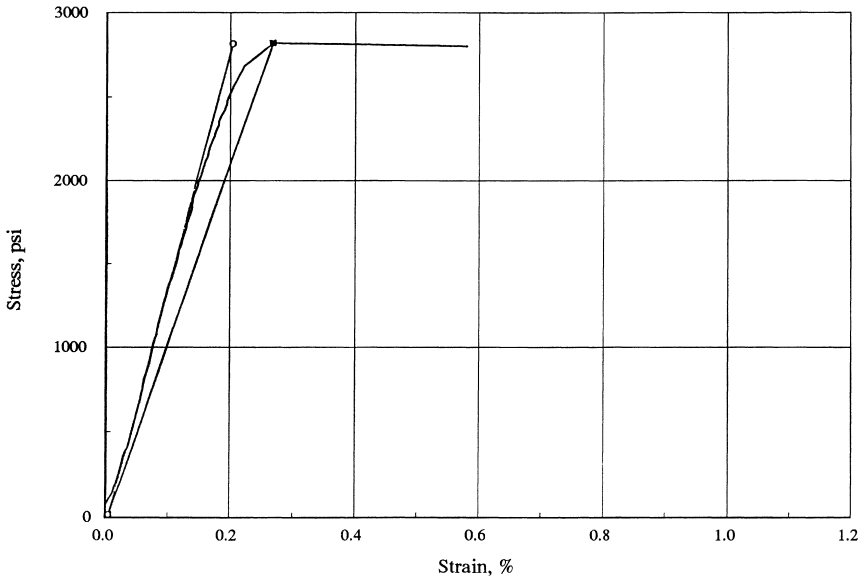


Figure 14 Compressive stress–strain data silica KN brick sample at 500°F.

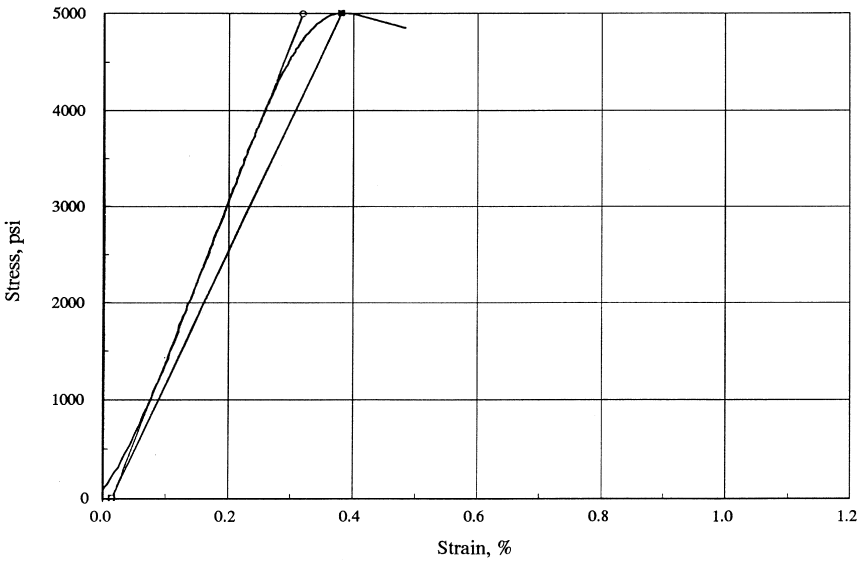


Figure 15 Compressive stress–strain data silica KN brick sample at 1000°F.

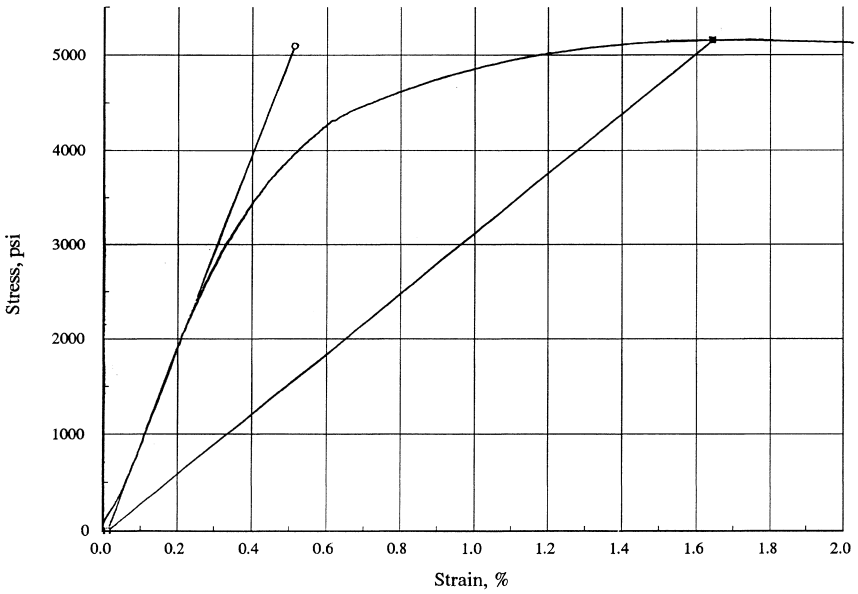


Figure 16 Compressive stress–strain data silica KN brick sample at 1500°F.

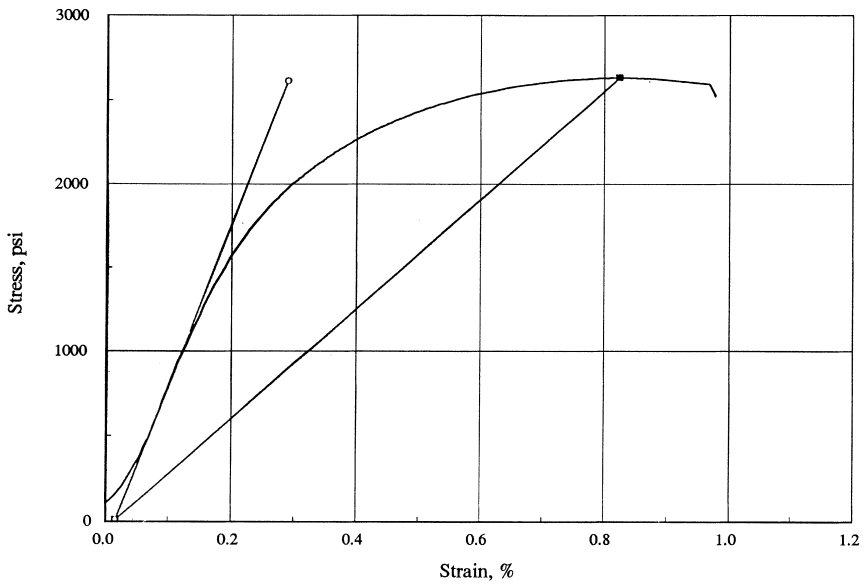


Figure 17 Compressive stress–strain data silica KN brick sample at 2000°F.

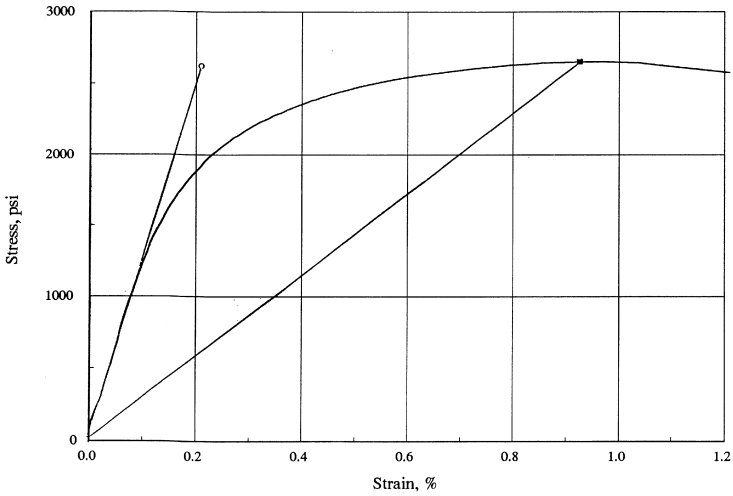


Figure 18 Compressive stress–strain data silica KN brick sample at 2200°F.

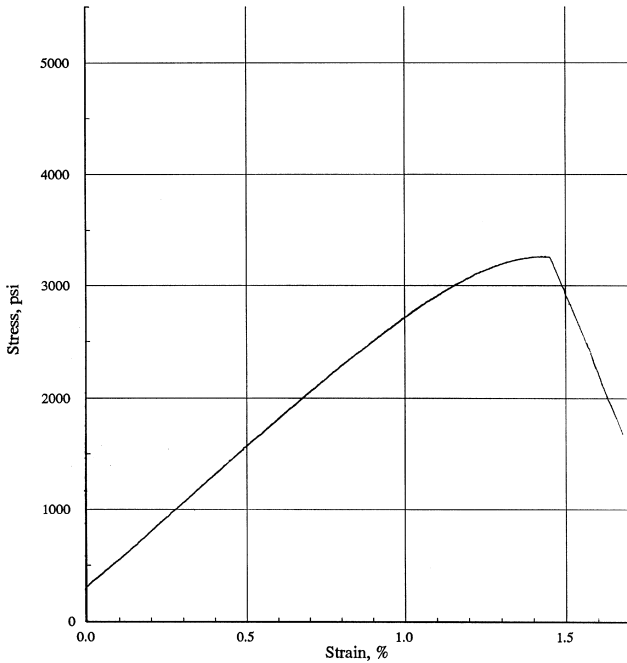


Figure 19 Compressive stress–strain data silica KN brick/mortar sample at room temperature.

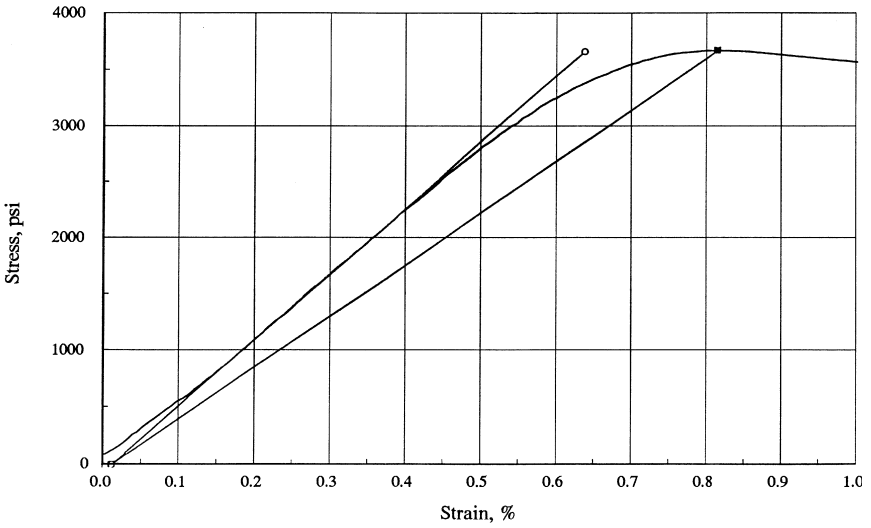


Figure 20 Compressive stress–strain data silica KN brick/mortar sample at 500°F.

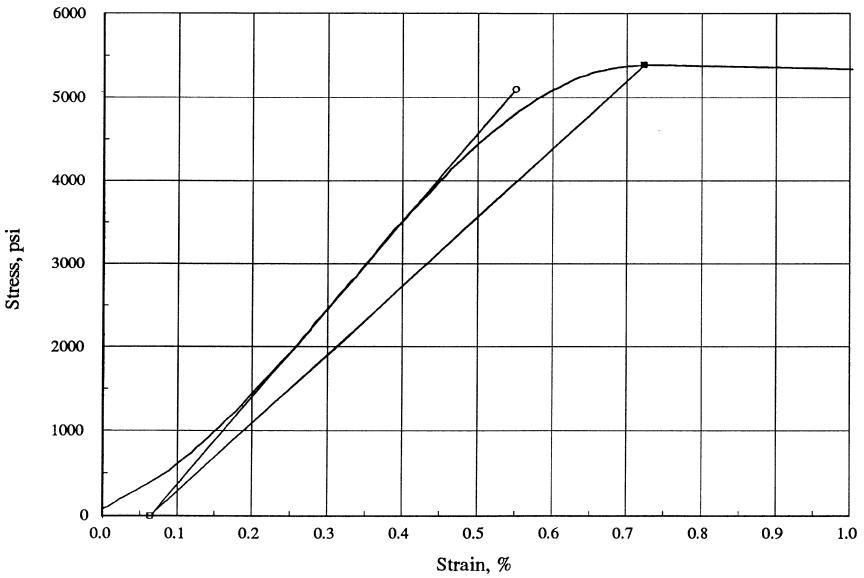


Figure 21 Compressive stress–strain data silica KN brick/mortar sample at 1000°F.

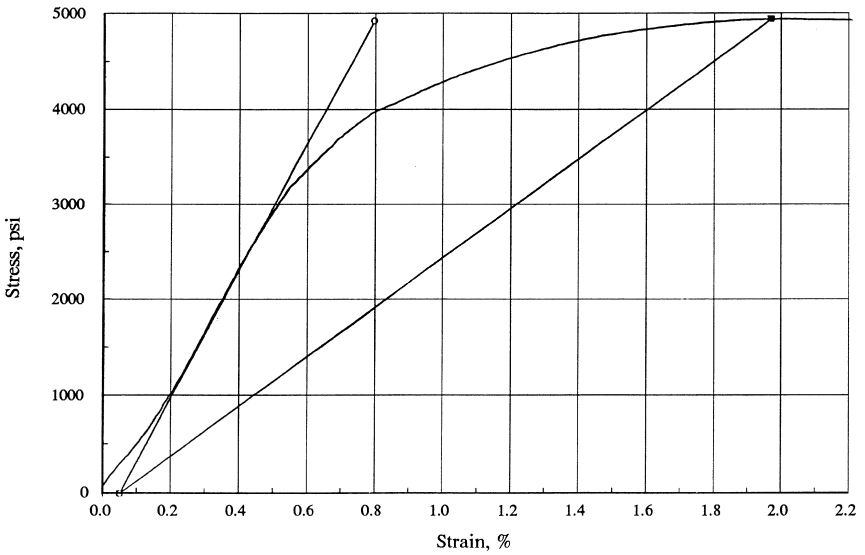


Figure 22 Compressive stress–strain data silica KN brick/mortar sample at 1500°F.

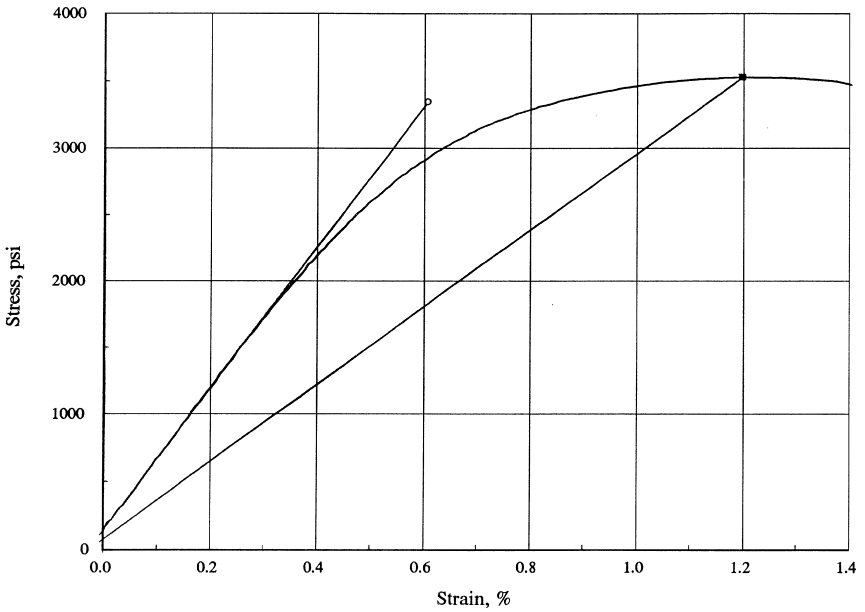


Figure 23 Compressive stress–strain data silica KN brick/mortar sample at 2000°F.

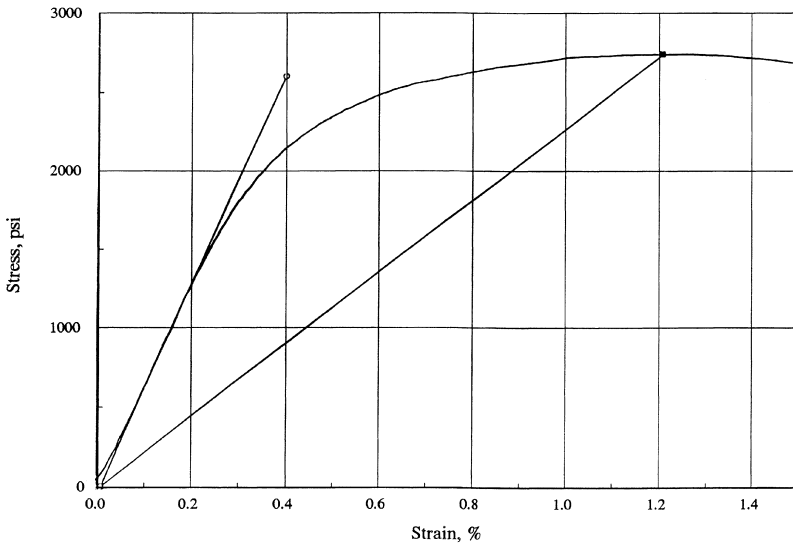


Figure 24 Compressive stress–strain data silica KN brick/mortar sample at 2200°F.

Figure 25 describes the thermal expansion of the silica KD brick-only and the silica KD brick/mortar composite samples. The mortar-only sample was also tested. The brick-only and the brick/mortar composite samples are similar except for temperatures above about 1100°F. The mortar softens considerably, as reflected in the mortar-only sample. Due to the confinement of the mortar within the mortar joint in the brick/mortar composite sample, the mortar maintains reasonable strength. This confirms that the true compressive stress–strain behavior of mortar must be tested with the mortar contained in the mortar joint (2). Containment of the mortar is an important and necessary parameter in testing the thermomechanical behavior of mortar.

Figure 26 describes the coefficient of thermal expansion as a function of temperature for the silica KD brick-only sample, mortar-only sample, and silica KD brick/mortar composite sample. Note the similarity of the brick-only and the brick/mortar composite samples. The confined mortar in the brick/mortar composite sample behaves in a similar manner as the brick-only sample. The mortar-only data curve reflects the importance of providing confinement to the mortar.

Figure 27 shows the silica KD brick-only sample and silica KD brick/mortar composite sample Young’s modulus, E_o , as a function of temperature. The maximum Young’s modulus is at 1000°F. As expected, the brick/mortar composite sample is softer. It should be noted that the brick/mortar composite Young’s

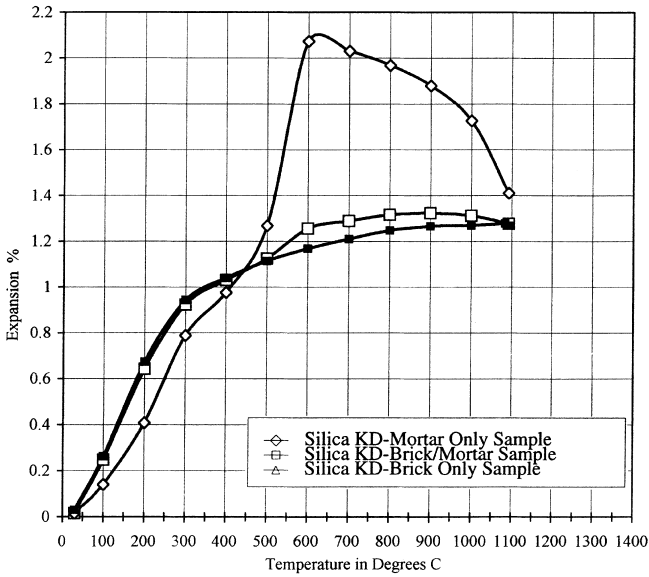


Figure 25 Comparison of expansion of silica KD composite, mortar-only, and brick-only.

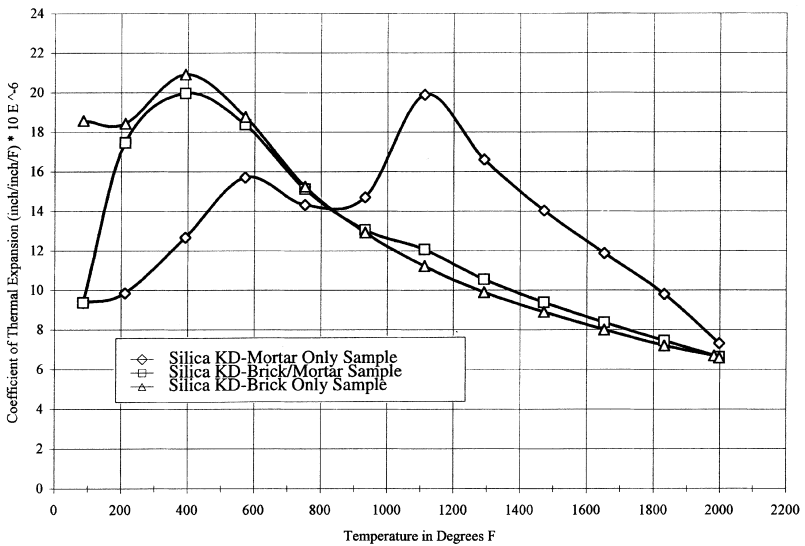


Figure 26 Comparison of coefficient of thermal expansion of silica KD composite, mortar-only, and brick-only.

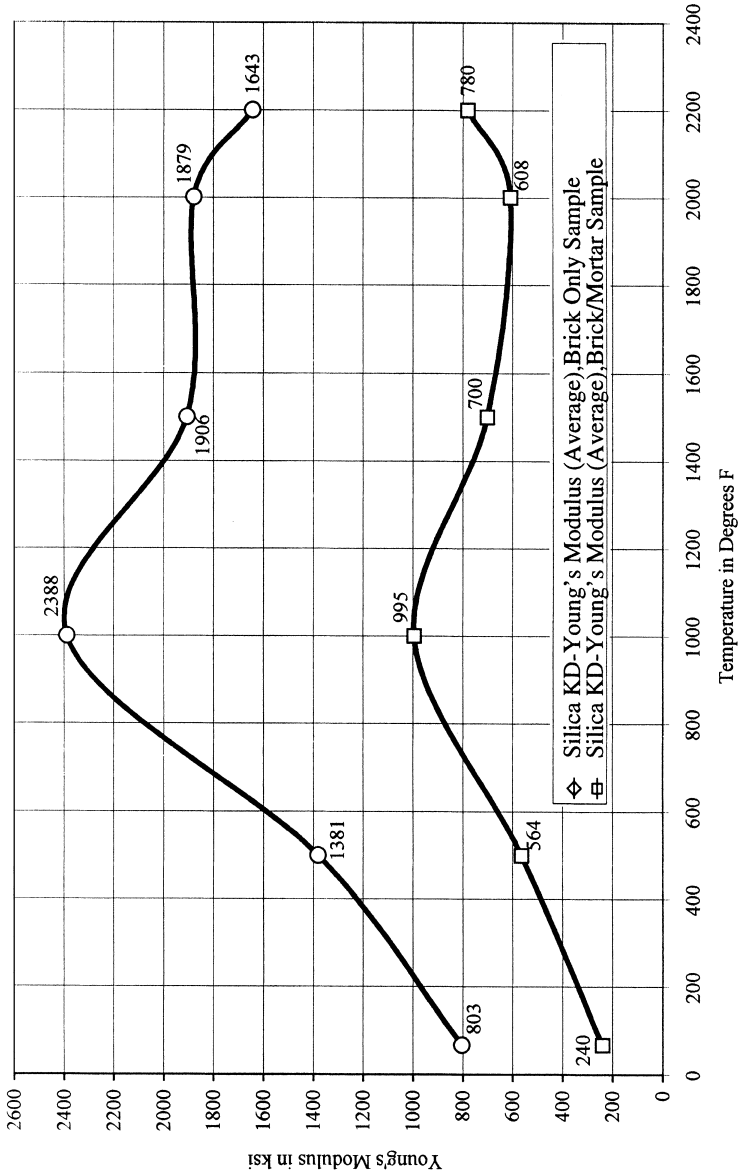


Figure 27 Comparison of Young's modulus—Silica KD bricks only and brick/mortar composites.

modulus is for the given split brick thickness (45 mm) and the mortar joint thickness (5 mm). With a different brick height-to-mortar joint thickness ratio, the brick/mortar composite Young's modulus (E_{mb}) will change. To determine Young's modulus for a different ratio, it is necessary to first determine Young's modulus of the mortar (confined Young's modulus). Equation (1) defines the confined Young's modulus of the mortar.

$$E_m = \frac{t_m(E_{mb})}{E_b} \cdot tm + (E_b - E_{mb})t_b \quad (1)$$

where E_m is the confined Young's modulus of the mortar, t_m is the mortar joint thickness, E_b is the brick Young's modulus, t_b is the height of the split brick, and E_{mb} is Young's modulus of the brick/mortar composite. Rearranging terms in Eq. (1), we can determine the composite Young's modulus for the revised brick height as shown in Eq. (2).

$$E_{mb} = (t_m + t_b)(E_b E_m) / (E_m t_b + E_b t_m) \quad (2)$$

Figure 28 shows the temperature-dependent MOR of the silica KD brick. As with the Young's modulus trend, the greatest MOR values are in the 1000 to 1500°F range.

Figure 29 shows the temperature-dependent crushing strength, S_c of the brick-only and brick/mortar composite samples. The brick-only samples reach maximum crushing strength in the 1500°F range. The brick/mortar composite samples reach maximum crushing strength at about 1000°F.

Figures 30, 31, and 32 show the creep behavior of the brick-only, mortar-only, and brick/mortar composite samples at 816°C (1500°F), 1094°C (2000°F), and 1372°C (2500°F), respectively. At all three temperatures the brick-only and brick/mortar composite samples exhibit insignificant creep. The mortar-only samples (no confinement) exhibit relatively considerable creep response. The creep tests also confirm that unconfined mortar tests do not replicate the true confined behavior of the mortar in the mortar joint.

IV. INTERPRETATION OF TEST DATA FOR SILICA KN

Figures 33 and 34 show the temperature dependent thermal expansion of the silica KN brick-only, mortar-only, and brick/mortar composite samples. The interpretive results are quite similar to the interpretive results of the silica KD tests. These results also show that the mortar-only (unconfined mortar) tests do not reflect the true confined thermomechanical behavior of mortar in mortar joints. Strength patterns as a function of temperature are also similar to the silica KD brick.

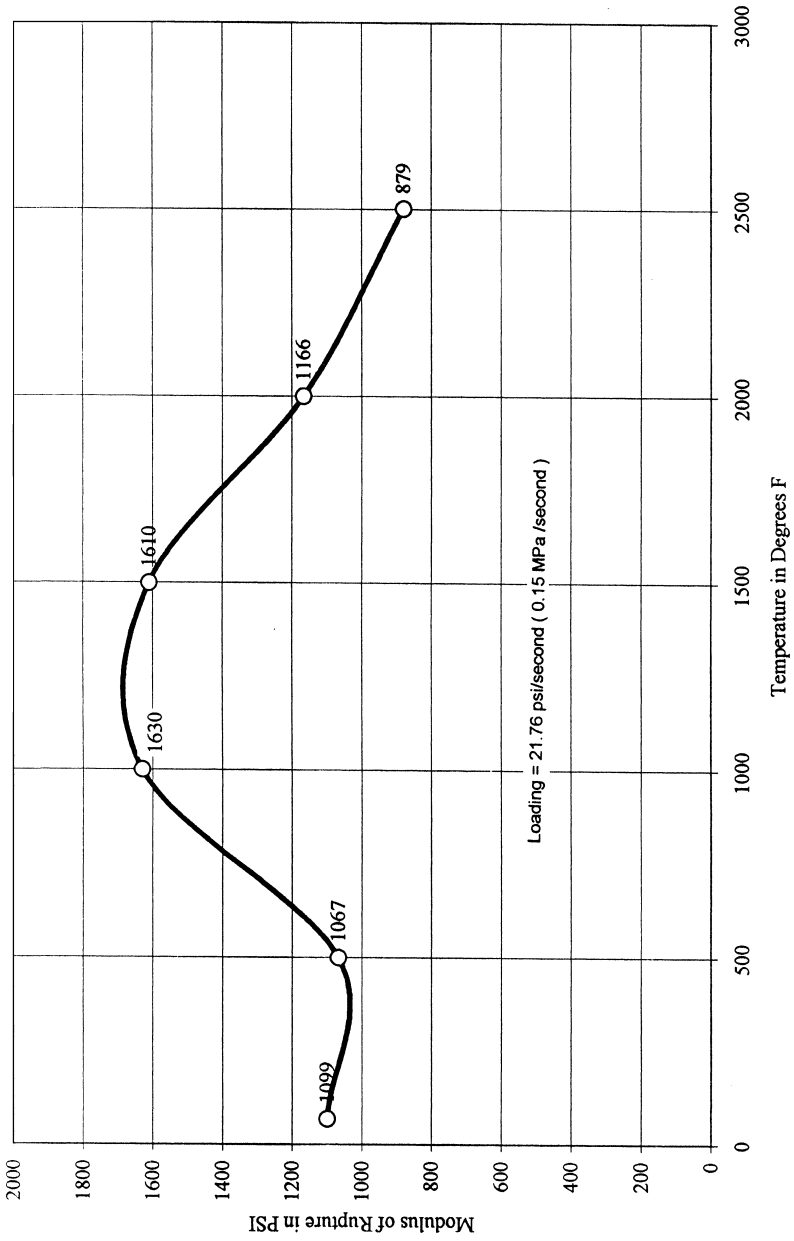


Figure 28 Modulus of rupture—silica KD bricks—average curve.

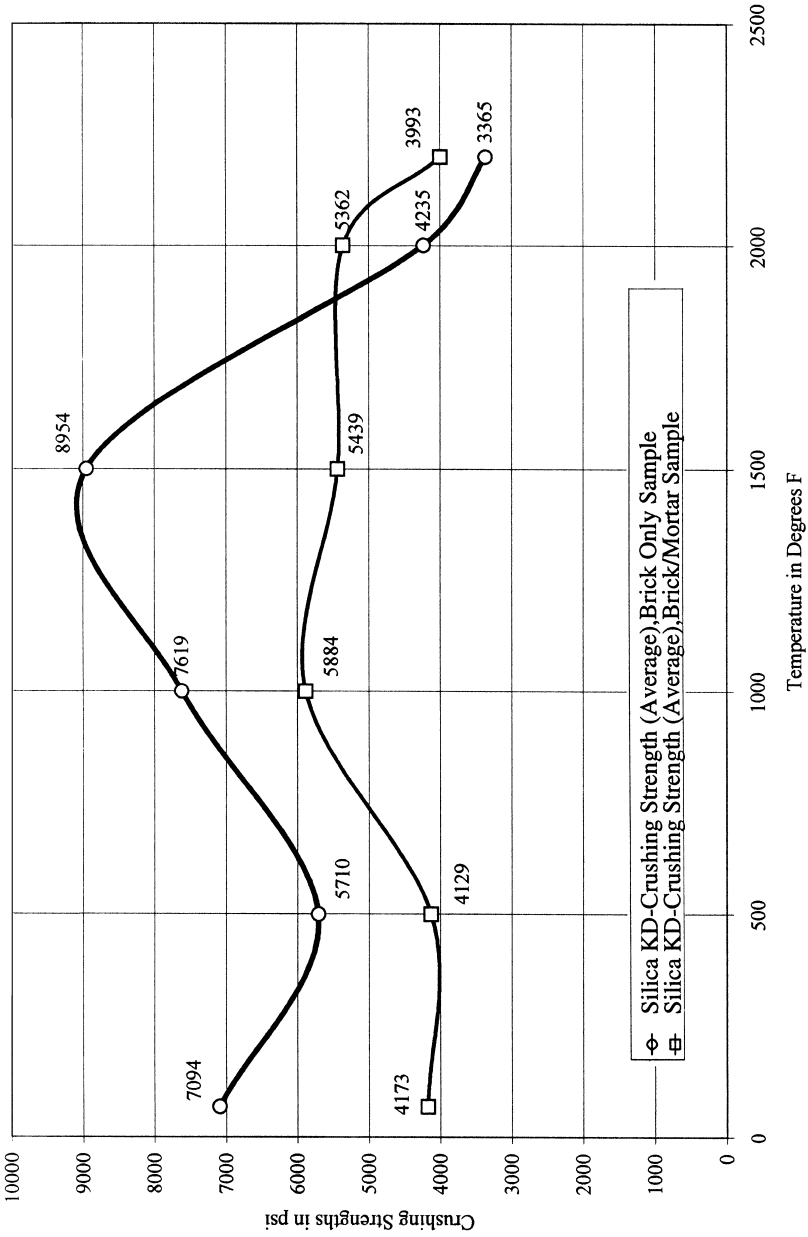


Figure 29 Comparisons of crushing strength of silica KD brick/mortar composite and brick-only.

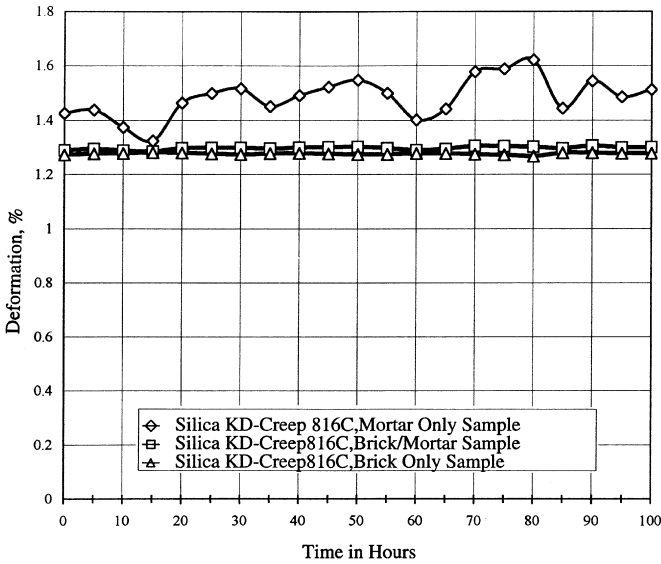


Figure 30 Comparisons of creep curves at 816°C of silica KD composite, mortar-only, and brick-only.

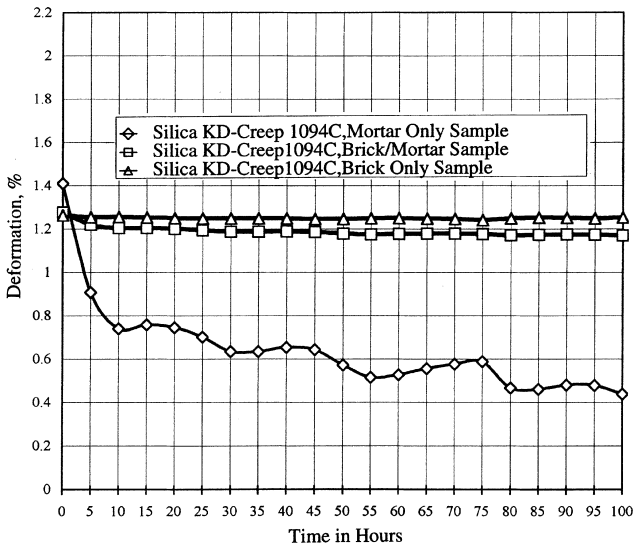


Figure 31 Comparisons of creep curves at 1094°C of silica KD composite, mortar-only, and brick-only.

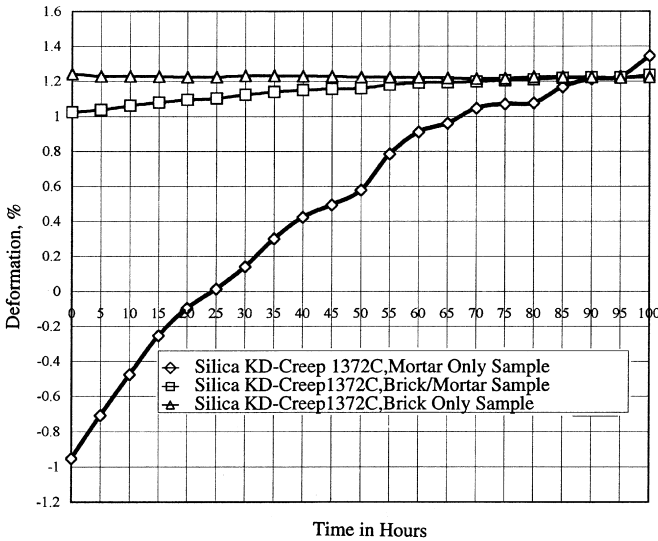


Figure 32 Comparisons of creep curves at 1372°C of silica KD composite, mortar-only, and brick-only.

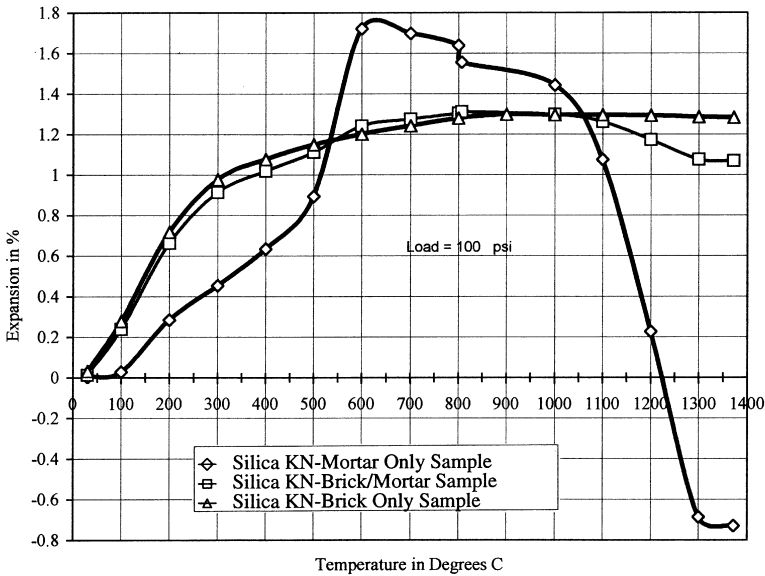


Figure 33 Comparisons of expansion of silica KN composite, mortar-only, and brick-only.

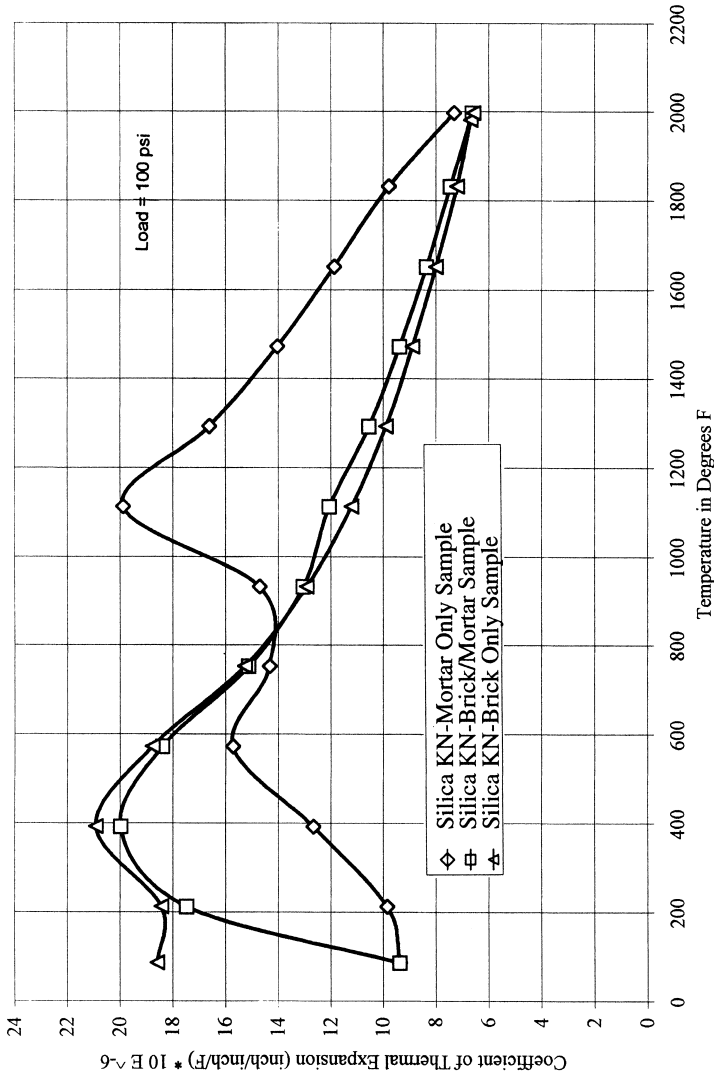
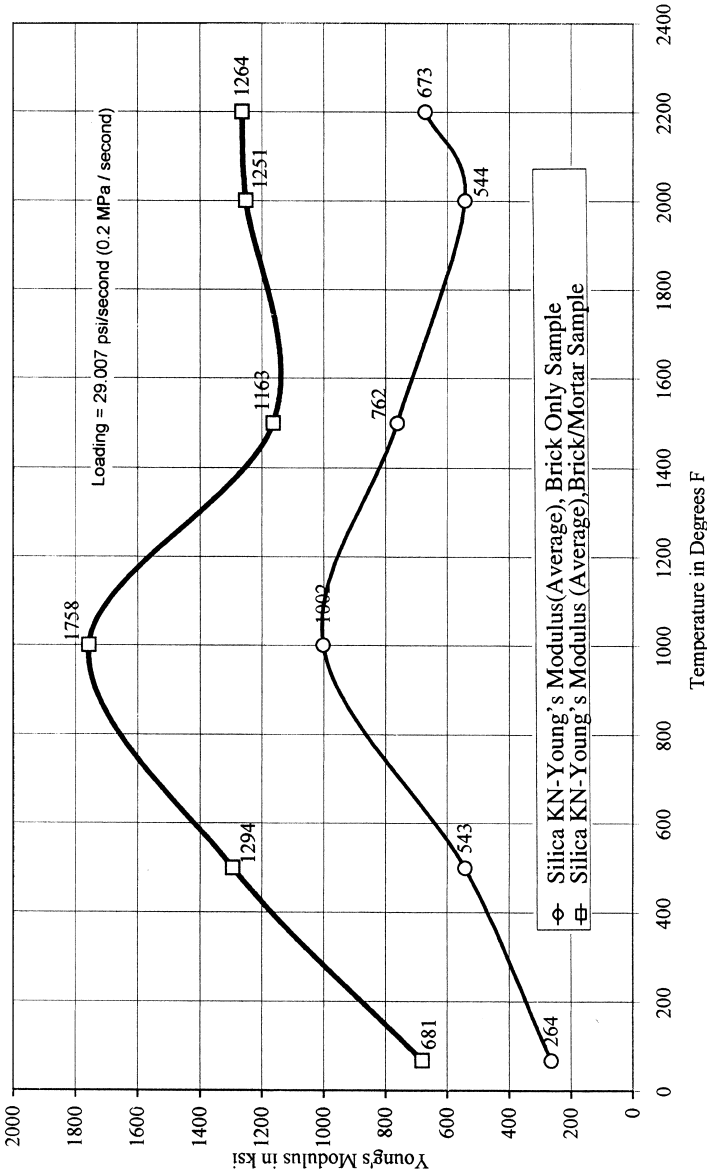


Figure 34 Comparisons of coefficient of thermal expansion of silica KN composite, mortar-only, and brick-only.



NB : Loading = 29,007 psi/second (0.2 MPa / second)

Figure 35 Comparisons of Young's modulus—silica KN bricks only and brick/mortar composites.

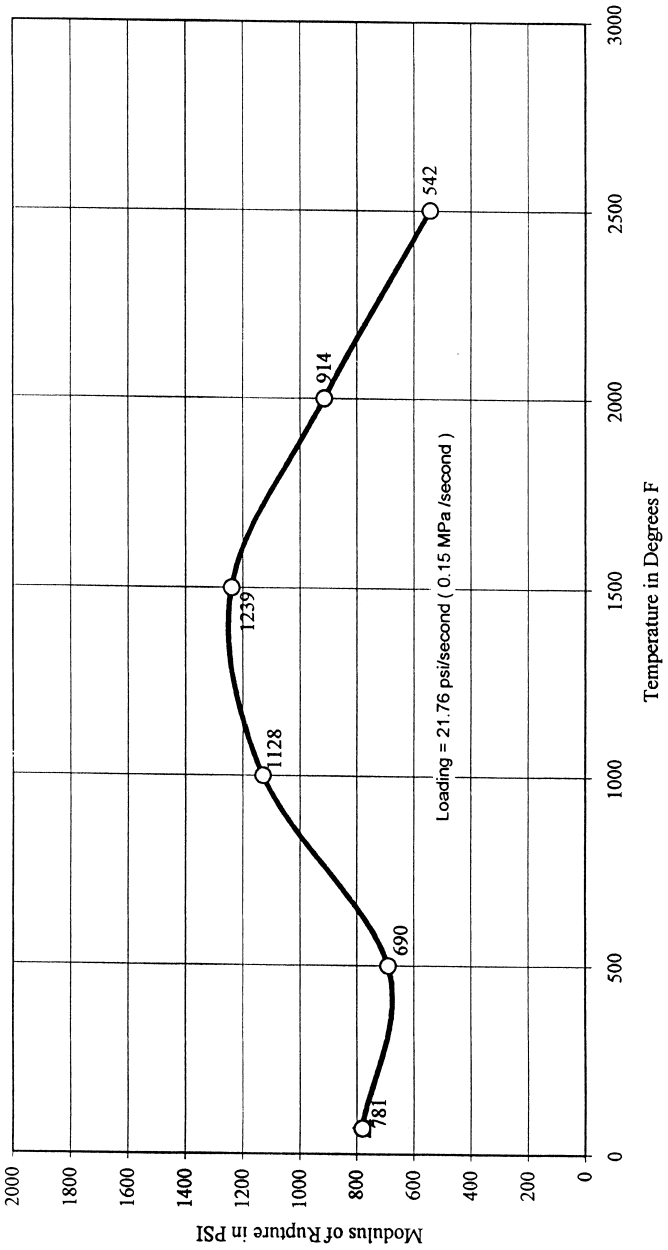


Figure 36 Modulus of rupture—silica KN bricks—average curve.

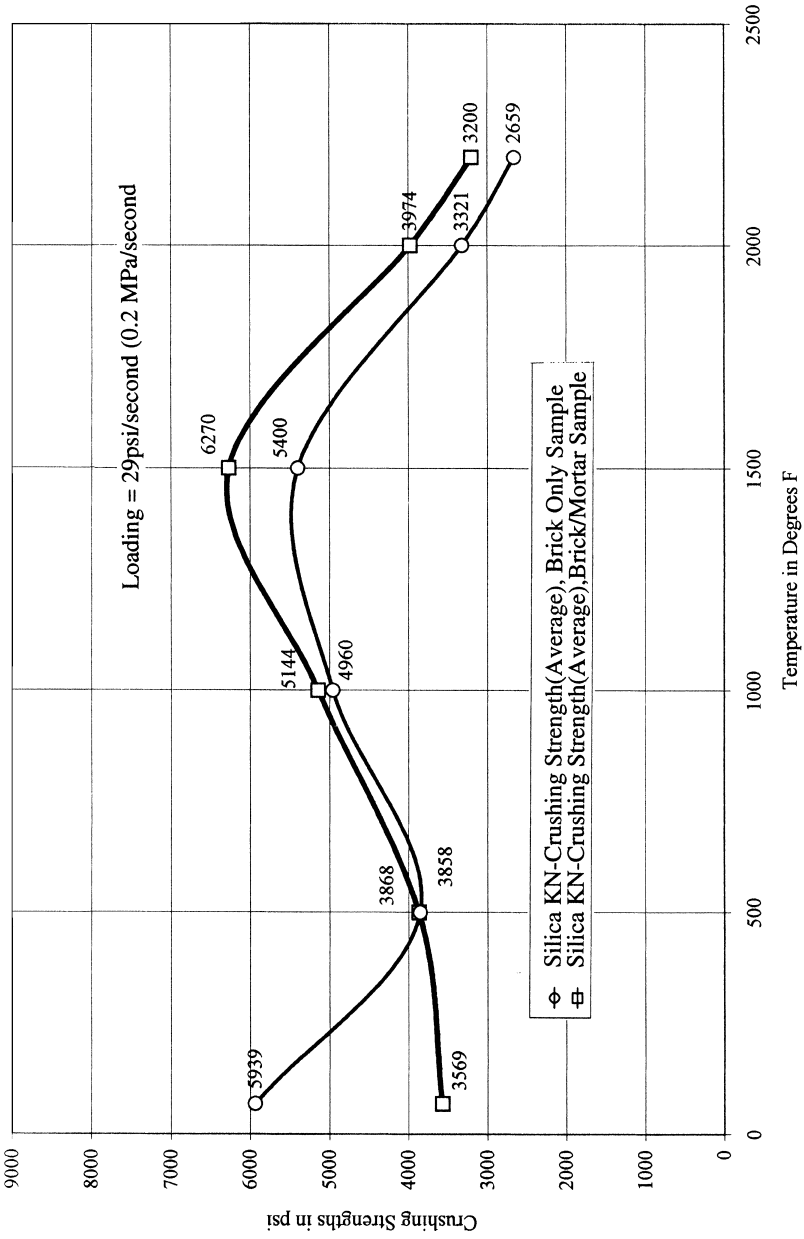


Figure 37 Comparisons of crushing strength of silica KN brick/mortar composite and brick/only.

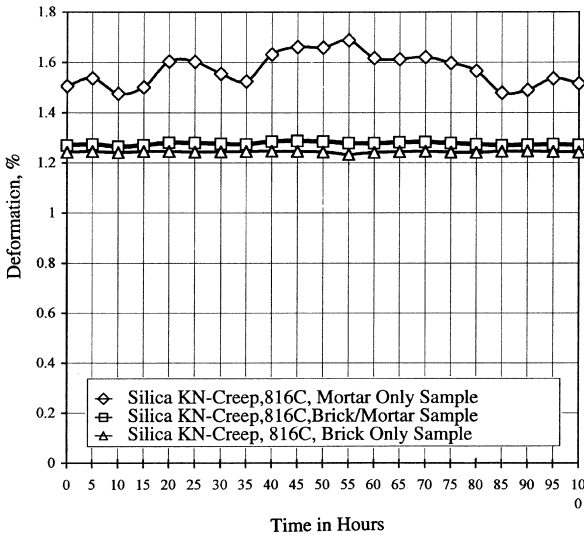


Figure 38 Comparisons of creep curves at 816°C of silica KN composite, mortar-only, and brick-only.

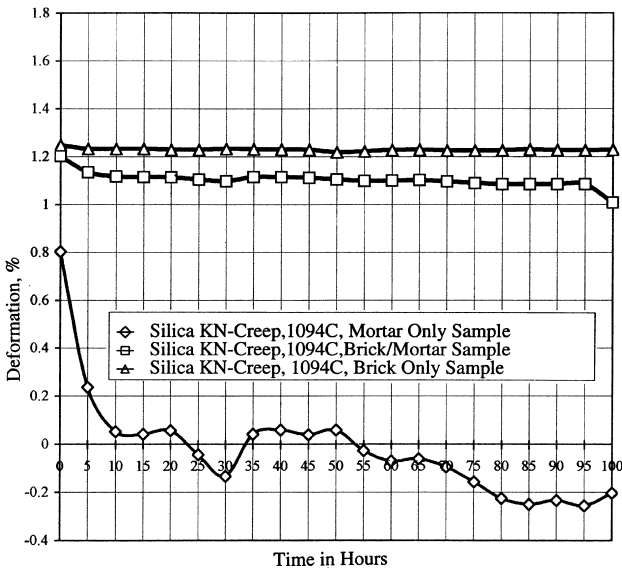


Figure 39 Comparisons of creep curves at 1094°C of silica KN composite, mortar-only, and brick-only.

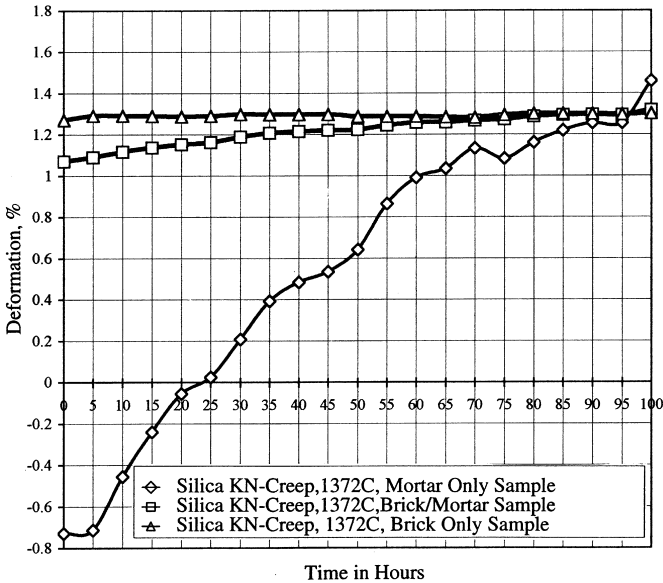


Figure 40 Comparisons of creep curves at 1372°C of silica KN composite, mortar-only, and brick-only.

Figure 35 shows the temperature-dependent MOE of KN silica brick. Note the room temperature MOE is not as high as at the 1000°F temperature. This data is MOE at temperature.

Figure 36 shows the temperature-dependent MOR of KN silica brick.

Figure 37 shows the temperature-dependent crushing strength of KN silica brick.

Figures 38 through 40 show the creep deformations of silica KN composity, mortar-only and brick-only.

V. POISSON’S RATIO OF KD AND KN SILICA BRICK

Figure 41 shows the test results variability in measuring Poisson’s ratio for KD and KN silica brick.

VI. THERMAL CONDUCTIVITY OF SILICA BRICK

Figure 42 is a plot of the thermal conductivity of silica brick. The solid line represents the expected upper bound values (for the higher-density silica brick). The

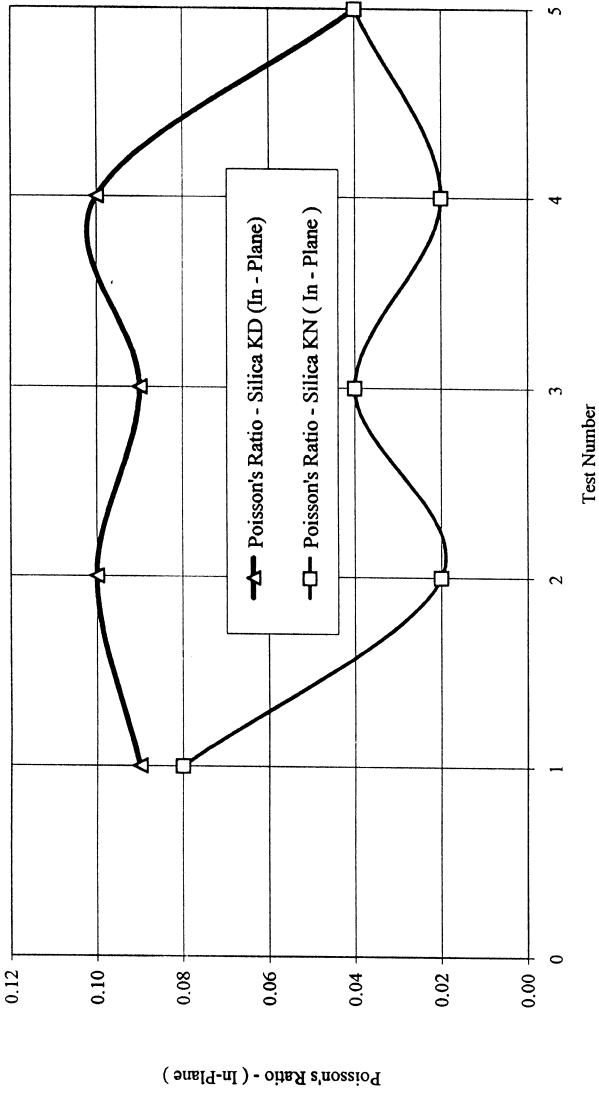


Figure 41 Poisson's ratio of silica KD and silica KN bricks.

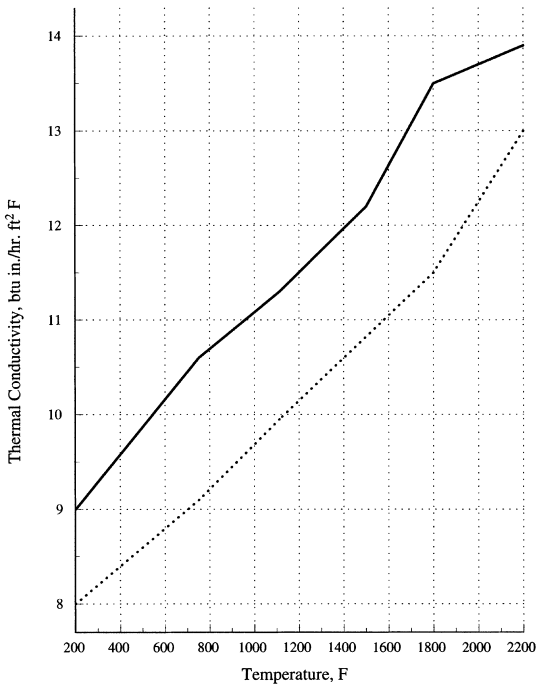


Figure 42 Thermal conductivity of silica brick.

dotted line represents the expected lower bound values (for the lower-density silica brick). These data were not determined by RWTUEV. Because of the variation in silica brick properties from manufacturer to manufacturer, the actual thermal conductivity data should be obtained from the supplier or brick manufacturer.

REFERENCES

- 1999 RUTUV Material Property Test Data, Set A, issue date May 7, 1999; Set B, issue date June 1, 1999; Set C, issue date June 29, 1999; Set D, issue date July 30, 1999.
 Schacht CA. Refractory Linings: Thermomechanical Design and Applications. New York, NY: Marcel Dekker, 1995.

7

Doloma Refractories

Colin Richmond

*LWB Refractories, York, Pennsylvania, U.S.A.**

I. INTRODUCTION: HISTORICAL BACKGROUND

The mineral dolomite is a double carbonate of calcium and magnesium [$\text{CaMg}(\text{CO}_3)_2$]. Dolomite is named after the French geologist Trancrede de Dolomieu, who identified it as a distinct mineral in the late 18th century. The name “dolomite” can refer to both the mineral and the rock contains a large percentage of the mineral. Theoretically, the mineral contains 30.4% CaO (54.3% CaCO_3), 21.7 MgO (45.7% MgCO_3), and 47.9% CO_2 . The formation of dolomite occurs by one of two methods. Primary dolomite has been formed from the direct precipitation from magnesium-rich solutions. Secondary dolomite has formed by impregnation of limestone with Mg-rich brines. The direct precipitation of dolomite occurs rarely under normal conditions so most deposits are thought to be of a secondary origin.

As other carbonate rocks, dolomite deposits are fairly common throughout the world. While dolomite is not as common as calcite (limestone, CaCO_3), it is considerably more abundant than magnesite (MgCO_3). Naturally occurring dolomites usually deviate only slightly from the 1 : 1 chemical ratio of calcium to magnesium. Most deposits occur in sedimentary rock sequences or their metamorphic equivalent, dolomitic marble. The rock dolomite usually contains some impurities that are often associated with accessory minerals. These impurities typically consist of silica, alumina, iron, manganese, sulfur, and phosphorous. Refractory-grade dolomites are usually high purity, which are considered to contain a minimum of 20% MgO (42% MgCO_3) and a maximum of 2.5% impurities (1).

**Current affiliation:* Independent Consultant, Ripon, North Yorkshire, England.

The use of dolomite as a refractory was first started in 1878 when dolomite rock was used as the linings in Open Hearths or Thomas converters (2). Dolomite stone was bonded with a sodium silicate binder and calcined in situ in the converter. As the increase for “basic” refined steel increased, the requirement to achieve better phosphorous and sulfur control was recognized and the use of the consumable dolomite hearth was replaced with linings of tarbonded doloma. In these early processes, much of the lining was intended to be consumed as part of the process; during these initial developments, purity of the doloma was not a consideration. In fact, the doloma used at this time was very impure, as calcining technology could not achieve adequate density or hydration resistance without high levels of iron oxide and silica. Even at these levels of impurities, oil or tar as binders was required to avoid hydration.

The increased usage of lime as a flux in steel making led to the replacement of doloma with magnesia, because poorly calcined magnesia was both more refractory- and more hydration-resistant than the low-purity doloma. Additionally, the doloma was no longer needed as a lime source for steel production. At this time, doloma was mainly used as a low-purity repair material for magnesia hearths.

During the 1930s, tar-bonded blocks comprising low-purity doloma were produced, and attempts to produce doloma of higher purity were also tried. Fired doloma bricks “stabilized” with silica were produced in the United Kingdom during this time, but with the technology available at the time it was still not possible to produce high-purity doloma. Rapid developments occurred during World War II with regards to doloma technology in Europe due to its availability and lower production cost as compared to magnesia. During the early 1950s, the introduction of the LD refining process came with medium- and high-purity tar-bonded and direct-bonded doloma bricks being used for LD converters and electric furnaces. The primary competition with doloma was magnesia. Improvements in the technology to make higher-quality magnesia grain and the moderately basic steel-making processes led to a decrease in doloma usage. The development of magnesia carbon refractories has resulted in all but eliminating the use of doloma in primary steel making (BOF, QBOP, BOS processes).

In the early 1960s, fired dolomite bricks had been developed for use in the burning zone of rotary cement kilns. Dolomite is chemically compatible with the cement-making process and readily acquires a protective coating with the clinker in the burning zone. The need for chrome-free linings in the cement-making process added impetus to penetration of dolomite refractories in this application.

II. HIGH-PURITY DOLOMITE FOR THE PRODUCTION OF DOLOMA REFRACTORIES

Despite the widespread occurrence of dolomite, there are only a limited number of dolomite deposits in the world that have satisfactory uniformity, purity, and

calcining behavior to be processed economically into a high-purity raw material suitable for the production of doloma refractories. The term “doloma” refers to the calcined dolomite. Refractory-grade doloma typically contains less than 2.5% impurities and greater than 97.5% CaO + MgO. Most high-purity dolomite deposits are difficult to calcine and sinter to high density and usually require special methods to yield an acceptable refractory-grade doloma.

Currently, high-purity doloma is produced in several European countries, Canada, and the United States, based on natural dolomite; “synthetic” dolomite is only produced in Japan and China. There are approximately 10 producers worldwide of all types of doloma.

Silica, iron oxide, and alumina are the most common impurities in high-purity doloma. Since the impurity levels are low and the melting points of the liquid phases are so high, the dolomite can be difficult to calcine. Temperatures in excess of 1850°C are usually required in order to achieve satisfactory density and hydration resistance. The microstructure of a typical high-purity doloma as shown in Fig. 1 consists of magnesia crystallites (3–5 microns in size) embedded in a matrix of lime.

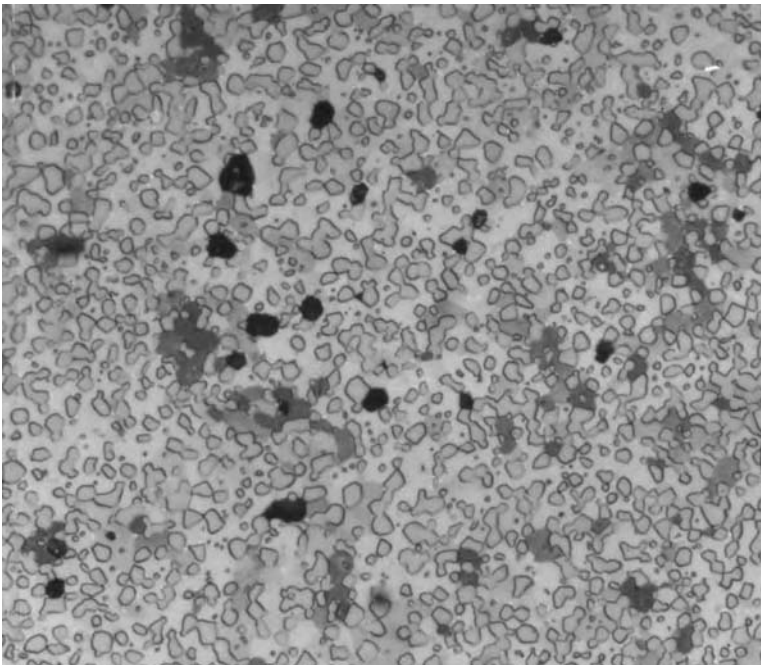


Figure 1 Microstructure of high-purity doloma grain.

The typical chemistry of dolomites used for doloma production are shown in Table 1.

The chemistry of Dolomite 2 corresponds to the upper limit of impurities that would be suitable for the production of doloma for refractory brick purposes. This dolomite would have to be dead-burned in such a way that there would be no significant pickup of impurities during the process (i.e., requires high-purity fuels).

High-purity doloma, which is produced today, is equal to or more refractory than magnesia products of up to 95% purity that are used for steel-making applications. Figure 2, the CaO–MgO phase diagram (3), indicates the range of composition within which most refractory-grade doloma falls; the lowest melting point in this system is 2370°C. While the presence of impurities will lower the initial melting, it is much higher than required for most steel-making applications. Table 2 shows the chemical and physical properties of a typical high-purity doloma material.

III. PRODUCTION OF DOLOMA FROM DOLOMITE

The carbonate (dolomite) is converted to the oxide (doloma) and sintered to the required density in either a rotary kiln or a shaft kiln operating at 1850°C or greater. There are basically two different production routes:

1. Single-pass process. In this process the dolomite rock is crushed to a suitable size for direct feed to the rotary or shaft kiln, with the calcination and densification being done in one single pass through the kiln. Only a few dolomites are suitable to be processed in this way.
2. Double-pass process. The dolomite is first crushed to kiln feed sizing and then passed through a kiln to complete the calcination stage. The resulting oxide (dolime) is then ground and pelletized to feed into a shaft or rotary kiln operating at 1850°C, or greater, to densify the doloma to required density. This double firing process is obviously more energy-consuming than the single-pass route.

Table 1 Chemistry of Typical Dolomite Raw Materials

Chemical analysis		
	Dolomite 1	Dolomite 2
CaCO ₃	55.00	54.30
MgCO ₃	44.50	44.60
SiO ₂	0.20	0.30
Al ₂ O ₃	0.10	0.15
Fe ₂ O ₃	0.30	0.55

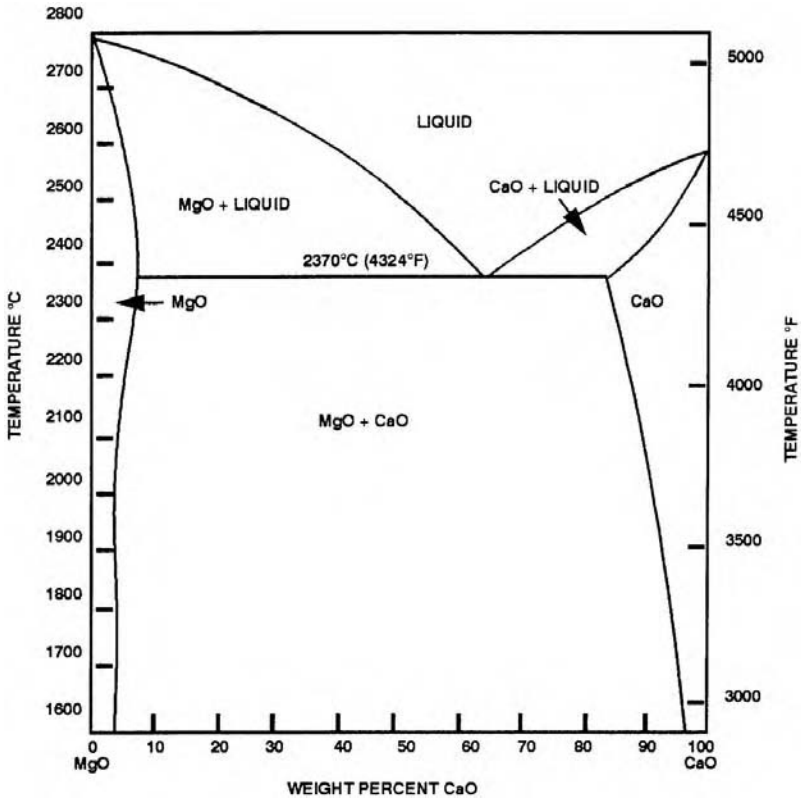


Figure 2 CaO–MgO phase diagram. (From Ref. 3.)

Table 2 Chemical and Physical Properties of a Typical High-Purity Doloma

Chemical analysis	
CaO	57.0%
MgO	41.0%
SiO ₂	0.70%
Al ₂ O ₃	0.50%
Fe ₂ O ₃	0.80%
Liquid phases present at 1600°C	2–3%
Physical properties	
Bulk density	3.25 g/cm ³
Open porosity	4%
Hydration resistance (ASTM C-492)	Less than 5%

IV. CHARACTERISTICS OF REFRACTORIES BASED ON HIGH-PURITY DOLOMA

In the last 20 years there has been a significant growth in the use of high-purity doloma refractories for steel applications and the burning and transition zones of kilns. In steel making this growth is primarily due to an increase in basic steel refining to produce higher-quality steel with precise metallurgical control. Doloma refractories are well suited for usage in many of these steel applications due to their high refractoriness and compatibility with basic slags.

In the case of cement, one of the big advantages of doloma-based refractories is to provide chrome-free lining configurations.

A. Metallurgical Considerations for Using Doloma

Doloma is an excellent refractory for use in many steel-making applications since it is thermodynamically stable to slags and metal. The two major constituents of doloma, CaO and MgO, are among the more stable of the refractory oxides. This can be seen by examination of the free energies of formation of various refractory oxides shown in Table 3. A doloma refractory containing less than 1% SiO₂ is far more thermodynamically stable than high alumina or even magnesite chrome refractories. Fruehan (4) shows that in ladle furnace applications involving aluminum killed steel, the Al in solution reduces the SiO₂ in the alumina brick according to the following equation:



Table 3 Free Energies of Formation for Various Refractory Oxides

	$\Delta G@1600^\circ C$ (Kcal/mole O ₂)
$2Ca + O_2 = 2CaO$	-205
$4/3Al + O_2 = 2/3Al_2O_3$	-175
$2Mg + O_2 = 2MgO$	-170
$Si + O_2 = SiO_2$	-140
$4/3Cr + O_2 = 2/3Cr_2O_3$	-110

Source: Ref. 5.

This reaction causes aluminum fade in the metal and can be a source of inclusions in the steel. The reduction of SiO₂ by the aluminum in the steel also raises the oxygen potential in the steel, which in turn inhibits desulfurization. The basic desulfurization reaction is given by



Therefore, the lower the oxygen, the better the desulfurization. Numerous studies (6–9) have shown the benefits that doloma-based refractories offer regarding desulfurization efficiency. Additionally, for desulfurization and inclusion removal, a fluid, highly basic slag is required. The optimum slag composition for these purposes is shown in Table 4. Doloma refractories are very compatible with the same slag practice that optimizes the refining processes used to produce clean and low-sulfur steel.

B. Slag Resistance

The good slag-resistant characteristics of doloma are a result of the presence of free lime not found in other refractories of lower basicity. In contact with slags not fully saturated with lime, a dense layer of recrystallized lime and di-calcium silicates forms on the hot face of the brick, limiting further slag penetration. Basically, the slag’s reaction with the lime stops penetration, slowing down overall wear. However, slags deficient in lime but high in R₂O₃ oxides can be quite aggressive to a doloma brick. This is due to the formation of calcium aluminates and/or ferrites that have melting points significantly below 1600°C (10).

C. Hydration Susceptibility

In any discussion of doloma refractories, one must consider the potential for hydration. The free lime portion of the doloma can react with atmospheric moisture, which can cause the material to powder and crumble. The degree of

Table 4 Optimum Slag Composition for Desulfurization and Inclusion Removal

Chemical composition	
CaO	60%
Al ₂ O ₃	25%
MgO	5–10%
SiO ₂	5–10%

hydration under set conditions of time, temperature, and relative humidity is dependent upon the amount of lime and impurities contained in the material, and the density of the grain achieved during the dead-burning process. The degradation of doloma grains by hydration in storage occurs in essentially two ways: (1) a formation of $\text{Ca}(\text{OH})_2$ on the surface of the grains and (2) the breaking apart of the grains into smaller particles. The main difficulties caused by doloma's pronounced tendency to hydrate are in the refractory manufacturing process and not in the products. By careful control at critical stages of manufacture and speedy use of the freshly processed doloma, the manufacturing difficulties can be minimized. A comparison of the hydration tendencies of natural doloma, synthetic doloma, and high-purity magnesite are shown in Table 5.

As can be seen, natural dolomite has a much better resistance to hydration than synthetic dolomite and in some cases not much worse than some high-purity magnesite.

Today, with modern packaging materials and techniques together with other means of protecting products, it is possible to store fired doloma products for up to two years and pitch or resin-bonded products for more than six months.

V. DOLOMA-BASED REFRACTORY PRODUCTS

A. Direct-Bonded Doloma Bricks (Fired)

Direct-bonded bricks are produced by pressing a combination of doloma grain fractions with an organic binder. Direct bonding between the doloma grains is achieved by firing the brick through a tunnel kiln. The organic binder provides green strength to the brick for handling and in the kiln, until the ceramic bond is developed. After firing in the tunnel kiln, the organic binder is completely burned out of the brick.

It is the lime phase of the doloma grain that provides the direct bond and is responsible for the chemical behavior of the brick. The microstructure of a fired doloma brick shows a high degree of direct bond, as Figure 3 shows.

Table 5 Hydration Resistance of Basic Refractory Material
(Based on ASTM C-492)

Material	Hydration resistance (ASTM C-492)
Natural doloma	3–5%
Synthetic doloma	25–30%
HP magnesite	0.3–2%

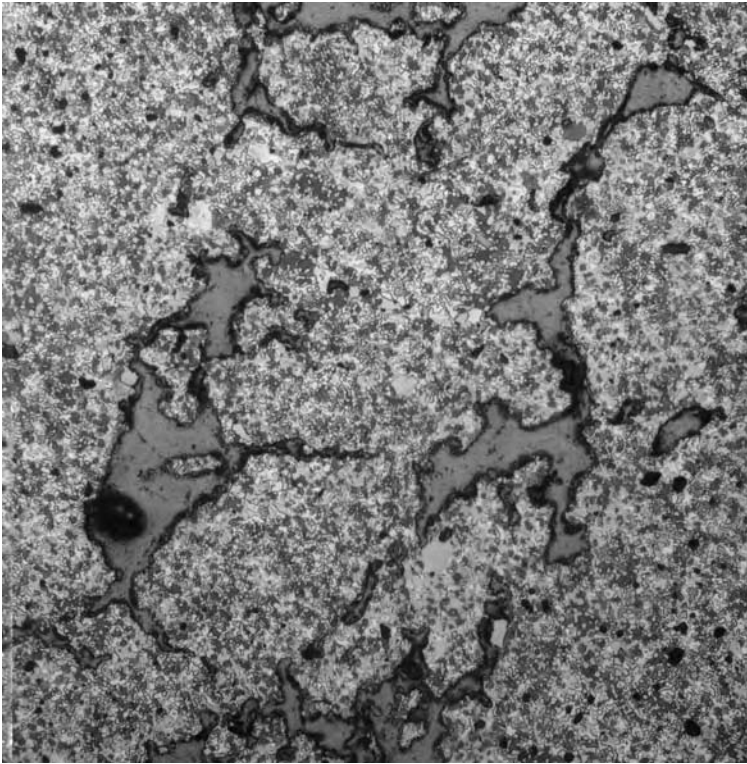


Figure 3 Microstructure of fired doloma showing direct bonding between doloma grains.

In the past there has been some reluctance to using direct-bonded bricks for steel-making applications because of their susceptibility to thermal shock. Significant improvement in the thermal shock resistance of the brick was accomplished through the addition of small amounts of zirconia. The enhancement is attributed to microcracking caused by the expansile formation of calcium zirconate as a result of reaction between the lime in the doloma and the zirconia. The microcracking is clearly illustrated in the microstructure shown in Figure 4.

Further improvements to the slag resistance of both direct-bonded and carbon-bonded doloma bricks have been made through the addition of high-purity magnesia. Doloma bricks that have been enriched with MgO are typically used in areas of ladles and AOD vessels where higher slag resistance is required. The chemical and physical properties of the direct-bonded bricks used in steel making are shown in Table 6.

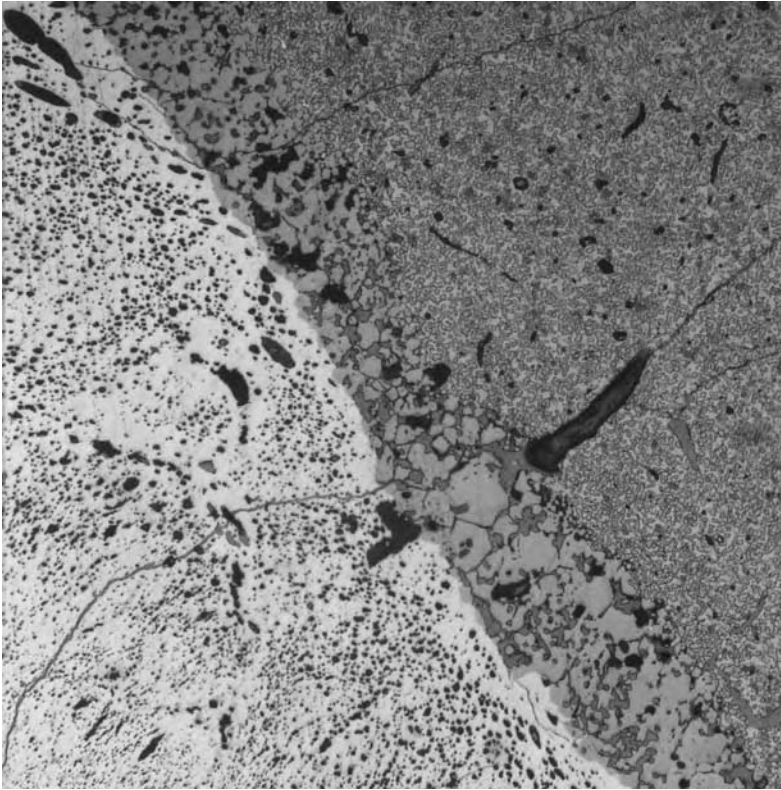


Figure 4 Microstructure of fired dolomite with zirconia addition showing microcracking associated with zirconia in the dolomite matrix.

A similar range of doloma-based products exists for cement applications, with a high proportion containing zirconia additions (up to 2% ZrO_2) because of the high risk of failure due to thermal shock in the operation. For the burning zone the products are based on doloma, but for the conditions in the transition zone MgO-enriched grades are required (60–80% MgO).

As indicated previously, fired dolomite brick has been used in cement kiln burning zones since the early 1960s, and in order to improve product performance, formulations have been developed incorporating ZrO_2 additions to improve the resistance to thermal shock. The use of zirconia for this purpose was first developed for cement kiln brick.

Formulations have been developed using magnesite additions to dolomite to extend its use into the transition zone of the cement rotary kiln. The use of the zirconia technology is also incorporated into these formulations.

Table 6 Chemical and Physical Properties for Various Direct-Bonded Doloma Brick

Chemical composition	Doloma			Doloma/MgO		
CaO	57.2	57.2	56.6	40.0	38.3	30.5
MgO	40.5	40.5	40.0	58.0	58.3	67.0
SiO ₂	0.9	0.9	0.8	0.8	0.8	0.7
Fe ₂ O ₃	0.9	0.9	0.9	0.7	0.6	0.3
Al ₂ O ₃	0.5	0.5	0.5	0.5	0.5	0.5
ZrO ₂	—	—	1.0	—	0.9	1.0
Physical properties						
Bulk density (g/cc)	2.80	3.00	2.85	2.95	2.95	3.05
Modulus of rupture (N/mm ²)	12.4	13.8	11.0	13.8	12.4	12.4
Hot modulus of rupture @ 1400°C (N/mm ²)	2.8	4.1	3.1	4.8	4.8	4.8
Porosity (%)	15.0	11.0	13.8	12.0	12.0	11.5
Application	Ladle	AOD	Ladle	Ladle AOD	Ladle AOD	Ladle AOD

B. Carbon-Bonded Doloma Bricks

Carbon-bonded doloma bricks can be subdivided according to the type of carbon precursor used. In the case of pitch-bonded bricks, the coal tar or petroleum pitch used to bond the doloma aggregate is a thermoplastic binder. Doloma bricks using pitch as the binder are typically tempered at 250°C to 3000°C to partially polymerize the binder. Resin-bonded doloma bricks are produced much like pitch-bonded bricks except a thermosetting phenolic resin is used instead of pitch. The important differences associated with the different binders are that the pitch-bonded graphitizes at higher temperatures, giving better oxidation resistance than the “glassy carbon” from the resin-bonded, but the latter exhibits much higher strength values and lower fume emissions during preheating. Carbon-bonded doloma bricks are used only in steel-making applications.

Doloma bricks with higher carbon contents are also available for steel-making applications. The higher carbon qualities are generally resin-bonded and contain a graphite addition. These bricks are used in impact pads, slag lines, and other high wear areas in steel-making vessels and ladles. The chemical and physical properties of the various resin-bonded doloma bricks are shown in Table 7.

Table 7 Chemical and Physical Properties of Various Resin-Bonded Doloma Brick

Chemical composition	Doloma	Doloma/C	Doloma/MgO/C
CaO	57.6	57.6	39.7
MgO	40.0	40.0	58.2
SiO ₂	0.8	0.8	0.8
Fe ₂ O ₃	0.9	0.9	0.7
Al ₂ O ₃	0.6	0.6	0.6
Carbon	3.0	6.0	6.0
Physical properties			
Bulk density (g/cc)	2.96	2.95	2.96
Cured modulus of rupture (N/mm ²)	22.4	15.5	17.2
Hot modulus of rupture (N/mm ²) @1400°C	4.8	4.8	5.2
Coked porosity (%)	12.8	12.0	12.0
Application	Ladle AOD	Ladle AOD	Ladle AOD

Carbon-bonded doloma refractories offer many advantages as linings in ladle furnace applications; however, there are factors to consider when using doloma.

Like all basic refractories, doloma bricks' thermal conductivity is higher than high-alumina brick. The consequence of this feature is that doloma linings are prone to develop open joints and to metal penetration.

For insulation and protection against possible breakouts, a high-quality safety lining is required in ladle furnaces. A high-alumina safety lining, either brick or monolithic (dry-vibrating) with a high resistance to carbon monoxide, is recommended since for most of the brick, sensitivity to sudden changes in temperature can still lead to spalling. This requires that preheating equipment is used for the initial burn-in and temperature maintenance during use.

A variety of ladle refining processes are used today. Examples of these are ASEA/SKF, Daido VAD, and VOD. Each of these ladle refining processes has its own chemical and mechanical wear mechanisms that are a characteristic of that process. In addition, variations in the operations and types of grades produced by a shop will affect the wear of the refractory lining. This requires that zoning by quality and lining thickness is done to optimize the refractory life for a particular process and shop. Lining designs combining doloma with magnesia carbon and high alumina, as backing linings, are also utilized.

C. Doloma-Based Monolithic Refractories for Steel Applications

A variety of doloma-based monolithic materials are designed to be used in conjunction with brick, and also monolithic lining materials or for maintaining and patching vessel linings.

Doloma monolithic materials used in conjunction with doloma and magnesia-based bricks for the construction of ladles, AODs and other steel-making vessels are typically classified as rams, mortars, plastics, and seals. These materials are able to withstand high temperatures, basic slags, and thermal shock. These brick accessories are based on combinations of doloma and magnesia aggregate depending on the application, and an organic thermo-setting binder system. Since the products are water-free, they can be safely used with hydratable brick.

Doloma-based monolithic lining materials are typically dry, free-flowing materials designed to be vibrated, poured, and/or tamped into place. Carefully controlled aggregate gradings are utilized so that a maximum installed density is achieved. Once installed, these materials form the working lining on which steel and slag are in direct contact. These types of materials are based on a combination of doloma and/or magnesia aggregates and various organic and inorganic binder systems. The main areas of use of these products are in tundish lining and electric arc furnace hearths.

Monolithic materials based on doloma that are used for lining maintenance are typically classified as gunning materials and/or hot patching products. Doloma-based gunning materials are applied when the furnace, ladle, etc. is hot to minimize the potential of hydration. Hot patching materials based on doloma, magnesia, and organic resin systems are also utilized for maintenance of electric furnace hearths, BOF vessels, and ladles.

D. New Developments in Doloma-Shaped Refractories

1. Introduction

Recent developments in doloma-based refractories have been based on their anticlogging characteristics and the potential for cleaner steels.

Steelmakers producing aluminum killed steels typically encounter alumina clogging in their continuous casting refractories. Alumina buildup can occur in the tundish nozzle, tundish slide gate refractory bore, submerged entry shroud (SES), and/or submerged entry nozzle (SEN). The former is typically associated with facilities that use tube changing devices. Other alloy additives to steel such as Ti and rare earth metals (Ce, La) can enhance alumina buildup or result in the deposition of other materials (titanium nitride, rare earth oxides). This is particularly important with Ti-containing steels, as the tiny (1–10 μm) Al_2O_3 inclusions

act as nuclei for other solubility or oxidation products. The ability for heterogeneous nucleation increases both the rate and extent of precipitation. This can result in certain stainless grades and ultralow carbon steel grades (11–14) to have a higher tendency to clog during casting. Alumina clogging can reduce the service life of the refractories, reduce casting productivity, and negatively affect the steel quality.

One method to reduce or eliminate alumina buildup on the refractory surface is to suppress the ability for the alumina to adhere to the refractory. Numerous reports have shown that lime-based refractories can reduce the tendency for buildup. The primary mechanism is that the alumina inclusions react with the lime and form low melting calcium aluminates that do not adhere to the refractory surface.

In the 1990s, trials of doloma-based refractories in the continuous casting of steel were started. It was felt that the high lime content (57%) of the doloma refractory would make it very effective in the prevention of alumina buildup during the continuous casting of aluminum killed carbon and stainless steels. Doloma graphite SENs and ceramic bonded doloma tundish nozzles have both been developed.

Doloma Tundish Nozzle. When aluminum killed steels are cast, the upper tundish nozzle is prone to clogging. Alumina inclusions in the molten steel deposit on the nozzle bore and restrict steel flow from the tundish. At this point the nozzle can be physically reamed open with a rod; however, this practice has an adverse effect on the steel quality, so generally the tundish is replaced by a new one.

Argon purging of the upper tundish nozzle is common when aluminum killed steels are cast. This practice is effective in reducing the rate of alumina buildup on the nozzle bore, but it does not prevent it. Clogging of the upper nozzle limits tundish life in some steel plants.

Doloma-based upper tundish nozzles, without argon purging, were developed in an effort to prevent clogging due to alumina buildup. The properties of the doloma nozzle are shown in Table 8. The doloma nozzles are based on

Table 8 Typical Analysis of a Fired Doloma Nozzle

Chemical analysis	MgO	CaO	SiO ₂	Al ₂ O ₃	Fe ₂ O ₃	ZrO ₂
(%)	38.9	55.9	0.9	0.6	0.9	2.8
Physical properties						
Bulk density (g/cc)	2.95					
Porosity (%)	14.0					

CaO and MgO with low levels of impurities (Fe_2O_3 , Al_2O_3 , and SiO_2). The nozzles are fired to high temperatures in order to develop a ceramic bond and have good erosion resistance. A ZrO_2 addition is made to the nozzle formulation to enhance thermal shock resistance.

There are two key features that make doloma a good candidate to prevent alumina clogging. One is the high level of free lime (57%) that can react with alumina inclusions, and the second is that the lime phase is continuous and readily available to react with these inclusions.

Results in practice have confirmed this theoretical potential of doloma to prevent clogging of nozzles in the tundish.

Doloma Graphite SENs. Doloma graphite (DG) pouring shrouds were developed in order to reduce and/or eliminate the tendency for alumina deposition in the SEN or SES. The DG tubes have been used primarily for casting stainless steels prone to alumina clogging and aluminum killed carbon steels that are also prone to this problem. Alumina graphite (AG) are typically used in these applications; however, alumina deposition is usually the limiting factor for their performance. Properties for several DG materials are shown as compared to a typical AG material in Table 9.

These products are exposed to extreme thermal shock conditions in use, and it has been shown (15) that doloma-based products can be produced to have extremely high resistance to thermal shock (as measured by R_{ST} values), higher even than the alumina-graphite application standard. In the case of doloma graphite products, the high resistance to thermal shock is most likely related to the presence of microvoids observed around the doloma grains in the microstructure. These microvoids develop during the manufacturing process

Table 9 Physical and Chemical Properties of DG Compared to AG

	DG-1	DG-2	AG
Chemical analysis (%)			
MgO	22.0	24.0	—
CaO	33.0	36.0	—
Al_2O_3	0.6	0.7	62
SiO_2	—	—	3.0
ZrO_2	—	—	4.0
C + SiC	40	35	24
Bulk density (g/cc)	2.26	2.34	2.23
Apparent porosity (%)	14.0	15.0	12.0
CCS (MPa)	15.9	14.5	32.0

and probably act in the same way as in other materials (e.g., magnesite-chrome and doloma-zirconia refractories).

The significance of the microvoids observed in doloma graphite may be exploited if similar structures can be developed in other types of refractory products.

VI. SUMMARY

Doloma-based refractories have been applied to the continuous caster to prevent alumina clogging when casting aluminum killed steel grades. Tundish nozzles based on doloma have been used at BOF shops that cast a variety of aluminum killed steel grades. It was found that the sulfur content of the steel was critical with maintaining the clogging resistance of the doloma nozzles.

The doloma nozzles have prevented alumina buildup and eliminated the use of argon in the tundish nozzle.

Doloma graphite SENs have been used by stainless steel producers to cast Ti modified and rare earth (Ce) stabilized stainless steels. The majority of these steel grades were 400 series. These grades were successfully cast without calcium treatment.

REFERENCES

- Hopkins D. Dolomitel. *Ceramic Bulletin* 1994; 74(6):95–96.
- Chesters JH. *Refractories: Production and Properties*. London, UK: The Iron and Steel Institute, 1973:177–207.
- Levin EM, Robins CR, McMurdie HF. *Phase Diagrams for Ceramists*. Columbus, Ohio: American Ceramic Society, 1964:102.
- Fruehan RJ. Physical chemistry and process dynamics or reactions in ladle metallurgy 1. *Jom-J Met* 1985; March:50–54.
- McGannon HE, et al. *The Making, Shaping and Treating of Steel*. 9th ed. Pittsburgh, PA: U.S. Steel, 1971:297–302.
- Bannenberg N. Demands on refractory material for clean steel production. Paper presented at the 8th Annual Colloquium on Refractories, UNITECR 95, Kyoto, Japan, Nov 1995, 36–59.
- Kosmideret H, et al. *Stahl U. Eisen*. 1979; 99(22):1215–1221.
- Sulton W. Selection of refractories for vacuum cast alloys: importance of refractory stability and chemical inertness. Preprint Investment Casting Institute Meeting, Scottsdale, AZ, 1978.
- Turkdogan ET. Clean steel technology—Inclusion control to improve steel castability, processing and performance in service. ISS-AIME Symposium, Birmingham, AL, Sept 1986.

- Griffin D, Loeffelholz M, Bennett J. The effects of slag composition on the wear of basic slag line refractories used in ladle furnaces. Paper presented at 1989 UNITECR Conference, Anaheim, CA, Nov 1989, 575.
- Bhamra MS, Rastogi R, Cramb AW. CISR Progress Report, 1999, 302–305.
- Ramacciotti A, Marino E. Proc. 42nd Electric Furnace Conference, 1985, 293–298.
- Oguri K, Ando M, Muroi T, Aoki T, Okumura H. Proc. UNITECR 93 Refractory Congress, 1993, 1119–1126.
- Iida I, Nakamura M, Yamanura T, Nomura O, Nakamura R. Proc. UNITECR Refractory Congress, 1997, 87–94.
- Cooper CF, Hoover DB, Richmond C. Apparatus for discharging molten metal in a casting device and method of use, U.S. Patent 5,885,520, March 1999.

8

Carbonaceous Refractories

Albert J. Dzermejko

Consulting Engineer, Schaumburg, Illinois, U.S.A.

I. INTRODUCTION

The objective of this chapter is to familiarize the user with carbonaceous-type refractories and provide basic characteristics and application information so that intelligent decisions can be made when incorporating these types into a lining design (1). Carbonaceous refractories behave differently than the typical ceramic refractories, primarily because carbonaceous types are conductive rather than insulating. All carbonaceous lining systems perform as a “conductive cooling system” as opposed to a classic definition of a refractory lining that is typically an “insulating system.” Consequently, proper cooling must always be utilized with any carbonaceous lining system to assist in maintaining refractory temperatures that are below the critical chemical attack temperature for mechanisms such as oxidation, alkali, CO degradation, or dissolution of the carbon by molten metal.

The words “carbon” and “graphite” are often used interchangeably in the literature, but the two are not synonymous. Additionally, the words “semigraphite” and “semigraphitic” are also similarly misused. The following describes the composition, processing, and major characteristics of these various carbonaceous materials.

II. CARBONACEOUS REFRACTORY MATERIALS

A. Carbon

The terms “carbon,” “formed carbon,” “manufactured carbon,” “amorphous carbon,” or “baked carbon” refer to products that result from the process of mixing

carbonaceous filler material particles such as calcined anthracite coal, petroleum coke, or carbon black with binder materials such as petroleum pitch or coal tar, forming these mixtures by molding or extrusion and conventionally baking these formed pieces in furnaces at temperature from 800°–1400°C to carbonize the binder. Conventionally baked carbon can be densified, and thus its permeability improved by the introduction of additional binders impregnated into the baked carbon under vacuum, and the resultant product rebaked to carbonize the impregnation. Multiple impregnations are possible to double or triple densify the end product. Each densification, however, adds to the cost of producing a denser product.

Some manufacturers also add special raw materials to the carbonaceous mix prior to baking to improve the end-product properties. Silicon carbide or silicon metal can also be added to improve permeability and abrasion resistance.

B. Hot Pressed Carbon

The Union Carbide Corporation developed a unique proprietary method of manufacturing carbon that is called the BP process or “hot pressing.” Carbon, as previously described, is a product containing carbon particles with a carbon binder, and hot pressed carbon is the same, except the manufacturing process is different. Unlike conventionally baked carbons that can take weeks to bake to volatilize the binders, this proprietary process of manufacturing “instant carbon” carbonizes the binders in minutes. In this hot pressing process, a special pressing/carbonizing method is utilized. The carbon particles and binders are mixed as before but are introduced into a special mold in which a hydraulic ram pressurizes the mixture while, simultaneously, an electric current is passed through the mold, carbonizing the binders. More importantly, as the binders volatilize, the hydraulic ram compresses the mixture that closes off the pores formed by the volatilizing gases as they escape. The resulting product is a very impermeable carbon that can be approximately 100 times less permeable than conventionally baked carbon. This impermeability is an important property that prevents furnace contaminants such as alkali and zinc vapor from penetrating into the hot pressed brick structure.

Additions such as silica and quartz are used to make this special hot pressed carbon more alkali resistant. Normally, alkali materials such as sodium and potassium react with normal carbon to form damaging lamellar compounds that “swell,” causing volume expansion and spalling of the carbon. However, these alkali materials react preferentially with the silica addition in hot pressed carbon and form compounds that do not “swell,” avoiding damaging volume expansion or spalling.

Hot pressing results in a higher thermal conductivity than conventional carbon, which makes this special hot pressed carbon a very successful metallurgical furnace hearth wall lining material. This is because the higher thermal

conductivity of the lining maintains a hot face temperature that is below the solidification temperature of the metal and slag, allowing the formation of a protective layer (skull) of frozen process materials of metal and/or slag on the hot pressed lining hot face. The solidified layer of metal and slag protects hot pressed carbon from the erosive wear from moving liquids and insulates the carbon, preventing chemical attack. The special hot pressing manufacturing process limits the size of these pressed carbon bricks to $450 \times 250 \times 115$ mm.

C. Graphite

The term “graphite,” also called “synthetic,” “artificial,” or “electrographite,” refers to a carbon product that has been additionally heat treated at a temperature between 2400° – 3000° C. This process is called “graphitization,” which changes the crystallographic structure and also changes the physical and chemical properties.

Graphite is also found in nature. This natural graphite is found in flake form and, if used in a refractory product, is usually part of a mixture with ceramic material or used for the binder. However, clay or ceramic bonded, natural graphite containing refractory is considered a ceramic product.

Artificial or synthetic graphite refractories begin as a baked carbon material, similar in manufacture to the carbon refractory material described previously. However, after carbonizing of the binder is completed, this baked carbon is then loaded into another furnace to be high-temperature-treated (to be graphitized). This graphitization changes the structure of not only the carbon particles, but also the binder. The resulting product contains graphitized particles as well as a graphitized binder.

There is no industry-wide system for designating the various grades of graphite that are commercially available. Each manufacturer has its own method and nomenclature to describe the available grades and varieties that are made for specific purposes or properties. These grades differ in their raw materials, grain sizes, purity, density, etc. For denser versions, the porosity of the material can be filled with additional binder materials such as tar or pitch by impregnation under a vacuum. The impregnated material can then be regraphitized, forming a denser and less porous product. Multiple re-impregnations/graphitizations can be performed to provide additional densification.

Purification can also be utilized to reduce the ash levels of graphite for high-purity requirements. Additionally, proprietary manufacturing methods and techniques can also be utilized to minimize ash (noncarbonaceous constituent) or iron contamination of graphites. Iron is a catalyst for oxidation of graphite in a carbon monoxide environment, so graphite intended for use as a refractory should contain relatively low ash and iron content.

D. Semigraphite

The term “semigraphite” is used to describe a carbonaceous product that is composed of artificial graphite particles, mixed with carbonaceous binders such as pitch or tar, and baked at carbonization temperatures of 800° – 1400°C . The resulting product is composed of carbon bonded graphite particles, in which the graphite particles were manufactured at temperatures close to 3000°C , but the binders have only been baked at the 800° – 1400°C range. The resulting product, a true “carbon bonded graphite,” is called semigraphite. Semigraphite exhibits higher thermal conductivity than the carbons, but because of its carbon binder, not as high as 100% graphite. Thermal conductivities of any carbonaceous product will vary with baking temperature and can be increased by rebaking at higher temperatures. Semigraphites can also be densified as was previously described for graphite and rebaked to carbonize the newly impregnated binder, reducing porosity and consequently permeability.

E. Hot Pressed Semigraphite

The proprietary “hot press” method of manufacturing brick can also be used to make true semigraphite products, utilizing graphite particles combined with carbon binder and other proprietary ingredients. The process is as described previously for hot pressed carbon.

F. Semigraphitized Carbon

The term “semigraphitized” refers to a baked carbon that has been additionally heat-treated at a temperature of between 1600° – 2400°C . This high-temperature baking process begins to change the crystallographic structure of the carbon and alters its physical and chemical properties. However, because this additional heat-treating occurs at temperatures below graphitization temperatures, the product is said to be “semigraphitized.” This product contains carbon particles and a carbon binder that are *both* semigraphitized. This is different than a semigraphite product that is composed of graphite particles with a *carbon* binder.

The resultant semigraphitized carbon, in which both particles and binder are semigraphitized, provides a material with higher thermal conductivity and chemical attack (from alkali or oxidation) resistance than either carbon or semigraphite materials. This is because alkalis and zinc attack the binder material first and the semigraphitized binder is more resistant to attack than the carbon binder of semigraphite.

Carbon and graphite have limitations (2) with regard to oxidation (burning). In air, particulate carbon burns rapidly at 500°C and in pure oxygen at 400°C and in CO_2 in excess of 600°C . Combustion of carbon in CO is not possible, which is

an important consideration in steel making. Hot steel-making vessels lined with carbon-bearing refractory brick can be severely deteriorated in a short period of time when not protected from air. Similarly, carbon or graphite electrodes in arc furnaces exposed to air, CO₂, or other oxidizing agents while hot will oxidize, which is the principal cause of deterioration.

Table 1 provides a summary of various carbonaceous refractories, classified by type.

III. CARBONACEOUS MATERIAL PROPERTIES AND CHARACTERISTICS

There is no industry-wide standard for designating the various grades of carbonaceous materials that are commercially available. Each manufacturer has its own method and nomenclature to describe the available grades and varieties that are made for specific purposes or properties. The following will help introduce carbonaceous products typically utilized as refractory materials.

A. Carbon

Typical carbon refractory material properties are shown in Table 2.

B. Graphite, Semigraphite, and Semigraphitized Carbon

Material properties typically will vary greatly, resulting from the differing raw materials and processing techniques used by the different manufacturers.

Table 1 Carbonaceous Refractory Types, Compositions and Baking Temperatures

Product classification	Characteristics		
	Baking temp. (°C)	Particles	Binder
Carbon	800–1400	Carbon	Carbon
Hot pressed carbon	Approx. 1000	Carbon	Carbon
Graphite	2400–3000	Graphite	Graphite
Semigraphite	800–1400	Graphite	Carbon
Hot pressed semigraphite	Approx. 1000	Graphite	Carbon
Semigraphitized	1600–2200	Semigraphitized carbon	Semigraphitized carbon

Table 2 Typical Carbon Material Properties

Property	Hot pressed bricks + silica addition	High-conductivity, conventionally baked, large blocks
Bulk density, g/cc	1.62	1.6
Crushing strength, kPa	30,500	44,000
Modulus of rupture, kPa	8,100	—
Ash, %	10 ^a	13
Permeability, m ³ Darcys	9	~200
Thermal conductivity, W/m ² K		
@600°C	18.4	11
@800°C	18.8	15
@1000°C	19.3	16
@1200°C	19.7	N.A.

^aAsh content includes quartz and silica addition to control alkali attack.

Note also the wide range in thermal conductivities of these materials, which, as was explained previously, depends upon their materials and processing temperatures.

Table 3 provides a limited list of various semigraphite and semigraphitized materials and their properties.

Table 4 summarizes typical material properties of graphite.

Tables 5 and 6 describe other parameters that have a direct effect on the properties of graphite materials. Table 5 illustrates the difference in material properties of graphite from two different manufacturers that reflects differing raw materials and processing methods or techniques. As can be seen from Table 5, the manufacturer has a profound influence on graphite properties due to differing manufacturing procedures, proprietary methods, and processes. This is primarily why there is no industry-wide standard for carbonaceous refractories.

Table 6 illustrates the effect of grain size, which also has a profound influence on material properties.

A critical consideration when designing a graphite-type lining system is heat flow. The greater the heat flow, typically the better the design. Table 7 tabulates the test results of heat flow measurements on mortar joints (cemented) versus machined contact (dry) joints.

Table 7 illustrates heat flow through differing graphite refractory interface conditions. The precision-machined joints (Tests 2 and 6) permitted between 8–16% higher heat flows than the mortared joints (Tests 1 and 5). In one case, however, the mortared joint (Test 3) permitted a 12% higher heat flow than the

Table 3 Typical Semigraphite and Semigraphitized Carbon Refractory Material Properties

Property	Semigraphites			Semigraphitized carbon			Hot pressed semigraphites		
	High-fired, conventional med. density	High-fired, conventional high density	High-fired, conventional med. density	High-fired, conventional high density	High-fired, conventional high density	Graphite + silica additive	Graphite w. no additives	Graphite + silicon carbide additive	
Bulk density, g/cc	1.62	1.73	1.65	1.75	1.80	1.79	1.87	1.87	
Cold crushing strength, kPa	25,000	36,000	27,000	38,000	31,000	33,000	48,000	48,000	
Ash, %	0.4	0.2	0.4	0.2	9.5 ^a	0.3	20 ^b	20 ^b	
Permeability m ³ Darcys	—	—	—	—	8	4	0.6	0.6	
Thermal conductivity, Wm ² K:									
@ 20°C	45	45	47	47	45	60	45	45	
@ 1000°C	32	32	32	32	32	32	32	32	

^aAsh content includes quartz and silica addition to control alkali content.

^bAsh content includes silicon carbide.

Table 4 Typical Graphite Material Properties

Properties	Graphite material description			
	Standard density, standard ash	Standard density, low ash	Medium density, low ash	High density, low ash
Bulk density, g/cc	1.63	1.67	1.72	1.80
Porosity, %	21	16	14	12
Ash, %	0.5	0.2	0.2	0.2
Cold crushing strength, kPa	20,000	28,000	40,000	51,000
Thermal conductivity, W/m [°] K:				
@20°C	150	140	15	160
@1000°C	70	70	75	80

machined joint (Test 4). This can partially be explained by the fact that the quality of any mortar application varies greatly as a function of the bricklayer, the bricklayer's technique, and tools and/or skills and can sometimes be so poor that heat transfer can be adversely affected. Conversely, a good mortar application can provide a beneficial heat-transfer effect.

Unfortunately, there is no way to predict the actual quality outcome of thousands of mortar joints in a typical refractory application, so some designers believe that joints should be minimized or mortar eliminated in favor of precision-machined contact. However, it should also be noted that properly prepared and applied mortar joints provide critical differential expansion compensation and actually enable mortared carbonaceous refractory linings to accommodate high differential stresses and avoid cracking. Machined contact joints provide

Table 5 Graphite Material Properties from Two Different Manufacturers

Property	Raw material manufacturer	
	A	B
Thermal conductivity, W/m [°] K	165	235
Thermal expansion, @ 20°C $\Delta l/120^\circ\text{C}$	2.4×10^{-6}	1.1×10^{-6}
Young's modulus, kPa	9.86×10^6	13.72×10^6

Table 6 Effects of Grain Size on Graphite Properties

Raw material size	Property	Value
Fine	Density, g/cc	1.55
Medium		1.54
Coarse		1.44
Fine	Thermal expansion, @20°C Δl/120°C	1.0×10^{-6}
Medium		1.4×10^{-6}
Coarse		1.9×10^{-6}
Fine	Flexural strength, kPa	17,900
Medium		8,300
Coarse		5,700

Table 7 Comparison of Heat Flow Through Graphitic Refractory Interface Conditions

Joint type	Test no.	Sample material	Joint composition	Longitudinal heat flow, Watts
Dry vs. mortared joints	1	Hot pressed	1.5 mm mortar	522
	2	semigraphite bricks	Dry (no mortar)	623 (16% higher) 617 (12% higher)
	3	Machined	1.5 mm mortar	
	4	semigraphite blocks	Dry (no mortar)	543 835
	5	Machined	1.5 mm mortar	906 (8% higher)
	6	graphite blocks	Dry (no mortar)	
Ram joint vs. machined contact to copper cooler	7	Machined semigraphite and 25-mm layer of graphitic ram	25-mm graphite ram layer	548
	8	Machined semigraphite block in contact with copper cooler	Dry (no mortar)	648 (15% higher)
Standard density graphite vs. premium density graphite vs. semigraphite	6	Machined graphite blocks	Dry (no mortar)	906 (30% lower)
	9	Machined premium graphite blocks	Dry (no mortar)	1176
	4	Machined semigraphite blocks	Dry (no mortar)	543 (11% lower)

no such protection unless the designer includes proper differential expansion compensation provisions.

The effect on heat flow of graphite versus dense graphite versus semigraphite (Tests 6, 9, and 4) is also evident in Table 7. The premium dense graphite blocks show a desirable significant increase in the heat flow because of their higher density and consequential higher conductivity.

In general, carbon, semigraphitized carbon, and sometimes semigraphite materials are normally utilized for the hot face of blast furnace hearth linings that are in direct contact with molten materials. Graphite materials are usually restricted to the backup lining to take advantage of their very high thermal conductivity and because they are more easily dissolved by molten iron from dissolution. Typically, ceramic refractories such as high alumina, mullite, and chrome corundum are used in the uppermost hearth pad layer as a wearing surface to minimize exposure of the carbon or semigraphite to molten iron and to provide an impermeable insulating crucible in which the “salamander” can reside.

C. Ceramic

Typical ceramic refractory materials used in the hearth wearing surface are shown in Table 8. Note that the thermal conductivities of ceramic refractories (insulating) are significantly lower than any carbonaceous refractory. The properties and characteristics of all ceramic refractories depend on the type, quality, and source of the raw materials utilized in their mix and the particle size makeup.

The fine particles in the mix form the ceramic bonding of the larger particles as the material is fired at high temperature. The fired refractory contains

Table 8 Typical Hearth Ceramic Refractory Properties

Property	Ceramic material			
	Hard-burned, superduty fireclay	60% alumina	Artificial mullite	Chrome corundum
Density, g/cc	2.24	2.40	2.45	3.43
Crushing strength, kPa	31,000	35,000	85,000	78,000
Porosity, %	13	22	19	8
Thermal conductivity, W/m ² K				
@500°C	1.9	2.0	—	—
@1000°C	0.9	1.7	1.8	2.3

Table 9 Critical Spalling Rates for Various Materials

Material	°C/min	°F/min
High duty	4	7
High alumina	5	9
Chrome corundum	5	9
Cast iron	50	90
Silicon carbide	50	90
Carbon	200	400
Semigraphite	250	450
Graphite	500	900

larger crystalline particles bonded together with glass or other small crystalline particles that have fused together during firing.

Critical spalling rates for various refractory materials are shown in Table 9 (3). All refractories will spall and crack if they are exposed to severe magnitudes of temperature fluctuations that exceed their “critical spalling rate.” Table 9 lists the critical spalling rates for a variety of refractory materials.

These critical spalling rates define the maximum temperature variations over time that the hot face of the refractory can survive without cracking. At higher rates, cracking will occur whether the temperature change is through heating or cooling. Note that carbonaceous materials can withstand much higher temperature fluctuations than ceramic materials, making them extremely valuable for applications subjected to severe thermal cycling.

IV. BLAST FURNACE HEARTH WALLS

Blast furnace hearth wall concepts and designs vary worldwide and provide totally different performance histories. However, the mechanisms of hearth wear are identical regardless of the region. These include chemical attack by alkalis and zinc vapor, slag, dissolution of the carbon by iron, oxidation, carbon monoxide degradation, and erosion by molten material movement. Additionally, operating practices, inadequate or improper cooling, furnace internal geometry, and lining configuration and composition can also intensify the effects of these wear mechanisms.

There are many reasons for the many different concepts, designs, and configurations utilized, including historical, evolutionary “solutions” that inadvertently have become accepted “standards” within a specific region. Yet the conservative nature of the Industry in general tends to avoid changing concepts or configurations that have been historically utilized, oftentimes for long-forgotten reasons.

Consequently, blast furnace hearth wall designers must properly identify and address all factors that can contribute to refractory wear, including the actual cause of the problem, not just the “symptoms.” For example, it has been a standard practice in some regions to increase lining wall thickness as a response to severe wall material loss, when the actual cause of the initial material loss was that the wall was originally too thick to be properly cooled or to accommodate differential stresses through its thickness!

Making the wall even thicker doesn’t solve the real problem of cracking and cooling loss. It only prolongs the period before wall wear would again reach a critical state, a sort of race of “mass against time”! Unfortunately, this kind of “mass vs. time” solution doesn’t eliminate the actual problem cause, which is cracking of the carbon and consequential degradation and ineffective cooling.

A thinner, highly conductive, and effectively cooled wall lining with proper differential movement compensation can eliminate the actual problem that causes the wear and allow a long-term, reliable campaign because differential movement and stresses are eliminated, preventing cracking. Consequently, effective heat transfer and thermal conductivity can be maintained throughout its lifetime, achieving and maintaining thermal equilibrium and resulting in a protective and insulating hot face accretion (skull).

In order to assist in this regard, a series of computer simulations were conducted to analyze the theoretical performance of two different hearth wall lining compositions and configurations, to demonstrate differing predicted performance outcomes for the same operating conditions.

Table 10 summarizes the thermal performance of various blast furnace hearth wall carbonaceous lining material concepts, utilizing a heat-transfer analysis of each hearth wall composition (Case 1 through Case 5).

Table 10 Carbonaceous Wall Lining Materials Performance Comparison

Case no.	Wall lining material	Condition	Carbon hot face temp.	Heat flux (kW/m ²)
1	Hot pressed carbon brick	Blow-in	821	11.4
2	Hot pressed carbon brick	Skull formation @ equilibrium	206	2.5
3	Large block carbon w/ceramic cup	Blow-in	700	6.3
4	Large block carbon w/ceramic cup	Crack formation, ram shrinkage, and deterioration	852	3.9
5	Large block carbon w/ceramic cup	Carbon and ram chemical attack	943	3.4

In Case 1, the initial blow-in (new) condition of a new hot pressed carbon wall section results in a high lining hot face temperature because molten materials would be in direct contact with the carbon so that heat flow is unimpeded by any hot face insulating accretion (skull).

In Case 2, the resultant achievement of a thermal equilibrium allows formation of an insulating skull formed from solidifying slag materials on the carbon lining hot face, resulting in a greatly reduced hot face temperature.

Case 3 represents a large, single-thickness block carbon wall lining in the blow-in (new) condition that includes a high-melting-point ceramic material on the carbon lining hot face intended for protecting the carbon.

Case 4 represents the deteriorated condition of Case 3 caused by stress cracking from differential thermal expansion of the large, single-thickness blocks that interrupts effective heat transfer through the carbon and thermal degradation of the ramming layer between the ceramic and the carbon.

Case 5 represents continued carbon and ram deterioration from chemical attack resulting from degradation and loss of thermal conductivity as lining material temperatures continue to rise unabated.

The primary reason for lining failure demonstrated in Cases 4 and 5 is the differential temperature cracking that interrupts heat transfer and results in chemical attack of the carbon and loss of thermal conductivity and consequential lack of a skull formation on the ceramic lining hot face. As a result, the ceramic lining absorbs heat because the deteriorating carbon cannot cool it effectively. Consequently the *cold* face of the ceramic becomes very hot versus time, further intensifying chemical attack of the carbon by alkalis and zinc vapor. Additionally, since the now hot “insulating” ceramic has become a heat source within the lining, it allows molten materials to penetrate into the stress cracks and joints of the carbon, causing dissolution of any exposed carbon and/or ram and consequential carbon loss and “break-out” possibilities.

The theoretical advantage of utilizing an “insulating” ceramic lining is lost because of ram deterioration and carbon block cracking, both of which interrupt heat transfer and result in carbon temperatures that exceed the “critical reaction temperature” for chemical attack by alkalis and zinc. Additionally, because the hot face ceramic cannot be sufficiently cooled because of the loss of continuity caused by the cracks and the loss of conductivity by the carbon, thermal equilibrium cannot be achieved. Thus, instead of providing “insulation,” the ceramic layer instead becomes hotter and hotter versus time as it absorbs heat from the molten materials and thus creates a “heat source” on the hot face of the carbon. This heat absorption by the “insulating” ceramic continues unabated until it reaches a temperature that is nearly the same as the molten materials in which the ceramic is exposed on its hot face. This is the same effect that would occur if a block of this insulating ceramic would be submerged in a ladle of molten metal, after which in a very short time, this “insulating” material would reach

an equilibrium temperature with the metal because it could not be cooled. Consequently, including an insulating type, ceramic hot face wall lining with the heat conducting carbon wall lining design, prevents the achievement of thermal equilibrium, because the ceramic actually becomes a heat source so that an insulating layer of solidified materials (skull) cannot form on its hot face.

V. CONCLUSION

Carbonaceous refractories behave differently than the typical ceramic refractories, primarily because carbonaceous types are conductive rather than insulating. All carbonaceous lining systems perform as a “conductive cooling system” as opposed to a classic definition of a refractory lining that is typically an “insulating system.” Consequently, proper cooling must always be utilized with any carbonaceous lining system to assist in maintaining refractory temperatures that are below the critical chemical attack temperature for mechanisms such as oxidation, alkali, CO degradation, or dissolution of the carbon by molten metal.

There is no industry-wide system for designating the various grades of carbonaceous materials that are commercially available. Each manufacturer has its own method and nomenclature to describe the available grades and varieties that are made for specific purposes or properties.

Carbonaceous materials exhibit excellent thermal conductivity, volume stability, chemical attack resistance, and thermal shock resistance, making them a valuable component for refractory applications. However, they must be properly cooled to assure long-term survivability in metallurgical applications.

Various methods can be utilized to accommodate internal stresses such as mortared joints or proprietary differential thermal expansion compensation, and carbonaceous materials can be combined in applications with various types of ceramic materials to take advantage of the best properties and characteristics of each.

REFERENCES

- Blast furnace refractory systems for the hearth, bosh and stack. UCAR Handbook. Columbia, TN: UCAR Carbon Company, Inc.
- Carniglia SC, Barna GL. Handbook of Industrial Refractories Technology. Park Ridge, NJ: Noyes Publications, 1992.
- DeBoer J, et al. History and actual state of lining and cooling systems at the Estel Hoogovens Ijmuiden blast furnaces. International Ceramic Review 1983; 32:16–18.

9

Spinel-Containing Refractories

S. Zhang and W. E. Lee

The University of Sheffield, Sheffield, England

I. INTRODUCTION

The minerals in the group of “spinel” are double oxides that crystallize in the cubic crystallographic system. They are generally indicated by the formula AB_2O_4 , where “A” is a divalent element such as Mg, Fe, Zn, Mn, Ni, Co, V, and Cu, and “B” a trivalent element such as Al, Fe, and Cr with reciprocal diadochal exchange. An enormous number of individual compounds (>200) and systems can justifiably be classified as spinels. Apart from those compounds closely related to the naturally occurring parent mineral spinel [i.e., magnesium-aluminate spinel, $MgAl_2O_4$ (MA)], there are many compounds that are structurally related (with greater or lesser variations), and there are also a broad range of solid solutions adhering to the same structure. Spinel associated with refractories systems include $FeFe_2O_4$, $FeAl_2O_4$, $FeCr_2O_4$, $MgFe_2O_4$, $MgAl_2O_4$, $MgCr_2O_4$, and their solid solutions. Some of their properties are listed in Table 1 (1). Among these spinels, $MgAl_2O_4$ and $MgCr_2O_4$ offer a good combination of physical and chemical properties such as high refractoriness, high mechanical strength, and high resistance to chemical attack, so they are consequently used to make a variety of spinel-containing refractories. Although $MgCr_2O_4$ -containing refractories are still being used in many areas, due to the carcinogenic nature of Cr^{6+} , they have been and are continuously being replaced by $MgAl_2O_4$ -containing refractories. Therefore, in this chapter, we emphasize the raw materials, processing, properties, and applications of $MgAl_2O_4$ -containing refractories.

The crystallography, stoichiometry, and typical properties of MA spinel will be described followed by a discussion of preparation methods of spinel powders and aggregates. The production, microstructures, and properties of several of

Table 1 Spinel Minerals Related to Refractories Systems

Mineral name	MgAl ₂ O ₄ Spinel	FeAl ₂ O ₄ Hercynite	MgCr ₂ O ₄ Picrochromite	FeCr ₂ O ₄ Chromite	MgFe ₂ O ₄ Magnesioferrite	FeFe ₂ O ₄ Magnetite
Composition (wt%)	MgO 28.3 Al ₂ O ₃ 71.7	FeO 41.3 Al ₂ O ₃ 58.7	MgO 21.0 Cr ₂ O ₃ 79.0	FeO 32.1 Cr ₂ O ₃ 67.9	MgO 20.1 Fe ₂ O ₃ 79.9	FeO 31.1 Fe ₂ O ₃ 68.9
Molecular weight	142.2	173.7	192.3	223.8	200.0	231.5
True density (g · cm ⁻³)	3.58	4.40	4.43	5.09	4.52	5.20
Melting point (°C)	2135	1450	2180	1770	1713 (incongruent melting)	1950
Linear thermal expansion (850°C) (%)	0.662	0.705	0.745	0.740	1.058	1.261

the most widely used spinel-containing refractories such as MgO–MA and Al₂O₃–MA system refractories, and newly developed spinel-containing refractories such as MgO–MA–MgTi₂O₅ and MgO–MA–ZrO₂ will be summarized. Finally, likely future work on development and application of spinel-containing refractories will be discussed.

II. SPINEL CRYSTALLOGRAPHY

The crystallographic structure of the MA spinel was determined independently by Bragg (2) and Nishikawa (3). It is simple cubic and belongs to space group Fd3m with eight formula molecules in one cubic unit cell. The oxygen ions form an almost perfect cubic close-packed array with the metal ions distributed among the resulting positions of fourfold and sixfold oxygen coordination. The maximum number of possible tetrahedral and octahedral sites is 64 and 32, respectively. The coordinates of the ionic positions for this space group are 8 positions of fourfold oxygen coordination at 8a, 16 positions of sixfold oxygen coordination at 16d, and 32 positions at 32e.

The 32 oxygen ions occupy the 32-fold positions, and the cations occupy the 8-fold and 16-fold positions. In MgAl₂O₄, 8 Mg²⁺ ions are distributed at the 8a positions, and the 16 Al³⁺ ions at the 16d positions, so only 1/8 of the tetrahedral cation sites are occupied by Mg²⁺ ions and 1/2 of the tetrahedral cation sites by Al³⁺ ions (Figure 1). Thus, the MA spinel structure has great potential to accommodate a number of other types of divalent and trivalent cations, allowing large deviations from stoichiometry and solid solution formation. The divalent and trivalent cations are usually limited to those with radii from 0.044–0.100 nm so that they can be accommodated in the tetrahedral and octahedral sites.

III. TYPICAL PROPERTIES OF MA SPINEL

As will be discussed in Section V, spinel can be synthesized using different raw materials and via different processes; therefore, the properties of synthesized spinels vary. Table 2, as an example, lists some typical properties of dense, sintered, stoichiometric spinel (4). Spinel has a higher melting temperature (2135°C) than Al₂O₃ (2054°C) but lower than MgO (2850°C). Its thermal expansion coefficient ($\sim 8.4 \times 10^{-6}/\text{K}$) is close to that of alumina ($\sim 8.8 \times 10^{-6}/\text{K}$), but much lower than MgO ($\sim 13.5 \times 10^{-6}/\text{K}$). Furthermore, it has superior hydration resistance than periclase and thus can be used in water-based castable systems.

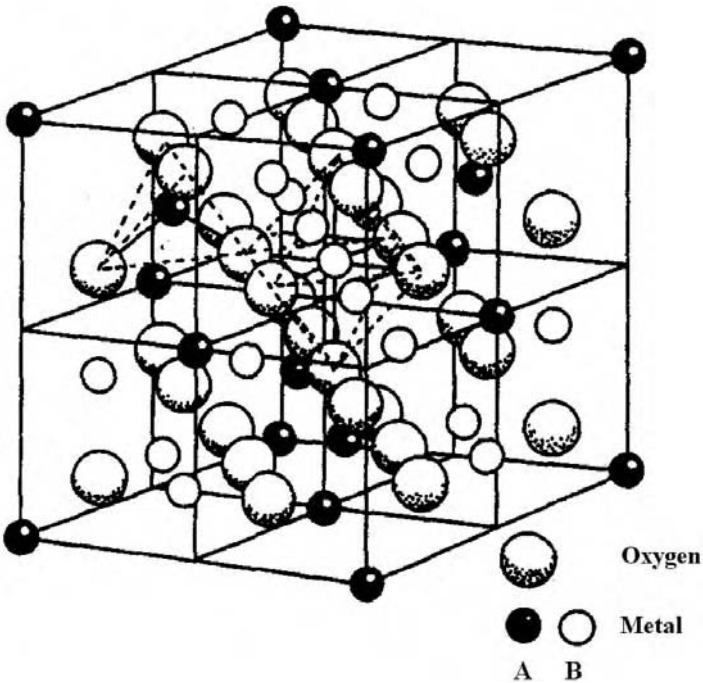


Figure 1 View of the spinel crystal structure.

IV. MA SPINEL STOICHIOMETRY

MA spinel has a range of stoichiometry discernable by its phase field in the MgO–Al₂O₃ phase diagram (Figure 2). Stoichiometric MA contains 28.3 wt% MgO and 71.7 wt% Al₂O₃. However, with increasing temperature, a wide range of nonstoichiometry may form in the system and the solid solubility of alumina in MA spinel is higher than that of magnesia at the same temperature. For example, the solid solubilities of MgO and Al₂O₃ at 1600°C are 2 and 6 wt%, respectively, but increase to 3 and 10 wt%, respectively, at 1700°C. Clearly, it is more likely that single-phase MA spinel is alumina-rich, and this can be indicated by the notation MgO · *n*Al₂O₃ where *n*, the number of moles of alumina, can be as high as 7.3 (5). MgO-rich spinel (*n* < 1) is, according to the phase diagram, theoretically achievable by quenching from very high temperatures (>1600°C), but more commonly MgO-rich spinel grain contains periclase and is located in the MgO-spinel binary phase field.

Table 2 Properties of Sintered, Stoichiometric MA Spinel

Melting point (°C)	2135
Thermal expansion ($\times 10^{-6}/^{\circ}\text{C}$)	
100°C	5.6
500°C	7.6
1000°C	8.4
1500°C	10.2
Thermal conductivity (W/mK)	
25°C	15
100°C	13
500°C	8
1000°C	5
Density ($\text{g} \cdot \text{cm}^{-3}$)	3.58
Young's modulus (GPa)	240–284
Bending strength (MPa),	
RT	110–245
1400°C	8–10
Hardness (GPa)	15

Source: From Ref. 4.

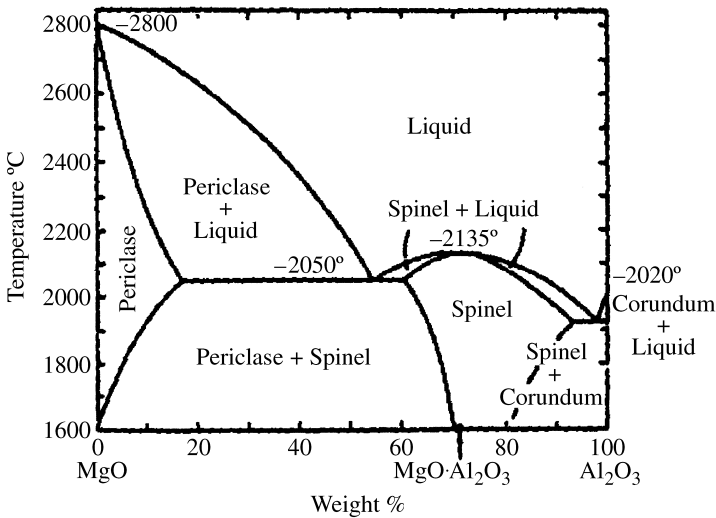


Figure 2 Phase diagram of the MgO–Al₂O₃ system.

In alumina-rich spinel, Al^{3+} replacing Mg^{2+} ions on tetrahedral sites with charge compensating cation vacancies on the octahedral sites accommodates the excess alumina stoichiometry range in the crystal structure. Because the ionic radius of Al^{3+} (0.050 nm) is also significantly smaller than that of Mg^{2+} (0.065 nm), doping with excess Al^{3+} leads to the formation of vacant cation sites, i.e., MA becomes cation deficient with a smaller unit cell volume. Figure 3 (5) shows that the spinel lattice constant decreases with increasing mole number of alumina. If the lattice constant of spinel is known, then using Figure 3, the amount of excess alumina in an alumina-rich spinel can be estimated. The cation vacancies formed in the alumina-rich spinel can accommodate many different cations, conferring spinel-containing composites with some interesting properties. For example, due to the accommodation of slag ions such as Fe^{2+} and Mn^{2+} by the spinel structure, spinel-containing refractories show improved slag penetration resistance, which will be discussed in detail in Section VI. In contrast to alumina-rich spinel, in MgO-rich spinel, enlargement of the spinel unit cell occurs with the formation of oxygen vacant sites, i.e., doping with excess MgO leads to the formation of an anion-deficient structure. In this case, the lattice constant increases slightly with increasing MgO content.

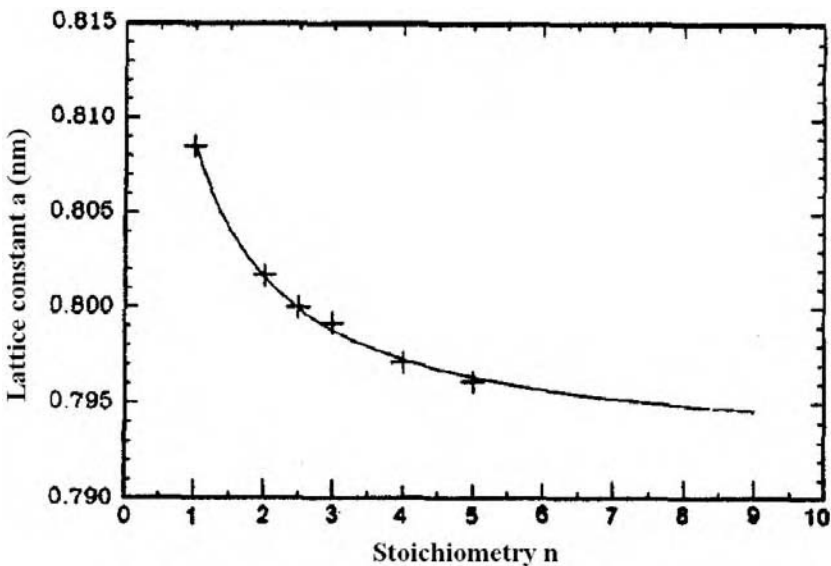


Figure 3 Lattice constant of spinel as a function of mole number (n) of Al_2O_3 . (From Ref. 5.)

Alumina-rich, stoichiometric, and MgO-rich spinels are all used by the refractories industry, and their stoichiometry affects sinterability, physical properties such as mechanical strength, and chemical properties such as slag corrosion resistance of spinel-containing refractories (see Section VI).

V. PREPARATION OF SPINEL POWDERS AND AGGREGATES

Spinel can be introduced into refractories in the following ways: (1) as preformed synthetic spinel powders in the matrix; (2) as preformed spinel aggregates; (3) by formation of in situ spinel by addition of Al_2O_3 to MgO-based refractories or MgO to Al_2O_3 -based refractories; and (4) by formation of in situ spinel by addition of a mixture of MgO and Al_2O_3 powders. Processes for the synthesis of spinel powders or aggregates will now be described.

A. Synthesis of Spinel Powders

1. Conventional Oxide Mixing (Solid–Solid Reaction)

MA spinel does not occur in nature and so commercial powders have to be synthesized using a wide variety of techniques. The oldest, simplest, and still most widely used method is the conventional oxide mixing (CMO), or solid–solid reaction, technique. With this technique, powdered MgO- and Al_2O_3 -bearing compounds (e.g., oxides, hydroxides, or carbonates) are mixed and pressed into pellets or some other shapes and then heated in a furnace at high temperature for prolonged periods. After synthesis, the product mass is crushed to aggregates or further ground to powders with the desired size distribution.

Spinel formation via CMO has been investigated extensively [e.g., (6)]. Initially, all the elements necessary to form the MA product are present at every interface between particles of MgO and Al_2O_3 . Therefore, small crystals with the spinel stoichiometry and structure are nucleated relatively easily on the surfaces of either MgO or Al_2O_3 grains (Figure 4). Once these initial spinel layers form, subsequent growth or thickening of the spinel product becomes much more difficult because, effectively, the two reactants, MgO and Al_2O_3 , are no longer in contact but are separated by a rather impenetrable spinel layer. To continue the reaction, a complex counterdiffusion process is thus required in which Mg^{2+} ions diffuse away from, and Al^{3+} ions diffuse toward, the MgO– MgAl_2O_4 interface and vice versa for the MgAl_2O_4 – Al_2O_3 interface. To preserve local electroneutrality during the reaction and throughout the product, it is necessary that, for every three Mg^{2+} ions that diffuse to the right-hand interface, two Al^{3+} ions must diffuse to the left-hand interface. The

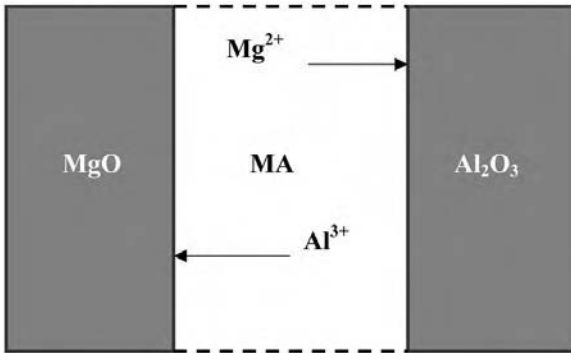
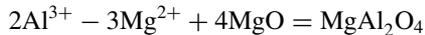


Figure 4 Formation of MA spinel product on the reactant MgO and Al₂O₃ grains by a counter-diffusion process.

reactions that occur at the two interfaces may be written, ideally, as

At the MgO/MgAl₂O₄ interface:



At the MgAl₂O₄/Al₂O₃ interface:



The overall reaction is: $4\text{MgO} + 4\text{Al}_2\text{O}_3 = 4\text{MgAl}_2\text{O}_4$

from which it can be understood that the right-hand interface should move three times as quickly as the left-hand interface (Figure 4).

Spinel formation reaction by this process is particularly slow because ions such as Mg²⁺ and Al³⁺ diffuse slowly. Defects are required, particularly vacant sites into which adjacent ions can hop. High temperatures are also required so that ions have sufficient thermal energy to, occasionally, vibrate or hop out of one site into an adjacent vacancy or interstitial site. Consequently, it can be difficult for solid-state spinel formation reactions to proceed to completion as the remaining reactants become increasingly separated from each other. A popular way of accelerating the reactions is to frequently regrind the partially reacted mixtures, which acts to break up reactant–product interfaces and to bring fresh reactant surfaces into contact. Alternatively, if gas- or liquid-phase assisted transport of matter can occur, the reactants may be brought together without the need for long-range solid-state diffusion. A small amount of gaseous or liquid transporting agent (mineralizer) may be effective in enhancing reaction rates.

Effective mineralizers for spinel formation reactions include fluorine- and boron-containing compounds. The former includes LiF, NaF, AlF₃, Na₃AlF₆,

ZnF₂, CaF₂, and BaF₂, whereas the latter includes, e.g., CaB₄O₇ and B₂O₃. These mineralizers can form liquid phases and/or help create cation vacancies, increasing spinel formation rate and decreasing its formation temperature. Figure 5 shows the effect of addition of LiF and a combination addition of LiF + CaCO₃ on spinel formation [after (7)]. Using 2 wt% LiF or 2 wt% LiF + 3.3 wt% CaCO₃ significantly increases the rate of spinel formation. Figure 6 shows the effect of additions of CaB₄O₇ or B₂O₃ on the spinel formation reaction [after (8)]. With increasing addition from 0 to 1.0 wt%, the content of spinel formed increases markedly. Figure 6 also shows that for the same amount of addition, CaB₂O₄ is more effective than B₂O₃, indicating that not only the type of mineralizer but also the amount is important to the spinel formation reactions.

2. Electrofusion

An electrofusion (EF) process is also used to synthesize spinel. Starting materials such as natural magnesite and calcined alumina are melted in an electric arc furnace to a temperature above the melting point of the mixture, so that MgO and Al₂O₃ react with each other to form spinel in the molten state. After reaction, the molten product is cooled to a solidified ingot that can be crushed to aggregates

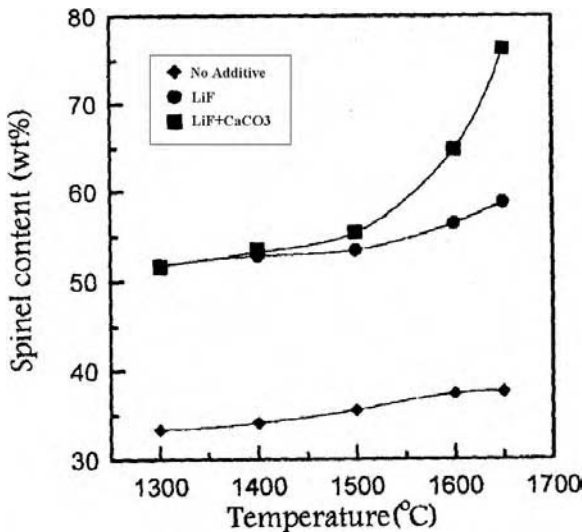


Figure 5 Effect of addition of LiF or LiF + CaCO₃ on the formation of spinel. (From Ref. 7.)

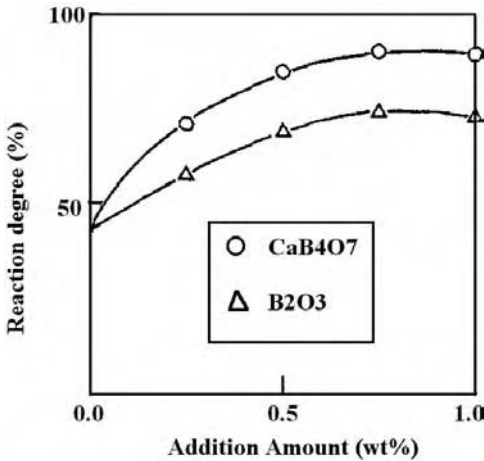


Figure 6 Effect of addition of CaB_4O_7 or B_2O_3 on spinel formation.

or further ground to controlled particle size distribution powders. The spinel formation reaction by EF is more complete than by CMO, and the spinel synthesized is usually purer and more homogeneous than by CMO due to volatilization of impurities. However, spinel powders prepared by EF have lower surface reactivity than by CMO, thus requiring even higher temperatures to densify them to aggregates or final products. Another problem with this technique is that very high temperatures ($\sim 2200^\circ\text{C}$) are needed, so the process is highly energy-intensive and thus financially expensive.

3. "Wet-Synthesis" Techniques

To prepare high-quality (uniform and reactive) spinel powders at lower temperature, several so-called wet-synthesis methods, including, e.g., *sol-gel* and hydrothermal synthesis processes, have been developed.

The starting point in the *sol-gel* technique is to prepare a homogeneous solution containing all the cationic ingredients. The solution is gradually dried and, depending on the species present, it may transform to a viscous sol containing particles of colloidal dimensions and, finally, to a transparent, homogeneous, amorphous solid gel, without precipitation of any crystalline phases. The gel is then fired at appropriate temperatures to remove volatile components trapped in the pores of the gel or chemically bonded organic-side groups and to crystallize the final product. The reagents for sol-gel synthesis of spinel are usually metal-organic compounds, especially alkoxides such as aluminium isopropoxide and magnesium ethoxide, or inorganic salts such as $\text{Mg}(\text{NO}_3)_2 \cdot 6\text{H}_2\text{O}$ and

$\text{Al}(\text{NO}_3)_3 \cdot 9\text{H}_2\text{O}$. Spinel powders prepared by sol-gel processes are pure, homogeneous, and highly reactive, and the synthesis temperature (as low as 800–1000°C) is much lower than CMO and EF. However, this synthesis technique often requires expensive (and environmentally unfriendly) organic precursors and solvents (9,10), and so is only applicable to niche cases and for small-scale products.

Synthesis of spinel powders using hydrothermal techniques involves reacting the MgO- and Al_2O_3 -bearing precursors in water/steam at appropriate pressures and temperatures. After reaction, the resulting spinel-forming precursors can be pyrolyzed at appropriate temperatures to obtain reactive spinel powders. Fujiyoshi et al. (11) recently synthesized MA spinel precursors by hydrothermally heating gibbsite and magnesium acetate $[\text{Mg}(\text{CH}_3\text{COO})_2]$ for 48 hr at 15.2 MPa and 200°C. They found that spinel could be prepared by heating the precursors at temperatures as low as 500°C. Similar to the sol-gel process, hydrothermal synthesis markedly decreases the spinel synthesis temperature while the resulting spinel powders are homogeneous and reactive. The drawbacks with this technique are that it sometimes uses similar precursors to the sol-gel process and requires a high-pressure autoclave. Furthermore, long reaction times are generally needed to complete the reaction (often several days).

4. Other Novel Synthesis Techniques

Besides “wet-synthesis” methods, another two novel methods have been used to synthesize MA spinel powders. These are mechanochemical alloying and molten salt synthesis (MSS).

In mechanochemical alloying, the appropriate raw materials (oxide, hydroxides, or carbonates) are mixed and co-milled by a high-energy milling machine. On milling a spinel-forming precursor forms from which fine spinel powders can be obtained by crystallization usually below $\sim 1200^\circ\text{C}$. Kim and Saito (12) investigated the effect of dry milling of a powder mixture of $\text{Mg}(\text{OH})_2$ and $\text{Al}(\text{OH})_3$ on spinel formation and found that MA spinel crystallized in a mixture ground for only 15 min at as low as 780°C.

The MSS technique uses low-melting salts as the reaction medium and/or reactants, thus permitting atomic-scale mixing of the reactants in the liquid phase. This, along with the quicker diffusion of species in the liquid medium, means the spinel formation reactions can be completed at a relatively low temperature and in a short time. Zawrah and Khesheh (13) co-melted $\text{Al}(\text{NO}_3)_3 \cdot 9\text{H}_2\text{O}$ and $\text{Mg}(\text{NO}_3)_2 \cdot 6\text{H}_2\text{O}$ at 500°C for 2 hr and later calcined the resulting mixture at 500–1000°C to prepare MA powders. They found that pure nanocrystalline (with a maximum size of ~ 10 nm) spinel powders can be obtained by calcining the mixture at 1000°C.

B. Preparation of Spinel Aggregates

Spinel aggregates used in refractories include fused aggregates and sintered aggregates. Fused spinel aggregates are produced by an electro-fusion process while sintered aggregates are usually made by either reaction sintering of Al_2O_3 and MgO (single-stage sintering) or sintering of partially spinelized powders or preformed spinel powders (double-stage sintering). Commercially, inexpensive Al_2O_3 and MgO sources may be used such as bauxite and brucite. Several research groups including Bradt et al. (14) and Cunha-Duncan and Bradt (15) have examined production of MA spinel aggregates from various types of readily available minerals.

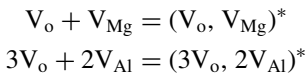
Compared to sintered spinel aggregates (especially those produced by one-stage sintering), electro-fused spinel aggregates are usually purer, denser, and more homogeneous. Furthermore, the spinel crystallite size in the aggregates is larger (up to mm) than in sintered aggregates. These features, along with lower surface reactivity, confer good slag penetration and corrosion resistance and high hot mechanical strength on refractories using fused spinel aggregates although they may lead to poorer thermal shock resistance than sintered aggregates.

Sintered spinel aggregates can be produced by either a single-stage or a double-stage sintering technique. However, it is usually difficult to produce dense spinel aggregates by single-stage sintering, i.e., by direct reaction sintering of a mixture of Al_2O_3 and MgO . The main reason for this is the large volume expansion ($5 \sim 8\%$) associated with spinel formation via $\text{MgO} + \text{Al}_2\text{O}_3 = \text{MgAl}_2\text{O}_4$. Thus, in single-stage sintering, even when a high sintering temperature (depending on the reactivity of the starting materials and their impurity levels, often $>1700^\circ\text{C}$) is used, the synthesized spinel aggregates are still porous. To obtain dense sintered spinel aggregates, the general practice is to use the double-stage sintering technique. In the first stage, partially spinelized or completely spinelized powders (i.e., preformed spinel powders) are prepared using the methods outlined in Section V.A, and in the second stage, the preformed powders are further sintered at high temperatures to obtain dense spinel aggregates.

Clearly, the sintering behavior of preformed spinel powders plays an important role in preparation of dense spinel aggregates (or products). Therefore, factors affecting sintering behavior of spinel powders will now be discussed. A key factor is the powder surface reactivity. The higher the surface reactivity of the preformed spinel powders, the better their sinterability. Fused spinel powders usually have poor surface reactivity, so they show poor sinterability. On the other hand, because of the higher surface reactivity of powders synthesized by processes such as “wet synthesis,” mechanochemical alloying, and molten salt synthesis, spinel densification can be completed at much lower temperatures. For example, Kong et al. (16) sintered MA spinel powders prepared by the

mechanochemical process and found that spinel could be densified to >96% theoretical density at a temperature as low as 1500°C. In the double-stage sintering process, the calcination temperature in the first stage is important, as it affects the surface reactivity and volume expansion associated with the spinel formation reaction. Generally speaking, with increasing calcination temperature, the spinelizing extent increases and thus the volume expansion associated with the spinel formation reaction decreases. However, increased calcining temperature usually decreases surface reactivity. Therefore, in double-stage sintering, an appropriate calcination temperature must be selected so that the spinel powders maintain a high surface reactivity but suffer from a minimum effect of volume expansion during the second-stage.

Spinel stoichiometry affects the sinterability of spinel powders since oxygen lattice diffusion through vacancies is the rate-controlling step and the oxygen vacancy (V_o) content is a function of stoichiometry (17). The oxygen ion is believed to be the slowest moving species for diffusion because it is large (0.14 nm) and has low diffusivity in both Al_2O_3 and MgO , which have close-packed oxygen sublattices similar to MA. The generation of oxygen vacancies extrinsically in nonstoichiometric MgO -rich compositions promotes oxygen lattice diffusion, and densification is consequently enhanced. In Al_2O_3 -rich compositions, however, oxygen vacancies are not likely to be the predominant defect species, even though their diffusion is the rate-determining sintering step. Al_2O_3 -rich compositions exhibit much lower densification rates than nonstoichiometric MgO -rich compositions, as expected from the low concentration of V_o . The reason for this is that the electrostatic attraction of neighboring oppositely charged point defects form defect clusters indicated by the following reactions:



The effects of additives on the sintering of spinel powders have also been extensively studied. As in spinel formation, fluorides such as LiF , ZnF_2 , BaF_2 , AlF_3 , and CaF_2 improve the sinterability of spinel powders by formation of a liquid phase. However, B_2O_3 , a strong mineralizer for spinel formation, hinders the densification of spinel powders. A similar detrimental effect is also found with V_2O_5 . The quicker crystal growth due to additions of B_2O_3 and V_2O_5 probably hinders the sintering process (18). TiO_2 is one of the most investigated additives for the sintering of spinel powders [e.g., (18,19)]. It is commonly accepted that addition of appropriate amounts of TiO_2 can significantly increase spinel densification. Increasing TiO_2 from 0 to 1.5 wt% gradually increases the sintered density (Figure 7) believed due to exsolution of alumina and dissolution of TiO_2 in spinel (19). Other additives that are effective in accelerating the sintering of spinel include $AlCl_3$, Y_2O_3 , Yb_2O_3 , Dy_2O_3 , Cr_2O_3 , MnO_2 , SrO , BeO , and ZrO_2 (or $ZrSiO_4$).

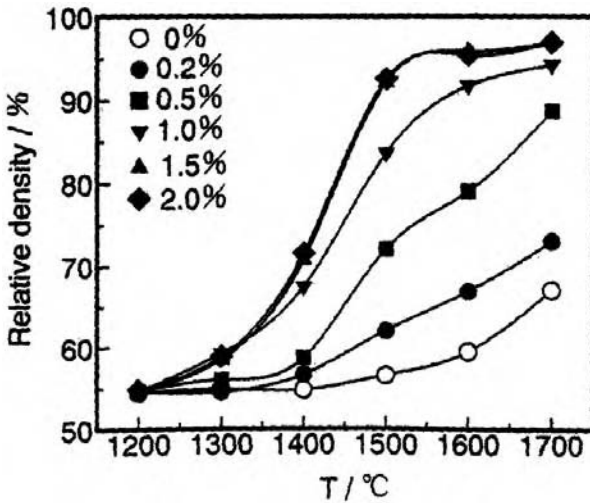


Figure 7 Effect of TiO₂ addition on the relative density of sintered spinel. (From Ref. 19.)

C. Commercial Spinel Materials

As described in Section B, spinel powders and aggregates used in refractories can be prepared using a range of materials and processes. Due to the differences in properties of the raw material, stoichiometry of spinel and synthesis processes, spinel powders and aggregates prepared for use in refractories exhibit differing properties and performance. Table 3 lists typical properties of some industrial spinel raw materials produced by sintering and electro-fusion processes. The main impurities in spinel raw materials include Na₂O, CaO, and SiO₂. Higher levels of impurities and porosity are found in reaction sintered spinels from bauxite and magnesite (Sintered MA4). Sintered MA1, MA2, and MA3 are pure sintered spinels produced by Alcoa with commercial designations MR66 (MgO-rich), AR78 (nearly stoichiometric), and AR90 (alumina-rich), respectively. MR66, due to its hydration tendency, is mainly used to make spinel-containing bricks, whereas AR78 and AR90 are more commonly used in castable systems. MR66, AR78, and AR90 are well sintered so that their density and porosity levels are close to those seen in fused spinel although their spinel crystallite sizes are smaller (a few 10's of μms). Figures 8 and 9 show the microstructures of AR78 and AR90 (20) revealing alumina laths and angular spinel crystallites in AR90 and angular spinel crystallites and light CA₆ and CMAS (CaO–MgO–Al₂O₃ · SiO₂) secondary phases in AR78.

Table 3 Chemical Compositions and Densities of Industrial Spinel Raw Materials

	Sintered MA1 (MR66)	Sintered MA2 (AR78)	Sintered MA3 (AR90)	Sintered MA4	Fused MA
Chemical composition (wt%)					
MgO	32.0–33.5	22.0–23.0	9.0–10.0	30.11	26.19
Al ₂ O ₃	~66	~78	~90	59.74	73.32
CaO	0.31–0.47	0.22–0.26	0.12–0.16	1.17	0.22
SiO ₂	0.06–0.12	0.08–0.12	0.03–0.10	4.31	0.06
Na ₂ O	0.02–0.04	0.06–0.12	0.13–0.17	0.03	0.17
Fe ₂ O ₃	0.15–0.25	0.10–0.20	0.05–0.08	1.45	0.04
TiO ₂	—	—	—	2.81	—
Bulk density (g · cm ⁻³)	3.26–3.29	3.25–3.29	3.38–3.42	3.00	3.48
Apparent porosity (%)	1.2–2.0	1.50–2.0	1.5–2.5	9.2	<1.5

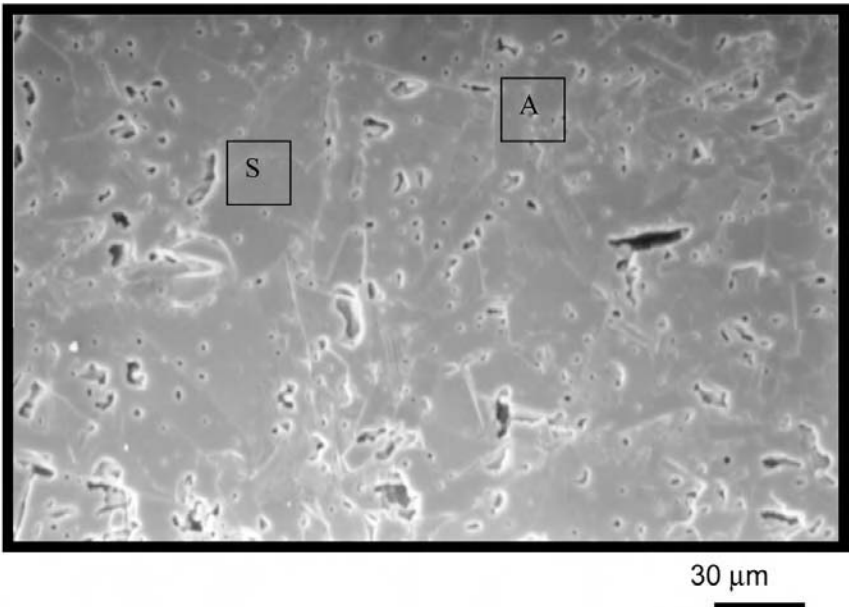


Figure 8 SEM image of AR90 showing angular spinel (S) and alumina laths (A). (From Ref. 20.)

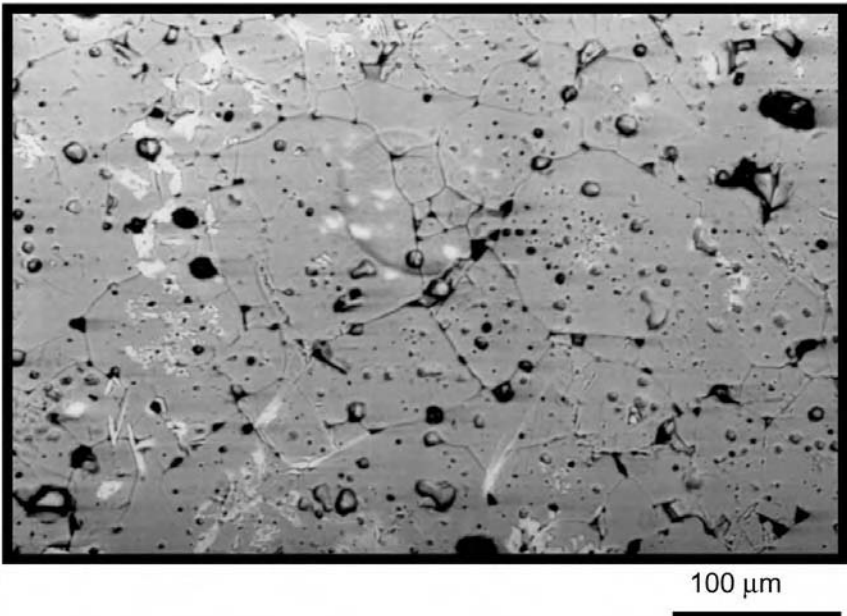


Figure 9 SEM image of AR78 showing angular spinel crystallites and lighter CaO-containing second phases. (From Ref. 20.)

VI. SPINEL-CONTAINING REFRACTORIES

A. Main Types

Modern spinel-containing refractories (neglecting MK chromium spinels) can be classified into the following main types: (1) MgO–Al₂O₃ refractories (including MgO–MA, pure MA, and Al₂O₃–MA); (2) MgO–Al₂O₃–TiO₂ refractories (including, e.g., MgO–MA–MgTi₂O₄ and Al₂O₃–MA–Al₂TiO₅); (3) MgO–Al₂O₃–ZrO₂ refractories (including MgO–MA–ZrO₂ and Al₂O₃–MA–ZrO₂); (4) MgO–Al₂O₃–SiO₂ (including, e.g., MA–M₂S and MA–A₃S₂) refractories; (5) MgO–Al₂O₃–CaO refractories (including, e.g., MA–CA₆) and (6) MA–carbon refractories (including, e.g., MA–SiC–C, Al₂O₃–MgO–C, and MgO–Al₂O₃–C).

B. MgO–MA Refractories

1. Historical Development of Sintered MgO–MA Bricks

The earliest MgO–MA bricks date back to the 1960s. Strictly speaking, they were simply improved magnesia bricks. In the first generation of MgO–MA

bricks, a small amount of alumina or bauxite powder, co-milled with MgO powder, was added to magnesia bricks. On firing, the co-milled MgO and Al_2O_3 reacted to form in-situ spinel. Compared with silicate (CMS or M_2S) bonded magnesia bricks (see Chapter 6, Magnesia Refractories in this book), this first generation of MgO–MA bricks had promising properties, including higher hot mechanical strength and much better thermal shock resistance. The early work also found that increasing Al_2O_3 content generally leads to better thermal shock resistance. However, with increasing level of Al_2O_3 , brick porosity also increased and when the Al_2O_3 content was above 10 wt%, it was difficult to make dense bricks. The improvement in thermal shock resistance with increasing Al_2O_3 content was found to be related to the mismatch of thermal expansion coefficients between MgO ($\sim 13.5 \times 10^{-6}$) and MA ($\sim 8.4 \times 10^{-6}$). Due to this mismatch, microcracks form between MgO and MA grains during cooling, assisting release of thermal stress and disrupting the microstructure, making crack propagation more difficult. The increase of porosity with Al_2O_3 content is related to the volume expansion (5 ~ 8%) associated with the spinel formation reaction from MgO and Al_2O_3 . For this reason, the amount of Al_2O_3 in the first generation of MgO–MA bricks was limited to be <10 wt%. The second generation of MgO–MA bricks, developed in the mid-1970s, used a preformed synthetic spinel grain to replace some MgO. The use of preformed MA grain instead of Al_2O_3 eliminated the thermal expansion caused by the formation of in-situ MA in the first-generation bricks, so a large amount of spinel could be introduced without significantly increasing the porosity. Nevertheless, in the second generation of MgO–MA bricks, the matrix remained unimproved because no spinel fines were present. To improve this, the third generation of MgO–MA bricks has been developed recently which contain spinel aggregates and spinel introduced in the matrix via direct addition of preformed spinel and/or alumina powders to form in-situ spinel. The third generation of bricks thus combine the main advantages of the first and second generations, so they show much better properties such as higher hot strength, higher slag penetration resistance, and higher thermal shock resistance and longer service life in many application areas. The morphologies of in-situ generated spinel are a complex function of a range of factors including local composition and temperature. Figure 10 shows several in-situ spinel morphologies including the characteristic angular habit and a tuber-like shape often seen in the presence of large amounts of liquid (21).

2. MgO–MA Bricks in Steel-Making Furnaces

Due to environmental concerns about formation of Cr^{6+} in MgO– Cr_2O_3 (MgO–MK) refractories, MgO–MK refractories previously used in many steel-making furnaces such as RH and VOD vessels have been, and are being, replaced by

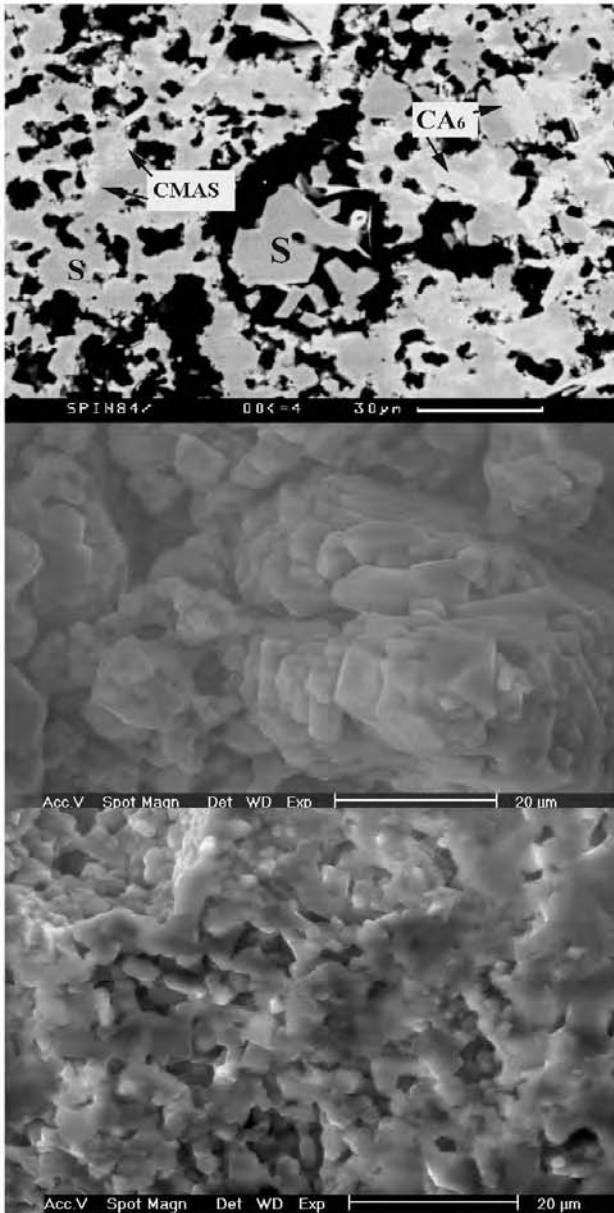


Figure 10 Various in situ spinel morphologies. (From Ref. 21.) The top picture shows angular (center S) and tuber-like (left S) spinel, the mid picture angular agglomerates and the bottom picture rounded spinel agglomerates.

high-quality MgO–MA refractories. Another reason for this replacement is that the properties and performance of second- and third-generation MgO–MA bricks are competitive with those of MgO–MK bricks. Table 4 shows some typical properties of MgO–MA and MgO–MK bricks used in the slag line of a VOD (VAD) ladle (22) illustrating that properties such as hot strength and corrosion resistance of MgO–MA bricks approach, or are better than, those of MgO–MK bricks.

Properties of MgO–MA bricks can be further improved by using fused aggregates to partially or completely replace sintered aggregates. An effective additive for improvement of properties of MgO–MA bricks is ZrO₂, which enhances hot strength slag corrosion resistance. Addition of ZrO₂ to MgO–MA bricks alleviates some problems attributable to spinel. Lime, from impurities in the magnesia-spinel bricks or from other sources such as slags, extracts the alumina within the spinel to form low-melting calcium aluminates. As a result, the hot strength of the MgO–MA will be decreased. However, when ZrO₂ is added, it reacts with lime to form high-melting (2550°C) because CaZrO₃ reaction between ZrO₂ and CaO is more thermodynamically favorable than reaction between Al₂O₃ and CaO, so avoiding formation of low-melting calcium aluminates. ZrO₂ can be incorporated in the form of single-phase ZrO₂ or in the form of Al₂O₃–ZrO₂ coexisting grain, but the latter appears more effective in improving the properties, because of formation of both CaZrO₃ and in-situ spinel. Gruver (23) showed that the modulus of rupture (MOR) of MgO–MA bricks at

Table 4 Properties of MgO–MA and MgO–MK Bricks Used in Slag Line of VOD (VAD) Ladle

	MgO–MA (No. 1)	MgO–MA (No. 2)	MgO– MK
Chemical composition (wt%)			
MgO	89	92	59
Al ₂ O ₃	10	7	10
Cr ₂ O ₃	—	—	19
Fe ₂ O ₃	—	—	8
Apparent porosity (%)	14.8	16.9	14.9
Bulk density (g · cm ⁻³)	3.06	2.98	3.17
Cold crushing strength (MPa)	78	58	85
Modulus of rupture (MPa)			
RT	16	11	15
1400°C	15.1	10.2	11
Wear ratio (Rotary slag test)	1.00	0.96	1.88

Source: From Ref. 22.

$\sim 1480^\circ\text{C}$ increased from 1.36 MPa (without addition) to 3.15 MPa (with addition of single ZrO_2) and 4.67 MPa (with addition of $\text{Al}_2\text{O}_3\text{-ZrO}_2$).

3. MgO–MA Bricks in Glass Tanks

The condensation zone of glass furnace regenerators is prone to attack. Although the temperature in this zone is not particularly high ($800 \sim 1000^\circ\text{C}$), the refractories are exposed to an extremely corrosive environment. The main corrosive agents in this zone include Na_2O , SO_3 , and Na_2SO_4 , which are introduced through the waste gases used. $\text{Al}_2\text{O}_3\text{-SiO}_2$ system refractories, e.g., high alumina and mullite-based refractories, are not suitable for application in this zone, since they react rapidly with alkalis to form low-melting phases. Magnesite or dolomite refractories are also not suitable, because MgO and CaO can react easily with SO_3 gas to form low-melting MgSO_4 and CaSO_4 , respectively. MA is most suitable in glass checkers because of its excellent resistance to these corrosive agents. Industrial trials showed that pure fused spinel bricks can achieve 10 years' service life (24) and pure spinel bricks (spinel-bonded spinel) should be ideal in such an application. These bricks are, however, expensive and have poor thermal shock resistance so that MgO -spinel bricks have been tried. As mentioned earlier, the thermal expansion mismatch between MgO and MA can lead to improved thermal shock resistance. However, due to MgO 's lower resistance to corrosive soda- and sulphate-containing compounds, especially SO_3 gas, MgO –MA bricks for such application need careful design. One strategy is using MgO as aggregates rather than as fines in the matrix; another is using enough spinel that the MgO clinkers are completely covered by spinel. Use of MgO -rich spinel to introduce MgO is effective because of the higher coverage of MgO by spinel. Table 5 lists

Table 5 Properties of Improved MgO –MA Bricks Used for Glass Furnace Regenerator

Chemical composition (wt%)	
MgO	76
Al_2O_3	15
CaO	1.3
SiO_2	3.2
Fe_2O_3	3.5
Porosity (%)	16–20
Density ($\text{g} \cdot \text{cm}^{-3}$)	2.85–3.00
Hot bend strength (MPa)	
1260°C	11.0
1400°C	1.0

Source: From Ref. 24.

compositions of MgO–MA bricks for these applications (24), and such bricks showed relatively good resistance to SO_3 and sulphate. No obvious corrosion was found except that secondary CMS phases in the bricks reacted to form Na–Ca sulphate (24).

In addition to sintered MgO–MA bricks, electro-fused MgO–MA blocks are being developed for application in the melting zones of glass tanks [e.g., (25)]. Such blocks are comprised essentially of ~ 60 mol% MA spinel with ~ 40 mol% MgO and a minor silicate boundary phase. The MgO is distributed bimodally as a fine co-precipitated phase locked within the spinel grains or as large primary MgO dendrites. Such refractories exhibit high strength with excellent high-temperature retention and extremely high creep and corrosion resistance; therefore, they may represent the ultimate superstructure option for high-temperature glass-melting tanks.

4. MgO–MA Bricks in Cement Kilns

MgO–MA bricks have also been developed and used to replace MgO–MK bricks in cement kilns. They are used in the burning (sintering), transitional and cooling zones, although the use of MgO–MA bricks to line the cooling and transitional zones is more common than in the burning zone, due to higher temperatures and more corrosive environment in the latter.

Bricks in the burning zone are protected from corrosion by an in-situ cement clinker coating that develops on the refractories surface (26). MgO–MA bricks originally developed for the transitional zone did not allow formation of such a coating and so were inappropriate for use in the burning zone. To use them in the burning zone, their coating formation and its adherence ability had to be improved.

Zongqi and Rigaud (27) found that fine crystalline spinel in MgO–MA bricks reacts with CaO from the cement forming low-melting phases and belite with good adherence. Lack of fine spinel crystals resulted in poor adherence. Impurities in MgO–MA bricks as well as deliberate additions are effective in improving coating formability. Using MgO and MA raw materials containing appropriate levels of impurity accelerates formation of coatings. For example, appropriate amounts of CaO and SiO_2 in the MgO aggregate can accelerate the formation of cement coatings. Additives such as Fe_xO , TiO_2 , and ZrO_2 (28–30) also improve coating quality. The added Fe_xO can react with CaO and Al_2O_3 from the cement clinker and refractories to form $\text{CaO–Al}_2\text{O}_3\text{–Fe}_x\text{O}$ liquid, contributing to the cement coating adhesion. Fe_xO can be added as Fe_xO or in the form of fused $\text{Al}_2\text{O}_3\text{–Fe}_x\text{O}$ or $\text{Fe}_x\text{O–MgO}$ grains. Addition of TiO_2 can also improve coating stability via formation of CaTiO_3 . ZrO_2 additions react with CaO from the cement clinker to form CaO-stabilized ZrO_2 and CaZrO_3 , which improve coating adhesion. Table 6 shows typical properties of MgO–MA bricks developed for the different zones of a cement kiln (31).

Table 6 Typical Properties of MgO–MA Bricks Recommended for Different Zones in Cement Kiln

	SP-8	SP-8D	SP-8C	SP-8C-3	SP-8-8	SP-8-11
Apparent porosity (%)	15.5	15.0	15.0	15.5	17.0	16.5
Bulk density ($\text{g} \cdot \text{cm}^{-3}$)	2.95	3.00	3.00	3.00	2.90	2.95
Cold crushing strength (MPa)	44	54	54	60	50	40
Refractoriness under load T_2 ($^{\circ}\text{C}$)	> 1700	> 1700	> 1700	> 1700	> 1700	> 1700
Permanent linear change (%)	+0.1	+0.1	+0.1	+0.1	+0.1	+0.1
Thermal expansion at 1000°C (%)	1.1	1.1	1.1	1.1	1.1	1.1
Chemical composition (wt%)						
MgO	81	81	79	80	81	86
Al_2O_3	18	18	17	17	18	11
Others	—	—	Fe_2O_3	$\text{Fe}_2\text{O}_3, \text{TiO}_2, \text{ZrO}_2$	—	—
Performance	Spalling resistance	Abrasion resistance	Coating adhesion	Thermal load resistance	Spalling resistance	Spalling resistance
Application zone	Cooling zone, transitional zone	Cooling zone	Sintering zone	Sintering zone	Transitional zone	Transitional zone

Source: From Ref. 31.

5. MgO–MA Castables

As well as MgO–MA bricks, MgO–MA castables have been developed. First-generation MgO–MA castables were developed using phosphate binders (32). Fused alumina clinkers were added to obtain a slightly positive permanent volume change once fired at 1600°C. Phosphate binders were supposed to improve the hydration resistance of MgO fines. On adding Al₂O₃, slag penetration resistance improved slightly, but structural spalling resistance improved significantly although hot strength deteriorated. Corrosion resistance tended to decrease with Al₂O₃ addition but was still better in basic slags when compared to a pure alumina castable.

Second-generation MgO–MA castables with similar MgO–Al₂O₃ clinkers have been developed using hydratable-alumina as a binder. The optimum size distribution of both MgO and Al₂O₃ is critical. When MgO and Al₂O₃ react to form in-situ spinel, as discussed in Section V.B, a volume expansion of 5 ~ 8% occurs, affecting the volume stability. By proper choice of reactive alumina, and control of the sintering process, it is possible to achieve a volume stable MgO–MA castable with 20–30% Al₂O₃. Adjustments (e.g., changing the particle size of added Al₂O₃ and adding preformed spinel) can be made to the formula, which allows control of the volume change at almost any given alumina content. The advantage of second generation MgO–MA castables is higher hot mechanical strength due to elimination of low-melting phosphates from the binder. Slag tests show that slag penetration resistance increases as alumina content increases although corrosion resistance decreases. In second-generation MgO–MA castables, either fused or sintered spinel clinkers with different stoichiometry can be used. Rigaud et al. (33) compared the effect of MgO-rich (MR66) and two Al₂O₃-rich spinels (AR78 and AR90) on the Modulus of Rupture (MOR) and corrosion resistance of MgO–MA castables, and found that castables using MgO-rich spinel had slightly higher MOR and better corrosion resistance than those using AR78 and AR90. The better corrosion resistance using MgO-rich spinel is attributed to the higher MgO content, as discussed by Zhang and Lee (34), since the solubility of MgO in silicate slag is lower than Al₂O₃. Bi et al. (35) verified that increasing Al₂O₃–MgO ratio in MgO–MA castables generally leads to better slag penetration resistance but poorer corrosion resistance.

To improve the flowability and hydration resistance of MgO fines, micro-silica is also used as binder, individually or along with hydratable alumina. However, its presence significantly decreases the castables' hot strength due to liquid formation. Calcium aluminate (CA) cement is sometimes used as well, although its addition also leads to formation of low-melting phases at high temperatures and thus decreases hot strength and slag corrosion resistance.

6. Corrosion of MgO–MA Refractories

The corrosion mechanisms of MgO–MA refractories depend on the environment in which they are used. In CaO–Al₂O₃–SiO₂ (CAS) model steel-making slags, if the slag Al₂O₃ content is high, it will react with MgO from the refractories to form a protective secondary spinel layer on the MgO surface, leading to indirect corrosion of MgO in the slag (Figure 11 after Goto et al. (36)). If the slag Al₂O₃ content is low, no continuous spinel layer forms on MgO; in this case, MgO will react with CaO and SiO₂ from the slag to form low-melting phases such as CMS and C₃MS₂ and then dissolve into the slag directly. If the slag CaO is high, MA from the MgO–MA refractories can react with it to form low-melting calcium aluminate phases; on the other hand, if the slag CaO is low, MA will react with CaO and SiO₂ from the slag to form low-melting phases such as C₂AS or CAS₂ and thus dissolve into the slag directly (37). Figure 12 shows schematically the corrosion process of an MgO–MA brick in a CAS slag (C/S = 1, Al₂O₃ = 20 wt%) (36). In such a slag, MgO dissolves in the slag indirectly via formation of a secondary spinel on its surface while MA dissolves in the slag directly.

In a more complex steel-making slag, e.g., an Fe- and Mn-containing CaO–MgO–Al₂O₃–SiO₂ (CMAS) slag, the corrosion mechanism will be slightly

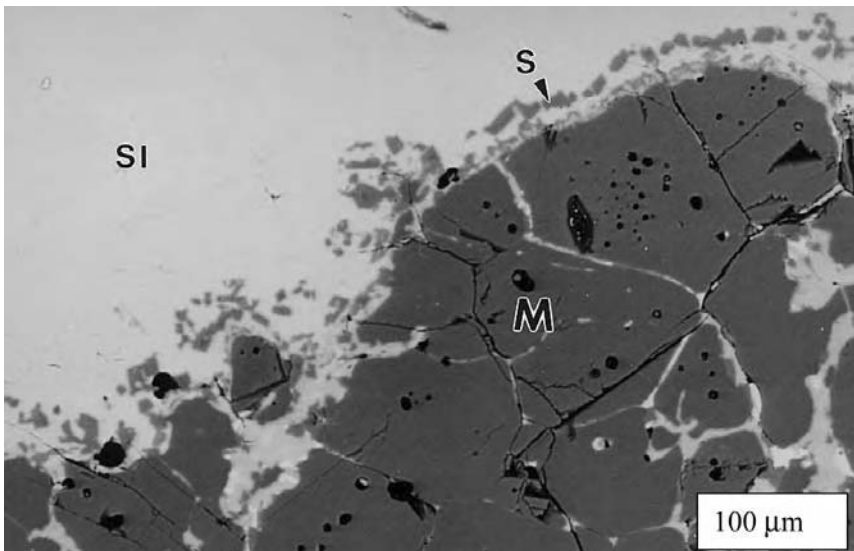


Figure 11 Angular spinel particles (S) precipitated adjacent a MgO grain (M) in contact with CAS slag (Sl). (From Ref. 36.)

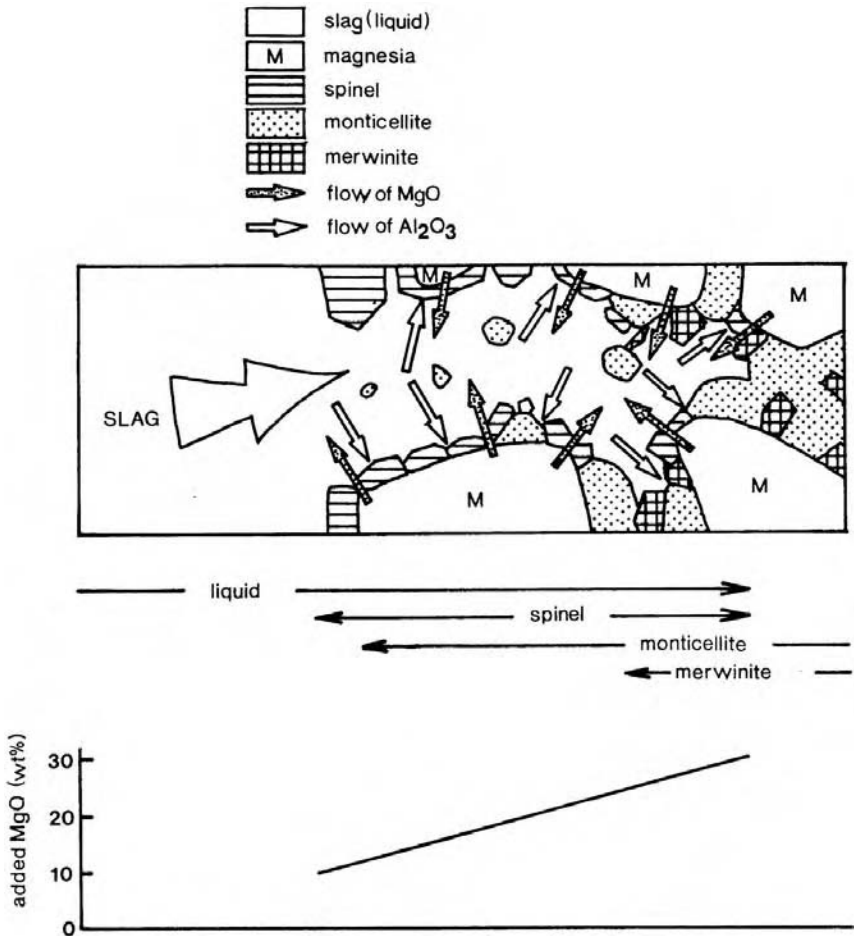


Figure 12 Schematic diagram of corrosion process of MgO–MA refractories in CAS slag. (From Ref. 36.)

different. Based on the corrosion mechanisms of MgO [e.g., (38)] and MA [e.g., (20,39,40)], the overall corrosion mechanisms of MgO–MA refractories can be predicted to be as follows. MgO in the refractories may dissolve into the slag via three routes: (1) reaction with slag Al_2O_3 to form a spinel layer so the MgO dissolves into the slag indirectly; (2) reaction with slag Fe_xO and MnO to form a magnesio-wustite so the MgO dissolves in the slag indirectly; and (3) reaction with slag CaO and SiO_2 to form low-melting phases such as CMS and C_3MS_2 , so in this case the MgO dissolves directly in the slag. In such a slag, MA from

the refractories may also dissolve in the slag in three ways: (1) reaction with slag Fe_xO and MnO to form a complex spinel $(\text{Mg},\text{Mn},\text{Fe})(\text{Al},\text{Fe})_2\text{O}_3$ and thus dissolve into the slag; (2) reaction with slag CaO to form low-melting calcium aluminates; and (3) reaction with slag CaO and SiO_2 to form low-melting CAS phases such as C_2AS and CAS_2 , so the MA dissolves directly in the slag.

C. Al_2O_3 –MA Refractories

Similar to the MgO –MA system, liquid formation temperatures in the Al_2O_3 –MA system are high (see Figure 2), so the refractories in this system also have high refractoriness. Due to the much lower thermal expansion coefficient of Al_2O_3 than that of MgO , the thermal expansion coefficients of Al_2O_3 –MA refractories are generally lower than those of MgO –MA refractories. Therefore, Al_2O_3 –MA refractories usually show better thermal shock/spalling resistance than MgO –MA refractories, although the mismatch between the thermal expansion coefficients of Al_2O_3 and MA is much smaller than that between MgO and MA.

Like MgO –MA refractories, Al_2O_3 –MA refractories are prepared as shaped bricks or monolithic castables. In recent years, extensive research and development work on Al_2O_3 –MA castables had led to their use in many areas such as steel-making ladles. Two Al_2O_3 –MA castable types are used: Al_2O_3 – MgO castables and Al_2O_3 –spinel castables. In the former, MgO is added to alumina-based castables to form in-situ spinel, and in the latter, preformed synthetic MA spinel is used instead of MgO . Due to the difference in the spinel used, these two kinds of castable show different microstructures, properties, and performances.

1. Al_2O_3 –Spinel Castables

Effect of Preformed Spinel Addition on Physical Properties. In Al_2O_3 –spinel castables, preformed spinel is used, so the volume expansion associated with the spinel formation reaction that occurs in Al_2O_3 – MgO castables is eliminated. As a result, compared with Al_2O_3 – MgO castables, Al_2O_3 –spinel castables usually show better thermal shock resistance.

Use of preformed spinel also improves the mechanical strength of Al_2O_3 –spinel castables. MacZura et al. (41) studied an Al_2O_3 –spinel castable containing 15 wt% alumina-rich spinel, 15 wt% CA cement, and 70 wt% alumina and found that hot MOR at 1400 or 1500°C became much higher than seen in alumina castables without addition of spinel. Vance et al. (42) made similar observations. Ko and Chan (43) studied the effect of spinel content on mechanical strength of Al_2O_3 –spinel castables and found that both cold MOR and HMOR of the Al_2O_3 –spinel castables increases with increased AR90 spinel content (Figures 13

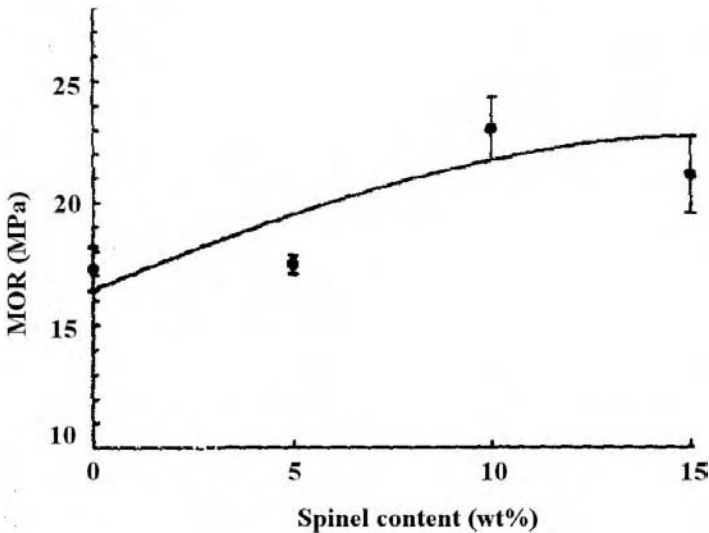


Figure 13 Effect of spinel content on the cold modulus of rupture of Al_2O_3 -spinel castables. (From Ref. 43.)

and 14). The enhanced mechanical strength of Al_2O_3 -spinel castables from the addition of preformed alumina-rich spinel was attributed to the reaction of CaO from the cement binder with Al_2O_3 in the preformed alumina-rich spinel forming calcium aluminate phases such as CA_6 , which improve the bond linkage between the CA_6 , alumina, and spinel grains in the matrix (41,43) as illustrated in Figure 15.

As well as mechanical strength, creep resistance of Low Cement Castables (LCC) and Ultra LCC Al_2O_3 -spinel castables is also significantly improved by addition of alumina-rich spinel (44), although it is not clear whether the improvement in bond linkage stated above is responsible for this or not.

Effect of Preformed Spinel Addition on Slag Penetration and Corrosion Resistance. Slag penetration and corrosion resistance of Al_2O_3 -spinel castables using preformed spinel has been extensively investigated in both laboratory and industrial trials. In general, addition of preformed spinel results in better slag penetration resistance since it is believed to make the local penetrating slag more viscous. The mechanism by which it achieves this is still the subject of debate but may be associated with dissolution of the spinel, affecting local slag composition, and/or the potential for the spinel to take up slag ions such as Fe^{2+} and Mn^{2+} . Nonetheless, depending on the properties of the preformed spinel, its effect on the slag penetration and corrosion resistance varies.

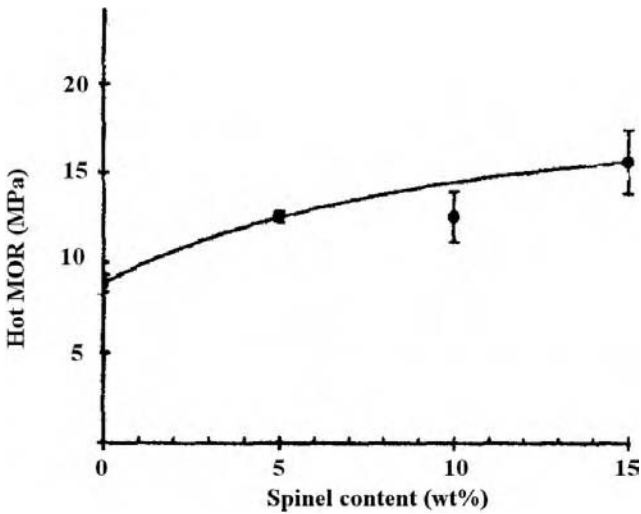


Figure 14 Effect of spinel content on the hot modulus of rupture of Al_2O_3 -spinel castables. (From Ref. 43.)

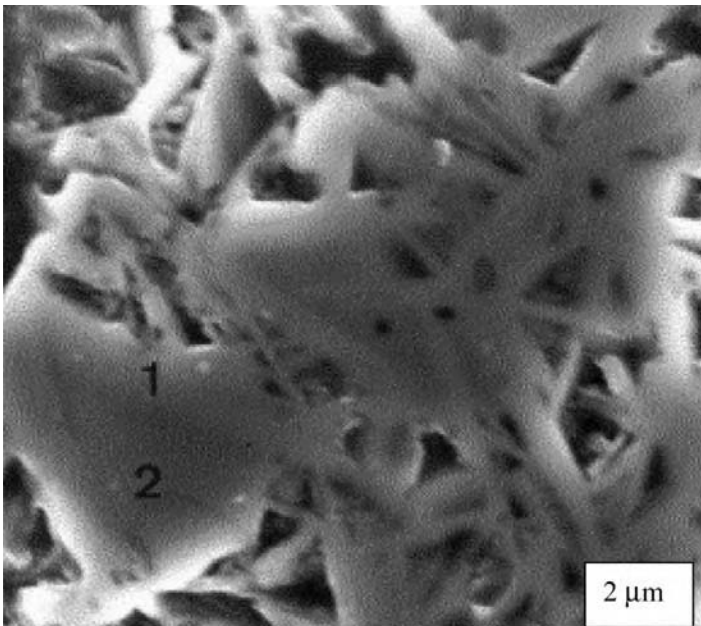


Figure 15 SEM image of the matrix of an Al_2O_3 -spinel castable containing interlinked spinel (2) and lighter CA_6 whiskers (1). (From Ref. 43.)

Spinel particle size has a clear influence on slag penetration resistance. Fine spinel powders generally lead to better slag penetration resistance than the use of coarse grain [Figure 16 after Mori et al. (45)], although the presence of the latter confers better behavior than in castables without spinel addition (46). Fine spinel grains can be more evenly distributed in the castables, especially in the matrix and, because of their higher surface reactivity, they can take up slag ions such as Fe^{2+} and Mn^{2+} or dissolve more efficiently than coarse spinel grain.

The level of spinel addition also plays an important role in inhibiting slag penetration and corrosion. As shown in Figure 17, if appropriate amounts of spinel are used, both slag penetration resistance and corrosion resistance of the castables can be improved (47). Others have also found similar results [e.g., (45, 48–50)]. Interestingly, although the compositions of the samples and slags these researchers used were different, their results all indicated that the spinel content corresponding to the best slag penetration resistance seems to be around 20 wt%.

Another important issue affecting slag penetration and corrosion resistance is the stoichiometry of the spinel used. Zhang et al. (51) investigated slag corrosion resistance of two alumina-rich spinel clinkers (AR78 and AR90) in a CMAS slag and found that alumina from AR90 reacts with CaO from the slag to form CA_6 , which makes the local slag at the slag–spinel interface become SiO_2 -rich and thus more viscous. As a result, AR90 shows better slag penetration resistance than AR78. Recently, Sarpoolaky et al. (20) compared the slag penetration resistance of these two types of spinel in an Fe- and Mn-containing

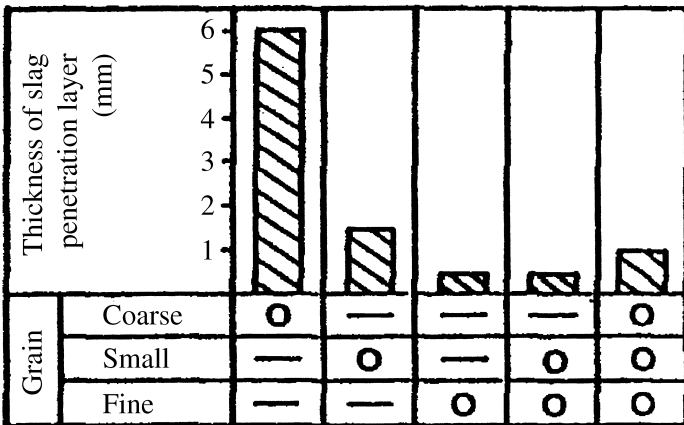


Figure 16 Effect of spinel particle size on slag penetration resistance of Al_2O_3 -spinel castables. (From Ref. 45.)

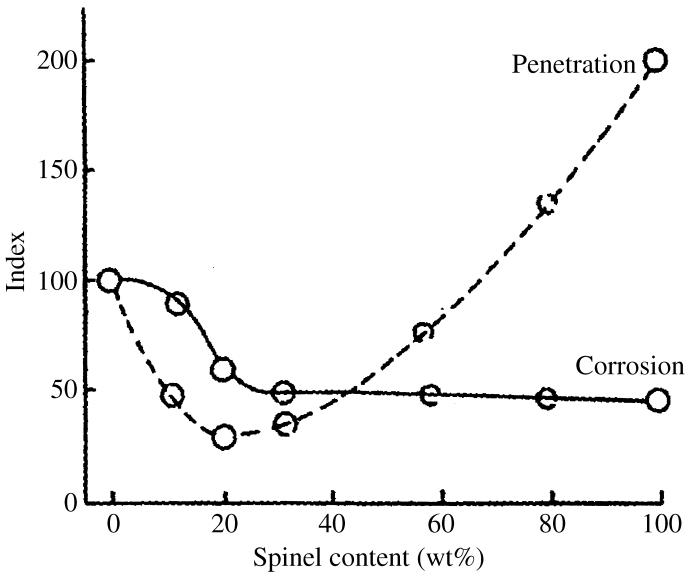


Figure 17 Effect of spinel content on slag penetration and corrosion resistance of Al_2O_3 -spinel castables. (From Ref. 47.)

CMAS slag. AR90 again showed better slag penetration than AR78. The reason is that AR90, due to its higher Al_2O_3 content, is able to form more cation vacancies than AR78, and thus can take up more Fe^{2+} and Mn^{2+} from the slag, leading to the formation of a layer of complex spinel so depressing slag penetration. Figure 18 shows X-ray element distribution maps at the interface of slag-AR90. It can be seen that a complex spinel layer containing Fe and Mn formed between the slag and uncorroded AR90. Cho et al. (40) compared the slag penetration and corrosion resistance of Al_2O_3 -spinel castables containing spinels with different stoichiometries (MgO-rich and Al_2O_3 -rich) in an Fe-containing CAS slag. They found that with increasing Al_2O_3 content in the spinel, the slag penetration resistance improved although the corrosion resistance became worse. Others have found similar results [e.g., (49, 52)]. Figure 19, for example, shows that with increasing Al_2O_3 in a spinel clinker (up to 90 wt%), the castable's slag penetration resistance increases. The improvement in slag penetration resistance with increasing Al_2O_3 content in the spinel is attributed to the increased concentration of cation vacancies in the crystal structure.

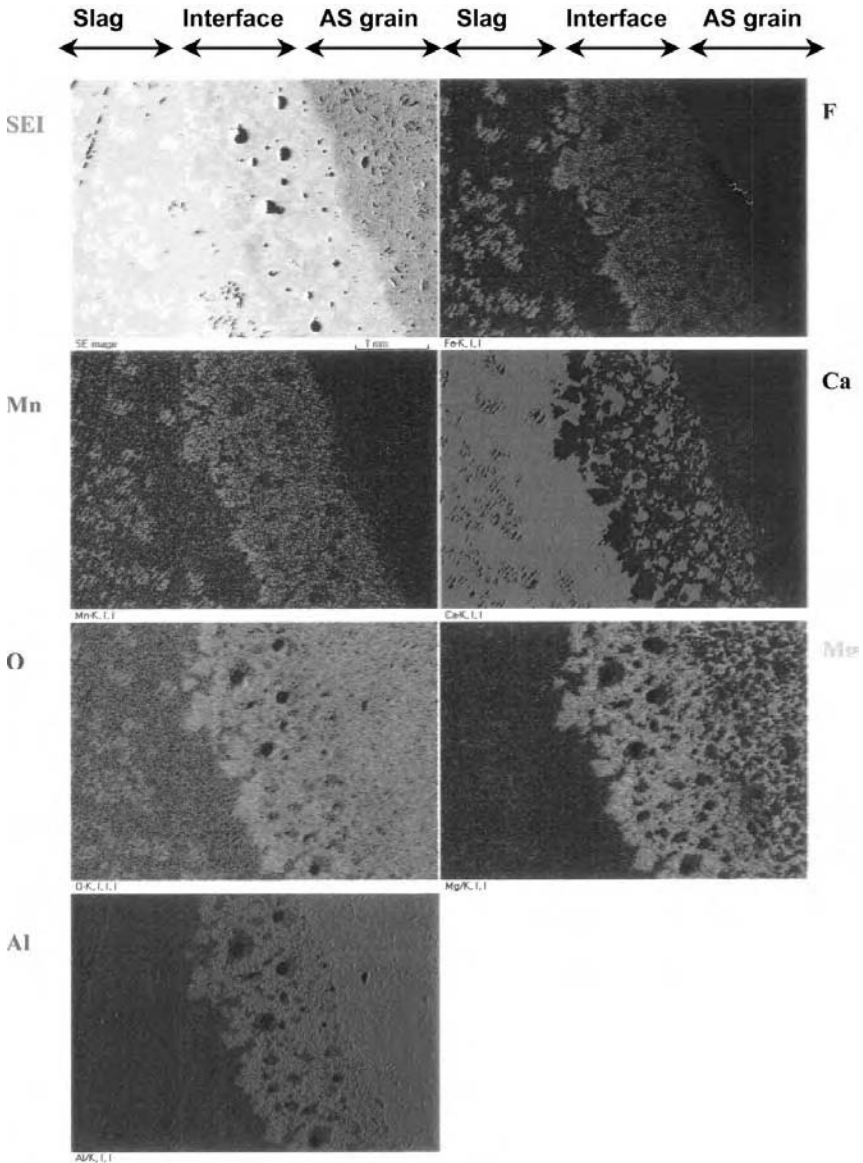


Figure 18 Elemental maps of area around the interface of slag/AR90. (From Ref. 20.) It is evident that the spinel takes up Fe^{2+} and Mn^{2+} slag ions.

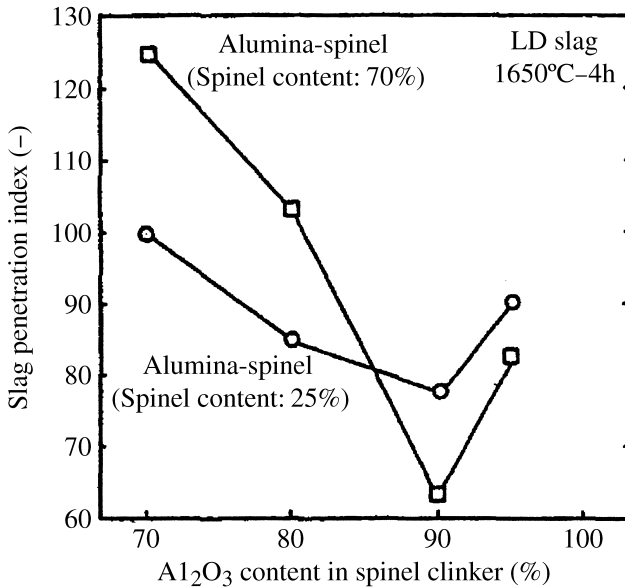


Figure 19 Effect of Al_2O_3 content in alumina-rich spinel on slag penetration resistance of Al_2O_3 -spinel castables. (From Ref. 49.)

2. Al_2O_3 -MgO Castables and Comparison with Al_2O_3 -Spinel Castables

In Al_2O_3 -MgO castables, both Al_2O_3 and MgO are used as the main raw materials, so spinel forms in situ at high temperatures. This type of castable is often used in applications such as the wall and bottom impact pad of a steel-making ladle (while the Al_2O_3 -spinel castables discussed in the previous section are used in the bottom area other than the impact pad).

In Al_2O_3 -MgO castables, MgO (instead of preformed spinel as in Al_2O_3 -spinel castables) is used. Due to the volume expansion associated with the spinel formation reaction from MgO and Al_2O_3 , Al_2O_3 -MgO castables show different microstructures and properties to those seen in Al_2O_3 -spinel castables.

The thermal expansion behavior of Al_2O_3 -MgO castables is related to the spinel formation reaction, which is affected by temperature and MgO content. The starting temperature for formation of in-situ spinel is $\sim 1000^\circ\text{C}$, and the spinel formation rate increases significantly with increasing temperature to

1200–1400°C (53,54). For this reason, at temperatures up to ~1000°C, the thermal expansion of Al₂O₃–spinel castables is similar to that of Al₂O₃–MgO, but with increasing temperature above 1000°C, Al₂O₃–MgO castables show larger thermal expansion. The MgO content also affects the thermal expansion of Al₂O₃–MgO castables. Due to formation of greater amounts of in-situ spinel, with increasing MgO content, thermal expansion of the Al₂O₃–MgO castables increases. As a result of the larger thermal expansion, Al₂O₃–MgO castables have poorer thermal shock resistance than Al₂O₃–spinel castables (55).

MgO content also significantly affects slag penetration and corrosion resistance of Al₂O₃–MgO castables. According to Itose et al. (56), with increasing MgO content up to ~9 wt%, slag penetration and corrosion resistance increases. Nakamura et al. (57) compared the slag resistance of Al₂O₃–MgO castables and Al₂O₃–spinel (with similar MgO content) and found that Al₂O₃–MgO castables showed better corrosion resistance than Al₂O₃–spinel castables (Figure 20), and thus Al₂O₃–MgO castables have longer service lives than Al₂O₃–spinel castables (58), although their thermal shock resistance is poorer. The better slag penetration and corrosion resistance of Al₂O₃–MgO castables over Al₂O₃–spinel castables was attributed to the higher surface reactivity of in situ formed spinel, which can take up slag Mn and Fe ions more efficiently than preformed spinel (54,59). Ko (60) found that slag penetration into Al₂O₃–spinel and Al₂O₃–MgO castables decreased with increased spinel MgO content, a result he attributes to spinel dissolution and MgO precipitation in the penetrating slag leading to increased local slag viscosity and reduced penetration.

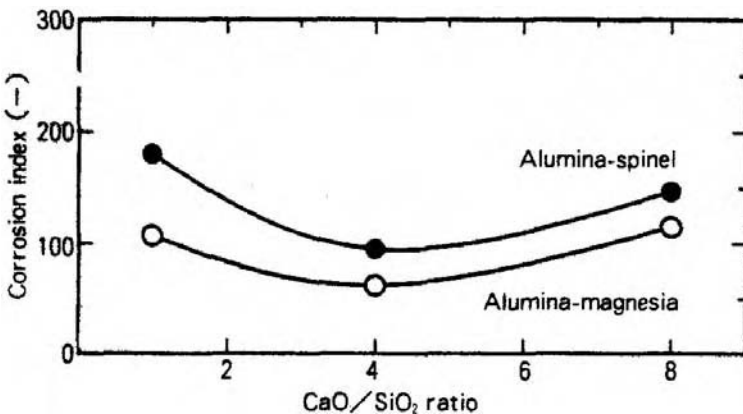
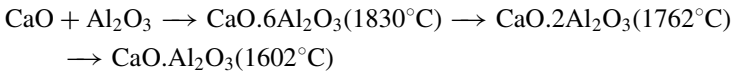


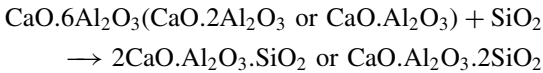
Figure 20 Al₂O₃–MgO castables show better slag corrosion resistance than Al₂O₃–spinel castables. (From Ref. 57.)

3. Corrosion of Al_2O_3 –MA Refractories

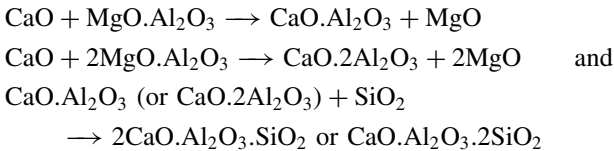
Depending on the slag composition, the corrosion mechanisms of Al_2O_3 –MA refractories are different. In an Fe- and Mn-containing CMAS slag, Al_2O_3 in the Al_2O_3 –MA refractories is initially attacked by the slag CaO via formation of calcium aluminates with melting temperatures shown in brackets according to



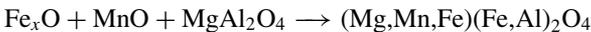
These calcium aluminates are further attacked by the slag SiO_2 via formation of low-melting CAS phases such as C_2AS (1593°C) or CAS_2 (1553°C) according to



On the other hand, MA spinel in the refractories is also attacked by the slag CaO to form calcium aluminates, which further react with the slag SiO_2 to form low-melting CAS phases, according to



or the spinel is attacked by the slag Fe_xO and MnO to form a low-melting complex spinel according to



Many groups have verified the above corrosion mechanism (e.g., (39,52,61–63). Figure 21 schematically shows the overall microstructure of an Al_2O_3 –MgO castable corroded by an Fe- and Mn-containing CMAS slag at 1600°C for 24 hr (52).

D. Spinel-Bonded Spinel Refractories

Pure spinel (spinel-bonded spinel, rebonded spinel) refractories have also been developed for specialist applications. They have much better resistance to alkalis than other spinel-containing refractories, so they can be potentially used in, e.g., glass industry furnaces (regenerator and melting furnaces), induction furnaces, and high soda waste-melting incinerators. Windle and Bentley (64) determined that rebonded spinel bricks exhibit exceptional tolerance to alkali in combination

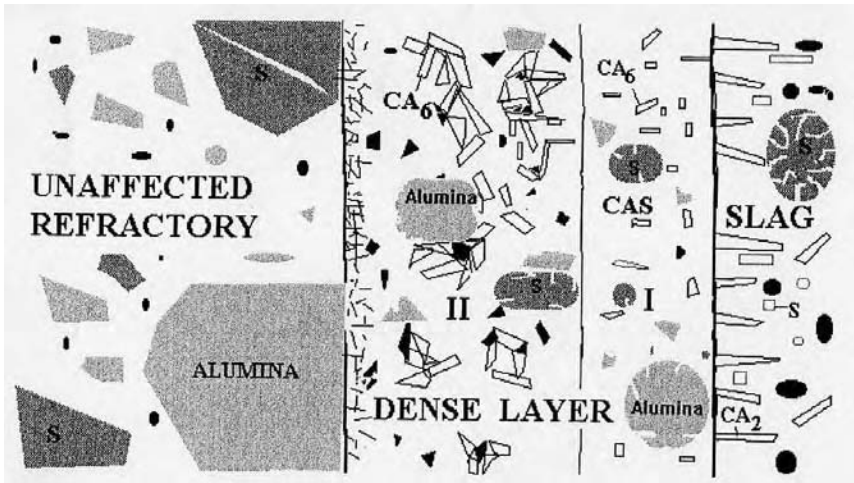


Figure 21 Schematic diagram of the general form of the corrosion front of Al_2O_3 -spinel castables. (From Ref. 52.)

with thermomechanical properties, which are ideal for crowns and superstructures of oxy-fuel fired glass melting furnaces.

E. $\text{MgO}-\text{Al}_2\text{O}_3-\text{ZrO}_2$ Refractories

The eutectic points corresponding to the two subsystems in the $\text{MgO}-\text{Al}_2\text{O}_3-\text{ZrO}_2$ system are all higher than 1800°C (1830°C for $\text{Al}_2\text{O}_3-\text{MgAl}_2\text{O}_4-\text{ZrO}_2$ and 1840°C for $\text{MgO}-\text{MgAl}_2\text{O}_4-\text{ZrO}_2$) (65). This fact, along with the unique properties of ZrO_2 , confers many excellent properties such as high refractoriness, mechanical strength, thermal shock resistance, and slag corrosion resistance on refractories in the $\text{MgO}-\text{Al}_2\text{O}_3-\text{ZrO}_2$ system. Consequently, $\text{MgO}-\text{Al}_2\text{O}_3-\text{ZrO}_2$ refractories have potential uses in many applications such as steel-making furnaces and waste-melting furnaces (66,67). Table 7 compares properties of $\text{MgO}-\text{MA}-\text{ZrO}_2$ castables developed by Sakamoto and Miyagishi with those of $\text{Al}_2\text{O}_3-\text{Cr}_2\text{O}_3$ castables currently used in waste-melting furnaces. $\text{MgO}-\text{MA}-\text{ZrO}_2$ castables show better corrosion resistance and spalling resistance and so may replace $\text{Al}_2\text{O}_3-\text{Cr}_2\text{O}_3$ castables in such applications.

F. $\text{MgO}-\text{Al}_2\text{O}_3-\text{TiO}_2$ Refractories

$\text{MgO}-\text{Al}_2\text{O}_3-\text{TiO}_2$ ($\text{MgO}-\text{MA}-\text{MgTi}_2\text{O}_4$) refractories have also been developed to replace $\text{MgO}-\text{MK}$ refractories used in RH-degasser vessels or to replace

Table 7 Properties of MgO–MA–ZrO₂ Castables Developed for Waste-Melting Furnaces

	MgO–MA–ZrO ₂	Al ₂ O ₃ –Cr ₂ O ₃
Chemical composition (wt%)		
ZrO ₂	5.0	—
Al ₂ O ₃	32.0	86.2
Cr ₂ O ₃	—	9.9
MgO	61.0	—
Water addition (%)	5.7	4.5
Apparent porosity (%)		
110°C × 24 hr	16.0	8.0
1000°C × 3 hr	20.0	10.0
1500°C × 3 hr	19.0	13.0
Bulk density (g · cm ⁻³)		
110°C × 24 hr	2.99	3.55
1000°C × 3 hr	2.91	3.45
1500°C × 3 hr	2.85	3.45
Cold crushing strength (MPa)		
110°C × 24 hr	39	69
1000°C × 3 hr	25	78
1500°C × 3 hr	34	147
Permanent linear change (%)		
1000°C × 3 hr	0.1	0.0
1500°C × 3 hr	0.5	0.2
Corrosion resistance index (slag C/S = 1.0), at 1600°C		
	129	100
Spalling resistance (JIS standard), at 1400°C		
	9	7

Source: From Ref. 66.

Al₂O₃–Cr₂O₃ refractories used in waste-melting furnaces. By selection of appropriate TiO₂–Al₂O₃ and total TiO₂ and Al₂O₃ content in the matrix, and addition of appropriate amounts of preformed spinel, MgO–Al₂O₃–TiO₂ refractories with excellent properties can be fabricated. Table 8 compares properties of developed MgO–Al₂O₃–TiO₂ bricks with those of MgO–Cr₂O₃ bricks (after (68)). Most of the properties of MgO–Al₂O₃–TiO₂ bricks are close to or better than those of the MgO–MK bricks. The bricks were trialed in RH vessels (mainly the lower vessel and snorkel) and showed longer service life than MgO–MK bricks. The better performance of MgO–Al₂O₃–TiO₂ bricks is attributed to the following factors: (1) TiO₂ and MgO in the bricks react with the slag CaO and Al₂O₃ to form high-melting CaO · TiO₂ and MA, respectively; (2) use of TiO₂ reduces slag wettability; and (3) TiO₂ forms a solid solution with MA

Table 8 Comparison of MgO–TiO₂–Al₂O₃ Bricks and MgO–Cr₂O₃ Bricks

	MgO–TiO ₂ –Al ₂ O ₃ Bricks				MgO–Cr ₂ O ₃ Bricks			
	A	B	C	Z	X	Y	Z	Z
Typical chemical composition (wt%)	MgO TiO ₂ Al ₂ O ₃ Cr ₂ O ₃	82.3 7.5 8.2 —	74.8 4.0 18.6 —	61.7	72.3	56.5	61.7	61.7
Apparent density (g · cm ⁻³)		3.53–3.53	3.52–3.53	3.51–3.51	3.65	3.83	3.81	3.81
Bulk density (g · cm ⁻³)		3.18–3.15	3.16–3.19	2.94–2.96	3.05	3.21	3.26	3.26
Apparent porosity (%)		10.8–11.3	9.7–9.8	15.4–16.4	16.5	16.2	14.3	14.3
Compressive strength (MPa)		92–94	67–86	53–72	54	62	69	69
Modulus of rupture (MPa)	R.T. at 1773°K	8.9–9.4 4.9–5.6	10.3–11.3 11.4–12.4	6.8–8.2 1.5–1.6	6.0 4.0	8.0 6.5	7.5 4.0	7.5 4.0

Source: From Ref. 68.

spinel, which takes up slag Fe_xO and MnO , increasing slag viscosity and suppressing slag penetration (69).

G. Spinel–Carbon Refractories

Spinel can be used in carbon-containing refractories to improve their properties. Similar to the oxide-based systems discussed above, spinel can be introduced by using preformed grain or by forming in situ.

Hamazaki et al. (70) investigated the effect of adding preformed spinel on properties of Al_2O_3 – SiC – C castables used in blast furnace troughs and found that additions of spinel improved corrosion resistance while having little effect on mechanical strength. The improved corrosion resistance was attributed to the high resistance of spinel against the alumina-rich slag formed by dissolution of Al_2O_3 from the castables in the original slag. However, the addition of spinel was found to be detrimental to the spalling resistance as it accelerated oxidation of SiC . Addition of small amounts (<5 wt%) of MgO to such castables was less beneficial because the MgO reacted with Al_2O_3 , CaO from the CA cement, and SiO_2 (SiC) to form liquid rather than in-situ spinel (71).

Addition of preformed spinels to both Al_2O_3 – C or MgO – C bricks also led to improved slag corrosion resistance. For example, addition of 20 wt% preformed stoichiometric spinel to MgO – C refractories improved their slag corrosion resistance by 48% (72). When MgO and Al_2O_3 are added to Al_2O_3 – C (i.e., Al_2O_3 – MgO – C) and MgO – C (i.e., MgO – Al_2O_3 – C) refractories, respectively, in-situ spinel forms in both refractories; as a result, both refractories show improved slag corrosion resistance although the MgO – Al_2O_3 – C refractories are more slag resistant than Al_2O_3 – MgO – C refractories. For this reason, the former are usually used in the slag lines of steel ladles whereas the latter are used in the wall.

H. Other Spinel-Containing Refractories

In addition to the spinel-containing refractories discussed above, other types of spinel-containing refractory, e.g., MA – M_2S , MA – A_3S_2 , MA – CA_6 , and MA – Al_2TiO_5 , are being developed and some promising results have been obtained. For example, M_2S –bonded MA bricks show very good alkali resistance (73) and MA – Al_2TiO_5 refractories show good thermal shock resistance (74).

VII. FUTURE WORK ON SPINEL-CONTAINING REFRACTORIES

Due to their excellent properties such as high refractoriness, mechanical strength, thermal shock resistance, and slag corrosion resistance, and environmentally

friendly nature, spinel-containing refractories are used extensively. Many traditional applications of MgO–MK refractories or Al₂O₃–Cr₂O₃ refractories, including steel-making furnaces (e.g., ladles, RH and EAF furnaces), glass tanks (e.g., regenerators), cement kilns (transitional, cooling, and burning zones) and waste-melting incinerators, have replaced MK- or Cr₂O₃-containing refractories with MA spinel-containing refractories. With improved and cheaper raw materials, improved processing, microstructures and properties, and development of new types, spinel-containing refractories will find increased application. Along with continuous improvement in the current synthesis techniques, novel synthesis techniques such as mechanochemical alloying and molten salt synthesis techniques may become significant, so that high-quality spinel raw materials can be prepared at lower temperatures and cost. In addition, microstructures, processing, and properties of currently used and newly developed spinel-containing refractories such as MgO–MA, Al₂O₃–MA, MgO–Al₂O₃–TiO₂ (MgO–MA–MgTi₂O₄) and MgO–MA–ZrO₂ will be further improved, so that they can be used to replace Cr₂O₃-containing refractories more efficiently. Finally, new types of spinel-containing refractories with excellent properties and performances (e.g., Al₂O₃–MA–Al₂TiO₅, spinel/nonoxide composite refractories, and spinel–carbon castables) will be developed, leading to new applications for spinel-containing refractories.

REFERENCES

1. Kitai T. Fundamental science of refractories: major components, their crystal structures and properties. Spinel Part 2. Taikabutsu 1994; 46(7):383–389.
2. Bragg WH. The structure of the spinel group of crystals. Philos Mag 1915; 30(176) : 305–315.
3. Nishikawa S. Structure of some crystals of the spinel group. Proc Math Phys Soc Tokyo 1915; 8 : 199–209.
4. Lee WE, Korgul P, Goto K, Wilson DR. Microstructural analysis of corrosion mechanisms in oxide-spinel steelmaking refractories. Proc. 2nd Intl. Symposium on Advances in Refractories for the Metallurgical Industries, Montreal, Canada, 1996 : 453–465.
5. Jing SY, Lin LB, Huang NK, Zhang J, Lu Y. Investigation on lattice constants of Mg–Al spinels. J Mater Sci Lett 2000; 19 : 225–227.
6. Carter RE. Mechanism of solid state reaction between MgO–Al₂O₃ and MgO–Fe₂O₃. J Am Ceram Soc 1965; 44(3) : 116–120.
7. Huang JL, Sun SY, Ko YC. Investigation of high-alumina spinel: effect of LiF and CaCO₃ addition. J Am Ceram Soc 1997; 80(12) : 3237–3241.
8. Hirai S, Murakami H, Katayama HG. Effect of additives on the formation of MgAl₂O₄ from MgO and Al₂O₃. J Japan Inst Metals 1991; 55(2) : 166–171.

9. Lee WE, Rainforth WM. *Ceramic Microstructures: Property Control by Processing*. London: Chapman and Hall, 1994.
10. Brinker CJ, Scherer GW. *Sol-Gel Science: The Physics and Chemistry of Sol-Gel Processing*. San Diego, CA: Academic Press, Inc., 1990.
11. Fujiyoshi K, Ishida S, Takeuchi N, Nanri H. Synthesis of whisker-like $MgAl_2O_4$ spinel from gibbsite and magnesium acetate. *Taikabutsu Overseas* 2002; 22(4) : 194–301.
12. Kim W, Saito F. Effect of grinding on synthesis of $MgAl_2O_4$ spinel from a powder mixture of $Mg(OH)_2$ and $Al(OH)_3$. *Powder Technology* 2000; 113 : 109–113.
13. Zawrah MFM, Kheshen AAE. Synthesis and characterisation of nanocrystalline $MgAl_2O_4$ ceramic powders by use of molten salts. *Trans Brit Ceram Soc* 2002; 101(2) : 71–74.
14. Bradt RC, Cunha FN, Resende WS, Pandolfelli VC. Synthetic magnesium aluminate spinel from the reaction of bauxites with brucite and magnesite raw materials. *Proc. Unified Intl. Tech. Conf. on Refractories*, Berlin, Germany. 356–358 (German Refractories Association, Aachen, Germany 1999).
15. Cunha-Duncan FW, Bradt RC. Synthesis of magnesium aluminate spinels from bauxites and magnesias. *J Am Ceram Soc* 2002; 85(12) : 2995.
16. Kong LB, Ma J, Huang H. $MgAl_2O_4$ spinel phase derived from oxide mixture activated by a high-energy ball milling process. *Mater Lett* 2002; 56 : 238–243.
17. Ting CJ, Lu HY. Defect reactions and the controlling mechanism in the sintering of magnesium aluminate spinel. *J Am Ceram Soc* 1999; 82(4) : 841–848.
18. Sarkar R, Das SK, Banerjee G. Effect of additives on the densification of reaction sintered and presynthesised spinels. *J Euro Ceram Soc* 2003; 29 : 55–59.
19. Yu J, Hiragushi K. Sintering of spinel added with titania. *Taikabutsu Overseas* 1999; 19(4) : 10–14.
20. Sarpoolaky H, Zhang S, Lee WE. Corrosion of high-alumina and near-stoichiometric spinels in iron-containing silicate slags. *J Euro Ceram Soc* 2003; 23(2) : 293–300.
21. Lee WE, Argent BB, Zhang S. Complex phase equilibria in refractories design and use. *J Am Ceram Soc* 2002; 85(12) : 2911–2918.
22. Ebisawa T, Takahashi T, Watanabe T, Watanabe Y, Hayama S. Test results of magnesia-spinel bricks used for slag line of VOD (VAD) ladle. *Taikabutsu* 1985; 37(6) : 335–340.
23. Gruver SP. Magnesia spinel refractory brick. United States Patent no. 6261983, 2001.
24. Kettner P, Christof G. MA-spinel brick in glass furnace regenerators. *Radex-Rundschau* 1986; 1 : 3–11.
25. Winder SM, Selkregg KR. Corrosion of refractories in glass-melting application. In: Bennett JP, Smith JD, eds. *Fundamentals of Refractory Technology*. 2001 : 195–221.
26. Lee WE, Moore RE. Evolution of in situ refractories in the 20th century. *J Am Ceram Soc* 1998; 81(6) : 1385–1410.
27. Zongqi G, Rigaud M. Adherence characteristics of cement clinker on basic bricks. *China's Refractories* 2002; 11(4) : 9–16.
28. Komatsu H, Arai M, Ukawa S. Current and future status of chrome-free bricks for rotary cement kilns. *Taikabutsu Overseas* 1999; 19(4) : 3–9.

29. Kaneyasu A. Trends of basic refractories raw materials—magnesia aggregates for chrome-free bricks. *Taikabutsu Overseas* 2000; 20(4) : 245–248.
30. Kajaita Y, Ozeki F, Honda T. The present and future of chrome-free linings for rotary cement kilns. *Taikabutsu Overseas* 2000; 20(4) : 266–270.
31. Itoh K, Ohta A. Chrome-free bricks for rotary cement kilns. *Shinagawa Technical Report* 1999 : 42 : 77–78.
32. Henry FW, Stendera JW. Producing basic refractories for steel applications. *Ceramic Industry* 1997; 2 : 29–32.
33. Rigaud M, Kovac V, Xing C. Spinel and forsterite bonded magnesia castables for steelmaking applications. *Iron Steelmaker* 1998; June : 33–37.
34. Zhang S, Lee WE. Use of phase diagrams in studies of refractories corrosion. *Int Mater Reviews* 2000; 45(2) : 41–58.
35. Bi Z, Zhou N, Zhong X. Relationship between composition and properties of MgO-spinel castables. *Proc. Unified Intl. Tech. Conf. on Refractories*. New Orleans, 33–39 (ACerS, Westerville, USA 1997).
36. Goto K, Argent BB, Lee WE. Corrosion of MgO-MgAl₂O₄ spinel refractory bricks by calcium aluminosilicate slag. *J Am Ceram Soc* 1997; 80(2) : 461–471.
37. Bates JL. Heterogeneous dissolution of refractory oxides in molten calcium-aluminum silicate. *J Am Ceram Soc* 1987; 70(3) : C-55–C-57.
38. Zhang S, Sarpoolaky H, Marriott NJ, Lee WE. Penetration and corrosion of magnesia grain by silicate slags. *Trans Brit Ceram Soc* 2000; 99(6) : 248–255.
39. Nilica R. Investigation to clarification of corrosion mechanisms of corundum and spinel. *Veitsch-Radex* 2000; 35–42.
40. Cho MK, Hong GG, Lee SK. Corrosion of spinel clinker by CaO-Al₂O₃-SiO₂ ladle slag. *J Euro Ceram Soc* 2002; 1783–1790.
41. MacZura G, Madono M, Kriechbaum GW, Sewell B. Low moisture regular corundum/spinel castables with superior properties. *Proc. Unified Intl. Tech. Conf. on Refractories*, Kyoto, Japan, 1995 : 179–186..
42. Vance MW, Kriechbaum GW, Henrichsen RA, MacZura G, Moody KJ, Munding S. Influence of spinel additives on high-alumina/spinel castables. *Bull Am Ceram Soc* 1994; 73 : 70–74.
43. Ko YC, Chan CF. Effect of spinel content on hot strength of alumina-spinel castables in the temperature range 1000–1500°C. *J Euro Ceram Soc* 1999; 19 : 2633–2639.
44. McConnell RW, Marra RA, Fullington FA. Benefits of sintered magnesium aluminate spinels in high purity castable refractories. *Refractories Applications and News* 2002; 7(2) : 23–28.
45. Mori J, Watanabe N, Yoshimura M, Oguchi Y, Kawakami T. Material design of monolithic refractories for steel ladle. *Bull Am Ceram Soc* 1990; 69(7) : 1172–1176.
46. Sarpoolaky H, Zhang S, Argent BB, Lee WE. Influence of grain phase on slag corrosion of low-cement castable refractories. *J Am Ceram Soc* 2001; 84(2) : 426–434.
47. Nagayi B, Matsumoto O, Isobe T, Nishiumi Y. Wear mechanism of castables for steel ladle by slag. *Taikabutsu* 1990; 42(8) : 418–426.
48. Yamamura T, Hamazaki Y, Kaneshige T, Toyoda T, Nishi M, Kato H. Development of alumina-spinel castable refractories for steel teeming ladle. *Taikabutsu* 1990; 42(8) : 427–434.

49. Yamamura T, Kubota Y, Kaneshige T, Nanba M. Effect of spinel clinker composition on properties of alumina-spinel castable. *Taikabutsu* 1992; 44(7) : 404–412.
50. Sumimura H, Yamamura T, Kubota Y, Kaneshige T. Study on slag penetration of alumina-spinel castable. *Proc. Unified Intl. Tech. Conf. on Refractories, New Orleans, 1997* : 97–101.
51. Zhang S, Sarpoolaky H, Lee WE. Dissolution of $MgAl_2O_4$ (MA) spinel grain in $CaO-MgO-Al_2O_3-SiO_2$ melt. *Proc. 44th Intl. Colloq. on Refractories, Refractories in Steelmaking, Aachen, Germany, 2001* : 64–67.
52. Korgul P, Wilson DR, Lee WE. Microstructural analysis of corroded alumina-spinel castable refractories. *J Euro Ceram Soc* 1997; 17 : 77–84.
53. Ahari KG, Lee WE, Habesch S. Spinel formation in cement-free castable bond systems. *Proc. 44th Intl. Coll. on Refractories, Refractories in Steelmaking, Aachen, Germany, 2001* : 160–163.
54. Fuhrer M, Hey A, Lee WE. Microstructural evolution in self-forming spinel/calcium aluminate-bonded castable refractories. *J Euro Ceram Soc* 1998; 18(7) : 813–820.
55. Chen SK, Cheng MY, Lin SJ, Ko YC. Thermal characteristics of Al_2O_3-MgO and Al_2O_3 -spinel castables for steel ladles. *Ceram Int* 2002; 28 : 811–817.
56. Itose S, Isobe T, Sugiyama K, Furukawa K. Optimum castable lining for steel ladle in Japan. *Proc Unified Intl Tech Conf on Refractories, New Orleans, 1997* : 165–174.
57. Nakamura R, Kaneshige T, Matsumura K, Sasaki H. The current status of ladle castables and application of clean shot system to steel ladles. *Shinagawa Technical Report* 42, 1999 : 7–14.
58. Kobayashi M, Kataoka K, Sakamoto Y, Kifune I. Use of alumina-magnesia castables in steel ladle sidewall. *Taikabutsu Overseas* 1997; 17(3) : 39–44.
59. Ko YC. Influence of the characteristics of spinels on the slag resistance of Al_2O_3-MgO and Al_2O_3 -spinel castables. *J Am Ceram Soc* 2000; 83(9) : 2333–2335.
60. Ko YC. Role of spinel composition in the slag resistance of Al_2O_3 -spinel and Al_2O_3-MgO castables. *Ceramics Intl* 2002; 28 : 805–810.
61. Reisinger P, Preßlinger H, Pissenberger E, Posch W. Evaluation of the interaction of different ladle slags with two different alumina castables. *Veitsch-Radex* 1998; 1 : 3–19.
62. Vezza TF, Richter T, Landy RA. Slag corrosion mechanism of cement-free Al_2O_3-MgO castables. *Proc. Unified Intl. Tech. Conf. on Refractories, New Orleans, 23–32 (ACerS, Westerville, USA 1997)*.
63. Ma Z, Janke D. Physicochemical and technological performance of alumina-spinel refractories for use in steelmaking. *Veitsch-Radex* 2000; 2 : 3–14.
64. Windle CJ, Bentley VK. Rebonded magnesia-alumina spinel products for oxy-fuel and alkali saturated atmospheres. *Proc. Unified Intl. Tech. Conf. on Refractories, Berlin, Germany, 1999* : 219–225.
65. Berzhnoi AS, Kordyuk RA. Melting diagram of the system $MgO-Al_2O_3-ZrO_2$. *Dopovidi Akad Nauk Ukr RSR* 1964; 4 : 506–508.
66. Sakamoto S, Miyagishi Y. Development of a Cr_2O_3 -free castable for waste melting furnaces (part 2). *Taikabutsu Overseas* 2001; 21(3) : 197.
67. Kida O, Miyaji T, Okamoto K, Sakamoto S. Development of Cr_2O_3 -free castables for waste melting furnace. *Taikabutsu Overseas* 2000; 20(3) : 217.

68. Obana T, Tsuchinari A, Shimizu I, Nakamori Y, Tokuchi K, Ishihara M, Sakakidani K, Shinagawa H. Application of chrome-free bricks to RH-degasser vessels. Proc. Unified Intl. Tech. Conf. on Refractories, Berlin, Germany, 1999 : 269–271.
69. Martino M, Curletto L, Bonifacino V. Some correlations between composition and characteristics in the field of chrome-free refractories for steel degassing, No. 11 on CD-Rom. Proc. Unified Intl. Tech. Conf. on Refractories, Cancun, Mexico, 2001 : 13.
70. Hamazaki Y, Kaneshihe T, Sumimura H, Namba M. The effect of spinel addition on Al_2O_3 -SiC-C castables. Shinagawa Technical Report 1998; 41 : 15–24.
71. Yoshimoto T, Suzuki T, Sugiyama K, Furukawa K. Effects of MgO Addition on Al_2O_3 -SiC-C castables, Proc. Unified Intl. Tech. Conf. on Refractories, New Orleans, 1997 : 5–14.
72. Ganesh I, Bhattacharjee, Saha BP, Johnson R, Rajeshwari K, Sengupta R, Rao MVR, Mahajan YR. An efficient MgAl_2O_4 spinel additive for improved slag erosion and penetration resistance of high- Al_2O_3 and MgO-C refractories. Ceram Int 2002; 28 : 245–253.
73. Khalil NM. Refractory aspects of Egyptian alum-waste material. Ceramics Intl 2001; 27(6) : 695–700.
74. Kim SW, Han BS, Kim HL, Lee HL. Sinterability and thermal shock characteristics of Al_2O_3 - TiO_2 -MgO ceramics. Yoop Hakhoechi 1999; 36(9) : 997–1005.

10

Refractory Castables

Leonard Krietz

Plibrico Company, Chicago, Illinois, U.S.A.

I. INTRODUCTION

In the family of monolithic refractories, refractory castables comprise a large group of materials that have evolved and grown significantly in the past 30 years. Progressing from rather simple mixes, refractory castables today comprise some very complex and technical formulations, finding use in a variety of very demanding and severe industrial applications. In this time period, refractory castables have gained in market share and, in many instances, have supplanted brick and shaped refractories and become, in many applications, the refractories of choice because of enhanced performance and ease of installation.

Refractory castables are premixed combinations of refractory grain, matrix components, bonding agents, and admixtures. The vast majority of castables are supplied as bagged, blended mixes though some very simple formulations are still field blended for use in low-temperature and noncritical applications. At the point of installation, the castable is mixed with a liquid (typically water) and vibrated, poured, pumped, or pneumatically shot into place to form a refractory shape or structure that becomes rigid because of hydraulic or chemical setting (1). The majority of refractory castables use a calcium aluminate cement as the bonding agent though in recent years other bonding systems have been employed. Common to all castables is the use of refractory aggregates and matrix components that may allow the refractory to be used to service temperatures of up to 1850°C.

Another class of monolithic refractory called a refractory gunning or gunite mix is very similar in formulation to a refractory castable, generally utilizing the same type of bonding agents. In fact, in some instances, refractory castables can also be dry gunned. In the dry gunning process, the dry blended formulation is

usually but not always predampened with a small amount of water to reduce dusting and begin cement/bond hydration. The dampened mix is charged into a gunite machine and conveyed through a hose by pneumatic pressure. At the end of the hose is a nozzle assembly where water is mixed into the air/refractory stream and the resulting mixture gunned onto the vessel shell or existing lining. While many of the physical property trends and hydration and setting attributes of refractory gunning materials are similar to those of refractory castables, refractory gunning mixes for the purposes of discussion in this chapter will be considered a distinct class of monolithic refractory and not specifically addressed.

II. TYPES OF REFRACTORY CASTABLES

Since refractory castables are a very large and diverse group of materials, they may be typed or classified in various ways or by a combination of characteristics. The primary division of castables is based on chemistry. This division separates the refractory castables based on alumina and alumino-silicate aggregates from the castables based on basic refractory oxides such as magnesite and dolomite. This division is fundamental in that different bonding systems are utilized in each category. In addition, the scope of application of basic castable products are more limited than that of the alumina- and alumino-silicate-based castables. The majority of basic castable products are used in areas where basic slag conditions exist such as in various steel, copper, and lead processing vessels. The tonnage sold of basic castables is also much smaller, accounting for approximately 20% of all refractory castables produced (2).

Alumina and alumino-silicate refractory castables may further be classified or typed in many ways. The American Society for Testing and Materials (ASTM) classifies alumina and alumino-silicate refractory castables in a very simplistic and general classification (3) that is a useful initial guide. In reality, refractory castables are typed or classified by a combination of the attributes listed in Table 1.

III. REFRACTORY CASTABLE COMPOSITIONS

A. Components

As mentioned, refractory castables are combinations of refractory aggregates, matrix components, bonding agents, and admixtures. The proportions of each component used vary in each castable composition to achieve the desired physical and chemical properties and characteristics for the intended castable application. The general range of component quantities in a refractory castable is shown in Table 2.

Table 1 Classification of Alumina and Alumino-Silicate Refractory Castables

-
1. Chemistry and/or mineralogy
 - a. Alumina content/refractoriness (i.e., superduty, 60% alumina, etc.)
 - b. Mineral base (i.e., mullite, fused silica, etc.)
 2. Density/thermal insulating value
 - a. Dense ($>1920 \text{ kg/m}^3$)
 - b. Medium weight ($1600\text{--}1920 \text{ kg/m}^3$)
 - c. Light weight/insulating ($<1600 \text{ kg/m}^3$)
 3. Cement content (by CaO from cement)
 - a. Conventional ($>2.5\% \text{ CaO}$)
 - b. Low cement ($1\text{--}2.5\% \text{ CaO}$)
 - c. Ultralow cement ($0.2\text{--}1\% \text{ CaO}$)
 - d. No-cement ($<0.2\% \text{ CaO}$)
 4. Flow/placement characteristics
 - a. Vibrating
 - b. Casting
 - c. Free-flow
 - d. Shotcrete
-

The refractory aggregates constitute the basic “skeleton” of the castable and account for the largest amount of the formulation. The sizing of the aggregates can range from 20 mm to 300 μm (50 Mesh) and are sized and proportioned to achieve the desired packing and particle size distribution. A wide variety of refractory aggregates is available, and castables can be formulated based on one or a combination of aggregates to achieve the desired chemistry, mineralogy, and physical properties. Tables 3 and 4 list the principal aggregates used in refractory castables.

In insulating and medium-weight refractory castables, lightweight aggregates are used in place of denser aggregates or are blended with dense aggregates to achieve the desired density and properties. Table 5 lists common insulating aggregates used in these castable compositions.

In order to “fill out” the particle sizing and to impart other desired attributes such as expansion control, chemistry/mineralogy modification, bond

Table 2 Refractory Castable Composition

1. Aggregate	40–80%
2. Modifiers	5–30%
3. Bond agents	2–50%
4. Admixtures	<1%

Table 3 Primary Alumina and Alumino-Silicate Aggregates

Aggregate	Al ₂ O ₃ /SiO ₂	Max. service limit ^a (°C)
Alumina—tabular or white fused	99 + %/0%	1870
Alumina—brown fused	94–98%/1–2%	1760
Bauxite—S.A. and Chinese	84–90%/5–7%	1760
Mullite—sintered or fused	74–76%/19–24%	1760
Bauxitic kaolin—calcined	58–70%/26–37%	1760
Andalusite	57–61%/38–40%	1760
Calcined kaolin and flint clay	40–47%/49–55%	1650
Pyrophyllite	13–30%/65–80%	1425
Fused silica	0%/99.7+%	1370

^aIn optimum castable formulation.

enhancement, etc., refractory fillers and/or modifiers are added to the castable composition. In many cases multiple fillers are used and in various particle size distributions. Fillers and modifiers can be finer-sized fractions of the same minerals used as aggregates or other minerals chosen for compositional enhancement. Table 6 lists the most common fillers and modifiers used in refractory castable compositions and their primary function. Many other and more exotic modifiers are routinely used in refractory castables for specific applications or operating conditions such as aluminum containment, slag resistance, thermal shock resistance, etc.

The types of bonding agents used in refractory castables have increased in number over the years though, in alumino-silicate castables systems, calcium aluminate cements are still the principal bonding agents. The available types of these cements are listed in Table 7. Specialized castables have been developed in the past 20 years using noncement bonds such as hydratable alumina, clay, silica and alumina gels, and chemical bonds such as monoaluminum phosphate, phosphoric acid, and alkali silicates. Basic castable systems rely on chemical or

Table 4 Other Dense Aggregates

Aggregate	Chemical formula	Ratio
Periclase/Magnesite	MgO	89–98%
Dolomite	CaO*MgO	56–59%/32–40%
Magnesium aluminate spinel	MgO*Al ₂ O ₃	26–32%/66–72%
Chromite	FeO*Cr ₂ O ₃ *Al ₂ O ₃	10–24%/33–46%/15–29%
Silicon carbide	SiC	90–99%
AZS	Al ₂ O ₃ *ZrO ₂ *SiO ₂	42–45%/36–37%/16–17%

Table 5 Insulating Aggregates

Aggregate	Aggregate density (kg/m ³)	Max. service limit (°C)
Vermiculite	64–128	1090
Perlite	140–190	1370
Haydite	720–1050	1200
Bubble fly ash	400–640	1200°–1525
Crushed insulating brick	480–960	1525
Lightweight clay grog	450–720	1650
Bubble alumina	540–610	1800

organic bonds, the most common of which are alkali silicates, sodium phosphates, mineral or organic acids, and resins.

To complete the refractory castable formulation, various types of additives or admixtures may be used to modify the flow/rheology characteristics of the castable, control setting behavior (retarding or accelerating), reduce casting water, stabilize/control the cement paste’s pH, or stabilize storage behavior.

Table 6 Common Refractory Fillers and Modifiers

Filler/Modifier	Chemical formula	Function
Fine milled aggregates	Various	Chemistry/mineralogy adjustment, bond modification/development
Alumina		
Calcined	$\alpha\text{-Al}_2\text{O}_3$	Chemistry adjustment, bond modification/development
Reactive	$\alpha\text{-Al}_2\text{O}_3$	Flow/rheology control, bond modification/development
Silica		
Quartz	SiO_2	Shrinkage control (~800°C)
Fume	SiO_2	Flow/rheology characteristics, bond modification/development
Kyanite	$3\text{Al}_2\text{O}_3 \cdot 3\text{SiO}_2$	Shrinkage control (1325°–1410°C), chemistry/mineralogy adjustment
Clay (fire, ball, bentonite)	Hydrated aluminosilicate	Filler, flow/rheology control
Zircon	ZrSiO_4	Reduce metal, slag, alkali attack
Graphite/Carbon	C	Reduce metal, slag attack
Fly ash	Varies	Low-temperature filler

Table 7 Calcium Aluminate Cement Types

	Chemistry (%)				Max. use temperature ^a (°C)
	Al ₂ O ₃	SiO ₂	CaO	Fe ₂ O ₃	
Low purity	36–48	3–9	35–40	7–16	1370
Medium purity—50	51–53	4–5	37–39	1–2	1540
Medium purity—60	57–59	4–5	33–35	1–2	1540
High purity—70	69–72	<0.5	27–29	<0.5	1870
High purity—80	79–82	<0.5	17–20	<0.5	1870

^aIn best aggregate system.

In many cases, multiple additives are used in a single formulation. Additives and admixtures are used in very small amounts, typically >0.2% and may possibly change in function by varying the quantity used. The proper use and control of additive/admixture combinations is an essential aspect of advanced castable mix design. Table 8 lists general types of additives and their function(s) in castable systems.

B. Aggregate and Particle Sizing

The aggregates and fillers/modifiers used in a refractory castable formulation are sized and proportioned to achieve a desired packing and particle size distribution. The packing and sizing of the components of the refractory castable will affect

Table 8 Common Additives/Admixtures Used in Refractory Castables

Additive	Function				
	Accelerator	Retarder	pH control	Water reducer	Rheology modifier
Lithium carbonate	×				
Calcium hydroxide	×		×		
Sodium carbonate	×		×		
Sodium bicarbonate			×		
Sodium citrate		×		×	×
Sodium phosphate(s)		×		×	×
Sodium polyacrylate				×	×
Polycarboxylate				×	×
Citric acid		×			
Boric acid		×			

the rheology of the castable mix during installation and the ultimate density and strength of the placed castable when in service. Particle packing has been studied since the 1930s (4), but the application of sophisticated particle packing systems in refractory castables only began to be applied in the 1970s when the first low-cement castable systems were being developed.

There are two primary approaches in aggregate sizing and particle packing used in refractory castables. These will be referred to as random and ordered systems (5). In a random system the aggregates are sized in broad mesh distributions and blended with the fillers/modifiers to obtain an “adequate” particle size distribution yielding acceptable rheology/flow on mixing and good physical properties. Most conventional dense and lightweight castables are formulated on this approach. In conventional dense castables, this means that acceptable flow on mixing is obtained with casting water amounts ranging between 8–15% (depending on aggregate base and cement type used) and resulting in porosities of approximately 22–30% (fired).

Ordered particle sizing systems are employed primarily in advanced castables to reduce water demand, impart desired rheological characteristics (such as vibratory/thixotropic flow or free flow/self-leveling behavior), minimize porosity, and maximize particle contact for enhanced bonding and optimum strength development and fracture resistance. In ordered systems, there are two distinct packing methods—gap sizing and continuous sizing.

Gap sizing relies on the mixing of two, three, four, or more tightly graded aggregate mixtures to achieve good packing density. The main disadvantage of this system is poor flow, and castables based on a gap sized aggregate distribution require intense vibration for consolidation and placement. Gap sizing does minimize casting water (typically 3.5–5%) and fired porosity (10–15%) and has been reported to impart good thermal shock resistance (6).

In continuous particle sized systems, the aggregate fractions are added in a relatively large number (or as a packaged blend) of closely sized screened fractions to fill out a continuous distribution curve such as proposed by Furnas (4) and illustrated in Figure 1. Continuous packing distributions have the advantage of very good rheologies at relatively low water contents, and good compaction with low shrinkage and high strength. In recent years, various continuous packing theories and approaches have been advanced resulting in castables with extremely fluid behavior. These “free flow or self-leveling” castables have had their rheology and flow improved, mainly by paying more attention to continuous packing in the subsieve and submicron particle fractions.

C. Bonding Mechanisms

Refractory castables must “set” or harden at room temperature. Either water or another catalyzing agent must activate the bonds used in castables. After

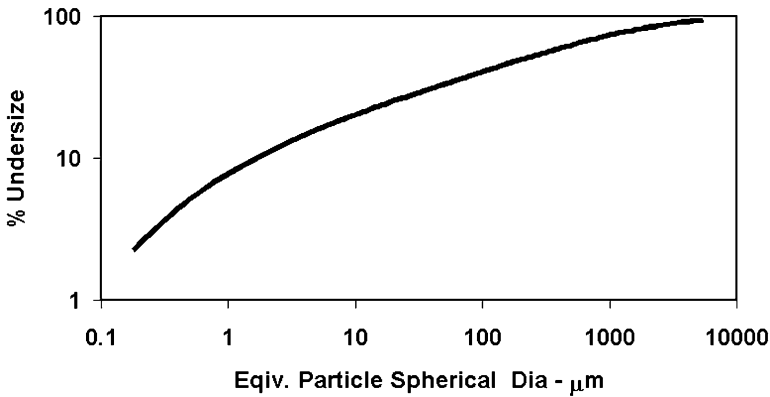


Figure 1 Continuous particle size distribution curve after Furnas.

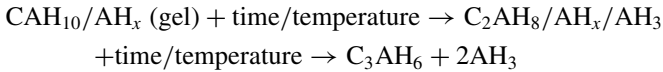
setting, a controlled heat-up procedure is generally required to dewater or dehydrate the bond as the refractory castable lined vessel or furnace is put into service.

The majority of alumina and alumino-silicate castables produced have historically been bonded with calcium aluminate cement. Extensive investigations on calcium aluminate cement hydration/dehydration have been carried out and reported over the years by various authors (7–9), and it is not the intention of this chapter to fully detail the cement hydration/dehydration mechanism but rather to provide an overview of the most important hydrating process. In the different grades of commercially available calcium aluminate cement, there are many mineralogical phases present and in various percentages. However, the principal and most important hydrating phase, common to all of them, is calcium monoaluminate— $\text{CaO} \cdot \text{Al}_2\text{O}_3$ or CA. Upon the addition of water in optimum ambient conditions, CA hydrates per the following equation:



where C = CaO, A = Al_2O_3 , and H = H_2O . C_3AH_6 is the normal, stable hydrate phase when cement curing temperatures of $>35^\circ\text{C}$ occur in the castable mass. While this curing temperature may seem high, it is generally attainable since cement hydration is an exothermic reaction. Quite often internal castable temperatures can reach temperatures of up to 75°C or greater especially in high-cement (20 + %) formulations. If a curing temperature of 35°C is not reached, the metastable hydrates of $\text{CAH}_{10} + \text{AH}_x$ (gel) ($<24^\circ\text{C}$) and $\text{C}_2\text{AH}_8 + \text{AH}_x + \text{AH}_3$ ($24^\circ\text{--}35^\circ\text{C}$) will form. These hydrates will convert to C_3AH_6 per the

following:



However, with this conversion to the stable hydrate there is a phase volume shrinkage that can disrupt the bond structure and lead to weakening of the bond.

When the castable is heated for the first time, the hydrated cement phase will undergo a dehydration process over a temperature range. Dehydration of the hydrated cement occurs over a temperature range from 210°C to 370°C, with the peak dehydration temperature for AH₃ at 230°C and for C₃AH₆ at 315°C. If the castable is heated too quickly and if released steam from the dehydrating cement cannot vent from the castable structure fast enough, internal pressure will build up in the castable and steam spalls or explosions can occur. Many advanced castables also contain fine powder additions and are packed to achieve maximum density, which reduces castable permeability and further complicates heat-up procedures. To help reduce the possibilities of bake-out spalls, it is quite common to use organic, synthetic fiber additions, which melt or burn out at low temperatures (typically <200°C) to help open the castable structure and ease the release of moisture. Polypropylene, acrylic, or polyester are the most common fibers used in lengths ranging from 3 mm to 10 mm and diameters of 15–40 μm. In any case, it is always recommended to consult the refractory castable manufacturer for the proper bake-out procedure for the specific castable used.

While calcium aluminate cement is still the dominant bond used, some alumina and alumino-silicate castables systems and basic castables utilize other bonding agents. In recent years, many cementless castables have been developed around a variety of bond systems.

One such bond is a hydratable alumina binder. This binder is referred to as a hydraulically setting, reactive, transitional alumina (γ or ρ Al₂O₃) and is finely ground for maximum reactivity and sometimes modified with an organic polymer to provide added low-temperature strength. A reported hydration mechanism is (10)



Moist curing of the castable is not required and is detrimental to green strength development with this bond system. It has also been reported that dehydration is easier with this bond that dehydrates between 200°C and 300°C (peak at 255°C). In reality, most castables utilizing this bond do have low permeabilities because of ultrafine particle additions, such as silica fume and reactive alumina, so again it is recommended to consult with the castable manufacturer prior to initial heat up of castables based on this bond system.

In another system, a colloidal silica solution is used to bond the castable (11). Hardening is achieved by the use of a small amount of a setting agent (<1%) such as magnesia, lime, or calcium aluminate cement. Again, dewatering is not as critical as with cement systems because the silica sol does not chemically attach the water. Dewatering of this system is reported to be completed at relatively low temperatures (<125°C).

Gel bonding, also referred to as gel casting (12), is another method of cementless bonding. In this case, setting and low-temperature bonding occurs because of a polymerization of organic monomers suspended in the casting liquid. Polymerization takes place either by a heat setting or by a chemical catalyst. Strength development in gel cast systems is dependent on temperature treatment and sintering rather than the initial bond. This results in a “weak” castable after polymer burnout (~250°C) until the ceramic bonding processes begin.

There are other bonding agents or binders used in castables that are referred to as chemical binders. A system that has seen an increasing use in recent years utilizes phosphoric acid or monoaluminum phosphate (MAP). Castables that use this system are supplied either as a two-component package—consisting of a dry component and liquid component (phosphoric acid or MAP) or a dry component and a damp/wet component (phosphoric acid or MAP premixed with a portion of the dry mix), or as a single-component mix using a dry MAP powder. Setting occurs by the use of an additive (in the dry portion of the castable) that reacts exothermically with the acid. Two commonly used setting additives that react with the phosphoric acid or MAP are powdered MgO (or MgO aggregate in basic castables), which forms a reaction bond phase of MgHPO_4 or $\text{Mg}(\text{H}_2\text{PO}_4)_2$ (13), and calcium aluminate cement, which forms a composite bond phase of $\text{Ca}(\text{H}_2\text{PO}_4)_2$ and $3\text{CaO}\cdot\text{Al}_2\text{O}_3\cdot 6\text{H}_2\text{O}$. The bond phases of MgHPO_4 or $\text{Mg}(\text{H}_2\text{PO}_4)_2$ and $\text{Ca}(\text{H}_2\text{PO}_4)_2$ will lose their chemically attached water at approximately 200°C.

Related to the use of phosphoric acid for bonding is the use of alkali phosphates (sodium phosphate) or alkaline phosphates (magnesium phosphate and calcium phosphate). These phosphates, especially sodium phosphate, find extensive use in bonding basic refractory castables since they can react with magnesite or dolomite aggregate and fines and stiffen the castable by coagulation. Many types of sodium phosphates are available, and setting time and setting hardness can vary depending on the phosphate used. Care must also be taken to minimize the quantity of sodium phosphate used since it can form low-melting reaction compounds, which will reduce the refractoriness of the castable. While sodium phosphates have been used in small quantities in advanced aluminosilicate castable systems for water reduction and flow control, a recent “innovation” has been to use a relatively large amount (1–4%) of a sodium phosphate such as sodium hexametaphosphate or sodium tripolyphosphate along with calcium

aluminate cement (13) to formulate refractory castables with excellent intermediate temperature (600° – 1000° C) strength and abrasion resistance.

Another bond used in basic castables and for producing acid resistant aluminosilicate castables involves the use of alkali silicates, either sodium silicate or potassium silicate. Alkali silicates will react with acids, salts, and metal hydroxides and stiffen or set by formation of a silica hydrogel. This gel will dewater continuously as temperature increases with complete dehydration at 350° C. Setting agents used to set alkali silicate bonded castables include sodium silicofluoride, aluminum polychloride, sodium phosphate, aluminum polyphosphate, magnesium polyphosphate, and calcium and magnesium hydroxides (13).

D. Flow Characteristics and Placement Methods

Historically, refractory castables have been mixed and placed in small quantities (<225 kg), by mixing by hand in a mortar box or in mechanical mixers such as paddle or drum mixers. Flow and placement consistencies were similar to that of a “stiff” mix portland cement civil concrete. Many conventional refractory castables are still placed this way. With the improvement in refractory castable technology, specifically starting with low-cement castable development, other placement methods and techniques have come into use. Early low-cement systems were either gap sized, requiring extensive vibration during placement (vibration cast), or “sticky” thixotropic materials, which use vibration assistance for flow and consolidation. Mixing of these early advanced castables was still done in small quantities, and placement was for the most part by “bucket brigade.” As the large-scale application of low- and ultralow-cement castables increased, so did castable placement technology. Second-generation advanced castables had improved flow with most of the mix “stickiness” removed. Mixer and batch placement size increased with paddle type and turbine type mixers being introduced that were capable of correctly mixing up to 1350-kg castable.

The need for faster placement of larger batches developed into two technological approaches and solutions. One was an equipment approach resulting in the successful development of specially designed refractory pumps (14) that were able to place up to $10\text{ m}^3/\text{hr}$ of advanced castable at distances of greater than 100 m. The other was a refractory castable approach resulting in free flow or self-flowing refractory castables (15) that could be used with readily available concrete pumps. Free flow castable systems are available today in both conventional and advanced types and are widely used. Pumping technology also exists, allowing for the placement of castables with extremely stiff flow consistencies.

In the 1990s, another placement method was developed to speed up placement of castables and eliminate expensive forming. Called refractory shotcreting or shotcasting, it combines many of the benefits of a “correctly” mixed castable

with the speed of gunning placement (14, 16, 17). In this method, a large batch of castable is mixed with the correct amount of water and charged into a pump. The castable is pumped similar to the method used in pump casting applications. However, at the end of the hose, a special nozzle assembly is employed. In this assembly, the castable is mixed with compressed air (at $\sim 0.4\text{--}0.5$ MPa) and a small amount of an “activator” or accelerator that begins a stiffening of the castable. The mixture is pneumatically “shot” onto the installation surface similar to the dry refractory gunning process. Because of the “activator” or accelerator, the castable mix begins to stiffen and allows the surface to be built up without forms. With proper anchoring and support systems, even overhead applications are possible.

Today, numerous castables are available in casting, free flow or shotcrete formulations. There are even commercially available “multi-viscosity” castables that allow a formulation to be placed by different methods by simply altering mixing water. The user should be aware that physical properties can vary between seemingly identical materials developed for different placement technologies and should always review available technical data.

IV. PHYSICAL PROPERTIES AND CHARACTERISTICS

As expected with a large, diverse group of materials, the physical properties and characteristics of refractory castables will vary between castable types and application purpose, i.e., insulating, conventional dense, low-cement, etc., and because of mineralogical and formulation differences among castables within a “group.” Formulation and composition differences (raw material sources) can produce significant variance in physical properties in seemingly “identical” materials (similar densities and reported chemistry). Generalized statements and data trends can be presented to provide an understanding of how the various castable types differ and what the primary attributes of each type are. The refractory castable user is cautioned to carefully evaluate potential materials, because material properties may differ between “similar” products produced by various manufacturers. There can also be exceptions to the anticipated physical property trends due to subtle and/or exotic compositional enhancements in a castable system.

A. Insulating Refractory Castables

The primary purpose of insulating refractory castables is to provide thermal insulation either as a backup lining or as a primary lining in nonsevere applications. As such, insulating castables are formulated for low relative thermal conductivity and not for strength or abrasion resistance. The vast majority of insulating castables

are alumino-silicate-based though high-alumina, high-purity “insulating” castables are produced for applications in very high-temperature environments (up to 1800°C) or in combustion atmospheres containing high concentrations of hydrogen. Alumino-silicate-based insulating castables are available in densities of 400–1450 kg/m³ with corresponding porosities of 45–85% and service temperature limits up to 1650°C. For alumino-silicate-based insulating castables, chemistry, specifically alumina content, has no apparent effect on thermal conductivity for castables with alumina contents between 12–60%. Density and porosity control the heat transfer. Generally, as density increases and porosity decreases, thermal conductivity will increase in a linear fashion. For very high-alumina insulating castables (>90% alumina), the crystalline alumina in the castable has a significant effect on thermal transfer. These thermal conductivity trends are illustrated in Figure 2. These curves represent thermal conductivity data obtained on the initial heat up of unfired insulating castables. A cool-down thermal conductivity curve is also shown in Figure 2. On cool down (or for a prefired castable) thermal conductivity will increase slightly (~5–10%) because of the dehydration of the cement bond phase.

B. Dense Castables

The category of refractory castables classified as dense castables represents a large and diverse group consisting of conventional-type castables and the various categories of advanced products. For the refractory user, the differences in the types of advanced castable are important to understand since dense refractory castables are used as structural components in furnaces and kilns, as primary lin-

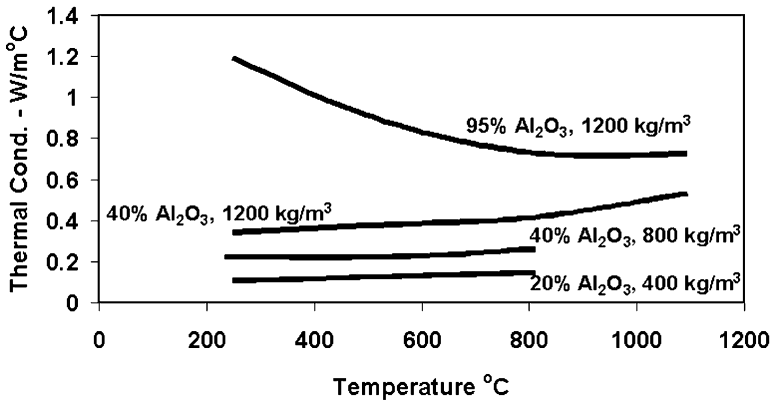


Figure 2 Insulating castables: thermal conductivity vs. density and chemistry.

ings in vessels containing molten metals and slags, in corrosive atmospheres, and in furnace areas experiencing physical abuse and abrasive conditions. Based on the intended application, different physical characteristics come into play when choosing the appropriate castable material.

1. Density, Porosity, and Permeability

Density of dense castables follows a simple trend—as the alumina content of the base aggregate(s) increases, so does density since higher-alumina raw materials are also denser. Particle sizing and packing also will influence density with castables based on ordered sizing being denser than materials based on random sizing. Porosity, on the other hand, does not depend as much on aggregate as it does on sizing, with gap sized systems having the lowest porosity and random systems having the higher porosities. A property that is related to porosity and that very much depends on particle sizing and packing is the permeability of the castable. In ASTM C71, permeability is defined as “the capacity of a refractory for transmitting a fluid or gas” (18). This property is important since the ability to safely dehydrate or bake out a refractory castable depends on its permeability. Permeability can also play a role in gaseous corrosion reactions. Permeability is measured per ASTM test method C577. While it is possible to measure the permeability of dense conventional castables with this test method, it is not possible to obtain flow measurements on many advanced castable types due to the amount of fine particles used in their formulation and the effect of the ordered particle packing systems employed. These advanced castables do have permeability, but it is below the limit that can be measured by the ASTM test. A recently developed technique and associated apparatus to measure the low permeability of advanced castable systems, called the vacuum decay method, has been developed and is being used to model dewatering behavior of these materials at the university research level (19). The low relative permeability of advanced castables and the difficulty or increased care in baking out field installations has led to the widespread and almost universal use of organic bake-out fibers (OBOF) to increase permeability and aid in water release especially in the critical dehydration range. Figure 3 illustrates the trend of low permeability of a low-cement castable and the increase achieved by the use of an OBOF addition versus the normal permeability of a conventional dense castable.

2. Hot Properties—Strength, Load Deformation, Creep, and Work of Fracture

It is easy to measure the strength of refractory materials at room temperature, and while this data is useful for quality assurance testing, it is of little importance

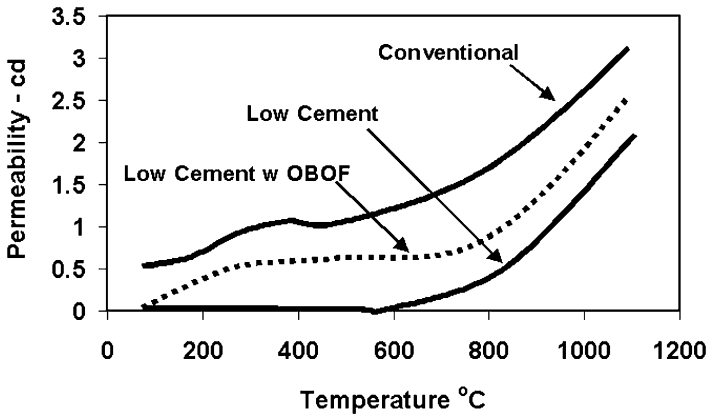


Figure 3 Superduty dense castables: relative permeability per ASTM C577.

when trying to evaluate a refractory castable for use in a high-temperature application. High cold strengths are impressive on paper but may mean a weak material at operating conditions. To truly evaluate the attributes of a refractory castable or any refractory for that matter, it is more important to be concerned with the hot measured properties.

Dense conventional castables are much stronger than insulating castables with strengths generally equaling those of normal firebrick of the same class. In dense conventional castables, hot strength behavior with increasing temperature is principally dependant on the cement type—low, medium-purity, or high-purity calcium aluminate cement, and the amount used in the formulation. With the exception of high-purity, high-alumina conventional castable formulations, the hot MOR (modulus of rupture measured at test temperature) of dense castables begins to decrease above 1100°C. Above this temperature, the calcium aluminate cement begins to react with silica in the castable and begins to form a phase called anorthite ($\text{CaO} \cdot \text{Al}_2\text{O}_3 \cdot 2\text{SiO}_2$ or CAS_2). Silica can be contributed from the aggregate(s) or from other matrix components. While anorthite has a melting point of 1553°C, in systems with other phases containing CaO and SiO_2 , liquid phase formation can begin at temperatures as low as 1170°C. In a silica-free, high-purity, high-alumina castable, the calcium aluminate cement is able to form the very refractory phase of calcium hexaluminate ($\text{CaO} \cdot 6\text{Al}_2\text{O}_3$ or CA_6) at high temperature. The hot strength of high-alumina castables of this type actually increases above 1350°C. Figure 4 illustrates these hot strength trends for dense conventional castables based on different calcium aluminate cements and aggregates.

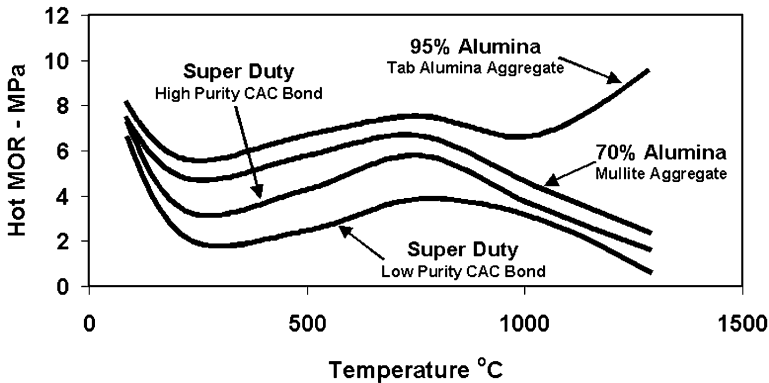


Figure 4 Dense conventional castables: hot strength per ASTM C583.

Because of the many types of advanced castables on the market today and due to the specialized development of many of these materials for specific uses, it is harder to characterize their strength development. The refractory manufacturer has less leeway in development of most dense conventional castables since they are viewed more or less as a commodity product (every manufacturer makes similar products) in the marketplace, and price dictates formulation constraints. This is sometimes true for “low end” (superduty, 50% alumina) advanced castable types in the low- and ultralow-cement classifications. However, application and performance criteria can and do call for the development and use of “premium” castables where the use of expensive formulations and exotic modifiers can modify physical properties and characteristics such as strength in specific temperature ranges that correspond to the anticipated service condition.

Most low-cement, ultralow-cement, and cement-free castables derive their enhanced strength from a combination of improved particle size distribution, reduced water demand, improved density, optimum cement/bond hydration, and the use of micro-sized additions, most notably silica fume and reactive alumina. Silica fume is used in the vast majority of these materials produced, contributing to particle packing, rheology, and, most importantly, to strength development (20, 21). While silica fume causes a significant strength increase especially in the sub-1300°C temperature range, it does react with the calcium aluminate cement in low- and ultralow-cement castables and contribute to anorthite formation at elevated temperatures (22), similar to what occurs in conventional alumino-silicate castables. The anorthite formation is minimized in low- and ultralow-cement castables due to the overall lower CaO content and by the use of reactive alumina in the formulation that will combine with some

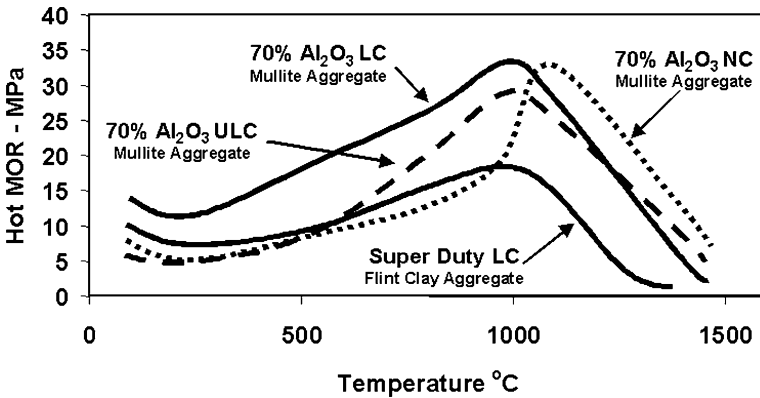


Figure 5 Fifty to 70% alumina advanced castables: hot strength per ASTM C583.

of the silica to form mullite. Cement-free castables do not experience anorthite formation (unless a lime-containing compound is used to “set” the system). The silica fume in these systems reacts with the reactive alumina and forms mullite as the stable bond phase at elevated temperature (23). Typical strength curves for commercially available low-cement (LC), ultralow-cement (ULC), and cementless (NC) castables is illustrated in Figures 5 and 6. Figure 5 shows the normal trend in hot strength development for the alumino-silicate-based

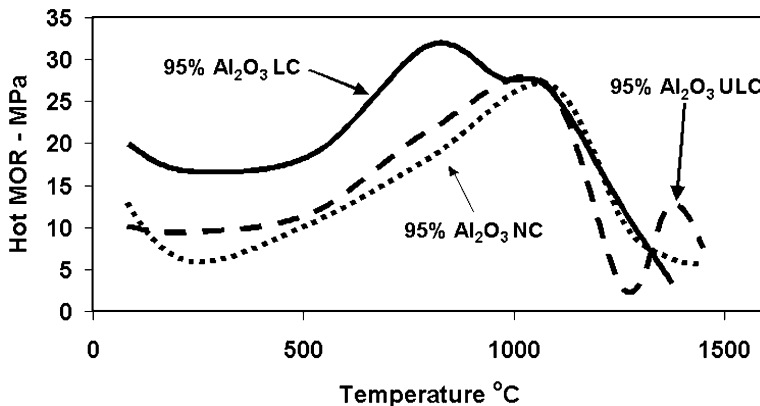


Figure 6 Ninety-five percent tabular alumina advanced castables: hot strength per ASTM C583.

castables. The superduty low cement because of aggregate and formulation limits, while much stronger than conventional castables, is not as strong as the “premium” 70% alumina, mullite-based, low-cement castable. In this castable, strength development is superior due to a premium aggregate and by the use of better, more expensive raw materials such as reactive alumina and micro-sized mullite. The difference in strength development or the optimum strength zones for low-cement, ultralow-cement, and cement-free castables is also illustrated. In comparing similar materials in these categories, we can generalize and say that alumino-silicate-based low-cement castables have the best strength development below 1100°C, while ultralow-cement castables and cement-free castables in this class develop and retain relatively higher strength at elevated temperatures.

A somewhat different trend in strength at elevated temperatures is noted in high-alumina advanced castables as exhibited in Figure 6. In this case, above 1200°C the ultralow-cement castable goes from being the weakest to the strongest in a very short temperature span. This illustrates a physical property effect due to proper formulation. In this case a correct balance of cement to silica fume results in an interesting bond phase development where mullite was able to crystallize from a liquid phase that was formed between 1100°C and 1300°C (24). This crystallization of mullite led to an increase in hot strength at 1400°C that would not have been predicted and is not experienced in low- or ultralow-cement castables based on alumino-silicate aggregates even when the same cement/silica fume ratio is maintained.

All these advanced castables discussed contained silica fume. There are specially reduced cement and cement-free systems for high-temperature and/or slag/metal contact applications that are based on high alumina and magnesium aluminate spinel aggregates and don't use a silica fume addition. These specialty castables can yield some very strong elevated temperature strengths (up to 15–20 MPa at 1450°C) though low-temperature strengths are not remarkable.

Typical hot strength curves for two other types of commonly used advanced castables are shown in Figure 7. Chemical bonded (CB) alumino-silicate and high-alumina castables find application because of their rapid set and quicker bake out. They generally develop adequate hot strength in the intermediate temperature range (<1100°C) but can lose strength rapidly above this temperature because of eutectic points of phases in their bond systems—typically the $\text{Al}_2\text{O}_3\text{--CaO--P}_2\text{O}_5$ or $\text{Al}_2\text{O}_3\text{--MgO--P}_2\text{O}_5$ systems. High-cement, low-moisture castables (HCLM) that contain relatively high-cement amounts (~20%) also contain silica fume and dispersants that allow them to flow and cast at 2–4% lower water amounts than conventional castables of equivalent cement contents. Their hot strength is very good and uniform from ambient conditions to 1100°C, which favors their use in many lower-operating-temperature applications (25). Above this temperature, again due

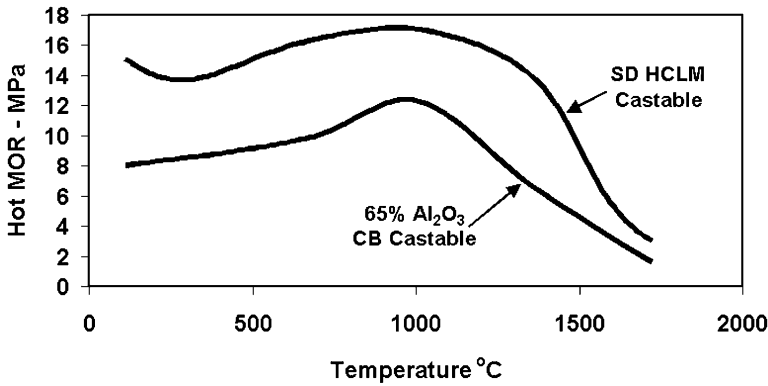


Figure 7 Chemical bond and high-cement, low-moisture advanced castables: hot strength per ASTM C583.

to anorthite formation, their strength decreases to levels equivalent to conventional dense castables.

Figure 8 exhibits hot load deformation data for dense conventional castables and low-cement castables as compared to similar grades of refractory brick. Once again the low-cement castables show their superior load-bearing properties compared to conventional castables and their brick counterparts. It is interesting that increasing alumina content in all three types of refractories shown (conventional castable, low-cement castables, and brick) does not yield the best deformation resistance. The refractories based on mullite aggregate have better load resistance, illustrating the point that mineralogy rather than

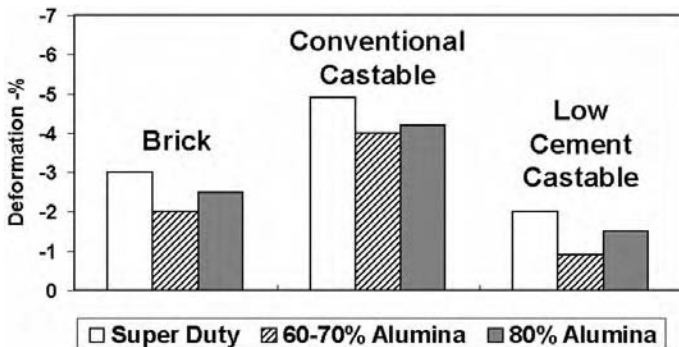


Figure 8 Hot load deformation per ASTM C16—0.17 MPa @1425°C.

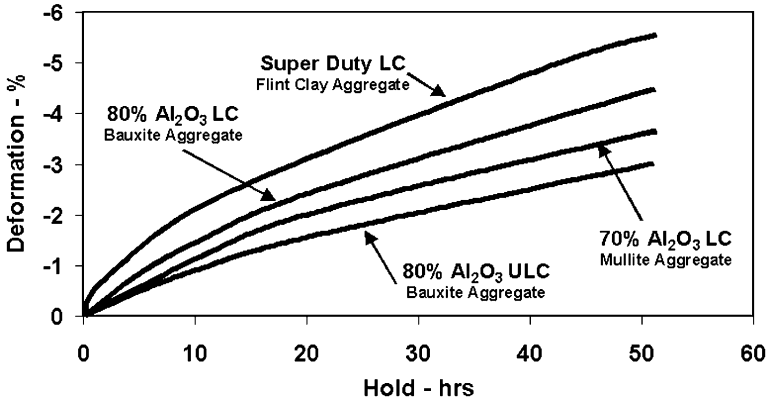


Figure 9 Creep per ASTM C832—0.17 MPa @1425°C.

chemistry is more important for developing better hot properties. This trend is again shown in the creep curves in Figure 9. Here the mullite-based, 70% alumina, low-cement castable again is better than the higher-alumina, low-cement one and only creeps about half of that of the superduty low-cement castable. Also illustrated is the benefit of an ultralow-cement castable in creep resistance at high temperature compared to its low-cement counterpart.

The fracture resistance of refractory castables, and refractories in general, is one of the more important attributes to be considered in the refractory selection process but, unfortunately, is probably the most nonreported property due to lack of available test equipment and a standard test method. It is a fact of life that a refractory lining will develop cracks during service, so it is important to know how well the refractory will resist crack growth propagation. Work of fracture (WOF) is a measure of the energy needed to propagate a crack through a material. This property is influenced very strongly by aggregate type, particle size distribution, and bond phase development. In many cases a relatively weaker castable or refractory as evaluated by modulus of rupture may be a more crack-resistant material and a better choice for an application. Subtle changes to a formulation or size distribution may not affect MOR as much as WOF, especially in advanced castable systems.

For dense conventional castables, the hot WOF trend is easily predicted, as cement and aggregate type have little effect on work of fracture (26), as illustrated in Figure 10. WOF for most alumino-silicate castables, regardless of the cement used, increases to a maximum at 1100°C and then decreases rapidly. The higher-strength, high-purity conventional castables have slightly higher WOF values though not in proportion to their hot strength. For example, the hot MOR of the

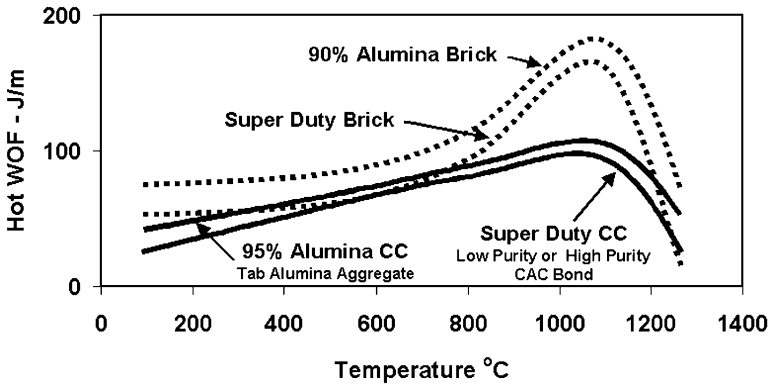


Figure 10 Dense conventional castables—hot work of fracture.

95% Al_2O_3 dense castable at 1100°C is over twice that of the superduty low-purity cement castable, but its hot WOF at the same temperature is only ~10% greater.

One can readily see the advantages of the advanced castable system over dense conventional castables and brick by comparing hot WOF values. Figure 11 plots the hot WOF of low-cement, ultralow-cement, and cement-free castables. The same trend is noted for these castables as was shown for hot MOR. The low-cement castables have the best fracture resistance below 1100°C, and the ultralow-cement and cement-free products yield better values at higher temperatures. Comparing this figure with the previous one also shows the superior fracture properties of this class of castables. The main advantage of these castables for the

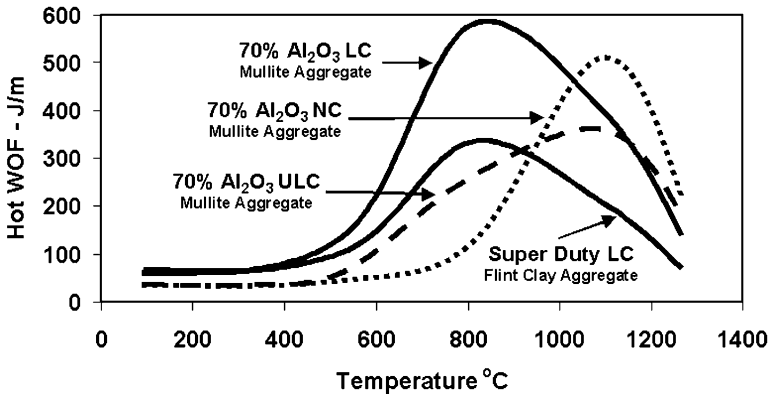


Figure 11 Fifty to 70% alumina advanced castables—hot work of fracture.

user is the fact that they are much tougher than other comparable refractories such as brick, plastic refractories, or conventional castables. The resistance to crack propagation also plays an important role in resistance to thermal shock and impact.

3. Abrasion Resistance

Many applications where refractory castables are used require that the castable be resistant to abrasion or erosion. Most of these applications are in the moderate- to low-temperature range ($<1100^{\circ}\text{C}$) and this allows the use of a room-temperature test for evaluation. The most universally used test method is ASTM C704, "Abrasion Resistance of Refractory Materials at Room Temperature" (27). While there have been attempts at developing hot erosion tests, none are consistently used or as accepted as C704. This test has been used for over 30 years to specify refractories for the petrochemical industry and has been accepted for providing useful data to predict or classify refractories for moderate temperature erosion environments. Dense conventional castables, for the most part, are "average" abrasion-resistant materials, having volume losses after testing of 20–40 cc. For abrasion-resistant applications, advanced castable systems such as low-cement, ultralow-cement, high-cement, low-moisture, and chemical bonded castables are used. Abrasion loss also varies with prefiring temperature and can reflect strength (MOR) variances. Figure 12 plots the cold abrasion loss of various castables versus prefiring temperature. Castables generally increase in abrasion loss as cement dehydration occurs, as illustrated by the conventional dense and even the low-cement castable. As the ceramic bonding/sintering process begins ($>600^{\circ}\text{C}$), measured abrasion loss decreases. High-cement, low-moisture castables go against this trend and retain a more uniform abrasion loss throughout the low- to moderate-temperature range (25), making them

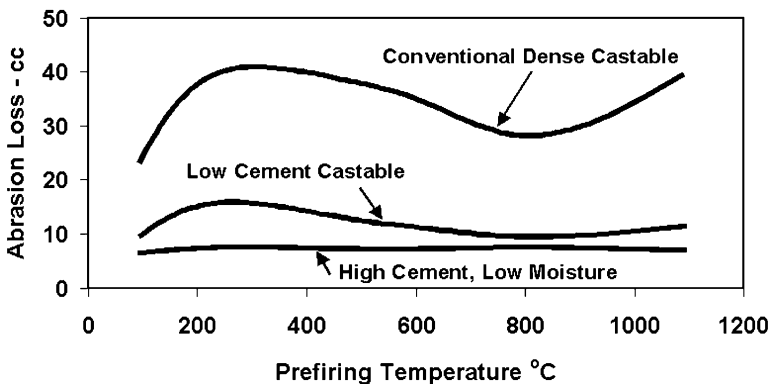


Figure 12 Superduty refractory castables—abrasion resistance per ASTM C704.

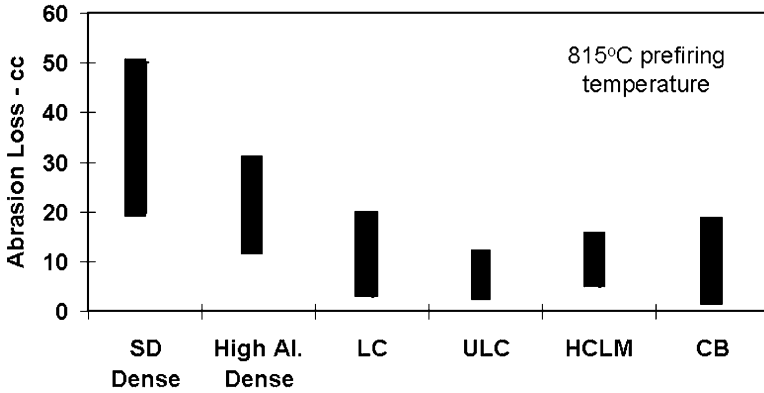


Figure 13 Refractory castables—abrasion resistance range per ASTM C704.

ideal for some petrochemical, mineral processing, and incineration applications. Figure 13 shows comparative abrasion ranges for the various types of refractory castables. It should be noted that the higher-alumina compositions in each class generally, but not always, have the lowest measured abrasion losses.

4. Thermal Conductivity

The thermal conductivity trend of dense alumino-silicate and high-alumina refractory castables is similar to that of refractory brick and is easy to predict: As alumina content and density increase, so does thermal conductivity. Figure 14 illustrates this for dense conventional castables. As with insulating

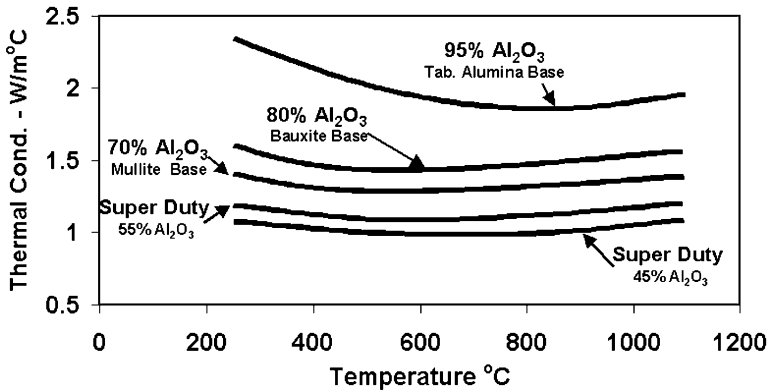


Figure 14 Dense conventional refractory castables—thermal conductivity.

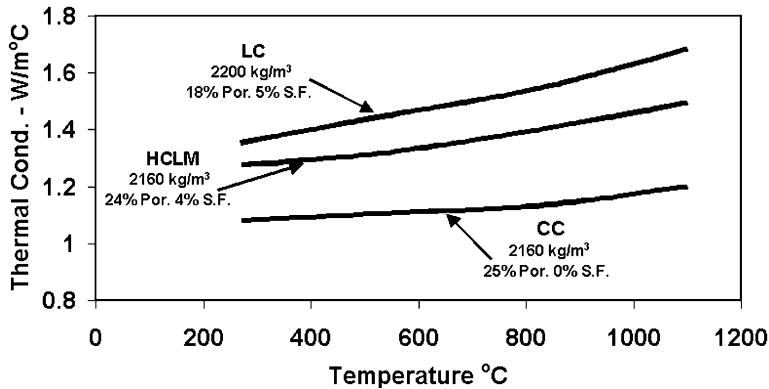


Figure 15 Fifty percent alumina dense castables—thermal conductivity.

castables, very high-alumina castables have a much higher thermal conductivity due to the higher amount of crystalline alumina.

Thermal conductivity for many advanced castables is significantly higher than their comparable conventional dense castable counterparts (28, 29). This is due partly because of their increased density and improved particle packing but primarily because of ultrafine powder additions, most notably silica fume. The ultrafine powders help reduce casting water and porosity, improve matrix continuity, and increase the crystalline content of the matrix. The exact mechanism of the thermal conductivity increase is not well researched, but the effect in thermal conductivity increase caused by silica fume is illustrated in Figure 15. This increase in thermal conductivity (20–30%) caused by a silica fume addition is illustrated for both low-cement (LC) and high-cement, low-moisture (HCLM) castables as compared to a conventional dense castable (CC). Typical thermal conductivities for other advanced castables based on different aggregates and bonds are shown in Figure 16.

V. FUTURE TRENDS IN REFRACTORY CASTABLES

For the past 30 years, refractory technologists have significantly improved refractory castable formulations, widening both the types of castables and the installation methods available. The improvement in their physical properties and characteristics have enabled castables to gain in market share and application at the expense of other types of refractories. In a recent report, an industrial market research firm predicted that castables would see the best sales growth in the refractory market over the next 5 years due to “superior performance character-

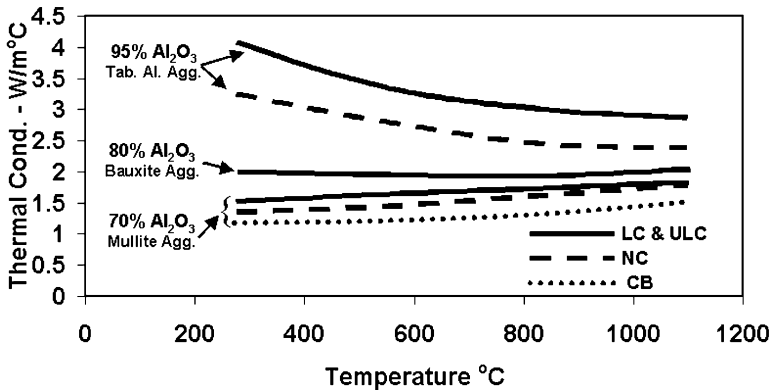


Figure 16 Advanced castables—thermal conductivity.

istic in an array of applications as well as from relative ease in installation” (30). Refractory producers are continuously improving both product quality and consistency. New advanced castables are continuing being developed and applied with the emphasis on engineering formulations for specific applications. This is evident in the new castable developed for metal contact in both the steel and aluminum industries, and it is expected that this development trend will spread to other industrial applications as well.

REFERENCES

1. C71-00 Standard Terminology Relating to Refractories. Annual Book of ASTM Standards Vol. 15.01. West Conshohocken, PA: American Society for Testing and Materials, 2001.
2. Refractories. Current Industrial Report MA327C(00)-1. Washington, DC: U.S. Census Bureau, 2001.
3. C401-91 Standard Classification of Alumina and Alumino-Silicate Castable Refractories. Annual Book of ASTM Standards Vol. 15.01. West Conshohocken, PA: American Society for Testing and Materials, 2001:75–76.
4. MacZura G, Gnauck V, Rothenbuehler P. Fine Aluminas for High Performance Refractories. Pittsburgh, PA: Aluminum Company of America, 1983:2–3.
5. German R. Fundamentals of particle packing theory. Proceedings of the 30th Annual St. Louis Section of the American Ceramic Society Symposium on Refractories, St. Louis, MO, 1994.
6. Homeny J, Bradt RC. Aggregate distribution effects on the mechanical properties and thermal shock behavior on model monolithic refractory systems. In: Fisher R, ed. Advances in Ceramics Vol. 13. Columbus, OH: The American Ceramic Society, 1985:110–130.

7. Kopanda JE, MacZura G. Production processes, properties, and applications for calcium aluminate cements. In: Hart LD, ed. *Alumina Chemicals Science and Technology Handbook*. Westerville, OH: The American Ceramic Society, 1990:171–184.
8. George CM. Aspects of calcium aluminate cement hydration. *Proceedings of the 30th Annual St. Louis Section of the American Ceramic Society Symposium on Refractories*, St. Louis, MO, 1994.
9. Robson TD. *High Alumina Cements and Concretes*. New York: John Wiley, 1962:51–68.
10. Hongo Y, Tuzuki Y, Miyawaki M. United States Patent 4,331,773. May 25, 1982.
11. Banerjee S, Connors CW Jr. United States Patent 5,147,830. Sept. 15, 1992.
12. Studart AR, Ortega FS, Innocentini MDM, Pandolfelli VC. Gelcasting high alumina refractory castables. *Ceramic Bull* 2002; 2:41–47.
13. *Technology of Monolithic Refractories*. Tokyo: Plibrico Japan Co. Ltd., 1999:172–175, 182–184.
14. Allen WG. Advanced equipment systems for refractory placement. *Proc. UNITECR 97*, New Orleans, 1997:523–530.
15. Masaryk JS, Steinke RA, Videtto RB. Development and use of low cement, self-flowing castables. *Proc. UNITECR 93*, Sao Paulo, 1993:527–538.
16. Cassens N, Steinke RA, Videtto RB. Shotcreting self-flow refractory castables. *Proc. UNITECR 97*, New Orleans, 1997:531–552.
17. Banerjee S, Harbin H, Reno E. Spray-gunning refractories. *Proc. UNITECR 97*, New Orleans, 1997:553–562.
18. C577-99 Standard Test Method for Permeability of Refractories. *Annual Book of ASTM Standards Vol. 15.01*. West Conshohocken, PA: American Society for Testing and Materials, 2001:99–102.
19. Moore RE, Smith JD, Sander TP, Severin N. Dewatering monolithic refractory castables; experimental and practical experience. *Proc. UNITECR 97*, New Orleans, 1997:573–582.
20. Myhre B, Hundere AM. Substitution of reactive alumina with microsilica in low cement and ultra-low cement castables, Part I: properties related to installation and demoulding. *Proc. UNITECR 97*, New Orleans, 1997:53–62.
21. Hundere AM, Myhre B. Substitution of reactive alumina with microsilica in low cement and ultra-low cement castables, Part II: the effect of temperature on hot properties. *Proc. UNITECR 97*, New Orleans, 1997:91–100.
22. Seltveit A. Microstructural aspects of microsilica blended high alumina cements. In *Ceramic Engineering and Science Proc.*, Vol. 7 No. 1–2. Columbus, OH: The American Ceramic Society, 1986:243–260.
23. Myhre B, Sunde K. Alumina based castables with very low contents of hydraulic compound. Part II: strength and high temperature reactions of “no-cement” castables with hydraulic alumina and microsilica. *Proc. UNITECR 95*, Vol. 2, Kyoto, 1995:317–324.
24. Myhre B, Hundere AM, Feldborg H, Odegard C. Correlation between mullite formation and mechanical properties of refractory castables at elevated temperature. *Proc. VIII Intl. Met. Conference*, Ustron, Poland: 1999:163–172.

25. Krietz LP, Fisher RE. Field performance and fracture behavior of low cement, conventional, and high cement, low moisture castables. Proc. UNITECR 89, Vol. 2, Anaheim, CA: 1989:1116–1126.
26. Fisher RE, Krietz LP. Bond variation effects on the fracture properties of fireclay castables. Proc. UNITECR 91, Aachen, 1991:272–275.
27. C704-99 Standard Test Method for Abrasion Resistance of Refractory Materials at Room Temperature. Annual Book of ASTM Standards Vol. 15.01. West Conshohocken, PA: American Society for Testing and Materials, 2001:127–133.
28. Krietz LP. Effect of silica fume on the thermal conductivity of low cement castables. Presented at the 87th Annual Meeting of the American Ceramic Society, Cincinnati, OH, 1985.
29. Monsen B, Seltveit A, Sandberg B, Bentsen S. Effect of microsilica on the physical properties and mineralogical composition of refractory concretes. *Advances in Ceramics*, Vol. 13. Columbus, OH: The American Ceramic Society, 1985:201–211.
30. Refractory News Vol. 9-01. Pittsburgh, The Refractories Institute, 2001:2.

11

Unshaped Refractory Products

Rudolf Krebs

St. Augustin, Germany

I. INTRODUCTION

In the United States, the year 1914 marked the opening of a new era in refractory technology with the manufacture of *specialties* or *monolithic refractories*. The term “specialties” was the official U.S. government term for the classification of unshaped and unburned refractory materials (1). During the 1920s and 1930s, important advances were made in new and improved monolithic refractories, and a big increase of the production of such refractories (especially plastics and rammings) took place during World War II. The demand for monolithic refractories of all kinds increased in the emergency “get-it-out-yesterday” atmosphere of World War II. One special wartime use of monolithic refractories was in dehydration plants, which produced millions of pounds of powdered eggs to be shipped to the American military and manufacturers. The production of ramming mixes, castables, mortars, and coatings increased by more than one third between 1937 and 1943 (1).

People often talk about *modern*, *intelligent*, and *innovative* refractory products and/or technologies. However, before an evaluation of these words can be made, it seems to be necessary to make a brief review of the “unshaped refractory history.” Table 1 shows some remarkable highlights of the last 88 years.

After the inventions of the “*plastic*” refractory in 1914 and the “*cast*”-able refractory in 1923, in the United States, there was a long pause until the mid-1950s, when the conventional *gunning technology* was established in Europe, too. As far as *prefabricated shapes* are concerned, the original idea was to make big prefabricated and pretreated blocks for quick installations and short heat-up times. The time of prosperity for this way of thinking was in the

Table 1 Highlights Regarding the Development of Unshaped Refractory Products

Time	Development	Type of installation
1914	Invention of plastic refractory	Ramming
1923	First patent on “cast-able” refractory	Casting
1950s	“Gun-able” refractories	Dry gunning
1970s	Invention of deflocculated castables	Vibrating
1970s	Prefabricated and pretreated shapes	Quick installation
1980s	Self-flowing castables	Self-flowing
1990s	Refractories for shotcreting	Shotcreting

1970s, when soaking pits and walls of pusher-type furnaces were lined with such big blocks within extremely short times. But today soaking pits have practically disappeared, and this technique ended simply due to the fact that in the steel plants the availability of the cranes could not be guaranteed.

One of the biggest steps ahead was the invention of *deflocculated castables*, which took place at the same time. This basic development was the assumption for all further developments in regard to the MCCs, LCCs, ULCCs, and NCCs. The development of *self-flowing* (SFC) and *shotcreting* (SCC) castables was a logical consequence. Both are *no-new-product types*: SFCs have the know-how to fill any space after casting without additional energy; products like SCCs were needed automatically after the introduction of the right equipment (which originally came from the civil building industry). However, it is a fact that both product types are deflocculated castables (2)!

II. DEFINITIONS, CLASSIFICATIONS, STANDARDIZATION

Shaped refractories like bricks were widely used for refractory linings before monolithics entered the market. And due to the fact that unshaped refractories were mostly used as repair materials, there was no need for standards or definitions in the beginning. Where properties were required, existing standards for bricks were applied. This “standard-free” state was no longer possible when monolithics gained a better image and were used more and more for new linings, too.

In Table 2 a historical summary is made in regard to the development of ASTM standards by showing the most relevant ones (3). It can be stated that according to the total production and consumption of refractories, the first standards were made for shaped refractories and applied later for monolithics as well. It can be also stated that in the United States, the necessity for standardizing monolithic refractories was more urgent. This can be traced back to the big increase

Table 2 History of Important Refractory Standards in the United States

ASTM standard	Content	Originally issued in	Type
C 20	Determination of app. porosity, water absorption, bulk density	1918	Shaped
C 24	Determination of refractoriness by pyrometric cones for bricks mortars, clay, etc.	1919	
C 113	Reheat change of refractory bricks	1934	
C 133	Cold crushing strength and modulus of rupture of refractories	1937	
C 134	Size, dimensional measurements, and bulk density of refractory bricks and insulating bricks	1938	
C 135	True specific gravity of refractory materials	1938	
C 179	Drying and firing linear change of plastics and rammings	1943	Unshaped
C 181	Workability index of plastic refractories	1943	
C 401	Classification of alumina and alumina-silicate castables	1957	
C 417	Determination of thermal conductivity of unfired monolithic refractories	1958	
C 860	Determining and measuring consistency of refractory concretes (e.g., "ball-in-hand test")	1977	
C 862	Preparing refractory concrete specimens by casting	1977	

of such refractories (especially plastics and rammings) during World War II (see ASTM C179 and C181).

Until the end of the 1960s, there was no unified European standardization. As already mentioned, existing standards for testing refractory bricks were applied in cases where properties of monolithics were necessary. Parallel to the work, which was made in the national standard bureaus like AFNOR, BS, and DIN, a very successful procedure was practiced by the creation of the so-called *PRE recommendations*. The PRE (Federation Européenne des Fabricants de Produit Refractaires) was formed in 1953 and is a federation of Western European producers of refractories presenting "technical recommendations produced in mutual agreement by all its members" (in 1976, 14 European countries were members of the PRE,

representing a total production of refractories of approximately 5.7 million tons (United States = 4.5 million tons, Japan = 2.7 million tons). The members were Austria, Belgium, France, Germany, Greece, Holland, Italy, Portugal, Scandinavia (Denmark, Norway, Sweden), Spain, Switzerland, and the United Kingdom. To avoid the development of any divergence of ideas between the refractories manufacturers belonging to PRE and the main users, mixed groups comprising members of the Iron and Steel and Refractories Industries were set up in 1969 under the name SIPRE (Siderurgie et PRE, or Steel Industry and PRE). Six working groups were organized. Their objectives were the attainment of an agreement between manufacturers and users on the procedures to be followed for determining the fundamental properties of refractories with a view to subsequent standardization of methods, both at national and international (ISO) levels (4).

In Europe much more time passed until the first tendencies for starting a standardization of unshaped refractories appeared. In February 1964, the PRE Bulletin No. 65 was published containing a first definition and classification of unshaped refractories and refractory mortars on a modest scale.

The most difficult items concerning standardization were the shape, the sizes of the shape, the method(s) for preparation, and the curing and treatment of test pieces, because we all know that without having a general test piece, no classification is possible. It is a matter of fact that, for example, the permanent linear change of a product depends on the shape and the sizes of the test pieces after a certain pre-firing temperature and soaking time. A standard brick shows a different PLC than a 2 in. cube or a 50-mm cylinder after firing at 1200°C for 5 hr. Therefore, most intentions made in the early 1970s were concentrated on this item.

During the early 1970s, a consensus could be found and first parts of the relevant PRE recommendations were published. Table 3 shows the results of the PRE activities as far as the unshaped refractories are concerned. In the data sheets for the products of the PRE producers, it was mentioned in most of the cases that data were obtained by applying the relevant PRE recommendations; the advantage was that these test procedures were accepted by the steel industry. According to the philosophy of PRE, the German DIN 51 010 was published in 1987 showing the same wording as the respective PRE recommendations.

Looking at Tables 1 and 2, it can be stated that during the 1970s, the biggest steps ahead were made in regard to unshaped refractories in Europe and in the United States. On the other side, it must be stated as well that in 1915 it was known how to measure the refractoriness of a product and how to determine the physical properties. But it took 28 years in the United States until the first "monolithic standard" was published (in Europe, it took more than 60 years).

In the mid-1980s, there was a need to create European standards (EN = Norme Européenne) to achieve easier communication and trading within the European Community. This referred to refractories, too. The CEN Technical

Table 3 PRE Recommendations Concerning Unshaped Refractories

PRE rec.	Content	First issue	Revised/ supplemented
42	Classification of prepared unshaped dense and insulating refractory materials	1978	
43	Provisional supplementary classification of dense and insulating refractory castables	1972	1978
44	Provisional supplementary classification of refractory ramming materials and mouldables	1973	1978
25	Control as received	1974	1984
26	Preparation of test pieces	1974	1984
27	Testing of the characteristics on unfired test pieces at ambient temperatures	1974	1986
28	Testing of the characteristics of test pieces during and after firing	1977	1986
45	Test on refractory mortars	1984	

Committee 187 was established with four working groups to set up the new standards. The first idea was to take the existing PRE recommendations that were approved and applied by users and producers for a long time and elaborate EN standards with a little updating. But it was found that some of the PRE members voted in the PRE meetings for the approval of the recommendations although they still practiced the testing according to their national standards in their countries—which differed very often significantly—especially as far as the monolithics are concerned. That was the main reason why the progress in working group 2 (unshaped refractories) was not as big as in the other three groups. However, now, after many meetings, tests, and discussions, the result is the issue of the EN 1402, which is subdivided into eight parts, as Table 4 shows.

Table 4 Subdivisions of EN 1402

EN 1402: Unshaped Refractory Products	
Part 1	Introduction and classification
Part 2	Sampling for testing
Part 3	Characterization as received
Part 4	Determination of consistency of castables
Part 5	Preparation and treatment of test pieces
Part 6	Measurement of physical properties
Part 7	Tests on preformed shapes
Part 8	Determination of complementary properties

The vocabulary and definitions, which will be used in the following text, are in accordance with this standard.

A. Definition

The term “unshaped refractory products” is the correct designation for the products in question, although words like “mixes,” “refractory mixes,” or “ramming mixes” are still used frequently today. However, the word “monolithics” is the more common term overseas. Compared to a refractory brick, the adjective “unshaped” also expresses the main difference. A brick generally has a specific shape, is prefired homogeneously, and is bricked or laid with suited mortars. In contrast, unshaped refractories are placed in larger sections, mostly behind shuttering. The furnace lining consists of these monolithics once they have hardened. The comparison of the quantity of joints for a brick lining and a refractory lining made of unshaped refractories justifies the word “monolithic.”

The general definition of monolithic refractories is found in the standard ISO 1927 (5) and in the European standard EN 1402-1:

Mixtures which consist of an aggregate and a bond or bonds, prepared ready for use either directly in the condition in which they are supplied or after the addition of one or more suitable liquids, and which satisfy the requirements on refractoriness given in ISO R 836. They may contain metallic, organic or ceramic fiber material. These mixtures are either dense or insulating. Insulating mixtures are those whose true porosity is not less than 45% when determined in accordance with EN 1094-4, using a test piece pre-fired to specified conditions.

Prefabricated refractory shapes are made of such products by casting, vibrating, or ramming. They are mostly thermally pretreated and can be taken into service immediately.

As far as the *nature of bond* is concerned, there are four types:

1. A hydraulic bond with setting and hydraulic hardening at ambient temperature
2. A ceramic bond with hardening by sintering during firing
3. A chemical bond (inorganic or organic–inorganic) with hardening by chemical, but not hydraulic, reaction at ambient temperature or at a temperature lower than that of a ceramic bond
4. An organic bond with binding or hardening at ambient temperature or at higher temperatures.

Of course, a lot of bonds are mixed bonds: This is, for example, the case with phosphate-bonded ramming materials (=chemical—ceramic) or materials for repairs with a hydraulic bond which contain besides calcium aluminate cements

also considerable amounts of clays (=hydraulic—ceramic). When several bonds are used together, the bond has to be designated according to the nature of that bond that plays the principal part during the hardening.

Before selecting a product, it is recommended to first check whether the material in question will require a special heat treatment for a proper setting or not. This will help to avoid unpleasant surprises and discussions about setting times, progress of the work, and the date of taking the furnace into operation. Very often additional “lost” shuttering is needed to support the setting of the material unless it has sufficient strength. This often happens with linings consisting of phosphate-bonded rammings or plastic mixes.

The mesh width of the finest sieve (ISO 565 series), through which at least 95% by mass of the material passes, is synonymous with the *maximum grain size* of the mixture. The *yield by volume* is the mass of material as delivered that is necessary to place 1 m³ of material, expressed in tons, to the nearest 1%.

B. Subdivision of Materials

The extensive product range of unshaped refractory materials can be subdivided as follows.

1. Refractory Castables

The family of the refractory castables is certainly the most important product group. Refractory castables can be either dense or insulating materials. The former relatively simple mixtures consisting of aggregates and calcium aluminate cements have been continuously improved so that they are on a very high technical level today. This called for differentiation. The dense castables are classified according to EN 1402-1 as follows:

Regular Castables. These are hydraulically bonded refractory castables containing cement; however, they do not contain a deflocculant.

Deflocculated Castables. Such cement-containing castables have to meet, in general, two requirements: They must contain

1. At least one deflocculating agent
2. A minimum of 2% by weight of ultrafine particles (less than one micron).

Ultrafine particles are, for example, pyrogenic microsilica or reactive aluminas. The family of the deflocculated castables is subdivided according to the content of CaO—and not (!) to the content of cement—as shown in Table 5.

This table shows that of course the amount of cement is decreasing parallel to the decrease of the CaO content. For example, an ULCC containing a 70%

Table 5 Classification of Deflocculated Castables

Category	Content (%) CaO	
	Minimum	Maximum
Medium-cement castable (MCC)	>2.5	—
Low-cement castable (LCC)	>1.0	<2.5
Ultralow-cement castable (ULCC)	>0.2	<1.0
No-cement castable (NCC)	0	<0.2

Al_2O_3 cement allows the addition of 3.3% cement maximum, and if a cement is used that contains 80% Al_2O_3 , the allowed quantity of cement is 5% only. The problems concerning strength development during the setting increase by decreasing cement content, as ULCCs and NCCs very often need additional heat to achieve sufficient green strength values.

Chemically Bonded Castables. These refractory castables contain one or more chemical bonds. After the addition of water or a suitable mixing liquid and an intensive mixing, they start setting mostly due to a neutralization process. By this it should be stressed that a clear differentiation between a chemically bonded castable and a deflocculated one of the NCC type is hardly possible. This can be also traced back to the fact that the nature of bonds has not been investigated in detail, respectively classified, so far.

2. Refractory Gunning Materials

As these materials can be installed very easily and efficiently, they increased their market share considerably. Refractory gunning materials can be subdivided into the following three groups:

1. Castables (dense or insulating), which are supplied dry and used after the addition of water during and/or before gunning
2. Deflocculated castables for the shotcreting process
3. Plastics for gunning, which are especially designed for gunning under high air pressure with special equipment, and are normally delivered in a “ready-to-use” state.

3. Refractory Moldable Materials

These moldable materials are usually described as plastic or ramming refractory materials.

Plastic Refractory Materials. The product group is demonstrably the oldest monolithic material. It was developed in the United States as “pliable firebrick” in 1914, and for a long period it was used as the standard material for the front installation of many types of furnaces (3). (The refractory castable was developed at a later stage; a first patent application in the United States was registered in 1923.)

Plastic refractory materials are supplied in mouldable, preformed blocks or slices and placed by ramming (manual or mechanical). An installation without shuttering is possible. They harden under the action of heat above ambient temperature.

Refractory Ramming Mixes. These are noncoherent materials, which are supplied in premoistened status or “ready-for-use.” After filling them behind a stable shuttering, they are installed by ramming (in special cases by vibrating, too). These materials can also be supplied in dry status together with a separate liquid binder. The “ready-for-use” consistency will be achieved by using a paddle mixer on-site.

Also, the refractory ramming mixes harden under the action of heat above ambient temperature.

4. Refractory Jointing Materials

This material group also belongs to the unshaped refractory products and is designed for laying and jointing or gluing refractory bricks or preformed blocks and also insulating products. The composition of these materials—consisting of fine aggregates and bonds—varies depending on the quality of the used bricks respectively on the field of application. These materials are delivered either dry or in a ready-to-use state. There are two main types:

1. Heat setting jointing materials, which harden at elevated temperatures by chemical or ceramic bonds
2. Air setting jointing materials, which harden at ambient temperature by chemical or hydraulic bonds.

5. Other Unshaped Refractory Materials

Dry Mixes. These materials are especially designed to be placed in the dry state by vibration or ramming. Due to their special grain size distribution, they reach a maximum compaction without adding any liquids. They may include a temporary bond (organic additives, sintering agents) but are eventually ceramic bonded by a further increase of temperature. These products are mainly used for the installation of induction furnaces, wear lining of tundishes, or transport ladles in foundries.

Injection Mixes. Such products have mostly a fine grading; they are “injected” by double-piston pumps, using pressures between 10 and 200 bar. They may be supplied ready-to-use or may require mixing on-site. Here a typical material is, for example, the so-called grouting mix that is injected through the steel jacket of the blast furnace to serve as rear-filling material in the remaining brickwork. The mix fills gaps and improves cooling efficiency.

Coatings. These products are mixtures of fine refractory aggregates and bond(s). They are usually supplied ready-for-use with a higher water or liquid content than is required for mortars. They are often designated as “coatings” and may have a ceramic, hydraulic, chemical, or organic bond. The mixtures are applied manually (with a brush or trowel), by pneumatic or mechanical projection, or also by spraying.

As already mentioned above, a remarkable overlapping can be stated here. Therefore, the following should be pointed out:

In boilers of power stations and waste incinerators, SiC-ramming mixes are installed by the “patching” method (by hand) between the studs. The thickness of the lining is often not more than 18 mm. To be exact, the ramming mix is actually being used as a “coating” for the water-cooled pipes. This example shows how difficult precise classification can be as several products can be placed or installed in different ways.

Tap Hole Mixes. These materials are especially designed for the filling and sealing of blast furnace tap holes. They are also supplied—like the plastic refractory materials—in extruded preformed blocks having a mouldable and plastic consistency containing refractory aggregates and several organic and ceramic bonds. These products usually have a carbon bond after firing or once in service.

Figure 1 shows a conclusion schematically.

C. Type of Chemical Composition

The subdivision of unshaped refractory products according to their chemical composition is in accordance with ISO R 1927:

Al₂O₃–SiO₂ products, consisting mainly of Al₂O₃, SiO₂, and aluminosilicates.

Basic products, consisting mainly of magnesia, doloma, magnesia-chrome, chrome ore, and spinel.

Special products, mainly consisting of oxides or nonoxide aggregates or others that are not mentioned above. These can include silicon carbide, silicon nitride, zircon and zirconia.

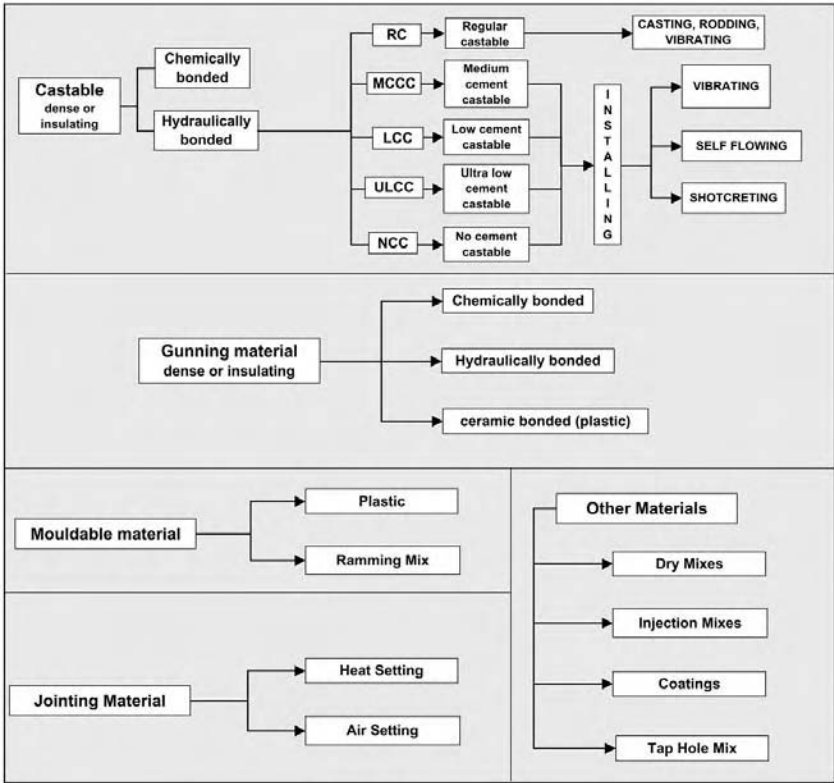


Figure 1 Subdivision of unshaped refractory products schematically.

Carbon-containing products, mainly consisting of aggregates mentioned under item 1.4.1, 1.4.2, or 1.4.3, which, however, contain more than 1% carbon or graphite.

D. Classification—Testing

One of the most important points of EN 1402 was the agreement about shapes and sizes of the test pieces. It was agreed to use for the preparation of test pieces the following three shapes:

1. Shape A = 230 mm × 114 mm × 64 mm (mainly for insulating products)
2. Shape B = 230 mm × 54 mm × 64 mm (previous standard shape for dense products)
3. Shape C = 230 mm × 64 mm × 64 mm (reference shape/test piece).

It is very important to point out that statements about the properties of unshaped refractory products depend on the shape of the test pieces and the standard being used. In other words, results determined on the basis of the EN standard cannot be compared with results determined on the basis of ASTM or JIS standards. As a result of international competition and more open markets, there is a growing necessity to quickly set up ISO standards, which apply worldwide. Positive efforts are being made. For example, ASTM standards, such as C704 (abrasion resistance) or C288 (CO resistance), have been included in the testing guidelines for unshaped refractory products for a long time (6,7). They have also been included in the EN 1402, Part 8.

In addition to the above-mentioned standards, a number of specifications exist, unfortunately. These specifications come from the petrochemical industry and deviate from EN and ASTM standards especially in regard to the shape of the test pieces. Here, too, harmonization would be in the best interest of all parties involved. Figure 2 demonstrates how many test pieces a producer of unshaped refractories has to prepare.

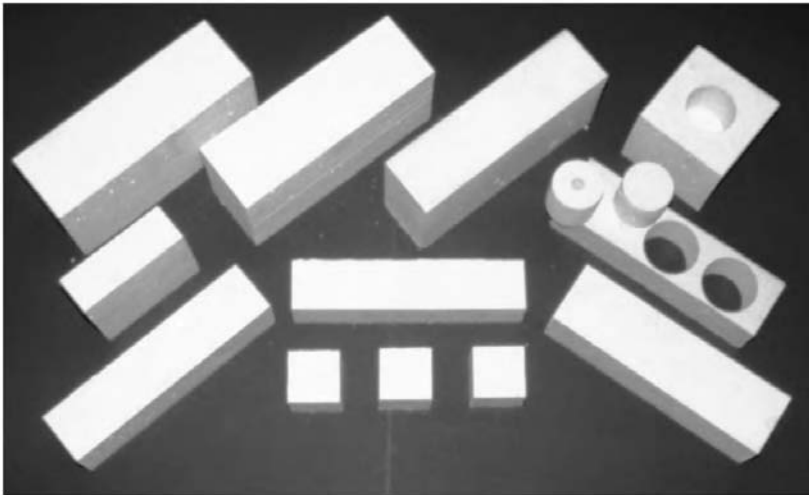


Figure 2 Collection of test pieces made of unshaped refractories. Description from left to right: (**Top**) Two bricks for measuring thermal conductivity ($230 \times 114 \times 76$ mm); Shape A according to EN; cup for slag tests ($100 \times 100 \times 100$ mm, hole 50 mm in diameter and depth). (**Middle**) Test piece for measuring abrasion resistance according to ASTM C 704 ($114 \times 114 \times 40$ mm); test piece according to special specifications for petrochemical industry ($230 \times 50 \times 50$ mm); drilled 50 mm cylinders out of a shape B (one with 12.5 mm hole for determination of Refractoriness Under Load or Creep Under Compression). (**Bottom**) Shape B according to EN; 3 cubes for petrochemical specifications ($50 \times 50 \times 50$ mm); Shape C according to EN.

The consumer is confronted with a confusing number of manufacturers and products with more or less fancy names. However, names or designations are not always in agreement with the performance capability of the refractory product and what is expected. Consequently, the “Verein Deutscher Eisenhüttenleute” (VDEh) (Association of the German Iron and Steel Engineers) published a code number key for unshaped refractory products. This code number key is provided in the form of a standard titled “Stahl-Eisen-Werkstoffblatt 916 (SEW)” and was universally accepted and applied by all concerned German-speaking countries (8).

The products are provided with a 12-digit code. The explanations of the digit positions in information sheet SEW 916 are given in Table 6.

The individual descriptions and properties are to some extent very differentiated. Consequently, this code system is quite explicit. This is also proven by the fact that digits 11 and 12 indicate the refractoriness under load classification temperature by way of a hot test and the permanent linear change after prefring.

Table 7 gives an example of how the code number key works for a regular dense refractory castable.

Looking at the above example, it is quite easy to define the main parameters (especially a hot one) of this castable. The coding system is also a help for making decisions, such as which product can be used for quick repairs in case of emergencies. The RUL classification Temperature is very near to the “real maximum service temperature,” although it has to be mentioned here that this property cannot be measured really.

It would have been a big advantage if an updated version of this code system could become part of EN 1402-1. It has provided such good service for many years. However, there were some different philosophies concerning classification within the European standardizing committee. The result is a classification according to certain temperature classes in combination with maximum

Table 6 Product Code of the VDEh for Unshaped Refractory Products (according to SEW 916)

Number of digits	Position in the code	Description and property
1	1	Type of product (e.g., castable, plastic, etc.)
1	2	State of delivery
1	3	Nature of bond
1	4	Type of installation
2	5 and 6	Raw material base
2	7 and 8	Percentage of main chemical component
2	9 and 10	Material required
2	11 and 12	RUL classification—Temperature

Table 7 VDEh Code of a Regular Dense Castable Based on Calcined Clay

VDEh—code	0 0 1 8 10 33 20 25
Decoding:	
1 = Type of product	0 = Dense castable
2 = State of delivery	0 = Dry for water addition
3 = Nature of bond	1 = Hydraulic
4 = Type of installation	8 = Vibrating
5 + 6 = Raw material base	10 = Chamotte, 30–45% Al ₂ O ₃
7 + 8 = Percentage, chemically	33 = 33–37% Al ₂ O ₃
9 + 10 = Material required	20 = 2.0 t/m ³
11 + 12 = RUL classific.—Temperature	25 = 1250°C

permanent linear changes after pre-firing, which is similar to ASTM C401 and shown in Table 8.

III. METHODS OF PLACEMENTS

The performance of a refractory lining will greatly depend on the type of installation and the quality of the unshaped refractory materials. This applies for laying

Table 8 Classification Temperatures According to EN 1402, Part 1

Criterion: Total linear change^a (determined in accordance with EN 1402-6)

Dense unshaped refractories	Insulating unshaped refractories
	Not applicable
	1000°C
Not applicable	1100°C
1200°C	1200°C
1300°C	1300°C
1400°C	1400°C
1500°C	1500°C
1600°C	1600°C
1700°C	1700°C
>1700°C	>1700°C
All types of castables <1.5% shrinkage	Castables <1.5% shrinkage
Shotcreting refractories <1.5% shrinkage	Gunnings <1.5% shrinkage
Gunning refractories <1.5% shrinkage	
Rammings <2.0% shrinkage	
Plastic refractories <2.0% shrinkage	

^aEquals PLC after drying + firing.

refractory bricks and even more so for the installation and curing of the unshaped refractories. Here humans have a great influence, and their actions are decisive for the quality of the furnace lining. Consequently, this chapter gives information on the most important general rules.

A. Concrete Work

After mixing with a suited liquid, refractory castables are generally installed by casting, rodding, vibrating, or self-flowing, which means casting without vibration. In some cases these materials can also be compacted by ramming, as was formerly often done with RC-type castables. In this case the results were also excellent.

Table 9 gives recommendations as to how the different types of refractory castables should be mixed and installed. This table cannot be considered as generally applicable or valid due to the multitude of available products; however, it should be a guideline. For example, it should be obvious that a paddle mixer cannot be used for so-called lightweight insulating castables, which contain aggregates in form of perlite and vermiculite. If a paddle mixer is used, the danger exists that these aggregates would be destroyed by abrasion. Bulk density and thermal conductivity of the product would increase. On the other hand, it is state of the art to prepare deflocculated castables in a paddle mixer only. This will ensure that the correct consistency for placement is obtained when the manufacturer's recommended amount of mixing liquid is used.

Inside and outside vibrators are used for compaction. The consistency of the castable requires special consideration if using outside vibrators. The refractory castable should never be adjusted to suit the vibrator. The vibrator must always be regulated in regard to the type of castable and the wall thickness. For example, MCC- and LCC-type castables often have a viscous consistency, which can be changed by adding more liquid. This will enable the user to install the castables with less suitable equipment, but in the end the user will also run the risk that the expected properties of the castables will not be achieved.

The packing units usually contain some kind of information on proper installation and working methods. In addition to this, informative brochures about the various installation techniques can be obtained from the refractory manufacturers as well. Due to the multitude of special factors requiring the attention of the user, it is recommended to request information directly from the manufacturer.

Every year the topic of cold temperatures arises. Many studies have been conducted in regard to castables and cold-weather conditions. The main points are summarized as follows:

The properties of a product are determined usually at room temperature, which is considered to be 20°C. At lower temperatures, for example near 0°C, the (mostly) exothermal setting process is delayed, i.e., the moulds cannot be

Table 9 Recommendation for Types of Mixer, Mixing Times, and Types of Installation in Function of the Type of the Castable

	Insulating castables			Dense castables				
	B.D. <1.2 g/cm ³	B.D. >1.2 g/cm ³	B.D. 2	RC	MCC	LCC	ULCC	NCC
Normal concrete mixer	yes	possible	possible	possible	no	no	no	no
Paddle mixer	no	possible	yes	yes	yes	yes	yes	yes
Mixing time after water addition (minutes) ^a	2	2	2-3	>3	≥3	≥3	≥4	≥4
Recommended type of installation:								
Casting	no	no	possible	no	no	no	no	no
Rodding	yes	yes	no	no	no	no	no	no
Vibrating	no	possible	yes	yes	yes	yes	yes	yes
Self-flowing ^b	no	no	no	possible	possible	possible	possible	possible

^aIn case of a two-component delivery, the components have to be mixed in a dry status for a minimum of 1 minute before water addition.

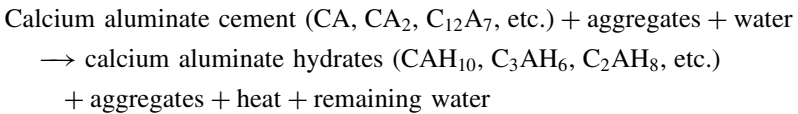
^bThe producer has to indicate if the castable is a self-flowing one; do not try to get a self-flowing consistency by the addition of too much water!

removed quickly, the initial strength is lower, which results in reduced strength values at higher temperatures.

An example: Comparing a RC-type castable with a cement content of 20% and an ULCC-type castable with 3% of the same cement. It is obvious that the ULCC type will need a relatively long time for setting and hardening at low temperatures. It is also not really helpful to use a warmer mixing liquid. For example, 5 l of mixing liquid per 100 kg only means 5 kg warm water facing 100 kg “ice-cold” material—this cannot have big effects. Refractory manufacturers often offer summer and winter versions of MCC- and LCC-type castables by adding accelerators or retarders. Nevertheless, certain on-site precautions will still be required despite these modifications. Further information can be found in the relevant literature.

As far as the curing of castables is concerned, the following general guidelines should be noted:

The setting procedure regarding refractory castables is exothermal—specifically for the insulating refractories and dense RC-type castables. The following *simplified* reaction serves to explain the process:



Insulating refractory castables and RC-type castables can get very hot during hydration. The temperature peak will depend on the quantity of castable, which has to be installed, on the ratio of the surfaces surrounded by moulds to the surface releasing water, and also on the moulded materials on their own. During this time (approximately 15 to 18 hr), the refractory castable must be protected against losing moisture (for example, by covering or sprinkling). Once the heat has disappeared, it is not necessarily required to continue to preserve moisture. If the ambient temperatures are high, however, it is still recommended to preserve moisture in any case. These refractory castables should be given approximately 48 hr’s time before starting any drying or heat-up procedures. The main reason for these measures is that calcium aluminates hydrate on a quantitative basis (see above equation).

Deflocculated castables contain lower amounts of cement, which produce a slight amount of heat. From this point of view, everything stated above can be limited to 24 hr in most cases. For ULCC- and NCC-type castables, the supply of heat will most likely be required to obtain sufficient green strength. Consequently, subsequent treatment of the castable will not be required in the sense described above. Special ULCC castables, which are installed in blast furnace trough systems, contain metallic additives and catalysts. These effect

an intensive exothermal reaction after the addition of water and installation of the castable. Hydrogen forms and creates capillaries by venting out of the castable structure. These capillaries assist the “self-drying” process and also the heat development. Furnaces lined in this way can be put into operation after a relatively short time.

B. Ramming

1. Plastic Refractory Materials

Plastic refractory materials are supplied in cardboard boxes already preformed in blocks or, more frequently, in slices. Depending on the thickness of the walls, the slices, or parts of a slice, which are broken off or cut out, are rammed into position. The ramming method is used to shape the mix better and to obtain the desired contour to fit its surrounding. Ramming is not selected in order to ensure better compaction of the mix, because it has already been properly compacted during its production. The material can be installed with pneumatic rammers or a heavy hammer weighing 1–1.5 kg. The rammer head should be a larger one and not small. The individual rammed layers must be scraped before installing the next layer. Because there is the danger of lamination, which effects spalling, it is always required to work vertically on the surface to be stressed later on.

The use of shuttering is not an absolute requirement for plastic refractories.

After completion, the surface is leveled and scraped with a board containing nails. This is not for trimming the surface alone, but for an easier drying out as well due to the bigger specific surface. To avoid uncontrolled shrinkage cracks, so-called shrinkage joints have to be made. An approximately 1-mm-thick steel plate is hit deep into the rammed material. Penetration must be at least one third of the entire thickness of the rammed section. The resulting segments should not have a side length above approximately 900 mm. For more complicated design (burners), the joint cut must be at the thinnest section.

To ensure better evaporation, venting holes are poked with a steel stud at distances of 150 to 200 mm (staggered). This steel stud should be at least 3 mm thick. It is best to poke all the way through the wall. The poking direction should be slightly upwards (approximately 30° – 45°).

2. Refractory Ramming Mixes

Refractory ramming mixes require very stable shuttering. Here, too, it is very important that ramming work is always conducted vertically on the surface to be stressed later on. The ramming mixes are filled behind the shuttering to a height not exceeding 50 mm. Each layer, having been poured into position, must be compacted with an appropriate pneumatic rammer. Continuous filling

during the ramming work, which must take work progress into consideration, will reduce lamination if working with proper pneumatic rammer heads. Generally, it is required to scrape the surface of each compacted layer. Typical technical data of a pneumatic rammer are as follows:

- Frequency: approximately 50 Hz at 6 bars
- Piston stroke: 120–180 mm
- Weight: approximately 5 kg

The piston rod should be polygonal or crowned in order to ensure better guidance of the rammer head. The recommendations given by the refractory manufacturers should be followed when selecting the size and shape of the rammer head. The size of segments to be rammed with ramming mixes is about the same as for segments filled with plastic refractory mixes.

C. Gunning

More than a third of all unshaped refractories will be installed by gunning. In a previous chapter the type of gunning was described; Table 10 makes a comparison between the old traditional dry gunning technique and the shotcreting method.

Table 10 Comparison of Regular Gunning and Shotcreting

	Dry gunning process	Shotcreting process
Type of product	Regular castables mostly	Deflocculated castables only
Equipment	Rotor or double chamber guns + compressed air	Paddle mixer + double piston pump + compressed air
Transport of castable	Dry to the nozzle through hose	Wet in “cast-able” consistency to the nozzle through hoses (metallic preferably)
Pressure during transport	Less than 6 bar	Sometimes more than 200 bar
Nozzle technique	Adding water through a water ring	Injection of compressed air + accelerator
Type of setting	“Normal” like typical for castables	Hardening very quick after hitting the wall
Dust development	Big as usual	No dust
Rebound	Big as usual	Under good conditions on-site—no rebound
Properties of the lining	As usual for regular castables	As cast or vibrated deflocculated castables

IV. PROPERTIES OF UNSHAPED REFRACTORY PRODUCTS

The multitude of refractory aggregates (for example, calcined clay, flint clay, andalusite, mullite, bauxite, fused white or brown alumina, sintered alumina, etc.) and the different grain sizes of these materials—in addition to the big variety of bonding agents, additives, and mixing liquids—enable endless combination possibilities in development work on unshaped refractory products. Therefore, a qualitative standardization is not really possible as it is the case for refractory bricks. As a result of the ENV 1402-1 standard, which now provides a more precise definition of the products, there will probably be adjustments on the market in the long run. If also considering economic aspects, suitable products will obviously be developed on the basis of all the available constituents.

The upcoming tables list typical commercial products and generally valid criteria.

A. Refractory Castables

Regular castables (RC type), which also include insulating and hydraulically setting gunning mixes, have a typical strength pattern depending on the degree of pre-firing. Figures 3 and 4 give examples of the progress of CCS and cold MOR for a typical chamotte-based castable with various types of calcium aluminate cements (CAC) and the same consistency (“W/C” = ratio of water to cement).

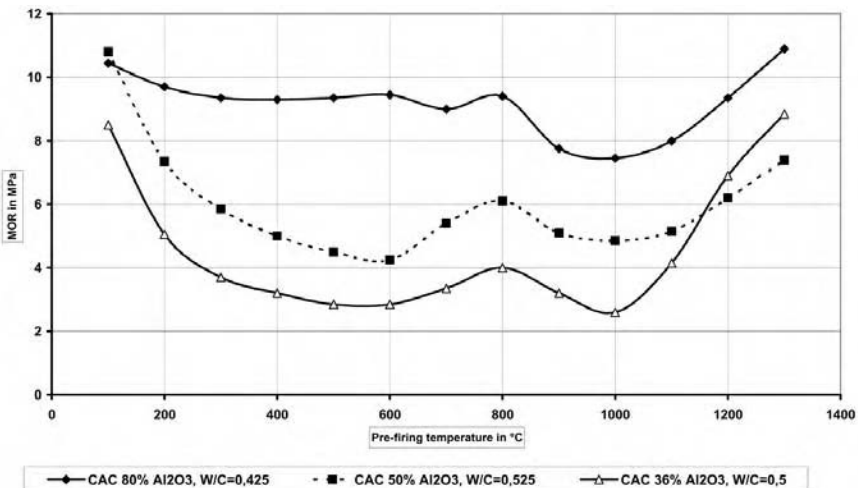


Figure 3 Cold MOR of a chamotte-based castable—type RC—with 20% CA-cement.

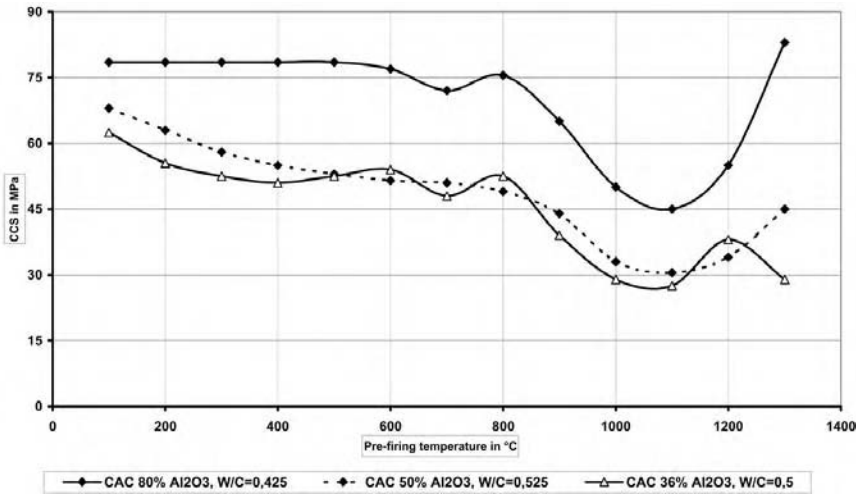


Figure 4 CCS of a chamotte-based castable—type RC—with 20% CAC of different grades.

Generally, the strength drops to a minimum after pre-firing at 1000°C to 1100°C. This decline in strength is due to the dehydration of the calcium aluminate hydrates and changes in pore size distribution. Increasing strength at temperatures above approximately 1100°C is the result of the formation of new minerals consisting of the components of high-alumina cements and aggregates. This can be equated with the start of a ceramic bond.

These correlations are typical for all regular refractory castables. The final strength will depend on the type of refractory castable; in other words, on the type of aggregate, grain structure, cement type, water-to-cement ratio, and installation technique.

The consistency becomes more “liquid,” and strength declines further with increasing mixing liquid content. Figure 5 illustrates the influence of the quantity of water on a refractory castable at 110°C and after 1250°C.

Figure 5 also shows which type of placement has to be applied at which water addition. If, for example, comparing the strength data after 110°C, which was obtained with 9 l water per 100-kg material (which had to be rammed), to the data recorded after using 14 l (having a consistency like a “soup”), one notices an appropriate 50% loss concerning CCS and approximately 35% loss regarding cold MOR. A comparison between unfired material and material pre-fired at 1250°C gives similar results. This is a good example of how the properties of a refractory castable can become worse through the use of too much water.

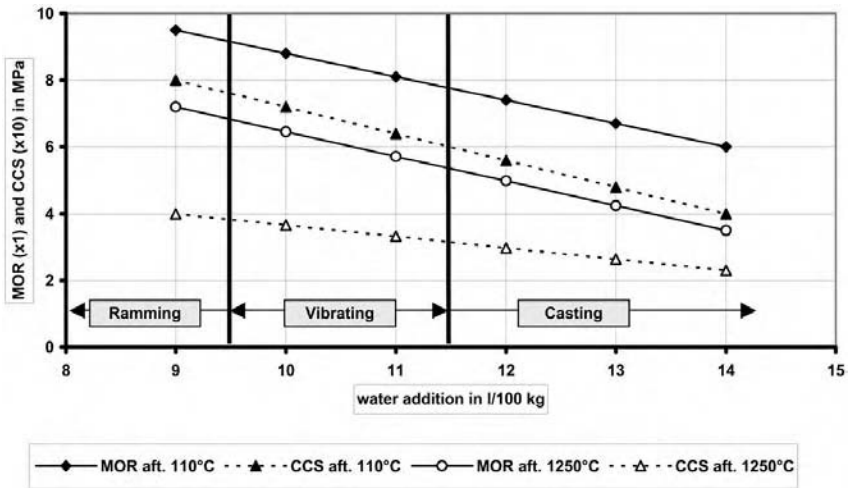


Figure 5 Influence of water addition on MOR and CCS of a chamotte-based castable, Type RC.

On the one hand, adding more water makes working with the refractory castables “easier.” On the other hand, there can be disadvantages in some cases (longer setting times, lower strength, higher shrinkage, and higher porosity, etc.). This is shown in Figure 6, where the influence of water addition (and type of placement) on B.D. and CCS is demonstrated.

In addition to the decrease of B.D. and CCS, there is also generally a significant increase of shrinkage by using too much water especially as far as lightweight products are concerned. And another very important correlation has to be mentioned: A loss of more than 0.2 g/cm^3 in B.D. is equivalent to a reduction of 0.1 W/mK for thermal conductivity!

Table 11 lists the properties of those standard insulating castables whose maximum service temperatures are between 950°C and 1800°C . The bulk density usually increases with rising maximum service temperature. This is due to the change of lightweight raw materials in the castables. Thermal conductivity and strength increase likewise, whereas apparent porosity, shrinkage, and permanent linear change decrease. The fact that the CaO and Fe_2O_3 contents drop can also be attributed to the raw material combination. However, the Al_2O_3 content increases. Apart from a few exceptions, this is generally the case.

As mentioned before, it was an absolute necessity for all producers to develop refractory castables with higher strength in the critical temperature range. Since the 1970s the so-called deflocculated castables have been available, and they have been improved continuously. The principle is to decrease the amount of cement,

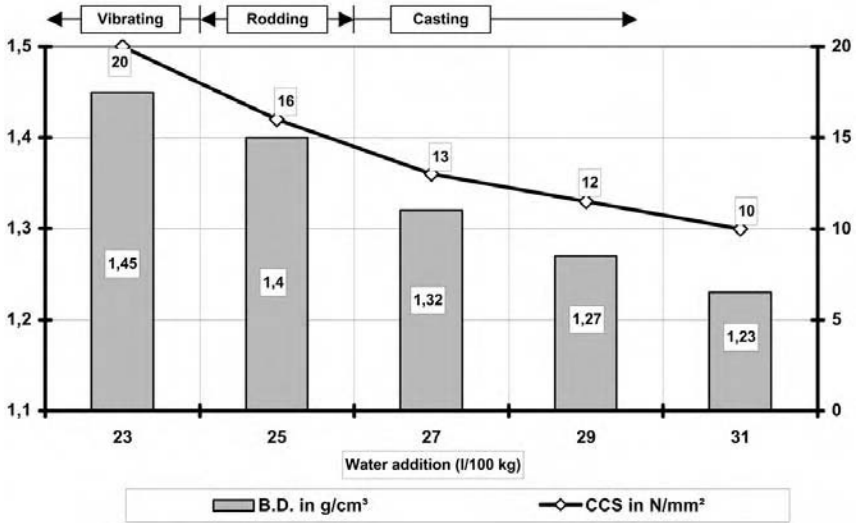


Figure 6 Influence of water addition on properties of LW-castables (after drying).

introduce raw materials with very high specific surfaces like microsilica or reactive alumina, and add deflocculants for reducing the water requirement.

Figures 7 and 8 illustrate current correlations concerning regular castables. Deflocculated MCC-type castables have more or less the same strength behavior as the RC types. However, the strength level is substantially higher and the strength drop less pronounced, as shown in Figure 7. LCC-type castables usually show a continuously rising strength curve at a generally high level without distinct maximums and minimums.

Figure 8 shows the CCS of castables based on andalusite/flintclay and on tabular alumina as regular castables RC and the deflocculated versions in each case. As far as flintclay/andalusite is concerned, the traditional RC type has poor strength. The MCC version shows similar tendencies as typical for the cement bonding—however, on a triple higher level. The LCC version is very similar to the MCC in this case.

Looking especially to the tabular alumina castables, it can be recognized that the ULCC version has relatively low strength at lower temperatures. Above 1100°C a strong and linear increase can be seen until 1700°C. Such behavior is typical for this type of deflocculated castables. The strength curve of the RC version is crossing the ULCC at 1200°C. Above this temperature, the strength is significantly lower than the one of ULCC. The LCC modification has a more or less “ideal” behavior. Until 1200°C the CCS is nearly constant on a high level (double of RC and ULCC). At higher temperatures the strength increases linearly, too, like the ULCC does.

Table 11 Technical Data of Different Insulating Castables

Product	A	B	C	D	E
Raw material base	Vermiculite	Vermiculite/exp. clay	Expanded clay	LW-chamotte	Bubbled-alumina
Max. service temp., °C	950	1100	1100	1300	1800
Water addition, l/100 kg	120	45	20	23	17
Al ₂ O ₃ , %	10	25	25	35	96
SiO ₂ , %	41	45	40	45	0.3
Fe ₂ O ₃ , %	4	9	8	5	0.1
CaO, %	27	14	11	10	3
After prefring at °C	800	800	1000	1200	1600
Bulk density, g/cm ³	0.4	0.9	1.4	1.4	1.5
App. porosity, %	88	58	45	45	48
MOR, N/mm ²	0.2	0.8	1.6	1.5	8
CCS, N/mm ²	0.2	2.0	10	6	18
P.L.C., %	-1.0	-0.3	-0.4	-0.4	±0
Therm. conductivity, W/mK	0.17	0.32	0.42	0.45	0.69

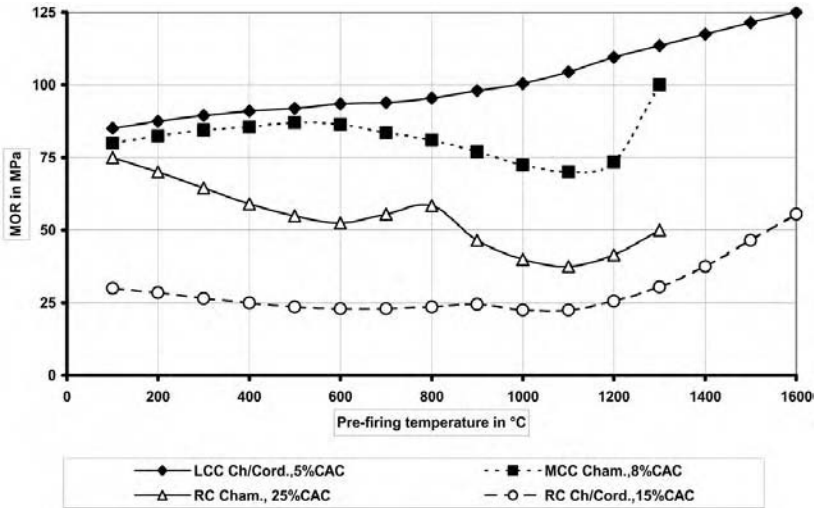


Figure 7 CCS of different castables; RC in comparison to MCC and LCC.

Table 12 lists properties of eight different industrial refractory castables and gives a comparison between RC- and MCC-type castables. Chamotte (A 1 + A 2), flint clay (B 1 + B 2), flint clay/fused brown alumina (C1 + C 2), and tabular alumina (D 1 + D 2) were selected to serve as examples of the raw material

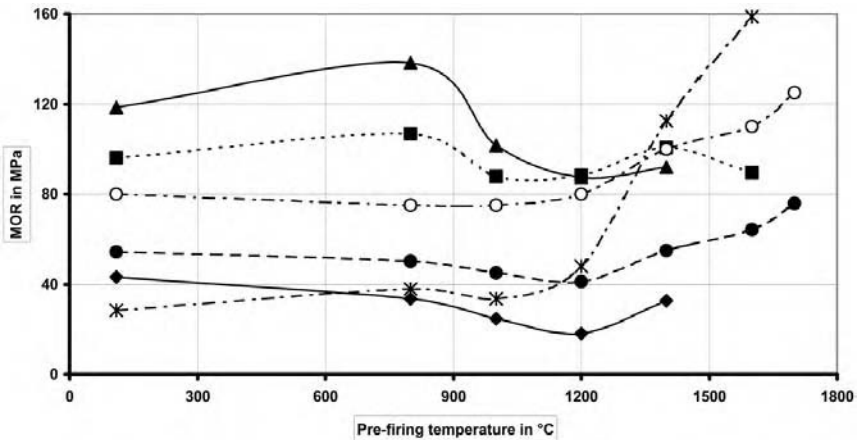


Figure 8 CCS-comparison of RC's and deflocculated industrial castables based on similar raw materials.

Table 12 Technical Data of Dense Castables, Comparison Between RC—MCC

Product	A 1	A 2	B 1	B 2	C 1	C 2	D 1	D 2
Type	RC	MCC	RC	MCC	RC	MCC	RC	MCC
Raw material base	Chamotte	Chamotte	Flintclay	Flintclay	Flintclay/ FBA	Flintclay/ FBA	Tab.- alumina 1800	Tab.- alumina 1800
Max. service temp., °C	1300	1300	1500	1500	1600	1600	7	5.5
Water addition, l/100 kg	13	9	11	6	9.5	6.5	71	93.4
Al ₂ O ₃ , %	38	35	49	51	69	71	95.6	3.4
SiO ₂ , %	47	53	45	43	27	25	<0.2	<0.2
Fe ₂ O ₃ , %	4	3.5	0.5	1.0	0.4	0.5	<0.15	<0.2
CaO, %	7.5	4.6	4.4	3.6	2.8	2.8	3.6	2.8
After prefiring at °C	1200	1200	1400	1400	1500	1500	1600	1600
Bulk density, g/cm ³	1.9	2.0	2.08	2.35	2.45	2.55	2.9	3.0
App. porosity, %	25	18	23	15	22	16	20	18
MOR, N/mm ²	4	9	6	14	8	12	15	24
CCS, N/mm ²	24	65	35	110	40	95	80	140
P.L.C., %	±0	-0.7	±0	-0.2	-0.2	-0.1	-0.2	-0.7

base. First, it should be pointed out that the addition of water for the MCC modification is far less than for the RC version. The same applies for the CaO content. B.D. and strength are substantially higher with MCC castables. However, the porosity is much lower.

From this it can be stated that deflocculated refractory castables generally possess the following characteristics in comparison to the regular ones:

- Lower amounts of mixing liquids
- Lower CaO contents
- Higher strength values
- Better erosion resistance
- Higher bulk densities
- Lower porosities
- Finer pore size distribution
- Higher thermal conductivity

These properties are made possible by the controlled introduction of raw materials with large specific surfaces, for example, microsilica. The selection of suited deflocculation systems is of further assistance. However, the hot properties (hot MOR, refractoriness under load, creep under compression, etc.) must be classified as a bit lower in comparison to the relevant RC. Microsilica, for example, leads to thermoplastic effects at high service temperatures. Consequently, LCC- and ULCC-type castables were developed by using other reaction partners (for example, Al_2O_3 and/or Cr_2O_3), which do not even contain SiO_2 . If these products, made from premium-grade raw materials, have been subjected to pre-firing at high temperatures, they can be compared to the corresponding high-fired, direct bonded bricks. Special additives, such as spinel or components forming spinel, will enable the attainment of special properties.

There will be promising applications for cement-free refractory castables in the future, too. The low green strength of these castables will be compensated for by superb properties in the hot state.

Table 13 shows some typical LCC- and ULCC-type castables. Product A is applied for high strength requirements up to 1300°C . Products B and C have provided good service results in hearths of rotary hearth, pusher-type, and walking beam furnaces. They have replaced the standard ramming mixes used previously. Product C is based on fused brown alumina and used for steel ladle coverings (lids), pouring lips, etc. Products E and F are ULCC-type castables. Despite high B.D. and strength, product E has good thermal shock resistance. Product F can be subjected to extremely high thermal stress due to its low SiO_2 content.

It is possible to manufacture deflocculated castables in self-flowing modifications. The better description of this exceptional property seems to be "self-leveling without segregation." The properties of such SFCs are generally similar to those castables applied by vibration (SFC = self-flowing castable). SFC-type

Table 13 Technical Data of Different Dense Castables, Type LCC and Type ULCC

Product	A	B	C	D	E	F
Type	LCC	LCC	LCC	LCC	ULCC	ULCC
Raw material base	Chamotte	Andalusite	Corundum/FBA	Corundum/FBA	Mullite	Tab.-alumina
Max. service temp., °C	1450	1600	1700	1700	1700	1800
Water addition, l/100 kg	5.8	5.8	4.4	3.8	5.8	4.2
Al ₂ O ₃ , %	48	57	80	90	77	99
SiO ₂ , %	47	38	15	8	21	0.2
Fe ₂ O ₃ , %	1.1	1.1	0.6	0.1	0.2	0.1
CaO, %	2.3	2.3	2.3	1.4	0.7	0.5
After prefiring at °C	1200	1400	1400	1600	1600	1600
Bulk density, g/cm ³	2.35	2.50	2.80	3.10	2.65	3.10
App. porosity, %	16	17	18	13	18	16
MOR, N/mm ²	13	9	10	30	10	20
CCS, N/mm ²	95	100	120	180	70	80
P.L.C., %	-0.2	+0.4	+0.1	-0.20	+0.70	-0.3

castables are specifically suited for “veneering” purposes; however, they can be used for new linings, too. Inside and outside vibrators often cannot be used for complicated designs (for example, single layer on water-cooled pipe walls with anchoring). In such cases, SFCs can be the better solution for a proper installation. Their properties follow the same rules, which were mentioned before.

B. Plastic Refractory Materials

Table 14 lists properties of typical plastic refractory materials. The ceramic bond is compared with the chemical (phosphate) bond. The latter will generally effect higher strength and B.D. However, after having been installed, the chemical bond mixes require heat in order to set. For this type of material it may be necessary to install extra shuttering for support.

The manufacturers of plastic refractory materials must make proper raw material compositions and operate strong extruders to ensure optimum properties. It is not easy to make a mouldable product with a workability index of approximately 15% to 20% considering the high density of this material.

C. Refractory Ramming Materials

Similar to the plastic refractory materials, ramming materials can have a ceramic or chemical (chemical ceramic) bond. Table 15 shows the properties of several ramming mixes, which, if installed properly, can be an excellent refractory lining. This is especially the case if liquid phases, slags, melts, etc., and thermal shock resistance are the main stress factors for the wear layer. The physical properties of these materials are comparable to those of dry-pressed refractory bricks. The production of ramming mixes is on the decline for two main reasons:

1. There are very few well-skilled operators who can install a ramming material properly without layers or free of lamination.
2. In addition to this, very stable shutterings are required on-site. This results in high installation costs.

However, refractory ramming materials are still used for the manufacturing of prefabricated shapes. This is done by hand ramming or by vibrating presses. In this case the mixes usually have a chemical bond. The preformed shapes are normally tempered at approximately 400°C and, consequently, have sufficient strength for any manipulation procedures until reaching the application site. If installed prefabricated and thermally pretreated shapes are not heated up immediately after installation, they will lose strength due to a hydration of the clay component. However, this loss of strength is compensated for without any disadvantages after heat-up.

Table 14 Technical Data of Different Plastic Refractories

Product	1	2	3	4	5	6
Raw material base	Flintclay	Chamotte/ andalusite	Bauxite/ FWA	Bauxite/ FWA	FWA/Tab.- alumina	FWA/Tab.- alumina
Max. service temp., °C	1650	1650	1700	1700	1750	1700
Nature of the bond	Ceramic	Chemical	Ceramic	Chemical	Ceramic	Chemical
Material required, t/m ³	2.35	2.55	2.80	2.9	3.0	3.15
Al ₂ O ₃ , %	51	59	84	84	91	91
SiO ₂ , %	44	35	12	11	7	4.5
Fe ₂ O ₃ , %	1	0.9	0.6	0.5	0.4	0.1
After prefring at, °C	1000	1000	1000	1000	1000	1000
Bulk density, g/cm ³	2.18	2.35	2.67	2.80	2.83	2.92
App. porosity, %	23	19	23	19	23	18
MOR, N/mm ²	3	10	5	13	5	20
CCS, N/mm ²	25	75	30	80	40	100
P.L.C., %	-1.4	-0.5	-1.4	-0.5	-1.3	-0.8

Table 15 Technical Data of Different Ramming Mixes

Product	1	2	3	4	5
Raw material base	Flintclay	Chamotte/ corundum	Mullite	Bauxite	Corundum
Max. service temp., °C	1450	1600	1700	1650	1800
Nature of the bond	Ceramic	Chemical	Chemical	Ceramic	Ceramic
Material required, t/m ³	2.5	2.65	2.55	2.80	3.25
Al ₂ O ₃ , %	50	62	70	80	95
SiO ₂ , %	47	34	28	15	4
Fe ₂ O ₃ , %	0.9	0.7	0.4	1.5	0.2
After prefiring at, °C	1350	1500	1500	1400	1500
Bulk density, g/cm ³	2.35	2.47	2.38	2.68	3.07
App. porosity, %	14	14	13	17	14
MOR, N/mm ²	9	8	13	7	10
CCS, N/mm ²	40	50	65	50	150
P.L.C., %	-0.6	±0	-0.3	+0.4	-0.4

D. Refractory Gunning Materials

Unfortunately, an applicable uniform standard for the sampling and testing refractory gunning materials does not exist so far in Europe. Nevertheless, it is quite common to gun panels or plates. After a subsequent curing time has elapsed, which depends on the specific material, samples are cut out of a panel like that shown in Figure 9.

These test pieces are subjected to testing and inspection according to the same procedures applicable for other unshaped refractory castables. For panels without sufficient green strength for cutting, a prefiring at a sufficient high temperature may be necessary. This procedure is valid generally for the preparation of test pieces of gunned plastic materials. Consequently, if comparing various data provided by several manufacturers, it is important to check if the data in the product information sheet refer to the gunned or, for instance, cast, trowelled, or rammed state.

Table 16 and 17 list properties of gunning materials. Table 16 includes insulating refractory gunning products A + B and plastic refractory materials C + D.

The dense refractory gunning products E, F, G, and H with hydraulic bond are shown in Table 17. These gunning mixes always have a higher porosity than the regular ones, which are rammed, respectively, cast. The higher porosity is based on the installation technique. Any rebound material of hydraulically setting products cannot be used again. The rebound of plastic refractory gunning mixes can be fed back continuously into the gunning machine if conditions on-site permit.

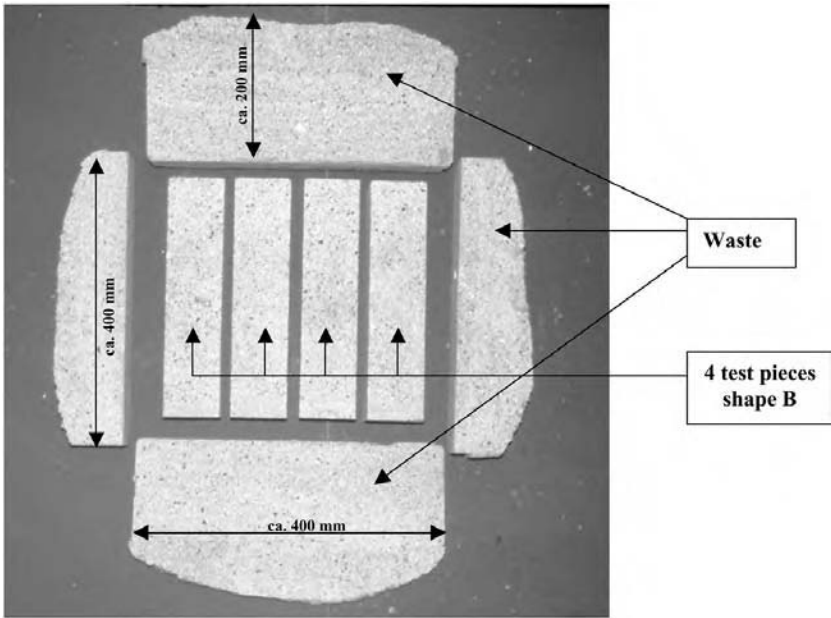


Figure 9 Cut test pieces, shape B, out of a panel.

Table 16 Properties of Insulating and Plastic Gunning Refractories

Product	A	B	C	D
Type of bond	Insulating hydraulic	Insulating hydraulic	Plastic ceramic	Plastic ceramic
Raw material base	Vermiculite	Bubbled alumina	Andalusite	Corundum
Max. service temp., °C	1100	1500	1600	1800
Al ₂ O ₃ , %	28	73	47	85
SiO ₂ , %	39	18	49	10
Fe ₂ O ₃ , %	9.3	0.7	1.2	1.0
CaO, %	15	7	0.2	0.2
After prefiring at, °C	1000	1400	1500	1600
Bulk density, g/cm ³	0.85	1.75	2.35	2.85
App. porosity, %	75	48	24	27
MOR, N/mm ²	1.5	5	8	6
CCS, N/mm ²	2	25	55	35
P.L.C., %	-1.5	-1.6	-0.7	-0.2

Table 17 Properties of Dense, Regular Dry Gunning Materials

Product	E	F	G	H
Type of bond	Dense hydraulic	Dense hydraulic	Dense hydraulic	Dense hydraulic
Raw material base	Chamotte	Andalusite	Corundum	SiC/chamotte
Max. service temp., °C	1400	1600	1650	1500
Al ₂ O ₃ , %	55	60	85	23
SiO ₂ , %	34	35	10	7
Fe ₂ O ₃ , %	0.7	0.9	0.6	0.5
CaO, %	7.7	2.3	1.8	5.8 (60% SiC)
After prefring at, °C	800	1400	1600	1400
Bulk density, g/cm ³	2.10	2.35	2.60	2.15
App. porosity, %	32	26	27	33
MOR, N/mm ²	9	4	8	5
CCS, N/mm ²	80	30	60	15
P.L.C., %	-0.2	+0.4	-0.9	-0.7

The loss of rebound must always be estimated in advance when calculating the required quantity of material for a gunned lining. This “lost” amount depends on several factors. It is possible to expect a so-called “usual rebound rate” (15%, for example). However, this rate can increase considerably when faced with difficult site conditions (gunning-above-head, hot gunning, anchor bricks, single-layer gunning, etc.). The gunning equipment is also an important factor (machine leaks, air pressure, water pressure, how far or high mix is transported, suitable prewetting of mix with water, etc.). Additionally, the experience of the gunning team (personnel) has also an effect on properties of the product in the wall and amount of rebound material.

Once an installation technique has been selected, it is important to use products best suited for this installation method. This applies specifically for gunning mixes. Conventional dense refractory castables should generally not be gunned (too high loss of rebound). Gunning castables should not be cast (low strength, high shrinkage, and porosity). Exception: Plastic gunning mixes can be installed also by ramming!

At the end of this chapter about gunning, it seems necessary to point out the superior properties of shotcreted refractories compared with ones that can be reached by the regular dry gunning method. This is shown in Figure 10, where three different curves are shown, which are explained as follows:

1. “as dry gunned” = standard gunning material (rich in cement), based on flintclay with 60% Al₂O₃, gunned with a MEYCO PICCOLA in gear 1

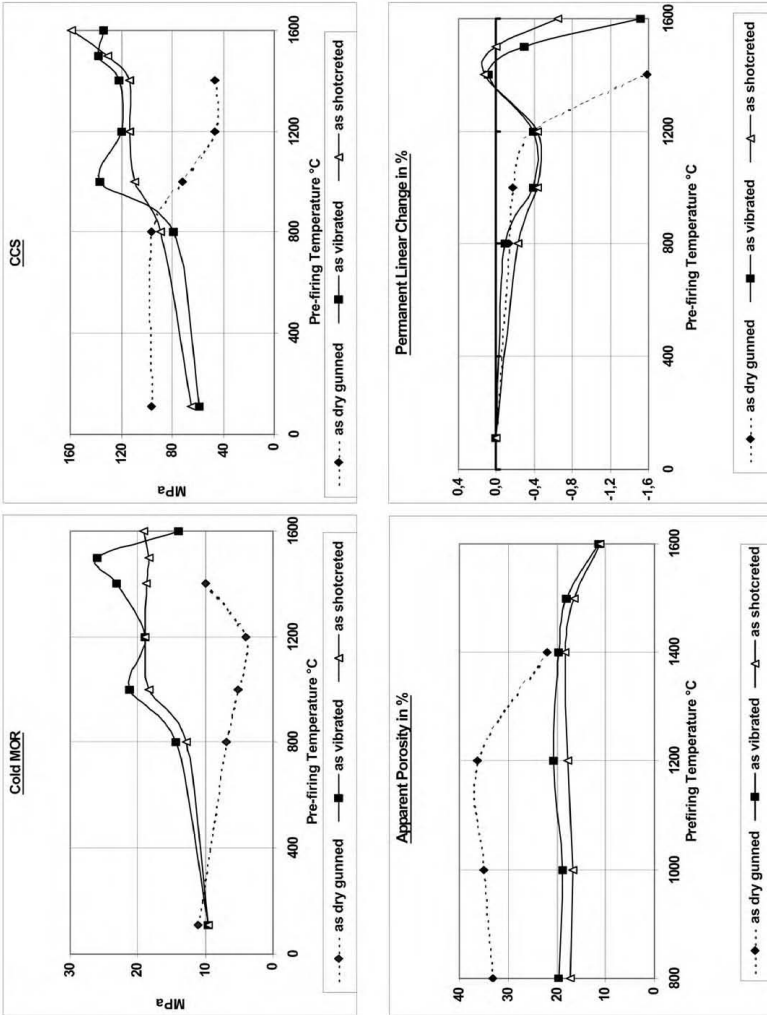


Figure 10 Comparison of physical properties after using different installation methods.

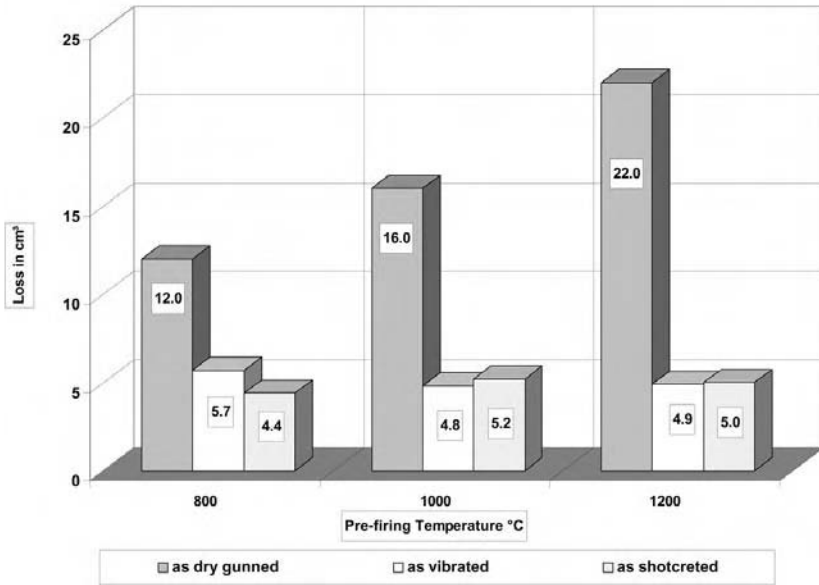


Figure 10 Continued.

2. “as shotcreted” = 60% Al₂O₃ LCC based on flintclay, shotcreted with PUMPMOR MX 10 after the addition of 6.2 l water/100 kg and using sodium silicate as an accelerator (flow = 231 mm after mixing with paddle mixer on machine, before entering the hopper)
3. “as vibrated” = same product with the same water addition vibrated in laboratory (flow = 210 mm after mixing in Hobarth mixer).

As far as the flow values are concerned, it can be noticed that obviously the mixing energy of a big paddle mixer (flow = 231 mm) is much better than the one of a laboratory mixer (flow = 210 mm).

During dry gunning, respectively, shotcreting, panels were gunned and test pieces—shape B—were cut according to Figure 9. Doing so, a comparison of physical properties after certain pre-firing temperatures could be made between the gunned and cut test pieces and the vibrated ones, which were also of the shape B type, of course.

Figure 10 shows the measured properties for MOR, CCS, PLC, and apparent porosity, and Figure 11 (see Sec. VII) shows the erosion loss, which was determined in accordance to ASTM C704.

Looking to the strength, it can be recognized that MOR and CCS show the same tendencies for shotcreting and vibrating, which are typical for LCCs

generally. On the other side, the strength behavior of the normal gunned product has the known decreasing tendency. The decrease will be stopped at higher temperatures above 1200°C; however, this has to be traced back to a strong sintering, which can be seen in the PLC diagram. Regarding the apparent porosity, it is remarkable that the one for regular dry gunning is about a third higher than that determined for shotcreting and vibrating.

Additionally, it can be stated that there is no significant difference whether the deflocculated castable will be installed by shotcreting or vibrating, as far as the measured properties are concerned.

The excellent physical properties of shotcreting and/or vibrating can be recognized also in Figure 10, where the erosion resistance is shown after prefring. After 800°C, the loss of material by erosion is more than double for dry gunning; after 1000°C, the loss is three times higher; and after 1200°C, the material loss increases to four times the value, which was determined for the shotcreting and vibrating technique. Finally it can be noticed that shotcreting and vibrating have no significant decrease or increase of erosion loss in function of the prefring temperature.

As said before, there are serious tendencies to develop and introduce so-called high-compact, high-strength, or high-density LCCs that can be gunned by using the standard equipments for dry gunning. The main target is to reach similar properties and to overcome the disadvantages of big equipment and a bigger team as well, which are necessary for shotcreting technology. Results of gunned panels are comparable with shotcreted or vibrated properties. However, the disadvantages of dust development and bigger rebound are not yet solved with the new dry gunning products. Due to the chemical additives and raw materials with big specific surfaces, there is a small range between “too wet” and “too dry” during the gunning of such products. If the upper range for water addition is exceeded, the gunned refractory wants to flow down, and if insufficient water is added, there will be a big dust development. Therefore, the advantages of shotcreting should be pointed out again.

No dust development.

Optimum wetting of all particles with water and homogeneous mixing in paddle mixers.

Only little or no rebound.

Quality of the lining can be compared with vibrated ones.

Big capacity! More than 10 tons/hr are possible on well-prepared job sites.

The products for shotcreting can be used also for vibrating—without any disadvantage.

E. Special Products

Tables 18 and 19 give examples of so-called special products, which are distinguished from the above-mentioned products due to their chemical composition or

Table 18 Properties of Different Special Unshaped Refractories, Part I

Product	A Ramming mix	B Ramming mix	C Dry mix	D Dry mix	E Tap hole mix
Raw material base	Zirconoxide	SiC/ bauxite	Calcined clay	FWA/ MgO	FBA/SiC
Max. service temp., °C	ca. 2200	1600	1100	1750	1600
Nature of bond	Ceramic	Ceramic	Ceramic	Ceramic	Organic
Al ₂ O ₃ , %	0.1	54	52	82	66
SiO ₂ , %	—	10	40	1.5	—
Fe ₂ O ₃ , %	0.1	1	0.6	—	0.4
CaO, %	—	—	—	—	—
SiC, %	—	18	—	—	18
C, %	—	14	—	—	6
MgO, %	—	—	—	14	—
ZrO ₂ , %	95	—	—	—	—
After prefiring at °C	1700	1400	800	1600	1400
Bulk density, g/cm ³	4.4	2.4	2.1	3.0	2.20
App. porosity, %	22	25	19	21	19.8
MOR, N/mm ²	3	2.5	2	-4	n.d.
CCS, N/mm ²	70	12	12	18	9.5
P.L.C., %	-0.7	-0.7	-0.2	+2.5	+0.3

installation method. All data were determined under the specific working consistency. Products containing SiC and C were fired in reducing atmosphere. Some of the application areas are listed in the tables.

1. Special Ramming Materials

The first-mentioned material “A” is a pure zirconia ramming mix, which provides good service results at extremely high service temperatures like in carbon black reactors. In addition to its high price, specific mention is made of the high B.D., which corresponds to a material requirement of approximately 4.5 t/m³. The second example “B” is a SiC–C-ramming material, which is occasionally used in blast furnace troughs but also in foundries.

2. Dry Mixes

Product “C” is based on chamotte and is used in aluminium foundries in ladles and smaller crucible furnaces. The spinel-forming dry mix “D” is based on fused white alumina and is suited for inductive melting of special steel alloys at high temperatures.

Table 19 Properties of Different Special Unshaped Refractories, Part II

Product	F Tap hole mix	G Casthouse castable	H Spinel castable	J Patching mix	K Patching mix
Raw material base	Bauxite/ SiC	FBA/SiC	FWA/ MgO	SiC	FBA
Max. service temp., °C	1550	1650	1800	1500	1750
Nature of bond	organic	ULCC	ULCC	inorganic	inorganic
Al ₂ O ₃ , %	36	71	93	1.5	93
SiO ₂ , %	—	4	1.2	7	3
Fe ₂ O ₃ , %	0.9	0.3	0.1	0.3	0.1
CaO, %	—	0.7	0.5	—	—
SiC, %	18	19	—	87	—
C, %	11	3	—	—	—
MgO, %	—	—	4.8	—	—
ZrO ₂ , %	—	—	—	—	—
Prefiring at °C	1400	1600	1600	1000	1200
Bulk density, g/cm ³	2.08	3.0	3.1	2.5	3.0
App. porosity, %	19.0	15	16	17	16
MOR, N/mm ²	n.d.	5	20	21	28
CCS, N/mm ²	11	50	150	120	130
P.L.C., %	+0.2	+0.2	+0.3	-0.7	-1.20

Here the quartzite-based dry mixes (also referred to as siliceous dry vibratables) have to be mentioned, too, which contain more than 95% SiO₂ generally and consist of quartzite grains and quartz sand having excellent grain size distribution and special shapes of the grains. Sintering at low temperatures is possible with the assistance of additives like boric acid or other low-melting agents. Some additives are functioning as a catalyst for the transition of α -quartz to cristobalite. These mixes are placed in induction furnaces for melting steel and brass.

3. Tap Hole Mixes

Both tap hole mixes “E” and “F” do not contain tar. They are resin bonded and mainly differ from each other in regard to their Al₂O₃–SiO₂ content of the raw material base. Here the higher strength—usually desired for unshaped refractory products—is not that important. Different criteria are essential for all tap hole mixes. These are correct consistency, setting, and carbonization at the right time, precisely controllable PLC, and “drilling capability.”

4. Special Refractory Castables

Two products, which are used quite frequently, were selected from the multitude of products.

The first-mentioned product “G” is a ULCC-type castable and based on fused brown alumina/SiC with approximately 3% carbon. It is applied in the casthouse of blast furnaces, especially in the pig iron trough. The second example “H” is a spinel-forming ULCC castable, which is used as wear lining in steel ladles.

5. Refractory Patching Materials

These are mixes installed as relatively thin layers on water-cooled and studded pipes. They are usually placed by hand (patching method). SiC mixes like product “J” are often used in boilers and waste incinerators due to their high thermal conductivity and good properties to resist slag attack. In incinerators today, temperature and time for burning out of particles increased due to the dioxin problem. Therefore, the risk of SiC oxidation increased, too. In such cases it is recommended to use refractory patching materials with a high Al₂O₃ content like shown in product “K” in the case of higher service temperatures; however, their thermal conductivity is significantly lower than that of SiC products.

V. THE ADDITION OF FIBERS

The definition of unshaped refractory products includes a statement that “they may contain organic, ceramic, or metallic fibers.” These fibers fulfill various objectives. Consequently, these additives will be described in brief.

A. Organic Fibers

These fibers generally serve as vaporization assistance for the drying and heat-up period in refractory systems. The dense and deflocculated refractory castables may experience explosionlike damage in the castable lining when a furnace is heated up too rapidly in the lower temperature range (at approximately 150°C to 250°C). The fibers most often used are made from polypropylene. These fibers form a system of communicating channels inside the castable structure. The fibers will already shrink below the boiling point of water and dissolve as the temperature increases. This permits easier evaporation of the lining. The general rule: The efficiency of the fiber increases with growing length and decreasing diameter (based on the same weight shares). Standard lengths are in the range of 6 to 12 mm and a diameter of 10 to 30 μm. Neither strength nor porosity of the product will change if the share of fibers is below 0.5% (in weight) in the dry mix.

B. Metallic Fibers

This concerns the addition of steel fibers. There are many reports on steel fibers in the literature (9). Steel fibers are wiredrawn, “centrifuged” out of the melt, or milled fibers made from blocks. The production of these fibers is directly related to the shape or geometry of the fibers. Consequently, it can be deduced that there are varying quantities of fibers per weight unit. The number of fibers per kg varies between 25,000 and 48,000 depending on the manufacturing method, shape, and alloy. Steel fibers with lengths of approximately 25 mm and 0.4 mm diameter are used most often. They can be straight, hooked, or corrugated, and they are mixed into a refractory castable with about 3% by weight. There is a common rule that the amount of steel fibers by volume shall not exceed 0.8% of the castable volume. This means, for example: If the B.D. of the castable is approximately 2 g/cm^3 , the addition of 3% in weight of the a.m. wire-type fibers corresponds to approximately 0.8% by volume.

Steel fibers improve the thermal shock rupture work. In other words, they improve the thermal shock resistance of the lining and its capability to stay in one piece upon rupture and act as a crack stopper. The thermal limits in refractories, of course, depend on the type of steel alloy and service conditions. Furthermore, they can still be effective under reducing atmospheres at temperatures above 1600°C like in gas lances for steel treatment. Under normal or oxidizing atmospheres, castables containing Cr–Ni-alloyed steel fibers should not be exposed to temperatures $> 1200^\circ\text{C}$.

However, it should be pointed out that the composition of the refractory castable matrix is of special significance, too. The chemical reactions between the main refractory matrix components like SiO_2 , CaO , and Al_2O_3 with the oxides, resulting from the steel oxidation, like Cr_2O_3 , NiO , Fe_3O_4 , and FeO should be taken into consideration.

Table 20 illustrates how adding steel fibers changes the properties of a refractory castable.

C. Ceramic Fibers

As mentioned before, the maximum service temperature for steel fibers under normal conditions is approximately 1200°C . Therefore, attempts have been made to reinforce unshaped refractory products with ceramic fibers in order to achieve positive effects at even higher temperatures.

Here one must differentiate between glassy and/or polycrystalline fibers, which are applied for the manufacture of insulating refractory products (mats/blankets, modules, vacuum-shaped components, etc.) and such fibers that are made by extrusion of raw materials including clay, mullite-based compositions, or Al_2O_3 (10). The latter type is subsequently fired (“ceramic studs”). They have

Table 20 Influence of Steel Fiber Addition on the Properties of Refractory Castables

Property	Changing
Water addition	Bit higher (approx. 0.1—0.15 l/100 kg)
Consistency, flow behavior	More “difficult”
Bulk density	Not significant
Porosity	Not significant
Modulus of rupture	Positive
Compressive strength	Not significant
Erosion resistance	Not significant
Thermal shock resistance	Positive
Thermal conductivity	Not significant
Permanent linear change	Tendency to expand
Thermal expansion	Bigger
CO resistance	—No changing for Cr–Ni–steel —Bad for carbon steel fibers

a diameter of one to several millimeters, whereas ceramic fibers have a diameter of approximately 2 to 5 μm.

In addition to the problems concerning mixing (dispersing of fibers, self-crushing, etc.), ceramic fibers and studs have not established themselves as suitable additives for the unshaped refractory products. They have certain reinforcing effects up to the point of ceramic bonding. However, upon further temperature increase, they react with the surrounding matrix as a refractory raw material. So they become an integral component of the refractory construction material and thereby lose the capability of reinforcing.

VI. PREFORMED SHAPES

Preformed shapes will be made normally from refractory castables and ramming mixes. These parts are usually pretreated thermally (dried, respectively, tempered) at the manufacturer’s plant and, consequently, they can be put in service more or less immediately. Often expense for moulds, installation, and heat-up on-site can be saved if applying preformed shapes wisely. The size of a preformed shape can vary greatly and is not a criterion for classification. For example, smaller furnaces with a complicated design can be lined more quickly with these parts than having to first install complicated shuttering. On the other hand, large-shaped sidewall elements or roof parts are suited as “shuttering” for the installation of insulating products. Preformed shapes, such as burners, injection lances for pig iron or

steel treatment, gas purging systems, or impact blocks for bottoms in steel ladles, can actually be better classified as “functional” refractory products.

If using preformed shapes, in regard to application and subsequent treatment of unshaped refractory materials, the consumers hand the problems over to the expert manufacturer. The advantages for the consumer include

Optimum processing.

No installation and removal of moulds and shuttering on-site.

Setting times are no longer required.

“Immediate” start of operation due to thermal pretreatment at manufacturer.

VII. DRYING AND HEATING UP

The drying and heat-up procedures can start once the furnace has been constructed and all treatment or finishing measures completed. The following general rules should be observed if longer time periods have elapsed (weeks or months) until first heating up:

1. The furnace must be subjected to draft conditions so that sufficient ventilation prevails. This will ensure that humidity is not too high and no hydrothermal conditions arise. Otherwise, alkaline hydrolysis is possible when using refractory castables. The result will be a carbonation and disintegration of the lining, beginning on the surface mostly (11).

2. Substantial reduction of strength was noticed on the surface of tempered shapes made from phosphate-bonded ramming mixes. From different reasons the furnace was not taken into operation. Half a year after the completion of the furnace, the surface could be grated by hand easily in a depth of approximately 15 mm. In this case the reason is not carbonation but rehydration of the meta-kaolinite due to hydrothermal conditions. The same strength as before can be restored if the furnace will be heated up.

3. Consequently, drying and heat-up should start immediately respectively 48 hours after the last concrete work! However, it should be taken into consideration that a refractory lining made of unshaped refractories has much more residual water than a brickwork.

Figure 11 shows the amount of residual water as function of the storage conditions.

This diagram will be explained as follows.

Test pieces shape B were prepared from two dense castables and three insulating castables with different bulk densities:

Based on tabular alumina, B.D. = 2.9 g/cm³, H₂O = 7 l/100 kg

Based on calcined clay, B.D. = 2.0 g/cm³, H₂O = 11 l/100 kg

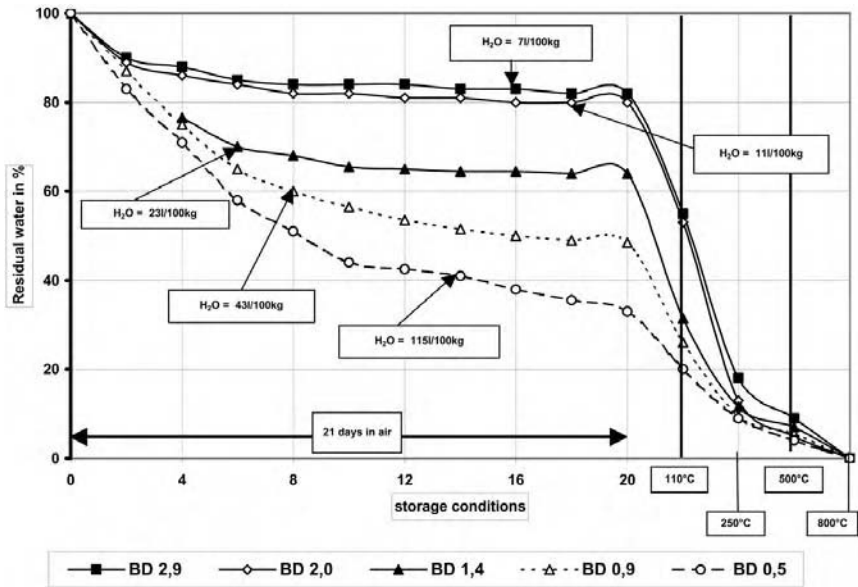


Figure 11 Dehydration of different dense and insulating castables (RC type).

Based on expanded clay, B.D. = 1.4 g/cm³, H₂O = 23 l/100 kg
 Based on exp. clay/
 vermiculite, B.D. = 0.9 g/cm³, H₂O = 43 l/100 kg
 Based on vermiculite, B.D. = 0.5 g/cm³, H₂O = 115 l/100 kg

The test pieces were put on a laboratory table in that way, so that all sides were in contact with air. They were weighed daily, and it needed 21 days until a constant weight was reached for all test pieces. Hereafter the test pieces were dried at 110°C for three days and at 250°C for three days also. The firing at 500°C, respectively at 800°C, were done in an electrically heated laboratory furnace.

Of course, they all needed different amounts of water for a proper flow. However, after each treatment the residual amount of water in percent was determined related to the initial water addition, which was set = 100%.

The a.m. diagram shows the results of dehydration. It is remarkable that both dense castables still have 80% residual water after **21 days storage in air**. The residual water decreases under this condition generally with decreasing B.D. Although the initial water addition was much higher for the lightweight castables than for the dense ones, the drying in air is much easier if the B.D. is low. This can be traced to the bigger pore sizes for LW products. The vermiculite-based product has after drying in air 35% residual water only!

This means, in practice, that after a long time drying in air, the residual amounts of water in linings—for example, in walls—must be bigger than 80% due to the fact that in furnaces normally *one side only* can dry out, and not all sides like for the test pieces.

It was surprising, too, that the two dense castables had approximately 50% residual water after **drying at 110°C**, whereas the water amounts of LW products were determined between 20 and 30% only. This is interesting so far as with decreasing B.D. the cement contents increase automatically. Due to this, the amount of calcium aluminate hydrates must be logically higher in LW products. Nevertheless, it seems to be a fact that it is easier to dry products with more cement, respectively hydrates, if the pore sizes are big enough!

After **drying at 250°C**, the residual water was determined for all castables with approximately 10%, except the tabular alumina-based dense castable, which had still 17% water after this temperature.

After 500°C the residual water was between 8% for the tabular alumina castable and 4% for the vermiculite castable. After **firing at 800°C**, weight losses of <0.5% were determined, which can be traced back to “loss on ignition” and which have nothing to do with residual water.

Deflocculated castables normally have significant lower cement contents, which also means less hydrates after installation and curing. Nevertheless, it has to be taken into consideration that the pore size distribution is much finer in such products than in regular castables. From Figure 11 it can be learned that the tendency for an easier drying out is strictly connected with increasing porosity, respectively increasing pore sizes, too. Therefore, the drying out and heating up of deflocculated castables is more dangerous. For further information, see also (12).

A similar investigation was made with clay-bonded products and different agents. From the following mixtures the same test pieces were rammed as described before (to avoid any influence on the results, the raw material base was fused white alumina):

clay + $\text{Al}(\text{H}_2\text{PO}_4)_3$ liq.	= type of bond, typical for phosphate-bonded ramming mixes; the liquid binder is mono-aluminumphosphate (MAP), which is a 50% hydrous solution
clay + water + $\text{Al}_2(\text{SO}_4)_3 \times 18 \text{H}_2\text{O}$	= typical for air-bonded plastic refractory, which contains approximately 3% aluminum-sulfate
clay + water	= pure ceramic bond without any chemical additive

The used clay (12% in weight) was a German refractory one with 41% Al_2O_3 , which is widely used in such products. Due to the fact that the raw material clay contains crystal water (for example, in kaolinite) and organic substances, which

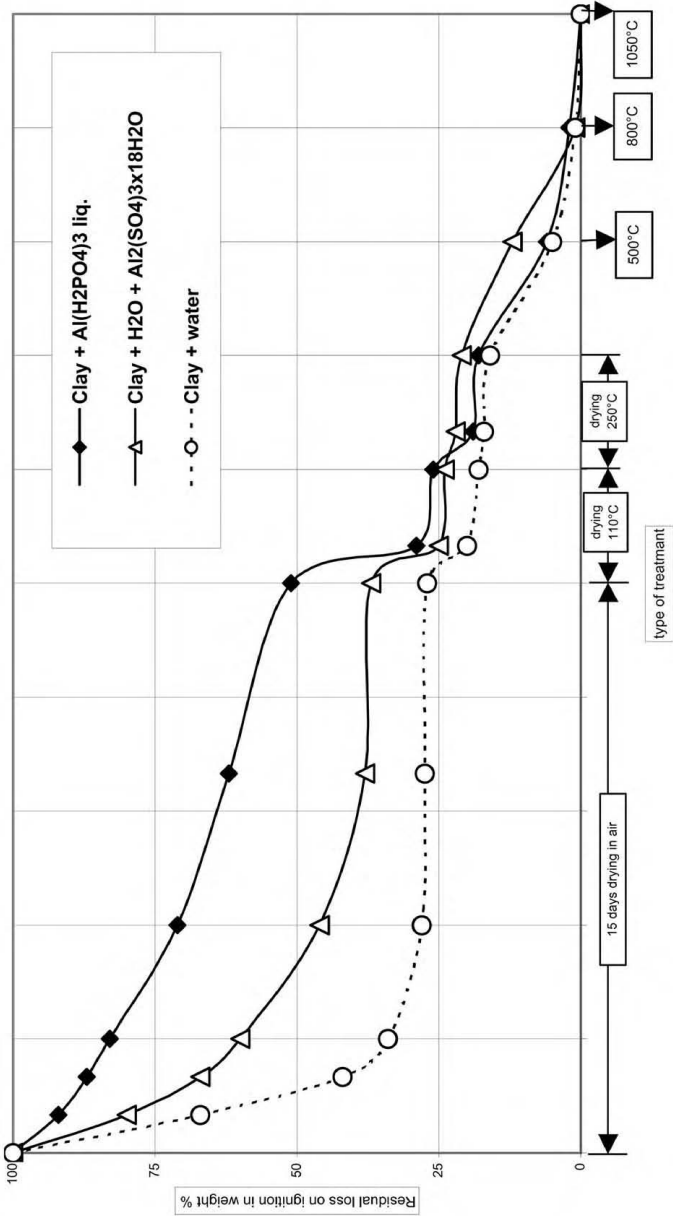


Figure 12 Loss on ignition versus pretreatment conditions of clay bonded mixtures.

are all parts of the loss on ignition of a mixture (including the water addition for getting the right workability), it was not possible in this case to determine the residual moisture after thermal pretreatments alone. Therefore the LOI of the mixtures in question was determined after a firing at 1050°C. These values were set at 100%. It was investigated now how big the percentage of LOI was under certain circumstances for the different clay mixtures.

Figure 12 shows the results.

Looking to the curve for **clay + water**, it can be seen that drying out in air is relatively easy. After 15 days, about 75% of the total LOI is reached, which is equal to the water addition more or less. The residual LOI is 26% only. From ambient temperature in air to drying at constant mass at 250°C, the LOI increases for 8% only, down to 18%. After 500°C the residual LOI is 5%, and after 800°C 2%.

The mixture with aluminumsulfate shows different behavior. After drying in air, the residual LOI is higher than the one for clay alone. This can be traced back to the fact that the 18-mol crystal water disappears at higher temperatures (86°C). After drying at 250°C and 500°C, the rest LOI is higher again because of the dissociation of the sulfate, which is theoretically finished at >770°C.

The phosphate-bonded modification was mixed with MAP only, which means no additional water was used. Drying in air results in 50% remaining LOI. After drying at 110°C, the water rest of the hydrous solution evaporates, and at higher temperatures $\text{Al}(\text{H}_2\text{PO}_4)_3$ loses the H_2O for the formation of AlPO_4 .

All the above-mentioned processes are combined with shrinkage of the capillary tubes. Therefore, the chemical and physical reactions of clay-bonded products also have to be taken into consideration during the first drying out and heating up.

The information about heat-up schedules, which is provided by the refractory manufacturers, must be read and followed precisely. An incorrect heat-up can have fatal results. The outcome can be an explosion-like destruction of the refractory lining.

REFERENCES

1. Krause CA. Refractories: The Hidden Industry of American Ceramic Society, 1987, (especially pp 52 and 76).
2. Krebs R. Modern solution of refractory problems with unshaped refractories. Proc. of UNITECR 1999, Berlin.
3. Krebs R. State of the art of the standardization of unshaped refractories in Europe. CN-Special Refractories. 1999; 6(3).
4. PRE Refractory Materials, Revision 1990, issued by PRE Zurich, Switzerland.
5. ISO 1927: Refractory products: prepared unshaped dense and insulating materials-classification.

6. ASTM C704-94: Abrasion Resistance of Refractory Materials at Room Temperature, 2001 Annual Book of ASTM Standards, Section 15.
7. ASTM C288-87: Disintegration of Refractories in an Atmosphere of Carbon Monoxide, 2001 Annual Book of ASTM Standards, Section 15.
8. STAHL-EISEN-Werkstoffblatt 916: Kennzeichnung ungeformter feuerfester und feuerbeständiger Erzeugnisse, Dec. 1984, issued by VDEh, Düsseldorf, Germany.
9. Braun M. Reinforcing Castables with Stainless Steel Fibres. *Interceram* 1980; 29.
10. Janes. Armierung von Feuerleicht-Erzeugnissen durch keramische Stifte, *Keramische Zeitschrift*, No. 6, 1989.
11. Hogue LD, Jackson WA. Nature of carbonation of hydrated calcium aluminate cements in castable refractories. *Ind Heat* 1997; Heft 8, S. 45–49.
12. Zhen-Xiang Gong, Mujumdar AS. Development of drying schedules for one-side-heating drying of refractory concrete slabs on a finite element model. *J ACS* 1996; 79:Heft 6, Seite 1649–1658.

12

Surface Chemistry as a Tool for the Development of Advanced Refractory Castables

André R. Studart and Victor C. Pandolfelli

Federal University of São Carlos, São Carlos, Brazil

I. INTRODUCTION

The surface chemistry of solid particles in a liquid medium is known to be of major importance for several distinct industrial processes, including food processing, soil conditioning, ore processing, formulation of paints and inks, pharmaceutical and cosmetic production, paper manufacturing, and ceramic fabrication (1–4). An understanding of some basic concepts of surface chemistry is therefore essential to improve the reliability and reproducibility of such processes and to enable the development of novel processing technologies (5–9). The common feature that makes surface chemistry principles so important for all these apparently diverse processes is the fact that they all involve the handling of suspensions (solid–liquid mixtures) containing colloidal particles ($< 1 \mu\text{m}$) of relatively high specific surface area ($> 1 \text{ m}^2/\text{g}$), which are more susceptible to the surface forces that take place at the solid–liquid interface. The magnitude of these surface forces controls the dispersion state of particles and the rheological behavior of colloidal suspensions.

Advanced refractory castables usually display a broad particle size distribution and, therefore, contain a large fraction of micron- and submicron-sized particles (0.1–100 μm) in combination with coarse aggregates ($> 100 \mu\text{m}$). Consequently, aspects of the surface chemistry and, thus, the dispersion state of the smaller particles (matrix) in water also play a major role in the processing and final properties of these refractory materials (10–15).

Particle dispersion has, in fact, been an important issue in refractory applications since the early years when crude fireclay used to be mixed with water to form a plastic material suitable for lining crucibles for melting metal and glass (16). However, little attention was given to this topic until the 1970s, when the need to develop refractory castables containing lower contents of calcium aluminate cement led to the addition of higher amounts of finely ground raw materials (e.g., silica fume and reactive alumina) to castables so as to increase the prefire mechanical strength of low- and ultralow-cement compositions. At that time, the appropriate dispersion of such fine raw materials using novel chemical admixtures (or dispersants) became a primary requirement to obtain refractory castables with lower cement content (16). In later years, new placing techniques utilizing self-flowing, pumpable, and innovative shotcrete castables were developed by tailoring the dispersion state of particles and selecting appropriate particle size distributions.

This chapter discusses the concepts of surface chemistry that have been applied to develop novel placing technologies and refractory castables with enhanced high-temperature properties. The main objective is to address the basic mechanisms underlying these developments rather than to provide detailed information concerning a specific installation process or class of castable. We expect this approach will provide useful guidelines to improve advanced castable processing and all refractory manufacturing processes where rheological properties and the dispersion state of particles are concerned. To this end, we have tried to present the sections of this chapter into a logical and comprehensive sequence. Section II discusses the inherent tendency of particles to form agglomerates, while Section III addresses the main mechanisms employed to inhibit this process. The agglomeration/dispersion mechanisms among particles are described, assuming that the earlier wetting and de-agglomeration processes were successfully conducted (4,17). The three following sections focus on the widely used electrostatic mechanism of dispersion, illustrating the development of electric charges on the surface of particles in water (Section IV), the repulsive force deriving from these charges to counterbalance the action of the attractive forces (Section V), and the method commonly used to measure the electric potential developed close to the charged surfaces (Section VI). It is worth mentioning that the physicochemical phenomena at the solid-liquid interface are outlined in a general, qualitative manner rather than with the rigorous approach used by colloidal scientists. Section VII describes the mode of action of dispersants, starting with their influence on the surface charge of particles (Part A), the effect of some of their features on the dispersion state and the rheological behavior of castables (Parts B-D), their most likely interactions with cement particles (Part E), and how they have been structurally designed to optimize the dispersion of advanced castables (Part F). Finally, Section VIII presents mechanisms to tailor the dispersion state of particles so as to produce castables with distinct rheological behaviors, homogeneous microstructures, and enhanced final properties.

II. DRIVING FORCE FOR AGGLOMERATION

The term “agglomerate” used herein denotes the relatively weak clusters of particles formed in the absence of efficient dispersing mechanisms. From this standpoint, agglomerates differ from the hard clusters of particles linked to each other by strong covalent bonds, normally referred to as aggregates.

Based on the above-mentioned aspects, one can readily conclude that particle agglomeration must result from a strong driving force, which justifies the need for efficient dispersing mechanisms. This driving force derives from the van der Waals attractive forces originated by the interactions between the permanent and/or induced inner electric dipoles of neighboring particles (1,3,18). This force is inherent to most particulate systems and can give rise to an attractive potential energy U_A , which depends on the separation distance among particles (D), according to the equation

$$U_A = - \frac{Ar}{12D} \quad (1)$$

valid for spherical equally sized particles at small separation distances (1,3). The variables r and A in this equation account, respectively, for the particle radius and the Hamaker constant.

Figure 1 shows the variation of the attractive potential energy U_A as a function of the distance D separating two alumina particles ($r = 0.25 \mu\text{m}$) in water. It can be noted that the potential energy U_A decreases continuously as the neighboring particles approach each other, indicating that the most thermodynamically stable condition (lower potential energy) is the close proximity (agglomeration) between the interacting particles. However, it must be kept in mind that, when the particles are separated by very short distances ($D \rightarrow 0$), an extremely strong repulsive force prevails over the attractive van der Waals potential (U_A), leading to a minimum in the potential energy curves known as the primary minimum (Figure 1). This strong repulsive potential energy at very short distances is caused by the interpenetration of the outer electronic orbitals of atoms present on the surface of neighboring particles.

The reduced level of potential energy of the primary minimum in comparison to that associated with Brownian motion ($\sim kT$) is the main driving force for particle agglomeration. For particles with a given radius r , the level of the primary minimum, and, hence, the tendency for agglomeration, depends on the Hamaker constant A [Eq. (1)]. Table 1 lists some Hamaker constants of different raw materials used in refractory applications. It can be seen that alumina particles display a strong driving force for agglomeration in comparison to other materials. This is probably one of the reasons for the major role of alumina particles in the dispersion of multicomponent castable systems (14).

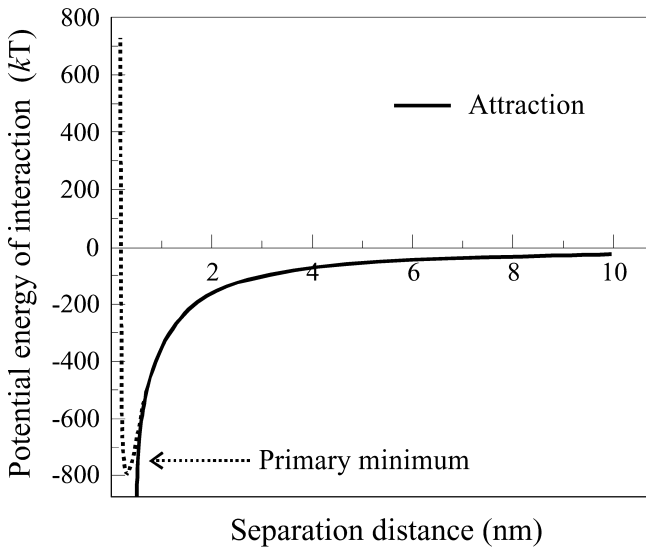


Figure 1 Potential energy as a function of the separation distance among noncharged particles ($r = 0.25 \mu\text{m}$, $A = 3.67 \times 10^{-20} \text{J}$), illustrating the strong driving force for agglomeration around the primary minimum (the repulsive potential energy expected at very small separation distances is schematically indicated by the dashed line).

Table 1 Hamaker Constants^a and pH at the Point of Zero Charge (pH_{PZC})^b for Various Refractory Raw Materials

Raw materials	Hamaker constant, A (10^{-20}J)	pH_{PZC}
Al_2O_3	3.67	7–10 ^d
SiO_2 (amorphous)	0.46	2–4
α -SiC	10.9 ^c	4–7 ^e
β -SiC	10.7	—
β - Si_3N_4	5.47	4–9 ^e
MgO	2.21	12–13
Mg Al_2O_4	2.44	—

^aSource: Ref. 18.

^bSource: Refs. 19–22.

^cValue obtained for 6H-SiC.

^dRange normally observed for Bayer aluminas.

^eValues significantly dependent on the surface treatment (21,22).

III. DISPERSION MECHANISMS

The agglomerates formed through the action of the van der Waals attractive forces exert a marked influence on the rheological behavior and final properties of refractory castables.

In terms of rheological properties, the main effects are due to the entrapment of water inside the newly formed agglomerates, which increases the suspension's effective solid loading and results in larger particulate units. This usually leads to an increase in the apparent viscosity and yield stress of the matrix suspension and, therefore, to a reduction of the castable's flowability (10). Higher water content is needed to increase the fluidity of castables in such cases, which may significantly reduce the matrix suspension's density and favor the segregation of dense and coarse aggregates.

The greater amount of water required by poorly dispersed castables also leads to a more porous final microstructure, reducing the mechanical, wear, and corrosion strengths of the refractory material. Additionally, the agglomerates thus formed usually reduce particle packing efficiency, further degrading the mechanical properties of castables.

Most of these drawbacks are overcome when dispersing mechanisms are activated to prevent particle agglomeration. The main approaches used for this purpose are known as the (1) electrostatic, (2) steric, and (3) electrosteric dispersing mechanisms. The electrostatic mechanism involves the development of electric charges on the surface of particles, inhibiting agglomeration through the formation of an electric double layer around the particles. In the purely steric mechanism, long-chain nonionic molecules are adsorbed at the particles' surface to prevent their close approach by a physical hindrance effect. The electrosteric mechanism simultaneously combines the electrostatic and steric features of the previous mechanisms by the adsorption of relatively long-chain charged molecules on the surface of particles. All these mechanisms are expected to provide a repulsive force that counterbalances the attractive effect of the van der Waals forces.

Since dispersion in refractory castables is usually accomplished by generating electric charges on the surface of particles, the following sections focus on the electrostatic and electrosteric mechanisms of dispersion.

IV. ELECTRIC DOUBLE LAYER

In the electrostatic and electrosteric mechanisms, the repulsive force required to overcome the attractive van der Waals forces is developed through the formation of the so-called electric double layer around particles. As previously mentioned, the buildup of this double layer starts with the generation of electric charges on the surface of particles.

Electric charges can readily appear on the surface of metal oxide particles in an aqueous medium through the reaction of the particle hydroxyl surface groups ($-\text{OH}$) with the H_3O^+ and OH^- ions in water (1,3). As shown in Figure 2a, at acid pH values, the hydroxyl surface groups tend to be protonated by the excess of H_3O^+ ions present in the aqueous medium, leading to positively charged particles. At basic pH values, on the other hand, the hydroxyl groups are most likely deprotonated by the OH^- ions, resulting in negative sites on the particle surface (Figure 2b). An intermediate condition may exist wherein the hydroxyl groups display the same reactivity with either H_3O^+ or OH^- ions, so that the number of positive charges equals the number of negative sites on the particle surface. The pH at which this electric neutrality occurs is known as the “point of zero charge” (PZC). The PZC is usually affected by the protonation/deprotonation ability of the $\text{M}-\text{OH}$ surface groups, which in turn depends on the charge/size ratio of the oxide metallic ion (M) (19). Table 1 presents the PZC values of some raw materials commonly used in refractory castables. The wide range of PZC values of these raw materials indicates their markedly distinct surface properties in water. In the case of nonoxide materials (SiC and Si_3N_4), the PZC is highly dependent on the surface treatment to which particles

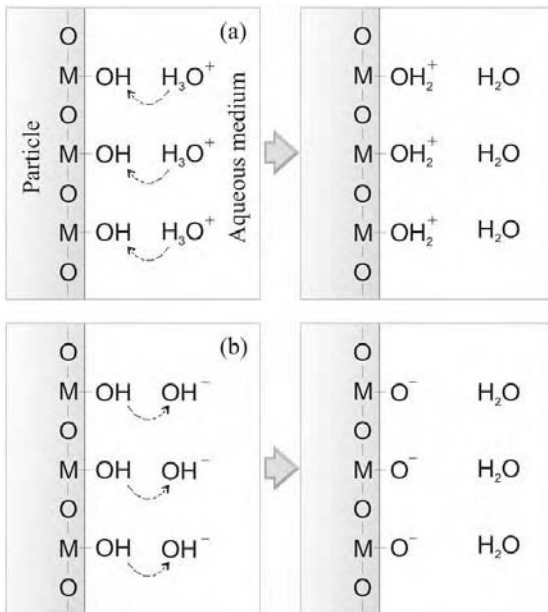


Figure 2 Simplified scheme showing the mechanisms of generation of (a) positive and (b) negative electric charges on the surface of oxide particles in an aqueous medium.

were submitted (20–22). A thin outer layer of SiO_2 is most often encountered in SiC and Si_3N_4 particles due to surface oxidation (20–22).

Electric charges can therefore easily originate on the surface of oxide particles by simply changing the pH of the aqueous medium to values differing from the powder's PZC. The charged sites developed on the surface of particles give rise to an electric potential ψ_0 that attracts many oppositely charged ions (counterions) present in the liquid medium, as schematically illustrated in Figure 3. Such counter-ions promote a screening effect on the surface potential ψ_0 , resulting in a continuous decay of the electric potential from the particle surface toward the bulk solution. Two main layers of counterions may be distinguished around the charged particle. The first, known as the Stern layer, contains the counterions that are rigidly attached to the particle surface through strong electrostatic interactions. These first counterions lead to a nearly linear reduction of the surface electric potential, resulting in the Stern potential ψ_s (Figure 3) (3). The second layer, called the diffuse layer, is formed by counterions that are loosely bonded to the charged particles due to the electrostatic repulsion caused by the ions of the Stern layer. The counterions in the diffuse layer promote a gradual and steady reduction of the Stern potential until the electric neutrality of the bulk solution is achieved, as illustrated in Figure 3.

The layer of charged sites on the particle surface, together with the (Stern and diffuse) layers of counterions, form the so-called electric double layer around particles. The following section describes the repulsive potential energy originating from the interaction between neighboring electric double layers and how this energy can be combined with the attractive van der Waals forces to predict the type of interaction between colloidal particles in a liquid medium.

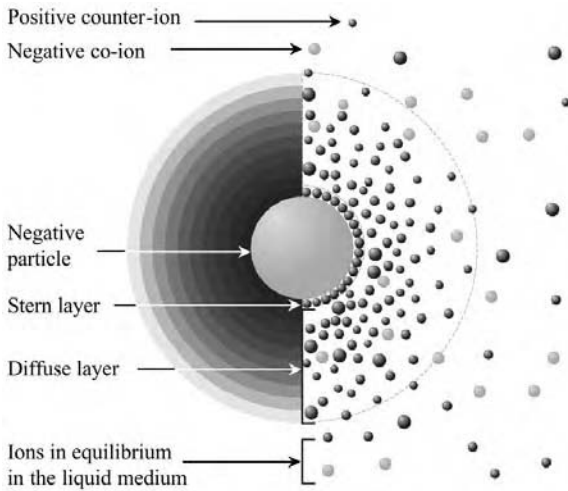
V. DLVO THEORY

The type of interaction between colloidal electrically charged particles in a liquid medium can be estimated by the DLVO theory (1–4,23). According to this theory, the extent of agglomeration in colloidal suspensions depends on the total potential energy of interaction between particles (U_T), which consists basically of a balance among the attractive (U_A) and repulsive (U_R) potential energies, as follows:

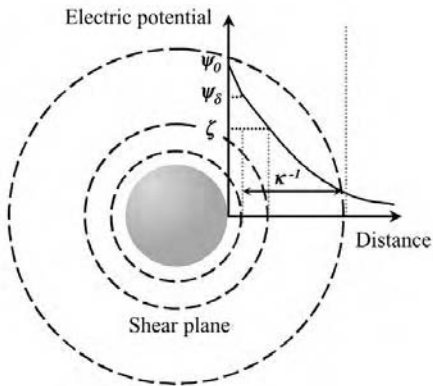
$$U_T = U_A + U_R \quad (2)$$

As discussed earlier herein, the van der Waals interactions usually account for the attractive potential energy (U_A), which is a strong driving force for particle agglomeration.

A repulsive potential energy (U_R) is therefore required to counterbalance the attractive van der Waals potential energy if agglomeration is to be prevented.



(a)



(b)

Figure 3 Schematic representation of the electric double layer developed around charged particles in an aqueous medium (surface potential ψ_0), illustrating (a) the cloud of counterions that form the Stern and diffuse layers, and (b) the electric potential decay through these layers that determines the Stern potential ψ_δ , the zeta potential ζ (at the indicated shear plane), and the double-layer thickness κ^{-1} .

In the case of the electrostatic dispersion mechanism, this repulsive potential energy arises from the overlap of the electric double layers of two approaching particles. This overlap significantly increases the concentration of counterions in the interparticle region, resulting in an osmotic pressure that tends to push the interacting particles apart. The repulsive potential energy that results from this interaction depends mainly on the distribution of electric charges (ions) around the colloidal particles. However, the complexity involved in calculating this spatial distribution of charges requires several assumptions to be made to estimate the potential energy owing to double-layer overlapping. For a simple case of equally sized spherical particles with a relatively low surface potential, separated by relatively large D distances, the potential energy, U_R , can be described by the following equation:

$$U_R = 2\pi\epsilon r\psi_\delta^2 \exp[-\kappa D] \quad (3)$$

where κ is the Debye parameter and ϵ is the permittivity of the liquid medium. The Debye parameter, which indicates the effect of the counterions of the liquid medium on the electric potential decay from the particle surface, is given by the equation:

$$\kappa = \left(\frac{2e^2 \sum n_0 z^2}{\epsilon kT} \right)^{1/2} \quad (4)$$

where e is the charge of the electron, k is the Boltzmann constant, T is the temperature, n_0 corresponds to the bulk concentration of each ionic species in the liquid medium, and z accounts for the species' charge number.

Based on the above considerations, one can then estimate the total potential energy of interaction (U_T) for the purely electrostatic mechanism by introducing Eqs. (1) and (3) in Eq. (2), as follows:

$$U_T = -\frac{Ar}{12D} + 2\pi\epsilon r\psi_\delta^2 \exp[-\kappa D] \quad (5)$$

The repulsive counterpart U_R from the above equation can be tailored to overcome the attractive potential energy U_A and then generate an energetic barrier in the U_T curve that inhibits particle agglomeration around the primary minimum, as illustrated in Figure 4.

The variables of the repulsive term [U_R in Eq. (5)] that exert a major effect on the profile of the U_T curve are the Stern potential ψ_δ and the Debye parameter κ , since the other parameters are usually constant for a given castable composition. To control the dispersion state of particles in refractory castables, it is therefore essential to understand the factors that determine the Stern potential and the Debye parameter.

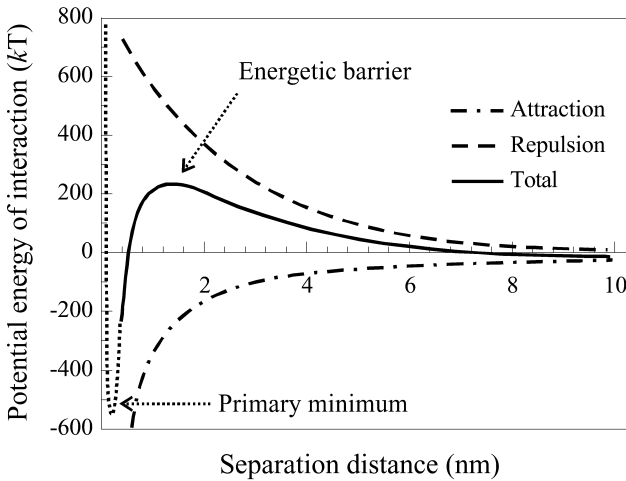


Figure 4 Total potential energy among particles as a function of their separation distance, showing the individual contributions of the attractive and repulsive potential energies. In this example, the repulsive counterpart was high enough to enable the formation of an energetic barrier against agglomeration around the primary minimum (electrostatic mechanism).

The Stern potential depends on the density of charges on the particle surface and the type and concentration of ions located in the Stern layer. Due to the difficulty of controlling the ions that compose the Stern layer, the most straightforward approach to increase the Stern potential is to provide a high surface charge density. As shown in previous sections, this can easily be accomplished by adjusting the suspension's pH to values differing from the particle point of zero charge (Table 1). Another approach that can be used to increase the Stern potential is to add to the solution charged molecules that specifically adsorb at the solid–liquid interface, providing additional electric charges on the particle surface. The next section describes the most important experimental techniques that have been used to assess the Stern potential of charged particles.

The Debye parameter κ , on the other hand, is mainly affected by the charge and concentration of ions in solution that screen the particles' Stern potential [Eq. (4)]. The ions that can contribute to increase the Debye parameter may be supplied by different sources, as, for example: impure raw materials; purposely added salts in shotcrete applications (Section VIII); partially or totally soluble particles (e.g., cement, dissolving powders); and dispersants that display low adsorption ability on the particle surface and remain dissolved in the

liquid medium. Conversely, some chelating agents may be added to the suspension to decrease the Debye parameter through precipitation and complexation mechanisms.

Alternatively, the screening effect of the ions dissolved in solution can be estimated by considering the inverse of the Debye parameter, κ^{-1} . This variable, commonly known as the double-layer thickness, indicates the distance from the particle surface where the electric potential decays to approximately 37% of the Stern potential. Hence, a reduction in the Debye parameter κ or an increase in the double-layer thickness κ^{-1} may aid the dispersion of particles by extending the range of action of the electrostatic repulsive forces.

Due to their strong influence on the Debye parameter [Eq. (4)], the charge number (z) and concentration (n_0) of ionic species in solution are usually combined in another parameter called ionic strength (I), as follows:

$$I = \frac{\sum n_0 z^2}{2} \quad (6)$$

The marked effect of the ionic strength and the Stern potential on the profile of the U_T curves is illustrated in Figure 5 for the case of two alumina particles ($r = 0.25 \mu\text{m}$) interacting in an aqueous medium. As can be seen, the formation of an energetic barrier against particle agglomeration requires the appropriate control of these two parameters, particularly of the Stern potential.

Figure 5 also reveals that a secondary minimum may occur in the potential energy curve, especially when the ionic strength of the liquid medium is increased at a fixed Stern potential. This secondary minimum is usually a relatively shallow energy potential well, which leads to a weak coagulation of particles if compared to the strong agglomeration that occurs around the primary minimum. Due to this feature, particles coagulated at the secondary minimum can sometimes be redispersed easily by applying a shear stress (energy) to the suspension sufficiently high to overcome the low attractive potential energy in this condition. As a result, suspensions containing particles coagulated around the secondary minimum often display a typical yield stress and are characterized by a pronounced shear-thinning rheological behavior. This characteristic of the secondary minimum, which may have several implications in the processing and final properties of refractory castables, will be discussed in Section VIII.

VI. ZETA POTENTIAL

Several experimental techniques have been used to measure the electric potential near the surface of charged particles in an attempt to estimate their Stern potential and predict the dispersion state of colloidal suspensions. The methods most

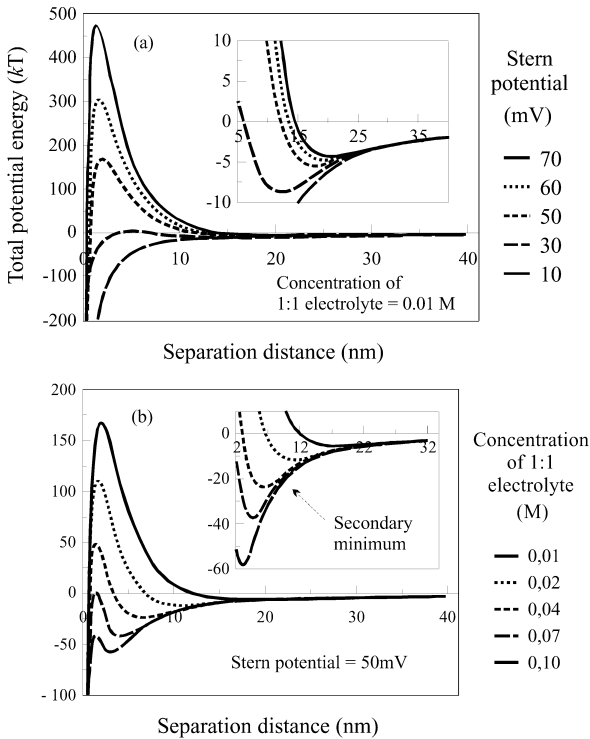


Figure 5 Effect of (a) the Stern potential and (b) the electrolyte concentration (or ionic strength) of the aqueous medium on the total potential energy of interaction among particles ($r = 0.25 \mu\text{m}$, $A = 3.67 \times 10^{-20} \text{J}$). The insets provide a magnified view of the potential energy curves, illustrating the secondary minimum that appears in high ionic strength and low Stern potential conditions.

widely applied for this purpose have been the electrophoretic and electroacoustic techniques (1–3).

The electrophoretic technique consists of applying an electric field to a diluted suspension and measuring the velocity developed by the charged particles in response to the voltage applied. The velocity data are then used to calculate the electrophoretic mobility of the particles in the liquid medium. The movement of charged particles induced by the electric field applied displaces the ions from the outer part of the diffuse layer, defining the so-called shear plane of the electric double layer (Figure 3). The electric potential at this shear plane can be calculated from the particle's electrophoretic mobility and is referred to as the zeta potential. Due to the proximity between the shear and Stern planes of the double layer

(Figure 3), the zeta potential value is usually considered representative of the Stern potential in most of the calculations performed to predict particle interaction.

Another method commonly employed to measure the zeta potential of particles is the electroacoustic technique, which involves the application of an oscillatory electric field to the colloidal suspension. As a result, an oscillatory relative displacement occurs between the charged core particle and the surrounding ions of the diffuse layer, giving rise to an acoustic response to the applied alternating electric field. The sound wave thus produced has been empirically correlated to electrophoretic mobility data so as to estimate the zeta potential of colloidal particles. A variation of this technique, in which a sound wave is applied to the suspension and an electric field is obtained as a feedback, is also widely used for zeta potential measurements. The main advantage of these electroacoustic methods is that they allow the zeta potential to be measured in concentrated suspensions, yielding a more realistic result in the case of high-solid loading systems.

Figure 6 presents the variation of zeta potential as a function of pH for some finely ground raw materials used in refractory applications. It is worth noting the markedly different zeta potential profiles of these raw materials, which reflects

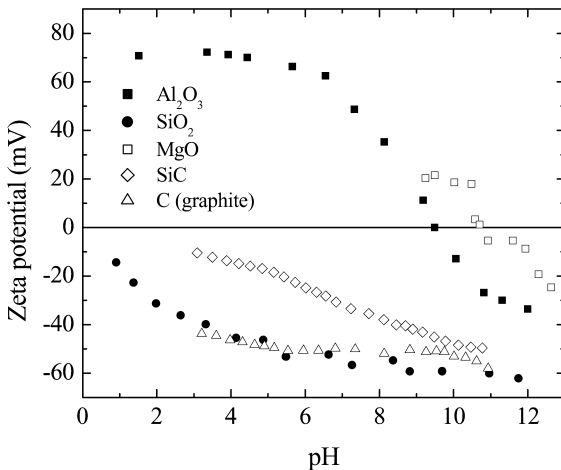


Figure 6 Zeta potential as a function of pH for some of the raw materials commonly used in refractory castables. In the case of graphite, a wetting agent was employed to enable the homogenization of the particles in the aqueous medium (after Ref. 14). The zeta potential data for MgO were taken from Ref. 24.

their distinct interaction with the H_3O^+ and OH^- ions of the aqueous medium, as discussed in Section IV.

VII. DISPERSANTS

As stated in earlier sections, the dispersion of refractory castables is usually accomplished by developing electric charges with the same signal on particle surfaces. However, a brief glance at the zeta potential curves of powders commonly used in refractory castables (Figure 6) reveals that it would be almost impossible to promote particle dispersion simply by controlling the suspension pH, since such raw materials display dissimilar surface charges over a very broad pH range. Even in the case of simple refractory compositions, substantial pH shifts are not expected to favor particle dispersion due to the large contents of acid/alkaline compounds usually required to change the pH of castables, which would substantially increase the ionic strength of the liquid medium.

Taking into account these factors, the most common approach to disperse refractory castables is the addition of specific charged molecules (dispersants), which can adsorb and provide charges with the same signal on particle surfaces. It should be mentioned that the charged sites of such molecules should be able to establish relatively strong interactions with the surface groups so as to actually modify the surface chemistry of particles. This can occur through the formation of either primary bonds or coordinated interactions among the dispersant molecules and the surface groups. This characteristic distinguishes the action of dispersants from that of the counterions of the Stern and diffuse layers, which, rather than reacting with the particle surface, simply exert a screening effect on the surface electric potential.

Due to the buildup of a layer of molecules on the particle surface, the above-mentioned approach usually leads to a steric effect, whose extent may vary according to the length and conformation of the charged molecules on the solid-liquid interface. Figure 7 indicates schematically the combined effect of the electrostatic and steric mechanisms on the potential energy curve between particles, illustrating the significant contribution of the steric mechanism (U_S) to the energetic barrier that prevents agglomeration.

This section presents a general overview on the mode of action of dispersants in refractory castables, focusing especially on the ability of these molecules to adsorb and modify the surface chemistry of particles (Parts A-C), the secondary effects that may arise from the addition of dispersants to the castable matrix (Part D), the possible interactions between dispersants and cement particles (Part E), and novel routes that have been applied to design the dispersant molecule in order to optimize the rheological behavior of castables and concretes (Part F).

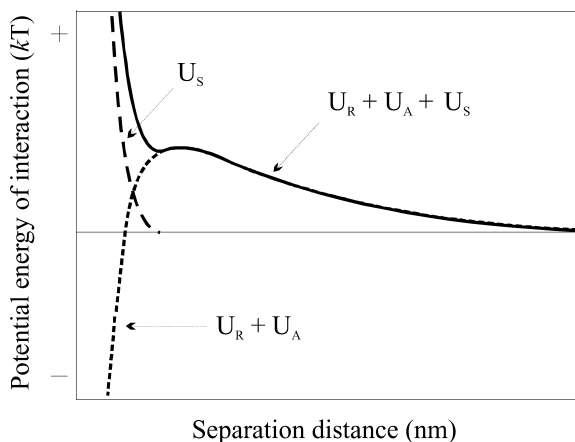


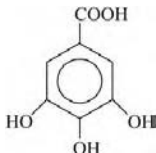
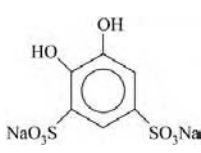
Figure 7 Schematic drawing of the interaction potential energy curve expected for electrosterically dispersed particles, indicating the energetic contribution of the steric layer (U_s) to the total potential energy curve ($U_s + U_R + U_A$). (Adapted from Ref. 1.)

A. Surface Modification

The dispersants most commonly used to modify the surface features of particles through the electrostatic/electrosteric mechanism can generally be classified as anionic or cationic species. When dissolved in water, the anionic dispersants possess mainly negative sites along the dissociated chain, whereas the cationic ones usually display positive charges throughout the molecule. Table 2 lists some dispersants commonly employed in refractory castables (e.g., carboxylates and phosphates) and examples of other anionic and cationic molecules that, although not yet fully exploited in refractory applications, may also display high dispersing ability. The dispersants shown in Table 2 have been further grouped into polymeric molecules (polyelectrolytes) and small aliphatic or aromatic compounds.

As can be seen, regardless of chain length, anionic molecules usually contain carboxylate ($-\text{COOH}$) (12,14,25–35), phosphonate ($-\text{PO}(\text{OH})_2$ or $-\text{PO}(\text{OH})\text{O}^-$) (36), sulfonate ($-\text{SO}_3\text{H}$) (37), and/or hydroxyl ($-\text{OH}$) (12,14,25,27–29,31,32) functional groups as major dissociable sites along the molecular structure. The cationic dispersants, on the other hand, usually have amines or amine-derived ($-\text{NH}-$ or $-\text{NH}_2$) groups that can be protonated in an aqueous medium. The extent of protonation/deprotonation of these functional groups is ruled by their dissociation constants pK_a , which correspond to the pH value when half of the functional groups have reacted with water to form charged

Table 2 Dispersants Commonly Used in Refractory Castables and Examples of Other Molecules That May Display High Dispersing Ability

	Compound	Structure	pK _a values ^a
Long-chain molecules			
Carboxylates	Salts of polyacrylic (R = H) or polymethacrylic (R = CH ₃) acid (M = Na or NH ₄)	$\left[\begin{array}{c} \text{R} \\ \\ \text{---C---CH}_2\text{---} \\ \\ \text{COOM} \end{array} \right]_n$	~4.75
Phosphates	Sodium hexamethaphosphate	$\left[\begin{array}{c} \text{O} \\ \\ \text{---P---O---} \\ \\ \text{ONa} \end{array} \right]_{n=13-20}$	—
Sulfonates	Beta-naphthalene sulfonate (M = Na or H)	$\left[\begin{array}{c} \text{R} \\ \\ \text{---} \langle \text{C}_6\text{H}_4 \rangle \text{---CH}_2\text{---} \langle \text{C}_6\text{H}_4 \rangle \text{---} \\ \qquad \qquad \qquad \\ \text{SO}_3\text{M} \qquad \qquad \text{SO}_3\text{S} \end{array} \right]_{n-1}$	—
Anionic	Sodium triphosphosphate	$\text{NaO}-\overset{\text{O}}{\parallel}{\text{P}}(\text{ONa})-\text{O}-\overset{\text{O}}{\parallel}{\text{P}}(\text{ONa})-\text{O}-\overset{\text{O}}{\parallel}{\text{P}}(\text{ONa})-\text{ONa}$	—
	Citric acid	$\begin{array}{c} \text{CH}_2-\text{COOH} \\ \\ \text{HO}-\text{C}-\text{COOH} \\ \\ \text{CH}_2-\text{COOH} \end{array}$	3.48, 4.50, 5.82, >14
Short molecules	3,4,5-trihydroxybenzoic acid (gallic acid)		4.26, 8.7, 11.45, >14
	Pyrocatechol-3,5-disulfonic acid disodium salt (Tiron)		—
	2-phosphonobutane-1,2,4-tricarboxylic acid (PBTCA)	$\begin{array}{c} \text{O} \qquad \text{CH}_2-\text{COOH} \\ \qquad \\ (\text{HO})_2-\text{P}-\text{C}-\text{COOH} \\ \\ \text{CH}_2 \\ \\ \text{CH}_2-\text{COOH} \end{array}$	3.74, 4.23, 5.14, 6.80, 9.05
Cationic	Polyethyleneimine	$\left[\text{---CH}_2\text{---CH}_2\text{---NH---} \right]_n$	—

^aSource: Refs. 13, 38, and 39.

sites on the molecule. Therefore, the development of charges on the dispersant molecule only occurs in castables displaying a pH close to or greater than the pK_a values of the molecule's functional groups. Table 2 shows the pK_a values of some of the molecules chosen as representative dispersants.

The ability of anionic and cationic dispersants to modify the surface characteristics of ceramic powders in water is shown in Figure 8. Zeta potential curves obtained for alumina and silica particles in either the presence or absence of dispersant were taken as illustrative examples. As can be observed, the adsorption of the anionic species onto the alumina surface causes a shift of the zeta potential curve toward acidic values, leading to negatively charged particles over a broad pH range. The opposite behavior occurs in the case of the cationic dispersant, whose adsorption produces a positive net charge on the surface of silica particles within a wide pH interval.

The net surface charge of particles after dispersant adsorption is given by the combination of the charges from the anchored dispersant molecule and those originally developed on the surface due to interactions with water (Figure 2). Therefore, five possible configurations may occur at the solid–liquid interface, depending on the pH of the aqueous medium, as schematically shown in Figure 9 for a hypothetical fully charged anionic dispersant. According to this figure, the adsorption of the charged molecules may (1) partially reduce the surface electric potential (ψ_0), (2) completely neutralize the electric potential ψ_0 , leading to the condition known as the isoelectric point (IEP), (3) reverse the surface electric potential, (4) develop an electric potential on originally neutral surfaces, or, finally, (5) further increase the surface potential ψ_0 . A comparison of Figure 8a and 9 reveals that the zeta potential curve obtained after dispersant

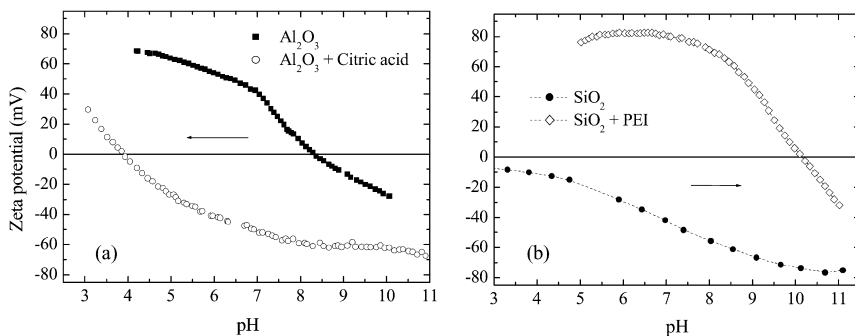


Figure 8 Examples of the effect of (a) anionic (0.06 wt% citric acid) and (b) cationic (0.33 wt% polyethyleneimine, PEI) dispersants on the zeta potential curve of alumina and silica particles, respectively. (The curves shown in graph *b* were kindly supplied by H. Wyss, ETH-Zürich.)

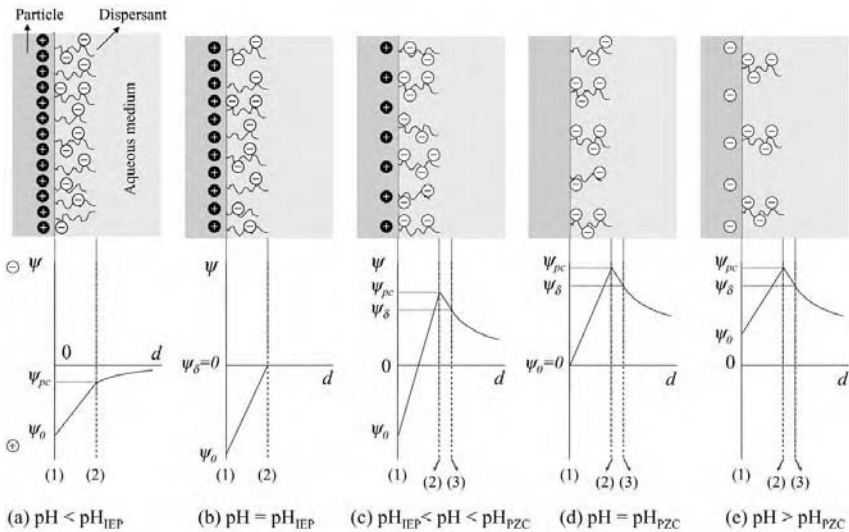


Figure 9 Electric potential profile at the solid–water interface resulting from the adsorption of electrically charged (anionic) molecules on the surface of oxide particles under various pH conditions. It is assumed that the adsorbed molecules shift the plane of charge from the particle surface to a distance equivalent to their molecular length. (Adapted from Ref. 2, where (1) is the surface plane, (2) is the plane of charge, (3) is the Stern plane, and ψ_0 , ψ_{pc} , and ψ_{δ} denote the electric potential at each of these planes.)

adsorption is a direct consequence of the distinct configurations that may occur at the solid–liquid interface.

According to the schemes shown in Figure 9, one would expect that the affinity between the dispersant molecules and the particle surface is considerably influenced by the pH of the aqueous medium. The following section describes the significant influence of pH on the adsorption ability of anionic molecules and how their functional groups can affect the pH range in which maximum adsorption occurs on the particle surface.

B. Adsorption Ability

The adsorption ability of anionic molecules on the surface of oxide particles is greatly dependent on the pH value of the aqueous medium, since the pH conditions control the type and density of charges on the particle surface (Figure 2) and along the adsorbing molecule (25–27). In the case of alumina particles, it has been shown (27) that such pH dependence is significantly influenced by the dissociation constants ($\text{p}K_a$ values) of the functional groups that constitute the

adsorbing molecule. Maximum adsorption is known to occur in a pH range close to the pK_a values of the molecule dissociable groups. Less adsorption is expected to take place at pH values lower than the pK_a value because of the absence of dissociated anchoring groups on the molecule. On the other hand, at pH values above the pK_a value, although the functional groups are fully dissociated, the lower density of positively charged sites on the alumina surface limits the adsorption of anionic molecules.

In addition to the pK_a value, the spatial arrangement of the functional groups also exerts a marked influence on the adsorption ability of anionic molecules. Carboxylate groups ($-\text{COOH}$), for instance, are known to form very stable configurations with the positive sites of alumina surfaces (27).

Compounds displaying carboxylate groups typically have low pK_a values (Table 2) and are therefore expected to adsorb preferentially under acid pH conditions on the alumina surface. Molecules predominantly containing hydroxyl groups, on the other hand, display much higher pK_a values (Table 2), which favor surface adsorption at basic pH values (38,39). Finally, molecules containing phosphonate groups (e.g., polyphosphate salts) may exhibit a wide range of pK_a values (from low to intermediate), which lead to maximum adsorption from acid to slightly basic pH conditions. Obviously, these pK_a ranges are susceptible to variations depending on the molecule side groups and should therefore only be considered as general guidelines for the selection of dispersants.

Due to the predominance of carboxylate groups in their molecular structure, citrate and polyacrylate molecules have low pK_a values and, thus, adsorb to a greater extent on alumina surfaces at lower pH values, as shown in Figure 10 (25,27).

Molecules displaying functional groups with intermediate to high pK_a values should therefore be chosen if one aims to improve the adsorption ability of the dispersant in the usual pH range of high-alumina castables ($8 < \text{pH} < 12$). Gallic acid (3,4,5-trihydroxybenzoic acid) is an example of a dispersant with such a characteristic (Table 2). This aromatic compound displays one carboxylate ($-\text{COOH}$) and three hydroxyl ($-\text{OH}$) groups around the benzene ring, which would favor adsorption on the alumina surface at basic pH values. Adsorption curves obtained for a similar molecule, namely 2,3,4-trihydroxybenzoic acid, on the alumina surface show that almost complete adsorption of this compound occurs within the alkaline pH range (Figure 10). The absence of ($-\text{OH}$) groups in the ortho position of the benzene ring (Table 2) is supposed to further aid the adsorption of gallic acid in comparison to 2,3,4-trihydroxybenzoic acid, since this steric configuration prevents the occurrence of unfavorable electrostatic repulsion between the carboxylate ion and the alumina surface (27). The probable enhanced adsorption ability of gallic acid at alkaline pH values was shown to have a positive effect on the dispersion of high-alumina castables (13). Although the pK_a values of the gallic acid molecule suggest that it might

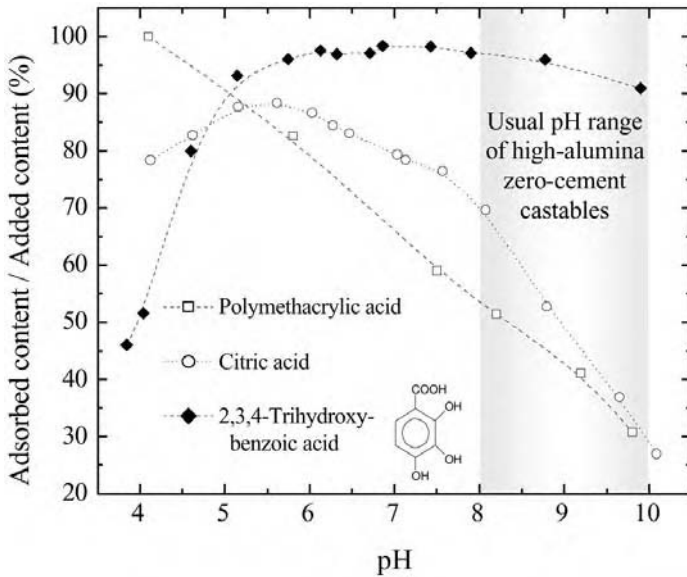


Figure 10 Adsorption behavior of polymethacrylic acid, citric acid, and 2,3,4-trihydroxybenzoic acid on the alumina surface as a function of pH. (Adapted from Refs. 26 and 27.)

not fully dissociate at the castable's pH (Table 2), higher absolute zeta potential values can be achieved with this dispersant in basic pH conditions in comparison to citric acid (13). Additionally, the minor content of nonadsorbed gallic acid molecules at the castable's pH results in a liquid medium with lower ionic strength. As a result, alumina suspensions and zero-cement castables containing gallic acid have been shown to achieve lower viscosity and higher free-flow values, respectively, than those prepared with citric acid, as revealed in Figure 11 (13).

C. Density of Charged Sites

The density of charged sites on the dispersant structure is another factor that exerts a major influence on molecule dispersing ability. Molecules containing a high density of dissociable functional groups can modify particle surfaces to a greater extent, since a greater number of charged sites will be attached to the particle for each functional group anchored on the surface. This usually results

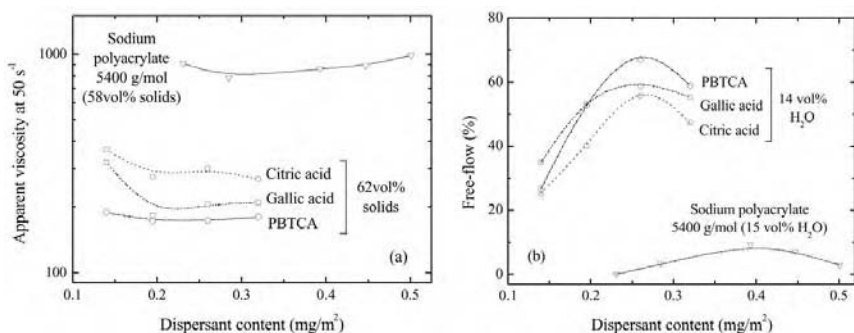


Figure 11 Example of the effect of distinct anionic dispersants on (a) the apparent viscosity of alumina matrix suspensions and (b) the flowability (free-flow value) of zero-cement alumina castables. (Adapted from Ref. 13.)

in higher zeta potential levels at a given pH and enables a considerable reduction of the particle's isoelectric point.

The effect of this characteristic can be visualized by evaluating, for example, the dispersing ability of 2-phosphonobutane-1,2,4-carboxylic acid (PBTCA) in comparison to that of citric acid (Table 2). This organic compound possesses one phosphonate and three carboxylate groups along its molecular structure, which provide a higher charge density per molecule than citrate ions. The PBTCA molecules also adsorb to a greater extent on the alumina surface at basic pH values, since the presence of phosphonate groups expands the molecule's pK_a range toward higher values (Table 2) (40,41). This improved adsorption efficiency combined with a higher density of charged sites per molecule has allowed for the preparation of alumina suspensions with lower viscosity and zero-cement castables with higher free-flow values than those attained with citric acid (Figure 11).

D. Secondary Effects

The examples described in earlier sections involved short-chain molecules with similar maximum lengths (0.5–1.0 nm), which presumably provide steric repulsive forces of a rather low magnitude. However, the use of polymeric molecules as dispersants may significantly enhance this steric contribution to particle dispersion. Furthermore, when these macromolecules display dissociable sites along their basic units (meres), high zeta potential values are usually attained, as shown in Table 3 for sodium polyacrylate. Therefore, these long-chain charged molecules would be expected to display a better dispersing behavior than that of short-chain molecules.

Table 3 Comparative Data Obtained for Alumina Suspensions Containing Citric Acid or Sodium Polyacrylate ($M_w = 5400$ g/mol) at Optimum Dispersing Conditions

Dispersant	ς (mV)	I (M)	IPS ^a (nm)	λ^b (nm)	τ_y (Pa)	η_{app} (mPa.s)
Citric acid	-31	0.14	26.2	0.5	2.3	342
Sodium polyacrylate	-67	0.20		19.3	10.1	817

^aObtained by applying the Westman and Hugill modified algorithm to the powder particle size distribution (from Ref. 12).

^bEstimated based on Refs. 30 and 36.

The zeta potential values (ς) were measured using diluted suspensions, whereas the ionic strength (I), interparticle separation distance (IPS), yield stress (τ_y), and apparent viscosity data (η_{app}) were either estimated or measured in 58 vol% solid-loading slurries (from Ref. 12).

Source: Ref. 12.

Figure 11, however, reveals that zero-cement alumina castables containing sodium polyacrylate as dispersant exhibit much lower flowability levels than those achieved using citric acid and other short-chain molecules. In principle, this contradicts the high zeta potential levels and the probably more pronounced steric effect obtained with sodium polyacrylate (Table 3). This unexpected behavior has been attributed to some secondary effects imparted by long-chain dispersant molecules, which tend to increase the viscosity and yield stress of matrix suspensions and, therefore, decrease castable flowability. These secondary effects occur mainly when the molecular length of the dispersant species remaining in solution is greater than or similar to the suspension interparticle spacing (IPS) (30). This condition is preferentially encountered in suspensions possessing high solid loading (as the castable matrix) or containing large contents of extended nonadsorbed molecules in solution. The most conspicuous secondary effects that may arise in the presence of long molecules in high solid loading suspensions are known as bridging and depletion flocculation (12).

Depletion flocculation is a phenomenon triggered by the difference in the concentration of nonadsorbed molecules in the region between particles (C_i) and that in the bulk solution (C_b), as schematically shown in Figure 12. When the molecules' length (λ) is similar or greater than the interparticle spacing (IPS), steric hindrance makes the access of molecules into the region between particles difficult. The difference in the concentration of nonadsorbed molecules, when $C_i < C_b$, produces an osmotic pressure along the poorly and highly concentrated regions in an attempt to establish a condition of equilibrium. Because molecules are unable to enter the interparticle region, the osmotic pressure tends to expel the less concentrated solution located between particles (C_i) toward the bulk solution. As a result, neighboring particles are pushed against each other, originating an attractive force between them (Figure 12). This mechanism

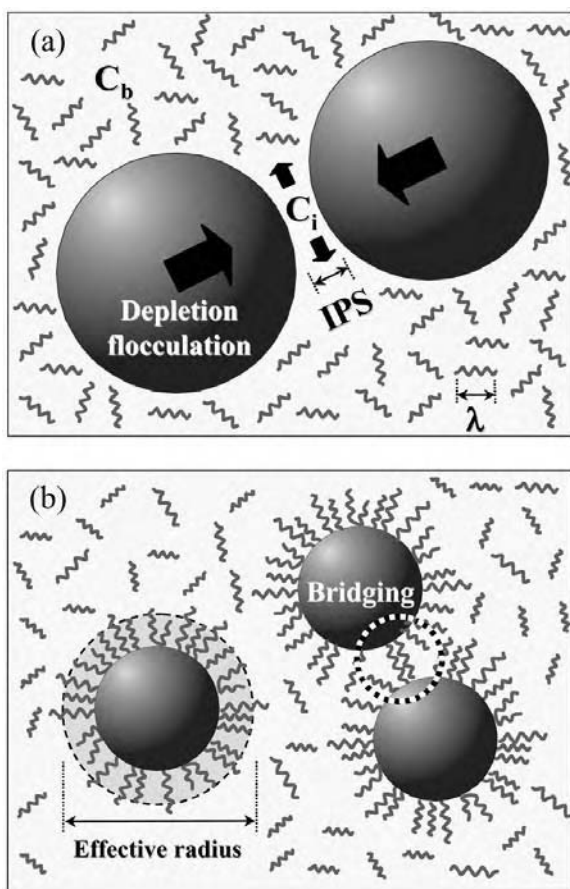


Figure 12 Schematic diagram presenting (a) the depletion flocculation and (b) the bridging effects that may occur when the interparticle separation distance (IPS) approaches the molecular length of nonadsorbed molecules (λ). C_i in figure (a) represents the concentration of nonadsorbed molecules in the region between particles, whereas C_b corresponds to the bulk concentration [molecules adsorbed on the particle surface are not included in Figure (a)]. Figure (b) also shows the particle's effective radius resulting from molecule adsorption.

constitutes an additional driving force for agglomeration not taken into account by the classic DLVO theory.

The bridging effect, on the other hand, occurs when the same molecule in solution adsorbs simultaneously on two different particles, forming a link between them (Figure 12). This mechanism is most likely activated when the

particle surface is not totally covered by dispersant and/or when particles and nonadsorbed molecules display electric charges with opposite signals. Under such conditions, the particle surface is still available for adsorption and the electrostatic attractive forces between nonadsorbed molecules and particles favor bridging. Like the depletion effect, bridging is another non-DLVO interaction mechanism that contributes to the formation of agglomerates and clusters in the suspension.

Table 3 shows that the extended chain length of polyacrylate molecules with relatively low molecular weight ($M_w = 5400$ g/mol) is, indeed, of the same order of magnitude as the average interparticle spacing of typical matrix suspensions. Although polyacrylate molecules may have different molecular lengths depending on the polymer's conformation (30,36,42), stretched conformations are likely to occur when the molecule is fully dissociated in solution ($\text{pH} \gg \text{p}K_a$), as is the case in high-alumina castables (12). Therefore, bridging and depletion flocculation are more likely to occur in castables containing such long-chain molecules. The restricted space available for motion in these systems (Figure 12) also favors hydrodynamic interactions and entanglement between particles and nonadsorbed molecules, further increasing the viscosity and yield stress of the matrix suspension (12,30). Another secondary effect imparted by long-chain molecules is the entrapment of a considerable amount of water in the steric layer formed around particles (Figure 12). This leads to an increase in the matrix's effective solid loading, which may also contribute to reduce castable flowability (12).

The molecular length estimated for citric acid and the other short-chain molecules previously described (0.5–1.0 nm) is about one order of magnitude smaller than the interparticle spacing of typical matrix suspensions, which reduces the chance of the above-mentioned secondary effects' occurring. This is the most probable reason for the higher flowability values obtained with these dispersants in zero-cement high-alumina castables (Figure 11), despite the lower zeta potential levels achieved with such small molecules (Table 3).

It is worth mentioning that the secondary effects associated with long-chain molecules can be minimized if the castable liquid medium displays high ionic strength, since the dispersant molecules tend to exhibit nonextended conformations in this condition. Additionally, the inferior zeta potential level obtained with short-chain molecules may not be sufficiently high to prevent particle agglomeration in high-ionic strength aqueous solutions. This condition is usually encountered in castables containing calcium aluminate cement or other highly dissoluble and impure raw materials. Therefore, the selection of additives for refractory castables cannot be considered a straightforward task, for the particularities of each specific composition must be taken into account and accurate control and knowledge of the raw materials employed are required.

E. Interactions with Cement Particles

An important constituent of refractory castables that has yet to be considered is the calcium aluminate cement. This raw material is known to strongly affect the dispersion state and rheological behavior of castables due to the various reactions occurring in the material as soon as it comes into contact with the admixing water (43–46). Therefore, an understanding of the effect of additives on the hydration process of cement particles is an essential requirement to optimize the rheological properties and working time of cement-based refractory materials.

In principle, all the concepts of surface chemistry previously described are also expected to be valid for cement particles. However, the highly dissolving and reactive nature of such particles introduces a dynamic and complex feature to the particle–water system. This makes it difficult to interpret the data obtained from cement-containing suspensions, which is probably the main reason for the paucity of publications available in the literature that focus on the interactions between additives and high-alumina cement particles. The concepts described herein are therefore based on studies performed in aqueous pastes of calcium silicate (Portland) cement, which have been more extensively researched in recent years due to their considerable importance for concrete technology (47–50). Although calcium aluminate and calcium silicate cements are known to display distinct reaction rates and form different hydration products, similar interactions between the cementitious phase and the chemical additives (admixtures) are expected to occur in aqueous suspensions.

To comprehend such interactions, it is important to first understand the hydration process of cement particles in water in the absence of additives. Calcium aluminate cements are known to readily dissolve in water, releasing increasing amounts of Ca^{2+} and $\text{Al}(\text{OH})_4^-$ ions in the liquid medium (43–46). This dissolution process continues until the concentration of these ions in the aqueous solution reaches a certain saturation level, at which point the ions tend to precipitate through a nucleation and growth mechanism to form hydrated phases. The precipitation of the first hydrated products decreases the concentration of ions in solution to levels below the saturation condition, favoring the further dissolution of cement particles. This leads to a cyclic process of ion dissolution-precipitation that proceeds until most of the anhydrous cement phase is reacted. It is important to note that heterogeneous nucleation of hydrates occurs on the surface of cement particles as soon as the dissolution process begins, leading to the formation of a surface layer of hydrated phases. Hence, this hydrated layer must be considered when predicting the interaction of cement particles with chemical admixtures and with other neighboring particles.

Figure 13 schematically illustrates some of the possible interactions that may take place between the dispersant molecules and cement particles in an aqueous medium. Such interactions may involve (47): (1) the adsorption of

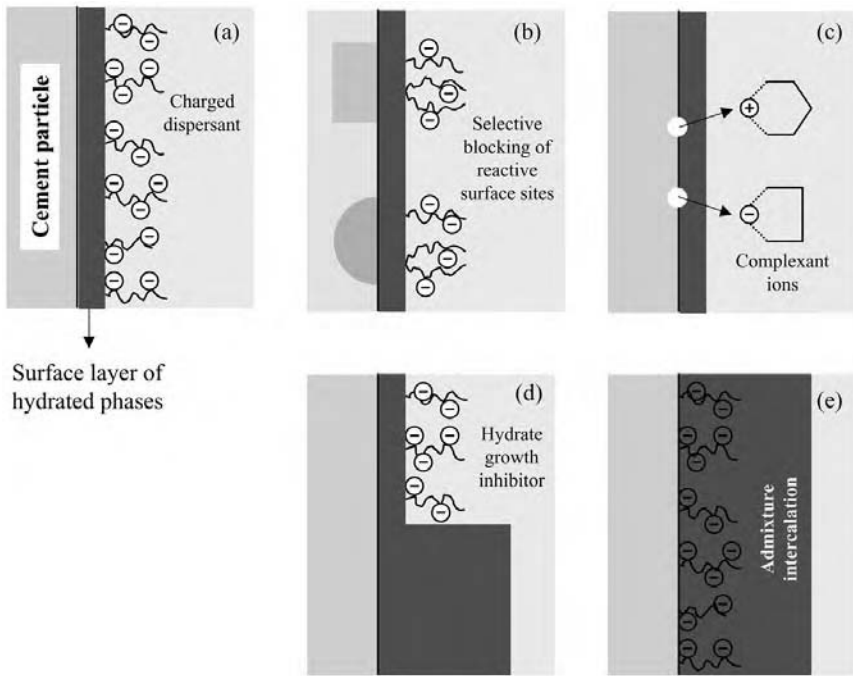


Figure 13 Schematic illustration of the cement–water interface, depicting the possible interactions that may occur between dispersant (anionic) molecules and cement particles. (Adapted from Ref. 47.)

dispersant molecules on the surface, leading to the earlier described mechanisms of dispersion, (2) the selective adsorption of molecules on reactive surface sites, locally blocking the dissolution of the anhydrous phase, (3) the complexation of dissolving ions by the nonadsorbed dispersant molecules, which may either retard the precipitation of new hydrated phases or further aid the dissolution process, (4) the inhibition of hydrate growth on the particle surface due to dispersant adsorption, and/or (5) the formation of hydrated phases that incorporate the dispersant molecule into its structure, leading to the so-called intercalation phenomenon.

The influence of some of the characteristics of dispersant molecules, such as chain length, charge density, and type of functional groups, on each of the possible interactions illustrated in Figure 13 is not yet fully understood. The lack of detailed investigations into this field is most likely due to the difficulties involved in setting up experiments to individually demonstrate the effect of given variables. Therefore, the selection of dispersants for cement-based refractory

castables must take into account all these possible interactions, in addition to the previously discussed parameters that affect particle dispersion.

F. Molecular Architecture

Despite the inherent complexity of cement-containing systems, the previous sections have shown that some of the features of dispersant molecules (e.g., length, charge density, functional groups) can generally be correlated with the type of interaction expected among particles. Hence, attempts have been made to design the molecular architecture of dispersants based on these general correlations, so as to optimize the dispersion state of particles in refractory castables and high-performance concretes.

A typical example of a dispersant molecule that has been designed for the production of cementitious materials with tailored rheological properties is the carboxylate-based polymer depicted in Figure 14 (50). This polymer displays a comblike structure containing dissociable sulfonate and carboxylate groups in the main backbone chain, to which lateral nonionic chains of polyethylene oxide of varying molecular weights are grafted. By adjusting the ratio of sulfonate to carboxylate groups in this molecule, one can, for instance, control the working time of high-performance concretes, since the sulfonate groups are known to specifically adsorb on highly reactive calcium aluminate phases (i.e., $3CaO \cdot Al_2O_3$), reducing the hydration kinetics of cement particles (47). The maximum length of the molecule can also be tailored by controlling the degree of polymerization of the backbone chain. This allows for the synthesis of molecules of sufficient length to provide efficient repulsive electrosteric forces, but still short enough to avoid the undesired secondary effects normally associated with long-chain dispersants (Part D). The most interesting feature of the comblike structure is that, once the maximum length of the backbone molecule has been established, polymeric chains of varying molecular weight (polyethylene oxide in the case of Figure 14) can be laterally grafted to this backbone to enhance

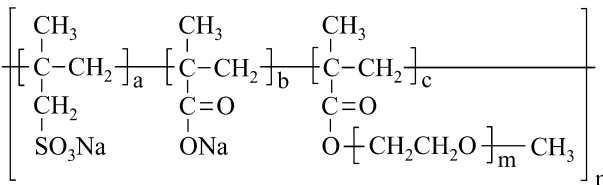


Figure 14 Example of a grafted polycarboxylate-based molecule whose molecular structure can be designed to optimize the dispersion of cement-containing materials. (Adapted from Ref. 50.)

the electrostatic/steric effect of the dispersant without necessarily increasing its maximum molecular length. This is expected to significantly improve the dispersing ability of the molecule, minimizing the occurrence of deleterious secondary effects on the castable matrix.

It is worth mentioning that the design of molecules with enhanced dispersing ability requires an adequate understanding of the effects of the dispersant's characteristics on the dispersion and rheological behavior of cement-containing suspensions. Other polymeric compounds that can be structurally tailored are expected to be developed as further investigations are conducted to better comprehend the interactions among dispersant molecules and cement particles.

VIII. TAILORING THE DISPERSION STATE OF PARTICLES

Although particle agglomeration may result in several deleterious effects on the flow and mechanical behavior of refractory castables, it can sometimes be deliberately induced to confer specific rheological properties on the material.

This is the case, for instance, of castables containing matrix particles with different specific densities (i.e., silica and alumina), which may be susceptible to phase segregation during transportation and placement. Such undesirable effects can be prevented by inducing particle coagulation around the secondary minimum of the potential energy curves (Figure 5). The weakly attractive forces that arise under this condition may also be useful to prevent settling and segregation of coarse and dense aggregates, since a yield stress is developed in the matrix suspension. This secondary minimum coagulation can be achieved easily by increasing the ionic strength (i.e., salt concentration) of the liquid medium in properly dispersed systems, as schematically illustrated in Figure 15.

The shear-thinning rheological behavior obtained through this weak coagulation may also be very important for pumpable castables in order to provide a certain cohesiveness to the material and avoid the typical shear-thickening tendency of fully dispersed concentrated systems.

The dispersion state of particles can also be tailored to impart the rheological changes required in shotcrete applications (51). This placing technique involves the sudden transformation of a highly fluid pumpable castable into a stiff and cohesive material capable of adhering to the wall under repair. One of the approaches that can be used to induce this abrupt rheological change is the coagulation of particles either in the primary or the secondary minimum of the potential energy curves (Figure 5). Figure 15 shows that this coagulation can be achieved by adding chemical admixtures that shift the castable's pH and/or increase the ionic strength of the liquid medium. It has been observed that secondary minimum coagulation may offer the advantage of providing more cohesive castables, which tend to reduce the so-called rebound effect (51).

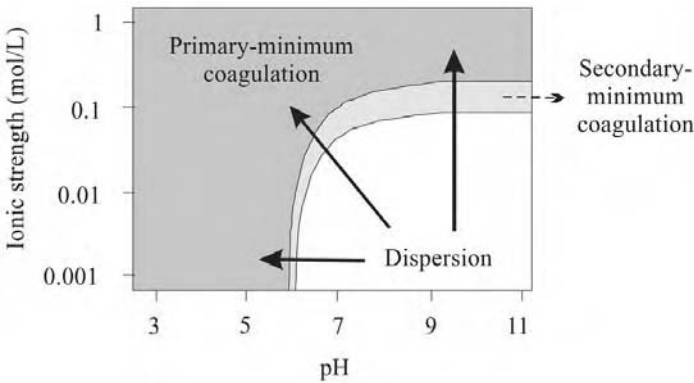


Figure 15 Stability limits for an aqueous alumina suspension containing 0.35 wt% of citric acid as dispersant, indicating (by arrows) the routes that may be used to impart secondary or primary coagulation among particles. (Adapted from Ref. 8.)

A few attempts have also been made to produce zero-cement self-flow castables through the appropriate control of the dispersion state of particles (9,52). The general idea, in this case, is to replace calcium aluminate cement for alternative coagulating agents in the castable composition in order to obtain refractory materials with minor contents of liquid ternary phases at high temperature (i.e., guelenite and anortite). Autocatalytic and enzyme-catalyzed reactions, as well as the gradual dissolution of partially soluble compounds, have been employed to promote particle coagulation in zero-cement castables by decreasing the system’s pH, increasing the liquid ionic strength, or promoting both mechanisms simultaneously, as shown in Figure 15. Zero-cement castables displaying homogeneous microstructure and minimal contents of low-melting-point phases have been obtained using this approach (9,52). Alternatively, such high-performance castables have also been produced by gelling the liquid medium around well-dispersed particles (53).

IX. SUMMARY

Basic concepts of surface chemistry are outlined in this chapter to understand the mechanisms that can be applied to optimize the dispersion and rheological behavior of advanced refractory castables. The modes of action of some dispersants are described to illustrate the effects of some of their molecular features (chain length, functional groups, charge density) on the dispersion state of matrix

particles. Possible interactions between the dispersant and cement particles are also discussed, although more extensive investigations are still required in this field. An understanding of some of these interactions and of basic principles of surface chemistry have enabled the design of special molecules with improved dispersing ability and better control over the kinetics of cement hydration. Finally, some examples are given of applications in which the particles' dispersion state can be tailored to provide highly homogeneous castables and allow for the development of innovative placing techniques.

Acknowledgments

The authors gratefully acknowledge FAPESP and ALCOA-Brazil for its financial support of most of the research involved in this work.

REFERENCES

1. Shaw DJ. Introduction to Colloid and Surface Chemistry. 3d ed. London: Butterworths, 1986:1–3, 148–212.
2. Hunter RJ. Introduction to Modern Colloid Science. New York: Oxford Science Publications, 1994:1–5, 227–322.
3. Hiemenz PC. Principles of Colloid and Surface Chemistry. 2d ed. New York: Marcel Dekker, 1986.
4. Nelson RD. Dispersing Powders in Liquids. Amsterdam: Elsevier, 1988:1, 39–54.
5. Lange FF. Powder processing science and technology for increased reliability. *J Am Ceram Soc* 1989; 72:3–15.
6. Lewis JA. Colloidal processing of ceramics. *J Am Ceram Soc* 2000; 83:2341–2359.
7. Sigmund WM, Bell NS, Bergström L. Novel powder-processing methods for advanced ceramics. *J Am Ceram Soc* 2000; 83:1557–1574.
8. Gauckler LJ, Graule T, Baader F. Ceramic forming using enzyme catalyzed reactions. *Mater Chem Phys* 1999; 61:78–102.
9. Studart AR, Valenzuela FAO, Pandolfelli VC, Tervoort E, Gauckler LJ. Enzyme-coagulated zero-cement refractory castables. *Am Ceram Soc Bull* 2002; 81(5): 26–31.
10. Studart AR, Zhong W, Pandolfelli VC. Rheological design of zero-cement self-flow castables. *Am Ceram Soc Bull* 1999; 78(5):65–72.
11. Studart AR, Zhong W, Pileggi RG, Bonadia P, Pandolfelli VC. Dispersion of microsilica-containing zero-cement high-alumina castables. *Am Ceram Soc Bull* 2000; 79(2):49–55, 84.
12. Studart AR, Gallo J, Pandolfelli VC. Dispersants for high-alumina castables. *Am Ceram Soc Bull* 2002; 81(4):36–44.
13. Studart AR, Pandolfelli VC, Tervoort E, Gauckler LJ. Selection of dispersants for high-alumina zero-cement refractory castables. *J Eur Ceram Soc* 2003; 23(7): 997–1004.

14. Oliveira IR, Studart AR, Pandolfelli VC, Menegazzo BA. Zero-cement refractory castables. *Am Ceram Soc Bull* 2002; 81(12): 27–34.
15. Studart AR, Pandolfelli VC. Thermomechanical behavior of zero-cement, high-alumina castables. *Am Ceram Soc Bull* 2000; 79(10):53–60.
16. Lee WE, Moore RE. Evolution of in situ refractories in the 20th century. *J Am Ceram Soc* 1998; 81(6):1385–1410.
17. Harnby N, Edwards MF, Nienow AW. *Mixing in the Process Industries*. 2d ed. London: Butterworth-Heinemann, 1997.
18. Bergström L. Hamaker constants of inorganic materials. *Adv Colloid Interfac* 1997; 70:125–169.
19. Parks GA. Isoelectric points of solid oxides, solid hydroxides and aqueous hydroxo complex systems. *Chem Rev* 1965; 65:177–198.
20. Si WJ, Graule TJ, Baader FH, Gauckler LJ. Direct coagulation casting of silicon carbide components. *J Am Ceram Soc* 1999; 82:1129–1136.
21. Premachandran RS, Malghan SG. Dispersion characteristics of ceramic powders in the application of cationic and anionic polyelectrolytes. *Powder Technol* 1994; 79:53–60.
22. Malghan SG, Pei PT, Wang PS. Analysis of surface chemistry of silicon nitride and carbide powders. In: Cima MJ, ed. *Ceramic Transactions, Vol. 26. Forming Science and Technology for Ceramics*. Westerville, OH: The American Ceramic Society, 1991:38–45.
23. Oliveira IR, Studart AR, Pileggi RG, Pandolfelli VC. Dispersion and packing of particles — Principles and Applications to Ceramic Processing (in Portuguese). São Paulo: Fazenda Arte, 2000.
24. Tari G, Ferreira JMF, Lyckfeldt O. Influence of magnesia on colloidal processing of alumina. *J Eur Ceram Soc* 1997; 17:1341–1350.
25. Hidber PC, Graule TJ, Gauckler LJ. Citric acid — a dispersant for aqueous alumina suspensions. *J Am Ceram Soc* 1996; 79:1857–1867.
26. Cesarano J, Bleier A, Aksay IA. Stability of aqueous α -Al₂O₃ suspensions with poly(methacrylic acid) polyelectrolyte. *J Am Ceram Soc* 1988; 71:250–255.
27. Hidber PC, Graule TJ, Gauckler LJ. Influence of the dispersant structure on properties of electrostatically stabilized aqueous alumina suspensions. *J Eur Ceram Soc* 1997; 17:239–249.
28. Sacks MD, Tseng T. Role of sodium citrate in aqueous milling of aluminum oxide. *J Am Ceram Soc* 1983; 66:242–247.
29. Luther EP, Yanez JA, Franks GV, Lange FF, Pearson DS. Effect of ammonium citrate on the rheology and particle packing of alumina slurries. *J Am Ceram Soc* 1995; 78:1495–1500.
30. Hackley VA. Colloidal processing of silicon nitride with poly(acrylic acid): II, Rheological properties. *J Am Ceram Soc* 1998; 81:2421–2428.
31. Biggs S, Scales PJ, Leong Y, Healy TW. Effects of citrate adsorption on the interactions between zirconia surfaces. *J Chem Soc Faraday T* 1995; 91:2921–2928.
32. Sumita S, Rhine WE, Bowen HK. Effects of organics dispersants on the dispersion, packing, and sintering of alumina. *J Am Ceram Soc* 1991; 74:2189–2196.

33. Guo L, Zhang Y, Uchida N, Uematsu K. Adsorption effects on the rheological properties of aqueous alumina suspensions with polyelectrolyte. *J Am Ceram Soc* 1998; 81:549–556.
34. Kamiya H, Fukuda Y, Suzuki Y, Tsukada M, Kakui T, Naito M. Effect of polymer dispersant structure on electrosteric interaction and dense alumina suspension behavior. *J Am Ceram Soc* 1999; 82:3407–3412.
35. Sindel J, Bell NS, Sigmund WM. Electrolyte effects on nonionic steric layers: Bis-hydrophilic PMMA–PEO diblock copolymers adsorbed on barium titanate. *J Am Ceram Soc* 1999; 82:2953–2957.
36. Leong YK, Scales PJ, Healy TW, Boger DV. Rheological evidence of adsorbate-mediated short-range steric forces in concentrated dispersions. *J Chem Soc Faraday T* 1993; 89:2473–2478.
37. Laucournet R, Pagnoux C, Chartier T, Baumard J. Coagulation method of aqueous concentrated alumina suspensions by thermal decomposition of hydroxyaluminum diacetate. *J Am Ceram Soc* 2000; 83:2661–2667.
38. Albert A, Serjeant EP. *The Determination of Ionization Constants*. 2d ed. London: Chapman and Hall Ltd., 1971.
39. Martell AE, Smith RM. *Critical Stability Constants*, Vol. 3. Other organic ligands. New York: Plenum, 1989.
40. Liu YQ, Gao L, Guo JK. Comparative study on the stabilizing effect of 2-phosphonobutane-1,2,4-tricarboxylic acid and citric acid for alumina suspensions. *Colloid Surface A* 2001; 193:187–195.
41. Liu YQ, Gao L, Yu L, Guo JK. Adsorption of PBTCa on alumina surfaces and its influence on the fractal characteristics of sediments. *J Colloid Interf Sci* 2000; 227:164–170.
42. Choi GN, Krieger IM. Rheological studies on sterically stabilized model dispersions of uniform colloidal spheres. II. Steady-shear viscosity. *J Colloid Interf Sci* 1986; 113:101–113.
43. Currell BR, Grzeskowlak R, Midgley HG, Parsonage JR. The acceleration and retardation of set high alumina cement by additives. *Cement Concrete Res* 1987; 17:420–432.
44. Mathieu A. Calcium aluminates and additives. Lafarge Fondu International, Internal Report, 1992.
45. Bunt N, Revais C, Vialle M. Additives in calcium aluminate cement containing castables. *Proc Unified Int Conf Refractories*, New Orleans, 1997:1347–1354.
46. Alt C, Wong L, Parr C. Measuring castable rheology by exothermic profile. *Proc Unified Int Conf Refractories*, Cancun, 2001.
47. Jolicoeur C, Simard MA. Chemical admixture-cement interactions: Phenomenology and physico-chemical concepts. *Cement Concrete Comp* 1998; 20:87–101.
48. Tanaka Y, Matsuo S, Ohta A, Ueda M. A new admixture for high performance concrete. In: Dhir RK, Hewlett PC, eds. *Radical Concrete Technology*. London: E & FN Spon, 1996:291–300.
49. Uchikawa H, Hanehara S, Sawaki D. The role of steric repulsive force in the dispersion of cement particles in fresh paste prepared with organic admixture. *Cement Concrete Res* 1997; 27:37–50.

50. Yamada K, Takahashi T, Hanehara S, Matsuhisa M. Effects of the chemical structure on the properties of polycarboxylate-type superplasticizer. *Cement Concrete Res* 2000; 30:197–207.
51. Pileggi RG, Marques YA, Vasques Filho D, Studart AR, Pandolfelli VC. Wet-shot-crete for refractory castables. *Am Ceram Soc Bull* 2002; 81(10): 51–56.
52. Studart AR, Pandolfelli VC, Tervoort E, Gauckler LJ. In-situ coagulation of high-alumina zero-cement refractory castables. *J Am Ceram Soc* 2002; 85(8):1947–1953.
53. Studart AR, Ortega FS, Innocentini MDM, Pandolfelli VC. Gelcasting high-alumina refractory castables. *Am Ceram Soc Bull* 2002; 81(2):41–47.

13

Thermomechanical Considerations for Refractory Linings

Charles A. Schacht

Schacht Consulting Services, Pittsburgh, Pennsylvania, U.S.A.

I. INTRODUCTION

The objective of this chapter is to provide guidance and understanding on the design and use of refractory linings with respect to structural behavior or often referred to as the mechanical behavior. Refractory linings, as typically used in industry, serve two dual purposes. First, refractory linings insulate the vessel or steel support structure from overheating and destruction of this support structure by the heat from the process contained within the refractory lining. Without the steel support structure the process is not contained and is not possible. Second, the refractories insulate the process and control the heat loss from the process. Controlling the heat loss controls the energy cost of the process. Therefore, most refractory linings are, not always but in most cases, exposed to and contain a process that creates heat, resulting in a temperature distribution throughout the lining system. The support structure contains and restrains the thermal growth or thermal expansion of refractory lining. As a result, the lining and support structure are also exposed to thermal expansion stresses. There are also gravity load (sometimes referred to as the dead load) stresses from the weight of the lining and structure. Usually the thermal expansion stresses are orders of magnitude greater than the gravity load stresses. Therefore, most attention is usually given to the thermal expansion stresses in both the lining and the support structure. Throughout this chapter it is typically assumed that the lining is supported by a steel structure. The term “lining system” is used to refer to combined refractory lining and the steel support structure. This chapter does not deal with the chemical behavior of refractories. The chemical effects on

refractories will most likely influence the mechanical material properties and thereby influence the mechanical behavior of the refractory lining. The chemical effects on the thermal and mechanical material properties can be determined by material tests.

This chapter provides information and the reasoning with respect to how to choose appropriate design features in a refractory lining system to minimize thermomechanical problems such as mechanical excessive distortions, excessive cracking, spalling, pinch spalling, and other signs of a deteriorating lining. It also covers how to choose the best refractory based on thermomechanical considerations. The mechanical behavior of most refractory materials is complex. The mechanical behavior of the refractory lining and the interaction with the steel support structure is also complex. These complexities lie in the nonlinear mechanical behavior of the refractory material and in the lining system. This chapter discusses the lining geometries that are frequently used in industry, the fundamental mechanical behavior of the nonlinear material properties of refractory material, and the lining system. Due to the page limitation the complete presentation on the thermomechanical behavior of refractory linings cannot be presented here. A more detailed and expanded presentation on the thermomechanical behavior of refractory linings and refractory materials is made in (1).

The information provided here will provide guidance and insight into to what to look for, what to expect, and what not to expect when inspecting a lining system. This chapter provides valuable guidelines when designing a refractory lining. Reliable lining system investigations require the use of computer methods such as finite element analysis (FEA). The observations made during lining system inspection often provide valuable information for the analytical investigations. Accurate thermal and mechanical material properties are also necessary for reliable FEA investigations. Since the lining and support structure interaction is typically nonlinear, the FEA computer program must have nonlinear features such as “elastic/plastic” material stress/strain behavior features as well as nonlinear “tension only” for either brick joints or the principal tensile stress regions in castables.

II. LOAD TYPES

Two fundamental types of loads (2) are imposed on refractory lining systems or for any type of structural system. The gravity load (a combination of dead load weight and live load weight) is classified as a “stress-controlled” load. Pressure loads are also stress-controlled loads. Typically, stress-controlled loads generate stress within the structure which is a function of the structure geometry. This type of load is usually the only load type considered such as in civil engineering buildings and bridges. For example, assume a stack of brick with a cross-sectional area

of A , height L , and unit weight of p . The compressive stress S_{SC} at the base of the brick stack can be calculated as

$$S_{SC} = AL_p/A \tag{1}$$

where AL_p is the total weight of the brick stack. It should be noted that the stress calculation only required the use of material density and the geometry of this simple structure.

The second type of load is called a “strain-controlled” load. A thermal expansion load is a strain-controlled load. Using the brick stack example, assume that the brick is restrained in the vertical direction by a steel structure. Let us also assume, for the simplicity of the calculation, that the thermal expansion is totally restrained. The compressive thermal S_{TC} in the brick stack is calculated as

$$S_{TC} = \alpha\Delta T (\text{MOE}) \tag{2}$$

The thermal strain “ ϵ ” developed is

$$\epsilon = \alpha \Delta T \tag{3}$$

where α is the coefficient of thermal expansion, ΔT is the temperature increase in the brick stack from ambient temperature at installation, and MOE is the modulus of elasticity of the brick. The brick was also assumed to remain elastic at the heated temperature for the simplicity of the calculation. In the case of the strain-controlled load, the material properties α and MOE were required. Also, α and MOE are assumed to be constant with respect to temperature.

The above example is used to define the two load types in refractory lining systems. Since refractory linings are primarily exposed to thermal expansion loads, it is important to have accurate static compressive stress/strain (SCSS) data in order to determine the MOE data. It will be shown in later discussions on the SCSS data that most refractory materials become softer (lower MOE) at higher temperatures and also become more plastic at higher temperatures. SCSS data curves obtained from laboratory testing are used to define the MOE property as well as the plastic behavior of the refractory material in question.

Another way to differentiate stress- and strain-controlled loads is to examine the creep response of the refractory lining when exposed to these two types of loads. Using the previous example, the refractory brick will continue to creep compressively when subjected to the gravity load until compressive creep failure occurs. That is, the gravity load will not diminish and the compressive creep will continue for the life of the lining until failure occurs. This is also true for pressure loads. For strain-controlled loads, such as thermal expansion loads, the creep will last until the thermal restraint strains are relaxed from the lining. Therefore, strain-controlled loads will result in creep over a finite period of time. At the end of the creep relaxation, the thermal stress will be reduced to a negligible value. The same reasoning for differentiating the stress- and strain-controlled

loads can be applied to high-temperature plastic deformation behavior of the refractory lining material. For stress-controlled loads, the plastic deformation will continue for the life of the structure or until an upper limit on the plastic stress threshold is reached. For the strain-controlled load, a finite amount of plastic deformation will take place equal to the restrained thermal strains.

III. REFRACTORY THERMAL AND MECHANICAL MATERIAL PROPERTIES

In the investigation of refractory lining systems, the analysis is typically done in two stages. Stage I is the thermal analysis. The thermal analysis can be simply steady-state thermal analysis or a transient thermal analysis. For a steady-state thermal analysis, only the thermal material property, thermal conductivity K , is required. For transient thermal analysis, the thermal material properties required include thermal conductivity, specific heat c and density p . In any thermal analysis other data needed are the external ambient temperatures, the emissivity of the external surfaces, the external wind velocity, and other boundary conditions data that are important to the thermal analysis.

Stage II is the thermal stress analysis. In this stage the basic mechanical material properties required are the modulus of elasticity (MOE), coefficient of thermal expansion (α), and Poisson's ratio (ν). Poisson's ratio defines the ratio of the displacement in the orthogonal directions within a material. For example, when a steel bar is stretched in tension, the bar increases in length in the direction of the load and decreases in width in the orthogonal direction. The ratio of the orthogonal displacement to the loaded direction displacement is Poisson's ratio. Basically, Poisson's ratio defines the orthogonal cross coupling of the material displacement behavior. For brittle materials, the value of 0.10 to 0.15 is often used. Note that steel has a Poisson's ratio of about 0.3.

As previously discussed, most refractory becomes plastic at higher temperatures. For example, a fired 70% alumina brick starts to become plastic at temperatures above 800 to 1000°F as shown by the static compressive stress/strain (SCSS) data plot in Figure 1. The MOE of a material is the tangent slope of the stress-strain curve (initial portion of the curve) obtained from the SCSS data. The higher-temperature SCSS data curves show the effects of the higher temperature. At the higher temperatures, the higher stress causes an increased plastic response of the refractory material. Therefore, the refractory material becomes more nonlinear at higher temperatures.

Another way to develop MOE data is by the sonic test methods. Fundamentally, the sonic method evaluates the MOE using the resonant frequency of the refractory sample. However, the sonic method tends to overpredict the MOE value. The primary reason is that the resonating sample is exposed to an

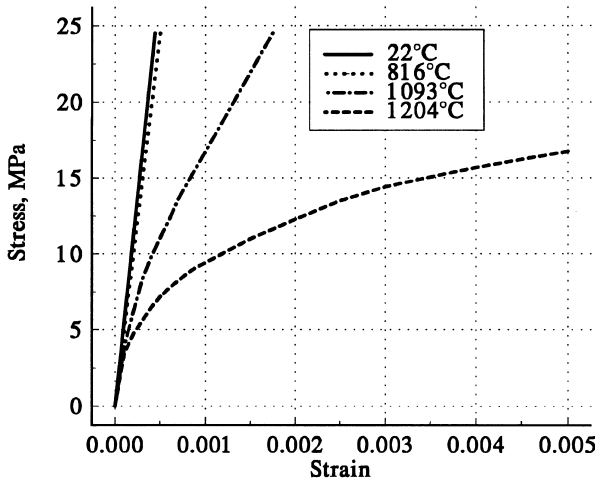


Figure 1 Static compressive stress–strain data for a fired 70% alumina brick.

extremely low stress–strain environment. Using an actual SCSS data curve, it means the MOE is tangent to the stress–strain data curve at an extremely low stress value where the data curve would have the greatest slope and no significant plastic response would be initiated. Typically, the refractory material is exposed to significant levels of thermal stress (several thousand psi). Also, the sonic method provides no information regarding the relationship between stress and strain. This method also provides no information about the plastic behavior of the refractory material.

IV. INFLUENCE OF STRESS STATE DIMENSIONALITY ON REFRACTORY STRENGTH

The compressive strength of refractory is influenced by the dimensionality of the compressive stress (3,4), as illustrated in Figures 2 and 3. Figure 2 shows the effective increase in the ultimate compressive crushing strength for a two-dimensional compressive stress state in the order of about 1.27 over the one-dimensional ultimate compressive crushing stress, f'_c based on the values of the two orthogonal principal compressive stresses, S_1 and S_2 . For three-dimensional compressive stress states (see Figure 3), the values of the ultimate compressive crushing strength can exceed six times f'_c .

The tensile fracture strength, however, is not altered by the dimensionality of the tensile stress state. A multidimensional tensile stress state will fracture in tension at the same value as the one-dimensional ultimate tensile stress, f'_t .

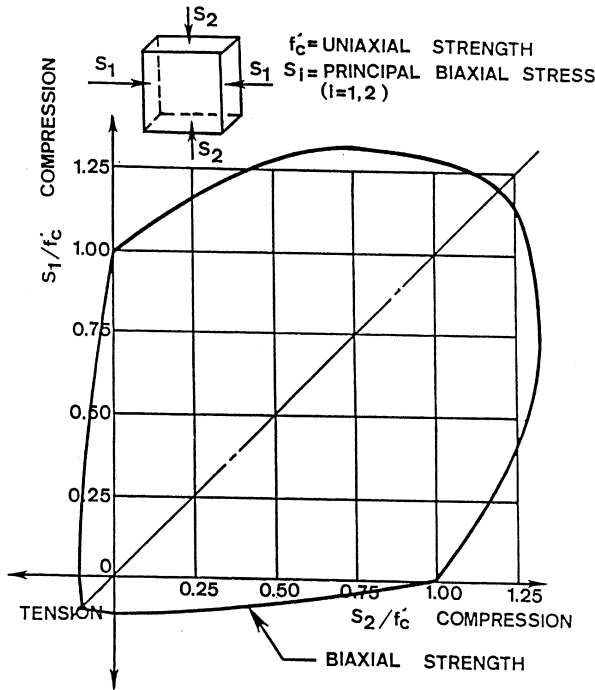


Figure 2 Ultimate strength of brittle material under biaxial stress.

Most lining systems are three-dimensional and therefore experience three-dimensional compressive thermal expansion states. This explains why refractory linings can resist large compressive thermal expansion forces that create stresses beyond the one-dimensional crushing stress. This also explains why the expansion force of the refractory lining system can cause distortions in the steel support structure and also why the refractory will not necessarily fail at high values of compressive stress.

V. CHOOSING THE BEST REFRACTORY

In selecting the appropriate refractory for the process application, various criteria are used. The refractory must be chemically compatible along with mineralogy and other considerations. The capability of the refractory to maintain its strength for the process temperature in question, resistance to thermal shock, and other strength considerations are used. ASTM tests can be used to rank the candidate

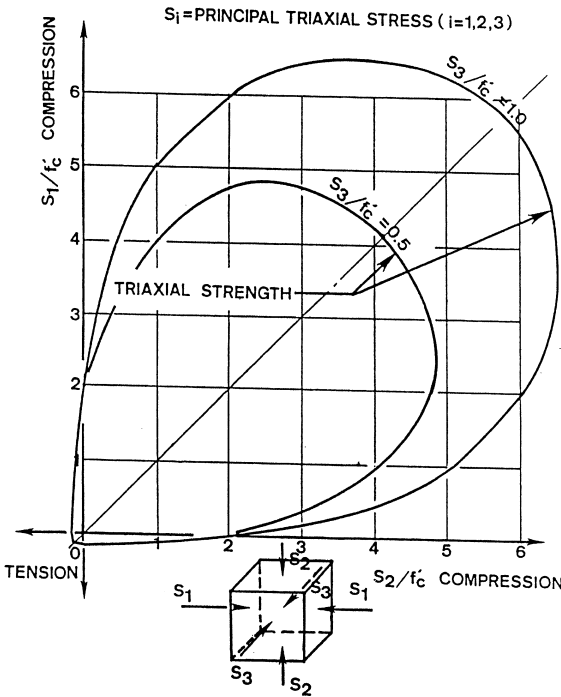


Figure 3 Ultimate strength of brittle material under triaxial stress.

refractory considered for the lining project. With regard to mechanical considerations, the ultimate crushing strength is sometimes used to rank the candidate refractories, with the refractory having the greatest ultimate crushing stress as being the best refractory. The following example is used to demonstrate that when considering mechanical properties, using the ultimate crushing stress provides only part of the necessary mechanical information needed to select the best refractory.

Let us assume there are two candidate refractory materials, Refractory A and Refractory B, chosen for the lining project. We will also assume that both materials have the same thermal material properties, meaning that both refractories have the same temperature profiles. For the mechanical material properties, we assume that both materials have the same coefficient of thermal expansion and Poisson's ratio. The only difference is in the static compressive stress-strain (SCSS) data. Figure 4 shows the hypothetical SCSS data curves for the two materials at an operating temperature T_0 . Since both materials have the same temperature and the same coefficient of thermal expansion, both materials have the same thermal strain, e_R . The ultimate crushing stress for Refractory A is f'_{CA}

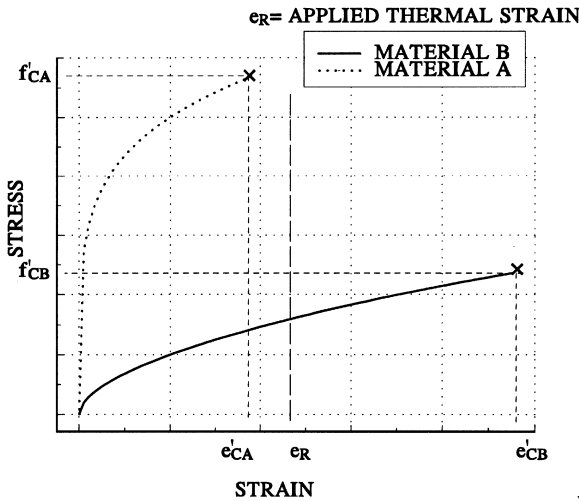


Figure 4 Stress–strain curves of two hypothetical refractory materials.

and is greater than Refractory B's ultimate crushing strength f'_{CB} . However, Refractory A is more brittle than Refractory B as reflected in the steepness of the stress–strain curve of Refractory A and the lesser ultimate crushing strain e'_{CA} of Refractory A. Refractory B has a much greater ultimate crushing strain, e'_{CB} . Note the e'_{CA} is less than the applied strain e_R of the lining. Therefore, Refractory A would crush while Refractory B would not crush. Refractory B has a considerable margin of compressive straining before crushing. Basically, Refractory B is a softer material than refractory A. Refractory B, based on thermomechanical considerations, would be chosen as the better refractory.

This example demonstrates that prudent interpretation should be given to the ultimate crushing stress data and that the SCSS data provide considerably more information when selecting the best candidate refractory. The SCSS data provide information on both the ultimate crushing stress and the corresponding ultimate crushing strain.

VI. THERMOMECHANICAL ASPECTS OF MORTAR JOINTS

Brick joints may be either mortared or dry (no mortar). In most cases refractory brick linings are installed with mortar in the brick joints. Based on the consistency of the mortar material and how the mortar is applied, the mortar joint

thickness can vary from less than 1 mm to several mm. Some brick linings are installed by dipping the brick in mortar slurry, while in other linings the mortar is troweled onto the brick joint face. A “battered joints” is when the mortar is mixed to a batter consistency and the mortar is troweled spread over the top surface of the brick course. The next layers of brick are in turn covered with the batter mix. Typically, the literature defines the use of mortar to bond the brickwork into a monolithic lining to provide more resistance to thermal shock and to provide a cushion at the brick joint, which has irregular surfaces. In actuality, mortar joints are rather weak in tension and cannot resist the magnitude of the tensile loads imposed on the cold face region in most lining systems.

Various types of mortars gain their strength by different means. There are heat-set mortars, air-set mortars, resin-bonded mortars, and phosphate-bonded mortars. Some mortars are given the generic name of chemically bonded mortars. Heat-set mortars exhibit shrinkage at temperatures around 950°F due to the softening and bonding of the fine mullite and glass grains. Air-set mortars tend to lose strength at temperatures over the 900 to 1000°F range due to the melting of the sodium silicate in the mortar. The sodium silicate gives the air-set mortar strength at temperatures below the 900 to 1000°F range. Phosphate- and resin-bonded mortars tend to be more stable at the temperatures above 950°F. That is, these latter two mortars expansion curves have a slight decrease in slope at temperatures above 950°F and up to about 1200°F.

Mortars are very soft compared to fired brick. Figure 5 (5,6) provides a comparison of SCSS data for homogeneous brick samples and brick samples with a 1.6-mm- (1/16-in.) thick phosphate bonded mortar joint. The mortar used was a phosphate-bonded mortar. The brick samples were 50-mm (2-in.) diameter by 100-mm (4-in.) long cored drilled from a fired 70% alumina brick made on an impact press. The strain in the samples was measured over the central 50-mm length. The joint surfaces in the brick were machined to provide a uniform mortar joint thickness. For the low-temperature range (20 to 815°F), the curves, at any selected strain value, show that the stress developed for the brick mortar sample is about 15% of the stress value for the homogeneous brick sample. For the higher-temperature SCSS curves, the mortar exhibits less stiffness. For any given strain, the stress developed for the higher-temperature brick mortar sample is around 70% of the stress for the homogeneous brick sample. The MOE for the brick mortar samples and the homogeneous brick samples was defined by using the slope of the initial portion of each curve. The mortar MOE_m is defined by the following equation:

$$MOE_m = MOE_{mb} t_m / t_b (MOE_b - MOE_{mb}) \tag{4}$$

where the subscript m relates to the mortar, mb to the brick/mortar sample, and b to the homogeneous brick sample. The thickness of the brick sample and mortar joint are t_b and t_m, respectively. Note that the thickness, t_b, of both homogeneous

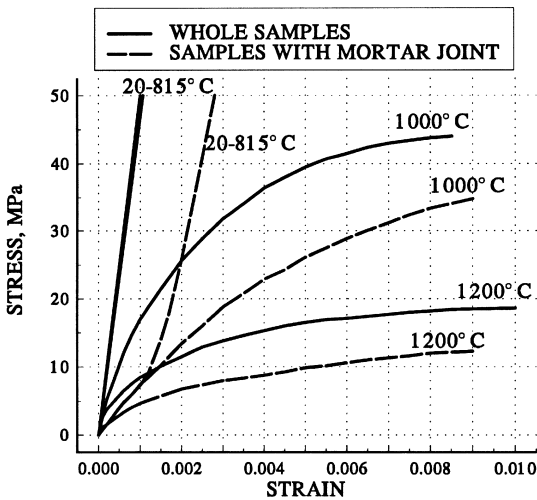


Figure 5 SCSS data for refractory with and without mortar joint.

brick and brick/mortar joint samples are 50 mm, as used in the Eq. (4) calculations. Table 1 provides the results of these calculations. The MOE values in Table 1 reflect the softer brick mortar samples over the homogeneous brick samples. The mortar is extremely soft. It should be noted that due to the high compressive and tensile stress levels, the tensile bond strength of the various mortars are destroyed due to the compressive crushing of the mortar grains when subjected to the operating stress conditions. The mortars tend to lose their tensile strength due to the crushing of the mortar grains.

The SCSS data also provide insight into the expansion allowance that the mortar joints provide. Table 2 uses the same data and shows the percentage of the compressive deformation that occurs in the 1.6-mm-thick mortar joint. As expected, greater deformations occur in the mortar joint at the higher levels of temperature and compressive stress applied to the mortar joint. It should also be noted that the compressive stress levels used in the SCSS tests are realistic based on field strain gauge measurements on cylindrical vessels lined with 70% fired alumina brick (6).

VII. THE FINITE ELEMENT ANALYSIS (FEA) METHOD

The most current state-of-the-art in analysis methods is the finite element analysis (FEA) method. The FEA method of analysis is conducted using finite element computer programs. Because of the nonlinear thermomechanical behavior of

Table 1 Summary of MOE of 70% Fired Alumina Brick and 70% Fired Alumina Brick with Mortar Joint

Data temperature, °C	Selected stress level	Secant MOE, GPa		
		MOE _b	MOE _{mb}	MOE _m , Eq. (4)
20–815	10	43.48	8.3	0.33
	25	46.30	12.76	0.56
	50	47.17	17.86	0.92
1100	10	18.52	7.14	0.32
	20	14.29	6.06	0.30
	30	10.91	4.62	0.24
1200	4	13.33	5.00	0.21
	8	9.41	2.67	0.11
	12	5.22	1.46	0.07

refractory linings, FEA computer programs are required to provide a reliable prediction of the thermomechanical behavior of the refractory lining. The term “finite element” refers to the analysis approach in which a finite (or small) mathematical element is used to represent stress–strain behavior over a finite portion of the structure of interest; in our case, a finite part of the refractory lining. A large numbers of these finite elements are assembled to represent the total structure of interest; in our case, the lining of interest. Numerous FEA computer programs have been developed by companies such as ANSYS, ALGOR, MSC, STAAD, COSMOS, and CFX to name a few. Each of these FEA programs is developed

Table 2 Summary of Calculated Phosphate Bonded Mortar Joint Compressive Deformation

Data Temperature, °C	Applied compressive stress, MPa	% Deformation of 1.6-mm-thick-mortar-joint
20–815	10	3.14
	25	4.25
	50	5.66
1100	10	3.20
	20	6.51
	30	12.48
1200	4	1.95
	8	7.39
	12	17.30

to solve similar or a different variety or class of engineering problems such as heat flow, acoustics, structural behavior, fluid and air flow, and others. Also, these programs have a wide range of finite element types! that is, one-, two-, and three-dimensional finite element types to represent the geometry of the structure or media of interest. Each program will most likely have similar and different types of a finite element to model the type of engineering problem unique to that FEA program. The following cylindrical lined vessel example shown in this chapter was solved using the ANSYS program (mechanical version). All of the FEA work the author of this chapter performed was done using the ANSYS Mechanical FEA program.

VIII. THERMOMECHANICAL BEHAVIOR OF CYLINDRICAL LININGS

The most used refractory lined vessel geometry in industry appears to be the cylindrical refractory lined vessel. In the steel industry, the blast furnace, blast furnace stoves, torpedo cars, steelmaking ladles (7), electric arc furnaces, degasser vessels, and cyclone dust collector are a few examples of cylindrical vessels. In the petrochemical industry, the petrochemical processing vessels are typically cylindrical. Fluid bed reactor vessel walls are typically cylindrical with a spherical vessel top. Many other basic industries use cylindrical refractory lined vessels such as rotary kilns and wood pulp process vessels.

The following example of a cylindrical refractory lined vessel is idealized to present the basic and fundamental features of refractory lining and the interaction of the lining with the steel vessel shell. Because of the frequent use of the cylindrical type of vessel geometry, it is important that the salient features of thermomechanical behavior of the cylindrical lining be identified. The other popular classical refractory lining geometries used in industry include flat wall lining systems, arch lining systems, conical lining systems, and spherical lining systems.

Figure 6 shows a finite element model of a typical brick in an idealized cylindrical lining. Only a single half-section of a typical brick is required to model the cylindrical lining since the half-section of brick represents the symmetric behavior of any location in the complete lining. The lining shown here is assumed to be a single thickness lining. Actual linings may consist of two or more layers of brick.

Figure 7 illustrates the idealized steady-state linear through-thickness temperature distribution in the refractory lining. Some refractory materials have temperature-dependent thermal conductivity and results in the need for a nonlinear thermal analysis and a resulting nonlinear through-thickness tempera-

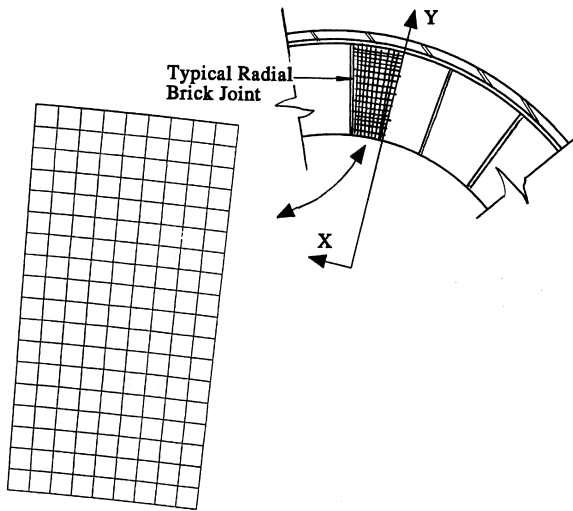


Figure 6 Finite element model of idealized cylindrical refractory brick lining.

ture distribution. As previously discussed, the first part of a lining investigation is the thermal analysis using the thermal material properties.

Figure 8 shows the temperature contour lines for the steady-state thermal analysis. Note the brick half-section was modeled with an element mesh of 9 elements across the width and 18 elements along the length. The element mesh chosen is typically based on the expected nonlinear stress-strain behavior of the refractory and the nonlinear “compression-only” behavior of the brick joint. In the case of castable systems, the circumferential width of the model is selected by trial solutions to determine the estimated maximum circumferential tensile stress that could be developed by the castable lining. Figure 8 is a line contour plot in which the letters on the contours represent a temperature at that location. Color contour plots are also available from most programs and provide a much better visualization of the temperature distribution, especially for more complicated temperature distributions.

The temperature data file is created from the thermal analysis. This file is used as input into the mechanical stress-strain model. The thermal model is, in most programs, converted to a mechanical model by replacing the thermal elements with the equivalent mechanical elements and converting the thermal material properties to mechanical material properties. In most cases the conversion from the thermal model to the mechanical model requires significant effort due to the addition of the nonlinear joint elements and the necessary additional

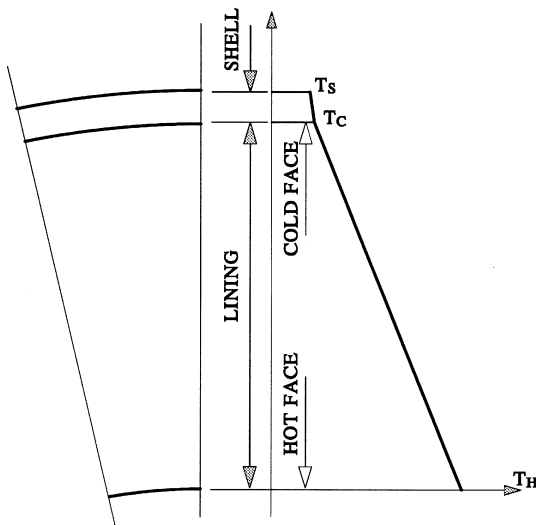


Figure 7 Idealized linear through-thickness temperature distribution.

displacement boundary conditions for symmetry. The mechanical behavior of the refractory material is nonlinear. Typically, the refractory material becomes plastic at higher temperatures. Therefore, nonlinear elastic/plastic stress–strain relationships are required in the model material for the refractory stress–strain behavior. Also, the brick joint, be it a mortar or dry joint, can only resist compression and will separate under a tensile load. Nonlinear “contact” elements are included in the mechanical model for the brick joints. These elements will simulate the “compression-only” behavior of the dry or mortar joint. This element will allow the joint to separate when the joint is subjected to a tensile or separating load.

Figure 9 illustrates the radial brick joint “compression-only” behavior. In this example the stress–strain behavior of the refractory material was assumed to remain totally elastic. As shown, a portion of the joint on the hot face end of the radial brick joint is in compression, and a portion on the cold face end of the brick is separated. The circumferential loading is a maximum at the lining hot face and decreases linearly to zero at an internal location of the brick joint. For actual elastic/plastic refractory behavior, the circumferential loading would be nonlinear. The internal location is where the joint begins to separate. This joint behavior can be explained fundamentally by considering the temperature of the various locations in the brick joint compared to the steel shell temperature and the coefficient of thermal expansion of the brick material and the steel shell.

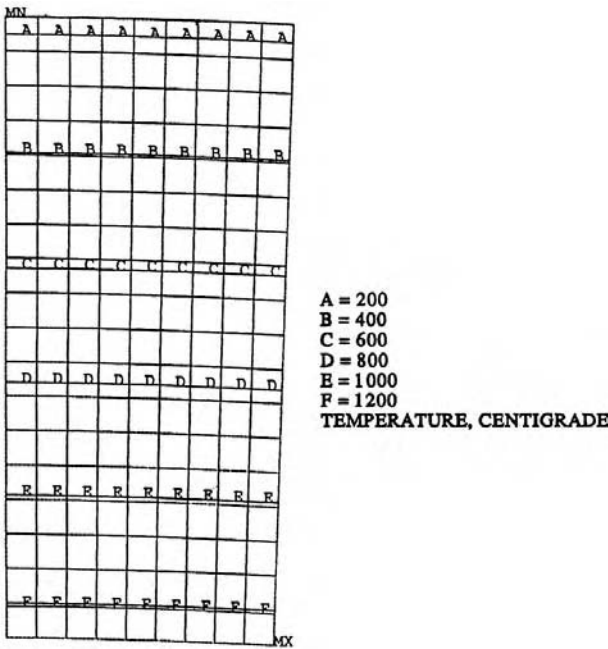


Figure 8 Temperature contour lines in cylindrical lining brick lining.

At the brick cold face (brick face against the shell) the temperature is usually equal or nearly equal to the steel shell temperature. If a high-alumina brick were used, the coefficient of thermal expansion of the alumina brick would be approximately half that of the steel shell (assuming carbon steel). Therefore, the steel shell will expand circumferentially twice that of the brick cold face. This implies that the cold face end of the brick radial joints will separate. The brick hot face temperature is typically several times that of the steel shell. Therefore, the circumferential expansion of the brick hot face will be greater than the steel shell. This implies that the brick radial joints will experience compressive loading. The lining will also expand radially against the steel shell. The steel shell will in turn restrain the brick lining expansion. The brick lining hot face will develop circumferential compressive stress. In addition, a radial compressive load will be developed between the brick cold face and the steel shell.

There will be an interior location of the restrained brick where the brick joint circumferential thermal expansion will be equal to that of the steel shell. This interior location will be where the compressive load in the joint ends and the joint begins to separate.

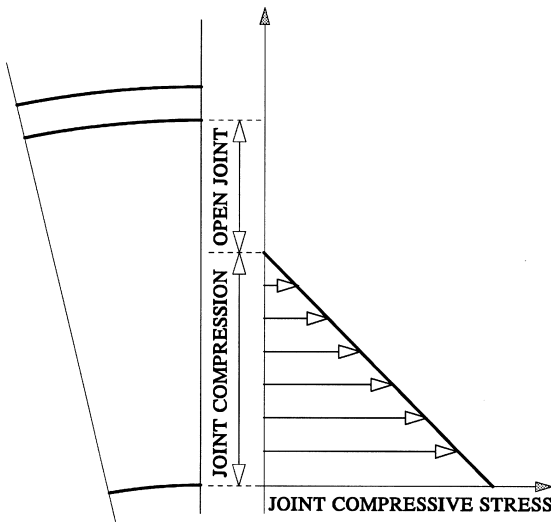


Figure 9 Idealized compression load-only condition of radial brick joint.

Figure 9 shows a linear decreasing circumferential load in the brick. This is typically the linear stress pattern that exists at lower temperatures in the lining such as during the early stages of the initial heatup. As the lining hot face continues to increase in temperature during the initial heatup, the refractory brick will become plastic and the circumferential forces in the hot face region (a short depth in from the hot face) will start to decrease while the lining hot face region continues to expand circumferentially. That is, the lining hot face will plastically deform under compression at the higher temperatures. At a cold shutdown the compressive plastic straining that took place at the maximum operating temperature will be seen as cracks in the lining hot face and in the lining hot face joints. The theoretical crack opening width should be equal to the amount of plastic straining that took place at the maximum operating temperature less the amount of elastic compressive strain that existed at the maximum heatup temperature. Provided the next heatup will be to the same operating temperatures, all of the cracks should close up. The cracks will close during subsequent heatup and should not be filled with a joint material during the cold shutdown condition. Filling the cracks means the lining hot face will be exposed to another cycle of compressive plastic straining. Continued compressive plastic straining in subsequent heatups after subsequent crack filling should eventually cause a mechanical deterioration of the lining refractory in the hot face region. For more extensive investigative computer studies on refractory lining systems of other geometries, refer to (1).

IX. DO'S AND DON'TS IN REFRACTORY LINING DESIGN AND USE

Several lining design features and use practices in refractory lining systems should be avoided. Investigative studies have shown that the following items have led either directly or indirectly to the deterioration of the refractory in lining systems. Some of these items may be obvious to some readers. However, for the sake of completeness and for the less experienced user and designer of refractory lining systems, all items are addressed here.

A. Thin Lining Design

Avoid thin refractory linings if possible. Thin linings are defined as linings that have a thickness such that the lining hot face temperature is not significantly greater than the temperature of the vessel steel shell. That is, the circumferential thermal growth of the steel shell is greater than the circumferential thermal growth of the refractory lining hot face. The thermal growth of the vessel shell will cause the lining to basically “tear apart” circumferentially as well as in the axial or orthogonal direction in the lining. When this takes place, process materials can penetrate the lining and assist in a more rapid deterioration of the lining. A thin lining is usually not restrained or at best only partially restrained, resulting in effectively a weaker refractory material more susceptible to tensile fracture during rapid temperature cycling. That is, there is no significant compressive stress–strain environment in the lining hot face region to offset tensile stress–strain conditions imposed in the hot face region due to cyclic operating temperatures.

B. Steel Plate Brick Support Ledges

Steel plate brick support ledges are often used in various types of lining geometries to support the lining or to restrain the thermal growth of the lining. Brick ledge plates are typically fabricated from the same type of steel used in the vessel shell plate. The ledges are then welded to the vessel shell plate. Ledge plates should be of such width (as measured perpendicular to the vessel shell plate) that the hot end of the ledge plate is not close to the lining hot face. If the ledge plate reaches too high a temperature, significant compressive plastic straining can take place at the hot face end, causing axial buckling in the ledge plate. The axial buckling can be due to excessive compressive thermal stress in the ledge plate or due to allotropic transformation (change in crystalline form) in the case of certain types of carbon steels. Certain types of carbon steels, when exposed to temperatures above 1200 to 1400°F, will cause allotropic transformation. Both effects can cause severe buckling of the ledge plate, resulting in deterioration of the refractory lining in the vicinity of the ledge plate. Ledge

plates should be of a width that only the cold end region of the refractory lining rests on the ledge. In addition, a compressible insulating blanket should be wrapped around the ledge plate for three reasons. First, the compressible blanket will minimize the thermal gradient effects in the lining resting on the ledge. Second, the blanket will soften the sharp edge of the ledge plate and minimize the load concentration on the lining. Both of these reasons will isolate the steel ledge plate from the refractory. The third reason is in regard to the temperature within the steel ledge plate. The blanket will reduce the temperature gradient within the ledge plate, thereby reducing the thermal stress within the ledge plate.

C. Steel Anchors in Monolithic Linings

Monolithic lining systems can consist of castable, plastic, or gunned refractories. Castables can be poured or vibrated. Vibrated castables are typically much stiffer than normally poured castables. Steel anchors are embedded in monolithic linings to make the monolithic lining more stable. The steel can be in the form of stainless steel wire anchors welded to the vessel shell plate. Anchors come in many complex configurations. (8). The more complex the configuration is, usually the greater the “pull-out” strength. Anchors can be as detrimental to the structural integrity of the refractory lining or can provide improved lining stability. Certainly without anchors there is always the question of lining stability. That is, will the lining remain as a monolithic lining? Although cracking is observed in the cold shutdown state of monolithic linings with steel anchors, the lining tends to remain as a monolithic. The incorrect use of steel anchors can also assist in the mechanical deterioration of the lining. The stainless steel anchors have a coefficient of thermal expansion of about two to three times that of the alumina-type refractory materials (see Table 3). This means that the stainless steel anchor is firmly embedded in the cold face side of the lining will expand more than the alumina lining and cause tensile fracture on the cold side of the lining. If the anchors are wrapped with mastic tape or coated with wax or plastic (7) that basically disappears at low temperatures so that the tensile fracturing due to this difference in expansion rates between the anchor and the refractory will not exist. However, tensile fracture cracks will still occur due to the through-thickness temperature gradient and the same thermo-mechanical response as previously discussed in cylindrical-type brick linings (see Figure 9). In the case of flat walls, the through-thickness temperature gradient will also cause cold face side tensile fracture. In order to minimize the amount of tensile fracture on the cold face side of the lining, coated or wrapped anchors for expansion allowance appears to be the best choice for the anchor design system. Steel anchor systems, such as steel mesh, should be avoided in the hot face side of the lining. The primary reasoning here, as in the cold face side, is the mismatch in the coefficient of thermal expansion between the steel anchor and

Table 3 Coefficient of Thermal Expansion of Lining System Materials

Lining system material	Coefficient of thermal expansion, ^a mm/mm/°C × 10 ⁻⁶
Stainless steel	17.0
Carbon steel	12.0
Alumina type refractory (60 to 70%)	6.8
Alumina type refractory (80 to 90%)	7.9
Magnesia type refractory (92%)	14.3

^aDivide by 1.8 to convert to in./in. °F.

the refractory lining. The steel anchors will expand more than the refractory causing the tensile fracture and severe distortions in the refractory, hot face region.

D. Lining Restraint

The dimensionality of the lining restraint is important in creating a stable lining. A stable lining means that the lining does not fracture easily and remains intact without large unrestrained movement in the bricks or castable. As previously discussed, anchors tend to keep the monolithic lining stable. A stable brick lining does not loosen and joints open. A cylindrical lining is an example of a well-restrained lining. Each brick is restrained in the circumferential, axial, and radial directions. This does not mean that expansion allowance is not used. Appropriate dimensional restraint means that the lining is contained and restrained in all directions and appropriate expansion allowance is used. The appropriate restraint means that the refractory has gained additional strength, as shown in Figures 2 and 3. The lining design has to consider the dimensionality of the restraint behavior in the heated condition. The lining is designed with as much three-dimensional restraint as possible compatible with the expansion allowance.

E. Flat Versus Cylindrical Lining Geometry

If one has a choice of selecting either a cylindrical or a flat lining (rectangular or square cross section) system, the cylindrical lining is the better choice. As shown above in the cylindrical lining example, the cylindrical lining is appropriately restrained in three directions, making the lining stable. The flat lining is, in turn, not well restrained. Typically, hangers are welded to the vessel flat wall plate to make the flat wall lining more stable whether it is a castable-, gunned-, or brick-type lining. The flat lining will tend to bulge inward (sometimes referred to as “thermal curl”) away from the vessel flat wall plate due to the through-thickness temperature gradient in the lining.

F. Minimize Cyclic Temperature to Minimize Lining Wear

Most materials tend to degrade when exposed to a cyclic environment. Refractory materials are no different. Cyclic heatup and shutdown of linings are detrimental to the refractory lining. Usually, any refractory lining system that is maintained at a constant temperature will last longer than a lining exposed to frequent heatup and shutdowns. The cyclic thermal straining will tend to degrade the refractory material. If the lining is exposed to high temperatures such that plastic straining is present, then the degradation becomes more severe. Therefore, cyclic heatup and shutdowns should be minimized as much as possible.

G. Design of Refractory Roof Hanger Support Systems

The design of refractory roof hanger supports should be designed such that they allow the in-plane expansion displacements of the refractory roof lining. The lining supports should not be connected rigidly and directly to the steel support system. In some cases the steel support is a steel shell plate. Stiff hanger systems welded directly to the vessel shell plate can cause undesirable distortions in the hanger system as well as in the steel support system. A rigidly connected hanger to the steel support will tend to overstress the refractory lining since the refractory hanger is typically embedded in the refractory lining. In the case of a steel plate support system with supports rigidly connected to the shell plate, the vessel shell plate can distort, resulting in deterioration of the surrounding refractory lining. Rigid refractory hanger systems are best designed with sliding-type connections between the hanger and the vessel shell plate. The key to a successful hanger support system is to allow for the in-plane thermal expansion of the lining relative to the plane of the support steel.

H. Use of Blanket and Board Materials for Expansion Allowance

Blanket and board materials are often used for expansion allowance materials in refractory lining materials (1). The lesser-density blankets allow a greater amount of expansion allowance because of the greater compressibility of these materials. Likewise, the more dense blanket and boards have less compressibility. The cylindrical refractory lining is used here as an example for the design of expansion allowance. Two types of refractory brick linings are used in this example, 70% fired alumina brick and a 60% magnesia brick. Also, the other parameters chosen here are the cylindrical vessel shell plate radius and the maximum process temperature. Table 4 summarizes the parameters used in the design of expansion allowance.

Table 4 Summary of Parameters Used in Expansion Allowance Example

Type of refractory brick	Coef. of thermal exp. of refractory brick, mm/mm °C and lining thickness, mm	Process temperature, °C	Vessel shell radius, mm	Vessel shell coef. of thermal exp. mm/mm°C	Vessel shell temperature, °C
70% Alumina	6.3×10^{-6} 229	1100	2200	11.7×10^{-6}	200
60% Magnesia	10.77×10^{-6} 229	1100	2200	11.7×10^{-6}	200

Blanket and board insulating material ranges in density from about 90 to 160 kg/m³ (6 to 16 pcf) and compresses to about 10 to 20% of the original unloaded thickness of these blanket materials, with denser material compressing to the lesser percentage (see Figures 10 and 11). A lightweight blanket of original thickness of about 6 to 7 mm will compress to about 0.6 to 1.4 mm. The maximum compression pressure load to cause this amount of compressive displacement is 10 to 20 MPa (1,450 to 2,900 psi). Once these low-density material have “bottomed out,” no more significant compressive displacement occurs. Board materials with densities in the range of 800 to 960 kg/m³ (50 to 60 pcf) will compress to only about 30 to 40% of their original thickness (see Figure 11). For these denser materials, the compressive load has a more gradual increase to the maximum compressive loads. The initial increase in compressive load starts at about 30% of the original thickness.

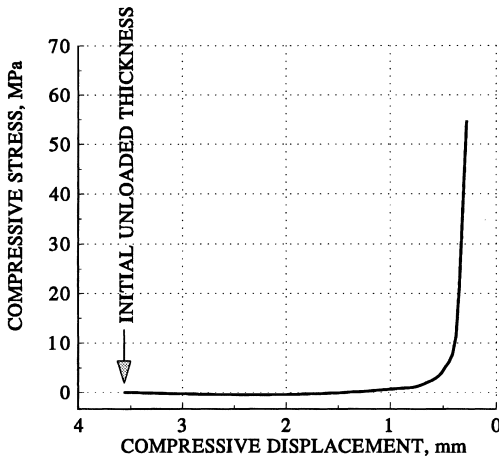


Figure 10 Compressive displacement-stress data for 160–190-kg/m³ blanket. (From Ref. 8.)

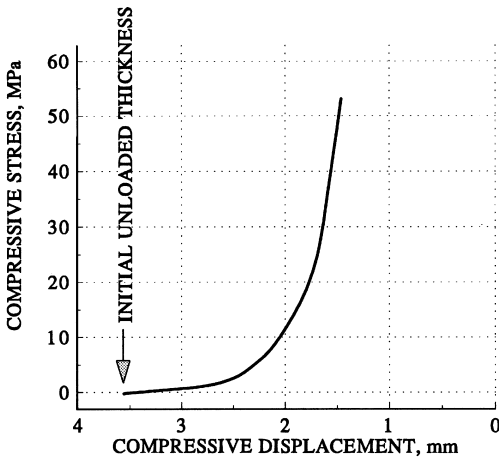


Figure 11 Compressive displacement-stress data for 800-kg/m³ blanket. (From Ref. 8.)

Table 5 summarizes the expansion allowance used for the typical range densities of blanket and board materials used as expansion allowance materials. Therefore, for a blanket material with a density of 160 kg/m³ and an initial thickness of 25 mm, the expansion allowance would be (0.94 × 25) 23.5 mm. Significant compressive thinning would occur in this lightweight blanket.

I. Alumina Lining Example

Using Table 4 parameters, the first example is for the 70% alumina lined vessel. The total expected difference in the radial displacement (ΔR_{DIFF}) between the hot

Table 5 Summary of Blanket and Board Compressive Behavior

Material density (<i>Q</i>)		Compressive pressure load range, MPa	Amount of expansion allowance, %C	^a Equation for estimating percent of thickness (C) used for expansion allowance
kg/m ³	pcf			
160	10	10–30	84	$C = 100 - 0.1Q^a$
560	35		44	
960	60		4	

^a*Q* is in kg/m³.

face region of the alumina lining and the carbon steel shell is

$$\begin{aligned} \Delta R_{DIFF} &= \Delta R_L - \Delta R_S & (5) \\ \Delta R_S &= R_L T_L \alpha_L - R_S T_S \alpha_L \\ &= (2200 - 229)1100 \times 6.3 \times 10^{-6} - 2200 \times 200 \times 11.7 \times 10^{-6} \\ &= 8.51 \text{ mm (3/8 in.)} \end{aligned}$$

To reduce the stress in the vessel wall without loss of lining restraint the 160 kg/m³ insulating blanket thickness of 6 mm is chosen to be placed between the lining cold face and the shell plate. This blanket will compress about (see Figure 12):

$$\begin{aligned} C &= 100 - 0.1 Q_B \\ C &= 100 - 0.1 \times 160 = 84\% \end{aligned} \tag{6}$$

Therefore, the remaining blanket thickness after compression is 6(1 - 0.84) = 0.96 mm. The thermal expansion allowance is 0.84 × 6 = 5.04 mm. The thermal expansion forces in the lining and shell are reduced to

$$F_{REDUCT} = \{(8.51 - 5.04)/8.51\} \times 100 = 41\%$$

of the original expansion loads without expansion allowance.

J. 60% Magnesia Example

Using Table 4 parameters for the 60% magnesia lined vessel, the total expected difference in the radial displacement (ΔR_{DIFF}) between the hot face region of the alumina lining and the carbon steel shell is

$$\begin{aligned} \Delta R_{DIFF} &= (2200 - 229)1100 \times 10.77 \times 10^{-6} - 2200 \times 200 \times 11.7 \times 10^{-6} \\ &= 18.21 \text{ mm (11/16in.)} \end{aligned}$$

As expected, the 60% magnesia lining expands more than the 60% alumina lining. To reduce the stress in the vessel wall without loss of lining restraint, the 160-kg/m³ insulating blanket thickness of 12 mm is chosen to be placed between the lining cold face and the shell plate. This blanket will compress to about 84% as previously calculated. Therefore, the remaining thickness after compression is {12 × (1 - 0.84)} = 1.9 mm. The expansion allowance is 12 × 0.84 = 10.1. The thermal expansion forces in the lining and shell are reduced to

$$F_{REDUCT} = \{(18.21 - 10.1)/18.21\} \times 100 = 44\%$$

of the original values.

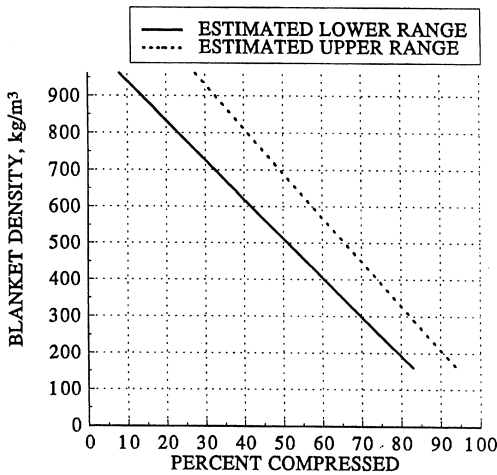


Figure 12 Estimated range of compressibility of blanket and board material.

It should be mentioned that these are example problems used to demonstrate the procedure for calculating expansion allowance. The actual lining system temperatures should be determined along with the thermal and mechanical material properties unique to the lining system being investigated. Field strain gauge tests along with FEA investigations should be made to establish the need for expansion allowance.

The previous two examples on lining expansion allowance used a blanket material laid in the circumferential direction between the lining cold face and the vessel shell plate. The expansion allowance can also be used in the radial joints in the brick lining. The relationship between the use of the circumferential allowance in the circumferential joint and the expansion allowance used in the radial brick joints originates with the basic equation of the circle:

$$C = 2\pi R \quad (7)$$

The expansion allowance in the circumferential direction ΔC (in the brick radial joints) and the expansion allowance in the radial direction ΔR (in the circumferential joint between the lining and shell) is

$$\Delta C = 2\pi\Delta R \quad (8)$$

Equation (8) shows that the amount of expansion allowance in the radial direction ΔR is

$$\Delta R = \Delta C / 2\pi \quad (9)$$

Therefore, the expansion allowance in the radial joints ΔC is 2π (about 6.28) times the radial expansion allowance ΔR . Continuing with the previous example for the 70% alumina brick, the number of radial joints is N . Assuming a total of 50 radial joints, the amount of expansion allowance per radial joint to accomplish the same expansion allowance is

$$\Delta C = 2\pi\Delta R = \Delta C = 2\pi \times 5.04 = 31.66 \text{ mm}$$

For each of the 50 radial joints, the expansion allowance in each radial joint is

$$\Delta C_J = 31.66/50 = 0.633 \text{ mm (0.025 in.) per radial joint}$$

Typically, the material used in the radial joints would not be a blanket material but rather a plastic material that would completely deteriorate at a low temperature of 150 to 200°C (300 to 400°F). Based on the portion of the lining radial joints that experience compressive loading (see Figure 9), the expansion allowance is not needed in the full length of the radial joint. The radial joint expansion allowance would start at the hot face end of the radial joint and extend inward to the location where the compressive load ends.

In most instances, the radial expansion allowance is preferred over the circumferential expansion allowance. The reason used is that the process material will not have an opportunity to penetrate into the radial joints with the radial expansion allowance.

X. SUMMARY AND CONCLUSIONS

Refractory linings are complex structures and made of complex refractory materials. When designing a refractory lining system, there are aspects of lining mechanical behavior that should be addressed.

1. There are two basic loads that are imposed on the lining, the gravity load and the thermal expansion load. The thermal expansion stresses are usually several orders of magnitude greater than the gravity load.

2. In order to have a stable lining it should be restrained in each of the lining major dimensional directions. A cylindrical lining would then be restrained in the circumferential, axial, and radial directions. The restraint results in two primary advantages to the lining behavior. First it makes a stable lining, and second it makes a stronger refractory.

3. Static compressive stress–strain (SCSS) data should be obtained on all candidate refractories. These data provide valuable information on which refractory has the greatest strain range, an important property for the thermal expansion strains.

4. Mortar joints are a form of expansion allowance. They will permanently compress. Expect some visual cracks in the cold shutdown condition of the lining.

5. For detailed investigations of refractory linings, computer analysis is required using the finite element method.

6. The cylindrical lining is one of the more frequently used lining geometries in most industrial operations. It is one of the more stable lining systems due to the nature of the lining restraint.

7. There are several do's and don'ts of lining design. The items listed should be carefully reviewed.

REFERENCES

1. Schacht CA. *Refractory Linings: Thermomechanical Design and Applications*. New York: Marcel Dekker, 1995.
2. Langer BF. Design values for thermal stress in ductile materials. *ASME Weld J Res Sup*. 1958; 37:411–418, Sept.
3. Griffith AA. The Theory of Rupture. *Proc. 1st Int. Con. Applied Mechanics*, Delft, The Netherlands, 1924:55–63.
4. Norton FH. *Refractories*. New York: McGraw-Hill, 1949:290–293.
5. Schacht CA. The effect of mortar joints on the thermomechanical behavior of refractory brick lining systems in cylindrical vessels. *AISE Spring Conference*, Birmingham, AL, March 1985.
6. Hartsock, MTS. Testing of Krial 70 HS Brick, Kaiser Aluminum & Chemical Corp., Lab. Service Report, March 21, 1984.
7. Schacht CA. Structural Behavior of Teeming Ladles Lined with High-Alumina Refractories. *AISE, Iron and Steel Engineer*, August 1984:33–40.
8. Crowley MS. Guidelines for Using Refractories in Circulating Fluidized-Bed Combustors. EPRI, Palo Alto, CA, 1991.
9. Cortney RL. Compressibility of Expansion Paper, Technical Memo, Kaiser Aluminum and Minerals Corp., (Natal Refractories and Minerals Corp., Proj. No. 49750, March 11, 1981.

14

Refractory Applications in Refineries and Circulating Fluid Bed Combustors

M. S. Crowley

M. S. Crowley Ltd., Crete, Illinois, U.S.A.

A number of process units in modern refineries depend on refractory linings to protect the shell from corrosion or erosion and to maintain an acceptable shell temperature. These units convert a feed stock of crude oil fractions into assorted components that are blended together to make gasoline, heater oil, jet fuel, etc. Temperatures may vary from near ambient to 1400°C (2550°F) or higher, with pressures ranging from vacuum conditions to around 2 MPa (300 psi). The atmosphere may contain corrosive agents such as hydrogen, sulfur compounds, salts, organic and inorganic acids, etc., which the refractory lining must resist. In addition, solid particles moving at high velocities may erode localized areas, especially when the particles must travel around a bend or corner, thus impacting the lining at a near-perpendicular angle. There are a number of papers listed in (1) and (2) that discuss various refractory requirements in refineries. Table 1 lists the properties of refractories commonly used in refining and petrochemical operations (1). Many of the properties vary, depending on the method of placement. Most process vessels are cylinders or spheres, and monolithic refractories (i.e., castables and plastics) typically are used due to their ease and speed of placement. The transfer lines that connect the vessels often must be lined with similar refractory materials to resist the process stream. This chapter deals with the units where refractories are essential components, that is, furnaces, boilers, catalytic cracking units, naphtha reformers, ammonia reformers, sulfur plants, incinerators, and circulating fluid bed combustors. In most cases, several different types of

Table 1 Typical Properties of Refractories Used in Refining and Petrochemical Operations

Products	Comment	Density, lb/ft ³	Compressive strength, lb/in ²	Modulus of rupture, lb/in ²	K-factor (see Notes)	Erosion loss, cm ³
Castables (Erosion-resistant)						
Standard	Without fibers	130–135	5,000–10,000	1,000–2,000	6–7.5	10–20
Gunned	Without fibers	120–140	4,000–12,000	1,200–1,800	5–8	8–16
Vibe-cast	Without fibers	140–170	5,000–15,000	1,000–1,200	7–10	4–10
Phos-bonded	Water is critical	165–170	4,000–9000	1,600–2,000	10–16	3–8
High-conductivity and special castables						
Standard cast	70–80% SiC	140–165	4,000–8,000	1,000–1,400	45–60	13–20
Gunned	70–80% SiC	136–160	3,000–12,000	1,000–2,000	50–65	7–10
Shock Resistant	Fused silica	115–125	4,000–12,000	700–1,400	4.5–6.5	8–20
Insulating castables (standard cast)						
Low-strength	Low k-factor	50–60	300–700	50–200	1.3–1.8	—
Mid-strength	Medium K-factor	80–90	400–1,100	200–250	2.5–3.5	—
Insulating castables (gunned)50–60						
Low-strength	Low k-factor	50–65	400–1,100	100–200	1.4–2.2	—
Mid-strength	Medium K-factor	85–90	1,100–1,700	300–400	2.7–3.6	—
Plastic-rammed						
High-alumina	65% Phos-bonded	155–157	1,000–2,000	1,200–1,400	5–6	13–15
High-alumina	70% Phos-bonded	163–169	1,900–2,000	1,600–2,000	8–9	7–8
High-alumina	85% Phos-bonded	170–180	4,000–7,000	1,900–2,400	11–14	6–8
SiC–80% SiC	Phos-bonded	160–168	1,700–3,400	1,100–1,300	60–70	12
Brick						
Super duty	40–45% Al ₂ O ₃	142–150	2,500–6,500	1,300–2,400	9–11.5	—
High-alumina	60% Mullite base	151–157	5,000–6,000	1,300–1,900	9–10	—

Notes: Thermal conductivity (k-factor) dimensions, Btu/(h-ft²-F)/in. Erosion loss per ASTM C704. Test conducted per ASTM methods. Mullite is an alumina-silica compound. Castables are tested without fibers, but use fibers in the field.

lining can be used successfully, and the final choice may depend on factors such as availability, speed of placement, and cost.

I. FURNACES

Generally, rectangular “boxlike” furnaces are used to preheat the oil before it is sent to the various process units. These furnaces usually only need to contain the hot flue gas and typically are not subject to corrosive or erosive conditions. Historically, the walls and ceilings of furnaces were often lined with high-temperature insulating block next to the shell covered with insulating firebrick, usually referred to as “IFB,” for the hot face. Figure 1 illustrates the need for adequate thermal expansion allowance with this type of lining. Failure to clean out and repack the expansion joints to keep them functioning resulted in buckling



Figure 1 Lining failure in furnace due to thermal expansion of insulating firebrick and inadequate allowance for expansion.

of the hot face. Floors use dense firebrick as the top layer to resist foot traffic and to support scaffolding. Thicknesses of each layer were usually determined by heat transfer calculations and desired shell temperatures and rounded up to the next-available standard thickness.

Combinations of dense and insulating castables have been used in some furnaces in place of insulating block and IFB. Unfortunately, poor anchorage of the dense castable occasionally has resulted in loss of the hot face layer, as seen in Figure 2. The design in Figure 3 is appropriate for units where severe mechanical impact, abrasion, or erosion is expected. A more detailed discussion of anchorage can be found in the literature (3,5). If no unusually severe mechanical damage is anticipated, a single layer of an intermediate-strength, medium-density castable is often the best compromise for maximum service life with good insulating value. Stainless steel fiber should be added to the castable in most cases for improved toughness and coherence (4). The fiber will improve the resistance to crack propagation even though the hot face is above 1000°C



Figure 2 Loss of furnace hot face lining due to poor anchorage.

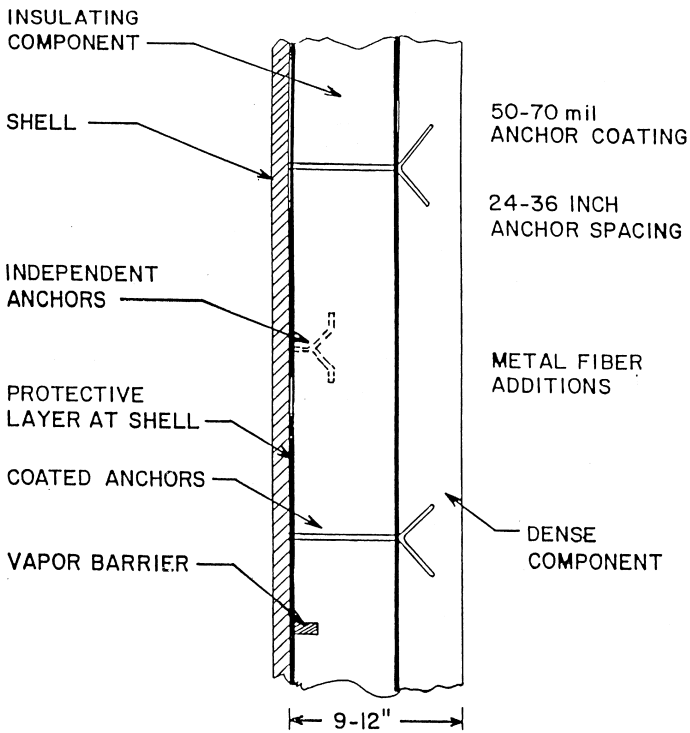


Figure 3 Lining design for areas of severe mechanical impact and erosion.

(1832°F) because the decreasing thermal gradient through the wall will ensure that the fiber in the cooler zone will remain effective.

Bridge walls of brick running down the center of the furnace may be used to achieve better control of the heat distribution inside the unit as seen in Figure 4. Care must be taken during shutdowns to clean out and repack the expansion joints to accommodate the thermal expansion that will occur when the furnace is brought on-line. Figure 5 shows the effect of inadequate expansion allowance in a division wall. It is imperative that all the expansion joints be fully functional to avoid buckling of the wall.

Many companies now prefer to use ceramic fiber modules or board and blanket systems due to their superior insulating value, ease of repair, and freedom from stringent curing requirements. Unlike castable linings, which must be heated slowly (e.g., <math>< 50^{\circ}\text{C}</math> per hour) to avoid explosive spalling during the initial dry-out, ceramic fiber linings can be safely heated at rates of several hundred degrees Celsius per hour (6). In addition, their flexibility allows them to bend



Figure 4 Stable lining and division wall in heater furnace.

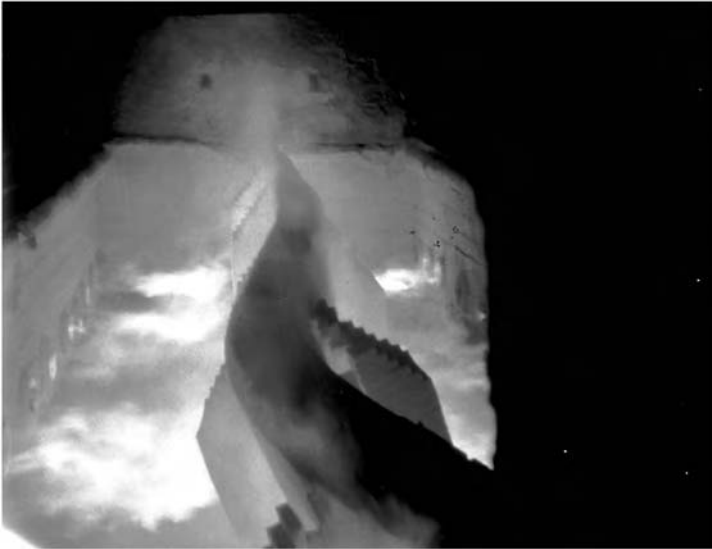


Figure 5 Unstable division wall due to lack of adequate thermal expansion allowance.

or compress when differential thermal expansion due to uneven heating causes the walls to move or flex. The poor erosion resistance of ceramic fiber, even to clean gas or air streams at high velocities, sometimes requires a zone of castable to withstand the localized service conditions as shown in Figure 6.

Modern boilers now have relatively few refractory lined areas due to the use of water-filled tubes (water walls) to convert the thermal energy to steam, which is used to drive a power turbine. Thin refractory linings on the tubes must be highly conductive to improve the thermal efficiency of the unit. These linings usually are based on silicon carbide due to its high thermal conductivity and may be fired tile or monolithic materials.

II. FLUID CATALYTIC CRACKING UNIT

One of the most essential units for the production of gasoline is the fluid catalytic cracking unit (FCCU), commonly called a “cat-cracker.” This unit, shown

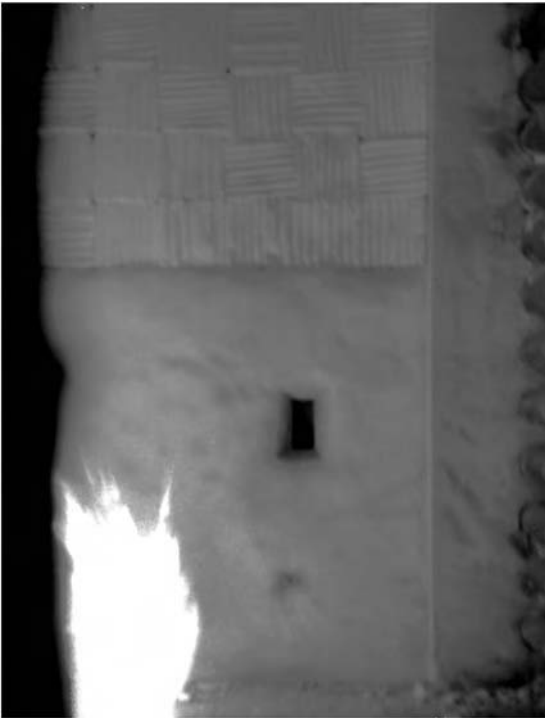


Figure 6 Lower castable zone to protect the refractory ceramic fiber from flame erosion.

schematically in Figure 7, consists of a regenerator and a reactor or disengaging chamber connected by refractory lined process lines (5). Both vessels have internal or external cyclones to separate the ultrafine catalyst from the gas stream. Each vessel requires a number of different refractory materials for various areas depending on the nature of the process atmosphere and the presence or absence of high-velocity particles. Typically, the areas of greatest concern are the regenerator cyclones and the spent catalyst return lines, where erosion is very severe and no coke deposition occurs to improve erosion resistance. Internal cyclone linings consist of 25 mm (1 in.) of extremely erosion-resistant refractory held in anchorage of stainless steel grid or gridlike independent anchors. Thermal conductivity is usually not a concern since the temperature is virtually the same on both the inside and outside of the cyclone and erosion resistance is the only consideration. The external cyclones and the spent catalyst transfer lines must have exceptional erosion resistance and lower the outside shell temperature to an acceptable level. A 100-mm (4-in.) lining of erosion-resistant castable is usually used for these locations.

Both the feed riser and the reactor linings will become coke-filled during operation and, their erosion resistance can increase up to 10-fold. While the feed riser is usually lined effectively with extremely erosion-resistant castable, attempts to use the same material in the reactor have not always been successful (7). The coke deposition results in very hard and brittle linings, which can spall during high stress periods caused by thermal fluctuations. Figure 8 shows two sections of a coked refractory fragment, before and after being fired to burn

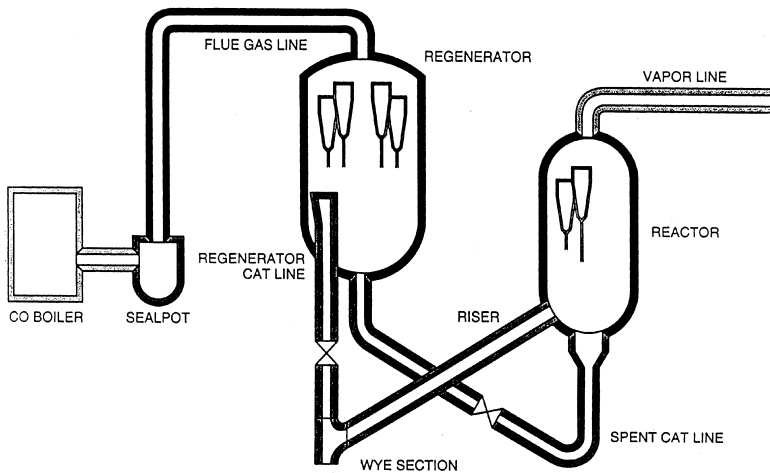


Figure 7 Typical fluid catalytic cracking unit.

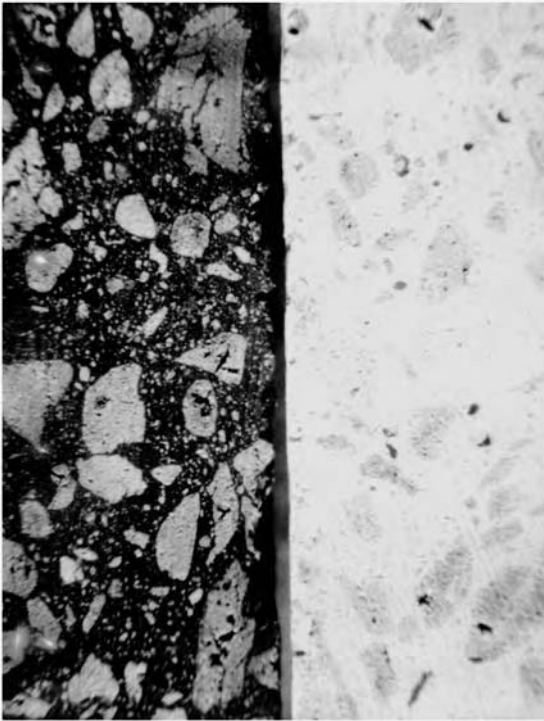


Figure 8 Coke-filled refractory castable before and after being fired to burn out the coke.

out the coke. Table 2 lists the changes that occur when a series of typical castables becomes coke-filled (7). A laboratory erosion test (ASTM C704) is used to differentiate between refractories with good to excellent erosion resistance. Test values of 5-cc volume loss or less usually are required before a material will be considered for trials in the field.

The walls of the vessels and the flue gas lines are often lined with medium-strength, medium-density refractories since there are few erosion problems and an acceptable shell temperature is the primary concern. Stainless steel fiber additions to the castable are strongly recommended since they have been shown to reduce maintenance costs. The elbows of the overhead flue gas lines may require better erosion-resistant materials because the flue gas can contain some catalyst dust that escapes from the cyclones. The cyclones are connected to a plenum chamber that is welded to the vessel head. The chamber collects the flue gases from the cyclones and transfers them to the overhead line. The plenum skirt has the same temperature on both sides and expands and contracts as the vessel temperature rises and falls. Castable refractory has been used to

Table 2 Physical Properties of Coked and Uncoked Refractory Concretes

Properties		High Strength	Dense	Semi- insulated	Insulated
Density, Gm/cc	Coked	2.89	2.40	1.97	1.56
	Uncoked	2.70	2.27	1.60	1.20
Cold crush Strength, MPa	Coked	170	145	72–123	29.60
	Uncoked	101	93.2	7.5–8.7	9.3
Porosity, %	Coked	7.6	7.0	0.8–1.7	nd
	Uncoked	27.0	22.0	41.5	43.0
Erosion loss, cc (C704)	Coked	2.9	3.16	6.5–7.9	nd
	Uncoked	5.5–6.5	6.4	42.6	nd

Notes: Coked samples were fired to 540°C in air to obtain the uncoked samples. A brief study of the thermal conductivity of an insulating refractory castable showed the coked sample was twice as conductive as the uncoked sample.

insulate the skirt and provide a cooling path for the critical weld of the plenum skirt to the vessel head. The outside lining usually requires extensive repairs at each turnaround due to the refractory cracking as the skirt expands and fracturing as the skirt shrinks upon cooling, as shown in Figure 9.

Refractory ceramic fiber is finding some use in insulating plenum skirts because of its ability to flex and accommodate movement in the plenum skirt. Care must be taken in designing some erosion protection for the lining due to the inability of ceramic fiber to withstand any erosive environment containing particulate material.

Slide valves are used to control flow in flue gas lines. The working faces are usually lined with an erosion-resistant plastic or castable refractory held in stainless steel grid or on independent anchors.

Seal pots are nonmechanical valves that use controlled water levels to regulate the flow of gas to the CO boiler. The refractory lining can change from a water-saturated condition at near-ambient temperatures to 700°C (1300°F) in less than 90 sec when the water level drops and hot flue gas starts into the CO boiler. The condition will reverse when water is put back into the pot. In this environment, materials with extremely good thermal shock resistance must be used to ensure maximum service life. Often, fused silica-based castables provide the best overall service.

III. NAPHTHA REFORMERS

Naphtha reformers operate in a hydrogen-rich atmosphere at temperatures around 535°C (1000°F) and at pressures up to 2 MPa (300 psi). Figure 10 is a cross



Figure 9 Fractured plenum skirt lining after repeated thermal cycling in regenerator.

section of a typical reformer lining and shows two layers of refractory castable, a dense, high-strength layer for mechanical integrity and an insulating layer for shell temperature control (8). Typical designs may call for low iron castables (i.e., <1% Fe) for the hot face to reduce the possibility of sulfur release during regeneration, which could poison the catalyst. A skirt to contain the catalyst bed may be welded to the shell. Thermal expansion of the bed during heating produces stresses at the weld, which can crack and allow hot, hydrogen-rich gas to flow next to the shell. Hydrogen gas at elevated pressures and temperatures above 430°C (800°F) can produce blisters and embrittlement in carbon and low-alloy steels. Special weld designs may be required to reduce the possibility of cracking at the skirt to vessel weld.

The thermal conductivity of refractories in hydrogen atmospheres increases significantly as hydrogen replaces air in the pores (9). Very light insulating castables (~30 lbs/ft³) may increase 3 to 4 times in thermal conductivity in a hydrogen-rich atmosphere at elevated pressures. Dense castables (~125 lbs/ft³) will increase around 50% due to the lower volume of pores as compared to insulating materials. No significant attack has been reported for hydrogen reactions with silica in naphtha reformers. This lack of reaction is probably due to the relatively low operating temperatures of naphtha reformers as compared to ammonia reformers.

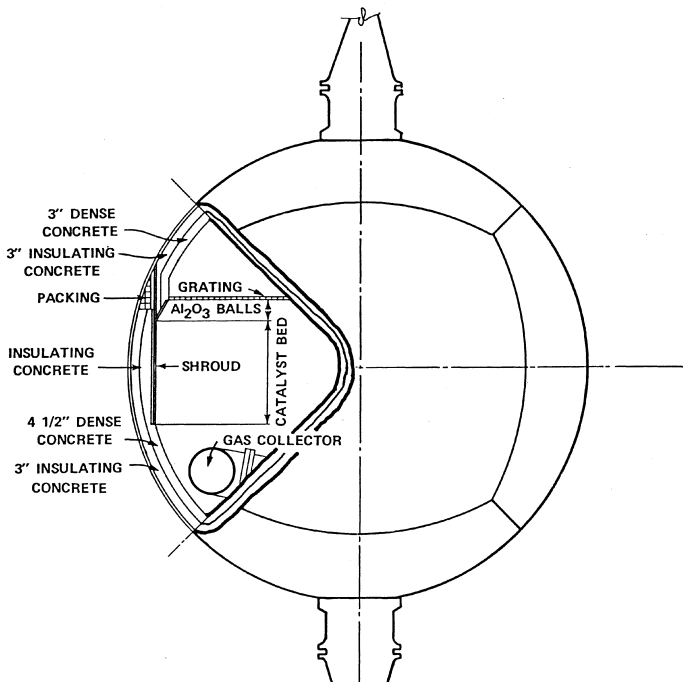
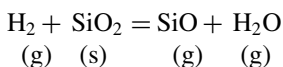


Figure 10 Cross section of refractory lining for naphtha reformer.

IV. AMMONIA REFORMERS

The secondary reformer in ammonia plants is shown schematically in Figure 11 and illustrates two lining designs (8). In the "fire-ball" area above the catalyst bed, the temperatures reach 1350°C (2460°F). The incoming hydrogen-rich gases are reacted with air to consume any residual methane and some of the hydrogen, leaving hydrogen, water vapor, carbon monoxide, and nitrogen. Early designs were plagued with silica carryover that fouled the heat exchangers. The deposits were found to be silica and silicon metal. It was determined that the hydrogen-rich process gas was attacking the mixture of silicates in the catalyst support media and the refractory walls. The reaction can be shown as



Thus, a solid and a gas react to form two gases (10). When the temperatures drop in the heat exchanger, the silicon monoxide undergoes disproportionation to

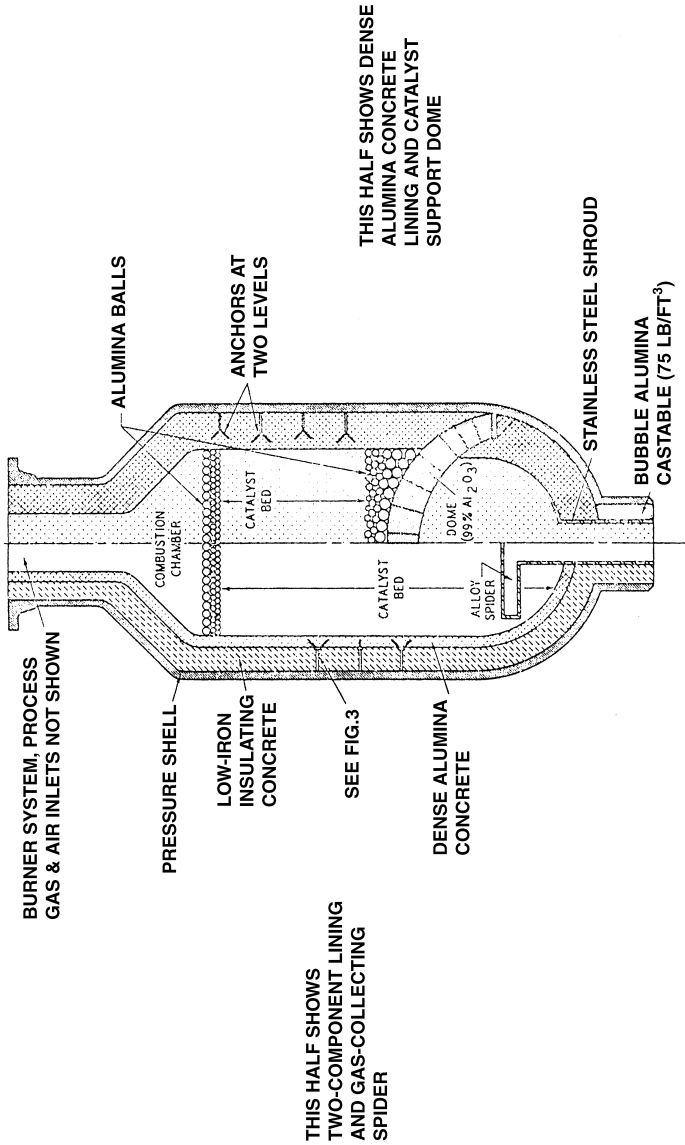


Figure 11 Two lining designs for an ammonia plant secondary reformer.

silica and silicon metal. The temperature required for silica loss in high-alumina refractories generally starts around 870°C (1600°F), as shown in Figure 12, and the weight loss increases exponentially as the temperature increases (11). Higher pressures and water contents decrease the silica loss. Current secondary reformer designs call for a dense, high-alumina castable for the hot face over an insulating castable layer.

The primary reformer is a conventional box furnace using insulating block and IFB or a refractory ceramic fiber system for the walls and ceiling. Dense, superduty brick over insulating block or over insulating castable usually forms the floor.

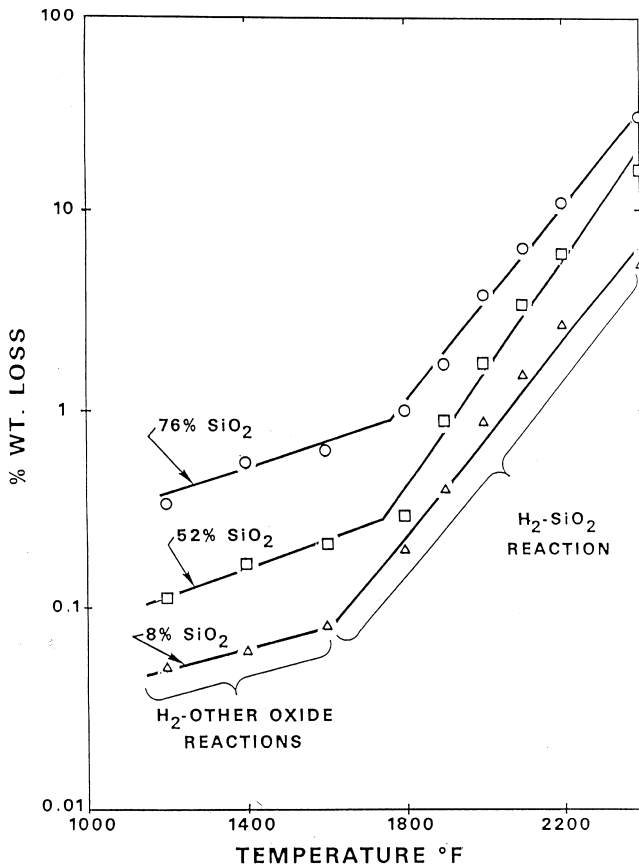


Figure 12 Silica loss as a function of temperature for several refractory specimens.

V. SULFUR PLANTS

Modern sulfur plants combust hydrogen sulfide and other sulfur containing gases to reclaim the sulfur and get rid of unwanted gases. The primary combustion unit is a horizontal cylinder with a large burner in one end and a heat exchanger on the other. Operating temperatures are around 1400°C (2550°F). The chamber is lined with high-alumina brick—frequently mullite-based—and may have a lining constriction, called a choke ring, toward the burner end that transforms the cylinder into two chambers. Near the burner is the intensive mixing chamber to ensure maximum combustion of the incoming gases. This zone is followed by a longer residence-time chamber to ensure complete combustion of all the gases. With proper refractory selection, the lining should last many years, since it only has to withstand the temperature and thermal cycling.

Figure 13 shows a sulfur combustor in which the choke ring of tabular alumina castable softened and fell onto the floor. The pile of refractory rubble deflected the burner flame toward the roof of the chamber and resulted in the roof bricks collapsing and exposing the shell to the operating temperatures. An analysis of the choke ring material revealed that the ring was not made of tabular alumina aggregate and pure calcium aluminate cement, a standard material with an effective use temperature of 1800°C (3275°F). Instead, the ring was made



Figure 13 Deformation and loss of refractory choke ring and lining in a sulfur combustor.

with an addition of silica fume to the conventional mix, an additive that provides excellent low- to intermediate-temperature strength and good working properties. Unfortunately, the addition of the silica fume radically changed the chemistry of the refractory mix. This change allowed the formation of anorthite, a low-melting-point phase that reduced the maximum use temperature to around 1250°C (2280°F) and resulted in extreme softening of the material at the designated operating temperature.

VI. INCINERATORS

Refineries generate significant quantities of waste materials that are most easily disposed of by incineration. Figure 14 shows a typical fluidized bed incinerator using sand as the bed material. The interior is lined with superduty fire brick and operates around 1000°C (1832°F). Thermal cycling and mild abrasion are the



Figure 14 Fluidized sand bed incinerator for refinery waste products.

primary service conditions for the refractory. Frequently, large clinkers of ash, primarily composed of sodium sulfate, are formed that can interfere with the operation of the unit. Periodic shutdowns are usually required to clean out the unit and replace any broken or missing brick. Excessive thermal cycling can result in sand wedging into the brick joints and causing “pinch spalling” and brick loss. The cyclones and flue gas lines will see some erosion from fine sand and some cracking from thermal cycling. Dense, high-strength castables over an insulating layer are usually used for these areas.

VII. CIRCULATING FLUID BED COMBUSTORS

Circulating fluid bed combustors (CFBCs) are commonly used for waste to energy power units, and as power generating systems using previously unusable fuels. Figure 15 illustrates a typical circulating fluid bed combustor with the critical areas identified (12). CFBCs are similar to fluid catalytic cracking units in refineries in that they contain circulating solids moving at high velocities in a hydrocarbon atmosphere at elevated temperatures. The primary differences involve temperature swings of 540°C (1000°F) or higher within a few minutes and high-velocity solids ranging in size from fine sand to marble-sized rocks.

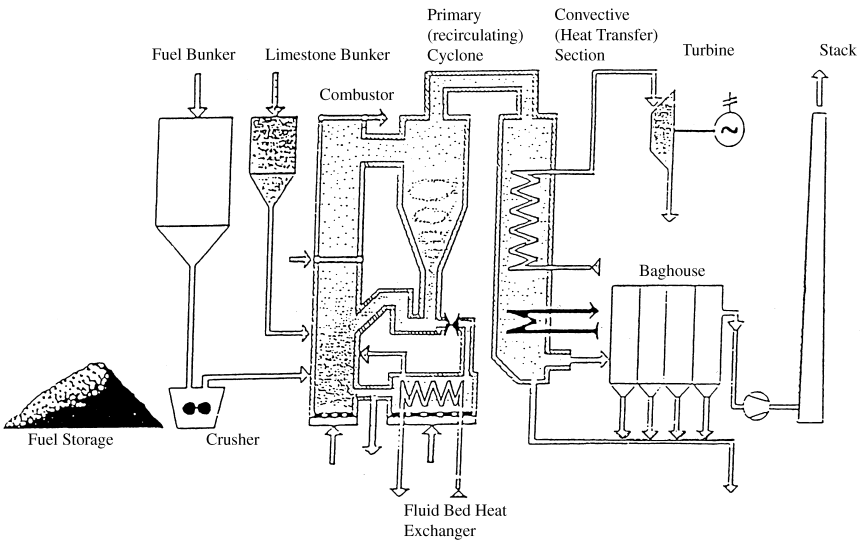


Figure 15 Typical circulating fluidized bed combustor.

Very large quantities of fossil fuels in America were mined decades ago and never used. These mountains of discarded coal were abandoned because they were not usable due to their high sulfur levels and ash contents above 50%.

Modern combustion methods now utilize ground limestone as a sulfur collector, forming calcium sulfate in the reactor bed. Figure 15 shows crushed fuel and limestone being added to the combustion bed above the fluidizing air grid where the fuel is consumed and the limestone reacts with the sulfur in the fuel (12). The flue gas containing some particulate material is transported up the combustor and into the crossover duct to the primary cyclone where the bulk of the solids are spun out and returned to the combustion bed through the dip leg and loop seal at the bottom of the cyclone. Portions of the fluidized bed must be continually drawn off in order to allow more fuel and limestone to be added without filling up the combustor. These reductions from the fluidized bed are either discarded or sent to an external heat exchanger before being discarded. The refractory lined areas include the combustion zone, the water walls, the combustor roof and cyclone inlet duct, the cyclone walls and cone, the dip leg and loop seal, the spent ash return line, the external heat exchanger, and the wind box below the combustion zone grid.

The combustion zone operates around 870°C to 1000°C (1600°F–1800°F) and is generally reducing (i.e., oxygen-deficient) in nature with a slight positive pressure. The main destructive agents are severe thermal shock and spalling resulting from periodic disruption of the fuel feed and the quench action of the water walls, which run continually. Abrasion and erosion from the input of fresh feed and recycled ash into the fluidized bed contributes to the attack. Lining materials low in iron or iron oxide are suggested to reduce the possibility of CO disintegration, a process that causes an internal disruption of refractories as carbon deposits on iron sites. Phosphate-bonded plastics using mullite-based aggregate have been used successfully to resist the erosion, thermal shock, and frequent temperature cycling found in the combustion zone.

The water wall area is not usually lined, since the majority of the heat transfer is expected to occur in this zone. The base of the tubes at the top of the combustor lining may have a silicon carbide tile or a thin layer of high-conductivity plastic refractory to reduce the erosion of the tubes as the ash slides down the tubes and hits the combustor lining. The water walls consist of a series of water-filled tubes connected by fins to form a solid wall that functions as a super heat sink. Any disruption in the feed flow results in a very sudden and severe temperature drop as the water wall drains the heat from the flue gas stream.

The combustor roof and cyclone inlet duct can see severe to moderate erosion and thermal cycling as the dust-laden gases turn to enter the cyclone. Two-component linings of an insulating layer protected by dense, erosion-resistant castable with stainless steel fiber and organic “burnout” fibers are often used in this area.

The cyclone lining is exposed to temperatures of 1000°C (1832°F) or higher, severe and rapid thermal cycling, and moderate to very severe erosion. Attempts to use a thick lining of dense castable over an insulating layer were not successful due to the repeated thermal cycling, thermal shock, erosion, and pinch spalling, which caused large sections to fall out. Attempts to replace these failed sections usually were not successful.

A current trend in cyclone linings is to use multilayer brick linings with an insulating layer next to the shell, insulating fire brick next, and an abrasion-resistant hot face layer of dense mullite-based brick. Units have also been made with the entire cyclone made of water wall sections with thin, silicon carbide-filled plastic refractory on studed tubes. Since the cone area lining actually rests on the metal shell, vibratory cast linings of low or ultralow cement-based castables have been used due to their excellent erosion resistance, low shrinkage, and good thermal shock resistance.

The cyclone dip leg and loop seal have often experienced severe problems due in part to poor installation workmanship. The service conditions, such as thermal shock, cycling, and severe erosion, are similar to those in the cyclone; however, the restricted access and tight working environment make proper installation very difficult. New units have the advantage of doing the installation in sections. Thus, the refractory lining can be vibration cast using dense erosion and shock-resistant castables over insulating castables. Dense brick linings also can be more easily installed before the sections are assembled. The spent ash return line from the loop seal to the combustion chamber is lined in the same fashion as the loop seal. Repairs are usually done using phosphate-bonded plastic refractory with additional anchorage if required.

The external heat exchanger and ash cooler areas require linings with excellent thermal shock and erosion resistance. Fused silica-based castables have been used in the division walls.

The wind box is below the combustion chamber grid and supplies the fluidizing air for the combustion zone bed. Erosion usually is not a concern, and a relatively thin insulating lining might be considered adequate for the service. However, new units may experience 20 to 30 cold starts in a year as run parameters are being developed. Lining/shell distortions and thermal shock fractures due to the repeated cold starts may call for a dense, low-expansion, thermal shock-resistant castable to provide an adequate service life.

In addition to utilizing discarded piles of high ash fuel, CFBCs are also used to obtain power from waste products such as scrap from lumber operations, animal and plant byproducts, and industrial waste. A major concern in selecting the refractories for a waste to power unit is the chemistry of the feedstock, which may contain high levels of alkalis, alkaline earths, and metallic compounds, which can react with the refractory lining to cause excessive expansion or shrinkage, low melting phases, and other disruptive actions. Extensive testing of the

proposed refractories in an atmosphere that truly reflects the actual combustion atmosphere is necessary to ensure that the unit will not immediately develop refractory problems.

A very high level of potassium vapor in a waste to energy plant caused the brick lining to expand and fracture due to the formation of kaliophilite from the reaction of the glassy matrix with the vapor. The kaliophilite/matrix reaction resulted in a large volumetric expansion and distortion of the brick. The problem was solved when the mullite-bonded brick was replaced with a phosphate-bonded brick.

REFERENCES

1. Brosnan DA, Crowley MS, Johnson RC. CPI drive refractory advances, *Chem Eng Oct*; 1998:110–120.
2. Hogue LD. Refractories for the Refining Industry, *Advances in Refractories for Incinerators, Waste Disposal and Petrochemical Applications, 27th Annual Symposium on Refractories*, St. Louis Section. The American Ceramic Society, May 23–24, 1991.
3. Crowley MS. Anchors for refractory concrete linings. *Oil and Gas Journal* 1982; 80:122–125.
4. Crowley MS. Steel fibers in refractory applications. *NPRA Refining and Petrochemical Plant Maintenance Conference*, paper #MC-81-5, February 17–20, 1981.
5. Harbison-Walker Refractories. *Modern Refractory Practice*. 5th ed. Pittsburgh, PA: Harbison-Walker Refractories, 1992:AP39–AP41.
6. Crowley MS, Johnson RC. Guidelines for installing and drying refractory concrete linings in petroleum and petrochemical units. *American Ceramic Soc Bull* 1972; 51:226–230.
7. Crowley MS, Schacht CA. A comparison of the thermo-mechanical properties of “As Installed” vs. “Coke Filled” refractories for fluid catalytic cracking units, *UNITECR '97*, 3:1643–1652, American Ceramic Society, 1997.
8. Bakker WT, Crowley MS. Requirements for ceramics in coal gasification processes. *Proc. of ERDA/FE-NSF Workshop on Ceramics for Energy Applications*, Columbus, Ohio, 1975:153–202.
9. Crowley MS. The effect of high-conductivity gases on the thermal conductivity of refractory concrete linings, Paper no. 64-PET31. *ASME Petroleum Mechanical Engineering Conference*, Los Angeles, CA, Sept. 20, 1964.
10. Crowley MS. Hydrogen silica reactions in refractories. *Am Ceram Soc Bull* 1967; 46:679–682.
11. Crowley MS. Hydrogen Silica Reactions in Refractories, Part II. *Am Ceram Soc Bull* 1970; 49:527–530.
12. Crowley MS, Bakker WT, Stallings J. Refractory applications in circulating fluid bed combustors. *Eleventh International Conference on Fluidized Bed Combustion*, ASME, Montreal, Quebec, Canada, April 21–24, 1991.

15

Byproduct Coke Oven Battery Heating Wall Refractories—Damage and Causes of Failure

Roger L. Rueckl

Independent Refractory Consultant, Apollo, Pennsylvania, U.S.A.

I. INTRODUCTION

The ovens in a slot-type byproduct coke oven battery are separated by the heating walls. The heating walls consist of a series of vertical and separate chambers called flues. A single heating wall can have from 24 to 34 flues. A mixture of preheated air and a fuel gas is introduced into the bottom of these flues. The combustion of this mixture inside the flue heats the wall from the inside, thereby heating the ovens separated by the walls. Each flue on each wall is equipped with an observation port or inspection hole on the battery top. Through these inspection holes, the conditions inside the flue can be observed and/or measured, for example, flue temperature. A battery can have nearly any number of ovens, from as few as 30 or 40, to as many as 70 or 80. There is always one more heating wall in a battery than there are ovens in a battery.

The coke oven battery is a refractory structure, contained within a steel and/or concrete exoskeleton. This exoskeleton is held together in the lateral direction by a series of tie rods between steel buckstays. The buckstays are vertical steel beams located on the ends of the heating walls between the ovens. In a longitudinal direction, the tie rods extend between the pinion walls on either end of the battery.

The coal to be coked is usually introduced into the ovens through openings in the roof of the battery called charging holes. The coal is charged as either “wet” coal, or “preheated” coal. When a battery is operated on “wet” coal, the

coal contains some moisture, as the name would indicate. In addition, wet coal is usually treated with some fuel oil, which aids in controlling the bulk density of the coal blend. All wet coal batteries are charged with a larry car, which is a vehicle with multiple bins or hoppers (the number of bins coinciding with the number of charging holes). These hoppers on the larry car are filled with coal. The larry car then travels along the length of the battery on rails, stopping over a specific oven, where the coal is fed into the charging holes of the oven. The emptying of the larry car hoppers may be by gravity alone or may be metered into the oven, for example, with a screw conveyor. Typically, on a wet coal battery at full production, an oven is pushed and charged about every 18 hours.

A battery operating on “preheated” coal has the coal cycled through a preheating system, where it is brought up to a temperature in the range of 180°C to 220°C prior to charging into the ovens. In the 1960s and 1970s, a number of batteries were constructed to use preheated coal. For a preheated coal battery, the coal can be charged pneumatically through a pipeline, on a conveyor system that spans the length of the battery, or from a hot larry car. Unfortunately, most of the preheated coal batteries have been abandoned, due to severe damage. A battery is designed to use either wet or preheated coal and, in most cases, cannot be readily switched over to operate on the other coal. On a typical preheat coal battery at full production, an oven will be pushed and charged about every 13 hours. Therefore, for the same oven volumes, a preheated coal battery will produce significantly more coke.

There are also other significant differences between wet and preheated coal. A preheated coal, ground to about the same fineness as a wet coal, has much lower intergranular friction; therefore, if poured into a pile, preheated coal will have a much lower angle of repose. In fact, preheated coal dropped on a flat surface will spread nearly like a liquid.

The battery has a pusher side and a coke side. On the pusher side of the battery there is a large machine, with an extendable ram used to push the coal converted to coke at the end of the coking cycle, from the slot-type ovens. The coke exits the ovens on the coke side of the battery, through a coke guide and into a quench car. The hot coke in the quench car is then water-cooled in a quench tower. Coke is a necessary component for the production of iron in a blast furnace.

The heating walls have traditionally been constructed of silica brick refractories (see Chapter 6). Silica is the refractory of choice primarily because, at normal coke battery operating temperatures, silica refractories are subject to minimal creep. Also, since nearly all of the expansion of silica brick takes place below about 650°C, during normal operation of a battery, the moderate temperature fluctuations of the walls have no effect on the volume stability of the refractory comprising the wall.

The silica refractories are manufactured as multiple asymmetric shapes, which are normally keyed or interlocked with each other by means of tongues

and grooves. A coke oven battery design can have well over 400 different shapes used in its construction. These shapes are installed with a silica mortar, which is primarily composed of the silica mineral quartz. In general, there are two types of mortar used, an air setting, which contains a small amount of sodium silicate, and a heat setting, which is basically the same mortar, but without the sodium silicate. Silica mortar of either type typically does not bond to the silica brick at normal battery operating temperatures. Therefore, it does not impart any strength to the wall.

Further, because the primary mineral constituent in the mortar is quartz, the mortar is not volume-stable. The quartz in silica mortar installed in an operating battery will slowly convert to the high-temperature forms of silica—tridymite and cristobalite—during normal battery operation. This conversion is accompanied by a significant increase in volume. This conversion happens first on the hotter flue side of the wall. This means that the mortar in the horizontal joints assumes a wedge shape; thicker on the flue side and thinner on the oven side of the wall.

A heating wall in a byproduct coke oven battery can be likened to a slab that is fixed all around its perimeter. The dimensions of a heating wall will vary, depending on the specific battery. Coke batteries are described as being a “3-meter battery” or a “6-meter battery.” This dimension refers to the height of the oven chamber and therefore the height of the surface of the wall. The length of the wall will also vary from something under 12 m to well over 15 m. The average thickness of the wall will fall within a relatively narrow range, from about 0.75 m to slightly more than 1 m.

The oven chambers are tapered along their length, and the walls are also tapered along their length. The ovens are wider on the coke side and narrower on the pusher side of the battery. The walls are wider on the pusher side and narrower on the coke side of the battery. The taper on an oven or a wall can vary from about 60 mm to nearly 90 mm.

Due to the unusual dilation curve for silica brick, the heating walls in a coke oven battery must be very slowly heated to prevent damage to the refractories. Once heated, the silica refractories can be expected to undergo 1.2% to 1.3% linear expansion. Almost all of this expansion will take place at temperatures below about 650°C. Therefore, the length of a wall can increase 15 cm to 20 cm during heatup, and the height can increase 6 cm to 8 cm.

Under normal operating conditions, the average typical internal flue temperatures will be in the range of 1325°C to 1375°C. Under the same typical conditions, oven temperatures will be in the range of 1065°C to 1120°C. However, there are temperature gradients in the battery. There is a vertical temperature gradient within each flue since the gas–air mixture is introduced and burned near the bottom of each flue. This vertical gradient is in the range of 40°C to 50°C. There is also a gradient in the average flue temperature from the pusher side to the coke

side. Since the oven is wider on the coke side, the heating wall must be hotter on the coke side. This “cross-wall” temperature gradient is in the range of 45°C to 50°C.

II. HISTORY OF BYPRODUCT COKE BATTERIES

Early byproduct batteries were small, having oven or wall heights of 3 m or less. These short batteries could have useful lives of 40 or more years. However, as oven height increased to 5 m, 6 m, and even greater than 7 m during the mid- to late 20th century, battery life became a cause of serious concern. Many of the taller batteries experienced premature failure, leading to their early abandonment, especially in North America.

Many tall batteries were abandoned after less than 10 years of service; some in as few as 3 or 4 years. Since the capital investment required for the construction of a large coke oven battery is substantial, these premature failures adversely affected the overall economics of iron and steel production. It is not unreasonable to say that the shortened life of coke making facilities in the latter part of the 20th century was one of the primary stimuli for the interest in direct steel-making research. If successful, direct steel-making would eliminate not only the coke ovens, but the blast furnaces as well, however, to date, direct steel-making has not proven to be a viable technology.

While the potential improved economics of the high-production, tall coke oven batteries were attractive to the industry, the track record of many of the tall ovens resulted in a hiatus in the construction of batteries during the late 20th century, particularly in North America.

III. HEATING WALL DAMAGE

A detailed study of the severely damaged and abandoned, 6-m, No. 2 Coke Battery at United States Steel’s Fairfield Alabama Works was done (1). This battery was designed by the then Firma Carl Still. It was a single divided battery with a large horizontal flue. This battery had been in operation for less than 4 years. This battery was operated on preheated coal, which was charged into the ovens by a hot larry car.

For this study, three of the heating walls were taken down, one tier or course of brick at a time, and all of the damage charted. All three of the walls displayed similar damage. The primary cause of damage was concluded to be flexure or movement of the heating walls in response to unbalanced differential pressure across the heating wall.

Earlier, a heating wall was compared to a slab that is restrained on all four sides. When a pressure is applied to one side of this slab or wall, areas of stress will be induced in the areas of the slab adjacent to the restrained sides. During wall flexure, these stressed areas will curve slightly as pressure is applied to the wall.

During flexure of a heating wall, the distribution and concentration of stresses in the walls refractories will be somewhat influenced by the basic design of the heating wall, and to specific details related to the keying or interlocking of the shapes and/or the courses of brick. There will be subtle differences in stress distribution among battery designs such as twin-flue, four-divided, double-divided, and single-divided.

The forensic study of the Fairfield battery showed that damaged bricks were present in the heating wall in the first five to seven flues from ends of each wall, in the first three courses of brick immediately in the bottom of the wall, and in the upper wall, in the area immediately below the horizontal flue—basically, around the periphery of the wall. In addition, the binder columns, which connect the two faces of the wall together and essentially form the individual flues, were found to be severely damaged near the ends of the walls. Damage, in the form of cracked brick, was usually associated with the areas of the individual brick that were interlocked, primarily at the tongues and grooves. Stress appears to concentrate in the interlocked or keyed areas and is not distributed uniformly through the whole brick shape.

The observations made during the forensic study of the three walls in the Fairfield coke battery indicated that heating wall damage was caused by wall flexure in response to unbalanced pressures on the heating wall. During flexure, a heating wall is distorted both horizontally and vertically. The wall damage is related to the bending stresses that are associated with areas of high wall curvature. In the horizontal cross section, the curvature occurs in the end flues, and also in an area four to six flues from the wall end. In the vertical section, curvature tends to take place near the bottom of the heating wall, and in the upper part of the wall.

Wall flexure behavior in the vertical section is, to some degree, dependent on the specific battery design. Stress distribution in the upper wall area will be different in a heating wall with a large horizontal flue opening, compared to a wall with a twin-flue design and its accompanying smaller horizontal opening and greater lateral continuity.

While other batteries were not studied with the same detail as the Fairfield battery, very similar damage patterns been observed in other coke batteries that were being partially dismantled prior to making repairs. Similar patterns of individual brick shape failure have been observed in at least six other coke batteries. In other words, wall flexure in response to unbalanced pressures on heating walls apparently accounts for much of the damage observed in coke battery heating walls, especially in regard to damage observed in end flues, and in the brick along the floor of the oven.

This premise would apply to all byproduct coke oven batteries, regardless of size or height. The greater the height of a heating wall, the less resistance to flexure. The ability of a heating wall to resist lateral pressure decreases as the inverse of the square of the wall height. In other words, a 6-m wall's ability to resist lateral force, and therefore flexure, is only about one quarter that of a 3-m wall.

IV. DEFINING THE CAUSES OF HEATING WALL FLEXURE

The existence of differential pressure across a heating wall, and the subsequent flexure of the wall, would mean that some part of the wall undergoes some movement. This movement would mean that stresses are being induced in the wall refractories. These stresses would be the greatest in the areas of the wall that realize the minimum radius of curvature during wall displacement. The level of stress and the ability of the refractory shapes to transfer the stress away from the high stress areas (i.e., areas of minimum radius of curvature) would determine whether failure of the refractory would occur. The failure either could be catastrophic or could occur slowly over time. Since the ovens in a normally operating coke battery are continuously charged and pushed, the stresses induced in a wall are cyclic, and possibly cumulative.

The movement of a heating wall is therefore indicative of the existence of a differential pressure between two ovens on opposite sides of the wall (2,3). Further, since the silica refractories are considered neither elastic nor plastic, the movement would indicate some level of stress in the wall's refractories. It is reasonable to suggest that increased displacement of a wall would indicate the potential for increased stresses. If this movement could be measured, the coincidence of the movement with other coke battery operating variables might be defined, and possibly control of the variables associated with movement might lead to means to minimize flexure, minimize wall damage, and maximize battery life.

Following the American Iron and Steel Institute's (AISI) sponsored Symposium No. 11 on "Tall Coke Ovens—Past, Present and Future" in 1983, the multicompany Task Force on Tall Coke Oven Collaborative Technology was formed. In 1985 this task force elected to sponsor a project on the measurement of movement of heating walls *in normally operating coke batteries* as a means of ascertaining when wall movement occurs. The project included the design and development of appropriate hardware to accurately monitor wall movement. The project was conducted in four phases, at four coke plants on five different operating batteries, over a period of about 6 years. In all, 13 field trips were made to gather data. Each of the four phases was carried out as a number of test series, with each test series having a specific objective.

The development of an on-line, nonintrusive sensor to monitor heating wall movement on an operating coke battery was a major part of the first phase of the project. The plan was to develop a sensor based on computer analysis of a video image of a target attached to the inside of a flue of a heating wall. This image was to be acquired by a precisely located and referenced television camera system aimed down a flue inspection hole on the top of the battery. The camera was mounted on a lockable gimbal equipped with highly accurate angular accelerometers. The camera system was enclosed in a very heavy, insulated and water-cooled container, which was bolted to the top brick paving of the battery over an inspection hole equipped with a quartz window. The camera system, in its container, was connected to a remotely located computer analysis system.

Ideally, the target to be monitored would be located at about two third's wall height, near where maximum movement would be expected. This target would be from about 11 to 13 ft (3.35 m to 3.96 m) below the top paving of a 6-m battery, where the television camera was positioned.

The sensor system was calibrated with a specially designed calibration frame. With this 18-ft tall frame with a precisely located simulated target, system accuracy as a function of distance to the target and magnification could be determined. At projected target distances of 11 to 13 ft between the camera system elevation and the target, the accuracy of the measurement system was better than plus or minus 0.003 in. (about 0.076 mm). The calibration was consistently repeatable and reproducible. The entire system was recalibrated prior to each field trip for data acquisition. In its final configuration, the sensor system was capable of taking measurements of a target's position automatically.

The measurement of heating wall movement on the different operating batteries produced consistent results. In all cases, when an oven was charged with coal, the walls adjacent to that oven moved away from the charged oven nearly instantaneously. It was found that from 40% to nearly 100% of the movement could take place within the first 30 minutes following the coal charge. A secondary movement might or might not follow the primary movement. Wall movement is reversed when the oven on the opposite side of the wall is charged, typically about one half the length of the coking cycle later. Therefore, heating wall movement is cyclic, is initiated by oven filling, and is correlated to oven charging and coal properties. The study was done in four parts, Phase I, Phase II, Phase III, and Phase IV.

A. Phase I

During Phase I, the sensor discussed above was not yet operable, and the deflection measurements were made using precision optical methods wherein the longitudinal position of a target inside the heating wall was referenced to a fixed benchmark on top of the battery. This method, while accurate, was labor-intensive and did not

readily allow for long-duration test series. The primary objective of this phase was to demonstrate that deflection or movement of a heating wall was related to events taking place in the ovens that were adjacent to that wall. This phase was conducted on a 6-m coke oven battery operating on preheated coal, which was conveyor-charged. Phase I was conducted in three test series.

The objective of the first series of Phase I was to measure the movement of an original wall in a 9-year-old battery, under normal operating conditions. That is, the No. 8 and 9 ovens on both side of the number 9 heating wall would be charged and pushed in a normal way. At the time this series was conducted, it was considered a series on a “damaged wall” at “low differential pressure.” The result of this series showed that the wall moved in response to the charging of the coal, Figure 1. On oven charging, the wall immediately moved away from the oven charged with coal and would continue to do so until the oven on the opposite side of the wall was charged. At that time the movement of the wall would be immediately reversed.

In Figure 1, as in other forthcoming graphs of wall deflection, the deflection of the heating wall and the percentage of time through the coking cycle of the two ovens that are adjacent to that wall are plotted. The ovens are charged when the cycle percentage is zero.

For the second series of Phase I, the objective was to monitor movement of the same No. 9 wall when one of the ovens was not always charged on schedule,

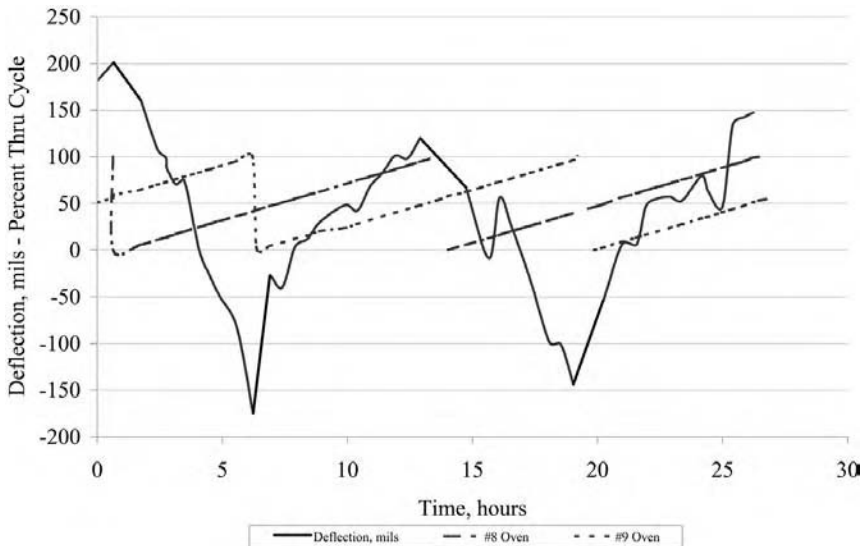


Figure 1 Phase I. Damaged wall, low, differential pressure.

and in fact would be at times held empty. At the time this series was conducted, it was considered to be a test of a “damaged wall” at “high differential pressure.” Further, the second oven was also left empty after its scheduled push, and for a period of about 7 hours, both ovens were empty. The deflection of the wall under these conditions is dramatically different when both ovens are normally charged (Figure 2). When the No. 8 oven was pushed and left empty about 8:45 into the series, the No. 9 oven was about 59% through its coking cycle. The wall continued to move away from the charged No. 9 oven until it was about 70% through its coking cycle, at which time the movement of the wall reversed, and the wall started to move toward the empty No. 8 oven and away from the charged No. 9 oven. When the No. 9 oven was pushed and left empty at the end of its cycle, the wall moved to essentially a neutral position. Both ovens were empty for about 7 hours, after which the No. 8 oven was again charged on schedule, at which time the wall moved rapidly away from the No. 8 oven.

This second series of Phase I would indicate that the carbonization gas pressures during the latter part of the coking cycle are less than the pressures derived during coal charging, or perhaps that the pressures derived from carbonization do not reach the wall’s surface! This series also showed that the inherent wall stiffness exceeds any carbonization gas pressure from the oven that was 70% through its cycle. This is indicated by the fact that the wall moved away from the empty oven, toward the charged oven at that time.

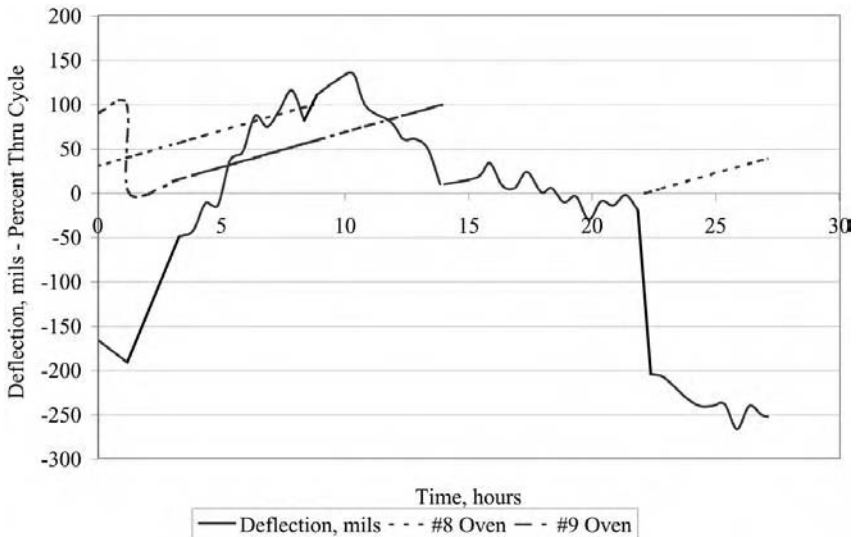


Figure 2 Phase I. Damaged wall, high, differential pressure.

For the third series of Phase I, the behavior of an undamaged wall between normally operating ovens was to be determined. The No. 3 wall of this battery had been completely rebuilt; however, on completion of the rebuilding, both the No. 2 and No. 3 ovens adjacent to the rebuilt wall could not be charged. However, the No. 2 oven was charged for nearly a month on a long coking time, while the No. 3 oven was empty. The No. 2 oven was charged 25 times against an empty No. 3 oven. The deflection test results showed that this “undamaged” wall had been damaged during its relatively short operating life. The flexure of the wall was asymmetrical—that is, the wall was more flexible toward the No. 3 oven, whereas movement toward the No. 2 oven was minimal (Figure 3). In spite of the damage to the No. 3 wall, its movement was still only about 40% of that of the No. 9 wall discussed above. Oven charging was again found to be the most important event initiating wall movement.

The three series of the first phase also showed that the absolute movement of a heating wall is also affected by the structural condition of the wall. The absolute movement of the No. 9 wall was greater than that of the No. 3 wall, indicating that the No. 9 wall was more flexible, apparently due to having sustained more damage through its longer service life.

B. Phase II

The on-line sensor, developed during Phase I was used throughout Phase II and all succeeding phases.

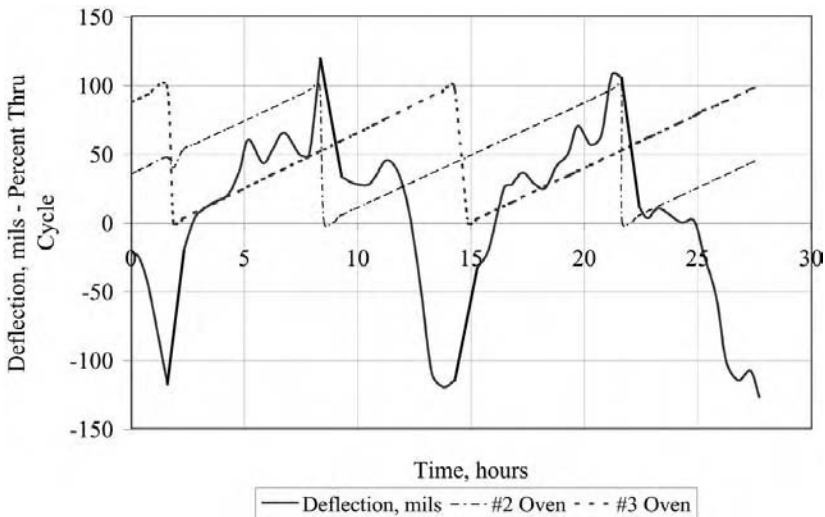


Figure 3 Phase I. Undamaged wall, low, differential pressure.

The original scope and objective of Phase II were to determine whether the location of a wall within the length of a battery affected wall movement and to determine whether charging variables and operating delays had any effect on wall movement. A 6-m battery of the same design as that in Phase I was to be used for Phase II. However, this battery was in a different plant and was operated on wet coal. The scope was redefined following the test series on the wall location. Because it was found that the full range of movement of the walls in this wet coal battery took place within the first two hours following oven charging, the emphasis was redirected toward coal variables, namely moisture and/or bulk density of the coal blend. It was theorized that gas pressure resulting from moisture/oil evaporation, in addition to the surcharge of the coal weight, would be related to wall movement within this relatively brief two-hour period.

The first series of Phase II showed that wall flexure is not related to the location of a wall within the length of a coke battery. While the absolute amount of wall movement varied, this was considered to reflect differences in the physical condition of the different walls. The deflection response was, however, different from that observed on a preheated coal battery. It was found that movement was again cyclic and directly related to oven charging. Also, nearly all of the movement, from one extreme position to the next extreme position, took place within two hours after an oven was charged. The movement on this wet coal battery took place in two stages, an immediate or primary movement, followed by a slower or a secondary movement to the extreme position. This observation raised questions regarding this behavior. It was at this time that the effects of vaporization of water and oil on the coal, as well as bulk density and weight of the coal charge, were considered as possible significant variables contributing to differential pressures on heating walls on normally operating coke batteries.

In the next three test series conducted as part of Phase II, an attempt was made to vary wall loading during charging and the period immediately following charging. These three series were to be (1) a low-bulk density series (Lo BD) in which the coal bulk density was lower than normal, (2) a high-bulk density series (Hi BD) in which the coal bulk density was higher than normal, and (3) a short-charge series (Sh Ch) in which the weight of the charge was less than that in normal operations.

Figure 4 shows the typical cyclic movement of the B18 heating wall during the high-bulk density series and its relationship to the coking cycle in the adjacent ovens. As stated earlier, ovens that are "0" percent through their cycle (left vertical axis) have just been charged. Time is plotted on the horizontal axis, this specific test series in Phase II was over 85 hours in length and consisted of five coal charges in the B18 oven and four coal charges in the B17 oven. The amount of wall deflection or movement is shown on the right vertical axis. The deflection of the heating wall as shown in Figure 4, as well as its relationship to charging of ovens adjacent to that wall, was typical for all phases and test series of this study.

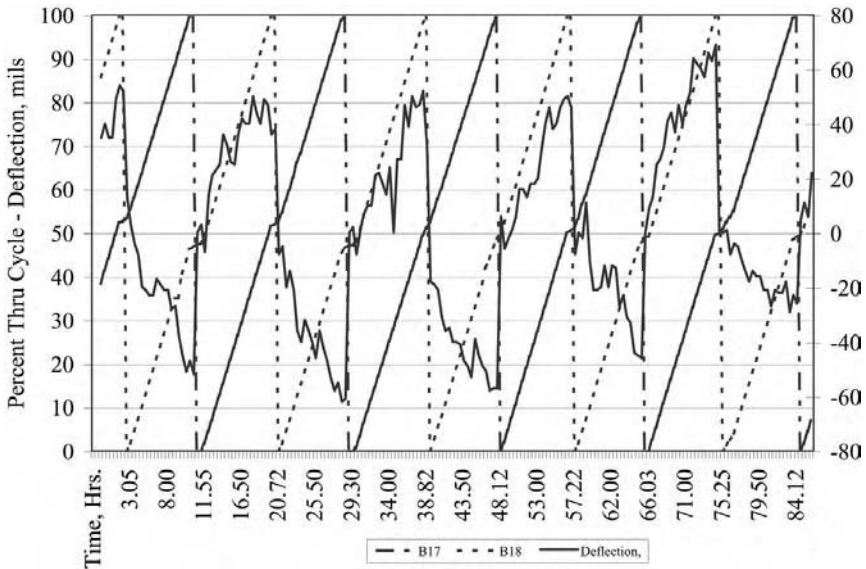


Figure 4 Phase II. Deflection versus time versus percent thru cycle.

The three series mentioned above showed that the amount of wall movement increases with increasing weight of the coal charge, and the duration of secondary movement increases with increasing bulk density of the coal. The following data from these three test series of Phase II were done on the same wall in the same 6-m coke battery over about a three-month period to minimize any effects of cumulative damage, and increasing wall flexibility.

Test series ^a	Bulk density, pcf	Oven charge weight, tons	Deflection, Mils		Time for secondary movement, Hours
			Primary	Total	
Lo BD	42.6	27.2	42	78	1:46
Hi BD	46.6	31.0	53	97	6:10
Sh Ch	44.3	26.1	33	60	2:5

^aLo BD = low bulk density; Hi BD = high-bulk density; Sh Ch = short charge. During the short-charge test, less coal than normally used was charged into the oven.

Note: Each of the above values is the average value for each of three test series for a specific wall in a specific coke battery at a specific coke plant.

Figures 5, 6 and 7 present the above data in graphic form. The relationships in these three figures can be defined by the following:

Figure 5: primary deflection, mils = (charge wt., tons \times 3.77) - 63.4
 $R = 0.9693$

Figure 6: total deflection, mils = (charge wt., tons \times 6.89) - 115.3
 $R = 0.9575$

Figure 7: wet bulk density, pcf = (log time, hours \times 7.312) + 40.869
 $R = 0.9986$

The relationship shown in Figure 7 might indicate the source of the pressure being applied to the wall, following the primary movement. The sustained pressure necessary to cause the sustained movement may be derived from the vaporization of the water and oil on the coal. The varying period and magnitude of the pressure may be a function of not only the volume of gas generated (higher bulk density is associated with greater amounts of liquids mechanically attached to the coal), but also its ability to escape through the coal bed (higher bulk density is also associated with lower bed permeability). The thermal conductivity of the coal bed, and therefore the rate at which it heats, may also further influence this reaction.

A fifth test series, in which the effect of operating delays was simulated, was conducted, again on the B18 wall. This was done because there were ques-

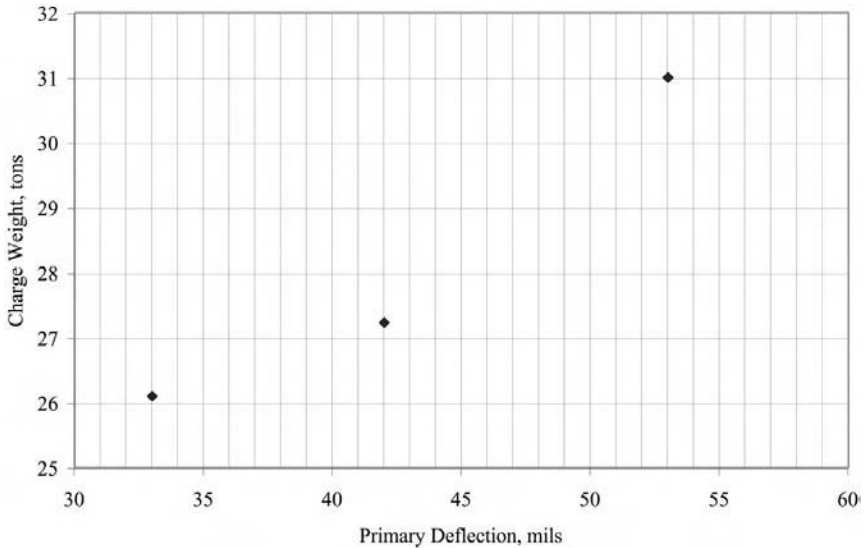


Figure 5 Phase II. Charge weight versus primary deflection.

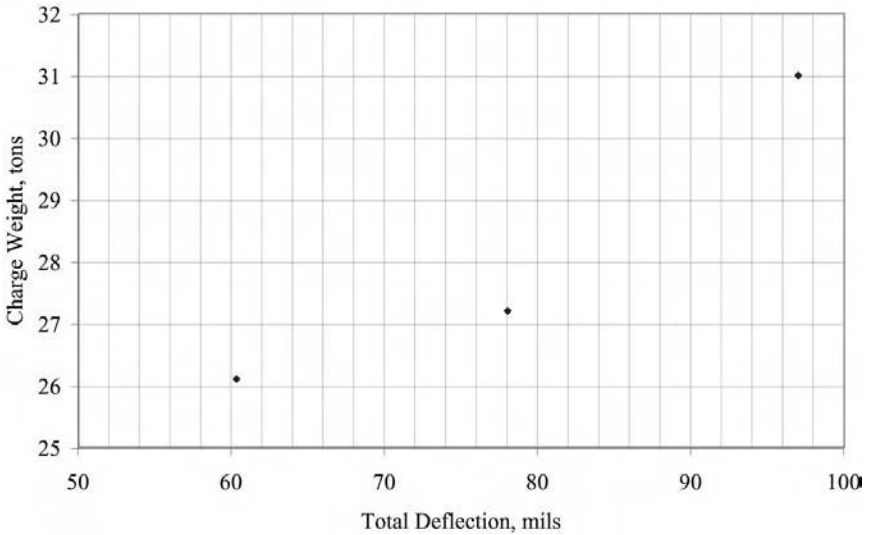


Figure 6 Phase II. Charge weight versus total deflection.

tions whether wall movement would be different if the oven opposite the one being charged was either not as far into its cycle, or further into its cycle than normal, or was even empty. Normally on this battery, the ovens opposite that being charged are about 48% and about 51% through their cycle. The operating delays simulated represent a variation of about plus or minus 3 hours from normal oven schedule.

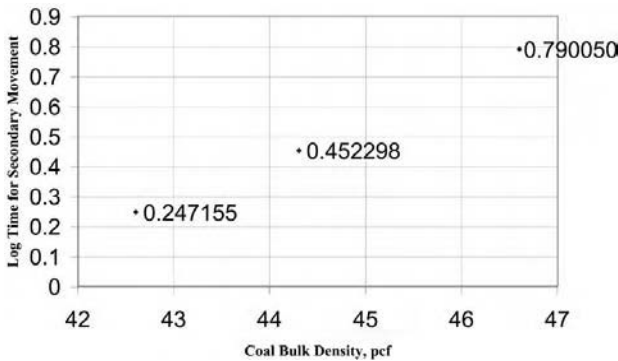


Figure 7 Phase II. Coal bulk density versus log time for secondary movement.

The fifth series of Phase II showed that there was virtually no difference in wall deflection attributable to operating delays. Even charges against an empty oven did not result in abnormal wall movement.

Therefore, the variables associated with the process of oven charging, the weight of the coal charge, the bulk density of the coal, and possibly with some physical/mechanical properties of the coal affects differential wall pressures, heating wall movement, and structural damage of the wall. Charging out of series by as much as plus or minus 3 hours from normal did not adversely affect wall flexure.

It must be noted that prior to the measurement of the movement of heating walls on operating coke oven batteries, prevalent theory was that the carbonization gas pressure, which develops when coal is heated through coking temperatures, was the primary cause of wall pressure. As a coking coal blend is heated, hydrocarbon gases evolve, and the coal fluidizes. The theory was that the fluidized coal contains the evolving gases in a sort of fluid envelope and that the increasing pressure inside of this envelope is transmitted to the heating walls, potentially resulting in movement of the heating wall. Carbonization gas pressures were not found to correlate with the movement of the heating walls in any of these three test series of Phase II. It would appear that any good blend of coking coals, with sufficient shrinkage, should not be considered a danger to the heating wall structure; however, bulk density and overall weight of the charge should be carefully watched.

For Phase II, which consisted of the five test series, a detailed study of the coal blends and their properties was made (4). In addition, internal gas pressures inside the charged coal were monitored with pipe probes located about 1 ft, 5 ft, 9 ft and 13 ft above the oven floor in some of the test series. The conclusions reached showed the following:

1. Peak internal gas pressures appeared to have no substantial effect on wall movement.
2. The duration and magnitude of the steam pressure peak appears to be related to wall movement.
3. The metallurgical properties of the coals and blends used during the Phase II test series were not a significant factor with respect to wall movement.
4. Movable wall pilot coke oven tests were inconclusive in predicting wall movement.

C. Phase III

The test series conducted for Phase III were basically designed to check the reproducibility of the series conducted in Phase II. This plan was adopted

primarily because the conclusions reached as a result of the Phase II tests differed significantly from previous theories and beliefs in regard to the sources of differential pressures that caused heating wall movement and damage.

The Phase III wall deflection measurements were made on another 6-m, wet coal, coke battery, at a different location from that in Phase II. Phase III consisted of four test series. The first series of Phase III was also a multiple-wall test. The deflections of five different walls across the length of the battery were measured. Oven charging again proved to be the primary event as related to wall movement; however, there were not two stages of movement on the Phase III battery. On this wet coal battery, the wall moved away from the oven just charged to near its extreme position in less than 30 minutes and then stayed at or near this extreme position until the other oven was charged, when the cycle was repeated (Figure 8). Again, slightly different levels in the magnitude of the deflection responses were measured among the five walls, and again these differences were attributed to different physical conditions of the various walls.

The data obtained during the second, third, and fourth test series of Phase III of the study essentially mirrored similar data obtained during Phase II. The data indicated as “normal” below are those from one of the walls in the five wall first series of Phase III. This same wall was then used for the next three series

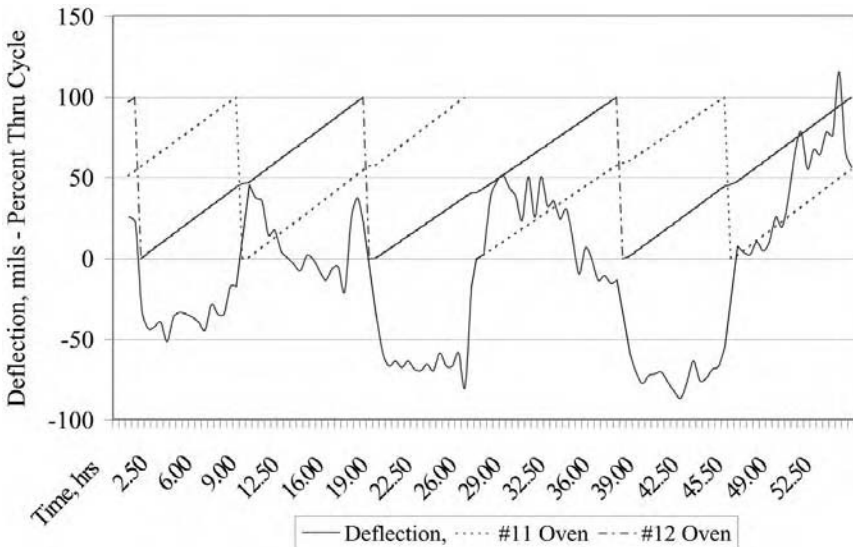


Figure 8 Phase III. High bulk density series.

as shown below. The following average data are from four of the test series of Phase III:

Test series	Average bulk density, pcf	Average charge weight, tons	Average deflection, mils
Normal	45.4	25.7	85
Lo BD	41.9	23.2	62
Hi BD	47.7	26.7	78
Sh Ch	45.4	22.6	47

These data are presented graphically in Figure 9. As can be readily seen, these data from Phase III are similar to the Phase II data shown in Figure 6.

D. Phase IV

In light of the apparent effect of liquids (water and oil) mechanically attached to the coal, their evaporation, and the restrictions on these vapors release from the coal bed in the oven, a company that specializes in characterizing properties and behavior of granular materials was consulted. A coal blend similar to that used throughout Phase II was evaluated. This study indicated that the rate at which the coal is charged into the oven could affect this component of the forces acting on the walls surface and cause wall movement and refractory stress.

Therefore, two test series on the same coke battery and on the same wall as used in Phase II were planned. For these series one of the larry cars was

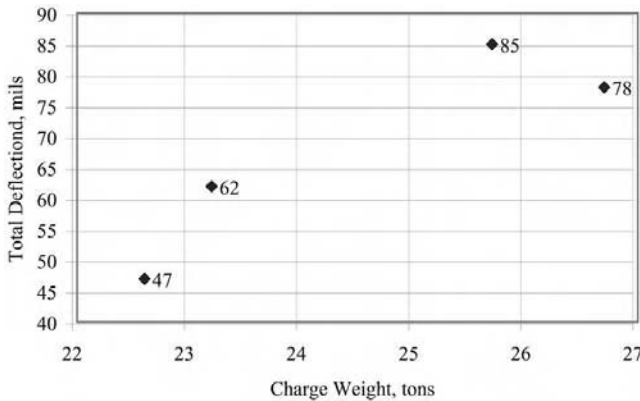


Figure 9 Phase III. Charge weight versus total deflection.

modified. More powerful motors were installed on the screw conveyors on the four hoppers of one of the larry cars, so that the conveyors could be slowed, thereby reducing the rate at which coal would be charged into the ovens. The two series were to be completed over eight consecutive days: four days at the normal charging rate, followed by four days at the lower rate of charging.

The normal charging rate on this battery is about 12 net tons per minute (tpm). With the normal charge weighing about 27 net tons, this equates to a charge time of about 2:15. By reducing the speed of the screw conveyors, it was possible to increase the charge time to an average of about 6 minutes and reduce the charging rate to about 4.5 tpm.

This reduction in the oven charging rate resulted in a reduction in the primary wall movement of about 10% and a reduction in total wall movement of about 12%.

Unfortunately, it was not possible to verify these results on another coke battery before the program was discontinued due to business conditions.

V. SUMMARY AND CONCLUSIONS

The heating walls in byproduct coke oven batteries exhibit a pattern of damage that is consistent with damage induced by flexure of the walls because of unbalanced pressures from the ovens on opposite sides of the wall.

The damage results because flexure induced stresses are concentrated in the areas of the wall that are adjacent to the fixed boundaries of the wall.

Within these areas of high stress in the wall, the distribution of stress between and among the wall component shapes is through the interlocking parts of each shape, thus the keys, tongues, and grooves tend to concentrate stress within each shape.

Wall flexure must be accompanied by some finite amount of wall movement; therefore, the measurement of wall movement during normal battery operations should define events or practices that cause wall movement, therefore damaging refractory stress.

The measurement of wall movement on different normally operating coke batteries gave consistent results. The charging of the coal into the oven was the single event that initiated wall movement, with 40% to 100% of the movement taking place within 30 minutes of charging.

The weight of the coal charge, thus bulk density, affected the magnitude of movement; increased weight of the coal charge increased wall movement and refractory stress.

Limited tests also indicated that with some coking coal blends, the rate at which the coal is charged can affect the amount of wall movement; movement decreased as charging rate decreased.

Internal gas pressures in the charged coal/coke have no substantial effect on wall movement. Further, movable wall pilot coke oven tests were inconclusive in predicting wall movement.

REFERENCES

1. McDermott JF, Rueckl RL. A forensic study of fairfield coke battery no. 2. Ironmaking Conference Proceedings 1986; 45:443.
2. Rueckl RL. The measurement of the deflection of coke battery heating walls and its significance. Ironmaking Conference Proceedings 1986; 45:269.
3. Rueckl RL. The relationship between some coke battery operating parameters and heating wall movement. Ironmaking Conference Proceedings 1989; 48:619.
4. Sich G, et al. Coking forces and heating wall movement. Ironmaking Conference Proceedings 1989; 48:635.

16

Testing of Refractory Materials

Sarah Baxendale

CERAM Research, Stoke-on-Trent, Staffordshire, England

Selecting the most suitable refractory materials to prolong service life and make a process more cost-effective is now more critical than ever in today's competitive climate. It is important to carefully assess materials to ensure that they are suitable for the environment and conditions in which they will operate.

Testing refractory materials is therefore an essential step in this selection and improvement process.

So why specifically test refractory materials?

To characterize new materials

For quality control of processes and products (1)

To help rank and select materials for a particular application and predict in service behavior (1)

To examine the effects of service conditions

For fault diagnosis

To establish properties required for mathematical modeling to compare current and new designs

A wide range of test methods is available to measure all aspects of refractory behavior, and worldwide an even greater range of methods exists within each test type. For example, in some cases different standards are followed depending on whether a material is a dense (having a true porosity of less than 45%) or insulating refractory (having a true porosity of greater than 45%). The majority of tests are characterized as national or international standards examples of which are shown in the table at the end of the chapter, while other tests are not yet featured.

Note: Special thanks go to Graham Oliver for his work on XRF, to Richard White for XRD and microscopy, and to Kevin Thomas for Poisson's ratio.

Figure 1 shows some examples of available tests for refractories. These tests generally fall into three functional areas, although, as we can see, some tests will fall into more than one category.

First come characterization/data sheet properties, of which we can see some examples. Most of these describe the fundamental properties of a material, for example, its structure, its chemistry, or its compressive strength at ambient temperature.

The information provided on material data sheets can, however, vary widely. Some refractory companies may provide detailed information covering a wide variety of tests, with references made to the particular test method by which the data were obtained. Only if this is the case is it possible to compare data for the same material types produced by different manufacturers. It should be remembered that data sheets report typical values and they should not be used to constitute a specification for a particular application. More emphasis should be placed on product definition sheets in which property limits are given.

These property types generally give very little insight into service performance.

Moving toward service-related properties such as pyrometric cone equivalent (P.C.E.), hot modulus of rupture (HMOR), and permanent linear change (P.L.C.) gives us a little more information on a product's maximum service temperature and stability on heating.

However, it is the combination of design data such as compressive and flexural stress–strain with thermal measurements that allows us to take that extra step from a material test piece to a working refractory lining or component. It allows us to study the thermomechanical behavior of materials.

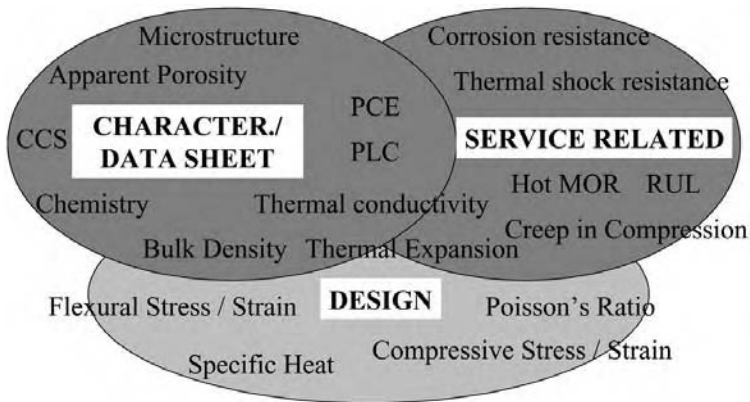


Figure 1 Testing of refractory materials.

In this chapter we review the refractory tests together with their purpose and limitations.

I. CHARACTERIZATION/DATA SHEET PROPERTIES

A. Chemical Analysis

Chemical analysis tells us which elements are present in a refractory. Generally, the quickest and most commonly used method is by X-ray fluorescence. The technique is based on the phenomenon that each element fluoresces characteristically when exposed to X-rays. The results for each element present are usually reported as oxides.

The definitive document for this technique is ISO12677: 2003, which appeared in 2003. The essence of the technique is the conversion of the ignited sample into a glass bead or button by fusing in a suitable lithium borate-based flux. Once treated in this way, all particle size and mineralogical effects that will lead to inaccuracies are destroyed. Hence, synthetic calibrations can be set up in a similar manner using synthetic mixtures of pure oxides or carbonates.

The technique is not viable for elements low in the periodic table (from fluorine downward) although there is research into the use of X-ray fluorescence for fluorine and boric oxide. To this end, a method has been developed for the determination of B_2O_3 , which allows either a wet chemical or inductively coupled plasma (ICP) finish, the latter being based on methods for the pottery industry. Another wet (colorimetric) method for the determination of Hexavalent chromium has also been produced. Finally, in the area of black and nitride ceramics, a series of standards is appearing that allow their characterization using a mixture of X-ray fluorescence, X-ray diffraction, and special chemical speciation methods.

B. Mineralogical Analysis by X-Ray Diffraction

X-ray diffraction (XRD) analysis provides a means by which different crystalline phases can be characterized and identified. X-ray diffraction works by diffracting incident X-rays along crystallographic planes. The angle by which X-rays are diffracted is in accordance with Bragg's law, in which

$$n\lambda = 2d \sin \theta$$

where

n is an integer value

λ is the wavelength of the diffracting X-ray

d is the spacing between successive diffracting planes in the crystal

θ is the angle between the crystallographic plane and the diffracted beam.

It is therefore possible using a monochromatic X-ray beam to measure the spacing of the crystallographic planes within a crystal from the diffraction peaks. Mineral characterization to such an extent is rarely used in a refractory context. More regularly, the unique diffraction pattern each mineral makes is used simply as a means of identification of presence in the sample.

In order to collect diffraction data from a sample, representative material is prepared as finely ground material and then presented to the X-ray beam in such a way that individual crystallites are randomly orientated. The resultant diffraction trace, as a plot of intensity against “ d ” spacing or against 2θ value, can be compared to traces of known material or published standard reference profiles enabling identification to be made. The International Centre for Diffraction Data (www.icdd.com) publishes reference patterns on an annual basis. Sophisticated search–match software to combine diffraction peak positions with chemical constraints for the system under examination can be employed.

Phase identification can be useful in cases of identification of unknown materials or products. Other examples of use may be confirmation that certain phases have formed during a firing process such as cristobalite in silica or that components have not broken down or removed during service.

Often phase identification is not enough and it is desirable to quantitatively determine the amounts of the different components within a sample. Examples of applications where this may be useful might include monitoring of product quality, modeling of mineralogy with process conditions, or determination of crystalline components that have significant effects on the property of the materials such as cordierite in kiln furniture. X-ray diffraction is inherently less quantitative than other analytical techniques such as X-ray fluorescence, but with careful use of standards, calibration, or processes such as standard addition, reasonably good results can be obtained.

Other applications of X-ray diffraction to refractories include accurate cell determination in cases where solid solution systems occur such as β -sialons ($\text{Si}_{6-z}\text{Al}_z\text{O}_z\text{N}_{8-z}$). Occasionally, it may be useful to determine the crystallite size of a material. This can be done by calculations based on the width of the peaks of diffraction peaks.

C. Microscopic Examination

Microscopic examination of refractories can range from simple hand lens examination to the use of sophisticated scanning or transmission electron microscopes with magnification in the order of many thousands of times. The purpose of examination is to increase the knowledge of microstructural properties of the

material. Examinations may be conducted on the surface of the refractory, internally to evaluate the normal structure, or across interfaces between materials or material and service environments to evaluate changes that occur. Naturally, it is essential to define the nature of the information that is being sought in order that the most effective approach can be taken. Generally, polished metallographic sections are made from refractory samples although geological thin sections may be appropriate. Polished sections provide greatly improved spatial resolution but reduced mineralogical information over thin sections. Selective etching techniques are employed to enhance features such as grain boundaries and increase contrast between phases and sometimes in phase identification.

Typical information that can be obtained from microscopic examination of refractories are parameters such as grain size, grain distribution, and mineralogy. However, many parameters are subjective in nature and therefore need to be examined in comparison with similar materials. Considerable experience is required if microstructures are to be correctly and objectively interpreted.

Some of the more subjective features are pore distribution, bond structure, degree of reaction, or dissolution and microcracking. In order to evaluate these parameters, it may be necessary to etch a sample to enhance grain boundaries or increase the contrast between components such as mullite and glass in refractory grog grain or corundum in calcined bauxite.

Some materials have characteristic microstructures that can be used for confirmation of their presence. For instance, fused magnesia, sintered magnesia, and seawater magnesia are structurally different. Similarly, calcined alumina, tabular alumina, and white fused and brown fused alumina all have very different characteristics.

In evaluating the microstructure of a refractory body it is necessary to examine grain structures, grain distribution, bond mechanisms, and degree and distribution of porosity. All the microstructural properties of the refractory will control the in-service behavior.

One vital method that can be applied to refractory sections is that of microanalysis in which small areas can be analyzed chemically after excitations with the incident electron beam. Microanalysis is normally used on polished sections while being examined by scanning electron microscopy. Analysis can be used to determine or confirm the composition of specific grains, particles, crystals, or bonds. By integrating the composition of grains or areas with spatial locations, reactions, diffusion profiles, and attack mechanisms can be evaluated particularly at interfaces.

D. Bulk Density and Apparent Porosity

The bulk density of a porous material is defined as the ratio of mass of the material to its bulk volume, whereas the apparent porosity is the ratio of open pores to the bulk volume of the material (2). The latter value is expressed as a

percentage. The Archimedian, evacuation method generally measures both bulk density and apparent porosity.

To measure these properties, the test piece is dried to constant mass, weighed in air, and then transferred to an airtight dessicator, which is then evacuated until a minimum pressure is reached. After the vacuum is maintained for a set time period, the liquid is introduced until the specimens are completely covered and to ensure open pores are filled. In most cases distilled water is used. However, for materials that may hydrate or if assessing ex-service materials, which may contain water-soluble corrosion products, then paraffin is preferable.

At atmospheric pressure, the specimens are reweighed while suspended in the liquid to determine the apparent mass, and then finally the soaked test piece is reweighed in air. Bulk density and apparent porosity are calculated as follows:

$$\text{Bulk density} = \frac{\text{mass in air}}{\text{soaked mass} - \text{suspended mass}} \times \text{liquid density}$$

$$\text{Apparent porosity} = \frac{\text{soaked mass} - \text{mass in air}}{\text{soaked mass} - \text{suspended mass}} \times 100$$

Bulk density and apparent porosity are generally used for quality-control checks. They have an effect on other properties such as thermal conductivity and thermal shock resistance of a material. Lower-porosity materials can often have greater resistance to chemical attack than their higher-porosity counterparts.

E. True Density and True Porosity

True density is the ratio of the mass of a material to its true volume, and the true porosity is the ratio of the total volume of open and sealed pores to the bulk volume expressed as a percentage (2).

The true density is often determined by a pycnometer method. A quantity of refractory material is ground finely to remove closed pores, and the dry mass of material in the pycnometer determined by comparative weighing. Following this, the pycnometer is partially filled with the test liquid followed by evacuation in a dessicator. The pycnometer is then completely filled with the test liquid and the temperature stabilized in a temperature bath prior to reweighing. Finally, the pycnometer is filled with the liquid alone and reweighed.

From these weight measurements, the true density is determined:

$$\text{True density} = \frac{\text{mass of ground material} \times \text{liquid density}}{\text{mass of pycnometer and test liquid} + \text{mass of material} - \text{mass of pycnometer, material, and liquid at controlled temperature}}$$

Density values are expressed in kg/m³ or pounds lbs/in.³

True porosity is then calculated from the results of the evacuation and pycnometer methods:

$$\text{True porosity} = \frac{\text{true density} - \text{bulk density}}{\text{true density}} \times 100$$

F. Cold Crushing Strength

The cold crushing strength of a material is the maximum load at failure per unit of cross-sectional area when compressed at ambient temperature.

$$\text{Failure stress} = \frac{\text{load (in Newtons or lbs)}}{\text{area (in square mm}^2 \text{ or in.}^2\text{)}}$$

Results are expressed in Newtons/mm² (megapascals) or lbs/in.².

Although variations existed previously, the preferred standard test piece size for determining cold crushing strength of dense refractories is a 50-mm cube or cylinder. To ensure good contact between the loading surfaces, the test piece should be carefully ground to specified tolerances and parallelisms to give consistent results. Test specimens are then loaded to failure at a specified rate.

Cold crushing strength is generally used for quality-control checks and does not give any specific indication of a material’s in-service behavior. Results on materials from within the same batch can differ with brick size and firing position in the kiln. A greater emphasis, however, would be placed on values falling below a minimum specified value since these may reflect a lesser degree of bonding. The results obtained can also differ depending on the method adopted. For example, dense products can be loaded directly between steel platens or between fiberboard placed between the platens and the specimen. The latter is the case in the ASTM (3) standard, whereas the opposite is true for the BS EN standard (4). This is often a source of variation between results obtained by different standard methods and can sometimes make comparisons difficult. An ISO standard using packing between samples and loading plates is now available. Packing is not generally used when testing insulation bricks and larger test specimens are used.

Table 1 shows some typical values of chemical analyses, bulk density, apparent porosity, and cold crushing strength for some common refractory materials.

G. Modulus of Rupture

The modulus of rupture is the maximum transverse breaking stress applied that a material can withstand before fracture (2). The property gives an indication of the bond strength of the refractory that results from its chemistry and mineralogy after production. Nominal test piece sizes include whole standard bricks

Table 1 Some Typical Properties of Selected Refractory Materials

Material	Al ₂ O ₃ %	SiO ₂ %	MgO %	TiO ₂ %	C %	Fe ₂ O ₃ %	SiC %	Cr ₂ O ₃ %	CaO %	Bulk density (kg/m ³)	Apparent porosity (%)	Typical cold crushing strength (MPa)
60% alumina brick	60	32.5	—	—	—	—	—	—	—	2600	17–28	39
50% alumina brick	51	44	—	—	—	—	—	—	—	2300–2550	18–28	55
42% alumina brick	42	51	0.5	1	—	3	—	—	0.5	2100–2350	20–22	41–90
Magnesite	0.8	2.5	92	—	—	1.8	—	—	2.3	2670–2950	17–24	34–55
Mag chrome	12	2.9	53	—	—	—	—	25	—	3080	16–22	38–55
Silica	0.7	96	—	—	—	0.7	—	—	2.3	2950–3050	20–25	28–34
Dolomite	2	3	37	—	—	1.5	—	—	55	1680–1870	16–22	48
1800°C convent. castable	94	0.2	—	—	—	—	—	—	3	2500–2800	—	55
1600°C low- cement castable	50	45	—	—	—	—	—	—	1	2400	—	75
Insulation brick	99	0.6	0.01	—	—	—	—	—	0.1	1440	—	17

Source: Ref. 1.

(230 mm × 114 mm × 76 mm or 64 mm) or bars of dimensions 150 mm × 25 mm × 25 mm. The test piece is placed between supports a set distance apart and loaded to failure at the center of the bar by a third loading arm. Loading rates differ for dense and insulating products. This three-point arrangement (Figure 2) is most commonly applied to refractory materials, although in some critical applications, although not standard practice, a four-point arrangement, where a greater volume of the test bar is placed under applied stress by two upper loading arms, is preferred. A four-point arrangement leads to lower overall failure stresses and gives an indication of the minimum failure stress of a material.

The calculations for modulus of rupture in three-point and four-point arrangements are shown below:

$$\text{Failure stress (3-point)} = \frac{3pl}{2bd^2}$$

$$\text{Failure stress (4-point)} = \frac{3pa}{bd^2}$$

where

- p = load in Newtons or lbs
- l = test span in mm or in.
- b = specimen breadth in mm or in.
- d = specimen depth in mm or in.
- a = distance between lower and upper loading points in mm or in.

Units of failure stress are Newtons/mm² (megapascals) or lbs/in².

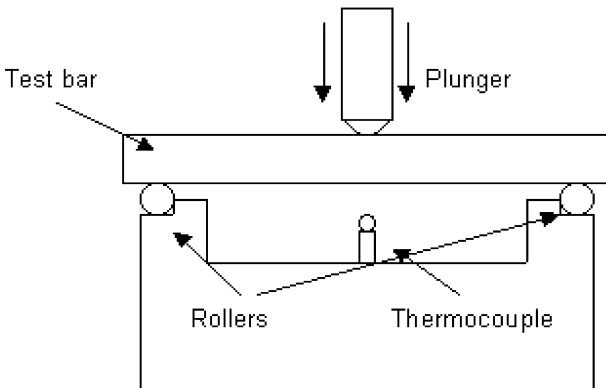


Figure 2 Three point bend arrangement for ambient and elevated temperature modulus of rupture testing.

It is much easier to measure bond strength in a flexural rather than tensile mode for refractories. Tensile tests are notoriously difficult to set up as any slight misalignment may give rise to erroneous results. Of course, flexural strength is not synonymous with tensile strength, but a reasonable, approximate relationship exists.

At ambient temperature, the modulus of rupture test is more generally used for quality-control purposes to ensure consistency between batches. The property, when measured at ambient temperature, again does not give any direct indication of in-service performance.

H. Permeability

The environments in which many refractory materials operate contain corrosive gases, which can penetrate a material and begin the process of corrosion. Assessment of the permeability of a material to gases is important in determining the potential susceptibility of a material to corrosion.

The degree of permeability is also a significant factor governing the ease with which water vapor can escape from monolithic blocks and structures when heated. Sometimes if a monolithic refractory is heated too quickly over critical temperature ranges during the initial dry-out and is low in permeability, the resulting pressure buildup can cause explosive spalling, leading to costly repairs and downtime. Fiber additions to monolithics, which are low in permeability, aid the escape of water vapor on heating.

Permeability therefore describes the rate of flow of a gas through a porous material per unit area (2).

Movement of gases through a material takes place under a pressure gradient, and this is reflected in the test method. Gas is passed through a test piece (nominally 50-mm diameter, 50-mm-high cylinder, or similar) that is placed in a gas-tight sample holder. Several measurements of the fall in pressure across the test piece are made at different gas flow rates. The pressure difference is measured using a manometer (3, 4).

The permeability is calculated using the following equation:

$$\mu = \frac{V}{t} \cdot \eta \frac{\delta}{A} \cdot \frac{1}{\rho_1 - \rho_2} \cdot \frac{2\rho}{\rho_1 + \rho_2}$$

where

μ = material permeability in m^2

V = volume of gas passing through the refractory, m^3

t = time taken for gas to pass through the refractory, sec

η = dynamic viscosity of the gas at the test temperature in Pa

δ = material thickness in m

A = cross-sectional area of the material in m^2

ρ = absolute gas pressure in Pa

ρ_1 = absolute gas pressure upon entering the material in Pa

ρ_2 = absolute gas pressure upon leaving the material in Pa

Permeability generally decreases as the temperature of a material is raised. This is probably a result of increased gas viscosity. For certain self-flowing castables it has been shown that permeability increases with heat treatment temperature due to structural changes.

Permeability of castable materials is also highly dependent on particle size distribution and water addition (6).

I. Pore Size Distribution

The apparent porosity of a material, as mentioned previously, can have a significant effect on the corrosion resistance of a material. It can also influence thermal shock resistance and thermal insulation capabilities. In addition to the amount of porosity in a material, it is also important to consider the nature of these individual pores, such as whether the pore volume or pore area comprises greater amounts of fine or coarse porosity and their relative proportions. Finer pores generally have a positive effect on the properties mentioned (7).

Measurement of this property is usually made by intrusion of small cubes of refractory by mercury under an increasing pressure. Initially under lower pressures the larger pores are filled, and subsequently the smaller pores as the pressure increases. Only open pores are considered.

Graphs such as cumulative pore volume or area versus pore diameter are plotted.

For two materials of equal apparent porosity, the refractory whose porosity comprises pores with an overall larger diameter may expect to be more easily penetrated by attacking corrosive media (as pressure is proportional to diameter) but may provide a lower surface area to volume ratio upon which corroding action could take place. The opposite situation would generally be true for fine pores. A greater pressure would be required to penetrate a smaller pore, but a larger surface area to volume ratio may lead to increased corrosion. Finer pores may also become blocked by invading media more quickly and further penetration into the refractory body may be prevented.

Convection currents are less readily set up in finer pores, which lead to greater insulation capabilities of a material, and thermal shock can also be reduced as a larger number of fine pores act as more effective crack stoppers than a smaller number of large pores.

J. Pyrometric Cone Equivalent (P.C.E.)

The pyrometric cone equivalent gives an indication of the refractoriness of a material, that is, its ability to withstand high temperatures in an unstressed situation. The method applies particularly to aluminosilicate materials. A standard refractory

cone shape is prepared from the test material and heated together with a number of standard cones in an oxidizing atmosphere at a specified rate. The purpose of the test is to identify the point at which the tip of test cone bends over. Its behavior is then compared to that of the standard cones. The most similar standard cone to the test cone gives a corresponding temperature rating. Sometimes the rating may be reported between two standard cone values if the softening point occurs between the two.

The endpoint obtained relates only indirectly to temperature. The value obtained corresponds to the heat input and is time-, temperature-, and atmosphere-dependent. Standard cone reference tables are available that correspond to a temperature equivalent specific to the test conditions. Orton, Seger, and ISO are examples of the cone rated systems used.

The pyrometric cone equivalent of a material is affected by the presence of impurities in the material such as iron and alkalis, which reduce the P.C.E. value, by acting as fluxes. Determination of the P.C.E. can ensure that a refractory selected for a particular application is operating well below the onset of melting.

K. Permanent Linear/Volumetric Change

This is a measure of the permanent changes in dimension of a refractory, whether it may be in terms of expansion or contraction, after heating ideally to an anticipated hot face service temperature or material classification temperature. This should indicate the maximum expected dimensional change in a stress-free condition.

Within the scope of the various test methods available, the change in dimensions is reported with corresponding test duration. Firing temperature and soak times at temperature may vary depending on the material and its operating conditions. Across the various methods available, the test piece size can be of a standard brick or rectangular prisms or cylinders.

Dimensions are measured at identified points on the test piece. The specimens are then fired in accordance with a specific heating schedule in an oxidizing atmosphere for the set duration. Minimum firing temperatures start around 800°C, and for dense refractories test duration is nominally 5 hours (4). The dimensions are remeasured following firing at the same identified points following firing, and the percentage change is calculated.

For linear changes, the result is expressed as follows:

$$\delta L = \frac{L_i - L_f}{L_i} \times 100$$

where

L_i = initial length

L_f = final length

The classification of insulating firebricks is dependent upon change in dimensions on reheating and material bulk density. An insulating material's linear change in dimensions should not exceed 2% at its particular classification temperature when fired for 24 hours (3). However, many user companies specify permanent linear change limits well below this value.

Low permanent linear and volumetric changes are generally desirable, as they indicate good material stability and minimize shrinkage to prevent loosening of a refractory lining in service. Also, ingress of corrosive material behind the hot face is prevented.

II. SERVICE-RELATED PROPERTIES

In addition to material characterization and physical tests used to describe refractory materials, there are several properties that are more relevant to the "in-service" performance of a refractory. Measurement of these properties gives a closer indication of how a material may act in a particular application.

A. Abrasion Resistance

In refractory applications such as the front end of a rotary cement kiln or the shaft of a vertical lime kiln, for example, the lining is subjected to high abrasive action from the charge material. In these regions it is important to install a material that can withstand the constant wearing action for long periods of time without a severe reduction in lining thickness.

It is therefore important to assess the abrasion resistance of candidate materials for such areas, that is, how well they can withstand mechanical rubbing or impact.

Assessments are often carried out by falling grit-type methods; an abrading medium is directed at a refractory test block for a set duration. Test specimens are weighed before and after testing, and results are expressed as the loss in material volume or by the calculation of an abrasability index based on loss in mass, material bulk density, and apparatus correction factor.

The abrasion loss from a material is highly dependent upon its density and porosity, the angle of impact, and the grain size and nature of the abrading media. Variation also exists between the outer skin of a refractory material and its interior, and tests take this into account. The abrasion loss generally decreases for fired refractories with increasing temperature as the material softens. However, for castable refractories, abrasion loss increases at elevated temperatures as the hydraulic bond is lost, but reduces again as a ceramic bond is formed (8).

Table 2 shows the variation of the abrasability index of some refractory materials at ambient temperature and 1000°C.

Table 2 Comparison of Ambient and Elevated Temperature Resistance to Abrasion by Falling Grit Method for a Range of Refractory Materials—Abradability Index

Refractory	Ambient	1000°C
85% alumina bauxite brick	62	20
59% alumina silliminite brick	230	75
44% alumina medium-duty firebrick	294	70
43% superduty blast furnace brick	45	20
39% alumina firebrick	394	100
Fusion cast alumina brick	72	38
Castable refractory	75	200

Source: Ref. 8.

With this in mind, tests for abrasion resistance are generally conducted at ambient temperature with standards for high-temperature tests now being withdrawn. Elevated temperature methods are often only used for research purposes (8).

B. Modulus of Rupture at Elevated Temperature

Modulus of rupture at ambient temperature was introduced earlier and, as indicated, is useful for quality assurance but gives little indication of in-service performance, unlike the same test carried out at elevated temperature. The nominal specimen size used in national and international standards for dense and insulating refractories is again 150 mm × 25 mm × 25 mm or similar, and support test span is approximately 125 mm. Specimen temperature is measured by a thermocouple placed centrally underneath the test bar. The specimens are heated to the test temperature at specified rates. Following a dwell for a set period at the test temperature, the samples are loaded to failure at a designated stress rate. The stress rate differs for dense and insulating refractories.

Figure 2 shows the test arrangement. Modulus of rupture varies with temperature. The greatest reduction in strength for most oxide refractories starts to occur beyond 1000°C as liquid formation increases.

Calculations for modulus of rupture are given in an earlier section.

C. Refractoriness Under Load

Refractoriness under load is the ability of a material to withstand specific conditions of load, temperature, and time (1). This is dependent on the softening point and the amount of glass or melt phase within the refractory system.

The specimen [50-mm diameter and 50-mm-high (4) or a prism 38 mm × 38 mm × 114 mm (3)] is placed in a furnace between refractory plates and in contact with a dilatometer system, which is in turn attached to an extensometer to measure deformation. A specified load is applied to the specimen, and the material is then heated to the maximum test temperature or until a particular percentage deformation is reached. Methods of measurement include EN 993-8:1997 and ASTM 832-00.

D. Thermal Shock Resistance

Thermal shock resistance is the ability to withstand rapid changes in temperature with minimal cracking (1). This situation may occur under conditions when the material is heated or cooled suddenly such as with submerged entry nozzles, under thermal cycling such as in the regenerators of a glass furnace, or when subjected to a severe thermal gradient such as with sliding gate plates. Incompatible changes in dimensions at these times may lead to failure in regions where local strain exceeds the tensile failure strain.

Table 3 lists the properties required for good thermal shock resistance (9), and Table 4 gives examples of three refractory material types that exhibit good thermal shock resistance and the features that lead to this (10).

Certain materials—for example, silica refractories—are more vulnerable to thermal shock if heated rapidly over temperatures where thermal expansion is high as a result of test changes. Test temperatures for silica can often differ from other refractory materials. Tests tend to take place at temperatures where expansion is high.

It is difficult to represent service conditions accurately in a laboratory test, because resistance is highly dependent on geometry, uniformity of heating, and

Table 3 Properties Leading to Good Thermal Shock Resistance

Property	Implication
Low thermal expansion co-efficient	Reduces stress associated with temperature gradient
High thermal conductivity	Conducts heat away and minimizes temperature gradients
High toughness/work of fracture	Reduces crack propagation
High strain to failure	Accommodates thermal stress
Low modulus of elasticity (i.e., stiffness)	Minimizes the stress associated with thermal expansion

Source: Ref. 9.

Table 4 Examples of Refractory Materials Showing Good Thermal Shock Resistance

Material	Properties giving good thermal shock resistance
Carbon	High strain to failure Low thermal expansion High thermal conductivity High work of fracture
Silicon carbide	High thermal conductivity Low thermal expansion
Castable (unfired)	High strain to failure Low thermal expansion

Source: Ref. 10.

the stresses imposed by the service conditions. However, several methods are used to measure thermal shock practically. These include assessment of

- Degree of cracking observed
- Number of cycles to failure
- Reduction in strength or modulus of elasticity (stiffness by resonant frequency technique)
- Calculation from several property measurements, e.g., Hasselman parameters (11).

The British Standard prism spalling test (14) subjects sections of refractory to successive heating and cooling cycles followed each time by loading of the sample to test resilience. Surviving samples progress to further cycles.

The ASTM thermal cycling method (ASTM C1171-96) (3) combines ultrasonic measurements and modulus of rupture at ambient temperature on 150-mm × 25-mm × 25-mm bars to assess performance. In this case, comparisons are between two separate sets of test pieces.

The ASTM ribbon burner (ASTM C1100-88) (3) thermal shock assessment is based solely on a nondestructive test measurement of the modulus of elasticity of the test samples before and after being subjected to the heating and cooling cycles.

Test samples are randomly supported 100 mm above a segmented line gas burner to form a closed panel, which is then subjected to cyclic rapid heating and forced air cooling for five cycles, each cycle consisting of 15 minutes' heating and 15 minutes' cooling. The hot face temperature reached can be between 815 and 1093°C. The modulus of elasticity of each sample is determined before and after testing, and the reduction in modulus calculated.

Sample sizes used can vary as long as all samples tested are the same size for different brands or product types. All samples should be 9 in. long but can be

sections of whole, standard bricks. Materials vulnerable to thermal shock damage are more significantly affected by changes in sample thickness (12).

The expected relative thermal shock resistance of materials, as mentioned above, can be calculated from measurement of a range of material properties. Hasselman (11) derived a series of parameters in an attempt to rank materials in order quantitatively. High calculated values of R are indicative of good thermal shock resistance.

R^{st} and R''' relate more closely to actual material behavior and take a fracture mechanical approach corresponding to situations of quasi-stable and unstable crack growth equations, respectively.

$$R^{st} = \left(\frac{\gamma_f}{\alpha^2 E} \right)^{1/2}$$

$$R''' = \left(\frac{E \gamma_f}{\sigma_f^2 (1 - \nu)} \right)$$

where

- γ_f = work of fracture (toughness)
- σ = modulus of rupture
- α = thermal expansion coefficient
- E = Young's modulus
- ν = Poisson's ratio

Work of fracture for refractories can be measured by methods such as chevron notch three-point bend test, whereby the energy required to produce and propagate a crack through a material is measured.

E. Corrosion Resistance

Refractory materials are used in a wide variety of applications and as a consequence encounter an equally wide range of molten, potentially corrosive media. As a result, numerous methods have been developed to assess corrosion resistance.

Test methods available are useful for comparing materials. However, many methods have limitations in that they do not reflect precise in-service conditions and generally are carried out at a single temperature, that is, no account is taken of the effect of thermal gradients on corrosion rates.

Tests for attack of refractories by molten agents are often described as either static or dynamic methods.

Static tests include the "crucible" or "cup" method whereby a corrosive agent is placed in a hollow within the refractory test piece or whereby a test finger is placed in a crucible of the corroding agent. The test pieces are then heated at a set rate to the test temperature and held there for a set duration. On cooling, the

degree of attack is then assessed visually or by examination of bond attack. Microscope sections can be prepared and the degree of attack examined. ASTM C621-84 (2001) (3) describes a static test to assess the corrosion resistance of glass contact refractories.

Dynamic test types include the rotating finger dip test, rotating panel tests such as BS 1902.5.13:1984 (4) and ASTM C874-99 (3) whereby test materials are cut to shape and are assembled in a rotating test furnace to form the hot face lining and slag drip test, ASTM C768-99 (3). Assessment of corrosion can be assessed by changes in material volume or thickness.

Tests that allow movement and flow of the corroding medium over the surface of the material prevent the formation of a protective boundary layer that would otherwise protect the material from further corrosion (13,14).

The corrosion resistance of a refractory to a particular medium at a specified temperature is influenced by a number of factors. These include their relative chemistries (corrosion series), microstructure, bulk density, apparent porosity, pore size distribution, permeability, and wetting angle.

F. Alkali Attack

There are many applications in which refractory materials are exposed to alkali vapors or melts. The crown of a glass melting furnace is just one example. Again, it is difficult in these tests to simulate precise service conditions. Sodium and potassium vapors are the most commonly encountered in refractory systems.

Assessments tend to involve suspension of the refractory over a crucible containing the alkali salts, e.g., ASTM C987-00 (3). Visual inspections, changes in weight, and microscopic assessment help in comparing materials.

G. Acid Resistance

Assessment of acid resistance is important for chimney linings, incinerators, and heavy clay and ceramic kiln linings. Methods such as BS EN 993-16:1995 (2001) and ISO 8890:1988 (1998) assess a material's resistance to attack by a boiling/condensing method.

H. Carbon Monoxide Resistance

Depending on their composition, many refractories may begin to deposit carbon when exposed to a carbon monoxide-rich atmosphere over a certain temperature range. The dissociation reaction is as follows (2):



Any free iron present acts as a nucleation site for deposition of carbon. The mechanism of the reaction typically involves the production of iron carbides.

It is therefore important to assess all refractories, which may operate under reducing conditions to ensure that they are resistant to attack by carbon monoxide. The optimum temperature for carbon deposition leading to bulk carbon growth, cracking, and finally disintegration of the refractory is generally between 400°C and 600°C. Figure 3 shows an example of a material that failed the test.

Assessment of refractories for resistance to carbon monoxide attack therefore takes place at 450°C (BS 1902-3.10) (4) and approximately 500°C for ASTM C288-87 (3) and ISO 12676:2000. Refractory prisms are placed in a sealed furnace into which a stream of carbon monoxide is introduced. The test pieces are visually inspected at regular intervals throughout the test duration, nominally 200 hours or until disintegration takes place, and their appearance noted.

Ideally, materials for use in reducing atmospheres should have a minimal content of iron that is free or potentially reducible.

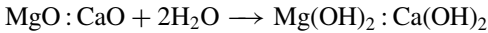
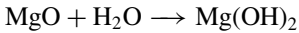
I. Hydration Resistance

Magnesia and dolomite, in both granular form and as shaped products, are susceptible to hydration. Even so-called dead burning of the material (firing to high temperatures to increase grain growth and hence reduce grain surface area) does not completely eradicate the problem. Hydration of these materials takes place via



Figure 3 Ramming material, which failed a CO test.

the following reactions leading to breakdown of the refractory structure.



The extent of the hydration reactions is dependent on temperature, exposure time, and degree of product susceptibility.

Assessment of the hydration resistance of basic bricks and shapes can take place in pressurized systems in an autoclave or pressure cooker or without pressure by storage in a humidity chamber. Generally, bricks with a minimum of three original surfaces are required. Specimens are examined after a set time period and results calculated or repeat tests take place until a specific total test time is reached or until the refractory disintegrates (3,4).

Hydration resistance of magnesia refractory grain sample is also measured via an autoclave method whereby the dried sample, of specified grain size fractions and known weight, is placed in the apparatus for a set duration or by suspension of the material in a flask containing boiling water with a condenser attached. Specimens are removed and dried to constant weight. Hydration tendency in some cases is recorded as the percentage of softened material passing through the sieve after the test (3,4).

Hydration resistance of dolomite grain is measured in a similar manner to magnesia except that the graded and dried sample is placed in a petri dish in a steam-humidity cabinet for a longer duration (24 hours). Following the test, the weight of the redried sample passing through a specified sieve size is given as a percentage of the total weight recorded after hydration (3,4).

J. Exudation Testing of Glass Contact Refractories

As we have seen, certain tests are only specific to particular refractory types but including these in a test regime to characterize a material can prevent catastrophic in-service problems. An example is the exudation testing of alumina–zirconia–silica (AZS) refractories, which form the side walls and superstructure of the melting tank of glass furnace. These materials, depending on how well oxidized they are during their production, can produce a glassy exudate when refired to a high temperature, which, if excessive, can contaminate the glass melt, producing vitreous and crystalline faults (13,14).

Comparison of chemical and physical properties of well- and poorly oxidized materials may reveal no apparent differences. However, firing discs or bars of material and then measuring the resulting change in volume may reveal a high exudation potential. An increase in volume results from exudation of the glass phase onto the disc surface. ASTM C1223-98 (6) gives details of this test type.

The maximum acceptance limit is around 2%, with higher values giving rise to increased risk of glass faults (13).

III. DESIGN PROPERTIES

Various chemical, structural, physical, in-service, and temperature-related tests for refractory materials have now been described. There is now a need to consider the combination of tests that provide us with properties, which additionally allow us to take that additional step from material test piece to a working refractory lining or component. This suite of tests allows us to study the thermomechanical behavior of materials and can be used in finite element modeling of refractory systems.

Test data required for modeling can be divided into two categories:

- 1. Data required to produce a thermal profile
- 2. Data required to produce a stress profile.

This is shown in Table 5.

As temperature increases there are changes in material thermal conductivity, strength, and stiffness. Materials expand or contract, and at high temperature material creep becomes significant.

We will now take a look at how some of these properties are measured and their importance in order to gain data to produce a mathematical model. Some examples of behavior of different types of refractory materials are given.

A. Thermal Conductivity

The thermal conductivity refers to the amount of heat flow through a material in unit time, per unit temperature gradient along the direction of flow and per unit cross-sectional area (2). The selection of a material with the most appropriate thermal conductivity for an application is essential. Sometimes a material of low conductivity is required to conserve heat and, in other cases, such as in areas of furnaces where the shell is cooled or contains internal water-cooled blocks, highly conducting materials are required for transfer of heat.

Thermal conductivity is also the most important parameter for producing a thermal profile through a refractory lining or component in mathematical

Table 5 Test Data Required for Thermomechanical Modeling of Refractory Structures and Components

Thermal profile	Stress profile
Thermal conductivity	Thermal expansion
Specific heat capacity	Bulk density
Emissivity	Stress-strain behavior in compression or flexure
	Poisson's ratio
	Creep

modeling. It is important to remember that thermal conductivity of a material is temperature-, density-, porosity-, and atmosphere-dependent.

Table 6 shows the range of thermal conductivities at a single temperature for a selection of refractory materials.

Thermal conductivity can be measured by several different methods, and some are reviewed here.

In **steady-state** methods, heat flow is measured through a thermal gradient between the hot and cold faces of the refractory. Heat flow and corresponding temperature rises are measured and conductivity calculated. The conductivity is quoted at the mean temperature between hot and cold face. Examples of this method are shown below.

1. *Calorimeter method*—This method can be used for measurements on low-conductivity insulating materials, but measurements of conductivities up to around 20 W/mK are also possible with this equipment. The results from the British Standard (BS 1902.5.5:1991) and ASTM method (C201) are often compared. The position of the calorimeter has the greatest influence on the conductivity values measured. Apparatus in which the calorimeter is positioned underneath the test sample, as in the ASTM method, yields lower conductivity values than when positioned above the test sample such as in the British Standard Method.

The British and ASTM panel methods were directly compared a number of years ago. The calorimeter positions lead to slight differences in the measurement of the heat flow. However, this work found that maximum discrepancies between these two tests did not exceed 5% (15,16).

2. *Split column method* (BS1902-5.8:1992) (4)—This method is used to measure values for the high thermal conductivity materials up to 80 W/mk such as those containing carbon, and the test can therefore be performed under

Table 6 Examples of the Range of Thermal Conductivity Values of Refractory Materials

Material	Thermal conductivity value (W/mK)
Low-temperature insulation panel	0.02
Insulation brick	0.15
Firebrick	0.80
High-alumina brick	1.50
Magnesia brick	5.00
Blast furnace carbon brick	13.50
Semigraphite carbon brick	30.00
High-conductivity graphite brick	107.0

argon or nitrogen atmosphere to prevent oxidation of carbon. The test specimen is sandwiched between two standard materials, and several thermocouples are positioned to measure the heat flow. The sides of the specimen are insulated to ensure that heat is not lost in that direction. Figure 4 shows a typical test setup.

In **transient methods**, measurements are taken after an input of heat, and the test materials are at a single temperature. Measurements can also be taken at ambient temperature, as small temperature rises are considered, which is not possible with steady-state gradient methods. Some examples of transient methods are discussed below:

1. *Cross array hot wire method* (BS EN 993-14:1998 and ISO 8894-1:1987) — In this method, two wires are welded together and sandwiched between the blocks of the test material. One is a heater, and the other is a thermocouple, and they lie in as cross arrangement. Hence the name. Power is fed to the hot wire for a short time, and the temperature rise measured. The temperature rise is related to the thermal conductivity of the material. This arrangement is more suited to measurement of materials with conductivities up to 2 W/mK.

2. *Parallel hot wire method* (BS EN 993-15:1998 and ISO 8894-2)—To extend the range of conductivities measured, the parallel hot wire method was devised. In this method, as its name suggests, the heater and thermocouple wires are arranged in parallel. This modified arrangement allows thermal conductivities up to 25 W/mk to be measured.

Eschner et al. (17) suggest differences in hot wire (transient) and calorimeter (steady-state) methods were about 10–15%, with hot wire values being higher. Further investigations by Davis and Downs on this subject suggested

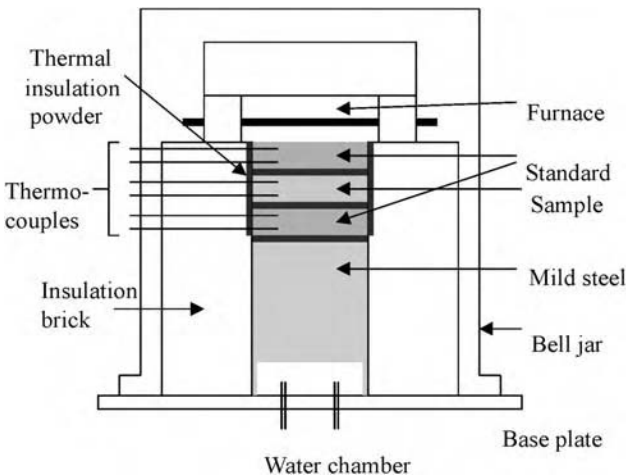


Figure 4 Split column thermal conductivity test arrangement.

that if sufficient care was taken with methods and specimen preparation, then a scatter of $\pm 2\%$ could be obtained for insulation materials rising to $\sim 5\%$ for higher conductivity materials (18).

Possible reasons for differing results in the techniques have been suggested, and these are as follows:

1. In the panel steady-state method, the conductivity is reported at a mean value between the hot and cold face. Wide temperature differences therefore exist compared to a narrow temperature difference in the hot wire, transient method. The effect is most marked with insulating materials (18).

2. In the panel steady-state method, heat flow is linear from hot to cold face of a refractory, whereas in the hot wire method, heat flow is in a radial direction from the heater wire. Therefore, if any material anisotropy exists, the latter method measures a mean conductivity of two directions (18).

Figure 5 compares steady-state and transient method thermal conductivity measurements.

While thermal conductivity results obtained may depend on the standard used, if care is taken with specimen preparation and test setup, it is possible to reduce variations within a particular material considerably.

As mentioned, the thermal conductivity of refractories often changes with temperature, and dense and insulating material types tend to behave differently with changes in temperature.

Figure 6 shows the variation of thermal conductivity with temperature for selection of dense refractories. For many dense refractories the conductivity decreases with increasing temperature for these materials. Heat flow through the solid by conduction predominates. As temperature increases, the thermal

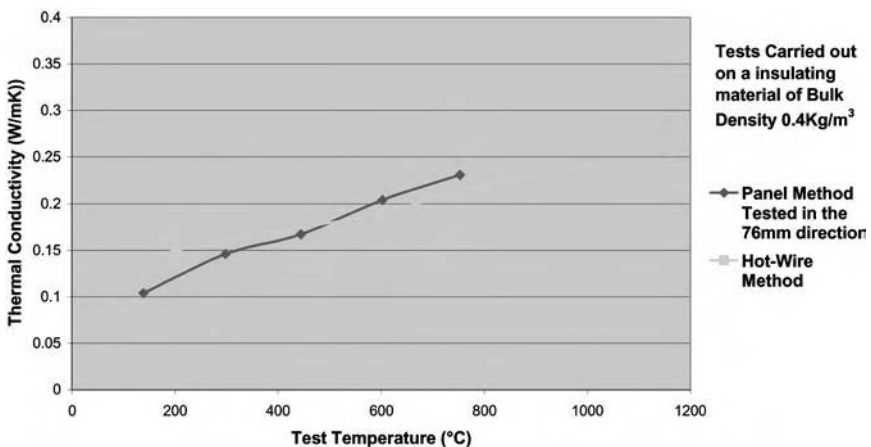


Figure 5 Comparison of panel calorimeter and parallel hot wire thermal conductivity techniques. (From CERAM data.)

energy of the solid also increases and vibration of phonons becomes greater. These increased vibrations cause more random than directional heat transfer and, as a result, heat flow rate and hence thermal conductivity reduce.

Figure 7 shows the variation with temperature for some lightweight refractory materials. In these materials the opposite is generally true in that thermal conductivity increases with increasing temperature.

In lightweight materials the gas within the pores has a greater influence on the thermal conductivity than in a dense refractory. At lower temperatures proportionally more heat transfer occurs through the solid phase as gas molecules are low in energy. As the temperature increases, heat flow through the gas phase increases as the number of collisions between gas molecules increases. As the temperature is raised further, first convection currents then radiation across the pores increase the effective heat flow and hence reduce the insulating capabilities of the material.

B. Specific Heat Capacity

The specific heat capacity is the ratio of heat capacity of a substance to the heat capacity of water. More specifically, it is the quantity of heat required to raise the temperature of 1 g of a substance by 1°C or 1°K.

Measurement is by observing the increase in temperature of water in a calorimeter when a specimen heated to a specific temperature is plunged into the water. Tests are nominally performed on a cylindrical test specimen. In-house procedures exist, but at present there are no standard refractory methods for measurement of this property.

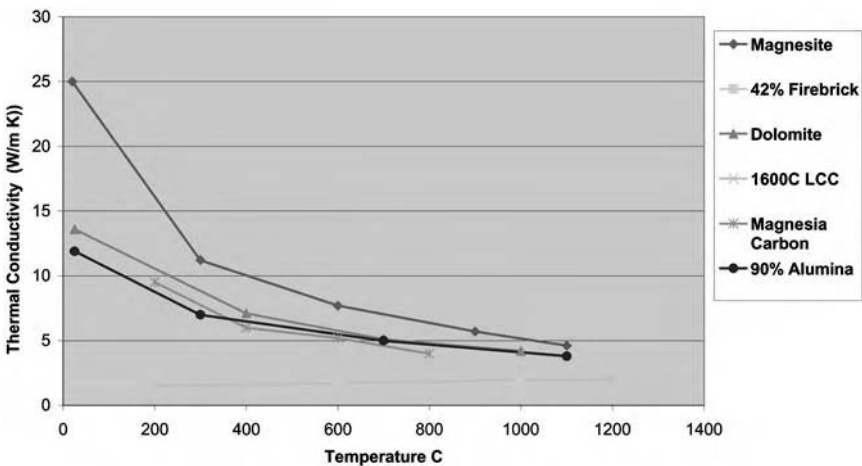


Figure 6 Thermal conductivities of dense refractories. (From CERAM data.)

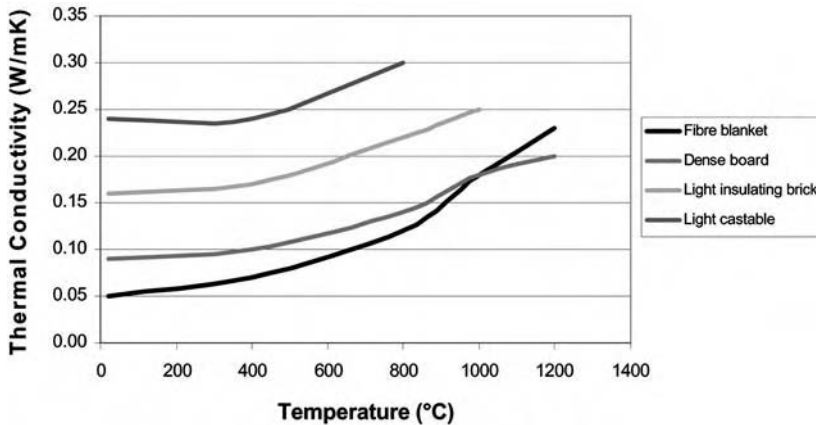


Figure 7 Thermal conductivities of insulating refractories. (From CERAM data.)

C. Emissivity

The emissivity of a material relates to how intensely radiative heat is reflected from its surface. Values range between 0 and 1 from a light, reflective to an increasingly dark, dull surface. Measurement is by a dual wavelength, calibrated optical pyrometer when an object is heated to a known temperature. No standard methods for refractories currently exist despite the influence of this property in many applications.

D. Thermal Expansion

Thermal expansion is the increase in dimensions of a material when heated. When no permanent change in dimensions is apparent after cooling, the expansion is said to be reversible. In a refractory lined vessel, stress builds up from the thermally generated strain. Measurement of thermal expansion is of key importance when designing refractory linings. Consideration must be given to the size and number of expansion joints required in a system. Linings need to close sufficiently on heating to prevent ingress of corrosive media, but a joint may be required to prevent high stressing between sections of the lining, which may lead to material failure.

Measurement methods vary. Both horizontal and vertical measuring techniques exist, and test piece sizes vary between 114 mm long \times 38 mm \times 38 mm in the ASTM standard test (3), which combines thermal expansion with a refractoriness under load test, down to small rectangular prisms of 55 mm \times 10 mm \times

10 mm in British standard tests (4). In the ASTM standard, the expansion is measured under a specified compressive stress.

Tests recording thermal expansion alone apply a temperature increase at a rate of between 1 k–5 k/min. From the expansion curve, the thermal expansion coefficient can be calculated as the amount of length increase per °C or °F over the specific temperature range or expressed as a percentage increase from the original length at ambient temperature. Figure 8 shows thermal expansion curves for a selection of refractories.

Not all materials expand linearly with temperature. The high, nonlinear expansion curve for silica stands out. The shape of this curve relates to the large volume expansions associated with quartz, cristobalite, and tridymite. Silica refractories must be heated carefully over the temperature range of 200–400°C due to greater rate of expansion.

E. Creep in Compression

Creep in compression is described as the plastic deformation of a refractory under a specific compressive stress over time. Again, as with refractoriness under load, the ability of a brick to withstand a load is dependent on the softening point and the amount of glass phase within the refractory system.

Measurement of creep is particularly important for materials selected for areas under contained load at high temperature, such as melting tank crowns of glass-making furnaces.

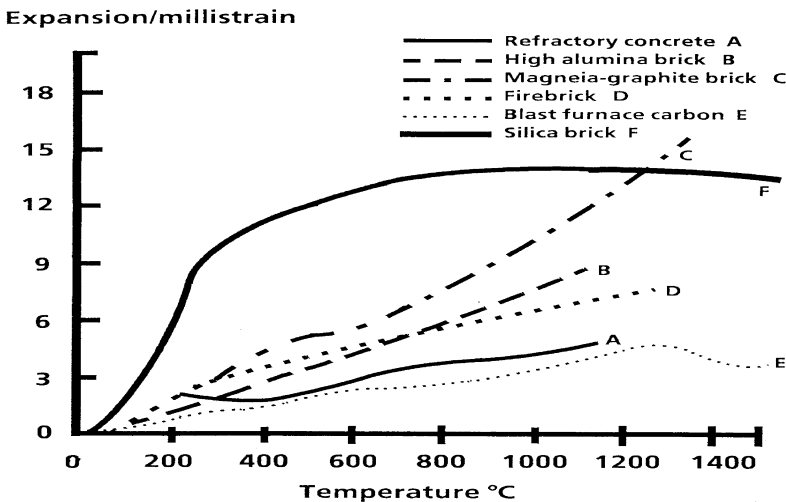


Figure 8 Thermal expansion of selected refractory materials. (From CERAM data.)

In the laboratory test a refractory specimen of nominal size 50 mm in diameter and 50 mm high is placed in furnace, in contact with a dilatometer system connected to an extensometer, and heated to the test temperature with a specific stress applied, nominally around 0.2 MPa for dense refractories. Once at temperature, the deformation of the sample over time is monitored. Results are represented graphically as a curve of creep percent versus time.

The total recorded creep over 25 hours should not exceed 0.2% at the proposed service temperature and loading conditions (19).

Application of creep data to finite element models will give a more accurate picture of stress levels over time at steady state.

F. Poisson's Ratio

Poisson's ratio is defined as the ratio of axial strain to diametral strain of a material. This parameter therefore defines the relationship between the effects of deformation in a direction perpendicular to the acting stress.

Measurement of dynamic modulus of elasticity (Young's modulus, E) and modulus of rigidity (G) can be determined by measurement of the fundamental longitudinal and fundamental torsional resonant frequencies of regular shaped test specimens. Resonant frequencies are detected by means of either a mechanical or electrostatic drive or detection technique by means of a commercially available apparatus.

The dynamic modulus of elasticity, E , is given by the formula

$$E = 4f^2 l^2 \rho \times 10^{-15} \text{ GPa}$$

where

f = the fundamental longitudinal resonant frequency (Hz)

l = the length of the specimen (mm)

ρ = the bulk density (Kg m^{-3})

The modulus of rigidity, G , is given by the formula

$$G = 4f^2 l^2 \rho F \times 10^{-15} \text{ GPa}$$

where

f = the fundamental torsional resonant frequency (Hz)

l = the length of the test specimen (mm)

ρ = the bulk density (Kg m^{-3})

F = the form factor (1 for a circular cylinder and 1.183 for a square cross section prism)

Poisson's ratio can then be calculated from the equation

$$\text{Poisson's ratio } \nu = \frac{E}{2G} - 1$$

where

E = the modulus of elasticity

G = the modulus of rigidity

Ambient temperature values for refractories are around 0.15. In comparison, values for metals are approximately 0.2–0.3, and rubber materials around 0.5. The property also varies with temperature.

G. Stress–Strain Testing in Compression and Flexure at Ambient and Elevated Temperature

Strength tests alone do not tell us everything about overall performance. Additional measurement of material deformation, however, provides more useful data, and curves of stress versus strain can be plotted. From the slope of these curves the static modulus of elasticity can be calculated. Modulus of elasticity by static loading, which takes into account the full strain range of material, is generally used for mathematical modeling. Dynamic modulus of elasticity, determined by resonant frequency methods, considers only the small strains around the origin of the stress–strain curves. This value is not generally appropriate for finite element calculations.

Compressive stress–strain data are required mainly for the modeling of refractory linings, whereas flexural stress–strain measurements are more often applied to individual refractory components such as sliding gate plates or kiln furniture.

From these tests, the failure stress and the static modulus of elasticity can be determined at various temperatures over the material's operating range. These data can then be applied to the mathematical model.

Figures 9 and 10 show examples of test arrangements used for measurement of these properties. With some modifications it is also possible to measure the properties of carbon-containing refractories (20). Tests are often performed on testing machines equipped with load cells and high-temperature furnaces.

For compressive stress–strain, the test specimen is placed between load columns in the furnace. A dilatometer system, to which the extensometer is attached, is located in the test specimen as shown. Other arrangements may use optical or averaging extensometers. This means the specimen deformation and hence strain can be measured. It is important to load the specimen slowly during the test to simulate the slow stress build due to thermal expansion in a refractory lining.

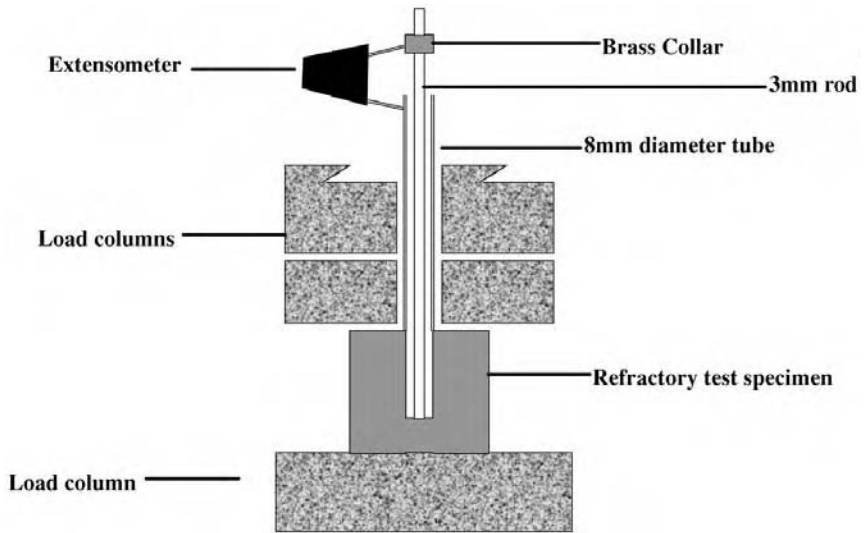


Figure 9 Compressive stress-strain test arrangement.

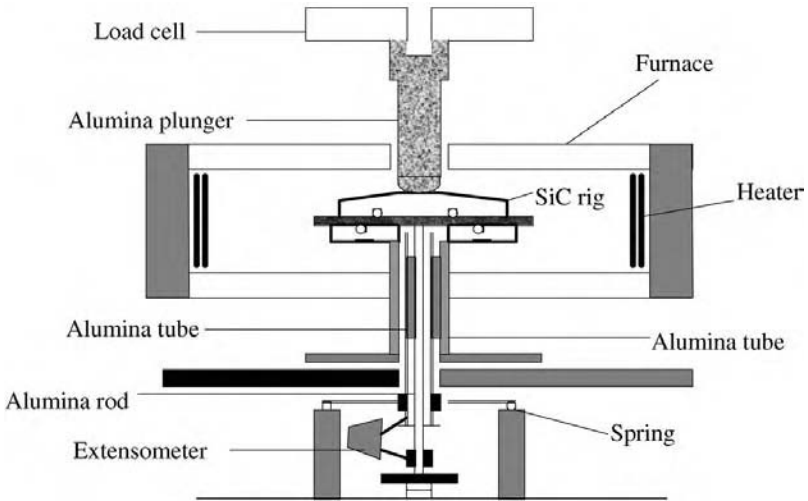


Figure 10 Flexural stress-strain 4-point arrangement.

The calculation of compressive failure load is shown in a previous section. Compressive strain is calculated as follows:

$$\% \text{Strain } \varepsilon = \frac{d}{h} \times 100$$

where

d = deformation (mm or in.)

h = specimen height (mm or in.)

Flexural stress–strain tests, as with modulus of rupture, can be carried out in either three- or four-point flexure. An alumina dilatometer attached to an extensometer, located under the test arrangement, measures specimen deformation and hence strains directly.

The calculations for failure stress in three- and four-point flexure were shown earlier. Material strain is calculated using the following formulas.

$$\text{Strain(3-point load)} = \frac{6dy}{L^2}$$

$$\text{Strain(4-point load)} = \frac{12dy}{(3L^2 - 4a^2)}$$

where

W = applied load (in Newtons or lbs)

y = specimen deformation (mm or in.)

L = test span (mm or in.)

b = specimen width (mm or in.)

d = specimen depth (mm or in.)

a = distance between the upper and lower loading points (mm or in.)

Examples of compressive and flexural stress–strain curves for a 60% alumina refractory measured at various temperatures are shown in Figures 11 and 12.

These graphs show how much stronger materials are in compression than flexure (or tension). The graphs also demonstrate the nonlinear relationship of refractory materials over the temperature range.

Stiffness, i.e., MOE, reduces in the majority of cases for refractories with increasing temperature.

There is currently no national or international standard for measurement of compressive and flexural stress–strain properties although the need has been recognized by the various standards bodies.

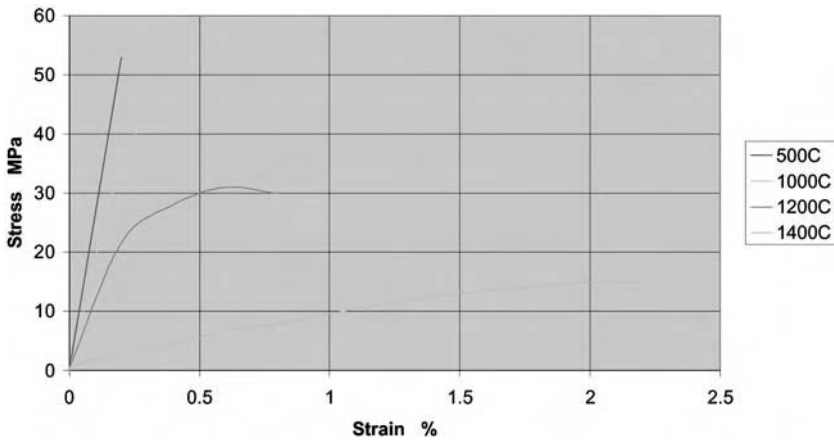


Figure 11 Compressive stress–strain of 60% alumina brick.

IV. SUMMARY

A review of the wide variety of the tests used to describe aspects of behavior for refractory materials has been undertaken.

In many cases for a specific property the method chosen can lead to some bias in the results obtained. However, if care is taken with sample preparation and test setup, then such effects can be reduced to a minimum, which would then make valid comparisons easier.

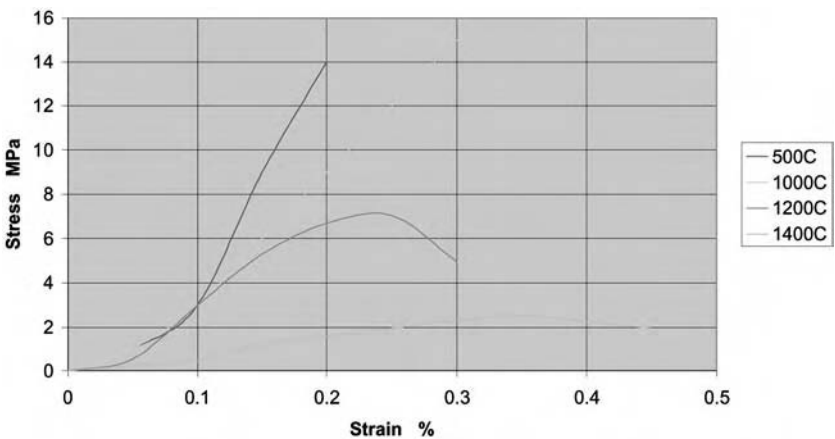


Figure 12 Flexural stress–strain of 60% alumina brick.

Table 7 Standards Available for Refractory Tests Featured (2003)

	Test method type	BS	CEN	ISO	ASTM
Chemical analysis	X-ray fluorescence			ISO 12677:2003	
	Alumino silicates	BS 1902.9.1:1987 (1996)			
	Silica	BS 1902.9.2:1987 (1996)			
	Wet chemistry				
	Alumino-silicates		EN 955-4		
	Chrome bearing	BS 1902.2.2:1974 (1995)	EN 995-3		
	Magnesites and dolomites		EN ISO 10058:1996	ISO 10058:1996	
	B ₂ O ₃ in magnesites	BS 1902.2.3:1976 (1995)			
	Chrome VI	BS 1902.9.3:1998			
Bulk density/ apparent porosity/true porosity	Vacuum pressure method of dense refractory shapes		EN 993-1:1995	ISO 5017:1998	ASTM C830-00
	Burned refractory brick and shapes—boiling water				ASTM C20
	Granular materials— boiling method				ASTM C357-94 (1998)
					(continued)

Table 7 Continued

	Test method type	BS	CEN	ISO	ASTM
Bulk density/true porosity	Solid refractories by wax immersion			ISO 5016:1997	ASTM C914-95
	Shaped insulating products		EN 1094-4:1995 (2001)		
Bulk density and volume	Dense shaped products	BS 1902.3.17:1990			ASTM C134-95 (1999)
	Insulation products				ASTM C134-95 (1999)
True density	Water immersion		EN 993-2:1995 (2001)	ISO 5018:1983(1998)	ASTM C135-96
	Pycnometer				ASTM C604-98
Powder density		BS 1902.3.5 1981 (1998)			
Grain bulk density			EN 993-17:1999	ISO 8840:1987	
			EN 993-18:2002		
			EN 993-5:2000	ISO 8995:1986 (1991)	ASTM C133-97
Cold crushing strength	Dense refractory		EN 1094-5:1995 (2001)	ISO 10059-1:1992	ASTM C133-97
	Shaped insulating products		EN 993-4:1997		
Permeability to gases	Ambient			ISO 8841:1991 (2001)	ASTM 577-99
	Elevated temperature	BS1902-10.2:1994			
Pore size distribution		BS 1902.3.16:1990			

Pyrometric cone equivalent	Fireclay and high-alumina refractories	EN 993-12:1997 (2001) (BS 1902-5.2:1997)	ISO 528:1983 (1998)	ASTM C24-01
Permanent dimensional change on heating	Dense shaped products	EN 993-10:1998 (2003) (BS1902-5.10:1998)	ISO 2477:1987 (1998)	ASTM C113-93 (1998)
	Shaped and insulation products	EN 1094-6:2000		ASTM C113-93 (1998) ASTM 210-95 (1999)
Abrasion resistance	Plastic /rammables			ASTM C179-85 (1999)
Modulus of rupture	Ambient temperature Ambient Elevated temperature	EN 993-6:1995 EN 993-7:2000	ISO 5014:1997 ISO 5013:1985 (1990)	ASTM C704-99 ASTM C133-97 ASTM C583-00
Refractoriness under load	Carbon-containing refractories	EN 993-8:1997 (2001)	ISO 1893:1989	ASTM C1099-92 ASTM C832-00
Thermal shock resistance	Ribbon burner test Thermal cycling Prism spalling method	ENV 993-11:1998 BS 1902.5.11:1986		ASTM C1100-88 ASTM C1171-96

(continued)

Table 7 Continued

	Test method type	BS	CEN	ISO	ASTM
Corrosion resistance	Rotary slag test	BS 1902. 5.13:1984			ASTM C874-99
Alkali attack	Drip				ASTM C768-99
	Static corrosion in glass				ASTM C621-84(2001)
Vapor attack	Aging of carbon refractories				ASTM C454-83 (1998)
Acid attack (sulphuric)			EN 993-16:1995 (2001)	ISO 8890:1988 (1998)	ASTM C987-00a
CO attack		BS 1902. 3.10:1981		ISO 12676:2000	ASTM C288-87
Hydration tendency	Dolomite	BS1902. 3.14:1996			ASTM C492-92
	Magnesite	BS1902.3.14:1996			ASTM C544-92
Exudation testing of AZS refractories	Basic bricks and shapes	BS1902.3.14:1996			ASTM C456-93 (1998)
					ASTM C1223-98

Thermal conductivity	Steady state Calorimeter	BS 1902.5.5:1991 (1996)		ASTM C201-98 (C202) (C182) (C417) (C767)
	Split column	BS 1902.5.8:1992		
Thermal expansion	Transient method			
	Parallel hot wire		EN 993-15:1998	ASTM C1113-99
	Cross array hot wire		ISO 8894-2:1990 ISO 8894-1:1987 (2003)	
Thermal expansion	Platinum resistance thermometer technique			ASTM C767-93
	Large test pieces			ASTM C832-00
	Shaped, fired refractory products. Horizontal method to 1100°C		BS 1902.5.4:1989 (1996) BS 1902.5.3:1990 (1996)	
Creep in compression	Shaped, fired refractory products to 1500°C		BS 1902.5.14:1992	
			EN 993-9:1997 (2001) ISO 3187:1989	ASTM C832-00

It is also difficult to accurately reproduce service conditions in test methods, and care should be taken with subsequent interpretation.

Various bodies and committees produce test standards for refractory materials. Table 7 summarizes the featured test methods available from British, CEN, ISO, and ASTM bodies.

Acknowledgments

Dr. Tex Palin, David Shepherd, Andrew Deighton, and John Cotton for reviews and comments. Paul Hodson and Kevin Thomas for compiling the table of standards.

REFERENCES

1. Herrell D, Palin FT. Refractories—Testing and General Properties, Mechanical Engineers Reference Book. 11th ed. 172–179.
2. Dodd A, Murfin D. Dictionary of Ceramics. 3rd ed.
3. Annual Book of ASTM Standards 2003. Vol. 15.01. Sect. 15.
4. British Standards Tests for Refractory Materials, British Standards Institute.
5. Pandolfelli VC, Innocenti MDM, Pardo ARF. Permeability of high-alumina self flow refractory castables, UITECR '99. Proc Unified Intl Tech Conf on Refractories. 6th Biennial World Congress/42nd Intl Colloq. On Refractories, Berlin, September 6–9, 1999:93–96.
6. Innocenti MDM, Studert AR, Pileggi RG, Pandolfelli VC. How PSD affects permeability of castables. *Am Ceram Soc Bull* 2001; 80(5):31–36.
7. Carswell GP. Pores for thought. *Refractories Journal* 1977; 52(6):7–19.
8. Malkin JT, Padgett GC. Abrasion of refractories at elevated temperatures. *Interceram* 1979; 28(Special Issue):228–233.
9. Cotton JW. Thermal Shock of Ceramics. CERAM research Web site.
10. Bell DA. Thermal Shock, Ceramic Technology International 1994. London: Sterling Publications Ltd, 1993:106–108.
11. Hasselman DPH. Thermal stress resistance parameters for brittle refractory ceramics, a compendium. *Bull Am Ceram Soc* 1970; 49(12):1033–1037.
12. Coppack TJ. A method for thermal cycling of refractories and an appraisal of its effect by a nondestructive technique. *J Br Ceram Soc* 1981; 80(2):43–46.
13. Evans G, Baxendale S. Refractory testing service. *Glass* 2000; 77(2):21–22.
14. Baxendale S, Farn S. Glass making refractories—the importance of corrosion assessment. *The Refractories Engineer* 2003; July:15–18.
15. Clements JF, Vyse J. A new thermal conductivity apparatus for refractory materials. *Trans Br Ceram Soc* 1954; 53:134.
16. Watson AF, Clements JF, Vyse J. A co-operative test on thermal conductivity. *Trans Br Ceram Soc* 1954; 53:156.

17. Eschner A, Grosskopf B, Jeschke P. Experiences with the hot wire method of measurement of thermal conductivity of refractories. *Tonind-Ztg* 1974; 98(9):212.
18. Davis WR, Downs A. The hot wire test—A critical review and comparison with the BS 1902 panel test. British Ceramic Research Association Technical Note No 286, February 1979.
19. Routschka G. *Refractory Materials* (Vulkan-Verlag Essen), 397.
20. Bell DA, Palin FT. Measurement of high temperature mechanical properties of refractories containing carbon, Unitecr 1989. Proc Unif Int Tech Conf on Refractories, Vol. 2, Anaheim, November 1–4, 1989:1219–1224.

Further Reading

1. Jarvis DA. Refractory testing provides valuable information, *Glass* 2001; 78(6):192–193.
2. Yang D, Blumm J. Viewpoint—testing times for refractories. *Asian Ceram Glass* 2001; December:39.
3. Moore RE. Significance and utility of refractories test data, third ECers. Proc 3rd European Ceramic Society Conf Vol 3. Engineering Ceramics, Madrid, September 12–17, 1993, Faenza Editrice Iberica SL, 1993:185–200.
4. Bell DA. Cold crushing strength—A waste of time? *Refract Eng* 2000; March:22.
5. Innocentini MDM, Silva MG, Menegazzo BA, Pandolfelli VC. Permeability of refractory castables at high temperatures. *J Am Ceram Soc* 2001; 84(3):645–647.
6. Innocentini MDM, Pardo ARF, Pandolfelli VC. Modified pressure decay technique for evaluating the permeability of highly dense refractories. *J Am Ceram Soc* 2000; 83:220–222.
7. Jena A, Gupta K. Materials pore sight—testing pore volume and flow through porous materials. *Mater World* 2002; 10(2):20–21.
8. Semler CE, Hawisher TH. Evaluation of thermal shock resistance of refractories using the ribbon burner method. *Am Ceram Soc Bull* 1980; 59(7):732.
9. Rogrigues JA, Pandolfelli VC, Rigaud M. Elevated temperature thermal shock parameters for refractories. *Interceram* 2002; 51(5):322–326.
10. Rodrigues JA, Pandolfelli VC. Thermal treatment temperature and its influence on the thermal shock parameters of refractory castables. *Interceram* 2002; 51(3):186–189.
11. Headrick WL, Moore RE. Sample preparation, thermal expansion and Hasselman's thermal shock parameters of self flow refractory castables. *Refract Appl* 2001; 6(4):5–7.
12. Fukushima Y, Kiyota Y, Takagi M. Evaluation of resistance to cyclic thermal shock of coke oven brick. *Refractories (Tokyo)* 2002; 54(2):86–87.
13. Crescent R, Rigaud M. Refractories testing: the usefulness of the rotary slag test. *Advances in Refractories for Metallurgical Industries*. Vol 4. Proceedings, Canadian Metallurgical Society; Canadian Inst. Mining and Metallurgy. Oxford: Pergamon Press, 1988:235–250.
14. Bell DA, Palin FT, Padgett GC. Effects of rapid heating on blast furnace refractories. *Steel Times* Feb. 1984; 212:65–66.

15. De Almeida M, Brook RJ, Carruthers TG. Thermal expansion of ceramics in MgO–CaO system. *J Mater Sci* 1979; 14(9):2191.
16. Le Parlouer P, Chan I. Calorimetry, dilatometry at high temperature: recent developments in instrumentation and applications. *Am Ceram Soc Bull* 2001; 80(7):31–37.
17. Okazaki M, Asuakura H, Minamizono H, Nataksukasa M. Development of a new thermal expansion measuring apparatus, *Refractories* (Tokyo) 2001; 53(3):136.
18. Hemrick JG, Moore RE, Wereszczak AA, Ferber MK. Creep behaviour and physical characterisation of fusion cast alumina refractories. Part 1. *Refract Appl* 2001; 6(4):9–11.
19. Hemrick JG, Moore RE, Wereszczak AA, Ferber MK. Creep behaviour and physical characterisation of fusion cast alumina refractories. Part 2. *Refract Appl* 2001; 6(3):8–10.
20. Wolters D. Testing refractories in reducing and non oxidising atmospheres. *Ind Ceramique* 1982;(766):804–808.
21. Schacht CA. Improved analytical procedures and material properties for predicting the thermomechanical behaviour of refractory linings and teeming ladles. *Ceramic Engineering and Science Proceedings* 1986; 7(1–2):209–219.

17

Refractory Lining Design and Installation

Charles A. Schacht

Schacht Consulting Services, Pittsburgh, Pennsylvania, U.S.A.

Michael Maupin

Maupin Enterprises, LLC, Northville, Michigan, U.S.A.

I. INTRODUCTION

Refractory lining design and installation are addressed here with respect to the thermal and mechanical behavior of the lining system. The chemical aspects of selecting refractory materials with respect to lining design and installation are not addressed here. Fundamentally, acid and basic processes dictate the type of refractory material (silica/acid and magnesia/basic) to be used. The primary purposes of refractory linings are to insulate the process temperature from the surrounding ambient temperature, to contain the product material, and to restrict the support structure (typically a steel structure) temperature to reasonable temperatures such that the steel maintains reasonable strength. Typically, carbon steel begins to lose strength and stiffness (yield stress and elastic modulus, respectively) at temperatures that exceed about 800°F (1). Based on the process temperature, the basic geometry of the refractory lining system, and the type of support structure, the second concern is the expansion forces developed in the lining and reacted by the steel support structure. This chapter describes the classical brick shapes, the primary classes of refractory lining geometries, the fundamental expansion behavior of each of the refractory lining geometries, the fundamentals of the need for lining containment, and the fundamentals in the use of expansion allowance material in the refractory lining system. Without appropriate lining containment, no expansion forces are developed and expansion allowance materials are of no use. Understanding the basic expansion behavior of each of

the classical refractory linings configurations also greatly assists in knowing where to place expansion allowance material and the amount of expansion allowance material. Compressible blanket and board materials and plastics sheets are often used as expansion allowance in refractory linings. Guidance is provided in the amount of compressive displacement that can be anticipated in these materials. Most refractories tend to soften, or go plastic, at elevated temperatures, as shown in Figure 1. Figure 1 is the static compressive stress–strain data (SCSS) for a 70% fired alumina brick. This behavior must be accounted for in the installation of expansion allowance. It should also be kept in mind that when the brick lining is installed, special care is given to making sure that the brick mortar joints are completely aligned. However, upon heatup of the brick, as expected, expansion occurs more on the hot face than on the cold face. As a result, misalignment occurs in the lining in the heated operating condition. The resulting compressive bearing loads do not occur over the complete brick bearing surfaces in the heated condition. Because of this behavior, “hinges” are developed in the lining in which a small portion of the brick bears the compressive load. These hinges occur at usually predicted locations based on the lining geometry. The locations of these hinges will be discussed, which will assist in the location of expansion allowance and also assist in zoning methods in the lining installation. That is, more crack-resistant brick should be placed in the hinge regions where higher operating stresses exist.

Castable lining systems are also addressed here in limited detail. Basically, monolithic castable linings will behave in the same fundamental

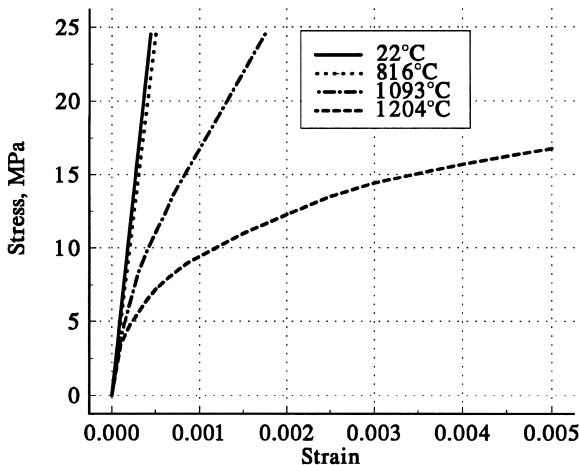


Figure 1 Compressive stress–strain data on a 70% alumina brick.

thermomechanical manner that brick linings behave. Brick linings have predetermined cracks (brick joints), where as castable linings do not.

II. REFRACTORY BRICK SHAPES

Refractory brick shapes are provided in several geometric shape definitions (2-4). Figure 2 describes these basic shapes. The shape name is defined below each shape. There are the straight, split, soap, wedge, arch, key, skew, circle, jamb, and semi-universal. Brick size is specified by the three orthogonal dimensions starting with the largest dimension proceeding to the smallest dimension. For example a 9-in. straight would be specified as $9 \times 4\frac{1}{2} \times 2\frac{1}{2}$, $9 \times 4\frac{1}{2} \times 2$, etc. The straight is a rectangular shape. Splits and soap use the same procedure for specifying the shape size. The split is basically a horizontal slice of the straight, parallel to the largest face. The soap is essentially a slice of the straight, perpendicular to the largest face. The wedge and arch shapes are specified, for example, as $9 \times 4\frac{1}{2} \times (2\frac{1}{2} - 1\frac{1}{2})$, with the taper on the smaller dimension. A key size would be specified as $9 \times (4\frac{1}{2} - 3\frac{1}{2}) \times 2\frac{1}{2}$, with the taper on the intermediate dimension. Note the A \times B \times C procedure in each case in which A is the largest dimension and proceeding to the smallest dimension C. There

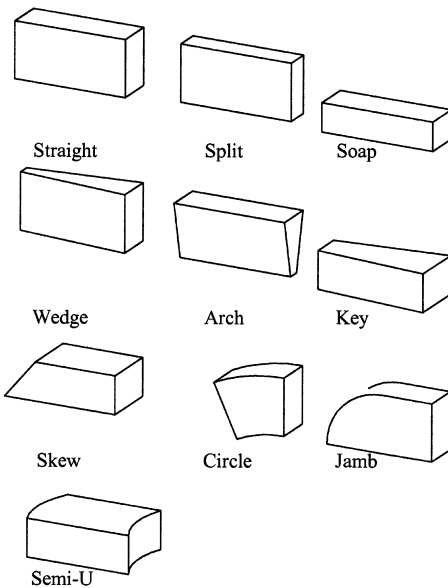


Figure 2 Primary shapes of refractory brick.

are several different skew shapes defined as end skew, edge skew, and side skew. Predetermined schemes using combinations of the arch or key brick are usually worked out by the supplier of the refractory shapes or the designer of the refractory lining to accommodate the desired radius of the cylindrical shaped lining or the arch roof or of any lining in question.

Special shapes are also produced for various industries. For example, in the steel industry, electric arc furnace (EAF) and blast furnace door jamb brick shapes are produced by some refractory manufacturers. Other special shapes include key shapes for blast furnace wall linings and arch-key and wedge-key shapes for EAF domes. These latter two shapes have a double taper (taper on both sides) that allows the brick to be laid to the desired contour of a dome. These two shapes are laid in various combinations to make up the desired dome radius. These shapes can be provided in various thicknesses such as 9 or $13\frac{1}{2}$ in. These shapes are also specified by a shape designation number that departs from the scheme defined above. As in cylindrical linings, combinations of the arch-key and wedge-key bricks are predetermined to make a desired dome radius. EAF refractory dome designs are being replaced by more efficient water-cooled steel domes (5). Fluid bed reactors also have interior process domes made of special refractory shapes. In these shapes, through-thickness holes are incorporated into the shape that allow hot gas flow in which the hot gas flows upward through the process dome and fluidizes the material resting on top of the dome. Fluid bed reactors and blast furnace stoves are examples of roof domes.

Steel-making ladles frequently use a two-layer brick lining (work lining and safety or permanent lining) in the ladle side wall. The brick lining against the steel shell side wall (safety) is typically a 3- to 6-in. refractory brick, and an insulation layer is sometimes used to help maintain the ladle's shell below critical temperatures. Sometimes a heat setting granular refractory material is used to create a monolithic layer in the ladle wall as well. The semi-universal shape (see Figure 1) has become a popular brick shape used for the work lining (lining wetted by the molten steel). This shape has rounded ends that allow an easier and faster installation to the cylindrical contour of the cylindrical steel shell. The semi-universal can typically vary from 3 to 9 in. in thickness. The semi-universal bricks are installed in a continuous spiral starting at the base of the wall and ending at the top of the wall. The installation is started at the base of the wall using special combinations of specially shaped bricks to the slope of the spiral. The semi-universal bricks are selected by a designation system defined by the manufacturer that defines the range of diameters that can be accommodated according to the diameter of the ladle wall. Semi-universal bricks are a variation in the shape of brick that can be installed in a range of shell diameters and still maintain tight joint integrity and tight contact with the backup lining or vessel shell. Ladle side walls are usually tapered in which the side wall radius increases from the base of the wall $\frac{1}{8}$ to $\frac{1}{2}$ in. per vertical ft of height,

causing the brick lining to be installed on a radius that increases with each course. The ladle steel shell wall radius can vary from about 45 in. (small ladles) to over 140 in. (large ladles) and in height from 8 to 15 ft. Some ladles are not round but are either elliptical or obround in shape, still tapering from top to bottom. Semi-universal shaped brick can be installed in the straight sections of the wall by as well as the curved sections by inverting the brick.

Steel-making ladle bottom linings are made in a variety of brick and types of refractory materials. Ladle steel shell bottom designs range from flat plate to elliptical dished plate. The flat bottoms are typically sloped to allow drainage of the molten steel to the discharge nozzle. Dished bottoms are also sloped. The molten metal discharges through a special slide gate design at the low side of the sloped bottom that is activated by an external mechanism located at the ladle bottom near the slide gate for discharging molten metal into the continuous caster. In dish bottoms a castable, plastic refractory, or heat setting fill refractory is used to establish a sloping flat surface for the brick shapes. The bottom brick can be straights of various dimensions, but other shapes are sometimes used. Full precast or cast-in-place castable bottoms are also used. The impact region of the molten metal on the bottom is often made up of either thicker refractory or of a more impact-resistant quality of refractory. The region between the bottom brick and the sidewall brick is filled with a plastic refractory or castable refractory. Special nozzle blocks are used at the discharge nozzle and around special porous plugs used for gas stirring. A plastic or castable refractory is used between the bottom straights and nozzle block or porous plug blocks.

Rotary kiln bricks or block shapes are typically arch, wedge, or circle shapes. The kiln lining includes a proper combination of one-half, two-thirds, and three-quarter splits. Manufacturers have predetermined the combination of kiln shapes for a desired kiln shell inside diameter.

It should be kept in mind that the vessel shell dimensions, such as the shell radius of a cylindrical vessel, may vary from those specified on the design drawings. Therefore, it may be prudent to provide actual vessel dimensions to the organization responsible for determining the combination of shapes in the lining.

Arch refractory linings are used in a variety of furnaces and tunnel kilns. Figure 3 describes the classical arch that is supported by skewbacks or skew shapes. A variety of skew shapes can be used to make a skewback.

Coke ovens are probably one of the most complicated refractory structures. For those not familiar with the steel-making industry, coke ovens are used to make coke (from coal) for processing raw iron from iron ore in a blast furnace. The coke ovens are made up of primarily silica block shapes (6). The shape design of the various silica block shapes make up the walls in the coke ovens. Hot gases flow internally through chambers in the walls. The walls are heated, which in turn heat the pulverized coal, converting the coal to coke. Silica bricks are used because of the very low expansion of the brick at higher temperatures,

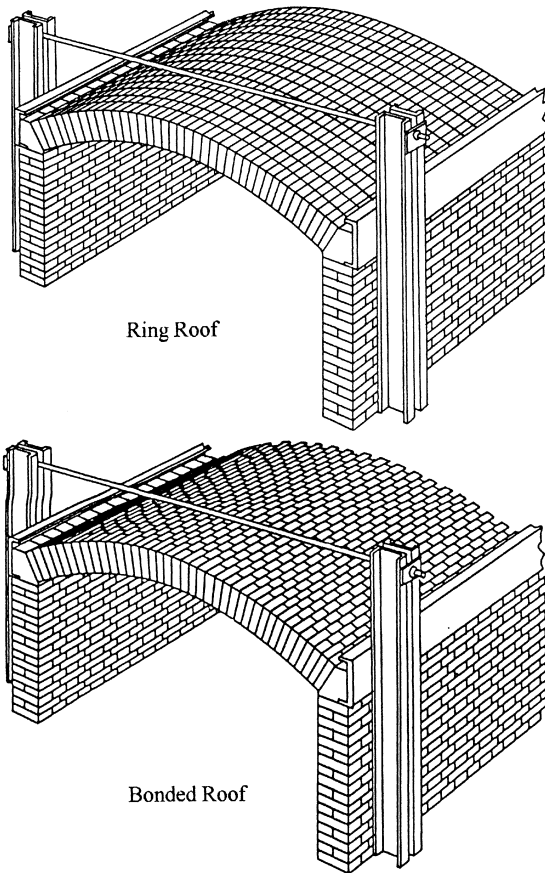


Figure 3 The refractory brick sprung arch. (From Refs. 2 and 3.)

giving a very stable structure in the operating temperature range of a coke oven. Special retaining mechanisms restrain the structure during initial heating when the refractory undergoes a large expansion.

III. TYPICAL LINING GEOMETRIES

Lining designs can be classified into five major geometries. They are arches, spherical domes, cylinders, cones, and flat walls. Each of these lining designs behaves in a unique way when heated to operating temperatures. That is, when the lining is heated and thermal expansion takes place, the lining will displace

and brick joints at certain locations will open. When the refractory bricks or blocks are heated, the bricks or blocks are distorted by the thermal expansion behavior and no longer fit the geometry of the lining. Therefore, brick or block joints will open. The portions of the lining brick joints that are in compression require quality mortar. The arch lining design can be used as an example to demonstrate this point. Figure 4a illustrates the unheated arch as installed with no loading and no hinges are formed. Figure 4b describes the spread arch (outward displacement of skewes). This would be equivalent to a heated arch having too much expansion allowance. Figure 4c describes the arch with insufficient expansion allowance. Note the hinges in Figure 4b and 4c form at the skewes and at the crown. In Figure 4b, the skew hinges are at the arch hot face and at the crown cold face. In Figure 4c, they are on the opposite sides of the arch. Because of the hinge formations at these regions, higher-quality brick should be used in these regions of the arch. In addition, the brick mortar joints are not in full use at these three regions. Even with a well-insulated arch with an insignificant through-thickness temperature gradient, these hinges will still occur based on the amount or lack of expansion allowance.

Refractory spherical domes form hinges at the base region of the dome (7), one at the skewback and one a short distance up from the skew as illustrated in Figure 5. This dome is restrained radially at the skew. The skew is in turn supported radially by a cylindrical steel shell and vertically by the cylindrical wall lining not shown. Other refractory dome investigations (8) have shown that the

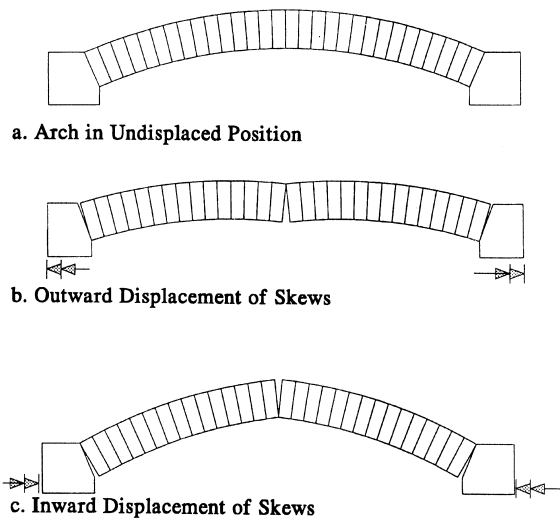


Figure 4 Hinge locations in a refractory arch.

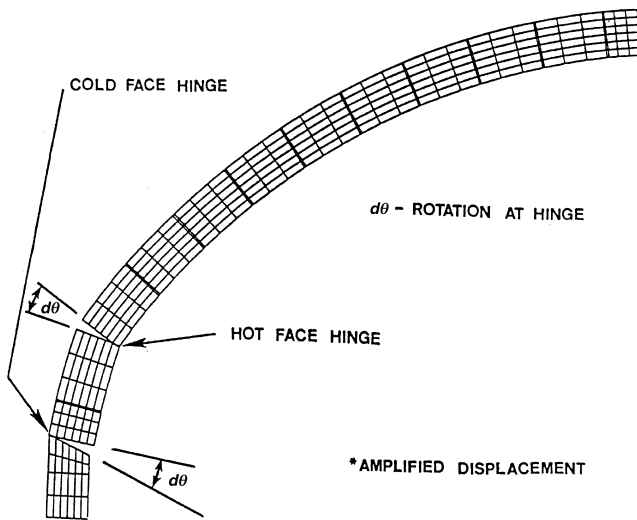


Figure 5 Hinge locations in a spherical refractory dome.

upper hot face hinge will migrate up and down in the brick joints above the skew due to cyclic heatup and cooldowns. The result is cyclic stresses in this lower portion of the dome. This helps to explain why the lower portion of the dome block tends to deteriorate faster than the rest of the dome. This lower region of the dome demands a higher-quality brick than the rest of the dome because of the cyclic stressing in this region. The mortar joints in the upper portion of the dome lining are in full bearing.

Cylindrical refractory lining systems are typical throughout industry. These types of linings consist of either a single or multiple lining systems inside a steel cylindrical shell. The steel shell provides the restraint as the lining inside expands due to the thermal heatup. Figure 6 illustrates the behavior of the radial brick joints. Typically, the joints compress on the hot face end region of the joint. At the cold face end the joints open. Therefore, the critical portion of the lining with regard to quality mortar joints is in the hot face region of the radial brick joints. The cold face ends of the mortar joints are considerably less important than the hot face end. The circumferential compressive stress results in a radial compressive load of the lining against the steel shell.

In some instances such as in steel-making ladles, the steel cylindrical side-wall shell has a taper in which the shell radius increases from the bottom to the top of the wall. The shell wall can be classified as a truncated cone section. The refractory lining, when exposed to a cyclic heating and cooling of the lining hot face, will cause the lining to progressively ratchet upward in the tapered shell.

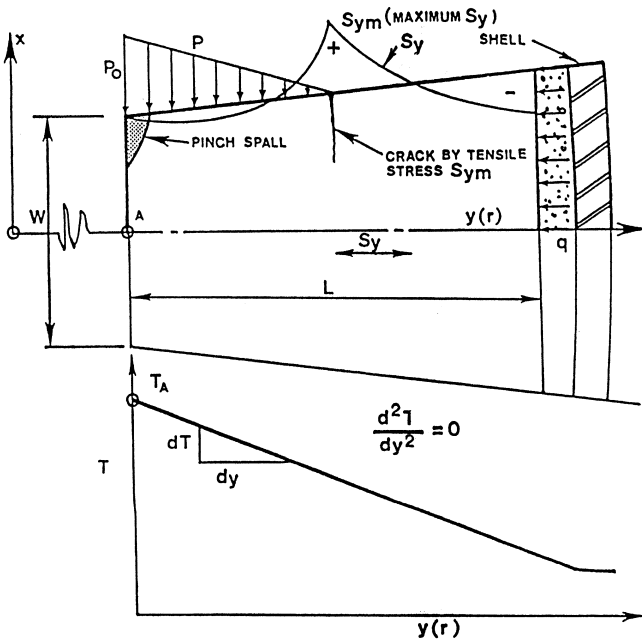


Figure 6 Stress behavior in cylindrical lining brick component with a linear temperature gradient.

Other examples of cylindrical lined vessels include blast furnaces, blast furnace stoves, basic oxygen furnaces, torpedo ladles, shaft kilns, multiple hearth furnaces, and rotary kilns. Some refractory lined vessels have refractory lined conical bottoms. When heated, the conical lining will want to displace upward. Therefore, the top mortar joint of the conical lining is critical. The cylindrical lining will be critical in restraining the upward expansion of the conical lining. At the ends of rotary kilns, restraint must be provided to contain and keep the kiln lining within the kiln shell.

Flat wall linings are not the most desirable type of lining but are necessary for rectangular shaped vessels. The hot face side of the lining brick joints (joints perpendicular to the hot face) will compress while the cold face end will open. Basically, the flat lining will tend to curl inward, away from the flat shell. Typically, the vessel steel walls consist of flat plate and are laced with stiffener members (Channel, I Beam, and WF Beam) on the exterior of the flat plate. Generally, anchoring of the refractory in a flat wall is required to keep resisting the inward force developed in the wall from heating. Specially designed anchors are used to anchor the refractory to the wall and may be made from metallic or ceramic materials, depending on the temperature and environmental conditions of the furnace. Examples of flat

walls are glass melting tanks, steel reheating furnaces, annealing furnaces, tunnel kiln walls, copper reverberating furnace, and steam boilers.

IV. EXPANSION ALLOWANCE

Expansion allowance is often used to reduce the expansion stress in the refractory lining. Expansion allowance is often used in lining systems made of magnesia and silica brick because of their high coefficient of thermal expansion. Approximate methods are used in which a percent of the full expansion displacement is taken for the amount of expansion allowance. Materials such as cardboard and plastic inserts are placed in brick joints that burn out at low temperatures. Compressible blanket of board materials are also used. Typically, low-density (10 to 25 pcf) blankets will compress to about 10 to 20% of their original unloaded thickness. Higher-density (50 to 60 pcf) board materials will only compress to about 80 to 90% of their original unloaded thickness.

Mortar joints can be taken into account as contributing to expansion allowance (8). The thickness of the mortar joints considered here are in the range of $1/32$ to $5/32$ in. (1 to 4 mm). Mortar joints approaching $\frac{1}{4}$ in. (6 mm) are used in some refractory lining systems such as coke oven walls.

In cylindrical refractory linings, expansion allowance can be used in the radial brick joints or in the circumferential joints. The relationship between the expansion allowance used in the radial joints for circumferential expansion allowance (Δ_C) and expansion allowance used in the circumferential joints for radial expansion allowance (Δ_R) is defined by the equation

$$\Delta_C = 2\pi\Delta_R = 6.28\Delta_R$$

That is, the expansion allowance used in the radial joints is an expansion allowance that affects the circumferential growth of the lining, whereas the expansion allowance used in the circumferential joint affects the radial growth of the lining.

In this example, assume a cylindrical lining that has an inside radius of 60 in. The lining is made of 57 magnesite bricks, each brick 6.61 in. in circumferential length. The operating temperature is 2000°F. In this example, 50% of the total hot face thermal expansion will be eliminated by expansion allowance material. The total circumferential thermal growth at the lining hot face (CE) is

$$CE = (\Delta T)(CTE)(C)$$

where ΔT is the increase in temperature from ambient, CTE is the coefficient of thermal expansion of the magnesite brick, and C is the circumference of the lining hot face. Therefore,

$$CE = (2000 - 70)(6.5E - 6)(2\pi \times 60) = 4.73 \text{ in.}$$

Using 50% expansion allowance, the total thickness of expansion allowance material used in the radial brick joints would be 4.73×0.50 , or 2.36 in. Using a 1/16-in.-thick plastic material that burns out at about 300°F, in 38 (two thirds) of the radial brick joints would amount to circumferential expansion allowance of

$$\Delta_C = 57 \text{ radial joints} \times 2/3 \times 1/16 = 2.37 \text{ in.}$$

If a layer of expansion allowance material were used instead, at the lining cold face, this radial expansion allowance material would have a thickness of

$$\Delta_R = \Delta_C/6.28 = 0.377 \text{ in. (about } 3/8 \text{ in.)}$$

Therefore, the use of 3/8-in.-thick radial expansion allowance material on the lining cold face is equivalent to using 1/16-in.-thick expansion allowance material in 38 radial brick joints. The use of expansion allowance at the cold face of the lining would allow the radial joints to remain in a more stable closed condition and minimize flow of process fluids or gases through the radial joints.

The use of plastic materials that burn out at a low temperature is perhaps better than a refractory blanket expansion allowance material. The blanket material may be easily compressed to a lesser thickness during installation, resulting in a loss of expansion allowance.

Expansion allowance in silica brick dome-type refractory linings is typically used only in the lower portion of the dome. The estimated portion of the dome above the skewback is in the lower quarter of the dome. Expansion plastic allowance material is placed in the vertical meridional joints. Domes made of alumina brick typically do not require expansion allowance.

V. LINING CONTAINMENT

It is important to remember that the refractory lining must be maintained in compression during service. This is especially important when liquid metal is to be contained. Consideration of the expected thermal gradient in the refractory wall and expansion behavior of those materials and the steel shell at the temperatures must be considered. If the steel shell expands too much at service temperatures, compression of the lining is lost, allowing failure of the lining. If allowances for expansion are not sufficient, the shell can be overstressed, causing shell damage and failure. Insufficient expansion allowance can also cause cracking and spalling of the lining refractory, leading to reduced lining life and failure of the lining.

Linings that are fully contained (or restrained) in all directions will result in a more successful lining. It has been shown that a fully contained lining is a stronger lining (7). An example of a well-contained lining is a cylindrical refractory lining on the interior of a steel shell with end restraints at both ends of the

cylindrical lining or a spherical refractory lining on the interior of a steel shell and end restraint from the skew. It is important that the installed lining have full containment since a well-contained lining is not only a stronger lining but also a more stable lining. Abrupt changes in lining thickness should be avoided since the hot face end of the thicker lining will not be contained. A transition in lining thickness can be accomplished by using corbelling, which allows a transition in the lining thickness and a transition of the expansion stresses from two extreme lining thicknesses. Any type of abrupt change in lining thickness in any type of lining geometry is not desired.

Changes in the lining refractory quality can also affect the structure much as dimensional changes. The differences in the properties of various refractories can change the heat flux and stress patterns in a lining. This is a normal practice where linings are zoned with different qualities of refractory, such as the slagline of a steel-making ladle. For example, a slagline using a 7-in. carbon bonded graphite bearing brick in the working lining, and a 3-in.-high alumina brick in the safety lining, has a calculated shell temperature of 845°F. With a 7-in.-high alumina lining as the working lining, it is calculated to have a 602°F shell temperature. This difference in shell temperatures can pose a problem because of stress imposed at the change boundaries because of differing expansion and strengths of areas of the steel shell. High-strength insulation materials allow reduction of shell temperatures without compression in service, enabling the lining to maintain compression and the shell to be kept at lower temperatures.

Hydraulic jacking is sometimes used in cylindrical linings as each layer of lining is installed. The jacking assures a tight lining and provides containment of each row. It is necessary to properly design for expansion in a lining installed in this way to ensure a proper stress distribution in the lining. Improper allowances will lead to spalling of the lining, damage to the shell, and loss of containment. If compressible blanket material is used as expansion allowance, then a portion of the expansion allowance is depleted because jacking compresses these blanket materials.

VI. STAGGERED JOINTS

Most refractory brick linings are installed with staggered joints. From the thermo-mechanical viewpoint, this is good practice since a torturous path is created for process gases and fluids. The compressive loading on the hot face of a properly restrained refractory lining also creates a mechanical seal to assist in preventing flow of the process gases and fluids to the back side of the lining. Typically, the backsides of the lining radial brick joints tend to open during the fully expanded condition of the lining. Therefore, the staggered joints are a valuable addition of mechanical seals. That is, the staggered joints allow the circumferential joints to act as mechanical seals. For example, staggered joints in a double-layered

cylindrical lining can apply to the radial joints or the circumferential joints. That is, a staggered thickness of the double-layer lining can be employed. However, with the staggered thickness of the double-layer lining, the radial joints cannot be staggered. The staggered radial joint of a double-lining system is the more popular lining system. Figure 3 shows that the bonded roof design of a sprung arch can be classified as an arch roof with staggered joints. Note also that the flat tunnel kiln walls have staggered joints along the length, height, and thickness of the wall.

VII. SELECTING THE BEST REFRACTORY

In selecting the best refractory for the applications, it is important to know the environment the refractory will be exposed to. The refractory engineer dealing with the chemistry aspects must make the appropriate decisions with regard to chemical compatibility with the process. Mechanical aspects should also be examined such as those listed in the ASTM Standards, Volume 15.01, Refractories; Carbon and Graphite Products; Activated Carbon. All of the refractory testing standards are too numerous to list here. The major groups for testing standards for refractories include General; Basic Refractories; Carbon–Carbon Ceramic Brick; Fireclay Refractories; Insulating Firebrick; Mortars, Plastics and Castables; and Silicon Carbide Refractories. The next major category is Manufactured Carbon and Graphite Products. The third category is Activated Carbon, and lastly Advanced ceramics. The refractory standard tests are established for bulk density and porosity, cold crushing and modulus of rupture at room and elevated temperature, thermal conductivity, thermal expansion, creep and modulus of elasticity (MOE), or Young's modulus by sonic method.

The sonic method used to determine the refractory MOE usually results in a conservative estimate (too high) of the refractory MOE when compared to the static compressive stress–strain (SCSS) data. The sonic tests also do not provide a complete stress–strain relationship over the full stress and strain range. That is, the sonic test provides the slope (MOE) of the stress–strain curve at a very low stress due to the nature of the sonic test. Often the three-point bending test is used to establish a stress–strain data curve. However, due to the very limited tensile strength, the data curve is very limited. According to available information, the tensile MOE and compressive MOE are not similar. Therefore, the stress–strain data curve from the three-point bending test leads a mix of tensile and compressive stress–strain behavior. The SCSS test provides the best stress–strain data curves for room and elevated temperature. The outstanding problem is that there is no ASTM standard for the SCSS test. A limited number of labs can conduct SCSS tests. The SCSS data curves provide the most accurate data to predict the compressive stress–strain behavior of a lining system (10). SCSS data on candidate bricks also provide valuable

information. These data can be used to choose the brick that has the greatest combined ultimate compressive stress and ultimate compressive strain.

Refractory materials generally have values reported for expansion as reheat expansion on supplier literature. It is important to understand that reheat expansion (contraction) is a simple test that gives values for the first heating of a refractory but does not report thermal expansion. Reheat expansion is sometimes called permanent expansion and occurs on first use of the refractory. The refractory can undergo changes to chemical, crystal, and mechanical properties during the initial heating. Thermal expansion, sometimes called reversible thermal expansion, is the change of size as the material is heated and the contraction when cooled. Both values are important to the performance of the refractory. Changes in material properties at temperature are especially important with castables, carbon-carbon refractories, and composite materials. Changes in these properties are usually not linear along the thermal gradient through the lining. Other properties important to the structure and performance of the lining are not linear as well, including strength and thermal conductivity.

VIII. CASTABLES

With respect to the thermal expansion behavior of castable linings, they can be defined as a brick lining without joint. Tensile fracture will be initiated in the same regions of hinge formation in a brick lining. The manner in which a castable is installed has a significant influence on the stiffness and strength of a castable (9). Vibrated castable is significantly stiffer than gunned castable. Both vibrated and gunned castable with steel fibers are less stiff than that without steel fibers. Since steel fibers have a greater coefficient of thermal expansion than most refractory types of castables, the thermal growth of the fibers is greater than that of the castable. As a result, tensile fracture cracks are developed in the castable in the vicinity of the fiber. Large vibrated monolithic sections of castable are not always better than the simply poured castable monolithic sections without vibration. The through-thickness temperature gradient can cause the large monolithic sections to thermally curl. With the higher stiffness and strength of vibrated sections, significant distortions and displacements will occur. Installing castable with steel fibers will not necessarily provide a stronger castable, but it will keep fractured pieces attached to the remainder of the lining. This is desirable to prevent clogging of various discharge openings in the vessel.

When using castables, it is important to consider the initial heating of the material. Castable undergoes considerable chemical changes during the initial heating, causing liberation of water from the refractory structure. Mechanical water that forms steam at 100°C (212°F) can place minor stress on the structure but is usually generated slowly and able to migrate through the porosity of the refractory body

without damage. Chemical water liberated from changes to the chemistry of the castable as the structure is subjected to heat is generally liberated at elevated temperatures. This causes rapid formation of high-energy steam at 400°C to 600°C. This steam can be explosive to the structure and cause considerable damage. In some cases, explosions, destructive to the structure and dangerous to surrounding personnel and equipment, are possible. The initial heating schedule should allow for very slow heating through the critical temperature range. The use of organic fiber in the castable has enabled castable refractory to be heated at faster rates by improving the ability of steam to migrate out of the structure without damage.

REFERENCES

1. Brockenbrough RL, Merritt FS, eds. *Structural Steel Design's Handbook*. 2nd ed. New York: McGraw Hill, 1994.
2. Harbison-Walker. *Handbook of Refractory Practice*. 2nd ed. Pittsburgh, PA, 1980.
3. Harbison-Walker. *Handbook of Refractory Practice*. 1st ed. Pittsburgh, PA: Indresco Inc., 1992.
4. Carniglia SC, Barna GL. *Handbook of Industrial Refractories Technology*. Park Ridge, NJ: Noyes Publications, 1992.
5. Fruehan RJ, ed. *The making, shaping and treating of steel. Coke and Ironmaking Volume*. 11th ed. Pittsburgh, PA: AISE, 1998.
6. Fruehan RJ, ed. *The making, shaping and treating of steel. Steelmaking & Refining Volume*. 11th ed. Pittsburgh, PA: AISE, 1998.
7. Schacht CA. *Refractory Linings: Thermomechanical Design and Applications*. New York: Marcel Dekker, 1995.
8. Schacht CA. Thermomechanical FEA Investigation of Contained and Noncontained Refractory Domes. American Ceramic Society 105th Annual Meeting & Exposition, April 27–30, 2003, Nashville, TN.
9. Alter WR. *Stress/Strain Testing of Refractories*. Livermore, CA: Kaiser Aluminum & Chemical Corporation, c. 1982.
10. Schacht CA, Abarotin EV. Structural Behavior of Teeming Ladles Lined with High-Alumina Refractories. Association of Iron and Steel Engineers 1983 Annual Convention. September 19–22, 1983, Pittsburgh, PA. August 1984 *Iron and Steel Engineer*, 33–40.

Index

- Abrasion, 1, 3, 447–448, 469, 472
- Acid attack, 470
- Acid resistance, 452
- Acidity and basicity, 40–41
- Aggregates, 17, 23, 28, 29, 30, 35, 226–229
 - fused, 226
 - sintered, 226–229
- Alkali attack, 452, 470
- Al₂O₃-MA refractories, 240–248
 - Al₂O₃-MgO castables, 246–248
 - Al₂O₃-spinel castables, 240–246
- Alumina, 337, 345, 351–355, 362, 439, 442, 448, 456, 459, 461, 464, 465, 466, 469, 472, 474
- Alumina-silica brick, 79–107
 - brief historical perspective, 80–81
 - 80% and 85% alumina brick, 99–101
 - 50% and 60% alumina class brick, 97–98
 - health and safety with, 106–107
 - insulating firebrick, 96–97
 - manufacturing of, 88–89
 - 90% and 99% alumina class brick, 101–103
 - properties and microstructure of, 89–94
- [Alumina-silica brick]
 - refractory raw materials, 84–85
 - changes on heating, 85–88
 - dehydroxylation of clay, 85–88
 - sillimanite and bauxite, 88
 - selected case studies, fireclay and high alumina, 103–106
 - semicordierite brick and kiln furniture, 94–95
 - 70% alumina brick, 98–99
 - technology of, 81–84
- Alumina, 17, 24, 34
- Alumino silicate, 17, 20
- Alumino silicates, 467
- Ammonia reformers, 406–407
- Anti-clogging characteristics, 195
- AOD process, 191
- Apparent porosity, 436, 439, 440
- Basic refractory, 17
- Biaxial stress state, 374
- Blanket and board expansion allowance, 388–390
- Blast furnace walls, 211–214
- Brazil test, 13
- Brick arch and dome hinges, 481–482
- Brick/mortar joint behavior, 378–379

- Bridge walls, 399
- Brittle, 16, 24, 26, 32
- Bulk density, 436, 439–440, 441, 442, 446, 447, 450, 452, 462, 463, 467, 468
- Byproducts coke oven battery, 415
 - AISI tall coke oven battery project
 - effect of charging rate, 432
 - effect of operating delays, 428, 429, 430
 - effects of wall stiffness, 423
 - two stage movement, 426, 430
 - wall location, 425, 430
 - wall motion sensor, 421
 - wall movement vs. charging, 421, 422, 425, 426, 427, 428, 429, 430, 431
 - wall movement vs. bulk density, 425, 426, 427, 428, 429, 430, 431
 - buckstays, 415
 - charging holes, 415
 - coke side, 416
 - coking coal
 - bulk density control, 416, 425
 - coal charging, 415, 416
 - coking pressure, 423, 429
 - preheated coal, 415, 416
 - wetcoal, 415
 - flues, 415, 419
 - heating walls, 415
 - dimensions, 417
 - number of, 415
 - thermal gradients, 417
 - wall taper, 417
 - refractories, 416
 - interlocking shapes, 417
 - quartz versions, 417
 - silica brick, 416
 - silica mortar, 417
 - thermal expansion, 417
 - heating wall damage
 - forensic study, 418
 - refractory stress, 418, 419
 - stress distribution, 419
 - unbalanced pressure, 418
 - wall flexure and movement, 418
- [Byproducts coke oven battery]
 - heating wall damage, cause of
 - cause of movement, 421
 - cyclic stresses, 420
 - induced stress, 418, 419
 - measure movement, 420
 - wall movement, 418, 419
 - history of, 418
 - machinery
 - door machine and coke guide, 416
 - larry car, 416
 - pusher machine, 416
 - quench car and tower, 416
 - operating temperatures
 - ovens
 - dimensions, 417
 - number of, 415
 - oven taper, 417
 - pinion walls, 415
 - pusher side, 416
 - tie rods, 415
- CaO-MgO phase diagram, 186
- Carbon, 201, 450, 453, 456, 457, 461, 464, 469, 470, 473
- Carbon bonding
 - chemical, 193
 - physical properties, 193
 - resin bond, 193
 - tar bond, 184
- Carbon monoxide attack, 453, 470 (*see also* CO attack)
- Carbon monoxide resistance, 453–454
- Carbonaceous refractory materials
 - blast furnace walls, 211–214
 - ceramic refractory comparison, 210–211
 - classification
 - carbon, 201
 - graphite, 203
 - hot pressed carbon, 202
 - hot pressed semigraphite, 204
 - semigraphite, 204
 - semigraphitized carbon, 204
 - comparison of heat flow, 209

- [Carbonaceous refractory materials]
composition and baking temperature, 205
grain size effect, 209
properties and characteristics
carbon, 205, 206
graphite, 208
hot pressed carbon, 206
hot pressed semigraphite, 207
semigraphite, 207
semigraphitized carbon, 207
- Case studies of corrosion, 53–75
- Castables, 17, 30, 35, 335, 336, 348, 442, 445, 447–448, 450, 459, 460, 472–473, 488–489
- Castable surface chemistry
agglomeration (*see also* Flocculation), 336–339, 341, 343, 345, 362, 363
alumina, 337, 345, 351–355, 362
castables, 335, 336, 348
installation of, 336
low-cement, 336
pumpable, 336, 362
rheology (*see* Rheology)
self-flowing, 336, 363
shotcrete, 336, 344, 362
ultralow-cement, 336
zero-cement, 354–356, 358, 363
cement, 344, 348, 359–363
calcium aluminate, 336, 358, 359, 361
dissolution, 360
hydration, 359, 361
chemical admixtures (*see* Dispersants)
coagulation (*see* Agglomeration)
counter-ions, 341, 343, 348
Debye parameter, 343–345
deflocculant (*see* Dispersant)
dispersant, 336, 344, 348–363
adsorption, 339, 344, 348, 351, 352–355, 360
anionic/cationic, 349–351, 353
architecture, 361, 362
charge density, 354, 355, 360, 361
conformation, 348, 358
- [Castable surface chemistry]
functional groups, 349, 353, 355, 360, 361
intercalation, 360
length, 348, 360–362
polyelectrolyte, 349
polymeric, 355
dispersion
mechanisms, 336, 339, 343, 348, 349, 362
of particles, 335–337, 343, 345, 348, 355, 361–363
DLVO theory, 341–345, 357
electric potential, double layer (*see* Layer)
surface, 341, 343, 345, 348, 351
Stern, 341, 343–347
flocculation
bridging, 356–358
depletion, 356–358
Hamaker constant, 337
ionic strength, 345, 348, 354, 358, 362, 363
isoelectric point (IEP), 351, 355
layer
diffuse, 341, 346–348
electric double, 339–341, 345, 346
steric, 358
Stern, 341, 344, 346, 348
measuring techniques, 346, 347
potential energy
attractive, 337, 341
repulsive, 341, 343
total, 341, 345, 348, 362
rheology
of castables, 336, 339, 348, 354–356, 358, 359, 361, 362
of suspensions, 335, 339, 345, 354–356, 358, 362
silica (*see* Silicon oxide)
silicon
carbide, 340, 341
nitride, 340, 341
oxide, 341, 351, 362

- [Castable surface chemistry]
 - surface
 - charges, 336, 339–341, 344, 346, 348, 352
 - chemistry, 335, 336, 348, 359
 - electric potential (*see* Electric potential)
 - forces, 335–337, 339, 345, 355, 361, 362
 - modification, 349–352
 - oxidation, 341
 - point of zero charge (PZC), 340, 341, 344
 - van der Waals (*see* Potential energy and Surface forces)
 - zeta potential, 345–348, 351, 354–356, 358
- Cement production applications, 192, 191
- Ceramic fibers, 327
- Ceramic properties, 9
- Chemical analysis of dolomite raw materials, 186
- Chemical analysis, 437, 467
- Chevron notch specimen, 21
- Choosing best refractory, 374, 487–488
- Circulating Fluid Bed Combustors, (CFBCs), 411
 - alkali attack, 414
 - high ash content fuels, 412
 - expansion joints, 399
 - erosion, 401, 402, 403, 413
 - fluid catalytic cracking units, (FCCUs), 401
 - coke filled refractories, 402, 403
 - properties of, 404
- CO attack, 470
- Cold crushing strength (CCS), 436, 441, 442, 468, 473 (*see also* Compressive strength; Compressive stress)
- Compressive strength, 436 (*see also* Cold crushing strength; Compressive stress)
- Compressive stress, 462, 464, 466 (*see also* Cold crushing strength; Compressive strength)
- Compressive stress-strain, 436, 463–464, 466
- Corrosion of refractories, 39–77
 - case studies of corrosion, 53–75
 - corrosion (phenomenological description), 42–47
 - reaction and temperature gradients, 43–44
 - thick wall, 45–47
 - thin wall, 44–45
 - corrosive environment, 39–41
 - equilibrium and phase diagrams, 47–49
 - laboratory slag tests, 75–76
 - porosity and corrosion, 41–42
 - refractory and slag compatibility, 40
 - acidity and basicity, 40–41
 - selected models for slag attack, 49–53
- Corrosion resistance, 436, 445, 451–452, 470
- Creep, 436, 450, 455, 462, 471, 474
- Cylindrical lining behavior, 482–483
- Coefficient of thermal expansion, 371
- Compressive strength, 5
- Compliance, 14
- Composites, 12
- Conductivity, 3, 7, 8
- Corrosion, 8, 9, 12
- Crack, 11–38
 - bridging, 28, 29, 30, 34, 35
 - friction, 30
 - growth resistance, 32
 - mouth opening displacement, 29, 30
 - opening displacement, 29, 30
 - process zones, 11, 19, 28, 29
 - stoppers, 19
 - wedging, 30
- Cylindrical lining behavior, 380–384, 387–388
- Data sheets, 436
- Density, 5, 439–441, 442, 446, 447, 450, 452, 456, 462, 463, 467, 468
- Design properties, 455–466
- Direct-bonded dolomite, 184
- Direct-bonded dolomite
 - chemical analysis, 193

- [Direct-bonded dolomite]
 - microstructure, 190
 - properties, 193
- Doloma
 - chemical analysis, 187
 - definition, 185
 - high purity, 186
 - physical properties, 187
 - synthetic, 185
- Doloma brick
 - hydration susceptibility, 189
 - slag resistance, 189
 - steelmaking, 188
- Doloma in steelmaking, 183
- Doloma-graphite SEN, 197
- Dolomite, 442, 454, 459, 467, 470
- Dolomite monolithics
 - repair materials, 195
 - safety linings, 195
 - working linings, 195
- Dugdale, 28
- Dynamic modulus of elasticity, 462, 463

- EAF dome, 478
- EAF door jamb, 478
- 80% and 85% alumina brick, 99–101
- Emissivity, 450, 460
- Equilibrium and phase diagrams, 47–49
- Erosion, 8, 9
- Exudation, 454–455, 470
- Expansion allowance examples,
 - 390–393, 484–485

- Fibers, 30
- Fiber blanket, 460
- 50% and 60% alumina class brick, 97–98
- Finite element analysis, 378
- Finite element modeling, 455, 462, 463
- Firebrick, 446, 448, 456, 459, 461
- Fireclays, 17, 24
- Fired doloma, 184, 196, 192
- Flat wall lining, 387, 483
- Flaw size, 17
- Flexural strength, 5, 6, 443
- Flexural stress–strain, 436, 464, 465, 466
- Flowability, 3

- Fluid bed reactor domes, 478
- Four point bend, 443, 464, 465
- Fracture, 11, 12
 - criterion, 32
 - nonlinear, 19, 26, 31, 34
 - toughness, 14, 16, 17, 20, 27, 35
- Frontal process zone, 20, 28
- Furnaces, 397
 - anchorage, 398
 - ceramic fiber use, 399
 - expansion allowance, 397
 - lining design, 399

- Glass contact refractories, 452, 454
- Grain bulk density, 468
- Graphite, 203
- Gravity load, 370
- Griffith equation, 14
- Gunning mixes, 10

- Hasselmann Parameters, 451, 472, 473
- Heatflow, 455, 456, 457, 458 459
- High purity doloma microstructure, 185
- Hot modulus of rupture (Hot MOR), 436
 - (*see also* Modulus of Rupture)
- Hot pressed carbon, 202
- Hot pressed semigraphite, 204
- Hydration resistance, 454, 470
- Hydration resistance
 - natural doloma, 190
 - synthetic doloma, 190
- Hydrocarbon, 3
- Hydrogen-silica reactions, 405, 406, 408

- Incinerators, 410
- Inductively Coupled Plasma, LC.P, 437
- I-integral, 11, 13, 14, 19, 20, 24, 25, 26
- Insulation, 441, 442, 445, 456, 458, 460, 468, 469

- Kinetic crack growth, 18

- Laboratory slag tests, 75–76
- Ladle refining applications, 194
- Lining containment, 485–486
- Lining design, 385

- Lining geometries, 480
 - Lining restraint, 387
 - Lining system, 369
 - Load types, 370
 - Loading rate, 15

 - Magnesia, 439, 454, 456
 - Magnesia carbon, 459
 - Magnesia chrome, 442
 - Magnesia graphite, 461
 - Magnesia refractories, 109–149
 - applications for, 138–144
 - industrial industries, 142–144
 - cement, 142
 - copper, 143–144
 - glass, 142
 - classification of, 136–138
 - by American Society for Testing and Materials, 138
 - by International Org. for standardization, 136–138
 - by other organizations, 138
 - refractory forms, 136
 - by U.S. Government, 136
 - definitions of, 109–110
 - examples of, 144
 - magnesia–carbon paradox, 126–128
 - manufacture of, 131–136
 - burning, 135
 - drying, curing, tempering, 135
 - final inspection, 135–136
 - post-treatments, 135
 - pressing or forming, 134
 - raw materials handling for, 131–134
 - batching of, 133
 - crushing, grinding, and screening of, 132–133
 - mixing of, 133–134
 - receiving, 132
 - specifying, 131–132
 - raw materials used in manufacturing of, 110–131
 - binders, 129–131
 - inorganic, 130
 - organic, 130–131
 - carbon black, 124–125
-
- [Magnesia refractories]
 - chrome ore, 118–121
 - characteristics of, 120–121
 - production of, 119–120:
 - Philippine chrome ore, 120;
 - Transvaal chrome ore, 119, 120
 - properties (chemical and physical) of, 118–119, 121
 - sources of, 119–120:
 - Philippine chrome ore, 120;
 - Transvaal chrome ore, 119–120
 - dead-burned dolomite, 129
 - dead-burned magnesium oxide, 111–118
 - characteristics of, 114–118:
 - bulk density, 117–118;
 - crystallite size, 117;
 - impurities, 114–117;
 - MgO content, 114;
 - thermal expansion, 118
 - production of, 112–113:
 - natural, 112–113;
 - synthetic, 113
 - properties (chemical and physical) of, 118
 - sources of, 111–112:
 - natural, 111–112;
 - synthetic, 112
 - doloma (*see* Dead-burned dolomite)
 - forsterite, 129
 - graphite, 125–126
 - magnesia (*see* Dead-burned magnesium oxide)
 - magnesia-chrome grain, 121–122
 - magnesite (*see* Dead-burned magnesium oxide)
 - magnesium aluminate spinel, 122–124
 - metals, 128–129
 - reasons for using, 128–129
 - types of, 128
 - MgO (*see* Dead-burned magnesium oxide)
 - nonoxides, 128–129
 - reasons for using, 128–129
 - types of, 128
 - periclase (*see* Dead-burned magnesium oxide)
 - pitches, 130–131

- [Magnesia refractories]
 - from coal, 130–131
 - from petroleum, 131
 - resins, 131
 - novolacs, 131
 - resoles, 131
 - steelmaking, 138–141
 - primary steelmaking, 138–141
 - basic oxygen furnaces, 139, 140–141
 - electric arc furnaces, 140, 141:
 - argon oxygen decarburization reactors, 140; open hearth furnaces, 139
 - secondary steelmaking, 141
 - degassers, 141
 - ladle metallurgical furnaces, 141
 - slide gate plates, 141
 - tundishes, 141
 - terminology related to, 110–111
- Magnesite, 442, 459, 467, 470
- Mathematical modeling, 435, 456, 463
- Mechanical material property, 372
- MgO enrichment, 191
- Microcracks, 28
- Microcracking in fired doloma, 191
- Microscopic examination, 438–439
- Microscopy, 435, 439
- Microstructure, 35, 436, 439, 452
 - fired doloma brick, 190
 - high purity dolomite, 185
 - microcracking, 191
 - zirconia additions, 191
- Mineralogical analysis, 437–438
- Modulus of elasticity (MOE), 152, 372, 449–451, 462–463
- Modulus of rigidity, 462, 463
- Modulus of rupture, 5, 13, 436, 441, 443, 444, 448, 450, 451, 464, 469 (*see also* Hot Modulus of Rupture)
- Mortar joint behavior, 376–378
- Mullite, 10
- Multiple cracking, 28
- Naphtha reformers, 404, 405
 - [Naphtha reformers]
 - thermal conductivity in hydrogen atmospheres, 405
 - 90% and 99% alumina class brick, 101–103
 - Nonporous, 3
 - Non-wetting, 2
 - Notched beam test specimen, 16, 22
 - Penetration, 2
 - Permanent linear change (P.L.C.), 436, 446–447, 469
 - Permanent volumetric change, 446–447, 469
 - Permeability, 444–445, 452, 468, 472, 473
 - Petrochemical, 6
 - Phosbonded plastic, 10
 - Plasticity, 16
 - Poisson's ratio, 436, 451, 462, 463
 - Pore size distribution, 445, 452, 468
 - Porosity, 5
 - Porosity and corrosion, 41–42
 - Powder density, 468
 - Properties of refractories, 396
 - Pumpable, 3
 - Pyrometric cone equivalent (P.C.E.), 436, 445–446, 469
- Quasi-static crack growth, 18
- Rammability, 4
- R-Curve, 11, 12, 19, 22, 29, 31–33, 35
- Refractoriness under load (RUL), 436, 448, 462, 469
- Refractory aggregates, 11
- Refractory and slag compatibility, 40
- Refractory brick shapes, 477
- Refractory castables
 - bonding, 265–269
 - composition, 260–270
 - physical properties, 270–283
 - types, 260
- Refractory properties, 442
- Resonant frequency, 450, 462, 463
- Roof hanger support, 388
- Rotary kiln lining, 479

- RST values, 197
 RWTUV, 151
- Scanning electron microscopy, 439
 Seal pots, 404
 Selected models for slag attack, 49–53
 Semicordierite brick and kiln furniture, 94–95
 Semigraphite, 207
 Semigraphitized carbon, 207
 Seventy percent alumina brick, 98–99
 Shaped, 3
 Silica brick, 442, 449, 461, 467
 CIC tests, 152
 modulus of rupture, 153
 silica KD, 151, 153
 creep response, 174–175
 hot crushing strength, 172–173
 MOE, 169
 MOR, 170
 SCSS data, 152, 153, 155–160
 thermal expansion, 167–168, 176
 silica KN, 151
 creep response, 176, 180–181
 hot crushing strength, 176, 179
 MOE, 176–177
 MOR, 176–178
 SCSS data, 152, 153, 155, 162–167
 thermal expansion, 172
 specimen size, 152
 test temperature, 152
 Silicate bridging, 28
 Silicates, 12, 15, 16, 29
 Silicon carbide, 450
 Slag, 12
 line, 12
 test, 9
 Slide valves, 404
 Sol-gel bonding, 7
 Spalling, 450, 469
 Specific heat capacity, 436, 450, 460
 Spinel containing refractories
 corrosion, 238–240, 243–249
 grain, 226–229
 microstructure, 229, 230, 232, 238, 242
 MgO-Al₂O₃ reaction, 222
 [Spinel containing refractories]
 MgO-MA refractories, 230–240
 castables, 237
 in cement kilns, 235–236
 corrosion, 238–240
 in glass tanks, 234–235
 in steelmaking, 231–233
 MgO-Al₂O₃-TiO₂ refractories, 249–252
 MgO-Al₂O₃-ZrO₂ refractories, 249
 phase Diagram
 electrofusion, 223–224
 hydrothermal, 225
 mechanochemical alloying, 225
 mixed oxides, 221–223
 MgO-Al₂O₃, 219
 molten salts, 225
 powder synthesis, 221–225
 sol gel, 224–225
 wet synthesis, 224–225
 properties 216, 217, 219, 228, 229, 233, 234, 236, 241, 242, 250, 251
 spinel
 crystallography, 217–218
 MA properties, 217, 219
 stoichiometry, 218, 220, 221, 227
 types, 215, 216, 230
 spinel-bonded spinel, 248–249
 spinel-C, 252
 Sprung arch design, 480
 Staggered joints, 486–488
 Stainless steel fiber, 403
 Static compressive stress/strain (SCSS)
 data, 372, 476
 for alumina brick, 373
 for silica brick, 155–167
 Static modulus of elasticity, 463
 Strain, 450, 461, 462, 463, 464, 465, 466
 Strain-controlled load, 370, 371
 Strain energy release rate, 20, 24, 26, 27, 31, 33
 Steels, 17
 Stress, 436, 441, 443, 446, 448, 449, 450, 455, 460, 461, 462, 463, 464, 465, 466, 472
 Strengths, 15, 18, 35

- Stress-controlled load, 370, 371
 Stress state dimensionality, 373
 Sulfur plants, 409
 silica fume additions, 410
 Surface energy, 23
- Tancrede de Dolomieu, 183
 Tensile tests, 443
 Thermal conductivity, 436, 440, 449,
 450, 455–460, 471, 473
 Thermal expansion, 436, 449, 450, 451,
 460–462, 464, 471, 473, 474
 Thermal material properties, 372
 Thermomechanical, modeling, 450
 Thermal shock, 6, 11, 13, 33, 35, 436,
 445, 449–451, 469, 472, 473, 474
 Thermal stress, 13, 17
 Thermo elastic, 18
 Thermomechanical behavior, 436, 455,
 474
 Three point bend, 443, 451
 Tough, 24, 26, 35
 Triaxial stress state, 375
 True density, 440–441, 468
 True porosity, 435, 440–441, 467, 468
 Tundish nozzles, 196
- Ultimate crushing strength, 152
 Unshaped, 3
 Unshaped Refractories
 ceramic fibers, 327
 chemical composition, 296
 chemically bonded castables, 294
 classification, testing, 297
 coatings, 296
 definitions, 292
 deflocculated castables, 293
 low cement castable LCC, 292
 medium cement castable MCC,
 293
 no cement castable NCC, 294
 ultra low cement castable ULCC,
 294
 dehydration of castables, 329
 dehydration of clay bonded products,
 330
- [Ultimate crushing strength]
 dry mixes, 295
 drying, 328
 European Standard EN 1402, 291
 heating up, 328
 injection mixes, 296
 maximum grain size, 293
 metallic fibers, 326
 methods of placement, 300
 concrete work, 301
 gunning, 305
 ramming, 304
 shotcreting, 305
 organic fibers, 326
 plastic refractory material, 295
 PRE, 289
 preformed shapes, 328
 properties of unshaped refractory
 products, 306
 castables, 306
 plastic refractories, 315
 refractory ramming material, 315
 refractory gunning materials, 317
 special products, 323
 refractory gunning materials, 294
 refractory jointing materials, 295
 refractory moldable material, 294
 refractory ramming material, 295
 regular castables, 293
 setting of castables, 303
 shotcreting, 319
 SIPRE, 290
 standardization, 288
 tap hole mixes, 296
 test pieces, 298
 VDEh code, 299
 vibrating, 3, 301
 yield by volume, 293
- Wake region, 19, 20, 28
 Wedge splitting test, 11, 24, 25
 Window glass, 17
 Work of fracture, 16, 18, 20–26, 29, 32
 Workability, 4
- Zirconia additions, 191, 192

about the book . . .

This reference comprehensively details the technical, chemical, and mechanical aspects of high-temperature refractory composite materials for step-by-step guidance on the selection of the most appropriate system for specific manufacturing processes — surveying a wide range of lining system geometries and material combinations to meet the day-to-day referencing needs of refractory manufacturers, designers, engineers, and consumers in industrial settings.

Covers a broad range of tests for the determination of the thermal, mechanical, strength, and resistance properties of refractories.

With contributions from international specialists with widespread experience in the field, this reference provides valuable recommendations on the design and installation of refractory lining systems...describes the most significant factors in castable lining design...provides examples of refractory lining systems utilized in a range of industries including petrochemical, glass, cement, and steel...considers the classification of load types, as well as issues related to refractories strength; compressive stress/strain data; arch, spherical, flat wall, and cylindrical lining behavior; and expansion allowance...highlights the latest developments in spinel-containing refractories and their application to steel, cement, and glass, manufacture...offers procedures to maximize the life of refractory lining systems...and contains detailed descriptions of laboratory testing methods for evaluation of refractory properties.

about the editor . . .

Charles A. Schacht is Consulting Engineer, Schacht Consulting Services, Pittsburgh, Pennsylvania. With more than 35 years of experience in the field, he is the author of numerous professional publications including *Refractory Linings* (Marcel Dekker, Inc.) and has lectured worldwide on the mechanical behavior of refractory linings. He is a member of the American Society of Civil Engineers, the American Society of Mechanical Engineers, the American Ceramic Society, and the American Institute of Mining, Metallurgical and Petroleum Engineers, among other organizations. Dr. Schacht received the B.S. degree (1960) in civil engineering from The Ohio State University, Columbus, and the M.S. (1968) and Ph.D. (1972) degrees in civil engineering from Carnegie Mellon University, Pittsburgh, Pennsylvania.

Printed in the United States of America



MARCEL DEKKER, INC.
NEW YORK • BASEL

ISBN 0-8247-5654-1



9 0000